



**UNIVERSITEIT
GENT**

Faculteit Wetenschappen
Vakgroep Geografie
Academiejaar 2006-2007

**The Use of Remote Sensing for Coral Reef Mapping
in Support of Integrated Coastal Zone Management
A Case Study in the NW Red Sea
Volume I**

**Het Gebruik van Teledetectie voor het Karteren van Koraalriffen
ter Ondersteuning van het Geïntegreerd Beheer van Kustgebieden
Een Gevalstudie in de NW Rode Zee
Volume I**

Tony Vanderstraete

Promotor: Prof. Dr. R. Goossens (Vakgroep Geografie, UGent)
Co-Promotor: Prof. Dr. T.K. Ghabour (National Research Centre, Cairo, Egypt)

Scriptie voorgedragen tot het behalen van de graad van
Doctor in de Wetenschappen: Geografie

‘A paradigm shift may be occurring in the evolution of the role of scientists in society from simply observers of the natural world with tenuous linkages to resource managers and the public, to partners in modern society’s quest for answers to pressing questions related to sustainable use and conservation of coral reef resources.’ (Crosby *et al.*, 2002: 121)

PREFACE

Tempus fugit! ... Time flies! It has been six years since I started my journey as a PhD student. Little I knew what was ahead of me. Sure enough I could explore an interesting and fascinating topic but many were the hurdles which had to be taken. Out of the plentiful ways in which remote sensing and coral-reef studies can be combined, what lead would I take? The difficulty, once chosen, to ignore the other, obviously interesting, topics and conversely, also to stay focused on the chosen path. What part would I play in this? Dig into the fundamentals of remote sensing and develop new algorithms or explore their applications? Finally, all pieces fell into place, the result of which is presented here.

Fortunately, I did not have to make this endeavour on my own and I would therefore like to acknowledge the numerous people who helped and supported me in their own but appreciated way. First and foremost, I would like to thank my promoter, Prof Dr Rudi Goossens, who scientifically guided me through the PhD process, not ignoring the social and humane dimensions either. I am greatly indebted to my co-promoter, Prof Dr Tharwat Ghabour, who supported and assisted in the field campaigns even in more difficult conditions. I express my gratitude to Prof Dr Morgan De Dapper who has put me on track of this research topic. I also acknowledge the 'Fonds voor Wetenschappelijk Onderzoek (FWO-Vlaanderen)' which has granted me a scholarship for the first four years of my PhD research.

My thanks go to Prof Dr Ann Vanreusel and Prof Em Dr Paul De Paepe for reviewing specific parts of my thesis and their useful comments and discussions. I sincerely pay tribute to Dr Beata Devliegher who tremendously helped me with the editing of the numerous figures presented. Many thanks also to all staff of VooDoo Divers who have made great efforts to make the field campaigns in Hurghada a success.

I would like to express my appreciation to all my colleagues and friends who were willing to lend me an ear especially during the less amusing stages I had to pass. Special thanks to all Boudewijners with whom I have spent countless pleasant hours and days. You are too numerous to name personally, with the risk to forget just one, but be aware of my sincere affection.

Finally, but not the least, I thank my parents and family who have supported my choices in life and had to live with mostly vague answers to their questions on what I was up to or what I exactly do at work. I hope you have a clearer view by now.

Many thanks to all of you and, surely, the best is yet to come.

ABSTRACT

Coral reefs are globally endangered: an estimated 58% are immediately threatened by coastal anthropogenic activities while during one single mass coral bleaching event in 1997/1998, more than 16% were killed worldwide. The situation in the NW Red Sea is especially worrisome as uncontrolled coastal development and tourism have already damaged numerous reef structures and may potentially endanger even more areas in future. If the coastal zone, conversely, is effectively managed and sustainably exploited, the coral reefs may trigger the development of the region with benefits to people and nature alike. The sustainable development of coral reefs is therefore acknowledged by international institutions, like the UN, and decision-makers at all levels of society.

Integrated coastal zone management (ICZM) becomes more and more accepted as the best procedure to handle this topic. An effective ICZM requires reliable baseline information on the current status of the coral reefs, on the actual human interferences with these natural resources and the underlying reasons for this handling, as well as a method to monitor changes in these elements. Obtaining this kind of information using in situ observations is very time and labour intensive and consequently also financially demanding. As a result, only small parts of the coral reef can be surveyed on a regular basis. Developing countries, which have a main interest in coral reef management, usually do not have the assets to collect these data and large stretches of reef remain totally unsurveyed. This is one of the reasons why management efforts in these countries usually remain unsuccessful. Here, remote sensing comes to the aid as it synoptically collects information over relatively large areas in a standardised format and this very cost-efficient. This study demonstrates the potential of remote sensing to map coral reefs, specifically aimed at supporting ICZM.

Although the research is focused on the reefs in the NW Red Sea and specifically the Hurghada region (Egypt), the developed methodology is intended to be worldwide applicable. The term remote sensing, in contrast, is restricted to passive, optical remote sensing from spaceborne platforms as these data are most readily available and affordable for developing countries; use has specifically been made of Landsat 5 TM, Landsat 7 ETM+, QuickBird and ASTER data. Other platforms such as SeaWiFS, MODIS or ENVISAT do provide useful information on the biogeophysical characteristics of the Red Sea, but current algorithms are developed for open-water conditions. The adaptation of these algorithms to fit the coastal coral-reef environment does not fit the timeframe of this work.

Based on the Landsat 7 ETM+ and QuickBird datasets, information has been derived on the bathymetric structure of the coral reefs by applying the depth-of-penetration-mapping method (Jupp, 1988), modified by Edwards (1999). This has respectively resulted in a bathymetric model at 30m resolution with a mean residual error of -1.13m and a Pearson correlation coefficient of 93%, and a spatially restricted model at 2.8m resolution with a mean residual error of -0.24m and a Pearson correlation coefficient of 90%. Despite some problems with dark substrates, both models depict a useful representation of the seabed topography; a view which is difficult to obtain using conventional bathymetric mapping procedures. Two alternative bathymetric mapping methods, being the ratio-transform method (Stumpf *et al.*, 2003) and a digital photogrammetric approach based on the stereoscopic ASTER data, have been tested as well but these have not resulted in acceptable bathymetric models.

Next, the distribution of coastal habitats has been defined using the Landsat 7 ETM+ and the QuickBird dataset by mapping the geomorphological zonation as well as the bottom-type composition of the reefs. Geomorphological zones have been delineated on a colour composite enhanced with the previously derived bathymetric models and both results give a clear overview of the complex reef structures in the NW Red Sea. Bottom types have been defined using a maximum-likelihood classification algorithm which has been improved by introducing textural information in the Landsat 7 ETM+ case; the QuickBird analysis has been ameliorated by calibrating the water-column correction technique over a seagrass substrate. Both classifications have also benefited from post-processing contextual editing. The bottom-type classifications provide an acceptable broad-level inventory of the main bottom types in the study area, being bare substrates, corals, seagrasses and algae. The higher spatial resolution of the QuickBird dataset has allowed more thematic detail and a subdivision could be made according to the density of the seagrass- and algae-dominated substrates. Information was however lacking to quantify these gradients. The accuracy assessments of both classifications, performed on the same detail level, have resulted in an overall accuracy of 60%. This value, however, only gives an indication of accuracy as the validity of this statistical measure may be questioned due to the limited number of evenly distributed control points. The bottom-type inventories and the geomorphological zonation maps have subsequently been combined into integrated coastal habitat maps.

The possibility to detect changes in land use/land cover and bottom-type distribution has also been investigated using a Landsat 5 TM dataset of 1987 and the Landsat 7 ETM+ dataset dating of 2000. Changes in coastal development have been defined by detecting expansions of the urban centre and the road network. Coral-reef bottom-type changes have conversely been

defined by applying a multi-component change detection algorithm (Pilon *et al.*, 1988). This multitemporal analysis has confirmed the booming coastal development in the region over the last two to three decades and has shown that the urban centre of Hurghada has increased from 5 to ca. 36km², mainly in a ribbon-like fashion along the coastline. This has resulted in important coastline changes and the massive destruction of fringing reefs. Further offshore, significant bottom-type changes have been detected as well, but information was missing to link these changes to the coastal development.

The remote-sensing-derived datasets are best integrated into a GIS to allow the further analysis of these data in conjunction with auxiliary datasets and the development of valuable ICZM decision-support products. The example has been given of a risk assessment map indicating the potential stress posed by coastal anthropogenic activities on the coral reefs in the Hurghada region. This map not only illustrates the threatened future of these coral reefs if mitigation rules are not imposed, but also supports the delineation of a multi-use MPA. A draft initial multi-use MPA zoning scheme has therefore been represented to exemplify the strength of remote sensing and GIS to support the ICZM process.

Although the accuracy of the derived products can be improved, the obtained results already represent valuable information on the configuration and composition of the coral reefs in the NW Red Sea which is difficult to obtain otherwise. As each dataset has its own merits and demerits, the best and most cost-effective approach would be multi-level sampling in which global datasets are applied to derive large-scale information on the biogeophysical parameters of the seas and oceans in which the coral reefs occur; high-resolution datasets, such as Landsat, are used to obtain broad-level information on the configuration and composition of the coral reefs on a regional to local scale; while very-high-resolution data, such as QuickBird, are employed to provide more detailed information on specific focus areas. These remote-sensing-derived data should then be incorporated in a Coral Reef GIS together with auxiliary information, e.g. from field observations, to further analyse and interpret the data. This GIS would then form a valuable information source for ICZM decision-makers to organise the coastal zone in order to balance economic development and nature conservation. Such an approach is not only urgently needed for the already seriously degraded coral reefs today, but even more to combat the grim future of coral reefs worldwide.

SAMENVATTING

Koraalriffen worden wereldwijd bedreigd: ongeveer 58% staat onmiddellijk onder druk door menselijk handelen in de kustzone terwijl gedurende één enkele massale *coral bleaching* in 1997/1998, meer dan 16% van de koralen gedood werden. De situatie is uitzonderlijk zorgwekkend in de noordwestelijke Rode Zee omdat ongecontroleerde kustontwikkelingsprojecten en toerisme daar reeds vele riffen beschadigd hebben en eventueel nog meer gebieden kunnen aantasten in de toekomst. Als de kustzone daarentegen efficiënt wordt beheerd en duurzaam ontgonnen, dan kunnen koraalriffen bijdragen tot de algemene ontwikkeling van de regio waarbij zowel de mensen als de natuur voordeel halen. De duurzame ontwikkeling van de koraalriffen wordt daarom erkend door internationale instellingen zoals de UN en beleidsmakers op zowat alle niveaus van de samenleving.

Een Geïntegreerd Beheer van Kustgebieden (GBK) wordt meer en meer gezien als de beste oplossing om deze doelstelling te bereiken. Een efficiënt GBK vereist in de eerste plaats betrouwbare basisinformatie betreffende de huidige toestand van de koraalriffen, de actuele antropogene invloeden op de koraalriffen en de achterliggende oorzaken ervan, maar ook middelen om de toekomstige evoluties van deze elementen op te volgen. Het verkrijgen van deze informatie door middel van in situ waarnemingen is zeer tijds- en arbeidsintensief en daarom ook financieel veeleisend. Ontwikkelingslanden, die uitermate belang hebben bij het behoud van de koraalriffen, hebben meestal niet de middelen om deze data te verzamelen en grote delen van de koraalriffen in de wereld werden daarom nog nooit onderzocht. Dit is een van de belangrijkste redenen waarom beheersmaatregelen in deze landen vaak zonder resultaat blijven. Teledetectie kan hier een uitkomst bieden aangezien dit toelaat om informatie synoptisch te verzamelen over relatief grote gebieden, deze data in een gestandaardiseerd formaat aan te bieden en dit alles op een zeer rendabele manier. Het doel van deze studie is dan ook het potentieel van teledetectie om koraalriffen in kaart te brengen aan te tonen, met speciale aandacht voor die informatie die het GBK kan ondersteunen.

Alhoewel dit onderzoek vooral gericht is op de riffen in de noordwestelijke Rode Zee, en specifiek op de regio rond Hurghada (Egypte), is de ontwikkelde methodologie bedoeld om wereldwijd toegepast te kunnen worden. De term 'teledetectie', daarentegen, is beperkt tot optische informatie geregistreerd door passieve sensoren aan boord van satellieten aangezien deze data zeer vlot beschikbaar is en eveneens betaalbaar voor onderzoekers en managers in ontwikkelingslanden. Er is voornamelijk gebruik gemaakt van Landsat 5 TM, Landsat 7 ETM+, QuickBird en ASTER data. Andere sensoren zoals SeaWiFS, MODIS of ENVISAT

leveren eveneens bruikbare informatie betreffende de biogeofysische eigenschappen van de Rode Zee, maar de huidige algoritmes toegepast op deze informatie werden voornamelijk ontwikkeld voor open water en het aanpassen ervan aan het kustmilieu waarin de meeste koraalriffen in de Rode Zee voorkomen, past niet in het tijds kader van dit onderzoek.

Informatie betreffende de bathymetrische structuur van de koraalriffen werd verkregen door het toepassen van de '*depth-of-penetration-mapping*' methode (Jupp, 1988), aangepast door Edwards (1999), op de Landsat 7 ETM+ en QuickBird data. Dit heeft respectievelijk geleid tot een bathymetrisch 30m resolutie model met een gemiddelde residuale fout van -1.13m en een Pearson correlatiecoëfficiënt van 93%, en een 2.8m resolutie model over een kleiner gebied met een gemiddelde residuale fout van -0.24m en een Pearson correlatiecoëfficiënt van 90%. Ondanks enkele problemen over een donkere ondergrond, bieden beide modellen een bruikbaar beeld van de topografie van de zeebodem; informatie die moeilijk te verkrijgen is door gebruik te maken van meer conventionele bathymetrische technieken. Twee alternatieve technieken, zijnde de '*ratio-transform*' methode ontwikkeld door Stumpf *et al.* (2003) en een digitaal fotogrammetrische benadering gebaseerd op de stereoscopische ASTER data, werden eveneens getest maar deze leverden geen bruikbare informatie op.

Ten tweede werd de ruimtelijke verdeling van de habitats bepaald op de Landsat 7 ETM+ en QuickBird beelden door het in kaart brengen van de geomorfologische rifstructuren en de benthische samenstelling van de koraalriffen. De geomorfologische structuren werden afgebakend op kleurencomposieten die versterkt werden door de eerder verkregen dieptemodellen toe te voegen. Beide resultaten leveren een duidelijk overzicht van de complexe geomorfologische structuur van de koraalriffen in de noordwestelijke Rode Zee. De benthische samenstelling werd gedefinieerd door het toepassen van een '*maximum-likelihood*' classificatie-algoritme op beide beelden. De classificatie van het Landsat 7 ETM+ beeld werd verbeterd door het inbrengen van textuur-informatie, terwijl de QuickBird classificatie positief beïnvloed werd door het calibreren van de waterkolomcorrectie met data verzameld over zeegrasbedden. Beide classificaties profiteerden eveneens van een contextuele bewerking gebaseerd op de algemene ecologische zonerings van koraalriffen. De bekomen classificaties bieden een aanvaardbare inventaris van de voornaamste bodembedekkingsklassen in de regio, zijnde onbedekte substraten, koralen, zeegras en algen. De hogere ruimtelijke resolutie van de QuickBird data laten een meer gedetailleerde classificatie toe en een onderverdeling in de zeegras- en algenklasse kan gemaakt worden op basis van hun densiteit. Informatie ontbrak echter om deze dichtheidsgradiënten te

kwantificeren. De validaties van beide classificaties, uitgevoerd op hetzelfde niveau van detail, leverden een algemene nauwkeurigheid op van 60%. Dit getal geeft echter slechts een indicatie van de nauwkeurigheid van de resultaten omdat de waarde van deze parameter zelf in vraag kan worden gesteld door het gebrekkige aantal homogeen verspreide controlepunten. De bodembedekkingsclassificaties en de geomorfologische zoneringskaarten werden daarna samengevoegd om te komen tot geïntegreerde kusthabitatkaarten.

Ten derde werd de mogelijkheid nagegaan om veranderingen in landgebruik en mariene bodembedekking vast te stellen door gebruik te maken van een Landsat 5 TM beeld van 1987 en het Landsat 7 ETM+ beeld dat dateert van 2000. De ontwikkeling van de kustzone werd bepaald door het bepalen van de uitbreiding van het stadscentrum en het wegennetwerk. Veranderingen in de mariene bodembedekking werden daarentegen gedetecteerd door het toepassen van het ‘*multi-component change detection*’ algoritme (Pilon *et al.*, 1988). Deze multitemporale analyse bevestigt de intensieve kustontwikkeling in de regio gedurende de laatste twee tot drie decennia en heeft aangetoond dat het stadscentrum van Hurghada gegroeid is van 5 tot ongeveer 36km², voornamelijk als lintbebouwing langsheen de kustlijn. Deze kustlijn is bijgevolg sterk veranderd en vele franjeriffen werden volledig verwoest. Verder zeewaarts zijn eveneens belangrijke veranderingen opgemerkt, maar de gegevens ontbraken om deze veranderingen te relateren aan de kustontwikkeling.

De informatie verkregen door middel van teledetectie wordt best geïntegreerd in een GIS om op die manier de data samen met bijkomende informatie te kunnen analyseren en waardevolle producten te ontwikkelen die het GBK kunnen ondersteunen. Een risicokaart werd als voorbeeld gegeven van een dergelijk afgeleid product waarbij de negatieve invloed van menselijk handelen in het kustgebied rondom Hurghada in kaart wordt gebracht. Deze kaart illustreert niet alleen de bedreigde toekomst van de koraalriffen in dit gebied als er geen bijkomende beheersmaatregelen getroffen worden, maar toont eveneens de mogelijkheid om deze informatie te gebruiken bij het afbakenen van een Mariene Beschermde Gebied (MBG) dat meerdere gebruikersgroepen toelaat. Een initieel ontwerpschema van een dergelijk MBG werd daarom ontwikkeld om de sterkte van teledetectie en GIS ter ondersteuning van het GBK proces aan te tonen.

Alhoewel de nauwkeurigheid van de bekomen resultaten nog enigszins verbeterd kan worden, bieden ze toch waardevolle informatie betreffende de configuratie en samenstelling van de koraalriffen in de noordwestelijke Rode Zee die anders heel moeilijk te verkrijgen is. Aangezien iedere dataset specifieke voor- en nadelen heeft, is een meerschalgige bendaring waarschijnlijk het meest efficiënt en rendabel waarbij globale datasets aangewend worden om

ruimschalige informatie te bekomen in verband met de biogeofysische kenmerken van de zeeën en oceanen waarin de koraalriffen voorkomen; hoge resolutie beelden, zoals Landsat, geanalyseerd worden om informatie te bekomen over de configuratie en samenstelling van de koraalriffen op een regionale tot lokale schaal; en zeer hoge resolutie beelden, zoals QuickBird, gebruikt worden om bepaalde focusgebieden in meer detail in kaart te brengen. Deze producten die door middel van teledetectie afgeleid werden, worden daarna best samen met aanvullende informatie, zoals verkregen uit veldwaarnemingen, geïntegreerd in een 'Koraalriffen-GIS' zodat de informatie verder geanalyseerd and geïnterpreteerd kan worden. Dit GIS zou dan een zeer bruikbare bron van informatie worden die door GBK beleidsmakers aangewend kan worden om de kustzone zo te organiseren dat economische ontwikkeling en natuurbescherming in balans worden gebracht. Een dergelijke benadering is niet alleen dringend nodig om de reeds beschadigde koraalriffen te beschermen, maar eveneens om de sombere toekomst van de koraalriffen wereldwijd te bestrijden.

TABLE OF CONTENTS

Preface

Abstract

Samenvatting

| | |
|---|-----|
| Table of contents | i |
| List of tables | xv |
| Acronyms | xxi |
| | |
| GENERAL INTRODUCTION | 1 |
| | |
| PART I CORAL REEFS | 9 |
| 1.1 What are coral reefs? | 11 |
| 1.1.1 Definition | 11 |
| 1.1.2 Coral physiology | 14 |
| 1.1.2.1 Coral anatomy | 14 |
| 1.1.2.2 Zooxanthellate corals | 16 |
| 1.1.2.3 Coral calcification | 17 |
| 1.1.2.3.1 CO ₂ environment | 17 |
| 1.1.2.3.2 Light-enhanced calcification | 18 |
| 1.1.2.3.3 Coral-reef building | 19 |
| 1.1.3 Global coral-reef distribution and limiting factors | 19 |
| 1.1.3.1 Long-term influence factors | 20 |
| 1.1.3.1.1 Darwin's Subsidence Theory (Darwin, 1842) | 20 |
| 1.1.3.1.2 Daly's Glacial Control Theory (Daly, 1915) | 21 |
| 1.1.3.1.3 Reef accretion under the influence of relative sea-level change | 21 |
| 1.1.3.2 Contemporary, physical limiting factors | 22 |
| 1.1.3.2.1 Temperature | 23 |
| 1.1.3.2.2 Light | 24 |
| 1.1.3.2.3 Salinity | 25 |
| 1.1.3.2.4 Wave energy | 25 |
| 1.1.3.3 Coral biogeography | 26 |

| | |
|---|----|
| 1.1.4 Coral-reef geomorphology | 27 |
| 1.1.4.1 Large-scale geomorphology | 27 |
| 1.1.4.1.1 Fringing reefs | 28 |
| 1.1.4.1.2 Barrier reefs | 28 |
| 1.1.4.1.3 Atolls | 28 |
| 1.1.4.1.4 Patch reefs | 29 |
| 1.1.4.2 Medium- to small-scale geomorphological zonation | 29 |
| 1.1.4.2.1 Reef crest | 29 |
| 1.1.4.2.2 Back reef/reef flat | 29 |
| 1.1.4.2.3 Fore reef | 30 |
| 1.1.4.2.4 Spur and groove systems | 30 |
| 1.1.4.2.5 Reef patch | 30 |
| 1.1.4.2.6 Lagoon | 30 |
| 1.1.4.2.7 Escarpment | 31 |
| 1.1.4.2.8 Bank/shelf | 31 |
| 1.1.4.3 Micro-scale morphology | 31 |
| | |
| 1.2 Coral-reef values | 32 |
| 1.2.1 Ecological values | 32 |
| 1.2.1.1 Biodiversity | 32 |
| 1.2.1.2 Seascape interrelations | 34 |
| 1.2.2 Socio-economic values | 35 |
| 1.2.2.1 Fisheries | 36 |
| 1.2.2.2 Tourism | 37 |
| 1.2.2.3 Coastline protection | 37 |
| 1.2.2.4 Coral reefs as pharmaceutical and biochemical resources | 38 |
| | |
| 1.3 Threats to coral reefs | 39 |
| 1.3.1 Natural disturbances | 41 |
| 1.3.1.1 Outbreak of <i>Acanthaster planci</i> | 41 |
| 1.3.1.2 Damage by storms, tsunamis, cyclones and hurricanes | 41 |
| 1.3.1.3 Coral bleaching | 42 |
| 1.3.2 Human-induced disturbances | 43 |
| 1.3.2.1 Coastal development | 43 |

| | |
|---|----|
| 1.3.2.2 Inland development | 43 |
| 1.3.2.2.1 Sedimentation | 45 |
| 1.3.2.2.2 Nutriphication | 46 |
| 1.3.2.3 Tourism | 49 |
| 1.3.2.4 Marine pollution | 49 |
| 1.3.2.5 Overfishing | 50 |
| 1.3.2.6 Destructive fishing | 51 |
| 1.3.3 Global change | 52 |
| 1.3.3.1 Ocean acidification | 54 |
| 1.3.3.2 Sea surface temperature rise | 56 |
| 1.3.3.3 UV-B radiation | 57 |
| 1.3.3.4 Sea-level rise | 58 |
| 1.3.3.5 Oceanic water circulation | 59 |
| 1.3.3.6 Atmospheric circulation, precipitation, and tropical storms | 60 |
| 1.3.3.7 Increased incidence of coral diseases | 61 |
| 1.3.3.8 Mass coral bleaching | 61 |
| | |
| 1.4 The future of coral reefs: tolerance, strategy shift, or phase shift? | 65 |
| 1.4.1 Physiological tolerance by current coral species | 65 |
| 1.4.2 Faster turnover | 66 |
| 1.4.3 Strategy shifts | 67 |
| 1.4.4 Phase shifts | 67 |

| | |
|---|----|
| PART II REGIONAL SETTING OF THE RED SEA | 69 |
| 2.1 Geography | 71 |
| 2.2 Geology | 73 |
| 2.2.1 Precambrian basement complex | 73 |
| 2.2.2 Paleozoic: continental conditions | 73 |
| 2.2.3 Mesozoic: marine conditions in the northern Red Sea | 74 |
| 2.2.3.1 Triassic (251-200 Ma) | 74 |
| 2.2.3.2 Jurassic (200-146 Ma) | 74 |
| 2.2.3.3 Cretaceous (146-65.5 Ma) | 75 |
| 2.2.4 Paleogene-early Neogene: northern Red Sea Rift initiation | 75 |
| 2.2.4.1 Paleogene pre-rift sedimentation | 76 |
| 2.2.4.2 Initiation of the northern Red Sea rift tectonics | 76 |
| 2.2.4.2.1 Rift phase 1: first stage | 77 |
| 2.2.4.2.2 Rift phase 1: stage shift | 78 |
| 2.2.4.2.3 Rift phase 1: second stage | 79 |
| 2.2.4.2.4 Rift phase 1: end | 79 |
| 2.2.5 Miocene: evaporites and contemporary terrestrial and coastal deposits | 79 |
| 2.2.5.1 Aquitanian (23-20.43 Ma) | 79 |
| 2.2.5.2 Burdigalian-Langhian (20.43-13.65 Ma) | 80 |
| 2.2.5.3 Serravallian-early Tortonian (13.65-11 Ma) | 81 |
| 2.2.6 Pliocene: re-activation of the Red Sea Rift (phase 2) | 81 |
| 2.2.7 Pleistocene: climate changes, tectonics, and coral-reef building | 83 |
| 2.2.7.1 Glacio-eustatic control | 84 |
| 2.2.7.1.1 Interglacial maximum | 84 |
| 2.2.7.1.2 Anaglacial transition phase | 84 |
| 2.2.7.1.3 Glacial maximum | 85 |
| 2.2.7.1.4 Cataglacial transition phase | 85 |
| 2.2.7.2 Tectonic control | 86 |
| 2.2.8 Holocene: a suitable coral-reef environment? | 86 |
| 2.2.8.1 Geotectonic setting | 86 |
| 2.2.8.2 Sea transgression | 88 |
| 2.2.8.3 Coral-reef formation | 88 |

| | |
|---|-----|
| 2.3 Climate and oceanography | 90 |
| 2.3.1 Climate | 90 |
| 2.3.1.1 Wind | 91 |
| 2.3.1.1.1 Winter | 91 |
| 2.3.1.1.2 Summer | 92 |
| 2.3.1.1.3 Land and sea breezes | 92 |
| 2.3.1.1.4 Effects of wind on coral-reef growth | 93 |
| 2.3.1.2 Air temperature | 93 |
| 2.3.1.2.1 Air temperature over the open sea | 93 |
| 2.3.1.2.2 Air temperature along the shores | 94 |
| 2.3.1.3 Air humidity and cloud cover | 96 |
| 2.3.1.4 Precipitation | 97 |
| 2.3.2 Oceanography | 99 |
| 2.3.2.1 Seawater temperatures | 99 |
| 2.3.2.1.1 Sea surface temperature | 99 |
| 2.3.2.1.2 Sub-surface temperature | 100 |
| 2.3.2.2 Salinity | 103 |
| 2.3.2.2.1 Surface salinity | 103 |
| 2.3.2.2.2 Sub-surface salinity | 103 |
| 2.3.2.3 Water flow | 105 |
| 2.3.2.3.1 Red Sea – Gulf of Aden water exchange | 105 |
| 2.3.2.3.2 General water flow in the Red Sea | 106 |
| 2.3.2.3.3 Surface currents | 107 |
| 2.3.2.3.4 Tides and other temporary sea-level changes | 108 |
| 2.3.2.4 Chemical oceanography | 110 |
| 2.3.2.4.1 Dissolved-oxygen content | 110 |
| a. Horizontal distribution | 110 |
| b. Vertical distribution | 110 |
| 2.3.2.4.2 Nutrient concentrations | 112 |
| a. Horizontal distribution | 112 |
| b. Vertical distribution | 113 |
| 2.3.2.5 Phytoplankton concentrations - primary production | 113 |
| 2.3.2.5.1 Horizontal distribution | 113 |
| 2.3.2.5.2 Vertical distribution | 115 |

| | |
|--|-----|
| 2.3.2.5.3 Light absorption | 116 |
| 2.3.2.6 Conclusions for coral-reef growth..... | 116 |
| 2.4 Coastal ecosystems..... | 118 |
| 2.4.1 Introduction | 118 |
| 2.4.2 Coral reefs | 119 |
| 2.4.2.1 Geographical aspects..... | 119 |
| 2.4.2.1.1 Coral-reef types | 119 |
| a. Fringing reefs..... | 120 |
| b. Barrier reefs..... | 120 |
| c. Atolls | 120 |
| d. Patch reefs | 120 |
| e. Coral carpets..... | 121 |
| f. Algal reefs..... | 122 |
| 2.4.2.1.2 Coral-reef distribution..... | 122 |
| a. Gulf of Suez..... | 122 |
| b. Gulf of Aqaba..... | 123 |
| c. Northern Red Sea | 123 |
| d. Central Red Sea..... | 123 |
| e. Southern Red Sea | 124 |
| 2.4.2.2 Ecological aspects | 124 |
| 2.4.2.2.1 Coral diversity | 124 |
| 2.4.2.2.2 Ecological zonation..... | 125 |
| a. Horizontal zonation | 125 |
| b. Vertical zonation | 127 |
| 2.4.3 Algae | 130 |
| 2.4.4 Seagrasses..... | 131 |
| 2.4.5 Mangroves..... | 133 |
| 2.4.6 Specific threats to Red Sea coastal ecosystems..... | 134 |
| 2.4.6.1 Natural threats | 136 |
| 2.4.6.2 Coastal development | 137 |
| 2.4.6.2.1 Land reclamation and water circulation changes | 137 |
| 2.4.6.2.2 Sewage | 138 |
| 2.4.6.2.3 Industrial pollution | 138 |

| | |
|---|-----|
| 2.4.6.3 Tourism | 140 |
| 2.4.6.4 Marine pollution..... | 140 |
| 2.4.6.5 Fisheries and destructive fishing activities..... | 141 |
| 2.4.6.6 Global change..... | 144 |

| | |
|---|-----|
| PART III ICZM AND REMOTE SENSING - A CASE STUDY: CORAL REEFS IN THE NW RED SEA..... | 147 |
| 3.1 Introduction..... | 149 |
| 3.1.1 Integrated Coastal Zone Management and remote sensing..... | 149 |
| 3.1.1.1 Multi-use marine protected areas..... | 153 |
| 3.1.1.2 Research and monitoring..... | 157 |
| 3.1.1.2.1 Remote sensing..... | 159 |
| 3.1.1.2.2 Geographic information system..... | 163 |
| 3.1.2 Study area..... | 164 |
| 3.1.2.1 Oil exploitation and transport..... | 165 |
| 3.1.2.2 Fishing pressure..... | 166 |
| 3.1.2.3 Tourism and coastal development..... | 167 |
| 3.1.2.4 Management..... | 171 |
| 3.2 Data and materials..... | 175 |
| 3.2.1 Satellite data..... | 175 |
| 3.2.1.1 Landsat 7 ETM+..... | 175 |
| 3.2.1.2 Landsat 5 TM..... | 176 |
| 3.2.1.3 QuickBird..... | 177 |
| 3.2.1.4 ASTER..... | 178 |
| 3.2.2 Field data..... | 179 |
| 3.2.2.1 Field surveys..... | 179 |
| 3.2.2.2 Tidal correction data..... | 180 |
| 3.2.3 Additional information sources..... | 181 |
| 3.2.3.1 Topographic maps..... | 181 |
| 3.2.3.2 Admiralty charts..... | 182 |
| 3.2.3.3 Software..... | 182 |
| 3.3 Data pre-processing..... | 183 |
| 3.3.1 Noise reduction..... | 184 |
| 3.3.1.1 Landsat 5 TM..... | 184 |
| 3.3.1.2 QuickBird..... | 186 |

| | |
|--|-----|
| 3.3.2 Geometric correction..... | 187 |
| 3.3.2.1 Landsat 7 ETM+..... | 187 |
| 3.3.2.2 Landsat 5 TM..... | 188 |
| 3.3.2.3 QuickBird..... | 190 |
| 3.3.2.4 ASTER..... | 192 |
| 3.3.3 Radiometric correction..... | 194 |
| 3.3.3.1. Conversion of DN to spectral radiance..... | 195 |
| 3.3.3.1.1 Radiometric calibration of Landsat 7 ETM+..... | 195 |
| 3.3.3.1.2 Radiometric calibration of Landsat 5 TM..... | 196 |
| 3.3.3.1.3 Radiometric calibration of QuickBird..... | 196 |
| 3.3.3.1.4 Radiometric calibration of ASTER..... | 197 |
| 3.3.3.2 Conversion of spectral radiance to apparent reflectance..... | 197 |
| 3.3.3.2.1 Landsat 7 ETM+..... | 199 |
| 3.3.3.2.2 Landsat 5 TM..... | 199 |
| 3.3.3.2.3 QuickBird..... | 199 |
| 3.3.4 Atmospheric correction..... | 200 |
| 3.3.4.1 Landsat 7 ETM+..... | 202 |
| 3.3.4.2 Landsat 5 TM..... | 203 |
| 3.3.4.3 QuickBird..... | 204 |
| 3.3.5 Water-column correction..... | 205 |
| 3.3.5.1 DIB correction method..... | 207 |
| 3.3.5.2 Implementation..... | 210 |
| 3.3.5.2.1 Landsat 7 ETM+..... | 210 |
| 3.3.5.2.2 Landsat 5 TM..... | 213 |
| 3.3.5.2.3 QuickBird..... | 214 |
| a. Sandy substrate sample points..... | 215 |
| b. Seagrass substrate sample points..... | 216 |
| 3.3.6 Masking..... | 218 |
| 3.3.7 Pan-sharpening..... | 219 |
| 3.3.7.1 Adaptive-intensity-matching-filter method..... | 220 |
| 3.3.7.2 Test case: pan-sharpening the Landsat 7 ETM+ dataset..... | 222 |
| 3.3.7.2.1 Data pre-processing..... | 222 |
| 3.3.7.2.2 Creation of a global intensity channel..... | 224 |
| 3.3.7.2.3 Application of a LMVM filter..... | 224 |

| | |
|--|-----|
| 3.3.7.2.4 Creation of individual pan-sharpened multispectral bands | 224 |
| 3.3.7.2.5 Additional pre-processing steps | 225 |
| a. Geometric correction | 225 |
| b. Water-column correction..... | 225 |
| c. Masking | 226 |
| 3.4 Bathymetric mapping | 227 |
| 3.4.1 Introduction | 227 |
| 3.4.2 Bathymetric mapping methods using remote sensing data | 228 |
| 3.4.2.1 Active remote sensing bathymetric mapping methods | 228 |
| 3.4.2.2 Passive remote sensing bathymetric mapping methods | 228 |
| 3.4.2.2.1 Bottom-reflection-based bathymetric mapping theory..... | 231 |
| a. Method of Jupp (1988) | 232 |
| b. Ratio-transform method | 234 |
| 3.4.2.2.2 Water-column-scattering-based bathymetric mapping theory | 234 |
| 3.4.2.3 Digital photogrammetrical approach..... | 236 |
| 3.4.3 Implementation..... | 239 |
| 3.4.3.1 Landsat 7 ETM+..... | 239 |
| 3.4.3.1.1 Modified DOP-mapping method..... | 239 |
| a. Methodology..... | 239 |
| b. Result..... | 242 |
| c. Residual analysis | 242 |
| 3.4.3.1.2 Ratio-transform method | 243 |
| a. Methodology..... | 243 |
| 3.4.3.2 Pan-sharpened Landsat 7 ETM+ | 245 |
| 3.4.3.2.1 Methodology | 246 |
| a. Calculation of DOP zones | 246 |
| b. Interpolation and calibration of depths within the DOP zones | 247 |
| 3.4.3.2.2 Result..... | 248 |
| 3.4.3.2.3 Residual analysis | 248 |
| 3.4.3.3 Landsat 5 TM dataset | 249 |
| 3.4.3.3.1 Methodology | 249 |
| a. Calculation of DOP zones | 249 |
| b. Interpolation and calibration of depths within the DOP zones | 250 |

| | |
|---|-----|
| 3.4.3.3.2 Result..... | 251 |
| 3.4.3.4 QuickBird..... | 251 |
| 3.4.3.4.1 Modified DOP-mapping method..... | 251 |
| a. Methodology..... | 252 |
| b. Result..... | 254 |
| c. Residual analysis..... | 254 |
| 3.4.3.4.2 Ratio-transform method..... | 255 |
| a. Methodology..... | 255 |
| b. Result..... | 257 |
| c. Residual analysis..... | 258 |
| 3.4.3.5 ASTER dataset..... | 258 |
| 3.4.3.5.1 Pre-processing..... | 258 |
| a. Contrast enhancement..... | 258 |
| b. Rotation..... | 259 |
| 3.4.3.5.2 VIRTUOZO 3.2 processing..... | 260 |
| a. Set-up..... | 260 |
| b. Model orientation..... | 260 |
| c. Epipolar images..... | 262 |
| d. Image matching..... | 262 |
| e. Match editing..... | 262 |
| f. DEM calculation..... | 263 |
| 3.4.3.5.3 Post-processing: refraction correction..... | 263 |
| 3.4.3.5.4 Result..... | 264 |
| 3.4.4 Discussion..... | 264 |
| 3.4.4.1 The effect of pan-sharpening the Landsat 7 ETM+ dataset..... | 264 |
| 3.4.4.2 Comparison of the modified DOP-mapping results of the Landsat 7 ETM+ and QuickBird dataset..... | 265 |
| 3.4.4.3 The applicability of the ratio-transform method..... | 266 |
| 3.4.4.4 General remarks on multispectral bathymetric methods..... | 267 |
| 3.4.4.5 Through-water digital photogrammetric approach..... | 270 |
| 3.4.5 Conclusions..... | 271 |

| | |
|---|-----|
| 3.5 Geomorphological classification..... | 273 |
| 3.5.1. Introduction | 273 |
| 3.5.2. Implementation..... | 275 |
| 3.5.2.1 Original Landsat 7 ETM+ dataset | 275 |
| 3.5.2.1.1 Hill-shading of the bathymetric map..... | 275 |
| 3.5.2.1.2 Construction of the DCC..... | 275 |
| 3.5.2.1.3 Geomorphological zonation | 276 |
| 3.5.2.1.4 Result..... | 277 |
| 3.5.2.2 Pan-sharpened Landsat 7 ETM+ dataset..... | 277 |
| 3.5.2.3 QuickBird dataset..... | 278 |
| 3.5.2.3.1 Methodology | 278 |
| 3.5.2.3.2 Result..... | 278 |
| 3.5.3 Discussion | 279 |
| 3.5.3.1 Effect of pan-sharpening | 279 |
| 3.5.3.2 General observations | 280 |
| | |
| 3.6 Bottom-type classification..... | 281 |
| 3.6.1 Introduction | 281 |
| 3.6.2 Methodology | 283 |
| 3.6.2.1 Pre-processing | 283 |
| 3.6.2.1.1 Correction for water-column effects | 283 |
| 3.6.2.1.2 Texture analysis..... | 284 |
| 3.6.2.2 Processing..... | 285 |
| 3.6.2.2.1 Bottom-type classification..... | 285 |
| 3.6.2.2.2 Accuracy assessment..... | 286 |
| 3.6.2.3 Post-processing..... | 289 |
| 3.6.2.3.1 Contextual editing | 289 |
| 3.6.2.3.2 Coastal habitat mapping | 290 |
| 3.6.3. Implementation..... | 290 |
| 3.6.3.1 Original Landsat 7 ETM+ dataset | 290 |
| 3.6.3.1.1 Pre-processing | 290 |
| a. Water-column correction..... | 290 |
| b. Texture analysis..... | 291 |
| 3.6.3.1.2 Processing..... | 291 |

| | |
|---|-----|
| a. Bottom-type classification..... | 291 |
| b. Accuracy assessment..... | 293 |
| c. Visual validation of integrating textural information..... | 295 |
| 3.6.3.1.3 Post-processing..... | 295 |
| a. Contextual editing | 295 |
| b. Coastal habitat mapping | 297 |
| 3.6.3.2 Pan-sharpened Landsat 7 ETM+ dataset..... | 298 |
| 3.6.3.2.1 Pre-processing | 298 |
| a. Water-column correction..... | 298 |
| b. Texture analysis..... | 298 |
| 3.6.3.2.2 Processing..... | 299 |
| a. Bottom-type classification..... | 299 |
| b. Accuracy assessment..... | 299 |
| c. Visual validation of integrating textural information..... | 300 |
| d. Validation of the pan-sharpening process | 301 |
| 3.6.3.3 QuickBird dataset..... | 302 |
| 3.6.3.3.1 Pre-processing | 302 |
| a. Water-column correction..... | 302 |
| b. Texture analysis..... | 303 |
| 3.6.3.3.2 Processing..... | 303 |
| a. Bottom-type classification..... | 303 |
| b. Accuracy assessment..... | 307 |
| c. Visual validation..... | 308 |
| 3.6.3.3.3 Post-processing..... | 310 |
| a. Contextual editing | 310 |
| b. Coastal habitat mapping | 312 |
| 3.6.4 Discussion | 313 |
| 3.6.5 Conclusions | 321 |
| 3.7 Remote sensing and biogeophysical parameters..... | 323 |
| 3.7.1 Ocean colour | 324 |
| 3.7.2 Sea surface temperature | 325 |
| 3.7.3 Sea surface salinity..... | 327 |
| 3.7.4 Sea surface currents..... | 329 |

| | |
|---|-----|
| 3.8 Multitemporal analysis | 330 |
| 3.8.1 Introduction | 330 |
| 3.8.2 Data processing | 332 |
| 3.8.2.1 Indication of LULC change..... | 332 |
| 3.8.2.2 Changes in coral-reef composition..... | 333 |
| 3.8.2.2.1 Image-differencing sub-procedure | 333 |
| 3.8.2.2.2 Landsat 5 TM classification | 333 |
| a. Geomorphological classification | 333 |
| b. Bottom-type classification..... | 334 |
| 3.8.2.2.3 Post-classification comparison..... | 335 |
| 3.8.3 Results | 336 |
| 3.8.3.1 LULC and coastline changes..... | 336 |
| 3.8.3.2 Coral-reef bottom-type change map..... | 337 |
| 3.8.4 Discussion | 337 |
| 3.8.5 Conclusions | 340 |
| | |
| 3.9 Risk assessment mapping..... | 341 |
| 3.9.1 ‘Reefs at Risk’ decision rules..... | 341 |
| 3.9.2 Application to the Hurghada study area..... | 342 |
| 3.9.3 Results and discussion..... | 344 |
| | |
| 3.10 Multi-use MPA zoning..... | 347 |
| 3.10.1 Specific multi-use MPA zoning scheme | 347 |
| 3.10.2 Initial draft MPA zoning plan | 350 |
| | |
| GENERAL CONCLUSIONS | 355 |
| | |
| REFERENCES..... | 367 |
| References PART I..... | 369 |
| References PART II | 387 |
| References PART III..... | 401 |

LIST OF TABLES

| | |
|---|-----|
| Table 1.1. Physical factors limiting hermatypic coral growth: minimum, maximum, mean and standard deviations | 23 |
| Table 1.2. Overview of the most common geomorphological forms of coral colonies | 31 |
| Table 1.3. Losses in gross revenue in terms of tourism, fishing and logging (in thousands USD) due to unsustainable use of the coral-reef resources..... | 44 |
| Table 1.4. Climate and environmental change observations and projections | 53 |
| | |
| Table 2.1. Air surface temperature over the Red Sea in 1° by 1° grid cells..... | 95 |
| Table 2.2. Mean monthly air temperatures for a number of weather stations along the Red Sea coast..... | 96 |
| Table 2.3. Mean monthly precipitation for a number of weather stations along the Red Sea coast..... | 98 |
| Table 2.4. SST over the Red Sea in 1° by 1° cells | 101 |
| Table 2.5. Surface salinity over the Red Sea in 1° by 1° cells | 104 |
| Table 2.6. Surface dissolved oxygen, phosphate, nitrate and silicate concentration in the Red Sea in 1° by 1° cells | 111 |
| Table 2.7. Average live coral cover percentages estimated on different reef zones along the Egyptian coastline | 127 |
| Table 2.8. Vertical ecological zonation (with indicator species) and average live coral cover percentages on northern Red Sea reefs | 129 |
| Table 2.9. Overview of seagrass species found in the Red Sea..... | 133 |
| Table 2.10. Overview of the most important human activities in the Red Sea region and their impacts on the coastal ecosystems | 136 |
| | |
| Table 3.1. Overview of the urban settlements along the Egyptian Red Sea coast with indication of major economic activities | 165 |
| Table 3.2. Number of fishermen active in Egypt's Red Sea fisheries..... | 166 |
| Table 3.3. Egyptian Red Sea fish catches (tonnes) between 1980 and 2003 | 167 |
| Table 3.4. Evolution of arrivals and overnight stays of non-resident visitors in Egypt between 1999 and 2003 | 168 |

| | |
|---|-----|
| Table 3.5. Assessment of fresh-water demand and supply in the Red Sea and South Sinai Governorate..... | 170 |
| Table 3.6. Overview of the main characteristics of the Landsat 7 platform and ETM+ sensor | 175 |
| Table 3.7. Specific information of the Landsat 7 ETM+ dataset used | 175 |
| Table 3.8. Overview of the main characteristics of the Landsat 5 platform and TM sensor. | 176 |
| Table 3.9. Specific information of the Landsat 5 TM dataset used..... | 176 |
| Table 3.10. Overview of the main characteristics of the QuickBird platform and sensor | 177 |
| Table 3.11. Specific information of the QuickBird dataset used..... | 177 |
| Table 3.12. Overview of the main characteristics of the Terra platform and ASTER sensor | 178 |
| Table 3.13. Specific information of the ASTER dataset used..... | 178 |
| Table 3.14. Overview of the three field campaigns made in the specific study area | 179 |
| Table 3.15. Overview of the tidal heights at the moment of satellite data acquisition..... | 181 |
| Table 3.16. Overview of specific spectral bands used per dataset according to algorithm... | 183 |
| Table 3.17. Mean DN values calculated in two sample sets at either side of a vertical scan error detected in the QuickBird dataset..... | 187 |
| Table 3.18. Overview of the parameters used to define the specific coordinate system..... | 188 |
| Table 3.19. Overview of residual errors for each GCP used for geocoding the Landsat 7 ETM+ subset | 189 |
| Table 3.20. Overview of the residual errors for each tie-point used for the geocoding of the Landsat 5 TM dataset | 189 |
| Table 3.21. Overview of the residual errors for each tie-point used for geocoding the multispectral QuickBird bands..... | 191 |
| Table 3.22. Overview of the residual errors for each tie-point used for geocoding the panchromatic QuickBird band | 191 |
| Table 3.23. Overview of the residual errors for each GCP used for the geocoding of the nadir ASTER VNIR bands | 192 |
| Table 3.24. Overview of the residual errors for each tie-point used in the geocoding of the ASTER 3b scene | 193 |
| Table 3.25. Spectral radiance range (in $W m^{-2} ster^{-1} \mu m^{-1}$) for the ETM+ sensor, specific for the dataset used in this study | 196 |
| Table 3.26. Landsat 5 TM calibration parameters to convert DN to radiance values | 196 |
| Table 3.27. Revised K-factors for 16bit products and effective bandwidths of the QuickBird multispectral bands..... | 197 |

| | |
|--|-----|
| Table 3.28. ETM+ mean solar exatmospheric spectral irradiance values | 199 |
| Table 3.29. Landsat 5 TM mean solar exatmospheric spectral irradiance values | 200 |
| Table 3.30. QuickBird mean solar exoatmospheric spectral irradiance values | 200 |
| Table 3.31. Determination of deep-water radiance on the Landsat 7 ETM+ dataset | 203 |
| Table 3.32. Determination of deep-water radiance on the QuickBird dataset | 205 |
| Table 3.33a. Variance within each Landsat 7 ETM+ radiance band | 211 |
| Table 3.33b. Determination of the attenuation ratios k_i/k_j for Landsat 7 ETM+ water column correction..... | 211 |
| Table 3.34. Comparison of COVs for Landsat 7 ETM+ before and after water column correction..... | 213 |
| Table 3.35a. Variance within each Landsat 5 TM radiance band | 214 |
| Table 3.35b. Determination of the attenuation ratios k_i/k_j for Landsat 5 TM water column correction..... | 214 |
| Table 3.36. Comparison of COVs for the radiometrically normalized Landsat 5 TM dataset before and after water column correction | 214 |
| Table 3.37a. Variance within each QuickBird radiance band..... | 215 |
| Table 3.37b. Determination of the attenuation ratios k_i/k_j for QuickBird water column correction..... | 215 |
| Table 3.38. Comparison of COVs for the QuickBird dataset before and after water column correction calibrated with sandy substrate points | 216 |
| Table 3.39a. Variance within each QuickBird radiance band..... | 216 |
| Table 3.39b. Determination of the attenuation ratios k_i/k_j for QuickBird water column correction..... | 217 |
| Table 3.40. Comparison of COVs for the QuickBird dataset before and after water column correction calibrated with seagrass substrate points | 217 |
| Table 3.41. Specific georeference system for the Landsat 7 ETM+ multispectral bands, based on scene characteristics, used in the pan-sharpening procedure | 223 |
| Table 3.42. Georeference system for the Landsat 7 ETM+ panchromatic band, based on scene characteristics, used in the pan-sharpening procedure | 223 |
| Table 3.43. Overview of the residual errors for each GCP used for geocoding the pan-sharpened Landsat 7 ETM+ dataset | 225 |
| Table 3.44a. Variance within each pan-sharpened Landsat 7 ETM+ band..... | 226 |

| | |
|--|-----|
| Table 3.44b. Determination of the attenuation ratios k_i/k_j for pan-sharpened Landsat 7 ETM+ water column correction | 226 |
| Table 3.45. Maximum DOP for TM bands 1, 2, 3 and 4 in optically clear water of the Great Barrier Reef..... | 233 |
| Table 3.46. Minimum, maximum and mean deep-water DN values for the original Landsat 7 ETM+ dataset | 239 |
| Table 3.47. Determination of the maximum DOP in Landsat 7 ETM + waveband 1, 2 and 3 | 240 |
| Table 3.48. Decision tree used to delineate the three exclusive DOP zones on the Landsat 7 ETM+ dataset | 241 |
| Table 3.49. Parameters needed for interpolating depth in each Landsat 7 ETM+ DOP zone | 241 |
| Table 3.50. Residual analysis of the Landsat 7 ETM+ bathymetric result..... | 243 |
| Table 3.51. Determination of L_i haze for the atmospheric correction of the Landsat 7 ETM+ bands 1 and 2..... | 244 |
| Table 3.52. Minimum, maximum and mean deep-water radiance values for the pan-sharpened Landsat 7 ETM+ dataset | 246 |
| Table 3.53. Determination of the maximum DOP in the pan-sharpened Landsat 7 ETM + waveband 1, 2 and 3 | 247 |
| Table 3.54. Decision tree used to delineate the three exclusive DOP zones on the pan-sharpened Landsat 7 ETM+ dataset | 247 |
| Table 3.55. Parameters needed for interpolating depth in each pan-sharpened Landsat 7 ETM+ DOP zone..... | 247 |
| Table 3.56. Residual analysis of the pan-sharpened Landsat 7 ETM+ bathymetric result ... | 248 |
| Table 3.57. Minimum, maximum and mean deep-water DN values for the Landsat 5 TM dataset..... | 249 |
| Table 3.58. Determination of the maximum DOP in the Landsat 5 TM band 1, 2 and 3 | 250 |
| Table 3.59. Decision tree used to delineate the three exclusive DOP zones on the Landsat 5 TM dataset..... | 250 |
| Table 3.60. Parameters needed for interpolating depth in each Landsat 5 TM DOP zone ... | 251 |
| Table 3.61. Minimum, maximum and mean deep-water DN values for the QuickBird dataset | 252 |
| Table 3.62. Determination of the maximum DOP in QuickBird band 1, 2 and 3 | 252 |

| | |
|---|-----|
| Table 3.63. Decision tree used to delineate the three exclusive DOP zones on the QuickBird dataset..... | 253 |
| Table 3.64. Parameters needed for interpolating depth in each QuickBird DOP zone | 253 |
| Table 3.65. Residual analysis of the QuickBird DOP-mapping bathymetric result..... | 254 |
| Table 3.66. Determination of L_i <i>haze</i> for the atmospheric correction of the QuickBird multispectral bands 1 and 2 | 255 |
| Table 3.67. Residual analysis of the QuickBird ratio-transform bathymetric result..... | 258 |
| Table 3.68. Overview of the GCPs used in the absolute orientation of the ASTER stereo-pair with the indication of individual errors in X, Y and Z..... | 262 |
| Table 3.69. Overview of mean RMS-errors of the absolute orientation | 262 |
| Table 3.70. Specific residual analysis of the resampled Landsat 7 ETM+ bathymetric result | 266 |
| Table 3.71. Specific geomorphological classification scheme for the Hurghada study area | 273 |
| Table 3.72. General hierarchical bottom-type classification scheme | 281 |
| Table 3.73. Schematic representation of an error matrix | 286 |
| Table 3.74. Minimum and maximum original Landsat 7 ETM+ DIB values | 291 |
| Table 3.75. Hierarchical bottom-type classification scheme applied on the Landsat 7 ETM+ dataset..... | 292 |
| Table 3.76. Mean and standard deviations for each bottom-type class derived from the original Landsat 7 ETM+ training sets | 293 |
| Table 3.77. Error matrix for the classification of the original Landsat 7 ETM+ dataset based on the DIB layers..... | 294 |
| Table 3.78. Error matrix for the classification of the original Landsat 7 ETM+ dataset based on the DIBs and the textural neo-channels..... | 294 |
| Table 3.79. Minimum and maximum pan-sharpened Landsat 7 ETM+ DIB values | 298 |
| Table 3.80. Mean and standard deviations for each bottom-type class derived from the pan-sharpened Landsat 7 ETM+ training sets | 299 |
| Table 3.81. Error matrix for the classification of the pan-sharpened Landsat 7 ETM+ dataset based on the DIBs | 299 |
| Table 3.82. Error matrix for the classification of the pan-sharpened Landsat 7 ETM+ dataset based on the DIBs and textural neo-channels | 300 |
| Table 3.83. Minimum and maximum QuickBird DIB values calibrated over sand (QB_DIB) and seagrass (QB_DIBsg) | 302 |

| | |
|--|-----|
| Table 3.84. Hierarchical bottom-type classification scheme applied on the QuickBird dataset | 304 |
| Table 3.85. Mean and standard deviations for each bottom-type class derived from the QB_DIB training sets | 305 |
| Table 3.86. Mean and standard deviations for each bottom-type class derived from the QB_DIBsg training sets | 306 |
| Table 3.87. Error matrix for the classification based on the QB_DIBs..... | 308 |
| Table 3.88. Error matrix for the classification based on the QB_DIBs and textural neo-channels..... | 308 |
| Table 3.89. Error matrix for the classification based on the QB_DIBsgs..... | 309 |
| Table 3.90. Error matrix for the classification based on the QB_DIBsgs and textural neo-channels..... | 309 |
| Table 3.91. Overview of the technical details of the SMOS and AQUARIUS sensors..... | 328 |
| Table 3.92. Minimum and maximum Landsat 5 TM DIB values | 334 |
| Table 3.93. Mean and standard deviations for each bottom-type class derived from the Landsat 5 TM training sets..... | 335 |
| Table 3.94. Extension of road network and urban areas in 1987 and 2000 as derived from the analysis of the Landsat 5 TM and Landsat 7 ETM+ datasets | 336 |
| Table 3.95. Coastline changes between 1987 and 2000 as derived from the analysis of the Landsat 5 TM and Landsat 7 ETM+ datasets | 337 |
| Table 3.96. Specific decision rules used to delineate risk zones in the Hurghada study area | 343 |
| Table 3.97. Overall risk assessment for the main bottom types occurring in the study area | 345 |
| Table 3.98. Overall risk assessment percentages for the study area, the Middle East*, and the world*..... | 345 |

ACRONYMS

| | |
|---------|---|
| AATSR: | Advanced Along-Track Scanning Radiometer |
| AGRRA: | Atlantic and Gulf of Mexico Rapid Reef Assessment |
| AIMF: | adaptive-intensity-matching filter |
| AIO: | ARGO Information Centre |
| ARSIS: | amélioration de la résolution spatiale par injection des structures |
| ASAR: | along-track synthetic aperture radar |
| AST: | air surface temperature |
| AVHRR: | Advanced Very High Resolution Radiometer |
| CASI: | Compact Airborne Spectrographic Imager |
| C-DOM: | coloured dissolved organic matter |
| CFC: | chlorinated fluoro-carbon |
| CORDIO: | Coral Reef Degradation in the Indian Ocean |
| CoRIS: | Coral Reef Information System |
| COTS | Crown-of-Thorns Starfish |
| CoV: | coefficient of variation |
| CRW: | Coral Reef Watch team |
| CZCS: | Coastal Zone Colour Scanner |
| DCC: | depth-improved colour composite |
| DHW: | degree heating week |
| DIB: | depth-invariant bottom index |
| DN: | digital number |
| DO: | dissolved oxygen |
| DOP: | depth of penetration |
| EEAA: | Egyptian Environmental Affairs Agency |
| EMR: | electromagnetic radiance |
| ENSO: | El Niño/Southern Oscillation |
| ERSDAC: | Earth Remote Sensing Data Analysis Center |
| ESA: | European Space Agency |
| GAFRD: | General Authority for Fish Resources Development |
| GAIW: | Gulf of Aden intermediate water |
| GASW: | Gulf of Aden surface water |
| GCP: | ground control point |
| GCRMN: | Global Coral Reef Monitoring Network |
| GEF: | Global Environment Facility |

| | |
|-----------|--|
| GIS: | geographic information system |
| GOES: | Geostationary Operational Environmental Satellites |
| GSFC: | Goddard Space Flight Centre |
| HEPCA: | Hurghada Environmental Protection and Conservation Agency |
| HIS: | hue-intensity-saturation |
| HPF: | high pass filter |
| ICAM: | Integrated Coastal Area Management |
| ICLARM: | International Center for Living Aquatic Resources Management |
| ICRAN: | International Coral Reef Action Network |
| ICRI: | International Coral Reef Initiative |
| ICRIN: | International Coral Reef Information Network |
| ICZM: | integrated coastal zone management |
| IGOS: | Integrated Global Observation Strategy |
| IOC: | Intergovernmental Oceanographic Commission |
| IOCCG: | International Ocean Colour Coordinating Group |
| INR: | intensity normalised ratio |
| IRI/LDEO: | International Research Institute for climate prediction/Lamont-Doherty Earth Observation climate data library |
| ISRS: | International Society for Reef Studies |
| ITCZ: | intertropical convergence zone |
| IUCN: | The World Conservation Union |
| JPL: | Jet Propulsion Laboratory |
| LAI: | leaf area index |
| LAT: | lowest astronomical tide |
| LIDAR: | Light Detection and Ranging |
| LMM: | local mean matching filter |
| LMVM: | local mean and variance matching filter |
| LPSO: | Landsat Project Science Office |
| LULC: | land use/land cover |
| MAB: | Man and Biosphere program |
| MARPOL: | International Convention for the Prevention of Marine Pollution from Ships |
| MCA: | multi-criteria analysis |
| MERIS: | Medium Resolution Imaging Spectrometer |
| MHWL: | mean high water level |
| MMM: | SST maximum monthly climatology |
| MODIS: | Moderate Resolution Imaging Spectroradiometer |
| MPA: | marine protected area |

| | |
|--------------|---|
| MS: | multispectral waveband |
| msl: | mean sea level |
| NASA: | U.S. National Aeronautics and Space Administration |
| NCEAS: | National Center for Ecological Analysis and Synthesis |
| NCICZM: | National Committee for Integrated Coastal Zone Management |
| NGO: | non-governmental organisation |
| NIR: | near-infrared wavelength |
| NLAPS: | National Land Archive Production System |
| NOAA: | U.S. National Oceanic and Atmospheric Administration |
| NOAA-AOML: | Atlantic Oceanographic and Meteorological Laboratory |
| NOAA NCDC: | National Climatic Data Center |
| NOAA NESDIS: | National Environmental, Satellite, Data and Information System |
| NOAA OSDPD: | Office of Satellite Data Processing and Distribution |
| NOAA SIS: | Satellite and Information Service |
| OSCAR: | Ocean Surface Current Analysis in Real-time |
| Pan: | panchromatic waveband |
| PAR: | photosynthetically available radiation |
| PCA: | principle component analysis |
| PCRF: | Planetary Coral Reef Foundation |
| PERSGA: | Regional Organization for the Conservation of the Environment of the Red Sea and Gulf of Aden |
| PIC: | particulate inorganic carbon |
| PIF: | pseudo-invariant feature method |
| PODAAC: | Physical Oceanography Distributed Active Archive Center |
| POES: | Polar Orbiting Environmental Satellites |
| POM: | particulate organic matter |
| PSU: | practical salinity units |
| RADAR: | Radar Detection and Ranging |
| REMSS: | Remote Sensing Systems |
| RMSE: | root mean square error |
| RSDW: | Red Sea deep water |
| RSOW: | Red Sea outflow water |
| RSSW: | Red Sea surface water |
| RSW: | Red Sea water |
| SAU: | Sea Around Us project |
| SBA: | satellite bleaching alert |
| SeaWiFS: | Sea Wide Field of View Sensor |

| | |
|-------------|---|
| SLP: | sea level pressure |
| SMOS: | Soil Moisture and Ocean Salinity sensor |
| SOOP: | ship of opportunity programme |
| SSC: | sea surface currents |
| SSH: | sea surface heights |
| SSS: | sea surface salinity |
| SST: | sea surface temperature |
| SWIR: | short-wave infrared wavelengths |
| TDA: | Tourist Development Agency |
| TOA: | top of the atmosphere |
| TCC: | true colour composite |
| TIR: | thermal infrared wavelengths |
| TMI: | TRMM Microwave Imager |
| TRMM: | Tropical Rainfall Measuring Mission |
| TSM: | total suspended matter |
| UAV: | Unmanned Airborne Vehicle |
| UNDP: | United Nations Development Programme |
| UNEP: | United Nations Environmental Programme |
| UNESCO: | United Nations Educational, Scientific and Cultural Organization |
| UNESCO CSI: | Environment and Development in Coastal Regions and in Small Islands |
| UNESCO WHC: | World Heritage Convention |
| USAID: | United States Agency for International Development |
| USGS: | United States Geological Survey |
| VNIR: | visible and near-infrared wavelengths |
| WTO: | World Tourism Organisation |

GENERAL INTRODUCTION

INTRODUCTION

Since the mid-1990s, concern is growing about the future of coral reefs. In 1993, Wilkinson estimated that about 10% of the world's coral reefs had already disappeared. The fast increasing population, predominantly in developing countries, and the anthropogenic use of the reefs as a natural resource were considered the main threats. To raise public awareness on the deteriorating state of coral reefs, the International Year of the Coral Reef was proclaimed by ICRI in 1997. Simultaneously, Bryant *et al.* (1998) published their Reefs at Risk report in which is stated that 58% of the coral reefs are immediately threatened by human coastal activities. Moreover, coral reefs globally underwent unseen mass bleaching during 1997/1998 -killing 16% of the world's coral reefs in only a few months (Wilkinson, 2000a)- an event which was associated with one of the severest ENSO cycles on record. This highlighted the increasing influence of global change on the health of coral reefs.

Coral reefs are not only one of the most spectacular marine ecosystems displaying an extremely rich biodiversity; they also offer valuable socio-economic resources and services to the people living along their coasts. The total, worldwide value of these resources (e.g. fisheries) and services (e.g. tourism or coastline protection) is estimated between 30 (Cesar *et al.*, 2003) and 375 billion USD per annum (Costanza *et al.*, 1997). Many people, especially in developing countries, heavily depend on the coral reefs as a food source and/or income provider. Tens of millions (Moberg and Folke, 1999) to over 1 billion (Hinrichsen, 1997; Bryant *et al.*, 1998; Whittingham *et al.*, 2003) people in Asia, for example, rely on coral reefs for at least part of their livelihood. At the 2002 Johannesburg World Summit on Sustainable Development, the world leaders, therefore, have recognised that the maintenance of healthy environments, including coral reefs, is essential to reduce poverty and to improve human health (UN, 2003).

Numerous initiatives, at all levels of society, have already been taken to attain the conservation and sustainable development of these coral-reef ecosystems. For an effective management and conservation strategy, accurate information is required on the ecology of the coral reefs as well as on the human exploitation of these resources. This requires both the collection of baseline data on the current status of the coral-reef ecosystem and on the present human interference, and a follow-up of potential future changes. Although a lot of research has already been done on coral reefs and their degradation, Bryant *et al.* (1998: 38) state that '*there is (still) a critical need for detailed monitoring and assessment of reef habitats in order to better document where and how coral reefs are threatened and to understand what measures are needed to safeguard them*'. Conventional field-observation methods, unfortunately, are very time and labour intensive and only small stretches of reef can therefore

be surveyed. As a result, many remote coral reefs have never or seldom been monitored. Here, remote sensing comes to the aid as it synoptically maps the world in a standardised manner. The ideal approach would be multi-level sampling in which information from different sources and levels of detail are integrated to obtain a comprehensive view on the subject. In this, a geographic information system (GIS) is optimally suited to combine and analyse these data layers.

The aim of this work is to demonstrate the usefulness of remote sensing as part of the array of tools to study coral reefs. Examined are the possibilities of remote sensing to derive information on the seabed bathymetry, to make an inventory of the dominant bottom types and their distribution over the main coral-reef geomorphological zones, and to determine major changes in the bottom-type composition over time. Emphasis is also put on the analysis of these remote-sensing-derived datasets in a GIS as a decision-support tool for the integrated coastal zone management (ICZM) of the coral-reef ecosystem. The examples are given of a risk assessment map, indicating future threats to the coral reefs, and an initial multi-use MPA zoning plan which has been developed based on the available remote-sensing-derived information. The term 'remote sensing' is restricted to satellite-based, optical, passive remote sensing, unless otherwise stated. Other remote sensing datasets, e.g. airborne LIDAR or hyperspectral data, may be useful as well, but these were either unavailable or too expensive at the start of the study. The costs of the remote sensing datasets can not be neglected as it is also intended to investigate the potential use of these data by developing countries in their day-to-day coral-reef management.

The Red Sea has been selected as study area, more specifically the northwestern Red Sea, i.e. Egyptian, coasts. The first reason to select this specific region is the threatened position of the coral reefs, mainly due to tourism and coastal development. Secondly, an easily accessible field-sampling area is preferred, as ground-truth data is needed to calibrate the remote-sensing methodology and to test the accuracy of the results. Therefore, the coastal zone near Hurghada has been chosen as focus area as it is conveniently accessible by plane from Belgium. As it also is one of the fastest growing coastal urban centres in the region, human activities have already negatively influenced the marine environment in the past and some of these still continue to affect the nearshore coral reefs. The selection of the NW Red Sea as study area also offered the opportunity to collaborate with scientists from the Egyptian National Research Centre (NRC) with whom the Geography Department of the Ghent University has a close, long-lasting partnership.

In order to correctly interpret the remote sensing data, knowledge on the ecology of a coral reef is required as well as an understanding of the physical environment in which it occurs, in casu the Red Sea. Part I gives a brief description of the coral-reef ecology with focus on the coral physiology (section 1.1.2) and the physical factors limiting their global distribution (section 1.1.3). Remark that the term ‘coral reef’ only implies the common warm- and shallow-water structures build up by coral animals. The geomorphological coral-reef zonation which result from the interaction between the coral ecology and the physical environment are reviewed in section 1.1.4. Next, an overview is provided on the values of coral reefs (section 1.2), both ecologically (section 1.2.1) and socio-economically (section 1.2.2), and of the main factors threatening their future (section 1.3). Details are given on natural threats (section 1.3.1), human-induced disturbances (section 1.3.2), and the effects of global change (section 1.3.3) with special attention to mass coral bleaching (section 1.3.3.8). To conclude this part, the main scenarios concerning the future of the coral reefs are briefly discussed in section 1.4.

Part II describes the physical environment the Red Sea is offering for coral-reef development. The available space for coral-reef growth in the Red Sea is largely defined by its geological setting (section 2.2). Within section 2.2, a concise summary is given of the geological evolution of the Red Sea region. Special attention is given to the northwestern Red Sea and emphasis is put on those elements critical for the current-day coral-reef distribution (section 2.2.8). The Red Sea is also a unique marine environment as it is almost completely surrounded by deserts. This is reflected in the climatic conditions in the Red Sea region (section 2.3.1). The oceanographic parameters (section 2.3.2) characterising the semi-enclosed Red Sea basin are favourable for coral-reef growth as well. Details are provided on seawater temperature (section 2.3.2.1), salinity (section 2.3.2.2), water flow (section 2.3.2.3), chemical parameters (section 2.3.2.4) and phytoplankton concentrations (section 2.3.2.5). The consequences for coral growth are summarised in section 2.3.2.6. Following, both the geographical (section 2.4.2.1) and the ecological (section 2.4.2.2) aspects of the coral reefs occurring in the Red Sea are examined. Other coastal ecosystems such as seagrasses (section 2.4.3), algae (section 2.4.4), and mangroves (section 2.4.5) are also discussed as there are many interrelations between these ecosystems. Finally, the specific factors threatening the Red Sea coastal ecosystem are highlighted in section 2.4.6. More detail on the Hurghada focus area is given in section 3.1.2.

Part III presents detailed information on the performed remote-sensing analyses and the integration of the derived products in a Coral Reef GIS as a decision-support tool for ICZM.

Before the effective procedures and results are discussed, an insight is provided in the concept of ICZM (section 3.1.1) and the role of remote sensing and GIS therein (section 3.1.1.3). Besides, an overview is given of the data and materials used which encompasses a brief summary of the main characteristics of the remote sensing datasets (section 3.2.1), a description of the ground-truth data collected (section 3.2.2) and an overview of the consulted auxiliary maps and software packages utilised to process the data (section 3.2.3). A diverse set of remote sensing data is examined on their potential for coral-reef research in the Red Sea. Some sensors are especially developed to derive information on marine biophysical parameters, such as the Sea Wide Field of View Sensor (SeaWiFS) and the Moderate Resolution Imaging Spectroradiometer (MODIS). An attempt has been made to process the plethora of SeaWiFS and MODIS data readily available for the region. The (multitemporal) analysis of these data, however, has shown very time consuming and did not fit the time frame of this research. Notwithstanding, a brief overview is provided of ocean colour (section 3.7.1), sea surface temperature (section 3.7.2), sea surface salinity (section 3.7.3) and sea surface current (section 3.7.4) products which are of interest to coral-reef science. When possible, examples for the Red Sea are presented. Although the other investigated satellite sensors (being Landsat 5 TM, Landsat 7 ETM+, ASTER, and QuickBird) are not primarily intended for marine research, their usefulness for the thematic study of the different aspects of a coral reef has been investigated. First, some additional pre-processing steps have to be taken. These steps include the noise reduction in the QuickBird and Landsat 5 TM datasets (section 3.1.1), the geometric correction of all datasets (section 3.1.2) as well as their radiometric correction (section 3.1.3), atmospheric correction (section 3.1.4) and water-column correction (section 3.1.5), and the masking of land and deep water (section 3.1.6). Secondly, the possibilities for bathymetric mapping (section 3.4) have been examined using the Landsat 7 ETM+, Landsat 5 TM, QuickBird and ASTER datasets. Of the different bathymetric mapping methods described in literature (section 3.4.2), the modified DOP-mapping method (Jupp, 1988; Edwards, 1999) and the ratio-transform method (Stumpf, 2003) have been tested on the Landsat 7 ETM+ (section 3.4.3.1), Landsat 5 TM (section 3.4.3.3) and QuickBird (section 3.4.3.4) datasets. While the Landsat data cover the entire Hurghada study area, the QuickBird dataset only depicts a more restricted part of the study area. The QuickBird dataset, conversely, allows to investigate the advantage of high spatial resolution. An alternative bathymetric mapping method based on digital photogrammetry is tested using the ASTER dataset which has unique stereoscopic properties in the third VNIR band (section 3.4.3.5). The different results are discussed and compared (section 3.4.4) and conclusions are

stated in section 3.4.5. Third, the geomorphological structures of the coral reefs in the (restricted) study area have been mapped using the Landsat 7 ETM+ (section 3.5.2.1) and QuickBird (section 3.5.2.3) datasets. In addition, the ecological distribution of the dominant bottom types on the coral-reef structures have been classified using these datasets (section 3.6). The obtained geomorphological zonation maps and bottom-type classifications have subsequently been combined into one single coastal habitat map. Methodologically, the advantages of incorporating textural information (section 3.6.2.1.2) and/or the contextual editing (section 3.6.2.2.1) of the obtained classifications have been examined. Specifically with the QuickBird dataset (section 3.6.3.3), alternatives for the calibration of the water-column correction technique has also been investigated in more detail. These techniques and the resulting products are discussed in section 3.6.4 and the conclusions concerning the bottom-type mapping are given in section 3.6.5. As the Landsat 7 ETM+ dataset also contains a panchromatic band with a spatial resolution of 15m, the advantages of pan-sharpening this dataset (section 3.3.7) have been analysed by comparing the bathymetric, geomorphological-zonation and bottom-type-classification results obtained over the restricted study area respectively using the QuickBird, the original and the pan-sharpened Landsat 7 ETM+ datasets (sections 3.4.3.2, 3.5.2.2 and 3.6.3.2). In addition, a multitemporal analysis has been performed to determine to what extent the augmented human activity in the region has altered the coastal environment (section 3.8). The Landsat 5 TM and Landsat 7 ETM+ datasets have been processed in a multi-component change detection procedure to determine changes in the marine bottom types. Besides, both datasets have been compared to estimate the expansion rate of the urban centre of Hurghada and the possible impacts on the shoreline and the adjacent coral reefs. To conclude, two examples of GIS analyses are given, being a risk assessment map based on the Reefs at Risk criteria defined by Bryant *et al.* (1998) (section 3.9) and an initial multi-use MPA zoning plan (section 3.10) which have been defined based on the previously described remote-sensing-derived products.

PART I

CORAL REEFS



1.1 WHAT ARE CORAL REEFS?

1.1.1 Definition

The term *coral reef*, basically, encompasses two components: first, the geological-geomorphological structure (the reef) and, secondly, the biological organisms responsible for the construction of the reef (the coral animals) (Veron, 2000; Kleypas *et al.*, 2001) as is exemplified by following selection of published definitions:

Levinton (1982: 394): ‘*Coral reefs are compacted and cemented assemblages of skeletons and skeletal sediment of sedentary organisms living in warm marine waters within water depths of strong illumination. They are constructional physiographic features of tropical seas consisting fundamentally of a rigid calcareous framework mainly composed of the interlocked and encrusted skeletons of reef-building (hermatypic) corals and crustose coralline algae.*’

Snead (1982: 42): ‘*A coral reef is defined as a complex organogenic framework of calcium carbonate (primarily of corals) that forms a rock eminence on the sea floor and customarily grows upwards to the tide limit.*’

Beer (1983: 185): ‘*Coral reefs, which occur in warm tropical waters, are a cemented mass of large interlocking coral and algal colonies buried in their original position by subsequent overgrowth on all sides.*’

Head (1987b: 129): ‘*Coral reefs are large masses of biogenic rock and sediment, capped with a thin veneer of living organisms, some of which, especially the corals and algae, produce the calcium carbonate of which the reef mass is composed.*’

Achituv and Dubinsky (1990: 1): ‘*... reefs are marine, biogenic wave-resistant carbonate structures, also known as bioherms, composed of shells or skeletons of hermatypic, or reef-building, organisms ... Coral reefs ... corals as the main hermatypic organisms.*’

Wilkinson and Buddemeier (1994: 20): *‘Highly productive coral communities occupy only a fraction of the surface of an entire coral reef system. The underlying limestone structure, the sediment dominated slopes and lagoon floors and the less attractive reef flats are products of present and past coral reef communities. These parts of a reef may also be covered by productive living communities. The term “coral reef” implies the larger system, but in discussions of the biological aspects of reefs or the reef community, the same words generally refer to the living community dominated by reef-building corals and calcifying algae.’*

Coch (1995: 371): *‘A reef is a ridgelike or moundlike wave-resistant structure occurring in the shallow waters along some coastlines ... built of the cemented skeletons of tiny animals called corals. These form coral reefs.’*

Hallock (1997: 13): *‘... a reef is a submerged hazard to navigation, usually a ridge of rock or sand at or near the surface of the water ... biogenic reefs are produced by biological as well as geological processes ... another term for a limestone structure or buildup produced by biological activity is bioherm. ... A coral reef is a rigid skeleton structure in which stony corals are the major framework constituents.’*

Hatcher (1997: 44): *‘... some general definition of a coral reef: a marine limestone structures built by calcium-carbonate secreting organisms which, with its associated water volumes, supports a diverse community of predominantly tropical affinities at a higher density of biomass than the surrounding ocean.’*

Freiwald (2002: 369): *‘In general, coral reefs form topographic highs on the basis of skeletal framework accretion which is enhanced by biological encrustation over dead surfaces, prolific sediment production and concurrent inorganic or biologically-controlled cementation. Destructive processes are dominated by rasping, grazing and boring organisms, and by high-energy hydrodynamics.’*

ICRIN (2002): *‘Coral reefs are massive structures made of limestone that is deposited by living things. ... The most important reef building organisms are corals.’*

Bellwood *et al.* (2004: 827): ‘Coral reefs ... are three-dimensional shallow-water structures dominated by scleractinian corals.’

CoRIS (2004b): ‘coral reef - a wave-resistant structure resulting from cementation processes and the skeletal construction of hermatypic corals, calcareous algae, and other calcium carbonate-secreting organisms.’

Davis and FitzGerald (2004: 354): ‘Reefs are a type of positive feature on the sea floor, generally in shallow water... an organic reef is a wave-resistant, organic framework.’

Concerning the geological aspect, a differentiation is made between a ‘reef’ formed by inorganic material, usually rock or sand, and an ‘organic reef’ or *bioherm* which is built up by organic material excreted by *hermatypic*, or reef-building, organisms. Emphasis is put on the fact that an organic reef is a ridge- or mound-like structure generally encountered in shallow tropical and subtropical waters and that it is an exceptionally wave-resistant, complex framework of limestone or carbonate build up to the sea surface.

Consequently, a coral reef is defined as an organic reef in which the main reef-building organisms are coral animals. This implies that other organisms are capable of building reefs as well. Examples are given by Snead (1982) and Davis and FitzGerald (2004) of serpulid reefs, bryozoa reefs, oyster and mussel reefs and sponge banks, but these organisms generally do not produce such large reefs as corals.

Although corals are the dominant reef-building organism in a coral reef, they are certainly not the only ones. The secondary role of encrusting coralline algae, especially, is emphasised in some definitions. The hermatypic corals are mainly responsible for the large coral-reef framework, while coralline algae fill the spaces in between and, in that way, consolidate the reef, making it more wave-resistant. Davis and FitzGerald (2004), therefore, even propose to use the term *coral-algal reef* instead.

Some definitions, especially the one given by Hatcher (1997) also stress the ecological meaning of a coral reef. Ecologically speaking, a coral reef also encompasses the entire community of species related to and supported by the coral reef. To differentiate from the geological-geomorphological structure, this is often referred to as the coral-reef ecosystem.

1.1.2 Coral physiology

1.1.2.1 Coral anatomy

At its broadest sense, the term ‘coral’ encompasses at least 7 Cnidarian orders (Head, 1987b). The most important reef builders, however, are the so-called ‘true’ (Head, 1987b), ‘hard’ or ‘stony’ corals which, taxonomically, belong to the order Scleractinia, subclass Anthozoa, class Zoantharia, phylum Cnidaria (fig. 1.1).

Like all cnidarians, scleractinian corals are *diploblastic*. Each polyp consists of two basic tissue layers: an outer *ectodermis* (or *epidermis*) and the *endodermis* (or *gastrodermis*) which surrounds a central cavity, the *coelenteron* or *gastrovascular cavity*. These layers are connected to each other by a fibrous layer, the *mesoglea* (fig. 1.2). In the case of stony corals, an additional differentiation is made between the *free epidermic layer* which is in contact with the water and the *calcioblastic epidermis* responsible for the excretion of the calcareous exoskeleton (Barnes and Chalker, 1990; Muller-Parker and D’Elia, 1997). The coelenteron is mainly responsible for the digestion of food particles and the exchange of gases and dissolved nutrients with the surrounding water (Muller-Parker and D’Elia, 1997). It has one opening, the *mouth*, which is surrounded by *tentacles* (Barnes and Chalker, 1990; Fautin and Romano, 1997). Like with other anthozoan polyps, but opposed to the other cnidarian classes, the tentacles of scleractinians are hollow, meaning that the coelenteron extends into them (Fautin and Romano, 2000).

The tentacles and epidermis are studded with microscopic stinging capsules, *nematocysts*. The possession of these intrinsic nematocysts is the defining characteristic of the phylum (Hessinger and Lenhoff, 1988; Fautin and Romano, 1997). With these *cnidae* and *tentacles* the cnidarians are capable of capturing prey. All cnidarians, therefore, are considered carnivorous. Because scleractinian polyps are sessile, they are believed to be passive predators (Fautin and Romano, 1997).

Within the gastrodermis of many anthozoans -and a small number of hydrozoans and scyphozoans- live symbiotic unicellular algae of which the exclusively marine dinoflagellates, termed *zooxanthellae*, are by far the most common (Fautin and Romano, 1997). Accordingly, a biological separation is made between *zooxanthellate*, i.e. having zooxanthellae symbionts, and *azooxanthellate* species. As will be shown in following paragraphs, this symbiotic relation has far-reaching ecological consequences for the species.

The class Anthozoa can be divided in two groups which are externally distinguished by the number and form of a polyp's tentacles. The subclass Alcyonaria (or Octocorallia) includes animals such as soft corals, sea fans, sea pens and blue corals. Most species of Alcyonarians form colonies and skeletons. The subclass Zoantharia (or Hexacorallia) includes sea anemones, 'stony' corals and black corals (Fautin and Mariscal, 1991; Fautin *et al.*, 2000). Two orders of living zoantharians have skeletons, being the Scleractinia and the Antipatharia. The rigid scleractinian skeleton, which lies external to the polyp that makes it, is composed of calcium carbonate in the crystal form aragonite (Milliman, 1974). The skeleton of an individual scleractinian polyp is known as a *corallite* (Fautin *et al.*, 2000). The antipatharian skeleton, in contrast, lies internal to the polyp that makes it (Fautin *et al.*, 2000).

Some species of the Scleractinia order are solitary, while others are colonial (Fautin *et al.*, 2000). When a coral is capable of forming colonies, and thus reefs, it is called hermatypic. Hermatypic corals were long-time believed to be confounded to the clear, shallow waters of the tropics, while *ahermatypic* corals, conversely, are found in all regions of the oceans, including temperate and polar regions, from relatively shallow waters down to 6,000m (Romano and Cairns, 2002). Recent advances in deep-water research, however, have proven the existence of reef structures built by cold-water azooxanthellate coral species at several hundreds meters deep along the margins of most oceans (Freiwald, 2002). These reefs, although generally not as stable and large as their warm- and shallow-water counterparts, may extend over many km².

The Scleractinian order is further divided in several suborders (Veron, 2000; Romano and Cairns, 2002) although this division has not been entirely defined yet. It is outside the scope of this work to provide an overview of the many families, genera and species comprising the scleractinian corals. For more detail on the taxonomy of zooxanthellate scleractinian corals is referred to Veron (2000)¹.

From this point onwards, the term 'coral' will only refer to hermatypic, zooxanthellate, scleractinian corals, unless otherwise stated. Subsequently, the term 'coral reef' will only be used to indicate the common warm- and shallow-water structures build up by these animals.

¹ Within the zooxanthellate scleractinian corals, Veron (2000) distinguishes 18 families, 111 genera and 794 species.

1.1.2.2 Zooxanthellate corals

Corals are heterotrophic as they can capture and directly ingest zooplankton and other particles from the water column. This is important for the provision of nitrogen, phosphorus and other nutrients essential for the coral's metabolism (Lesser, 2004a). Zooxanthellate corals, nevertheless, derive most of their energy and nutrients through the symbiosis with zooxanthellae.

The zooxanthellae exclusively occur in membrane-bound vacuoles in the gastrodermis cells (fig. 1.2). On average, more than one million algal cells per cm² are counted, though this number greatly varies spatially as well as temporarily (Muller-Parker and D'Elia, 1997). The symbiotic dinoflagellates, zooxanthellae, were long believed to belong to one single pandemic species, *Symbiodinium microadriaticum*, but recent research has already differentiated eight phylogenetic clades (Coffroth and Santos, 2005). Although many hosts are specific for a particular symbiont type, different dinoflagellates can occur within one species and even within one polyp colony (LaJeunesse, 2002; Knowlton and Rowher, 2003).

During photosynthesis, the zooxanthellae produce oxygen and organic products such as amino acids, glucose, glycerol and small peptides of which 95% (Muscatine, 1990) is delivered to the coral host using this energy for respiration, growth and deposition of its carbonate skeleton (Muscatine, 1990; Coch, 1995). In return, the coral provides shelter to the algae and supplies them with compounds essential for photosynthesis. These components are CO₂ from the animal's respiration and crucial plant nutrients, mainly ammonia and phosphate, derived from the metabolic waste products of the coral (Coch, 1995; Muller-Parker and D'Elia, 1997). Zooxanthellae, consequently, also help the coral to remove its wastes.

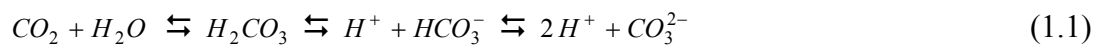
More and more studies, however, indicate the break-up of this symbiotic relation by one of the partners under less than ideal circumstances. This leads to the well-known phenomenon of bleaching. The symbiotic relation, therefore, might have been too often considered as a cooperative relationship, while it should be better regarded as a reciprocally selfish association (Herre *et al.*, 1999) beneficial to both partners, but easily broken when environmental conditions become less favourable. Nevertheless, the symbiosis with a primary producer, like the zooxanthellae, enables the coral to survive in a nutrient-poor environment (Hoegh-Guldberg, 2000; Lesser, 2004a). Moreover, the availability of algal photosynthates is taken as the prime reason for the rapid rates of

skeletal growth typical for hermatypic corals (e.g. Barnes and Chalker, 1990; Muller-Parker and D'Elia, 1997; Buddemeier *et al.*, 2004).

1.1.2.3 Coral calcification

1.1.2.3.1 CO₂ environment

The secretion of calcium carbonate by the coral polyps is first of all dependent on the CO₂ concentration in the surrounding water. In formula 1.1 is shown how CO₂ combines with water to form carbonic acid (H_2CO_3) which, subsequently, is easily dissolved as bicarbonate (HCO_3^-) or carbonate (CO_3^{2-}):



The total dissolved inorganic carbon concentration is the sum of the carbon in these four states. How much CO₂ is dissolved in water and which state predominates depends primarily on temperature, pressure and concentrations of other dissolved materials. In general, tropical surface waters hold less CO₂ than temperate or polar waters (Hallock, 1997).

Calcium carbonate (CaCO₃), consequently, is precipitated in the following way:



The more CO₂ is dissolved in the water, therefore, the more readily the water can dissolve CaCO₃. Since calcium ions (Ca^{2+}) and bicarbonate ions (HCO_3^-) are both abundant in seawater, modern tropical ocean-surface waters are more conducive to the precipitation of CaCO₃, whereas deeper and colder ocean waters are more apt to dissolve CaCO₃ (Hallock, 1997).

As the precipitation of one mole of CaCO₃ generates one mole of CO₂, there has been debate whether coral reefs are a source or a sink of atmospheric CO₂. Nowadays, consensus has risen that, like rainforests, a coral reef may be seen as a sink for atmospheric CO₂ on a geological time scale but that, in the view of future global change and on time scales of interest to humans, coral reefs must rather be regarded as

an additional source of atmospheric CO₂ (e.g. Smith and Buddemeier, 1992; Ware *et al.*, 1992; Chisholm and Barnes, 1998).

1.1.2.3.2 *Light-enhanced calcification*

The excretion of calcium carbonate by a coral polyp occurs from its calcioblastic epidermis. As coral calcification certainly continues in the dark, there is solid evidence that reef-building corals have a basic calcification mechanism that is not directly dependent upon photosynthesis (Head, 1987b; Barnes and Chalker, 1990). Nevertheless, there is ample proof that calcification rates are much higher during daytime and even differences between cloudy and cloud-free days have been noted (Levinton, 1982; Head, 1987b). This effect is called light-enhanced calcification (Barnes and Chalker, 1990).

As a consequence, the photosynthesis by the endosymbionts plays an important role in the amelioration of the calcification process. As there is still debate about the exact link between calcification and photosynthesis, four hypotheses, currently, are proposed:

1. CO₂ is taken from the coelenteron by the algae to support photosynthesis. As is seen from formula 2, any process that removes CO₂ from the system promotes the precipitation of CaCO₃ (Coch, 1995; Adey, 1998; Buddemeier *et al.*, 2004);
2. By the act of photosynthesis inorganic nutrients, especially phosphates, are consumed by the algae. These nutrients are known to inhibit the calcification process (Levinton, 1982; Barnes and Chalker, 1990);
3. As calcification is a very energy consuming process, the deliverance of photosynthates from the algae supports the coral in this process (Levinton, 1982; Barnes and Chalker, 1990);
4. Some organic products delivered by the algae are considered vital components in the construction of the organic calcium carbonate matrix without which the skeleton could not be built (Levinton, 1982; Barnes and Chalker, 1990).

The most fundamental requirement appears to be the creation of an isolated environment in which calcification can occur (Barnes and Chalker, 1990).

1.1.2.3.3 Coral-reef building

To form its skeleton, the polyp produces a basal plate and subsequently a cup, the *calyx*, in which it is embedded. Later on, the polyp starts to reproduce asexually by budding forming the coral colony in which the polyps are connected to one another by the *coelenchyme* (Fautin and Mariscal, 1991). In fact, a coral colony consists of a thin organic layer of coral tissue overtopping the growing underlying coral skeleton. Vertical growth rates of individual coral colonies widely vary from one species to another. Harriott (1999), for example, has reviewed growth rates ranging from 2 to 185mm per year.

Although corals are the most important contributors to the carbonate skeleton of the reef, massive reef accretion can not be solely ascribed to the production of calcium carbonate by scleractinian corals. Also numerous crustose coralline algae and other calcium carbonate-producing algae contribute to the reef growth (Levinton, 1982). According to Spencer and Viles (2002: 30), coral-reef growth occurs '*at the physiological level of coral-zooxanthellae symbiosis; at the site scale of secondary calcification, sedimentation and cementation infills in the locally created framework; and at the reef scale, with the vertical and lateral growth of the reef margin and the sedimentary infill of associated back reef and lagoon environments.*' After bio-erosion processes have been taken into account (Spencer and Viles, 2002), the average vertical growth rate of an entire coral reef varies between 1 and 10mm per year depending on the dominant coral associations and the position on the reef (Smith and Buddemeier, 1992).

1.1.3 Global coral-reef distribution and limiting factors

Spalding *et al.* (2001) estimate the total area of coral reefs in the world at 284 300km² based on in situ observations and remote sensing data. This only represents 0.089% of the world's oceans and less than 1.2% of the world's continental shelf area. Figure 1.3 shows the global distribution of the coral reefs. Coral reefs are clearly confined to a broad zone encompassing the tropics and subtropics, although remarkably absent in some areas like the coasts of South America and the west coast of Africa. This general pattern is largely explained by a number of long-term, geological, influence factors as well as certain contemporary, physical, limiting factors largely related to the ecological requirements of the coral-algae symbiosis.

1.1.3.1 Long-term influence factors

1.1.3.1.1 Darwin's Subsidence Theory (Darwin, 1842)

The geology of a coral reef has since long been studied. Already in the 19th century, attention was paid to these fascinating structures. One of the most prominent, and still relevant, theories is the Subsidence Theory developed by Charles Darwin in 1842. With this theory, Darwin tried to explain the formation of the deep-water atolls he observed in the Pacific Ocean on his voyage on H.M.S. Beagle between 1831 and 1836.

It was already known before Darwin that modern corals, generally, do not exist in water any deeper than roughly 100m (Hubbard, 1997). How then could the Pacific atolls been formed as they are surrounded by water several thousands meters deep? To explain this apparent incompatibility, Darwin regarded tectonic subsidence of the Earth's crust as the main factor influencing the geological evolution of a coral reef.

Darwin (1842) stated that each reef originally starts as a fringing reef growing on the shore of high volcanic islands (fig. 1.4). As these islands subside, the *fringing reef* grows upwards, forming a barrier reef further offshore. When this process continues, the lagoon between the *barrier reef* and the high volcanic island becomes wider and deeper. Ultimately, the central volcanic island will totally disappear below the sea surface, leaving an encircling barrier reef which now forms an *atoll*. Subsidence was thus regarded as the "renovating agency" (Darwin, 1842) determining the existing form of atolls: without it, lagoons would fill, reefs widen and, eventually, featureless reef banks would form (Steers and Stoddart, 1977).

Later on, Darwin extended his theory to include continental fringing and barrier reefs, which he considered to differ in no material way from open-ocean reefs (Steers and Stoddart, 1977). In his explanation of the general distribution of coral reefs, he connected fringing reefs to tectonically stable coasts, while barrier reefs were taken as characteristic for subsiding shores (Hubbard, 1997).

Although Darwin's ideas were confirmed by deep core drillings in oceanic atolls (e.g. Ladd and Schlanger, 1960; Hubbard, 1997), the hypothesis that subsidence is the universal and sole factor influencing the evolution of coral reefs no longer holds.

1.1.3.1.2 *Daly's Glacial Control Theory (Daly, 1915)*

An alternative to Darwin's Subsidence Theory was formed by Daly in 1915, who regarded Pleistocene sea-level changes, independent of tectonic subsidence, as the sole factor determining the formation of modern reefs. He founded his theory on the observation that, in most of the areas he examined, many lagoon floors are situated at approximately the same depth between 50 and 90m. He explained this by linking the lagoon floors to wave-cut platforms created during a global drop in sea level associated with a Pleistocene glacial. The inner high island would then be subject to marine erosion and wave-cut benches could be formed (fig. 1.4). If sea level rose again, the corals recolonise the platforms and, for ecological reasons, grew faster on the outer rims of the banks. If the island was not totally abraded, a barrier reef forms, otherwise, an atoll was formed surrounding a lagoon platform (Steers and Stoddart, 1977; Hubbard, 1997).

Daly's theory, as well, lost its role as a universal explanation for the creation of barrier reefs and atolls; especially after the criticism by W.M. Davis (1923) who pointed to the lack of cliffed coastlines behind barrier reefs in the Pacific, which would normally be formed if Daly's theory was correct. Since then, nevertheless, sea-level changes, whatever their cause, have become more and more regarded as a major controlling factor for the evolution and formation of modern reefs (Steers and Stoddart, 1977; Hubbard, 1997).

1.1.3.1.3 *Reef accretion under the influence of relative sea-level change*

The general pattern of reef development under changing sea-level depends both on the rate of sea-level rise compared to the upward accretion rate of the reef, and on the time span during which sea level rises faster than the ability of the reef to grow upwards (Hubbard, 1997).

The different ways in which coral reefs could react on a relative sea-level change, intrinsically a sea-level rise, have first been described by Neumann and Macintyre (1985) who have distinguished a *keep up*, a *catch up*, and a *give up* scenario:

- 'keep up' reefs are able to maintain their crest at or near sea level throughout their history;
- 'catch up' reefs are initially left behind by a sea-level rise, but then recover, usually after the rate of sea-level rise has slowed down;

- 'give up' reefs are reefs that, for different reasons, simply stop accreting. This can be the result of a sudden rise in sea level which increases water depth to a point where net reef carbonate production could no longer keep up; a sudden change in oceanographic conditions such that the environment is no longer conducive to rapid carbonate production; noncarbonated sedimentation; or a combination of these factors.

Hubbard (1997), alternatively, proposes slightly different scenarios on how coral reefs react to sea-level rises (fig. 1.5):

- *prograding reef*: if the rate of the sea-level rise is lower than the reef growth rate, the reef will grow upwards whenever possible; otherwise it will form horizontal extensions;
- *vertical accretion reef*: if the sea-level rise equals the reef growth rate, the reef will grow upwards;
- *retrograde, backstep or drowned reef*: if the sea-level rises faster than the reef grows, the reef will retrograde, backstep or, ultimately, drown if the rise persists at the same rate or if the resulting sea-level rise was too large to catch up.

Sea-level fluctuations have occurred throughout geological time, with glacio-eustatic changes dominating most of the late Pleistocene. With each rise and fall of the sea level, reefs living near the sea surface, were alternately flooded or exposed. This results in a series of reefs, each built upon the remnants of its predecessor. As a result, modern reefs as they appear today occur wherever a suitable substrate becomes available, whatever its origin. Moreover, they could only be formed since the last transgression of the sea about 10,000 years ago. Therefore, in most cases, they only form a thin veneer on top of older limestone deposits (Steers and Stoddart, 1977; Hubbard, 1997; Buddemeier *et al.*, 2004).

1.1.3.2 Contemporary, physical limiting factors

Corals need specific environmental conditions in order to survive and, as important, to form massive carbonate structures. The most important physical limiting factors for hermatypic corals are temperature, light, salinity, and wave energy (table 1.1).

Table 1.1. Physical factors limiting hermatypic coral growth: minimum, maximum, mean and standard deviations (after: Kleypas et al., 1999b)

| | minimum | maximum | mean | standard deviation |
|---|----------------|----------------|-------------|---------------------------|
| <i>weekly temperature (°C)</i> | | | | |
| mean | 21.0 | 29.5 | 27.6 | 1.1 |
| minimum | 16.0 | 28.2 | 24.8 | 1.8 |
| maximum | 24.7 | 34.4 | 30.2 | 0.6 |
| <i>monthly salinity (PSU)</i> | | | | |
| minimum | 23.3 | 40 | 34.3 | 1.2 |
| maximum | 31.2 | 41.8 | 35.3 | 0.9 |
| <i>monthly maximum depth of light penetration (m)</i> | | | | |
| mean | 9 | 81 | 53 | 13.5 |
| minimum | 7 | 72 | 40 | 13.5 |
| maximum | 10 | 91 | 65 | 13.4 |

1.1.3.2.1 Temperature

As temperature influences the CO₂ absorption capacity of the water, it has its consequences for the calcification process of hermatypic corals. Temperature, therefore, is the most important factor for the latitudinal distribution of coral reefs (Snead, 1982; McClanahan, 2002). Long time, it was generally accepted that coral reefs are restricted to water temperatures ranging between 18 and 30°C (Veron, 1986; Coch, 1995; Hubbard, 1997). Based on a recent review of 1000 coral-reef sites listed on Reefbase, Kleypas *et al.* (1999b), in contrast, found that coral reefs occur in seas and oceans with temperatures ranging from 16 to 34.4°C (table 1.1).

However, with the exception of one coral-reef site in Japan occurring at minimum temperatures of 16°C (Fujiwara *et al.*, 2000), the 18°C monthly minimum isotherm globally forms the boundary between shallow-water coral reef and non-reef coral communities (McManus and Vergara, 1998; Kleypas *et al.*, 2001). A possible upper temperature boundary to coral-reef formation is still debated, but the former upper limit of 30°C is becoming more and more regarded as erroneous (Kleypas *et al.*, 2001).

As can be seen in figure 1.3, the lower temperature boundary corresponds with an abundant coral-reef zone stretching between approximately 30°N and 30°S around the equator (Snead, 1982; Coch, 1995; Souter and Lindén, 2000; Davis and FitzGerald, 2004). The absence of coral reefs along the western coasts of the African and American continents may largely be explained by the occurrence of cold upwelling streams (figure 1.6). On the eastern continental shelves, coral reefs, in contrast, may extend north of the 30° latitudinal border because of warm ocean currents; examples

can be found in Japan and Bermuda as a result of the Kuroshio Current and the Gulf Stream respectively.

1.1.3.2.2 Light

The second, if not the most important limiting factor for hermatypic corals is the availability of light. Light will not directly dominate the latitudinal distribution of corals, but is very important for their vertical distribution. As light is primordial for photosynthesis by the symbiotic algae, corals are restricted to clear, shallow water. As photosynthesis positively influences coral calcification, it has been shown that under reduced light conditions corals produce more fragile skeletons which are more subject to breakage (Yentsch *et al.*, 2002). Two elements are important for the availability of sufficient light: incoming solar irradiance at the water surface, changing daily as well as seasonally, and water transparency (Yentsch *et al.*, 2002).

Because light rapidly attenuates in water, the *photosynthetically available radiation* (PAR) becomes quickly restricted with depth. The light spectrum also changes as longer wavelengths, e.g. infrared light, are more rapidly attenuated than shorter wavelengths. As a result from a certain depth, depending on the water quality, only blue wavelengths are available for photosynthesis. Zooxanthellae, normally, adapt to these changes in the light field by changing the characteristics of their photosynthetic systems (Muscatine, 1990; Muller-Parker and D'Elia, 1997; Yentsch *et al.*, 2002). These changes include an increase in the light-harvesting ability of the photosynthetic units, e.g. by an increase in the size or number of pigments, and/or an increase in the rate of carbon fixation (Muller-Parker and D'Elia, 1997).

Corals, generally, occur up to a depth of 40 to 60m (Beer, 1983; Wilkinson and Buddemeier, 1994; Coch, 1995; Spencer and Viles, 2002), although some have been reported to occur at depths of 100m and more in exceptionally clear waters. These corals, however, are generally small and solitary and their calcification rate is highly restricted (Snead, 1982; Beer, 1983; Schlichter *et al.*, 1985; Head, 1987b; Muscatine, 1990; Hoegh-Guldberg, 2000). At a certain depth, i.e. the *compensation depth*, photo-acclimation can no longer compensate the decline in light availability and the photosynthetic production just balances the respiration by the coral-algal symbiont ($P/R = 1$) (Head, 1987b). Coral growth below this depth, thus, becomes impossible or, at least, severely restricted. The compensation depth, however, is species and even

colony dependent (Yentsch *et al.*, 2002) and a strict depth limit to coral growth can not be drawn.

The clarity of the water not only depends on the attenuation coefficient of the water, but is also highly influenced by runoff bringing suspended sediments and nutrients into the coastal waters (Wilkinson and Buddemeier, 1994; Hoegh-Guldberg, 2000). Increased turbidity is considered as one of the main reasons why coral reefs do not extensively occur near large river mouths like the Amazon and Orinoco in east South America or the delta of the Indus and Ganges-Brahmaputra in South Asia (Snead, 1982; Coch, 1995) (figure 1.3).

Another element related to light availability is the amount of UV radiation capable of penetrating the water (Wilkinson and Buddemeier, 1994) as it greatly influences the distribution and physiology of both reef plants and animals (Jokiel, 1980). In normal conditions, both host and symbiont have developed a range of protective mechanisms to deal with an excess in UV-radiation (Jokiel, 1980; Falkowski *et al.*, 1990; Muller-Parker and D'Elia, 1997). Recently, concerns have however risen about the influence of the thinning stratospheric ozone layer on the incoming UV radiation and the ability of the coral-algal symbionts to adapt to the changing situation².

1.1.3.2.3 Salinity

Corals, globally, occur in a salinity range between 32 and 40PSU (Veron, 1986; Hoegh-Guldberg, 2000), although coral reefs also thrive in exceptionally high and low salinity conditions (41.8 and 23.3PSU respectively) as was found by Kleypas *et al.* (1999b) (table 1.1). More important than average salinity concentrations, however, are sudden decreases in salinity due to high freshwater input by rivers or torrential rains (Hoegh-Guldberg and Smith, 1989; Souter and Lindén, 2000). Decreased salinity is seen as a second factor for the disappearance of massive coral reefs in front of large river mouths (Coch, 1995; Hubbard, 1997).

1.1.3.2.4 Wave energy

Sufficient wave and current energy is a final factor determining the presence and distribution of coral reefs: currents are responsible for the distribution of coral larvae over short to long distances (Andrews and Pickard, 1990), while sufficient wave action is necessary to provide food and oxygenated water to the sedentary polyps, to

² For a further discussion, see section 1.3.3.3.

prevent smothering of the polyps by sediments, and to remove waste products from the coral system (Snead, 1982; Head, 1987b; Coch, 1995; Hubbard, 1997; Davis and Fitzgerald, 2004; Nybakken and Bertness, 2005). Too strong waves and currents, conversely, may prohibit or inhibit reef formation (Snead, 1982).

On the scale of a single reef, the benthic zonation of coral associations is highly regulated by wave energy and light availability (Achituv and Dubinsky, 1990; Hubbard, 1997; Davis and FitzGerald, 2004). Maximum rates of reef accretion and productivity, therefore, are found between 5 and 15m depth (Snead, 1982), while highest coral diversity occurs in a zone between 15 and 30m (Huston, 1985). Much local variation, however, exists in the composition of the coral associations. More detail on this benthic zonation pattern, therefore, will only be given in section 2.4.2.2.2 when dealing with the ecological zonation of the Red Sea coral reefs.

1.1.3.3 Coral biogeography

Coral diversity patterns may be expressed at the family, genus and species level (Veron, 2000) (Fig. 1.7). The lower the taxonomic level, the more recent the differentiation has taken place. The family diversity is related to geological events such as continental drift or mass extinctions and, therefore, no clear regional differences are noticeable (fig. 1.7a). At the generic level, a clear difference is visible between a well-defined Indo-Pacific centre of diversity and a much less diverse Caribbean region (fig. 1.7b). This pattern mainly results from the geological closures of the Thetys Sea and the Central American Seaway. Most ancient taxa only survived in the Indo-Pacific and, as a consequence, many genera only evolved, and remained, in the Indo-Pacific (Veron, 2000). From the central Indo-Pacific, generic diversity remains more or less stable across the Indian Ocean, while clearly attenuating eastwards into the Pacific.

Diversity patterns can be most clearly noticed at the species level (fig. 1.7c). A clear species diversity centre is evident in South-East Asia with distinctive attenuation in all directions. This centre of diversity is mainly the result of a confluence of widespread species, rather than a high number of regional endemisms. This may be explained by the global surface current pattern transporting watermasses, including coral larvae, from all over the Indo-Pacific region to this area. Moreover, the many thousands of islands and shallow shelves in South-East Asia provide a very suitable habitat for coral growth.

The latitudinal attenuation of diversity not only results from decreasing temperatures leaving less corals able to survive, but may also be attributed to the general poleward

direction of the major oceanic surface currents, connecting the subtropics with the tropical centre of diversity but not vice-versa. Remote areas, therefore, are less diverse but generally have a relative high number of endemisms. New species may evolve in these isolated locations but are unable to disperse to other regions due to the unfavourable currents.

Species diversity remains mostly uniform in the tropical Indian Ocean with the Red Sea as a secondary centre of diversity (Veron, 2000), although largely isolated at the outer edge of the Indian Ocean (Behairy *et al.*, 1992; Spalding *et al.*, 2001). Diversity in the tropical Pacific, in contrast, shows a clear attenuation pattern away from the centre. The diversity level in the Caribbean and Atlantic Ocean only equals the most remote Indo-Pacific reefs.

Based on a degree of regional similarity taking into account the number and identity of coral species, Veron (2000) distinguishes 15 coral biogeographic provinces as shown in figure 1.8. Differences between the provinces largely reflect their regional proximity, the more the provinces are interconnected through oceanic currents, the higher their similarity. Consequently, largest differences can be found between the Indo-Pacific and the Caribbean-Atlantic regions (Veron, 2000; Nybakken and Bertness, 2005). Within the latter region, the Caribbean/Gulf of Mexico province is the most distinctive. The far-eastern province in the Indo-Pacific also has unique characteristics, as does the Red Sea albeit to a lesser extent. Least differentiation can be made between the central Indo-Pacific provinces.

1.1.4 Coral-reef geomorphology

1.1.4.1 Large-scale geomorphology

The terminology of large-scale coral-reef geomorphology is largely based on the sequence of reef types differentiated by Darwin in 1842. Differentiation, therefore, is made between four reef morphologies: fringing reefs, barrier reefs, atolls, and *patch reefs*. Current-day use of this terminology in coral-reef geomorphology, however, does not imply Darwin's subsidence theory. As shown by Snead (1982) and Kennedy and Woodroffe (2002), respectively in the case of atolls and fringing reefs, different mechanisms may lead to similar coral-reef morphologies. Different other, more detailed classifications have been proposed, e.g. the classification scheme by Maxwell and Swinchatt (1970) (fig. 1.9),

although most of them are based on specific local environmental conditions and can not be applied worldwide.

1.1.4.1.1 Fringing reefs

Fringing reefs are the most common and basic reef type. These coral reefs edge the shoreline of islands and continents and, by definition, do not include a deep *lagoon* between the land and the reef (Snead, 1982; Beer, 1983; Achituv and Dubinsky, 1990; Davis and FitzGerald, 2004) (fig. 1.10). With time, however, the reef flat may become hollowed out to form a shallow, lagoon-like channel (Achituv and Dubinsky, 1990; Head, 1987b) (fig. 1.11). Occasionally, living corals are able to establish themselves once more in this area; forming a double fringing reef structure (Beer, 1983; Kennedy and Woodroffe, 2002).

1.1.4.1.2 Barrier reefs

Barrier reefs are similar to fringing reefs as they border the shoreline, but they occur at much greater distances from the land and a deep and wide channel or lagoon has formed between both (Snead, 1982; Beer, 1983; Achituv and Dubinsky, 1990; Davis and FitzGerald, 2004) (fig. 1.12). This lagoon may range in width from 0.8 to 16km and more, and can be 50 to 80m deep (Snead, 1982). Most barrier reefs have open passes which act like tidal inlets permitting the exchange of water between the lagoon and the open sea (Davis and FitzGerald, 2004). Barrier reefs, commonly, are asymmetrical in section (fig. 1.12), being steeper at the seaward side but gently sloping to the interior with a *back reef* often dotted by small *reef patches* and coral heads (Snead, 1982).

1.1.4.1.3 Atolls

Atolls are ring- or horseshoe-shaped reefs surrounding a lagoon (fig. 1.13). They are not connected with any land except for an occasional island of purely coral formation (Snead, 1982; Beer, 1983; Achituv and Dubinsky, 1990; Davis and FitzGerald, 2004). As with barrier reefs, each section of the atoll is asymmetrical with a clear difference between the leeward and the windward side of the atoll in which the latter is generally steeper and broader (fig. 1.13). Snead (1982) makes a further differentiation according to the formation history of the atoll:

- *shelf atolls*: atolls grown up as open patch reefs or remnants of earlier patch reefs;

- *compound atolls*: atolls grown out of barrier reefs or patch reefs in areas where large continental shelves have slowly subsided;
- *oceanic atolls*: atolls, as described by Darwin, associated with a subsided volcanic high island.

1.1.4.1.4 Patch reefs

Patch reefs, also called platform, shelf, bank, hammock, pinnacle or table reefs (Snead, 1982; Davis and FitzGerald, 2004), are isolated reef platforms of various shapes and sizes commonly found in water of moderate depth on continental shelves or in lagoons (Snead, 1982; Beer, 1983; Davis and FitzGerald, 2004).

1.1.4.2 Medium- to small-scale geomorphological zonation

On a medium to small scale, coral reefs are further subdivided into different geomorphological zones. These zones are the result of the interaction between the reef system and the physical forces acting in the marine environment. As the geomorphological aspects of a coral reef are closely linked to its ecology/biology, care should be taken not to mix both aspects in the definition of the geomorphological zones (Mumby and Harborne, 1999a).

The geomorphological classification scheme used in this work is based on the hierarchical schemes developed by Mumby and Harborne (1999a; b) and Coyne *et al.* (2003), for the reef systems in Belize and Hawaii respectively, who in their turn took advantage of the work done by Holthus and Maragos (1995). A differentiation is made between the back reef, the reef flat, the reef crest, the fore reef, the spur and groove systems, the patch reef, the lagoon, the escarpment, and the bank/shelf. These geomorphological zones have been identified in figures 1.10, 1.12 and 1.13 respectively on a fringing reef, a barrier reef, and an atoll.

1.1.4.2.1 Reef crest

The reef crest is the shallowest part of the reef, often emergent at low tides. The reef crest absorbs much of the wave energy and is an important coastal defence. The zone separates the fore reef from the back reef/ reef flat.

1.1.4.2.2 Back reef/reef flat

The back reef is the shallow zone between the reef crest and the lagoon. It is usually formed by a pavement of hard substratum with or without rubble. In the case of a

fringing reef, where no lagoon is present, the area between the shoreline and the reef crest is called the reef flat (Coyne *et al.*, 2003).

1.1.4.2.3 Fore reef

The fore reef is the area from the seaward edge of the reef crest downwards. Mumby and Harborne (1999a; b) quantified the slope of the fore reef to be lower than 45°. The lower part of the slope, generally from depths of 50m downwards, is less steep than the upper part as it commonly consists of reef debris or dead in situ reef framework (Davis and FitzGerald, 2004).

1.1.4.2.4 Spur and groove systems

Spur and groove systems are specific parts of the fore reef where a structure of alternating *spurs* (or *buttresses*) -formed by accreting hard corals and calcifying green algae- and deeper *grooves* -usually containing sand or bare rock- has formed. This system is believed to be created as a response to wave action (Davis and FitzGerald, 2004). Mumby and Harborne (1999a; b) made a further subdivision into:

- a low relief spur and groove: the spurs are generally less than 5m in height. These are almost vertical walls, commonly located immediately seaward of the reef crest;
- a high relief spur and groove: the spurs are generally more than 5m in height. These are much larger structures than the above and are usually situated near the lower edge of the fore reef, near the escarpment.

1.1.4.2.5 Reef patch

Reef patches are isolated coral formations in the lagoon or on the bank/shelf. This reef zonation is not easily distinguishable from a patch reef on the large-scale level, as only the areal extent of the feature differs. The term reef patch is also used for reef parts originally formed by hard corals, but which are now colonised by other organisms (Mumby and Harborne, 1999a; b).

1.1.4.2.6 Lagoon

The lagoon is the shallow area, relative to the deeper water of the bank/shelf, between the shoreline and the back reef of a barrier reef, or the shallow area encircled by an atoll. This zone is generally protected from high-energy waves by the reef crest. A depth limit of 12m is proposed by Mumby and Harborne (1999a; b) to differentiate between shallow and deep lagoons.

1.1.4.2.7 Escarpment

An escarpment, generally, is defined as any part of the seafloor where slopes are in excess of 45° (Mumby and Harborne, 1999a; b). It is often associated with the drop-off wall of barrier reefs and atolls.

1.1.4.2.8 Bank/shelf

The bank or shelf zone is defined as the relatively undeeper area of the continental shelf which is not in direct relation to the reef structure.

1.1.4.3 Micro-scale morphology

On the micro scale, each coral colony is characterised by its own morphology. Although this morphology is mostly species specific, it may also change dependent on varying environmental conditions (e.g. depth or wave energy) such that a single species may be manifested in several morphologies, while one morphology may be developed by several distinctive species. Table 1.2 gives an overview of the most common forms distinguished.

Table 1.2. Overview of the most common geomorphological forms of coral colonies (after: Veron, 2000; CoRIS, 2004a)

| colony morphology | description |
|---------------------------------|---|
| branching or arborescent corals | corals with tree-like branches |
| digitate corals | singled branched, finger-like, corals |
| table corals | table-like structures of fused branches |
| elkhorn corals | corals with large, flattened branches |
| foliose or laminar corals | broad plate-like corals |
| encrusting corals | corals forming thin surface layers |
| submassive corals | corals with an encrusting base and protruding knobs, columns (columnar) or wedges |
| massive corals | ball-shaped or boulder-like corals |
| mushroom corals | corals resembling attached or unattached tops of mushrooms |
| cup corals | cup-shaped corals |

1.2 CORAL-REEF VALUES

1.2.1 Ecological values

1.2.1.1 Biodiversity

Coral reefs are considered as one of the most spectacular marine ecosystems on earth as they are characterised by a tremendous biodiversity and, in many places like the Red Sea (Head, 1987b), a high level of endemism³. For this reason, coral reefs are often referred to as the rainforests of the marine world. According to Reaka-Kudla (1996) already 93,000 different species living on coral reefs are described worldwide, although this is only a small percentage of the total of one to nine million species estimated to be associated with coral reefs (Reaka-Kudla, 1996). The difference between the estimate and the actual number of known coral-reef-associated species, points to a very high undocumented biodiversity.

The diverse group of species associated with a coral reef interact with each other in a very complex way. A simplified representation of a trophic web in a typical coral-reef community is shown in figure 1.14. Generalised, the coral-reef community's diversity can be divided into three main components: the suprabenthic fishes, the sessile epibenthic organisms responsible for the reef structure and the cryptofauna living inside this framework (Reaka-Kudla, 1996; Adey, 1998).

Since long, ecologists and biologists have tried to explain how a coral-reef community can support such a high level of diversity. First, the idea existed that coral reefs generally evolve to a system of well-ordered ecological climaxes under benign environmental conditions with limited fluctuations in the physical and chemical parameters (Odum, 1971; Brown, 1997b; Spencer and Viles, 2002). Later on, more and more acknowledgment was given to the dynamic interaction between coral reefs and such natural disturbances, physical as well as biological. By the 1960s and 1970s, reefs were considered as non-equilibrium systems whose structure consists of a temporal mosaic of communities in different stages of recovery from various disturbances. This concept is best represented by the *intermediate disturbance hypothesis* worked out by Connell (1978). Consequently, the high diversity supported by coral reefs is maintained by this

³ in terms of total coral reef related biodiversity, not only the number of coral species

system of intermediate disturbance (Connell, 1978; Brown, 1997b; Spencer and Viles, 2002; Lesser, 2004a). Each stage, however, was still considered as a transition phase until the coral-reef system eventually returns to its original equilibrium (*single-equilibrium*) after the disturbance has ceased (fig. 1.15) (Nyström *et al.*, 2000).

Recently, ecological thinking has moved away from these *neo-equilibrial* or *quasi-equilibrial* models (Spencer and Viles, 2002) and coral reefs are now more seen as dynamic systems, fluctuating around an average, the coral-reef *stable state*, never reaching a climax state even if environmental conditions remain constant (Scheffer and Carpenter, 2003). Moreover, the coral-reef system is not considered as the only possible stable state. It is assumed that multiple stable states (*multi-equilibrium*) exist and that the system may shift from one state to another (Done, 1992; Knowlton, 1992; McCook, 1999; Nyström *et al.*, 2000; Scheffer and Carpenter, 2003). Such a *phase shift* may occur after a sudden dramatic disturbance but may also result from gradual environmental changes. In the latter case, small changes may have little effect until a critical threshold is reached after which the system quickly and dramatically shifts to another state. Alternatively, these gradual changes may not apparently alter the system, but make it more susceptible to an additional disturbance with which, under the original conditions, the system could have easily coped (Scheffer and Carpenter, 2003).

This concept is exemplified in figure 1.16. In this schematic representation, the ball symbolizes the state of the ecosystem and the curve depicts the different possible stable states (valleys) and the possibility of the system to shift to another stable state. In figure 1.16a, the system is situated in one stable state and it is difficult to move to the other stable state on the left. In figure 1.16b, environmental changes have reduced the resilience of the system -the hilltop has lowered- and the system becomes more susceptible to disturbances. In figure 1.16c, the resilience of the system is reduced to a point where additional changes or a sudden dramatic event results in a phase shift. Finally, the system shifts to the alternative stable state as shown in figure 1.16d (Holling *et al.*, 1995; Nyström *et al.*, 2000; Scheffer and Carpenter, 2003).

In terms of biodiversity, a coral-reef system is described as a *shifting steady-state mosaic* (Bormann and Likens, 1979; Done, 1999) defined as ‘*a regional population of reef communities that are diverse and changing, but in which all of the important types and components are always represented*’ (Buddemeier *et al.*, 2004: 7). In other words, biodiversity is kept at such a high level partly due to the dynamic interaction of the reef environment with the different disturbances. As different parts of the coral reef are, or

have been, subject to different disturbances, they show a distinctive species composition, thus attributing to an overall high coral-reef biodiversity.

The most common phase shift observed on coral reefs is a change from dominance by corals to dominance by fleshy macro-algae, although other transitions have been reported as well (Bellwood *et al.*, 2004). The best known and studied example probably is the dramatic coral-algal phase shift which occurred on many Caribbean reefs in the late-1980s, commonly linked to growing anthropogenic disturbances, especially overfishing and excessive nutrients supply (e.g. Brown, 1997b; Nyström *et al.*, 2000; Scheffer and Carpenter, 2003) (fig. 1.17a).

Bellwood *et al.* (2004) present a model exemplifying the possible transitions between different ecosystem states on a coral reef (fig. 1.17b). Healthy coral dominated reefs become progressively more vulnerable as their resilience is affected by different disturbances (dashed lines). If their resilience is dramatically altered, the system may slide to another stable state. As the resilience of progressively less diverse stable states decreases, the system can quickly slide to a 'lower' stable state. The ability of the system to recover to the original coral-dominated situation, on the contrary, decreases markedly.

A coral-dominated system, consequently, may shift to another stable state dominated by non-coral organisms whenever the original disturbance regimes changes; the ecosystem resilience is reduced; or a combination of both occurs (Nyström *et al.*, 2000). The system, however, is not able to return easily to the original state nor is it sufficient to restore the initial environmental conditions, as has become clear from several case studies on coral reefs. This irreversible effect is known as *hysteresis* (Scheffer and Carpenter, 2003). Besides, when a stable state 'lower' than the coral-dominated state has been reached, the system, commonly, can no longer support the initial high biodiversity levels. Major concern, therefore, is growing that human interaction with the disturbance regime influencing coral reefs changes the ability of the corals to cope with them and eventually will lead to more dramatic phase shifts, ultimately resulting in great losses in biodiversity (Brown, 1997b; Nyström *et al.*, 2000; Buddemeier *et al.*, 2004).

1.2.1.2 Seascape interrelations

Early studies of coral-reef ecology were mainly focussed on open ocean atolls (Nyström *et al.*, 2000; Spencer and Viles, 2002). Ecologists of this period (e.g. Sargent and Austin, 1949; Odum and Odum, 1955), therefore, regarded coral reefs as unique marine ecosystems as they are highly productive although often surrounded by water poor in

nutrients necessary for primary production (Adey, 1998; Hoegh-Guldberg, 2000). For this reason, the coral reefs, often described as oases in an ocean desert, were regarded as closed, fragile climax systems (Hoegh-Guldberg, 2000). Over time, when more elaborate studies became available and coral reefs near continental margins were examined as well, the ecological view on coral reefs has changed (Hatcher, 1997; Spencer and Viles, 2002). Nowadays, coral reefs are more regarded as an open system in close relation with other ecosystems, although they may occur in an isolated, open ocean environment as well (Ogden, 1997). The complex mosaic of interacting ecosystems -in casu coral reefs, seagrass beds, and mangroves- of the coastal zone is referred to as the *seascape* (Ogden, 1997).

Two schemes, represented in figures 1.18 and 1.19, show how the different ecosystems in the seascape may interact. Ogden (1997) differentiates three types of interactions: biological interactions, physical interactions, and fluxes of nutrients and organic material. The best known biological interactions are the diurnal and/or nocturnal *foraging* patterns of different species which migrate from one ecosystem to another (Ogden, 1997), and a *nursery* relation where many coral-reef-associated species spawn and/or grow up in a sheltered seagrass or mangrove environment (Ogden, 1997; Dorenbosch *et al.*, 2004; Mumby *et al.*, 2004). The physical interactions are mainly linked to the creation of a suitable environment for the associated ecosystems. Mangroves and seagrass beds, on the one hand, are considered important for the development of coral reefs along continental shores as they may interrupt large freshwater discharges, stabilise salinity levels in the coastal zone, and act as buffers or sinks for high sediment and/or nutrient concentrations in terrestrial runoff (fig. 1.19). Coral reefs, on the other hand, protect the coastline against high wave action and erosion and, as such, create lagoons and sedimentary environments that favour the growth of mangroves and seagrasses (Ogden, 1997) (fig. 1.19). Although most seascape ecosystems are regarded as open systems, fluxes of nutrients and organic materials are considered limited (Ogden, 1997).

1.2.2 Socio-economic values

Coral reefs are not only important for their biodiversity and their key role in the tropical marine biosphere; they are also very valuable socio-economic resources. In Asia alone, tens of millions (Moberg and Folke, 1999) to over 1 billion people (Hinrichsen, 1997; Bryant *et al.*, 1998; Whittingham *et al.*, 2003) depend on coral reefs for part of their livelihood as these

reefs are main fishing grounds and attractors of large numbers of tourists. In this way, they generate important contributions to the national income of many countries. This is especially important as two-thirds of all countries with reef areas are developing countries; one quarter of which even belongs to the least developed category (Whittingham *et al.*, 2003; UNDP, 2004). Coral reefs also protect human settlements and the hinterland from marine erosion and the worst effects of storms and surges. Besides, more and more importance is given to coral reefs as potential sources of medicines and other biochemical products. The total yearly value of resources and services provided by reefs worldwide, as a result, is estimated between 30 (Cesar *et al.*, 2003) and 375 billion USD (Costanza *et al.*, 1997).

Moreover, coral reefs also have a high immaterial value as they are often influencing the socio-cultural organisation of many indigenous people living near coral reefs (Whittingham *et al.*, 2003). To give just one example, traditional coral-reef fishing usually is a cooperative activity involving the entire village, including women, children, and the elderly. As such, fishing activities, and thus coral reefs, can be regarded as consolidating parts of the social structure of the village (Birkeland, 1997a).

1.2.2.1 Fisheries

Fishery is not merely significant for the national income of a country; it is often an important, if not the only source of proteins for people living in developing countries (Wilkinson and Buddemeier, 1994) as up to 25% of the total fish catch is provided by coral-reef-associated fisheries (Jameson *et al.*, 1995; Bryant *et al.*, 1998). This percentage, most probably, is even underestimated as much fish is caught by subsistence fishermen and never officially recorded (Souter and Lindén, 2000).

The potential sustainable yield of fishes, crustaceans and molluscs related to coral reefs is estimated at 9 million metric tons per year (Jameson *et al.*, 1995). The standing stock of coral-reef fishes is remarkably higher than on other demersal fishing grounds (Russ, 1984; Birkeland, 1997a), but still relatively low compared to the highly productive upwelling oceanic areas. Coral-reef fishing grounds, however, are very vulnerable for overexploitation due to their complex ecosystem structure (Wilkinson and Buddemeier, 1994; Birkeland, 1997a), so care should be taken to exploit them sustainably.

Besides, different reef related organisms are harvested for the curio, jewellery, and live fish trade. According to the Global Marine Aquarium Database a total of 1471 species of fish, 1410 species of stony coral and 500 species of invertebrates other than corals are traded as marine ornamentals (Wabnitz *et al.*, 2003). Most species are collected in South-

East Asia and transported to the USA, EU and Japan. Closely linked is the trade in live fish supplying exclusive restaurants, especially in China and Japan (Moore and Best, 2001; Wabnitz *et al.*, 2003).

The harvesting of aquarium animals probably is the highest value-added part of coral-reef fishery (Wabnitz *et al.*, 2003). Currently, the live marine aquaria trade is estimated at 200 to 330 million USD annually (Wabnitz *et al.*, 2003). If managed sustainably, this could support many coastal communities in developing countries where other options for revenue generation are often limited (Wabnitz *et al.*, 2003). Collecting and trading ornamental marine species, unfortunately, is often associated with damaging fishing techniques and potential overharvesting of some species. More details on the problems related to fishing and the live fish trade are given in sections 1.3.2.5 and 1.3.2.6.

1.2.2.2 Tourism

Yearly, more and more tourists are attracted to the coral reefs and the associated beaches. As a result, tourism is the fastest growing economic sector associated with coral reefs and is expected to double within the next couple of years (Hoegh-Guldberg, 2000). This evolution already has occurred in the southern parts of the Egyptian Sinai with the number of tourist rooms increasing from under 600 in 1988 to over 6,000 in 1995 and even 16,000 in 1999 (Spalding *et al.*, 2001).

Tourism is the most important source of foreign income for many small island nations, most of them catalogued as a developing country (Souter and Lindén, 2000; Davenport and Davenport, 2006). In Palau, a small Pacific island state consisting of more than 300 islands with a population of about 20,000 (CIA, 2004), for example, coral-reef-related tourism brings in about 13 million USD per year (Birkeland, 1997a). In the Caribbean, where millions of visitors annually spend their holidays, the tourism industry is responsible for about half the gross national product -valued at 8.9 billion USD in 1990- and employs 350,000 people (Jameson *et al.*, 1995).

1.2.2.3 Coastline protection

Coral reefs are protecting the adjacent coastline against erosion, surges and other impacts of waves and storms (Bryant *et al.*, 1998; Souter and Lindén, 2000). 1km² of coral reef, for example, has been estimated to prevent about 2,000m² of erosion per year along the erosion-sensitive coasts of western and southern Sri Lanka (Berg *et al.*, 1998; Whittingham *et al.*, 2003). Birkeland (1997b), as well, has shown the different impacts of

a typhoon for areas in Guam with and without adjacent coral reefs. Cesar (1996) has estimated the costs, over a period of 25 years, of destroying 1km of coral reef in Indonesia between 137,000 and 1,200,000 USD due to losses in fisheries, tourism and the loss of natural protection.

In this way, coral reefs not only protect human infrastructure like villages, harbours or industrial plants, but they also protect the often very fertile hinterland and create save waters for navigation and fishing (Whittingham *et al.*, 2003). Moreover, they provide an ideal environment for typical coastal habitats like mangroves and seagrass beds which are important nursery ground for commercially interesting fishes (Birkeland, 1997a; Bryant *et al.*, 1998; Souter and Lindén, 2000).

Although some anecdotal evidence from Sri Lanka (Fernando *et al.*, 2005; Liu *et al.*, 2005) points to increased inland damage on places where coral reefs have been damaged or removed, in general, they were largely unable to stop the huge waves generated by the December 26th, 2004 tsunami in the Indian Ocean (Obura and Abdulla, 2005; Wilkinson *et al.*, 2006). Mangroves and coastal forests, in contrast, are believed to have given much more protection (Wilkinson *et al.*, 2006).

1.2.2.4 Coral reefs as pharmaceutical and biochemical resources

Pharmaceutical companies, in their search for new medicines, as well, are becoming more and more interested in the enormous diversity of coral-reef-associated species (Adey, 2000). Corals are especially promising as they produce a large array of chemicals to protect themselves against predators and other disturbances in their environment (Bryant *et al.*, 1998). Already, valuable pharmaceuticals derived from coral-reef-related species are used in the treatment of cardiovascular diseases, asthma, tumors, skin cancer, leukaemia, and viral and bacterial infections (Carte, 1996; Fenical, 1996; Birkeland, 1997a), and about half of all new cancer drug research is assumed to focus on marine organisms (Fenical, 1996; Maragos *et al.*, 1996). Besides, coral carbonate is used for human bone grafts (Bryant *et al.*, 1998) and as aids in bone marrow-transplants (Birkeland, 1997a). Coral reefs also are a reservoir of biochemically important substances and are used in many industrial applications of marine biotechnology, e.g. in the development of biodegraders, antifouling and anticorrosion substances, biosensors, biocatalysts, biopolymers and many other potentially important compounds and products (Zilinskas and Lundin, 1993).

1.3 THREATS TO CORAL REEFS

With an increasing global human population, more and more people will rely on coral reefs as a natural resource to support their livelihoods. Unfortunately, the interaction between humans and the reef ecosystem is not always sustainable. Although coral reefs are able to deal with natural disturbances, they often show signs of degradation after anthropogenic interference. The major difference between many natural and human-induced disturbances probably is the persistence of the latter (Nyström *et al.*, 2000). While natural disturbances normally occur in a pulsed manner (Connell, 1997), human-induced disturbances, regularly, are more persistent and tend to accumulate slowly or occur so frequently that little time remains for the reef system to recover (Brown, 1997b; Connell, 1997; McCook, 1999; Nyström *et al.*, 2000).

Human activities may damage coral reefs directly or they may adversely disrupt the ecological interactions within the coral-reef ecosystem and/or the seascape (Nyström *et al.*, 2000; Knowlton, 2001). Besides, anthropogenic activities may alter the temporal and spatial scales of the natural disturbance regime (Nyström *et al.*, 2000). This could lead to the transformation of the natural disturbance into a more persistent disturbance or even a chronic stress. In addition, this may also suppress or remove the natural variation in the system which is essential for maintaining the natural dynamics of the coral reef (Holling and Meffe, 1996; Nyström *et al.*, 2000).

Human-induced disturbances mainly are the result of coastal development activities; inland development projects, pollution and erosion; marine pollution; overexploitation of the coral-reef resources; and destructive fishing practices (Wilkinson and Buddemeier, 1994; Bryant *et al.*, 1998). The two greatest worldwide threats generated by human activities are identified to be pollution, especially due to excessive sediment and nutrients in terrestrial runoff, and unsustainable fishing activities (Bryant *et al.*, 1998; Wilkinson, 1998; Spalding *et al.*, 2001; Hughes *et al.*; 2003).

In 1993, Wilkinson estimates that about 10% of world's coral reefs had already disappeared and that an additional 30% might totally collapse within the next two decades (Wilkinson, 1993; Jameson *et al.*, 1995). Five years later, Bryant *et al.* (1998) already estimates that 58% of the coral reefs in the world are under medium to high risk of being damaged by human activities. Until the mid-1990s, these anthropogenic threats were considered the most important negative influence factors and, as a consequence, coral reefs

near human settlements were considered the most threatened (e.g. Smith and Buddemeier, 1992; Wilkinson and Buddemeier, 1994).

This point of view radically changed after the massive coral bleaching event in 1997/1998 which was closely linked to one of the severest El Niño events in human history (e.g. Reaser *et al.*, 2000; Wellington *et al.*, 2001; Hughes *et al.*, 2003). According to Wilkinson (2000a), an additional 16% of the coral reefs worldwide were destroyed by this single mass bleaching event. While it is assumed that these coral reefs will recover, this process will be slow and about half of them are not expected to recover in the next 50 years (Wilkinson, 2000a). From that moment onwards, coral-reef scientists became more and more aware of the negative effects of global change.

The natural resilience of coral reefs, thus, becomes more and more pressured by a complex interplay of many disturbances, natural as well as human-induced, local as well as global, direct as well as indirect. The result of these interacting disturbances, however, is not well understood yet, although more and more evidence points to a synergistic, devastating effect (Nyström *et al.*, 2000). Consequently, the regenerative capacity of the coral reef will be severely reduced and, therefore, phase shifts might become more frequent in the near future (Nyström *et al.*, 2000; Hughes *et al.*, 2003; Bellwood *et al.*, 2004).

It is believed that under the current scenario of a fast growing global human population, predominantly in developing countries (Wilkinson and Buddemeier, 1994), and a changing global climate, coral reefs will become severely threatened if our interaction with coral reefs - and nature in general - will not change drastically (fig. 1.20). Green and Bruckner (2000), for example, show that in the Caribbean, 97% of the coral diseases reported are related to reefs moderately to highly impacted by human activities. Worldwide, coral-reef degradation will generate severe economic losses which will be especially worrisome for the local economies in developing countries (Souter and Lindén, 2000; Bellwood *et al.*, 2004). Eventually, this could lead to the use of even more destructive methods to extract the increasingly scarce resources (Holling and Meffe, 1996; Cesar *et al.*, 2003; Buddemeier *et al.*, 2004). The loss of the coral-reef ecosystem, ultimately, may even have consequences for the entire human population, especially if the potential of the reef system as a pharmaceutical resource is taken into consideration (Adey, 2000).

1.3.1 Natural disturbances

Under normal conditions, coral reefs interact with a wide range of natural disturbances. Some of the most common natural threats to the integrity of a coral reef are considered to be outbreaks of *bio-eroders*, for example Crown-of-Thorns starfishes (*Acanthaster planci*); storms, tsunamis and hurricanes; coral diseases; and stress-related bleaching (Wilkinson, 1998; Souter and Lindén, 2000).

1.3.1.1 Outbreak of *Acanthaster planci*

One of the best documented examples of bio-erosion probably is the recurrent population explosions of the Crown-of-Thorns Starfish (COTS), *Acanthaster planci*, in the Indo-Pacific region (e.g. Faure, 1989; Brown, 1997b). The damage caused can be very severe, as can be seen in an example on the Great Barrier Reef after the outbreak of *Acanthaster planci* in the period 1981-1989. Approximately 10% of the coral reefs showed extensive, high mortality and declines in coral cover from 78% to 2% over a six month period were observed in some sites (Brown, 1997b). The precise cause of these *Acanthaster planci* outbreaks, however, is not yet fully understood (Brown, 1997b; Souter and Lindén, 2000).

As most bio-eroders appear less sensitive to the environmental changes than *bioconstructors* and even seem to benefit from the deterioration of the coral-reef system (Spencer and Viles, 2002; Fabricius, 2005), such bio-eroder outbreaks may be triggered by human activities and become more frequent and severe in the future.

1.3.1.2 Damage by storms, tsunamis, cyclones and hurricanes

The destruction of coral reefs by storms or hurricanes is mostly mechanical. Damage may result from the removal of all growing corals over relative large areas, often several km²; the selective destruction of the fast-growing branching species in an even wider area; and the provision of large amounts of coarse sediment interrupting coral-reef growth and settlement (Stoddart, 1971). Vertically, the direct physical damage from storm waves is mostly restricted to less than 20m depth, although coral blocks falling down the steep forereef slopes may cause severe damage at much greater depths (van Woosik *et al.*, 1991; Brown, 1997b).

Indirectly, the torrential rainfall associated with these storms may locally lower the salinity level of the sea water for days or even weeks, potentially causing physiological stress to the corals (Stoddart, 1971). Excessive rainfall on the mainland, on the other hand,

may result in augmented runoff loaded with sediments making the water more turbid, while the sediment particles may even smother the coral polyps. Nutrient levels in the water may also be augmented due to the terrestrial runoff or due to the breakdown of moribund tissues in the water following the storm (Brown, 1997b).

Tsunamis may damage coral reefs through 3 mechanisms: waves may physically damage the coral reef and move the coral rubble; the resulting increase in sediment may smother the corals; and the retreating waves may bring along additional sediment and debris from the land (Wilkinson *et al.*, 2006). The damage to the coral reefs in the Indian Ocean caused by the December 26th, 2006 Tsunami proves to be very patchy and diverse and is largely related to the position of the reef in respect to the seabed bathymetry and the wave direction (frontal or sheltered), to the normal natural environmental conditions (frequency of heavy currents, tropical storms) and the overall health status of the coral reef concerned (healthy or already affected by other disturbances) (Obura and Abdulla, 2005; Wilkinson *et al.*, 2006). Damage was greatest in regions closest to the origin of the tsunami, i.e. Indonesia, Thailand, the Andaman and Nicobar Islands, and Sri Lanka. Most of the coral reefs, however, appear to have escaped serious damage and are expected to recover within 5 to 10 years, provided environmental conditions do not deteriorate (Wilkinson *et al.*, 2006).

1.3.1.3 Coral bleaching

Coral bleaching is a natural stress reaction used by the coral polyp to protect itself from changing physical, chemical or biological conditions (Hoegh-Guldberg, 2000) including reduced salinity levels, fluctuations in light intensity, increased sea water temperatures, bacterial infection, and contamination from a wide variety of pollutants (Brown, 1997b; Muller-Parker and D'Elia, 1997; Souter and Lindén, 2000). The bleaching either results from the expulsion of the endosymbiotic zooxanthellae, from the loss of pigment in the zooxanthellae, or from both (Souter and Lindén, 2000; Douglas, 2003; Lesser, 2004a).

Although corals may recover after bleaching (Douglas, 2003), the potential physiological and ecological effects are wide-reaching as bleaching mainly results from the disruption of the basic symbiotic relationship with the zooxanthellae. Physiologically, bleaching has been shown to reduce coral growth, the rate of calcification and the reproductive capacity of corals. Ecological effects may range from reduced resilience resulting in replacement of sensitive coral species by more stress-resistant species or,

ultimately, a phase shift to dominance by non-coral organisms (Brown, 1997b; Souter and Lindén, 2000). More attention will be given to this topic in section 1.4.

1.3.2 Human-induced disturbances

1.3.2.1 Coastal development

According to Bryant *et al.* (1998), 30% of the world's reefs are threatened by coastal development. The damage to reefs may be directly or indirectly linked to nearby shoreline alterations. Direct physical damage is caused by land reclamation; by construction of shoreline protection infrastructure, harbours, airports, and tourist resorts; by dumping spoils into the water; or by mining the reef areas for construction materials, mainly sand and limestone (Wilkinson and Buddemeier, 1994; Bryant *et al.*, 1998; Souter and Lindén, 2000; Buddemeier *et al.*, 2004). These direct disturbances, although often very severe, usually have only a localised impact.

Indirect effects of coastal development, usually, are more damaging. Some examples are: increased turbidity of the water due to algal blooms resulting from nutrient-rich sewage releases or due to the disturbance of sediments during shoreline construction; coral-algal phase shifts or outbreaks of COTS caused by excessive nutrients from urban sewage (Faure, 1989); hot-water discharges and toxic pollution by desalinisation plants (Hoepner and Latteman, 2002), mines and other industrial activities; or the alteration of the coastal water circulation resulting in a changed coastal erosion pattern and a loss of connectivity with sources of coral recruits (Bryant *et al.*, 1998; Souter and Lindén, 2000; Buddemeier *et al.*, 2004). More details on some of these threats are provided in following section.

1.3.2.2 Inland development

One example, out of many, of how inland development causes damage to coral reefs is given by Hodgson (1997) for the El Nido village on Palawan Island (Philippines). In this study, an economical study is made on how inland logging would affect the economic value of the nearshore coral reefs in terms of tourism and fishing revenues. Hodgson (1997) has developed two scenarios: one wherein a logging ban has been imposed (scenario 1), and a second wherein logging continues unaltered (scenario 2). Table 1.3 gives an overview of the gross revenue, over a ten year period, to the village from logging, fishing and tourism. Under the second scenario, although income from logging is

preserved, the total gross revenue is markedly lower than under the first scenario. This clearly illustrates how logging would affect the coral reefs and, consequently, drastically diminishes income from tourism and fisheries. Under scenario 1, in contrast, the revenues generated by the coral reefs clearly outpace the losses made by banning inland logging.

Table 1.3. Losses in gross revenue in terms of tourism, fishing and logging (in thousands USD) due to unsustainable use of the coral-reef resources (after: Hodgson, 1997; Cesar *et al.*, 2003)

| | Scenario 1 | Scenario 2 | (Scenario1-Scenario2) |
|--------------|-------------------|-------------------|------------------------------|
| tourism | 47,415 | 8,178 | 39,237 |
| fisheries | 28,070 | 12,844 | 15,226 |
| logging | 0 | 11,375 | -11,375 |
| total | 75,485 | 32,397 | 43,088 |

Poor agricultural practices, deforestation, and/or intensification of agricultural techniques all result in augmented terrestrial runoff loaded with sediments, nutrients⁴ and pollutants (Smith and Buddemeier, 1992; UNEP-PERSGA, 1997; Bryant *et al.*, 1998; Fabricius and Wolanski, 2000; Souter and Lindén, 2000). Special attention is recently given to the potential negative consequences of wildfires. Wildfires may not only block the sunlight for many weeks, Abram *et al.* (2003) also ascertain an increased iron concentration in the coastal waters after the large 1997 Indonesian wildfires. This iron fertilisation is taken responsible for an extra-ordinary red tide which led to massive coral death by asphyxiation. As tropical wildfires are expected to become larger and more frequent due to the increasing human population (Eaton and Radojevic, 2001; Siegert *et al.*, 2001), this may become a serious threat to coastal marine ecosystems in the next century (Abram *et al.*, 2003).

The individual effects of sedimentation, nutrification⁵, and pollution, however, are often difficult to separate as these elements co-occur in the runoff water (McLaughlin *et al.*, 2003; Fabricius, 2005). This, especially, is the case for pollutants like herbicides or pesticides which often have devastating consequences, even at very low concentrations, but are difficult to trace (Buddemeier *et al.*, 2004).

⁴ Nutrients: all inorganic and organic forms of nitrogen (N) and phosphorus (P) (Szmant, 2002)

⁵ nutrification: an increased influx of nutrients; as opposed to eutrophication describing a more complex process involving organic production and accumulation, and the nutritional status of a community (Nixon, 1995 in: Szmant, 2002)

1.3.2.2.1 *Sedimentation*

Sediments, in suspension as well as deposits, may damage the corals and the coral-reef communities in many ways (Wilkinson and Buddemeier, 1994; Woolfe and Larcombe, 1999; Fabricius and Wolanski, 2000; McLaughlin *et al.*, 2003; Buddemeier *et al.*, 2004; Fabricius, 2005):

- corals respond to low concentrations of settling suspended sediments by physically removing the particles or by excreting *mucus*. This takes a lot of energy from the coral system and, eventually, when the sediment concentration increases, corals may die;
- acute high levels of settling sediment may disable the corals to remove the particles all together and they become smothered;
- the soft tissues of the coral may be damaged through abrasion by the sediment particles;
- chronic stress to the coral-reef system may result from a continued elevated suspended sediment load which reduces the water clarity and, consequently, the light energy available for the photosynthetic calcifying organisms; and
- large packages of unconsolidated sediment deposited on the seafloor may inhibit the settlement of new coral larvae which, generally, require a stable bottom.

The time, and thus the energy, required to remove the sediment particles varies between taxa and colony shapes (Stafford-Smith, 1993). Therefore, coral reefs do occur in sediment-rich environments, although then, they are usually dominated by a few, relatively large, individual coral colonies belonging to only a limited number of species (Fabricius and Wolanski, 2000; Fabricius, 2005).

As the terrestrial water discharge and the associated sediment load is one of the most altered parts of the global water cycle (Vörösmarty and Sahagian, 2000), many reefs, potentially, may shift to such less diverse systems in future. A differentiation in this global trend must however be made depending on the scale of the river's drainage basin (McLaughlin *et al.*, 2003; Buddemeier *et al.*, 2004). In larger river systems, the tendency is to dam the river. This will regulate the river outflow and, generally, diminishes the suspended sediment load reaching the sea which would be beneficial to the coral reefs occurring near these river mouths. New coral reefs, conversely, are unlikely to colonize these deltaic and estuarine areas as corals can not easily settle on the soft sediment bottom. Greater negative impacts, unfortunately, are likely to take

place in small coastal basins which are generally less managed and where land conversion and deforestation quickly increases erosion and runoff.

1.3.2.2.2 Nutriphication

Excess of dissolved inorganic nutrients in the water may have different direct physiological effects on the corals, mainly induced by interaction with the endosymbiotic zooxanthellae (Adey, 1998; Koop *et al.*, 2001; Szmant, 2002). The kind of effect depends on the coral species, the dose level, and the type of nutrient (nitrogen or phosphorus) (Koop *et al.*, 2001).

When the amount of additional nutrients is low, most coral biotic processes remain significantly unaffected (Wilkinson and Buddemeier, 1994; Koop *et al.*, 2001) except for the coral reproduction rate (Koop *et al.*, 2001; Szmant, 2002). As the coral reproduction rate even reduces at a small increase in nutrient levels, this may have far-reaching effects on the coral-reef system (Fabricius, 2005).

When higher levels of nutrients come into the water, different biotic responses are observed up to the point where the coral dies (Koop *et al.*, 2001). Controversy exists about whether or not increased nutrient levels reduce coral growth. According to McClanahan (2002), nitrogen as well as phosphorus inhibits calcification and coral growth, with phosphorus being more influencing than nitrogen. Koop *et al.* (2001), in contrast, have observed that adding high amounts of nitrogen does stunt coral growth, whereas adding phosphorus to the system increases calcification and the linear extension rate of the corals. However, they have noticed that the skeletal density of these extensions is reduced, leaving them more susceptible to breakage (Koop *et al.*, 2001).

In general, short term increases in dissolved inorganic nutrient concentrations are not believed to have large direct effect on the individual coral colonies, although chronically increased levels may hinder the coral metabolism and reduce the calcification rate (Fabricius, 2005). When nutrients occur as *particulate organic matter* (POM), in contrast, they may have a beneficial effect on coral growth and calcification, provided the levels of POM are only slightly or moderately increased (Fabricius, 2005).

Nutriphication, moreover, does not only directly interfere with the physiology of the coral; it may also have some indirect effects on the coral-reef community as a whole. It has been noted that increased nutrient concentrations improve the

environmental conditions for filter feeders which generally bore into the reef substratum (Smith and Buddemeier, 1992; Knowlton, 2001; McClanahan, 2002; Szmant, 2002). External coral predators such as Crown-of-Thorn starfishes, as stated previously, also benefit from increased nutrient conditions. As a result, whether or not nutrients decrease or increase the calcification rate of corals, bio-erosion of the reef structure is likely to increase with elevated nutrient concentrations (Risk *et al.*, 1995; Holmes *et al.*, 2000; McClanahan, 2002; Fabricius, 2005).

Excessive nutrient loadings, in addition, may result in mass phytoplankton blooms in the water column (Souter and Lindén, 2000; McClanahan, 2002; Buddemeier *et al.*, 2004). Water turbidity, consequently, increases and the available light energy decreases, inhibiting the physiological functioning of the corals (Fabricius, 2005). Ultimately, the corals may become asphyxiated due to the elevated biochemical oxygen demand by the phytoplankton or may get killed by the release of hydrogen sulphide by some phytoplankton species (Grigg and Dollar, 1990; Smith and Buddemeier, 1992).

Besides, augmented nutrient concentrations improve conditions for fast-growing algae with high organic but low inorganic carbonate production (McClanahan, 2002; Fabricius, 2005). Together with the erosion of the reef structure, this could trigger a phase shift towards a state dominated by macro-algae (Adey, 1998; McClanahan, 2002). The idea that nutrification may be responsible for a coral-algal phase shift stems from the central paradigm that coral reefs occur in a nutrient-limited environment and that the algae occurring on these reefs, therefore, are limited in their growth. Consequently, if nutrient supply to the reefs increases, the algae would proliferate and potentially outcompete the corals as the dominant species on the reef (Adey, 1998; Koop *et al.*, 2001; McClanahan *et al.*, 2002; Szmant, 2002).

Recent studies, however, have shown that many other elements determine the balance between coral and algal growth (fig. 1.21) such that nutrification as a sole factor is rarely the trigger for a coral-algal shift (McCook, 1999; Koop *et al.*, 2001; McClanahan *et al.*, 2002; Szmant, 2002; McClanahan *et al.*, 2004; McManus and Polsenberg, 2004) except maybe in very extreme situations (Smith *et al.*, 1981; Knowlton, 2001; Szmant, 2002, McManus and Polsenberg, 2004). Physical disturbances, such as siltation and/or resuspension of sediment; hurricanes; outbreaks of COTS; bleaching events or unsustainable fishing, all may contribute to the shift from corals to algae as the dominating species (McManus and Polsenberg, 2004). The

complexity of the interactions between all these influencing elements is best illustrated in the conceptual model depicted in figure 1.21.

Of all these influences, fishing pressure is considered the second, if not the most important factor as algal growth is not only controlled by the available nutrients but also by the abundance of grazing herbivores. Normally, excess algal growth would be quickly controlled by increased herbivore grazing. If the grazers, however, are not sufficient in numbers, due to a natural cause or due to overfishing, algal communities will grow to a more adult stage, possibly outcompeting corals as the dominant species (Lewis, 1986; McManus and Polsenberg, 2004).

In studies where the influence of herbivory and nutrients are compared, herbivory is almost always indicated as the most important factor causing the coral-algal phase shift (Miller *et al.*, 1999; McManus *et al.*, 2000; Knowlton, 2001; McClanahan *et al.*, 2002). Miller *et al.* (1999) even notice that a coral-algal phase shift could occur due to overfishing without an additional increase in nutrients, while nutrification, in contrast, could only create a favourable environment for macro-algae if the reefs are also subject to overfishing. A combination of overfishing and nutrification, on the other hand, does not necessary guarantee a phase shift either (McClanahan *et al.*, 2002).

The ability of a coral reef to withstand nutrification, therefore, is likely depending on the integrity of the food web. In a healthy reef, any excess in nutrients may be passed to the next trophic level, and will ultimately be removed from the system. In a reef where natural herbivory is reduced, however, biomass is accumulated at the primary production level, leaving the opportunity to the algae to dominate the reef (McManus and Polsenberg, 2004). In fact, any factor that leads to coral death or reduced levels of herbivory will advantage algal colonisation (Szmant, 2002).

To conclude, the effects of sedimentation, nutrification, and pollution not only depend on the duration and the severity of the event, but also on the geographical and biological conditions in which the coral reef occurs (Fabricius, 2005). Reefs which are already deteriorated or which occur in a less favourable environment, e.g. on a shallow lagoons or at deeper reef slopes, are likely to be more vulnerable.

1.3.2.3 Tourism

Dive-related tourism is one of the fastest growing businesses in the world (Cesar *et al.*, 2003), with around 1 million new divers trained each year (Davenport and Davenport, 2006). Tourism, unfortunately, is indirectly responsible for many, often uncontrolled, coastal development projects and destructive fishing activities (Bryant *et al.*, 1998; Davenport and Davenport, 2006). Besides, tourists, and especially SCUBA-divers and snorkellers, also cause direct damage to coral reefs. This damage mainly results from walking on the reef flats (Neil, 1990; Rodgers and Cox, 2003); breakage of corals and stirred up sediments during diving or snorkelling (Tratalos and Austin, 2001); anchor damage; and souvenir collection (Jameson *et al.*, 1995; UNEP-PERSGA, 1997; Bryant *et al.*, 1998; Zakai and Chadwick-Furman, 2002). The level of damage is not only related to the number of divers visiting the reefs (Zakai and Chadwick-Furman, 2002; Cesar *et al.*, 2003), but also to the behaviour and the level of experience and education of the diver (Rouphael and Inglis, 1997; Davenport and Davenport, 2006).

The devastating effects this may have on the coral reefs are illustrated by the example of Sharm el Sheik in the Egyptian Red Sea: between 1997 and 2002, almost 30% of the live hard coral cover has been destroyed, predominantly by the negative impacts of diving tourism (Wilkinson, 2002a). The damage, however, varies locally as the morphological constitution of the reef, i.e. branching or more robust species, will determine its sensitivity (Rouphael and Inglis, 1997).

1.3.2.4 Marine pollution

Oil spills and the deliberate discharges of oily ballast water are the main sources of marine pollution (Bryant *et al.*, 1998), although, for long time, these were not considered as a severe threat to coral reefs (e.g. Bryant *et al.*, 1998). Recent studies, however, prove that oil polluted corals may show acute lethal as well as chronic sublethal effects (Shigenaka, 2001; McClanahan, 2002). The sublethal effects of oil exposure are numerous, the most important of which appear to be reduced levels of reproduction and larval recruitment on the affected sites (Guzmán and Holst, 1993; Shigenaka, 2001). Besides, oil pollution may hinder the primary production of the zooxanthellae by blocking the sunlight, or the production of mucus to remove the oil particles may exhaust the coral's energy (Shingenaka, 2001).

Whether or not corals recover from the pollution mainly depends on the persistence of the pollution and on the constitution of the oil spill (Shigenaka, 2001). Based on a review of different studies made on this topic, Shigenaka (2001) concludes that a short exposure - less than half an hour- to extreme concentrations of oil is far less toxic to the corals than a longer- several hours to days- exposure to low concentrations. Even more remarkable, although direct coating increases the severity of the impact, it is especially the water-accommodated fraction of the oil which causes acute mortality or long-term physiological effects (Shigenaka, 2001).

Other sources of marine pollution exist as well, one example being toxic pollution due to anti-fouling paint used on many marine vessels. This becomes especially worrisome in the case of a ship-grounding as, next to the acute and chronic toxic effects of the paint on the sessile organisms, coral recruitment on the damaged site is seriously reduced for a long time (Negri *et al.*, 2002). On another level, coral reefs are also physically damaged by the movement of derelict fishing gear across the reef's surface (Donohue *et al.*, 2001).

1.3.2.5 Overfishing

Although coral reefs are one of the most productive marine communities, they only generate relatively small amounts of sustainably harvestable biomass (Birkeland, 1997b; Buddemeier *et al.*, 2004). Besides, many reef organisms are long-lived and must reach a certain age or size before they reproduce. Fishing of large consumable or economically interesting individuals will thus have a disproportionate impact on the group (Buddemeier *et al.*, 2004). Coral reefs, therefore, are especially vulnerable to overexploitation (Birkeland, 1997b). This has been shown by Pandolfi *et al.* (2003) who have discovered that many reef ecosystems were already substantially degraded before 1900. The main reason for this early decline is indicated to be overfishing, although land-derived pollution could have acted synergistically in some locations (Jackson *et al.*, 2001; Pandolfi *et al.*, 2003). This proves that the effect of fishing is already marked at relatively low intensities of fishing (Roberts, 1995). Bryant *et al.* (1998) estimate that, today, 36% of the world's reefs are potentially threatened.

As a minimum effect, overfishing causes shifts in fish size, abundance, diversity, and/or species composition, and may ultimately lead to the extinction of the target species (Roberts, 1995; Bryant *et al.*, 1998; Souter and Lindén, 2000). In some parts of the world, like the Philippines, not only fish, but also many mollusc species and other edible invertebrates are fished to extinction (Souter and Lindén, 2000). Moreover, as shown

previously, the removal of key herbivorous or predator species indirectly causes large-scale ecosystem changes and result in a phase shift towards a macro-algae dominated system (Roberts, 1995; Bryant *et al.*, 1998; McManus *et al.*, 2000; Souter and Lindén, 2000).

1.3.2.6 Destructive fishing

In recent years, more and more destructive fishing techniques become used although these destroy the very own resource the fishermen rely on. The main incentives for these unsustainable practices are the growing pressure to subsist an increasing poor population (McClanahan, 1995; Wilkinson, 1998; Souter and Lindén, 2000), and the international trade putting high amounts of money on some desirable fish (Wilkinson, 1998; Best and Bornbush, 2001; Moore and Best, 2001). The latter is especially worrisome as these fisheries are not restricted to reefs close to settlements, but even affect the most remote reefs, especially in Southeast Asia and the west Pacific (Bryant *et al.*, 1998; Moore and Best, 2001).

Destructive fishing practices cause direct damage to the reef structure and habitat (Roberts, 1995; Bryant *et al.*, 1998) mainly through the application of blast/dynamite fishing, fishing with poisonous chemicals, damaging netting techniques, or non-selective fishing (Wilkinson and Buddemeier, 1994; Bryant *et al.*, 1998; Wilkinson, 1998; Souter and Lindén, 2000). This damage can be very severe as is illustrated by an economic assessment made by Cesar (1996) in Indonesia. He estimated that over a 25 year period, and a 10% discount rate, the net losses due to destructive fishing techniques could reach between 140 000 and 1.2 million USD per km² of reef (Cesar, 1996).

Blast or dynamite fishing is a widespread fishing technique (Souter and Lindén, 2000) mainly applied for subsistence fishing but also for the ornamental aquarium trade (Moore and Best, 2001). This is not only a non-selective fishing method, killing undesirable fish, but especially is destructive for the reef structure itself (Souter and Lindén, 2000). As a result, the coral community and the associated faunal community completely locally changes (Riegl and Luke, 1998) as the explosion not only completely destroys the reef structure at the place of impact but also blasts corals of the rocky substratum in a large halo around it (Riegl and Luke, 1998). What is more, an unstable rubble substratum is created inhibiting the recruitment of young coral colonies for a relatively long time (Riegl and Luke, 1998; Fox *et al.*, 2003). Pet-Soede *et al.* (2000) have calculated the costs of blast fishing to the Indonesian society to be as much as four times higher than the direct

benefit to the fishermen. Net losses after 20 years could amount to more than 300 000 USD per km² in areas with a high potential value for tourism and coastal protection, and around 33,900 USD per km² in less valuable areas. This results in a total estimated foregone benefit of 3.8 billion USD during the last 25 years, solely due to blast fishing (Pet-Soede *et al.*, 2000).

Fishing techniques using poison to stun fish are mainly applied to collect living species for the aquarium trade and the live food market (Bryant *et al.*, 1998; Moore and Best, 2001; Wabnitz *et al.*, 2003). Although legally prohibited, it is widespread, especially in the remote and difficult to control areas of Southeast Asia (Bryant *et al.*, 1998). Most often, cyanide is used (Wabnitz *et al.*, 2003). Although fish are rarely killed, high mortality rates are recorded post-capture (Wabnitz *et al.*, 2003) and the poison used may kill non-target reef organisms, including corals (Jones and Hoegh-Guldberg, 1999; Moore and Best, 2001). Moreover, the coral-reef structure is often physically broken to ease access to fish hiding in the reef, or to harvest pieces of 'live rock' for the aquarium and curiosa trade (Moore and Best, 2001; Wabnitz *et al.*, 2003). This fishing technique is not without risk to the divers themselves either (Wabnitz *et al.*, 2003).

Physical damage to the reef structure is also caused by damaging netting techniques such as *muro-ami*⁶ and kayak-drive netting techniques where either a weighted scare line or a trashing palm frond is used to scare the fish out of the reef structure (Souter and Lindén, 2000). Fine-meshed gill nets and traps are also often used on reefs (Wilkinson, 1998) and, although these do not damage the reefs directly, it is a highly non-selective fishing method catching unwanted fish as well as immature juvenile fish.

1.3.3 Global change

Most current-day scleractinian genera originated in the Middle Triassic (Stanley, 2003) and coral reefs have survived dramatic and sometimes unexpectedly rapid (Broecker, 2000; Folland and Karl, 2001) climate changes in the past. Based on geological evidence, consequently, coral reefs, as an ecosystem, are not expected to become globally extirpated due to the current climate change (Smith and Buddemeier, 1992; Brown, 1997a; Hoegh-Guldberg, 2000). Therefore, until the mid 1990s, scientists did not consider global climate change as a serious threat to coral reefs (e.g. Wilkinson and Buddemeier, 1994; Wilkinson,

⁶ Muro-ami: a fishing technique in which a weighted net is dragged across the reef by a group of swimmers while smashing the reef in order to scare the fish into the net.

1998). Changes in the climate regime were believed to have only local effects, mainly by aggravating the effects of human disturbances (Smith and Buddemeier, 1992; Wilkinson, 1998).

Geological evidence, on the other hand, also indicates that the recovery of the coral-reef ecosystem often had taken thousands or even hundreds-of-thousands of years. After the last Glacial Maximum, 10,000 years ago, the thin veneer of modern corals has taken 6,000 years to grow since the Holocene maximum sea level (Wilkinson, 1998). The effects of global change to coral reefs, therefore, become very severe if they are considered on a temporal and spatial scale relevant for humans depending on these reefs for their livelihood (Smith and Buddemeier, 1992; Hoegh-Guldberg, 2000).

Recent studies, moreover, indicate that the future climate will be completely different from most paleoclimatic conditions. The magnitude and speed at which climate will change in the near future are expected to be substantially larger than most changes in the past (Hughes *et al.*, 2003). CO₂ concentrations and temperature, for example, are anticipated to rapidly exceed conditions which prevailed over the last 500,000, if not millions of years (Watson *et al.*, 2001). Table 1.4 provides an overview of the most important climate and environmental changes, relevant to coral reefs, predicted to occur within the next century.

Table 1.4. Climate and environmental change observations and projections (based on: Watson *et al.*, 2001; ¹Mclean and Tsyban, 2001; ²Schubert *et al.*, 2006)

| Variable | observed | | projected | | |
|------------------------|----------|------------|-------------|------------------------------|--------------------------|
| | 1880 | 2000 | 2050 | 2100 | 2300 |
| CO ₂ (ppmv) | 280 | 368 | 463–623 | 490–1250 | |
| global mean temp. (°C) | | +0.4-0.8 | + 0.8-2.6 | +1.4-5.8 | |
| tropical SST (°C) | | + 0.6 ±0.2 | | ~ + 1.0-2.0 (¹) | |
| sea level (m) | | + 0.1-0.2 | + 0.05-0.32 | + 0.09-0.88* | + 2.5-5.1 ⁽²⁾ |

* considered an underestimation according to new observations (Schubert *et al.*, 2006)

^o under a scenario in which global warming is limited to 3°C

The earlier viewpoint on the effect of future climate change on the prevalence of coral reefs definitively changed after the mass coral bleaching event of 1997-1998 which has been linked to one of the severest El Niño/Southern Oscillation (ENSO) events in history (Reaser *et al.*, 2000; Wellington *et al.*, 2001; Hughes *et al.*, 2003). Worldwide, even the most remote reefs were affected by bleaching and approximately 16% of the corals were killed (Wilkinson,

2000a). From then on, more and more research is done towards the consequences of global change and the mechanisms responsible for coral reef deterioration. A brief summary of the results of these studies is given in following sections.

1.3.3.1 Ocean acidification

The present atmospheric CO₂ concentration is already the highest since the last 400 000, if not millions of years (McClanahan, 2002; SCOR-IOC, 2004) and is expected to increase rapidly in the coming decades (fig. 1.22). By 2065, the atmospheric CO₂-concentration is supposed to double the pre-industrial level of 1880 (table 1.4) (Kleypas *et al.*, 2001; Watson *et al.*, 2001). Through the atmosphere-ocean interaction, the rising level of atmospheric CO₂ causes *ocean acidification*, i.e. a significant drop in the pH of the ocean surface water (SCOR-IOC, 2004; Kleypas *et al.*, 2006; Schubert *et al.*, 2006). When atmospheric CO₂-concentration reaches 650ppm, a decrease in the average pH by 0.30 units compared to pre-industrial values is expected (Caldeira and Wickett, 2005).

Subsequently, oceanic uptake of CO₂ and consequently lowered pH levels drastically decrease the saturation states of the carbonate minerals calcite, aragonite, and high-magnesium calcite (Kleypas *et al.*, 2006; Schubert *et al.*, 2006). Corals use aragonite to build up their exoskeleton, and can only extract it from the seawater when the water is supersaturated with it (Schubert *et al.*, 2006). The aragonite saturation state, unfortunately, is one of the first to be adversely affected by the acidification (Kleypas *et al.*, 2006; Schubert *et al.*, 2006). As a result, reef-building organisms will encounter difficulties precipitating CaCO₃ and their calcification rates will decrease (Wilkinson and Buddemeier, 1994; Kleypas *et al.*, 1999a; Hoegh-Guldberg, 2000; Buddemeier *et al.*, 2004; Langdon, 2004; SCOR-IOC, 2004).

Steffen *et al.* (2004) (in: Schubert *et al.*, 2006) have simulated the changing degree of aragonite saturation⁷ under the predicted global change (fig. 1.23). Locations with an aragonite saturation below 3.5 are considered only marginally suitable for reef-building, while values below 3 are not suitable at all (Schubert *et al.*, 2006). Figure 1.23 clearly shows a shrinkage of the optimal environment for coral-reef growth by 2065 (Guinotte *et al.*, 2003; Schubert *et al.*, 2006). A marginal environment, however, not necessary implies a total extinction of coral reefs (Guinotte *et al.*, 2003). The largest nominal decreases in aragonite saturation are expected to occur in waters currently in high saturation

⁷ The degree of aragonite saturation indicates the relative proportion between the product of concentrations of calcium and carbonate ions and the solubility product of aragonite (Schubert *et al.*, 2006).

conditions, i.e. warm tropical and subtropical waters such as the Red Sea (Kleypas *et al.*, 1999a). It, however, is unlikely that these waters will become undersaturated with respect to calcium carbonates under the predicted climate scenarios (Kleypas *et al.*, 2006). Effects, conversely, will be much worse at high latitudes and in upwelling regions as aragonite undersaturation is expected to arise by the end of 21st century (Orr *et al.*, 2005; Kleypas *et al.*, 2006). Alarming new data also indicate an intensified effect in coastal waters (Andersson *et al.*, 2006), although additional research is required to confirm these preliminary findings (Kleypas *et al.*, 2006).

Several laboratory studies have examined the effect of a doubling of the CO₂ concentrations on the precipitation of carbonate by reef organisms. Decreases in calcification rates compared to pre-industrial rates range from 3 to 37% for individual coral species and from 20 to 54% for entire coral-reef communities⁸ (see for references: Buddemeier *et al.*, 2004; Gleason, 2004; Langdon, 2004). Gleason (2004) has even found that reef organisms stopped excreting CaCO₃ when CO₂ level exceeded 1200ppmv, a value reached in the most extreme scenario predicted for 2100 (table 1.4). Translated to real world conditions, and under a doubled CO₂ scenario, coral calcification rates are estimated to decrease with an average 30% (Kleypas *et al.*, 1999a) by the middle of this century, while rates up to 60% are assumed for the entire reef community (Kleypas *et al.*, 2006). With even more extreme rises in atmospheric CO₂, carbonates may become totally dissolved in some places (Kleypas *et al.*, 1999a; Kleypas *et al.*, 2001, Buddemeier *et al.*, 2004).

When the calcification rate of the corals decreases, the calcifying organisms will grow slower or will form less dense skeletons (Schubert *et al.*, 2006). The reefs, subsequently, become more susceptible to (bio)erosion; they will be more vulnerable to physical damage; and their ability to keep up with rising sea level will be limited (Smith and Buddemeier, 1992; Kleypas *et al.* 1999a; Hoegh-Guldberg, 2000; Kleypas *et al.*, 2001; Hughes *et al.*, 2003; Buddemeier *et al.*, 2004; Kleypas *et al.*, 2006). As can be derived from the wide range of results in the above mentioned studies, the response to decreases in carbonate saturation state is clearly species-specific and some coral species may be more resilient than others (Kleypas *et al.*, 1999a).

Moreover, increasing CO₂ concentrations may also fertilize algae on the reefs, or may give a competitive advantage to non-calcifying reef organisms (Smith and Buddemeier,

⁸ thus including calcifying organisms other than hermatypic corals

1992; Wilkinson and Buddemeier, 1994; Kleypas *et al.* 1999a). Consequently, increases in atmospheric CO₂ become an important environmental stressor, potentially causing an entire phase shift on its own (Langdon, 2004). Evidently, reefs experiencing stress, and therefore already encounter problems in balancing their CaCO₃ budget, will be much more vulnerable (Kleypas *et al.*, 1999a).

1.3.3.2 Sea surface temperature rise

Global sea surface temperature (SST) has increased by $0.6 \pm 0.2^{\circ}\text{C}$ over the last 100 years, and by the year 2100, tropical SST is predicted to have increased by an additional 1 to 2°C (table 1.4) (Watson *et al.*, 2001).

Rises in sea temperature are often thought to be the primary cause of coral bleaching (Brown, 1997a). Not an average increase in sea temperature is devastating for the coral reefs, but rather an increase in the magnitude and duration of periods with higher than normal temperatures (Wilkinson and Buddemeier, 1994; Hoegh-Guldberg, 2000; Souter and Lindén, 2000; Wilkinson, 2000b; Kleypas *et al.*, 2001; Lesser, 2004a; b). On average, corals bleach when temperatures are 2 to 3°C above long-term summer maximum for several weeks (Lesser, 2004a) though corals may already bleach when a temperature rise of 3 to 4°C occurs for only 1 or 2 days, or, conversely, when a temperature rise by only 1 to 2°C persists for several months (Smith and Buddemeier, 1992). Under the predicted SST rise, bleaching will very likely take place more frequently in this century (Hoegh-Guldberg, 2000). This topic is discussed in more detail in section 1.3.3.8.

Thermal-induced bleaching is mainly regarded as the result of photo-inhibition of the photosynthetic production by the zooxanthellae (Jones *et al.*, 1998; Souter and Lindén, 2000; Lesser, 2004b). Under normal conditions, the rate of photosynthesis by the zooxanthellae increases with the amount of available light until a threshold, or *saturation point*, is reached at which the extra light energy can no longer be used (Falkowski *et al.*, 1990; Hoegh-Guldberg, 2000; Yentsch *et al.*, 2002). This excess energy is then surpassed through non-photochemical pathways (Souter and Lindén, 2000). However, when corals and their zooxanthellae are under a thermal stress, this dissipating mechanism is interrupted and the zooxanthellae can no longer lose the excess photosynthetic energy. As a consequence, reactive oxygen groups are produced which have lethal effects on the zooxanthellae and their hosts (Jones *et al.*, 1998; Souter and Lindén, 2000). To prevent intoxication, the coral expels its zooxanthellae and bleaching takes place (Souter and Lindén, 2000).

Importantly, thermal-induced coral bleaching should also be placed in the context of the seasonal variation in density and pigment content of the endosymbiotic algal cells (Douglas, 2003; Lesser, 2004a; Skirving, 2004). As zooxanthellae densities are shown to be lowest after the annual SST high (Stimson, 1997; Fitt *et al.*, 2000), the longer the season of high seawater temperature lasts, the more bleaching could occur (Douglas, 2003).

Rises in global SST, conversely, may increase the coral-reef distribution as in some mid-latitude areas, minimal temperatures will become higher than 18°C in winter (Kleypas *et al.*, 2001; Precht and Aronson, 2003). If the maximal temperature rise of 2°C by 2100 (table 1.4) is taken as a base, an approximate 2.5 to 3.5% increase in potential coral-reef habitat area is assumed (Kleypas *et al.*, 2001). This effect, however, is expected to be counteracted by the equatorward migration of the boundary between reefbuilding and non-reefbuilding corals due to the lowered carbonate saturation states in the oceans (Kleypas *et al.*, 2001) (fig. 1.23). A significant expansion of potential reef habitat by global warming, therefore, will presumably not take place (Kleypas *et al.*, 2001; Buddemeier *et al.*, 2004).

A rise in SST will also affect other global phenomena such as sea level, tropical cyclones, ocean currents, and precipitation patterns (Harley *et al.*, 2006; Schubert *et al.*, 2006). These global changes are further discussed in their corresponding sections.

1.3.3.3 UV-B radiation

Stratospheric ozone concentration has significantly decreased, mainly resulting from the anthropogenic emissions of chlorinated fluoro-carbons (CFCs) (Watson *et al.*, 2001). This led to an increase in the amount of harmful UV-B radiation reaching the sea surface (Madronich *et al.*, 1998; McClanahan, 2002; McKenzie *et al.*, 2002).

This is especially worrisome as UV-B irradiance in the tropics is already high due to the naturally thinner ozone layer and the smaller solar zenith angles all year through (McKenzie *et al.*, 2002). Besides, the optical properties of tropical waters allow UV radiation to reach depths of 15m and more (Gleason and Wellington, 1993; Lesser, 2004b). The penetration of UV-B radiation is also favoured by the low phytoplankton concentrations in most coral-reef waters and may be enhanced by reduced mixing of the water column under El Niño conditions (Anderson *et al.*, 2001; Yentsch *et al.*, 2002; Lesser, 2004b). Therefore, while nominal changes in ozone concentration in the tropics

are insignificant compared to higher latitudes (McKenzie *et al.*, 2002), even these small decreases will have important consequences (Lesser, 2004a).

The effects of increasing UV-B radiation may be similar to photo-inhibition by thermal stress (Gleason and Wellington, 1993), but may also result in DNA damage of the host tissue (Anderson *et al.*, 2001; Lesser, 2004a). Under normal conditions, zooxanthellae, as well as their symbiotic hosts, produce UV-absorbing compounds and enzymes to protect themselves from these lethal effects (Jokiel, 1980; Falkowski *et al.*, 1990; Häder *et al.*, 1994; Muller-Parker and D'Elia, 1997; Salih *et al.*, 2000). However, the concentration of these compounds has been shown to decrease upon exposure to elevated temperatures (Lesser *et al.*, 1990; Lesser, 1996; Lesser, 2004b). Sea temperature rises may thus induce both thermal and UV-B-related coral bleaching.

1.3.3.4 Sea-level rise

A sea-level rise due to the combined effects of thermal expansion of the ocean water and addition of water from melting icecaps and glaciers is predicted between 0.09 and 0.88m by the year 2100 (table 1.4; fig. 1.24), though Schubert *et al.* (2006) assume this to be an underestimation. They predict a sea-level rise by 2.5 to 5.1m by the year 2300 under a scenario in which SST will not have risen more than 3°C by that time.

Sea level, on the one hand, will thus rise on average by 0.9 to 8.8mm per year, while, on the other hand, individual corals growth by 2 to 200mm per year (Done, 1999; Harriott, 1999) and the entire coral-reef system vertically accumulates⁹ between 1 and 10mm per year (Smith and Buddemeier, 1992). The fastest growing species will have no problem to keep up with the predicted sea-level rise and they will probably take advantage of the additional growth space (Wilkinson and Buddemeier, 1994; Buddemeier *et al.*, 2004). If slow-growing corals, in contrast, are forced to grow at higher rates in order to keep up with the sea-level rise, they may produce less dense carbonate structures and become more vulnerable to erosion (Hoegh-Guldberg, 2000).

Whether or not coral-reef systems will drown under these conditions is equivocal as, to start with, the above rates are believed to be an underestimation. The entire reef system, consequently, will only be able to keep up with the slowest predicted sea-level rises. With greater sea-level rises, most reefs will probably become situated slightly deeper than is currently the case (Buddemeier *et al.*, 2004) and will only be able to catch up over time

⁹ i.e. net gain: taking effects of (bio-)erosion into account

when sea-level rises do not accelerate in future. As the reef structures will be situated deeper in the water and become more vulnerable to erosion, they will no longer be able to protect the coastline from erosion and storms (Wilkinson and Buddemeier, 1994). The consequent increase in suspended sediments will pose extra stress on the reefs (Buddemeier *et al.*, 2004). Although coral reefs are thus assumed to survive sea-level rises *sensu strictu*, some reefs, eventually, may become weakened by additional stresses, and drown (Knowlton, 2001). Some new areas, conversely, may become available for coral colonisation (Knowlton, 2001) provided a suitable, stable, substrate is present (Done, 1999).

1.3.3.5 Oceanic water circulation

Oceanic water circulation exerts an important control on the marine erosion and sedimentation patterns, as well as on primary physical and ecological variables such as temperature, salinity or nutrient levels, which are important for the global distribution of corals (Smith and Buddemeier, 1992). Besides, the circulation patterns also influence the dispersal of coral larvae and, in this way, the connectivity between the individual coral-reef ecosystems (Veron, 2000). Any change in the oceanic water circulation patterns may thus have serious effects on the local, regional, and global distribution of coral reefs, especially as the water movement also affects the interaction between human disturbances and coral reefs (Smith and Buddemeier, 1992).

One global phenomenon, namely the occurrence of warm ENSO phases (which have been proven to intensify under the predicted global change), has already shown to cause changes in the oceanic water circulation. During an El Niño, the NE monsoon over the Indian Ocean weakens, causing wind still conditions, reduced surface currents and a resultant stratification of the water column (Wilkinson, 2000b). The clear skies and the stability of the vertical water circulation may lead to lower phytoplankton concentrations and allow the seawater to heat up to depths of 30m and more. These effects, on their turn, enable UV-B radiation to penetrate deeper than usual (Reaser *et al.*, 2000; Wilkinson, 2000b; Hendee, 2004; Skirving, 2004). A reduced oceanic water flow, under the influence of a weakened monsoon system, thus creates coral bleaching conditions (McClanahan, 2002; Skirving, 2004).

On an even larger scale, the *global ocean thermohaline circulation* is assumed to become suppressed due to a decreasing seawater density caused by increasing temperature and freshwater input (Manabe and Stouffer, 1993; Cubash and Meehl, 2001; Broecker,

2003; Buddemeier *et al.*, 2004; Schubert *et al.*, 2006). This would, consequently, affect the global atmospheric circulation pattern, the global oceanic circulation, and different upwelling patterns (Broecker, 2000; Vellinga and Wood, 2002; Buddemeier *et al.*, 2004). These effects and the time frame in which they would take place, however, are still debated (Schubert *et al.*, 2006).

1.3.3.6 Atmospheric circulation, precipitation, and tropical storms

Global change, naturally, also causes changes in the atmospheric circulation and the associated weather patterns. Uncertainty, however, remains about what the precise effects will be and where these will be most pronounced (Huntington, 2006). More and more evidence, nonetheless, is put forward of an intensification of the water cycle, resulting in increased precipitation and consequent runoff (Huntington, 2006). Many regional differences, however, are observed (Huntington, 2006), such that, generally stated, dry areas are assumed to become drier and wet areas wetter (Watson *et al.*, 2001; Buddemeier *et al.*, 2004).

Tropical precipitation, in the region between 10°S and 10°N, has already increased by 0.2-0.3% per decade over the past century and the frequency of intense rainfall is very likely (90 to 99% chance) to increase over most areas (Watson *et al.*, 2001). Coastal coral reefs, therefore, will become subject to more discharge of nutrients, sediments and contaminants (Wilkinson and Buddemeier, 1994; Watson *et al.*, 2001; Buddemeier *et al.*, 2004). Locally, increases in precipitation, and especially the intensity of rainfall associated with tropical storms, may also lower the salinity, even on the most remote reefs, causing physiological stress to the coral polyps (Wilkinson and Buddemeier, 1994; Watson *et al.*, 2001; Buddemeier *et al.*, 2004).

Secondly, higher air and sea surface temperatures are projected to increase the intensity of annual monsoons and ENSO events (Watson *et al.*, 2001; Huntington, 2006). Consensus is rising that this will also increase the duration and intensity of tropical storms, i.e. hurricanes and typhoons, (Cubash and Meehl, 2001; Buddemeier *et al.*, 2004; Emanuel, 2005; Schubert *et al.*, 2006) while a predicted increase of their frequency (Hughes *et al.*, 2003) remains more controversial (Emanuel, 2005; Huntington, 2006; Schubert *et al.*, 2006). The effects tropical storms may have on coral reefs have been discussed in section 1.3.1.2.

1.3.3.7 Increased incidence of coral diseases

An important indirect effect of global change appears to be the worldwide increasing incidence of coral diseases (Richardson, 1998; Harvell *et al.*, 1999; Hoegh-Guldberg, 2000; Knowlton, 2001; McClanahan, 2002; Hughes *et al.*, 2003). This phenomenon has been attributed to a variety of human induced changes like higher nutrient concentrations, increased dust transport and sedimentation, toxic chemical pollution, reduced water circulation, and international traffic which functions as a vector for global pathogen dispersal (Harvell *et al.*, 1999; Barber *et al.*, 2001; Lipp *et al.*, 2002; McClanahan, 2002; Buddemeier *et al.*, 2004; Fabricius, 2005).

However, as most outbreaks of coral diseases are highly correlated with increased sea surface temperatures (Kushmaro *et al.*, 1998; Thompson *et al.*, 2001; Rosenberg and Ben-Haim, 2002), SST is believed to be the most dominant factor (Harvell *et al.*, 2002; Rosenberg and Ben-Haim, 2002). Reasons for this could be that higher SST increases the sensitivity of the host to the pathogen; the virulence of the pathogen; the frequency of transmission via a vector; or a combination of these elements (Rosenberg and Ben-Haim, 2002). In any case, as seawater temperature is expected to rise in the next decades, coral diseases are likely to become more prevalent.

Rosenberg and Ben-Haim (2002) even suggest that bacterial diseases are the main causes of mass coral bleaching in the last decade. They argue that the bleaching response of the corals is not directly the result of thermal-induced photo-inhibition rather it results from an outbreak of coral diseases due to the creation of an ideal thermal-determined environment for the pathogens. This could explain the patchy bleaching patterns observed which can not be easily explained by the conventional temperature/UV radiation theories (Rosenberg and Ben-Haim, 2002).

1.3.3.8 Mass coral bleaching

Since the 1980s, bleaching has occurred more frequently and over much larger geographical areas -involving entire reef systems and biogeographic provinces- than ever before (Glynn, 1991; Buddemeier and Fautin, 1993; Stone *et al.*, 1999; Hoegh-Guldberg, 2000; Wellington *et al.*, 2001). While only three records of bleaching events are known for the period 1976-1979, Williams and Bunkley-Williams (1990) (in: Wellington *et al.*, 2001) have documented 60 bleaching events in the period 1979-1990, and this trend continues in the recent decade (Hoegh-Guldberg, 2000). Since 1979, 6 bleaching events

were associated with massive coral mortalities all over the world (Hoegh-Guldberg, 2000). These major events are referred to as *mass coral-bleaching events*.

As already mentioned in section 1.3.3.2, the severity of a bleaching event and the consequent mortality, is primarily linked to the duration and extremity of temperature extremities surpassing the long-term summer maximum for several days or weeks. This explains why corals may also bleach in areas like the Persian Gulf where corals have adapted to high average temperatures (Buddemeier *et al.*, 2004). The increase in frequency and severity of mass coral-bleaching events, therefore, is strongly related to intensified El Niño phases (e.g. Goreau *et al.*, 2000; Hoegh-Guldberg, 2000; Reaser *et al.*, 2000). Before SST increased during the last century, corals and their zooxanthellae are believed to have lived well within their thermal limits and they, therefore, could easily cope with relative large SST fluctuations. With a SST increase of $0.6\pm 0.2^{\circ}\text{C}$ (table 1.4) over the last 100 years, corals are now living almost near their upper thermal limits. As a result, from the 1980s onwards, El Niño disturbances have become capable of pushing SST over the thermal limits of most coral species, resulting in mass coral bleaching (fig. 1.25) (Hoegh-Guldberg, 2000; Souter and Lindén, 2000).

While increased SST, generally, is considered as the main cause for coral bleaching (Goreau *et al.*, 2000; Hoegh-Guldberg, 2000; Souter and Lindén, 2000), other factors play an important role as well. Solar radiation, PAR as well as UV-B radiation, is believed to be a second, dominant factor (Jones *et al.*, 1998). In the case of mass bleaching events, the two are often considered to act synergetic, exacerbating the bleaching response of the coral polyps (Fitt *et al.* 2001; Wellington *et al.* 2001; Douglas, 2003; West and Salm, 2003; Fitt, 2004; Hendee, 2004). An important modulating role is given to calm weather which is usually associated with El Niño conditions (Stone *et al.*, 1999), as already shown in section 1.3.3.5.

The severest and most widespread mass bleaching event on record took place in 1997/1998 (Wilkinson, 2002b) and was linked to one of the most extreme ENSO cycles ever documented. Bleaching was coincident with the El Niño phase in the southern hemisphere, while most bleaching in the northern hemisphere developed during the following La Niña in the summer of 1998 (Wilkinson, 2000a). Coral bleaching, nevertheless, did also occur in the southern hemisphere under La Niña conditions (Wellington *et al.*, 2001). Approximately 16% of the world's coral reefs were effectively killed (Wilkinson, 2000a); the central and northern Indian Ocean, South-East and East Asia, and the western Pacific being the most affected (Goreau *et al.*, 2000; Wilkinson,

2000a). Coral mortality was relatively less severe in the Caribbean and Central Pacific regions (Wilkinson, 2000a) where the 1998 bleaching event was comparable to the previous one in 1995 (Goreau *et al.*, 2000).

Following, an example is given of how a mass coral bleaching event migrates through the oceans and is related to global atmospheric and oceanographic circulation patterns. Bleaching was first reported in the southernmost part of the Indian Ocean in late 1997 and it reached its peak in the southern Indian Ocean between February and April 1998 (Wilkinson, 2002a). Bleaching then followed the calm *Intertropical Convergence Zone* (ITCZ) northward until it reached the northern Indian Ocean between May and June 1998, and the Persian Gulf and southern Red Sea between July and September 1998. The corals suffered most during the summer period when SST extremes exceeded the long-term maximum with 1 to 2°C; a situation which lasted for weeks or, in some regions, even months. Bleaching usually started only 4 to 6 weeks after the passing of the solar zenith, thus indicating the importance of the heat persistence (Goreau *et al.*, 2000; Wilkinson, 2000b). 4 years after the event, coral recovery is slow to moderate in most places and full convalescence is expected to take several decades (Wilkinson, 2002b). The total socio-economic costs, over a 20-year period, of the 1998 bleaching event in the Indian Ocean, are estimated at more than 8 billion USD, assuming that most reefs will not recover during this period. These costs, primarily, result from damage due to coastal erosion (2.2 billion USD), tourism losses (3.3 billion USD), and fishery losses (1.4 billion USD) (Westmacott *et al.*, 2001).

As a result of predicted SST rises and increased ENSO intensities, coral bleaching events are assumed to occur more often and be more lethal in the next century (Hoegh-Guldberg, 2000). If SST rises as predicted (table 1.4), mass coral bleaching will even result from normal seasonal temperature changes, without the need of a major trigger like an El Niño phase (Hoegh-Guldberg, 2000). Donner *et al.* (2005) project that, within the next 30 to 50 years, coral bleaching with the severity of the 1997-1998 event will become an annual or biannual event for the vast majority of the world's coral reefs. South-East Asia, the Caribbean, and the Great Barrier Reef are assumed to be the first regions affected (Hoegh-Guldberg, 2000).

When bleaching events become more frequent and severe, the damage to coral reefs worldwide will become critical to the survival of the ecosystem (Hoegh-Guldberg, 2000). Not only will the chances of coral mortality increase, sublethal impacts of coral bleaching such as a reduced reproductive and recruitment capacity and a reduced calcification rate

and consequent coral growth will threaten the ecological functioning of the coral reefs as well (Hoegh-Guldberg, 2000; Souter and Lindén, 2000; Douglas, 2003). The reaction of the coral species on these changing environmental conditions, however, may differ according to their physiology and their location on the reef. Corals with branching growth forms, rapid growth rates, and thin tissue layers are more sensitive to bleaching and are often the first to die, usually within a month after the peak temperatures occurred (Goreau *et al.*, 2000; Loya *et al.*, 2001; Buddemeier *et al.*, 2004). Encrusting and massive, slow-growing, and often thick-tissued species, conversely, are less sensitive and usually bleach only when the extreme temperature period lasts for months (Goreau *et al.*, 2000). They, commonly, also have a higher recovery capacity (Loya *et al.*, 2001; Buddemeier *et al.*, 2004). Geographically, the position on the reef is of importance, as sheltered corals and corals lower on the reef front have been observed to be less bleached compared to fully exposed species (Hoegh-Guldberg, 2000).

1.4 THE FUTURE OF CORAL REEFS: TOLERANCE, STRATEGY SHIFT, OR PHASE SHIFT?

Whether or not coral reefs will survive as we know them today depends on the nature and the intensity of the stress and on the frequency of its occurrence or, in other words, the time the coral is given to recover. Done (1999) identifies 4 different ways in which corals might respond to increasingly stressful and/or more frequently disturbed environments: corals may tolerate the changed environment; they may respond via a faster turnover rate; a strategy shift may take place towards more resilient species; or a total phase shift towards non-coral organisms may arise.

1.4.1 Physiological tolerance by current coral species

When the stress factor is relatively benign, the coral species may be able to tolerate it. This *physiological tolerance* is often species and location dependent, though the reasons for these species-specific responses are still poorly understood (Berkelmans and Willis, 1999; Goreau *et al.*, 2000; Loya *et al.*, 2001; Hughes *et al.*, 2003). Secondly, the ability of the coral species to *acclimate* or *adapt* to the changing environmental conditions should not be disregarded (Goreau *et al.*, 2000; Wellington *et al.*, 2001), although this ability is still debated (Hughes *et al.*, 2003; Donner *et al.*, 2005).

In the case of *acclimation*, corals surviving a stressful event are assumed to have acquired a certain tolerance to the conditions promoting this stress (Douglas, 2003). Acclimation then involves the active modification of the intrinsic metabolic processes in order to better perform in the new environmental, e.g. temperature, conditions (Hoegh-Guldberg, 2000). The fact that corals appear to be as close to their thermal limits as 20 years ago when the first mass coral bleaching events took place could indicate that corals are not able to acclimate. This is attributed to two elements. First, extreme temperatures only occur during part of the year, often with a lag of different years in between, so that the thermal acclimation by the coral during one bleaching year would be lost by the time thermal maxima were exceeded again. Secondly, as temperature is predicted to rise steadily in coming years, the acclimation to the new conditions during one year, would not be sufficient to cope with the thermal conditions the years to come (Hoegh-Guldberg, 2000; Douglas, 2003).

Adaptation involves the natural selection of stress tolerant individuals in the population which are able to survive and breed under the changing conditions (Hoegh-Guldberg, 2000). The geographical and species variation in bleaching sensitivity, for instance, is empirical evidence that corals have adapted to different temperature stresses in the past (Hoegh-Guldberg, 2000; Hughes et al, 2003). Corals in the Arabian Gulf, for example, do not bleach at temperatures where corals from outer regions would. This gives at least circumstantial evidence of *local adaptation* (Hughes *et al.*, 2003). However, adaptation, or genetic change in general, normally takes several hundreds to thousands of years to evolve. The observation that most corals seem to be near their upper thermal limits since the temperature rise of the last century could prove that they have not been able to adapt, at least not in such a short time period. They, probably, will not be able to adapt or acclimate over the next 100 years either, as climate is expected to change more dramatically and rapidly than ever before (Goreau *et al.*, 2000; Hoegh-Guldberg, 2000; Hughes *et al.*, 2003; Buddemeier *et al.*, 2004).

A special place in the discussion about adaptation by corals is taken by the *Adaptive Bleaching Hypothesis* of Buddemeier and Fautin (1993). They have stated that coral species respond to a stressful condition by expelling their original endosymbiotic zooxanthellae -they bleach- in order to replace them by a new mix of symbionts better suited to the changed conditions. This controversial theory is still heavily debated and, while some observations seem to prove this hypothesis (e.g. Baker, 2001; Kinzie *et al.*, 2001), most scientists remain sceptic about its validity especially when they take the vast coral mortality after the recent mass coral bleaching events into account (e.g. Hoegh-Guldberg, 2000; Hoegh-Guldberg *et al.*, 2002; Douglas, 2003; Hughes *et al.*, 2003).

1.4.2 Faster turnover

If the frequency and/or the intensity of the disturbances increases, the corals will no longer be able to fully recover and the population composition will become skewed towards younger, smaller specimen. This will not necessary cause a deterioration of the coral-reef system, although it will affect the 3-D architecture of the reef and, most likely, also the mode and rate of reef accretion and erosion (Done, 1999).

1.4.3 Strategy shifts

With an even more disturbed environment, many coral species will no longer be able to survive and more resilient species will replace the most vulnerable species. This change in species composition may also result from the different ability of corals to migrate to more benign locations or to adapt to future changes (Wilkinson, 2000b; Hughes *et al.*, 2003). The dominant direction of such a *strategy shift*, however, is ambivalent: while coral bleaching could favour the survival of slow-growing, massive coral species (Goreau *et al.*, 2000); increasing storm intensity or predator outbreaks could stimulate the occurrence of fast-growing species (Done, 1999). As with the faster turnover of species, a strategy shift may have its effects on the structural complexity of the reef and, subsequently, on the entire reef fauna and flora (Done, 1999; Souter and Lindén, 2000; Hughes *et al.*, 2003).

1.4.4 Phase shifts

Ultimately, if most corals die or are not capable to reproduce, a *phase shift* may occur, replacing them by other non-coral organisms, most probably macro-algae (Done, 1999; Goreau *et al.*, 2000; Hoegh-Guldberg, 2000; Westmacott *et al.*, 2001). The example of coral-algal phase shifts under increased nutrification and fishing pressure has profoundly been described in section 1.3.2.2.2.

A satellite-style map of the Red Sea region, showing the sea in dark blue, the Nile river delta in the north, and the surrounding landmasses of Africa and the Arabian Peninsula in shades of tan and brown. The text is overlaid in the center.

PART II
REGIONAL SETTING
OF THE RED SEA

2.1 GEOGRAPHY

The Red Sea basin is over 2250km long and 450km wide measured along a line passing through Dahlak Ghebir and Farasan, narrowing to 240km at Ras Muhammad in Sinai (Braithwaite, 1987) (fig. 2.1). It is bounded by the uplifted shoulders of the African and Arabian shields. These fringing mountains, mainly consisting of Precambrian rocks, rise highest on its western shores in Eritrea where the coastal escarpment exceeds 2700m and in the east, in Yemen, where the escarpment reaches up to 3760m. In front of the marginal escarpments, gently sloping rocky platforms with sand and gravel outwash plains have been formed, ranging in width from 5 to 30km (Braithwaite, 1987).

Within this basin, the Red Sea proper is 1932km long (Braithwaite, 1987) extending in a SSE direction from Suez in the north to the Bab el Mandab in the south. With approximately 354km, it is at its widest near Massawa, quickly narrowing southwards to 29km at Bab el Mandab, and more gradually northwards to about 180km before it branches into the narrow Gulf of Aqaba and Gulf of Suez (Braithwaite, 1987). Through the narrow Bab el Mandab in the south, the Red Sea is connected to the Gulf of Aden and the Indian Ocean. North of the entrance to Bab el Mandab, the Hanish Sill¹⁰, with a maximum depth of 137m (Siddall *et al.*, 2002), restricts the deep water circulation and enhances the isolated position of the Red Sea.

Morphologically, the Red Sea consists of two shallow continental shelves on either side of a *main trough* (fig. 2.2). These shelf zones are very narrow in the northern parts of the Red Sea, only extending over several tens of metres or less. In the southern part of the Red Sea, these continental shelves are much larger and extend over several tens of kilometres offshore. The main trough stretches from about 15°N to 24°N at depths of 600 to 1000m (Ghebreab, 1998). Within the main trough, a narrow central *axial trough* is distinguished, only 5 to 30km wide and characterized by steep walls and an irregular bottom topography (Cochran, 1983). The greatest depths, locally over 2000m (Braithwaite, 1987), can be found in hot-brine pools situated within this axial trough.

The Gulf of Aqaba is a deep trough consisting of three separate pull-apart basins (Friedman, 1985). It has an irregular bottom topography with an average depth of 1250m (Said, 1990a), although depths up to 1850m occur near its eastern side (Said, 1990a). It is separated from the Red Sea by the Sill of Tiran, 250-260m deep (Said, 1990a; Sheppard *et al.*,

¹⁰ Sill: a submerged ridge at relatively shallow depth separating the basins of two bodies of water (Merriam-Webster Online Dictionary)

1992). The continental shelf which characterizes the Red Sea does not occur in the Gulf of Aqaba, except in the south (Said, 1990a). The Gulf of Suez is much shallower and flat-bottomed with maximum depths of 50 to 75m (Said, 1990a). It has no sill at its connection with the Red Sea (Sheppard *et al.*, 1992).

2.2 GEOLOGY

2.2.1 Precambrian basement complex

The construction of the *Arabian-Nubian Shield*, the basement complex for the entire Red Sea region, has been ascribed by Ghebreab (1998) to the accretion of a series of interoceanic island arcs resulting from the collision between the East and West Gondwanas during late Precambrian (1100-542 Ma¹¹) times (Hassan and Hashad, 1990). The Arabian-Nubian Shield is a metamorphic complex which mainly includes schists, metaquartzites, and gneisses (Braithwaite, 1987) and is characterised by igneous intrusions, mainly granites, emplaced in Phanerozoic times (Hassan and Hashad, 1990). This basement complex is currently exposed in the uplifted shoulder escarpments bordering the Red Sea basin (Braithwaite, 1987).

Another characteristic feature of the Precambrian Red Sea fold belt is the development of northwesterly strike-slip fracture zones (Kazmin *et al.*, 1978; Ghebreab, 1998). These structural features determined the evolution of the Red Sea rifting which started in the late Paleogene (Ghebreab, 1998; Montenat *et al.*, 1998b). In the northern Red Sea, these structural features can be divided in four main fault groups (Jarrige *et al.*, 1986a; Montenat *et al.*, 1998b):

- N140-N160 (*Clysmic*) faults (Hume, 1921) which are parallel to the axis of the basin and commonly occur on the margins where they often border large fault blocks;
- N00-N20 (*Aqaba*) faults which are parallel to the Aqaba-Dead Sea fault and are well developed in the Gulf of Suez and southern extension of the Gulf of Aqaba;
- N100-N120 (*Duwi*) faults which comprise large corridors of faults occurring locally along the rift margins;
- N40-N60 (*cross-faults*) faults which are perpendicular to the rift axis and only occur in the Gulf of Suez.

2.2.2 Paleozoic: continental conditions

The general absence of Paleozoic (542-251 Ma) marine sediments indicates that throughout this era, most of the Arabian-Nubian Shield was emerged and subject to erosion and continental sedimentation (Braithwaite, 1987). Marine incursions did occur, but these,

¹¹ Date derived from the International Stratigraphic Chart 2004 (see annex I)

commonly, were short-lived and restricted to the margins of the Arabian-Nubian Shield (Braithwaite, 1987; Behairy *et al.*, 1992). In the northern Red Sea region, Paleozoic strata are largely limited to the northwest of Egypt (Klitzsch, 1990), although some thinner Silurian (444-416 Ma) sequences occur in the southwest of Egypt (Klitzsch, 1990) and a subsidence zone started to develop in the Gulf of Suez region during the Carboniferous (356-299 Ma) (Braithwaite, 1987).

Since the Upper Devonian, Laurasia and Gondwana converged and in the early Carboniferous, this intraplate compression started to result in the regional uplift of the Arabian platform and, to a more limited extent, of northeast Africa (Klitzsch, 1990; Schandelmeier and Reynolds, 1997). This uplift was related to the *Hercynian orogenic phase* recognised in many parts of the world. The uplift continued in the late Carboniferous and due to the significant fall in sea level, the raised areas were eroded (Klitzsch, 1990; Schandelmeier and Reynolds, 1997). Until the late Permian, regional uplift in southern Egypt, Sudan and the Horn of Africa continued, leading to an increased exhumation of the basement rocks over large areas (Schandelmeier and Reynolds, 1997). The Arabian platform, in contrast, became relatively stable and witnessed extensive deposition of carbonates (Braithwaite, 1987; Schandelmeier and Reynolds, 1997).

2.2.3 Mesozoic: marine conditions in the northern Red Sea

During the Mesozoic (251-65.5 Ma), the northern Red Sea region witnessed an important marine transgression from the northeast, which was associated with the formation of the *Neothetys* (Sengor, 1979; Schandelmeier and Reynolds, 1997).

2.2.3.1 Triassic (251-200 Ma)

The Triassic seas only reached the northeasternmost part of Egypt and the Sinai and Gulf of Suez region was under the influence of tidal flat and deltaic sedimentation (Kerdany and Cherif, 1990). Most of the Arabian-Nubian Shield remained emerged (Schandelmeier and Reynolds, 1997).

2.2.3.2 Jurassic (200-146 Ma)

The start of the Jurassic period was marked by a new transgressive phase and the Arabian-Nubian Shield became largely submerged in the south and southeast; creating a southern shoreline across the Red Sea region from Massawa to Jizan (Behairy *et al.*, 1992;

Schandelmeier and Reynolds, 1997). During this period, the forming of the Indian Ocean was initiated (Schandelmeier and Reynolds, 1997). Many sequences of this period include red or brown sandstones commonly referred to as *Nubian Sandstone*, although this name has no precise age connotation and includes deposits ranging in age from Carboniferous to Upper Cretaceous, and possibly even Eocene (Furon, 1963). Facies distribution suggests that the central area between the southern and the Sinai shorelines remained emerged (Braithwaite, 1987).

2.2.3.3 Cretaceous (146-65.5 Ma)

The transition between Upper Jurassic and Lower Cretaceous was characterised by a strong drop in sea level (Kerdany and Cherif, 1990; Schandelmeier and Reynolds, 1997) and an uplifting of the Arabian-Nubian Shield (Said, 1990a), which resulted in severe erosion. Following, the northern Red Sea region underwent four transgressive cycles in the Cretaceous period (fig. 2.3). The Aptian, Cenomanian, and Coniacian transgressions gradually extended further across northern Sinai with an increasingly distinct trough over the Gulf of Suez region where marine or semi-continental sandstones accumulated (Said, 1990b). During the Campanian-Maastrichtian transgression, corresponding to a worldwide sea-level rise (Kerdany and Cherif, 1990), the embayment along the Gulf of Suez significantly enlarged southwards, at least as far as the Sudanese border (Said, 1990b; Behairy *et al.*, 1992; Braithwaite, 1992; Schandelmeier and Reynolds, 1997). Towards the end of the Cretaceous, waters shallowed again due to the uplift of northern Sinai and northeastern Egypt which was related to the generation of the Syrian Arc folds (Braithwaite, 1987; Kerdany and Cherif, 1990).

2.2.4 Paleogene-early Neogene: northern Red Sea Rift initiation

The Cenozoic era is markedly different from the previous as the Red Sea Rift started to form. Although the exact timing is still debated, most authors now situate the onset of the actual rifting in the northern Red Sea in the late Oligocene, between 25 and 30 Ma ago (Morgan, 1990; Bosworth *et al.*, 1998; Ghebreab, 1998; Purser and Bosence, 1998). Rifting is believed to have started somewhat earlier in the southern Red Sea region (Ghebreab, 1998; Montenat *et al.*, 1998a) when a crack propagated westward from the early Indian Ocean (Carlsberg) Ridge spreading centre (Girdler, 1991).

2.2.4.1 Paleogene pre-rift sedimentation

The Paleocene was ushered in by a transgression which pushed its way along the northwestern shores of the current Red Sea basin, across the southern borders of Egypt into north Sudan (Said, 1990a). The maximum transgression occurred during the late Paleocene (Said, 1990a) and lasted well into the early Eocene. Nowadays, Eocene outcrops, several thousand metres in thickness, cover about 21% of the surface area of Egypt (Said, 1990a) forming carbonate mountain scarps along both shores of the Gulf of Suez and central and north Sinai (Braithwaite, 1987; Said, 1990a). South of the Gulf of Suez, not much Eocene rocks, however, have been found (Braithwaite, 1987). From the late Eocene onwards, the sea almost completely retreated from the northern Red Sea region and a new phase of erosion started (Said, 1990a; Behairy *et al.*, 1992), removing the Mesozoic sedimentary cover from the Red Sea mountain range (Kerdany and Cherif, 1990).

2.2.4.2 Initiation of the northern Red Sea rift tectonics

Most evidence of pre-rift sediments indicates that rift development was not preceded by an initial stage of *thermal doming* (Morgan, 1990; Patton *et al.*, 1994; Montenat *et al.*, 1998a;b). On the contrary, it was preceded by a stage of planation and weathering (Montenat *et al.*, 1998a) so that the rift started in a relatively low-lying continental plate interior lacking notable relief situated at, or near, sea level (Garfunkel and Bartov, 1977; Sellwood and Netherwood, 1984; Steckler, 1985; Coleman and McGuire, 1988; Montenat *et al.*, 1998b). Marine waters, as a result, would reach most of the sub-basins within the rift very early in their development (Bosworth *et al.*, 1998).

When rifting started in the late Oligocene, the margins totally emerged and became eroded, whereas the Red Sea trough, which now underlays the coastal plains, began to receive considerable marine deposits (Behairy *et al.*, 1992). The onset of the syn-rift sedimentation was earlier on the eastern margin of the rift (Chattian) than on the western margin (Aquitania), indicating an important asymmetry of the rifting (Dullo *et al.*, 1983; Purser and Hötzl, 1988; Montenat *et al.*, 1998a).

Plate tectonics were the main driving force behind the opening of the Red Sea Rift. Several authors (Morgan, 1990; Behairy *et al.*, 1992; Sheppard *et al.*, 1992) have determined an overall anticlockwise rotation of the Arabian shield by approximate 7° relative to the African continent, about a pole of rotation in the central or south-central

Mediterranean Sea. The associated spreading and rifting resulted in the widening of the Red Sea at a net rate of about 0.02m per year (Behairy *et al.*, 1992). The rift, however, did not progress far enough to completely separate Sinai from Africa (Morgan, 1990).

Different models have been proposed to explain the rifting evolution of the Red Sea, varying between the two extremes of passive versus active rifting (Morgan, 1990; Bosence, 1998; Ghebreab, 1998). Each theory, however, failed to explain the evolution for the total length of the Red Sea (Ghebreab, 1998). Therefore, only a review of the main phases of the rifting in the northern Red Sea–Gulf of Suez region is given. Although there is controversy between advocates of a single-phase and a two-phase spreading evolution for this region as well (Ghebreab, 1998), most authors consider a *two-phase spreading* with a large intermittent phase of relative stability as the most probable evolution (Braithwaite, 1987; Sheppard *et al.*, 1992; Ghebreab, 1998). The first phase was situated in the late Oligocene-early Miocene and witnessed a transition from an early rift stage running simultaneously in the Gulf of Suez and the northern Red Sea to a later stage in which the Gulf of Aqaba–Dead Sea Wrench Fault dominated the Red Sea rifting. The middle to late Miocene, subsequently, was characterised by relative tectonic stability after which the Red Sea Rift reactivated (second phase) in Pliocene times (5 Ma) due to active seafloor spreading. More details on the first rifting phase are given in this section, while the second rifting phase is discussed in section 2.2.6.

2.2.4.2.1 Rift phase 1: first stage

The early (late Oligocene – early Miocene) stages of rifting in the northern Red Sea and the Gulf of Suez are considered to be simultaneous events (Bartov *et al.*, 1980; Morgan, 1990), with the Gulf of Suez being formed as the northern segment of the Red Sea Rift (Bosworth *et al.*, 1998). The Gulf of Aqaba had not yet been formed and was only represented by a large fracture separating the Gulf of Suez from the Red Sea area (Meshref, 1990). The Gulf of Suez-northwestern Red Sea Rift underwent a complicated structural evolution (fig. 2.4), including an initial episode of wrenching, followed by different episodes of extensional tectonics (Jarrige *et al.*, 1986b; Jarrige *et al.*, 1990; Montenat *et al.*, 1998b). During this time, the margins moved apart at an approximately 0.13m a year per flank (Braithwaite, 1987; Behairy *et al.*, 1992).

A first episode of strike-slip faulting took place in the late Oligocene to Aquitanian (Montenat *et al.*, 1998b; Morgan, 1990) and was accommodated by movements along many closely-spaced, inherited faults (Bosworth *et al.*, 1998; Montenat *et al.*, 1998b).

The wrench tectonics probably were diachronous; being older (Oligocene) in the Red Sea and younger (Aquitanian-early Burdigalian), but more accentuated, in the Gulf of Suez (Montenat *et al.*, 1998b). This resulted in the partition of large, slightly tilted rhomb-shaped blocks with relatively minor basin subsidence (Montenat *et al.*, 1998b) (fig. 2.4a), perhaps reflecting the inherent strength of the pre-lift (i.e. Precambrian) lithosphere (Bosworth *et al.*, 1998). Magmatic activity also occurred during this early episode (Braithwaite, 1987; Behairy *et al.*, 1992; Montenat *et al.*, 1998b) mainly along the eastern side of the rift (Montenat *et al.*, 1998a). In the Gulf of Suez and Red Sea, these volcanics occurred as scattered, small-sized magmatic bodies in contrast to the large and repeated outflows in the southern Red Sea area (Behairy *et al.*, 1992; Montenat *et al.*, 1998b) attaining Oligocene lava piles of 240 to 1463m thick (Braithwaite, 1987).

A second episode is distinguished between the late Aquitanian and the early Langhian, witnessing normal faulting without any evidence of strike-slip movements (Montenat *et al.*, 1998b). The Gulf of Suez and northern Red Sea area, subsequently, entered a period of rapid extension and increased marine depths (Steckler, 1985; Evans, 1988; Steckler *et al.*, 1988). Large rift margin escarpments, however, were not developed until about 23-21 Ma (Omar *et al.*, 1989), indicating that uplift accompanied or only slightly preceded the lateral extension (Bosworth *et al.*, 1998). The extensional tectonics began with the formation of largely antithetically (20-25°) tilted blocks, predominantly bounded by Clysmic faults, albeit locally complicated by the interference of other fault directions (fig. 2.4b) (Montenat *et al.*, 1998b). As a result, different groups of tilt blocks with opposite dips were separated from one another by Aqaba or Duwi faults which had previously acted as strike-slip faults bounding the late Oligocene-Aquitanian rhomb-shaped blocks (Jarrige *et al.*, 1986a).

This episode was followed by the formation of a *horst and graben* tectonic pattern created by the break-up of the tilt-blocks due to a longitudinal cutting or cleavage of many block crests by, predominantly, synthetic faults (fig. 2.4c) (Montenat *et al.*, 1998b). Some blocks were simulataneously rotated (<5°), though this tilting was only of minor importance (Montenat *et al.*, 1998b).

2.2.4.2.2 Rift phase 1: stage shift

The rate of extension in the Gulf of Suez markedly dropped by about 14 Ma (Garfunkel and Bartov, 1977; Angelier, 1985; Steckler, 1985), corresponding to the

final shift of the Sinai-African Plate boundary to the Gulf of Aqaba-Dead Sea transform system, leaving the Gulf of Suez as an essentially aborted rift (Steckler and ten Brink, 1986; Steckler *et al.*, 1988; Ghebreab, 1998). This shift resulted from a change in motion direction between Arabia and Nubia which was caused by the prolonged opening of the Gulf of Aden in an almost NNW-SSE direction (Meshref, 1990). When the NE-SW Gulf of Aqaba-Dead Sea strike-slip fault extended further south into the northern Red Sea, it became the dominant tectonic movement and the main orientation of the northern Red Sea rifting subsequently changed (Dewey and Sengor, 1979; Quennell, 1984; Morgan, 1990; Ghebreab, 1998).

2.2.4.2.3 Rift phase 1: second stage

From the middle Miocene onwards, the left-lateral shear on the Aqaba-Dead Sea fault system accommodated the continued extension of the northern Red Sea Rift (Bartov *et al.*, 1980). The predominance of synthetic faults resulted in a general flexure of the margins towards the axial part of the Red Sea Rift basin, which marked the beginning of the centripetal migration of subsidence and coincided with the maximum subsidence of the rift (fig. 2.4d) (Moretti and Colleta, 1987; Bosworth *et al.*, 1998; Montenat *et al.*, 1998b). The combination of the abovementioned tectonic episodes, finally, resulted in a complex *zigzag* structural pattern (Garfunkel and Bartov, 1977; Jarrige *et al.*, 1986a).

2.2.4.2.4 Rift phase 1: end

During the Seravallian, basin extension and subsidence ceased or slowed down (Braithwaite, 1987; Morgan, 1990; Montenat *et al.*, 1998b) and the northern Red Sea region became relatively stable although rift shoulder escarpments were still uplifted and minor faults and unconformities were locally formed (Bosence, 1998).

2.2.5 Miocene: evaporites and contemporary terrestrial and coastal deposits

2.2.5.1 Aquitanian (23-20.43 Ma)

Only limited marine Aquitanian sediments were deposited in the northern Red Sea (Said, 1990a) as a regional sill separated the southern end of the Gulf of Suez from the Red Sea proper, such that waters of the Mediterranean could not reach the Red Sea basin (fig. 2.5)

(Said, 1990a). The Red Sea Rift basin, in stead, was filling up with a thick layer of clastic sediments subaerially deposited in alluvial fans (fig. 2.5, 2.6b) (Said, 1990a). The presence of easily weathered rock fragments within this layer indicates that these deposits were the product of rapid erosion of the rising rift escarpments (Braithwaite, 1987). Tidal flats along the shoreline, in addition, were characterised by high rates of evaporation, resulting in the development of salt and gypsum deposits (Braithwaite, 1987).

2.2.5.2 Burdigalian-Langhian (20.43-13.65 Ma)

The maximal marine transgression of the Miocene epoch occurred during the Burdigalian (Said, 1990a) to early Langhian (~16 Ma) (Perrin *et al.*, 1998) such that the northwestern Red Sea basin was connected with the Mediterranean basin via the Suez Strait (Said, 1990a; Bosworth *et al.*, 1998) (fig. 2.7). Only the crests of some fault blocks remained emerged (Said, 1990a; Bosworth *et al.*, 1998).

After a short reefbuilding period in the Aquitanian, a second period of more extensive, shallow water coral reef building took place in the northern Red Sea and Gulf of Suez area during a relatively brief time interval around 16 Ma (Braithwaite, 1987; Bosworth *et al.*, 1998; Perrin *et al.*, 1998). This time interval was associated with the maximum of the middle Miocene sea-level highstand and a phase of warm global climate (Perrin *et al.*, 1998). Besides, the Red Sea Rift subsidence slowed down, forming a more stable environment in which corals could develop (Bosworth *et al.*, 1998).

The reefs were characteristic for an *arid land-locked subtropical-temperate setting* (Taviani, 1998) where full reef growth was limited by a combination of periods of increasing salinity and, perhaps, low temperatures only allowing the formation of short-lived fringing reefs of modest size (Sun and Esteban, 1994). Moreover, the reef distribution (fig. 2.8) and development within the region was governed by the tectonic movements of the early rift phase and the associated sedimentation patterns. Coral reefs, therefore, typically occurred on subaquatic paleohighs, e.g. horsts and fronts of fan deltas. Along the western coastline, they preferentially developed on the northeastern side of fault blocks as, there, they were facing the open marine water of the axial rift zone and were sheltered from the siliciclastic sediments from the southwest rift shoulder. These steep northeast facing footwall slopes, however, seemed to have limited reef progradation (Perrin *et al.*, 1998) and, as a result, coral assemblages were restricted to small-sized fringing reefs, thin biostromes, and shallow marine facies with scattered coral colonies (Perrin, *et al.*, 1998; Taviani, 1998). The coral diversity was consequently poor (Purser *et*

al., 1990; Sun and Esteban, 1994), although apparently at the same level as coral assemblages in the western Mediterranean basin (Perrin *et al.*, 1998).

2.2.5.3 Serravallian-early Tortonian (13.65-11 Ma)

Coral reefs and their coral fauna became totally extinct within the Gulf of Suez-northern Red Sea region during the Serravallian (Said, 1990; Bosworth *et al.*, 1998; Perrin *et al.*, 1998; Taviani, 1998) as a result of an increasing restriction of marine conditions. This was directly related to the gradual closure of the Suez Strait, probably due to both eustatic and tectonic movements (Perrin *et al.*, 1998), isolating the Gulf of Suez and the northern Red Sea basin from the Mediterranean basin (Braithwaite, 1987; Perrin *et al.*, 1998).

As the connection with the Mediterranean closed, the flow of water towards the Red Sea basin was no longer adequate to keep up with the evaporation and it was only a matter of time before sea level quickly fell such that extended marine areas became shallow. Braithwaite (1987) and Behairy *et al.* (1992), however, assume that the basin was rarely drying up completely. Sedimentation in the basin correspondingly changed from open and marginal marine conditions to an evaporitic, silled-basin setting (fig. 2.6c-d) (Hassan and El-Dashlouti, 1970; Robson, 1971; Braithwaite, 1987; Bosence, 1998; Orszag-Sperber *et al.*, 1998). With continuous evaporation, salinity in the basin increased to levels at which sulphates and halites are produced (Braithwaite, 1987). Such evaporite deposits were formed throughout the middle and late Miocene (Said, 1990a). These evaporites were mainly deposited in hypersaline waters which remained in the centre of the basin. Due to the prolonged restricted marine conditions, evaporite deposits could build up to 3000m in thickness in the southern part of the Gulf of Suez (Fawzy and Abdel Aal, 1984) and even exceeded 4000m in the offshore areas of the Red Sea basin. The lateral extent of these salt deposits, in contrast, was not very large (Behairy *et al.*, 1992) as the marine environment was restricted to the central axial trough. No evaporites were deposited in the northern Gulf of Suez and on local structural highs (Said, 1990a) as these remained totally emerged from the sea.

2.2.6 Pliocene: re-activation of the Red Sea Rift (phase 2)

Subsidence was renewed in the late Miocene to Pliocene (Steckler, 1985; Evans, 1988; Steckler *et al.*, 1988) although with markedly lower horizontal extension rates (Bosworth, 1995) averaging 1.5-1.6mm a year in the southern Red Sea (Roeser, 1975). The Gulf of

Aqaba-Dead Sea Wrench Fault, in contrast, underwent a lateral displacement of 45km, one of the largest in its evolution (Morgan, 1990; Sheppard *et al.*, 1992). Subsidence became increasingly focused along the axis of the rift during this time (Bosworth *et al.*, 1998), while the Suez isthmus continued to be uplifted (Behairy *et al.*, 1992; Braithwaite, 1987). As a result, the connection to the Mediterranean was permanently closed. However, because of an important sea-level rise, the Pliocene Indian Ocean could overflow the Hanish Sill in the late Tortonian (Said, 1990a). Renewed influx of normal marine water, consequently, occurred from the southern Red Sea and deposition switched to mixed evaporite-marginal marine settings (Bosworth *et al.*, 1998). From this time onwards, marine biota changed from typical Mediterranean to Indo-Pacific associations (Braithwaite, 1987). This is still recorded in current-day coral reefs which all have an Indo-Pacific origin.

Within the northern Red Sea basin, sediments accumulated and covered the Miocene sequences (fig. 2.6e). Pliocene facies were mainly shallow-marine siliciclastics and carbonates (Orszbag-Sperber *et al.*, 1998), although alluvial siliciclastic sediments were more common towards the margins (Braithwaite, 1987). These alluvial deposits resulted from heavy-rain erosion on the bordering rift escarpments and could form packages of 300-400m thick (Behairy *et al.*, 1992). Marine sediments reached considerable thicknesses as well, ranging from about 300m in the north, to 1000-1500m in the south (Braithwaite, 1987; Behairy *et al.*, 1992; Orszbag-Sperber *et al.*, 1998). These packages were attained over a relatively short time interval, ~3 Ma (Orszbag-Sperber *et al.*, 1998), implying that the rate of post-Miocene sedimentation was generally larger than that of the Miocene (Braithwaite, 1987; Purser and Philobos, 1993). The thickness of post-Miocene sediments and the absence of interruptions in sedimentation also imply that there was important continued subsidence, especially along the axis of the rift (Orszbag-Sperber *et al.*, 1998). In addition, lavas were emplaced in the central trough; and still are as the seafloor spreading is continuing (Braithwaite, 1987).

These Pliocene and subsequent Pleistocene sediments formed a marked contrast with the evaporites underneath (Braithwaite, 1987). Due to the partially heavy loading of these thick sediment packages, the underlying Miocene salt deposits became mobile and started to flow upwards, forming *salt domes* (Braithwaite, 1987; Behairy *et al.*, 1992; Bosworth *et al.*, 1998). This *salt diapirism* was enhanced by the high temperatures in the deep underground, up to 180°C (Braithwaite, 1987), which were related to the active seafloor spreading. Within the diapirs, thicknesses of the salt deposits were substantially increased, whereas the layer quickly thinned out laterally (Braithwaite, 1987). These diapirs, consequently, forced the overlying

layers upwards, forming structural highs which are important for the present-day distribution and geometry of coral reefs in the region (Braithwaite, 1987; Behairy *et al.*, 1992; Bosworth *et al.*, 1998).

Within this general context, three distinct zones are recognized in the Gulf of Suez and the northern Red Sea (Coletta *et al.*, 1988; Steckler *et al.*, 1988; Meshref, 1990; Bosworth, 1995). In the northern and central parts of the Gulf of Suez, terrigenous sediments were deposited, mostly undisturbed by post-Miocene tectonics. This indicates that these areas were tectonically stable or, in other words, that the Red Sea Rift reactivation had not reached these areas. The southern Gulf of Suez, conversely, exhibited post-Miocene halokinetic diapirism and the reactivation of Miocene fault blocks which resulted in numerous NW-SE domal and anticlinal structures, all indicating that this region was still in rifting phase 2 (Orsbag-Sperber *et al.*, 1998). The northern Red Sea also underwent abundant post-Miocene movements related to rejuvenated Miocene faults and evaporite remobilization, both parallel and oblique to the axis of the rift. In addition, the region was affected by a regional dip of 5 to 20° towards the axis of the rift and by frequent discharges of basement-derived conglomerates, both reflecting the continuous opening of the Red Sea basin and the uplift of its periphery. This region, however, is now considered to be in a *post-rift* phase as the above movements mainly result from an isostatic adjustment of the passive margin (Orsbag-Sperber *et al.*, 1998).

The late Pliocene, finally, was characterised by regression and a dramatic increase in precipitation (Said, 1990a). This marked the beginning of a period with strong climate changes characterising the Pleistocene.

2.2.7 Pleistocene: climate changes, tectonics, and coral-reef building

The Pleistocene environment was highly determined by frequent oscillations in sea level and climate changes related to glaciations in the higher latitudes (Braithwaite, 1987). During the Pleistocene, about 30 sea-level fluctuations are distinguished in the Red Sea region (fig. 2.9) (Plaziat *et al.*, 1998). These sea-level and climate changes have had thorough consequences for the sedimentation, erosion, and coral-reef-building patterns in the region (Taviani, 1998). Five successive Pleistocene coral reef terraces (400ka, 330-290ka, 250-170ka, 135-115ka and 7-6ka), which are now situated above mean sea level (msl), have been discriminated by Taviani (1998), recording Pleistocene sea-level highstands. A number of submerged Pleistocene coral terraces have been detected as well, representing relative sea-level

lowstands (Brachert and Dullo, 1990; Behairy, *et al.*, 1992; Gvirtzman, 1994). However, this succession of coral-reef terraces could not be totally ascribed to glacio-eustatic controls, as the Red Sea basin was still subject to tectonic movements. In following sub-sections, a short description of these two influencing, and interfering, processes is given.

2.2.7.1 Glacio-eustatic control

Each glacial cycle can be divided into four distinct phases (fig. 2.10), each of them having specific environmental settings and consequent influences on potential coral reef building (Plaziat *et al.*, 1998).

2.2.7.1.1 Interglacial maximum

Each interglacial maximum can be more or less compared to modern environmental conditions of a relatively high sea level, warm SST, an arid climate, and consequent limited runoff. Such glacial phases, therefore, were ideal for localised coral-reef growth (Plaziat *et al.*, 1998). The sea-level highstand would favour marine erosion of the prominent parts of previously formed coastal alluvial fans, allowing fringing reefs to develop along narrow terraces (Sheppard *et al.*, 1992; Plaziat *et al.*, 1998). The arcuate form of some current-day coral reefs is a testimony of these ancient terraces (Plaziat *et al.*, 1998).

2.2.7.1.2 Anaglacial transition phase

During the following period of anaglacial cooling, the climate became subarid with contrasting seasons (Plaziat *et al.*, 1998). In the beginning of this phase, this led to the planar erosion of the upper parts of the alluvial fans, deposited in earlier times, and consequently augmented terrestrial sediment transport, mostly through debris flows and sheet floods (Plaziat *et al.*, 1998). As a result, new fanconglomerates were deposited at the foot of the basement escarpments, notably near the opening of oblique, E-W oriented, fault-related valleys (Behairy *et al.*, 1992; Plaziat *et al.*, 1998). These fans could attain a radius of hundreds of metres to kilometres and thicknesses of at least 10m, depending on the size of their catchment area (Plaziat *et al.*, 1998). The relatively small catchment areas of most wadis, the extent of the associated alluvial fans, and the coarse siliciclastics found within (Braithwaite, 1987) suggest that these anaglacial phases were relatively long and characterised by intense seasonal rainfall (Plaziat *et al.*, 1998). The fan deposits would form new substrates for reef growth in

later episodes of higher sea level (Behairy *et al.*, 1992; Sheppard *et al.*, 1992), although Braithwaite (1987) suggest that reef growth might as well have been contemporary with the deposition of these siliciclastics.

In the course of the anaglacial phase, due to growing glacial caps at the poles, the sea level dropped further, increasing the erosion potential. Narrow valleys, consequently, were cut deep into the fanconglomerates and the adjacent reef flats (Braithwaite, 1987; Plaziat *et al.*, 1998); the largest of which forming new fan deltas at their mouth (Behairy *et al.*, 1992; Plaziat *et al.*, 1998). These valleys, nowadays, form *marsas* or *sharms*¹² near the mouths of second-order wadis (Behairy *et al.*, 1992; Sheppard *et al.*, 1992). Some of the largest sharms go down to 60-65m below present-day msl, indicating spectacular sea-level drops in the past (Sheppard *et al.*, 1992).

2.2.7.1.3 *Glacial maximum*

The glacial maximum was a new period of aridity. In contrast to interglacial maxima, it was typified by global sea-level lowstands (Braithwaite, 1987) as evaporation continued while seawater inflow from the Indian Ocean was severally, if not completely, restricted at the Hanish Sill (Taviani, 1998). The resulting high salinity level, combined with temperature drops (Ivanova, 1985) and the disruption of the internal organisation of the reefs during the sea-level changes, killed most of the coral-reef fauna in the Red Sea (Taviani, 1998).

Some authors (Braithwaite, 1982; Sheppard *et al.*, 1992) have pointed to the effect of karst erosion on the exposed coral-reef limestone surfaces during these periods of sea-level lowstands. According to Braithwaite (1987: 40), 'echo-sounding around reefs on the Sudanese coast suggests that the seafloor within these reef areas consists of gently sloping surfaces at 20 to 30 m depth, punctuated by roughly circular closed depressions at 5-60m depth, probably solution pits', typical for karst erosion surfaces. This karst surface would then determine some of the topographical features of the present-day reef systems throughout the Red Sea (Behairy *et al.*, 1992).

2.2.7.1.4 *Cataglacial transition phase*

During the following cataglacial warming, renewed humidity progressively supplied the fluvial drainage system (Plaziat *et al.*, 1998). Alluvial sediments, consequently, filled the linear incisions and prohibited coral-reef growth, although contemporary reef

¹² drowned valley

deposits have been found as well (Braithwaite, 1987). This, again, suggests that sediments which are not firmly consolidated could still become a suitable substrate for coral growth (Sheppard, 1981; Hayward, 1982; Hopley *et al.*, 1983; Perry, 2006).

2.2.7.2 Tectonic control

As in the Pliocene, the Pleistocene tectonic evolution differed between the northern part of the Gulf of Suez, its southern part, and the northern Red Sea basin. The northern part of the Gulf of Suez and the Suez Isthmus remained stable, such that the connection with the Mediterranean basin remained closed (Plaziat *et al.*, 1998). The southern Gulf of Suez, conversely, was marked by a considerable degree of instability (fig. 2.11) presumably associated with a modern reactivation of rifting northwest of the Aqaba-Dead Sea fault, rather than directly linked to strike-slip faulting along this fault line (Plaziat *et al.*, 1998). After a severe, mid-Pleistocene uplift, in the order of 25-40m (Plaziat *et al.*, 1998), the tectonic situation in the northern part of the Red Sea became relatively stable during the last 100-200 ka (Plaziat *et al.*, 1998; Taviani, 1998), although the regional eustatic uplift and the dipping of 5 to 20° of the rift shoulder escarpments towards the basin axis continued, as well as the deepening and widening of the axial basin related to the active seafloor spreading (Plaziat *et al.*, 1998). In between the uplifted escarpments and the sinking axial basin, the coastal plains seemed to have coincided with a stable transition belt (Plaziat *et al.*, 1998). Rifting in this belt, however, did not totally cease, but was restricted to the local uplift, in the order of 3 to 5m, of some fault blocks (Plaziat *et al.*, 1998).

2.2.8 Holocene: a suitable coral-reef environment?

2.2.8.1 Geotectonic setting

The Red Sea Rift is not a stand-alone system but forms part of a complex and diversified Neogene geotectonic system (fig. 2.12a) which includes the *Gulf of Aqaba-Dead Sea Wrench Fault*, connected with the *Syrian Arc folds* and the *Taurus and Zagros orogenic belts* to the N-NE, and the *Gulf of Aden* and the *East African Rift* in the south (Ghebreab, 1998; Montenat *et al.*, 1998b). Through the Gulf of Aden, a connection across the *Owen Fracture Zone* exists with the *Carlsberg Ridge* in the northwestern Indian Ocean (Braithwaite, 1987; Behairy *et al.*, 1992). The eastern branch of the East African Rift appears to have evolved by crack propagation southwards from a stress concentration

point situated in the *Afar region* (fig. 2.12b), a weakness zone where the southwest corner of the Gulf of Aden joins the Red Sea (Girdler, 1991). This point forms the *Nubia-Somalia-Arabia triple junction*.

The Red Sea Rift is not tectonically homogeneous (Ghebreab, 1998), and can be divided into five distinct zones (fig. 2.12b). Each zone is characterised by a different morphology and structure which appear to represent different stages in the development of a continental margin and the establishment of a mid-ocean-ridge spreading system (Cochran, 1983; Cochran *et al.*, 1986). From north to south, these zones are (Ghebreab, 1998):

- (1) an inactive rifting zone underlying the northern and middle parts of the Gulf of Suez;
- (2) a zone of late-stage *continental rifting* (from 23°20'N to 27°N) in which a broad trough without a recognisable spreading centre is present, co-existing with a number of small, isolated deeps (black dots on figure 2.12b) (Cochran *et al.*, 1986). Active seismicity is registered in the median zone of the northern Red Sea (Morgan, 1990) associated with the spreading at a rate of 5mm per year; possibly increasing to 6mm per year or more at the junction with the Gulf of Suez (Meshref, 1990). Localised uplift of Pleistocene coral terraces similarly reflects continued tectonic deformation (Andres and Radtke, 1988; Bosworth and Taviani, 1996). Although localised, this uplift can be very dramatic with sudden coastline rises up to a few metres above present sea level, as has been recorded after the Shadwan 1969 earthquake (Kebeasy, 1990). Micro-earthquake studies (fig. 2.11b) also indicate that sinistral oblique-slip tectonic movements are still active in the southern part of the Gulf of Suez (Dagget *et al.*, 1986; Jackson *et al.*, 1988; Morgan, 1990);
- (3) a transition zone (between 20°N and 23°20'N) which is made up of a series of deeps alternated with shallow inter-trough zones (Searle and Ross, 1975);
- (4) a zone of *active seafloor spreading* (from 15°N to 20°N) characterised by a well-developed axial trough resulting from normal seafloor spreading during at least the last 5 Ma (Girdler and Styles, 1974; Roeser, 1975; LaBreque and Zitellini, 1985); and
- (5) a zone of *active rifting* representing the future line through the Danakil Depression (Afar) along which the southern Red Sea is due to propagate.

2.2.8.2 Sea transgression

From around 15,000 BP (Milliman and Emery, 1968), sea level started to rise markedly, departing from the Last Glacial Maximum lowstand at circa 120m below present msl (Gvirtzman *et al.*, 1977; Sheppard *et al.*, 1992). A Holocene maximum high was reached at about 6400-5400 BP when sea level was about 0.5-1m above present msl (Chappell, 1983; Gvirtzman, 1994; Plaziat *et al.*, 1995; Bosence *et al.*, 1998; Plaziat *et al.*, 1998). This short period of sea-level highstand is often associated with an abrasion coral-reef surface at about 0.5m above current msl (Plaziat *et al.*, 1998; Taviani, 1998). During the last 5000-5500 years, sea level slowly dropped again unto its current-day position (Chappell, 1983).

2.2.8.3 Coral-reef formation

The current Red Sea coral fauna is the result of a Holocene recolonization of the basin after complete extinction during the Last Glacial Maximum (Gvirtzman *et al.*, 1977). Present-day coral reefs, therefore, are believed to be only a thin carbonate veneer formed over the last 6000-7000 years on older reef structures (Braithwaite, 1987; Behairy *et al.*, 1992). The total Pleistocene and Holocene reef-complex limestones, in contrast, are about 200m thick (Berry *et al.*, 1966), thus illustrating the potential of reef communities to repeatedly colonize the changing coastal morphologies (Plaziat *et al.*, 1998). The distribution of Holocene coral reefs is strongly controlled by the geotectonic setting of the Red Sea, the Pleistocene sediment patterns, and the contemporary ephemeral siliciclastic input from the hinterland through the wadi systems (Dullo and Montaggioni, 1998).

The tectonic control on the morphology of most reefs in the northern Red Sea is demonstrated by their orientation parallel to the main axis of the rift. In addition, most reefs have almost vertical foreslopes from shallow waters up to 50m depth, predominantly representing the fault planes of the graben structures (Dullo and Montaggioni, 1998). Besides, all along the northwestern Red Sea coast, exposed Holocene reef flats occur between 0.2 and 0.5m above current msl (Dullo and Montaggioni, 1998). These emergent reefs have been dated by Dullo and Montaggioni (1998) between 5500 and 3900 BP. Two types are distinguished: stepped, horizontal terraces fringing the continental coastline and gently seaward-sloping surfaces around islands (Dullo and Montaggioni, 1998). These, respectively, have been linked to sharp rapid uplift, evaporite tectonics and/or block rotation (Bosworth, 1994). Besides uplift, Dullo and Montaggioni (1998) have also

recognised recent low-amplitude subsidence in the region. Especially along the northeastern Red Sea shorelines, dead, undisturbed in situ coral heads, pavements, and molluscan assemblages have been found at depths between 0.20 and 1.20m below mean low tide level. C¹⁴ dating indicates these were flourishing coral reefs between 4600 and 2000 BP (Dullo and Montaggioni, 1998).

Due to post-Miocene sedimentation, the influence of the rift tectonics inherited from the Miocene, however, is largely diminished and has been masked out in many areas (Plaziat *et al.*, 1998). The formation of alluvial fans during more humid climate periods has resulted in new substrate for coral-reef colonisation and has locally pushed reef growth seawards from the coastline. Due to the arcuate form of most of the alluvial fans, the belt of modern reefs situated in front of them exhibits the shape of barrier reefs. Where reefs have developed along the seaward margins of the fans, the reef framework protects the siliciclastic sediments from being eroded and redistributed by marine processes (Roberts and Murray, 1983). Furthermore, the mobilisation of Miocene evaporitic deposits created localised halokinetic movements resulting in salt diapirs which influence the morphology and distribution of some coral reefs. Such reefs typically have circular or semicircular outlines (Dullo and Montaggioni, 1998).

Present-day drainage patterns, finally, control the small-scale morphology of the reefs, which is indicated by small channels and furrows displaying a similar pattern and orientation as the drainage system on land (Gvirtzman *et al.*, 1977; Dullo, 1990). The fact that reefs do not flourish in or even colonize these channels suggests that land-derived siliciclastics are still transported through these pathways. Because of the variable flood intensities, sediment delivery through these channels is often localised and restricted to the distributional channels. Sediment inundation further afield, therefore, is generally incomplete such that the damaged coral reefs will be rapidly recolonised (Hayward, 1982).

2.3 CLIMATE AND OCEANOGRAPHY

The Red Sea is set in a very unique environment as it is almost completely situated amidst deserts or semi-deserts although stretching out between 12° and 30°N (Edwards, 1987). Air temperatures over most of the region, consequently, are relatively high throughout the year and precipitation is scarce (fig. 2.13). Because of this low precipitation level and the orographic structure of the Red Sea Mountains, no major rivers have their runoff directly to the Red Sea (Purser and Bosence, 1998b) (fig. 2.14). The Red Sea proper is also one of the warmest and saltiest seawater bodies found anywhere in the world (Edwards, 1987). Besides, it is hydrographically very stable, with only small but important seasonal changes (Sheppard *et al.*, 1992), and nutrient levels are low even compared to other ocean basins (Edwards, 1987). Combined with the limited terrestrial runoff, this results in low turbidity levels. The following discussions on the climate and oceanography of the Red Sea are mainly derived from the summary given by Edwards (1987) supplemented with some additional information from more recent publications.

Remark that the Red Sea is also very well known for the occurrence of hot-brine pools at depths greater than 2000m. These are very interesting marine environments not yet completely understood, but given that these have no direct effect on the coral reefs occurring in the top 100m of the water column, they are beyond the scope of this work.

2.3.1 Climate

The climate of the Red Sea region is largely controlled by the distribution of and changes in atmospheric pressure over North Africa, Asia and the Mediterranean region (Edwards, 1987). Although these pressure cells markedly change over the year, the weather over the Red Sea shows a remarkable uniformity. Edwards (1987) attributes this stability to two factors, namely the desert climate zone in which the Red Sea is located, and the topographic setting of the Red Sea basin. Although distorted by seasonal pressure changes, most of the airflow to the region originates from the NE Trade Winds. Upwind to the northeast of the Red Sea, most of the area is desert or semi-desert land so the air brought to the region is mostly dry and warm throughout the year. Secondly, the high mountainous escarpments along the Red Sea basin ensure that the prevailing wind predominantly blows along the length of the sea. The wind direction, therefore, remains virtually unchanged throughout the year, resulting in stability of the air mass over the Red Sea.

Notwithstanding this general stability, a differentiation can be made between a warmer and a cooler season (Edwards, 1987). These seasons roughly correspond to the summer and winter season in the northern hemisphere temperate regions. The 'winter' season runs from mid-October to mid-April, while the 'summer' season occupies the rest of the year. In winter, a regional difference in weather conditions exists between the northern and southern part of the Red Sea.

2.3.1.1 Wind

The dominant wind fields of the Red Sea region are associated with the global air pressure cells of the eastern mid-latitude northern hemisphere. A marked difference in wind direction exists between winter and summer, especially in the southern Red Sea (fig. 2.15) (Edwards, 1987; Sheppard *et al.*, 1992; Johns *et al.*, 1999).

2.3.1.1.1 Winter

In winter, as can be seen on figure 2.15a, two zones of high pressure dominate North Africa and Asia respectively, while in southern and central Africa, a low pressure zone prevails which extends as a narrow low pressure trough over the central Red Sea. This low pressure trough is situated around 18-20°N in January, and migrates to the south in early spring and back in late autumn (Sheppard *et al.*, 1992). In this area of convergence, winds are light and variable and periods of calm weather frequently occur.

The centre of the Asian anticyclone is situated above Mongolia, with ridges of high pressure extending to the Arabian Peninsula. The NE Monsoon, associated with this anticyclone, determines the climate over southern Asia and the Indian Ocean. Winds over the Indian Ocean are mainly easterly and the ITCZ is pushed south of the equator. Orographic influences in the Gulf of Aden deflect the easterly winds and steer them up the Red Sea where the now southeasterlies flow to the area of low pressure over the central part. The southern part of the Red Sea is thus covered by S-SE winds during winter.

The northern part of the Red Sea is protected from the NE Monsoon by the central low pressure zone and the weather is mainly dominated by the North African anticyclone. Winds are mainly NW to N but may be disturbed by passing low pressure troughs associated with W-E migrating Mediterranean cyclones. These troughs swing from northwest to southeast and ahead of such fronts, the wind backs from north

through west, to southwest and even south and may become quite strong. As the front passes, squalls frequently occur with a veering of wind back to NW or N, or sometimes even NE (Edwards, 1987). These troughs may also bring local rains to the northern Red Sea.

2.3.1.1.2 *Summer*

In summer, the Mongolian anticyclone is replaced by an extensive low pressure area centred over northwest India, Iran and the Persian Gulf (fig. 2.15b). The ITCZ migrates northwards until it lies along the southeast coastline of Arabia, passes up the Gulf of Aden, and then crosses into central and northern Africa (Sheppard *et al.*, 1992). South of the ITCZ, the SW Monsoon builds up, while north of it, a high pressure zone over the Mediterranean region dominates the weather. As a result, weak northwesterly winds prevail over the whole Red Sea region which completely lies north of the ITCZ (Edwards, 1987; Sheppard *et al.*, 1992; Johns *et al.*, 1999).

2.3.1.1.3 *Land and sea breezes*

Adding to this basic pattern, local wind systems make the situation more complex. Land and sea breezes are the most important as they alter the wind direction in the coastal areas as compared to the open ocean. These *thermionic winds* (Sheppard *et al.*, 1992) are diurnal winds and result from the differential heating and cooling of the sea and the surrounding deserts.

The sea breeze, a flow of air from the sea towards the land due to higher daytime air temperatures above the desert, develops during the day and usually reaches its maximum in the early to mid-afternoon. The wind direction is not perpendicular to the coast as could be theoretically expected, but strikes obliquely along the coast because of the influence of the main wind field. During summer, the sea breeze is mainly between N and NE along the African shore, while on the Arabian side, the sea breeze is generally coming from the NW (Sheppard *et al.*, 1992). In the Gulf of Suez and the Gulf of Aqaba, the water body is much smaller such that the sea breeze, mostly with a northerly direction, is less developed (Edwards, 1987).

The reverse land breeze, resulting from the higher warmth capacity of the sea, infrequently occurs at night (Sheppard *et al.*, 1992). The land breezes are usually coming from W to NW on the African shore and reach their maximum speed around

dawn. The change from one land to sea breeze generally occurs around 8 a.m. and 8 p.m. local time and last for about one to two hours (Edwards, 1987).

2.3.1.1.4 Effects of wind on coral-reef growth

Generally, wind speeds in the Red Sea region are low and do not have large effects on reef growth. The sea breeze, nonetheless, influences the distribution and the development of coral reefs as, apart from occasional storms, these winds are the strongest experienced in the Red Sea (Behairy *et al.*, 1992). The effect is most noticeable in the structure of the reefs, who tend to grow into the prevailing wave direction (Sheppard *et al.*, 1992). This, for example, can be noted in the structure of the coral reefs offshore Hurghada, where many reef crests are lined up perpendicular to the northeasterly waves. Strong sea breezes may also force water shoreward, submerging reef flats which would otherwise be left dry. Land breezes, in contrast, may have devastating effects as they are highly desiccative and often very intense (Sheppard *et al.*, 1992). Reef flats, consequently, may become exposed, leading to widespread mortality and community disturbance in shallow areas (Morley, 1975; Loya, 1976).

Tropical storms normally do not develop on the Red Sea (Stoddart, 1971), but exceptional wind conditions may also have disturbing effects on the reef systems. Strong summer breezes, for example, may lead to exposure of the upper parts of the reefs, whereas strong winter winds, associated with passing low pressure troughs, may drastically decrease SST for several days, leading to massive coral mortality (Behairy *et al.*, 1992).

2.3.1.2 Air temperature

2.3.1.2.1 Air temperature over the open sea

Over the open sea, a general latitudinal air surface temperature (AST) –i.e. air temperature at sea level- gradient is noticed with annual mean temperature increasing from north to south (table 2.1). As can be seen on figure 2.16 and table 2.1, maximum values, however, are not recorded in the extreme south of the Red Sea but around 16°N. South of this latitude, temperature is slightly decreasing under the growing influence of the Gulf of Aden air circulation. Seasonal AST differences are recorded over the entire Red Sea; lowest temperatures are registered in February and highest

temperatures in August. The mean annual AST range, however, differs: it spans about 6-7°C in the southern part, increasing to 10°C near the entrances of the Gulf of Suez and the Gulf of Aqaba, and according to Edwards (1987), this range even becomes larger in the northern parts of these Gulfs due to stronger influences of the surrounding land.

When compared to mean monthly SST¹³ for the entire Red Sea, AST over the open sea is generally lower in winter and higher in summer (fig. 2.17). In summer, AST is almost 1°C higher than SST over the entire Red Sea. Differences between AST and SST are slightly larger in winter, although, then, important latitudinal differences occur. South of about 17°N, AST and SST only differ by ca. 0.5°C. To the north, this difference increases to about 2°C in the northern extremity of the Red Sea and even more in both the Gulf of Suez and the Gulf of Aqaba (Edwards, 1987).

Daily AST has been recorded for Daedalus Reef (approx. 25°N-36°E), giving an indication of the daily AST range over the open sea (Edwards, 1987). A mean diurnal range of 4°C was registered from December to April and a range of 5°C in all other months except for July, when 6°C was registered. These records are believed to be representative for the entire Red Sea, although diurnal ranges probably become larger towards the northern and southern extremities (Edwards, 1987).

2.3.1.2.2 Air temperature along the shores

The temperature regime along the coasts is marked by a high degree of *continentality* along the entire length of the Red Sea. This is evident in a larger annual (respectively 8-9°C in the south and 11-14°C in the north) and diurnal temperature range than over the open sea in the same latitude. The increased seasonality from south to north seen in open-sea AST is also noticed in the coastal temperature regimes (fig. 2.13). The general annual air temperature pattern which emerges from table 2.2 is that along the entire Red Sea coast, mean air temperature is below the offshore air temperature in winter, while the reverse prevails during the summer. Sea breezes, consequently, are most likely stronger in summer, whereas land breezes are more likely to develop in winter. The summer period stretches from April to September from Hurghada to Port Sudan, but tends to lengthen southwards.

¹³ An overview of the mean monthly SST is given in 2.3.2.1.1

Table 2.1. Air surface temperature over the Red Sea in 1° by 1° grid cells (da Silva et al., 1994)

| latitude | longitude | AST January °C | AST February °C | AST March °C | AST April °C | AST May °C | AST June °C | AST July °C | AST August °C | AST September °C | AST October °C | AST November °C | AST December °C | AST annual mean °C |
|---|-----------|----------------------|-----------------------|--------------------|--------------------|------------------|-------------------|-------------------|---------------------|------------------------|----------------------|-----------------------|-----------------------|--------------------------|
| 27.5N | 34.5E | 19.6 | 19.4 | 20.4 | 22.1 | 25.0 | 26.5 | 28.2 | 29.1 | 27.8 | 26.3 | 24.1 | 20.8 | 24.1 |
| 26.5N | 34.5E | 20.9 | 20.6 | 21.6 | 23.3 | 26.2 | 27.4 | 29.1 | 30.0 | 28.6 | 27.1 | 25.1 | 21.9 | 25.2 |
| 26.5N | 35.5E | 20.9 | 20.7 | 21.6 | 23.4 | 26.3 | 27.4 | 29.1 | 29.9 | 28.6 | 27.0 | 25.1 | 22.0 | 25.2 |
| 25.5N | 35.5E | 21.7 | 21.5 | 22.4 | 24.1 | 26.9 | 28.0 | 29.5 | 30.4 | 29.0 | 27.5 | 25.8 | 22.9 | 25.8 |
| 25.5N | 36.5E | 21.9 | 21.6 | 22.5 | 24.3 | 27.0 | 28.1 | 29.6 | 30.4 | 29.1 | 27.6 | 26.0 | 23.1 | 25.9 |
| 24.5N | 35.5E | 22.2 | 21.9 | 22.8 | 24.6 | 27.1 | 28.2 | 29.7 | 30.5 | 29.2 | 27.8 | 26.2 | 23.4 | 26.1 |
| 24.5N | 36.5E | 22.4 | 22.1 | 23.0 | 24.8 | 27.3 | 28.4 | 29.8 | 30.6 | 29.4 | 28.0 | 26.4 | 23.7 | 26.3 |
| 23.5N | 36.5E | 22.9 | 22.6 | 23.4 | 25.2 | 27.5 | 28.6 | 30.0 | 30.7 | 29.7 | 28.4 | 26.8 | 24.2 | 26.7 |
| 23.5N | 37.5E | 23.1 | 22.8 | 23.6 | 25.4 | 27.7 | 28.8 | 30.1 | 30.8 | 29.9 | 28.6 | 27.0 | 24.5 | 26.9 |
| 22.5N | 36.5E | 23.4 | 23.1 | 23.9 | 25.6 | 27.7 | 28.9 | 30.3 | 30.9 | 30.0 | 28.8 | 27.2 | 24.8 | 27.1 |
| 22.5N | 37.5E | 23.4 | 23.1 | 23.9 | 25.6 | 27.7 | 28.9 | 30.3 | 30.8 | 30.0 | 28.8 | 27.2 | 24.8 | 27.1 |
| 22.5N | 38.5E | 23.9 | 23.5 | 24.3 | 26.0 | 28.1 | 29.2 | 30.6 | 31.1 | 30.4 | 29.3 | 27.6 | 25.3 | 27.5 |
| 21.5N | 37.5E | 24.3 | 23.9 | 24.6 | 26.3 | 28.3 | 29.5 | 30.8 | 31.3 | 30.6 | 29.5 | 27.8 | 25.6 | 27.7 |
| 21.5N | 38.5E | 24.5 | 24.1 | 24.8 | 26.5 | 28.5 | 29.6 | 31.0 | 31.3 | 30.7 | 29.8 | 27.9 | 25.8 | 27.9 |
| 20.5N | 37.5E | 24.9 | 24.4 | 25.1 | 26.8 | 28.7 | 29.8 | 31.3 | 31.6 | 30.9 | 30.0 | 28.2 | 26.2 | 28.2 |
| 20.5N | 38.5E | 25.1 | 24.6 | 25.3 | 27.0 | 28.9 | 30.0 | 31.4 | 31.6 | 31.0 | 30.2 | 28.3 | 26.3 | 28.3 |
| 20.5N | 39.5E | 25.2 | 24.7 | 25.4 | 27.1 | 29.1 | 30.1 | 31.5 | 31.6 | 31.1 | 30.3 | 28.3 | 26.5 | 28.4 |
| 19.5N | 37.5E | 25.4 | 24.9 | 25.6 | 27.2 | 29.1 | 30.2 | 31.6 | 31.9 | 31.2 | 30.4 | 28.6 | 26.6 | 28.6 |
| 19.5N | 38.5E | 25.4 | 24.9 | 25.6 | 27.2 | 29.1 | 30.2 | 31.6 | 31.8 | 31.2 | 30.4 | 28.5 | 26.6 | 28.6 |
| 19.5N | 39.5E | 25.6 | 25.2 | 25.8 | 27.5 | 29.4 | 30.4 | 31.8 | 31.8 | 31.4 | 30.7 | 28.5 | 26.8 | 28.7 |
| 19.5N | 40.5E | 25.7 | 25.3 | 25.9 | 27.7 | 29.6 | 30.5 | 31.9 | 31.8 | 31.4 | 30.8 | 28.4 | 26.9 | 28.8 |
| 18.5N | 38.5E | 25.9 | 25.5 | 26.1 | 27.8 | 29.6 | 30.6 | 32.0 | 32.2 | 31.6 | 30.8 | 28.8 | 27.1 | 29.0 |
| 18.5N | 39.5E | 25.9 | 25.5 | 26.0 | 27.8 | 29.6 | 30.6 | 32.0 | 32.0 | 31.6 | 30.8 | 28.6 | 27.0 | 29.0 |
| 18.5N | 40.5E | 26.0 | 25.6 | 26.2 | 28.0 | 29.9 | 30.8 | 32.1 | 32.1 | 31.6 | 30.9 | 28.6 | 27.1 | 29.1 |
| 17.5N | 39.5E | 26.2 | 25.8 | 26.4 | 28.2 | 30.0 | 31.0 | 32.2 | 32.4 | 31.8 | 31.1 | 28.8 | 27.2 | 29.3 |
| 17.5N | 40.5E | 26.1 | 25.8 | 26.4 | 28.2 | 30.0 | 31.0 | 32.1 | 32.2 | 31.8 | 30.9 | 28.6 | 27.1 | 29.2 |
| 17.5N | 41.5E | 26.1 | 25.8 | 26.4 | 28.4 | 30.2 | 31.1 | 32.1 | 32.1 | 31.8 | 31.0 | 28.4 | 27.1 | 29.2 |
| 16.5N | 39.5E | 26.3 | 26.0 | 26.6 | 28.4 | 30.1 | 31.2 | 32.4 | 32.5 | 32.0 | 31.2 | 28.9 | 27.3 | 29.4 |
| 16.5N | 40.5E | 26.1 | 25.9 | 26.5 | 28.4 | 30.1 | 31.2 | 32.2 | 32.2 | 31.8 | 31.0 | 28.6 | 27.1 | 29.3 |
| 16.5N | 41.5E | 26.1 | 25.9 | 26.6 | 28.5 | 30.3 | 31.3 | 32.2 | 32.2 | 31.9 | 31.0 | 28.4 | 27.0 | 29.3 |
| 15.5N | 40.5E | 26.2 | 26.0 | 26.7 | 28.6 | 30.3 | 31.5 | 32.3 | 32.4 | 32.0 | 31.1 | 28.6 | 27.1 | 29.4 |
| 15.5N | 41.5E | 26.1 | 25.9 | 26.7 | 28.5 | 30.3 | 31.5 | 32.2 | 32.2 | 31.9 | 30.9 | 28.3 | 26.9 | 29.3 |
| 14.5N | 42.5E | 25.7 | 25.7 | 26.6 | 28.4 | 30.3 | 31.7 | 31.9 | 31.7 | 31.8 | 30.4 | 27.9 | 26.5 | 29.1 |
| Gulf of Aden | | | | | | | | | | | | | | |
| 12.5N | 43.5E | 25.4 | 25.4 | 26.4 | 28.1 | 30.2 | 31.9 | 31.5 | 30.8 | 31.4 | 29.6 | 27.3 | 26.0 | 28.7 |
| 12.5N | 44.5E | 25.3 | 25.4 | 26.4 | 28.0 | 30.1 | 31.9 | 31.4 | 30.7 | 31.2 | 29.3 | 27.2 | 25.9 | 28.6 |
| 12.5N | 45.5E | 25.2 | 25.4 | 26.4 | 28.1 | 30.1 | 31.9 | 31.3 | 30.6 | 30.9 | 29.0 | 27.1 | 25.9 | 28.5 |
| AST MONTHLY MEAN for RED SEA | | 24.4 | 24.1 | 24.8 | 26.6 | 28.7 | 29.8 | 31.1 | 31.4 | 30.7 | 29.6 | 27.6 | 25.6 | |

The diurnal range of air temperature on the coasts is also substantially larger than over the open sea as recorded at Daedalus Reef. The difference between the mean daily maximum and mean daily minimum usually is lowest in winter months, about 7-9°C, and increases towards midsummer when ranges of 13-15°C are common. These diurnal ranges are influenced by different factors, one of the most important being the occurrence and strength of sea breezes (Edwards, 1987).

Table 2.2. Mean monthly air temperatures for a number of weather stations along the Red Sea coast (source: IRI/LDEO, 2000)

| °C | Jan | Feb | Mar | Apr | May | Jun | Jul | Aug | Sep | Oct | Nov | Dec | mean annual |
|---------------------|-------------|-------------|-------------|-------------|-------------|-------------|-------------|-------------|-------------|-------------|-------------|-------------|-------------|
| Hurghada | 15.7 | 16.5 | 18.9 | 22.4 | 25.7 | 28.4 | 29.4 | 29.8 | 27.9 | 24.9 | 21.0 | 17.2 | 23.1 |
| Quseir | 18.0 | 18.6 | 20.7 | 23.3 | 26.2 | 29.1 | 29.7 | 30.1 | 28.2 | 25.9 | 23.0 | 19.4 | 24.3 |
| Port Sudan | 23.1 | 23.0 | 24.0 | 26.4 | 29.3 | 31.9 | 33.7 | 33.9 | 31.9 | 29.3 | 27.3 | 24.6 | 28.2 |
| Tokar | 24.1 | 24.5 | 25.9 | 27.8 | 30.4 | 34.0 | 35.6 | 35.1 | 34.0 | 31.0 | 28.3 | 25.6 | 29.7 |
| Assab | 25.5 | 26.2 | 28.0 | 30.2 | 31.8 | 33.2 | 34.8 | 34.4 | 32.8 | 30.8 | 28.4 | 26.5 | 30.2 |
| Elat | 15.2 | 16.9 | 20.0 | 24.2 | 28.3 | 31.6 | 32.8 | 32.9 | 30.6 | 26.8 | 21.5 | 16.5 | 24.8 |
| Al Wajh | 18.6 | 18.8 | 21.3 | 24.4 | 26.6 | 28.0 | 29.2 | 29.4 | 28.2 | 26.5 | 23.5 | 20.1 | 24.5 |
| Yanbu | 19.8 | 20.0 | 24.1 | 27.1 | 29.8 | 31.6 | 32.3 | 32.0 | 31.8 | 29.9 | 25.2 | 22.3 | 27.2 |
| Jeddah | 23.5 | 23.7 | 25.4 | 27.6 | 29.9 | 31.4 | 32.0 | 32.0 | 31.1 | 29.5 | 27.3 | 25.0 | 28.2 |
| Jizan | 25.9 | 26.3 | 27.9 | 30.2 | 32.1 | 33.4 | 33.4 | 33.0 | 32.5 | 31.2 | 28.7 | 26.0 | 30.1 |
| mean Red Sea | 20.9 | 21.4 | 23.6 | 26.4 | 29.0 | 31.3 | 32.3 | 32.3 | 30.9 | 28.6 | 25.4 | 22.3 | |

2.3.1.3 Air humidity and cloud cover

Although air brought to the region is fairly dry as it originates from desertic or semi-desertic areas, the very high evaporation rate¹⁴ raises the humidity¹⁵ of the lower layers of the atmosphere. Over the open sea, the average annual humidity is about 70% with a range of $\pm 5\%$, while only a maximum diurnal range of 4% has been recorded. Along the coasts, humidity is usually lower than over sea and generally increases from north to south. This pattern, however, is highly influenced by both the occurrence of land and sea breezes and the local air temperature range. Mean monthly humidity values along the Egyptian coast, for example, are around 50% throughout the year for morning observations and some 5 to 10% higher in the afternoons. The mean humidity at Perim Island, in contrast, rises to more than 80% in the morning throughout the year, but falls to 60-65% in the afternoon (Edwards, 1987).

¹⁴ Evaporation averages 2060 ± 220 mm per year for the entire Red Sea (Sofianos *et al.*, 2002).

¹⁵ Humidity is expressed as relative humidity, i.e. the amount of water vapour present in the air as a percentage of the amount required for saturation at the same temperature.

In the higher atmosphere, cloud cover generally is low over the Red Sea. The mean daily cloud cover is never more than 50% at any location and over large areas cloud cover is often less than 25% for months in a row. A differentiation has to be made for areas north and south of the 20°N parallel. To the north, the cloudiest months are from December to March when more than 25% cloud cover is to be expected for 30 to 40% of the time. Cloud amounts of 5/8s or more only occur in 10% of the observations but may reach 20% in the Gulf of Suez in March. This cloud cover is associated with passing fronts. For the remainder of the year, cloud cover is very small with long cloudless periods from June to September. Cloudiness only increases in August near the southern edge of the area. South of 20°N, the cloudiest are the summer months from June to September. In July and August, cloud coverage exceeding 25% occurs for 30% of the time around 20°N, increasing to 60% of the time further south. These clouds are associated with the summer monsoon over the western Indian Ocean. The clearest months in this part of the Red Sea are October and November when less than 20% of the observations show more than 25% cloud cover (Edwards, 1987).

2.3.1.4 Precipitation

As can be seen in figure 2.13 and table 2.3, annual rainfall over the Red Sea generally is low throughout the year, although some regional differences occur. Rainfall may amount to 25mm per year (Edwards, 1987) in the northern Gulfs but is completely restricted to the winter months when Mediterranean depressions are passing. The rain usually falls as heavy squally showers, sometimes accompanied by thunderstorms and hail, although longer periods of drizzle are not uncommon either (Edwards, 1987). By the time the depressions reach the north of the Red Sea proper, they have lost most of their rain-producing activity. The northwestern shore of the Red Sea, up to 22°N (Edwards, 1987), is virtually rainless throughout the year. According to the information in table 2.3 and assumed by Edwards (1987), the eastern shore is slightly more humid. Over the northern Red Sea itself, scarce rainfall is also more regular, amounting to 10-15mm per year (Edwards, 1987).

Precipitation increases in the central part of the Red Sea, which is related to the zone of convergence between the Northwesterlies and Southeasterlies in winter (Edwards, 1987). Total mean annual rainfall amounts to 158,5mm in Suakin and increases to 184.6mm in Massawa. Most of the rainfall is restricted to the winter, from October to February, with a southwards enlarging rainy season. Local differences may however occur

as seen, for example, in Tokar where only a mean annual precipitation of 81.6mm is received. High amounts of rain associated with local heavy thunderstorms, in addition, may also fall sporadically in July and August (Edwards, 1987). South of the zone of convergence, the amount of rainfall decreases again, e.g. a mean annual precipitation of 45.3mm in Assab, and appears to be more evenly distributed throughout the year.

Table 2.3. Mean monthly precipitation for a number of weather stations along the Red Sea coast (source: IRI/LDEO, 2000)

| mm/year | Jan | Feb | Mar | Apr | May | Jun | Jul | Aug | Sep | Oct | Nov | Dec | Mean annual |
|--------------|------|------|------|------|-----|-----|-----|-----|-----|------|------|------|-------------|
| El Tûr | 1.9 | 1.3 | 1.8 | 0.3 | 0.2 | 0.0 | 0.0 | 0.0 | 0.0 | 0.8 | 2.3 | 4.5 | 13.1 |
| Hurghada | 0.2 | 0.4 | 1.1 | 0.2 | 0.1 | 0.0 | 0.0 | 0.0 | 0.0 | 0.3 | 0.4 | 1.3 | 4.0 |
| Quseir | 0.1 | 0.0 | 0.1 | 0.1 | 0.2 | 0.0 | 0.0 | 0.0 | 0.0 | 0.9 | 1.5 | 0.6 | 3.5 |
| Suakin | 14.4 | 2.9 | 0.9 | 1.0 | 1.9 | 0.2 | 8.0 | 5.7 | 0.1 | 20.9 | 70.7 | 31.7 | 158.5 |
| Tokar | 16.9 | 3.9 | 0.8 | 1.4 | 2.6 | 0.8 | 6.1 | 4.4 | 0.6 | 6.0 | 22.0 | 16.2 | 81.6 |
| Aqiq | 41.8 | 12.5 | 4.9 | 1.1 | 0.9 | 0.3 | 1.3 | 2.7 | 0.3 | 3.5 | 31.6 | 41.7 | 142.5 |
| Massawa | 31.7 | 28.2 | 14.3 | 11.6 | 5.2 | 0.1 | 5.7 | 8.6 | 3.1 | 17.0 | 20.6 | 38.6 | 184.6 |
| Assab | 5.9 | 4.0 | 2.5 | 1.7 | 0.3 | 0.1 | 9.3 | 4.8 | 2.9 | 0.6 | 3.5 | 9.6 | 45.3 |
| Al Wajh | 1.6 | 7.1 | 3.8 | 0.5 | 1.6 | 0.0 | 0.0 | 0.0 | 0.0 | 8.7 | 5.4 | 14.0 | 42.8 |
| Yanbu | 4.0 | 0.9 | 29.2 | 7.9 | 0.0 | 0.0 | 0.0 | 0.0 | 0.7 | 0.2 | 13.4 | 7.3 | 63.6 |
| Jeddah | 11.3 | 4.5 | 4.2 | 1.1 | 1.0 | 0.0 | 0.1 | 0.0 | 0.1 | 0.6 | 18.2 | 16.2 | 57.4 |
| mean Red Sea | 11.8 | 6.0 | 5.8 | 2.4 | 1.3 | 0.1 | 2.8 | 2.4 | 0.7 | 5.4 | 17.2 | 16.5 | 72.4 |

The values given above and in table 2.3 are averaged from incomplete NOAA NCDC precipitation datasets mean values. The total annual amount of rain, however, is of little consequence to the marine environment; of more importance is the intensity of the rainfall. When examining the original datasets¹⁶, monthly precipitation values appear to be highly variable and for many stations along the Red Sea coasts, months and even years pass without any rainfall. Within the rainy months, rainfall is usually restricted to heavy showers lasting only for a couple of hours. These intense showers may have serious effects on fringing coral reefs. As the surface of the coastal plains mainly consists of sands and silts (Plaziat *et al.*, 1998) making the desert soil almost impermeable, heavy rainfall will run off as sheet floods, transporting enormous amounts of sediment (Plaziat *et al.*, 1998). These flash floods may cause locally important coral-reef smothering and even coral mortality (Behairy *et al.*, 1992; Sheppard *et al.*, 1992).

¹⁶ These datasets can be found at: <http://ingrid.ldeo.columbia.edu>

2.3.2 Oceanography

The volume of the Red Sea has variously been estimated between 200,000 and 250,000km³ (Edwards, 1987; Sheppard *et al.*, 1992). As rainfall is extremely sparse and no permanent rivers enter the Red Sea, the total fresh water input is estimated to be less than 200mm per year (Sheppard *et al.*, 1992). Evaporation, in contrast, is very high at 2060 ± 220mm per year (Sofianos *et al.*, 2002), resulting in a very considerable water deficit which can only be made up by inflow from adjacent seas. The exchange of water between the eastern Mediterranean and the Red Sea via the manmade Suez Canal is insignificant and evidence even points to an overall outflow from the Red Sea (Edwards, 1987; Sheppard *et al.*, 1992). As a result, the replacement water has to come from the Indian Ocean and the Gulf of Aden through the Bab el Mandab.

Due to the water deficit and the lack of fresh water input, the total Red Sea salinity is very high and tends to increase by 0.13PSU per year (Edwards, 1987). This is not counteracted by the inflowing water from the Gulf of Aden as this water itself has a salinity of about 36.5 PSU, but rather is countered via the discharge of highly saline waters out of the Bab el Mandab (Sheppard *et al.*, 1992). Because the Red Sea is located in a largely desert environment, SST is also relatively high. Even below 250-300m, the water remains at a constant temperature of about 21.5°C (Sheppard *et al.*, 1992). When compared to other tropical waters where temperature drops to 10°C and less below 200-300m, the Red Sea can be considered as a unique deep water body having an extremely stable and high temperature (Sheppard *et al.*, 1992). As far as the constituents of the sea water are concerned, concentrations in the Red Sea are very low, but their distribution is not believed to differ significantly from other oceans (Edwards, 1987).

2.3.2.1 Seawater temperatures

2.3.2.1.1 Sea surface temperature

Generally, the open-water mean SST throughout the year increases from north to south, although in the extreme south of the Red Sea, SST is usually decreasing again because of the inflow of cooler water from the Gulf of Aden (fig. 2.18 and table 2.4). The area of maximum SST varies seasonally, being located around 18°-19°N in winter (November to February) and around 13-14°N in summer (August to September). A marked difference of 2-2.5°C is also noted between the Arabian and the African coast,

with the eastern coast being warmer than the western shore at the same latitude (fig. 2.18).

Lowest SST in the Red Sea is measured in February: an average of 17.5°C is found in the extreme north of the Gulf of Suez (Edwards, 1987); 21-22°C in the northern Red Sea; and ca. 26°C in the south. SST starts to rise throughout March and April, and in May, SST ranges from 24°C in the north to approximately 30°C in the temperature maximum. In summer, a maximum SST of more than 32°C is already reached in June in the south (Edwards, 1987), whereas in the northern part, the highest SST of about 29°C is only attained in August. Little changes during September but from October onwards, SST starts to fall with 2°C a month.

On average, monthly SST variability is limited to 2°C from mean (Edwards, 1987). Two exceptions exist at both extremities of the Red Sea. At the northern end of the Gulf of Suez, temperatures may drop 5 to 6°C lower than the monthly means between November and February, when cold northerly winds create an overturning of the water. At the southern end near Bab el Mandab, SST may become lower than usual in summer when the SW Monsoon causes upwelling of cooler water from the Gulf of Aden. SST variability, consequently, increases and the temperature range may reach up to 9°C in August.

The situation along the shores can be considerably different. In the shallow coastal areas, where depths are less than 50m, a higher temperature than over the open sea is recorded in summer and somewhat lower temperatures occur in winter. Figure 1.19 shows the example of the coastal waters near Jeddah as recorded by Jones *et al.* (1987).

2.3.2.1.2 *Sub-surface temperature*

Below 250-300m depth, the whole Red Sea is filled with water with a constant temperature of about 21.5°C. Because the surface water of the Red Sea proper is at all times warmer than this deep isothermal water layer, an intermediate layer exists in which temperature drops. The temperature gradient within this layer varies seasonally according to changes in temperature at the sea surface. Throughout this intermediate layer, the temperature gradient is not constant; three different sub-layers can be determined (Edwards, 1987). Immediately beneath the surface, the water column is mixed by wind-related turbulences.

Table 2.4. SST over the Red Sea in 1° by 1° cells (da Silva et al., 1994)¹⁷

| latitude °N | Longitude °E | SST January °C | SST February °C | SST March °C | SST April °C | SST May °C | SST June °C | SST July °C | SST August °C | SST September °C | SST October °C | SST November °C | SST December °C | SST annual mean °C |
|---|-----------------|----------------------|-----------------------|--------------------|--------------------|------------------|-------------------|-------------------|---------------------|------------------------|----------------------|-----------------------|-----------------------|--------------------------|
| 27.5N | 34.5E | 21.6 | 21.1 | 20.9 | 22.1 | 24.0 | 25.9 | 27.6 | 28.6 | 27.9 | 26.8 | 25.2 | 23.1 | 24.6 |
| 26.5N | 34.5E | 22.8 | 22.3 | 22.2 | 23.3 | 25.1 | 26.7 | 28.3 | 29.2 | 28.5 | 27.5 | 26.1 | 24.1 | 25.5 |
| 26.5N | 35.5E | 22.9 | 22.4 | 22.3 | 23.4 | 25.2 | 26.7 | 28.4 | 29.3 | 28.4 | 27.5 | 26.1 | 24.2 | 25.6 |
| 25.5N | 35.5E | 23.7 | 23.1 | 23.1 | 24.2 | 25.9 | 27.3 | 28.8 | 29.7 | 28.9 | 28.0 | 26.7 | 24.8 | 26.2 |
| 25.5N | 36.5E | 23.9 | 23.3 | 23.2 | 24.4 | 26.0 | 27.4 | 28.9 | 29.8 | 29.0 | 28.1 | 26.8 | 25.0 | 26.3 |
| 24.5N | 35.5E | 24.2 | 23.5 | 23.6 | 24.7 | 26.3 | 27.6 | 29.0 | 29.9 | 29.1 | 28.3 | 27.0 | 25.2 | 26.5 |
| 24.5N | 36.5E | 24.4 | 23.7 | 23.8 | 24.9 | 26.5 | 27.8 | 29.2 | 30.0 | 29.2 | 28.5 | 27.2 | 25.4 | 26.7 |
| 23.5N | 36.5E | 24.7 | 24.1 | 24.2 | 25.3 | 26.8 | 28.1 | 29.4 | 30.2 | 29.5 | 28.8 | 27.6 | 25.9 | 27.1 |
| 23.5N | 37.5E | 25.0 | 24.3 | 24.4 | 25.5 | 27.1 | 28.3 | 29.6 | 30.3 | 29.7 | 29.1 | 27.8 | 26.1 | 27.3 |
| 22.5N | 36.5E | 25.1 | 24.5 | 24.6 | 25.7 | 27.3 | 28.4 | 29.7 | 30.4 | 29.8 | 29.2 | 28.0 | 26.3 | 27.4 |
| 22.5N | 37.5E | 25.1 | 24.5 | 24.6 | 25.7 | 27.3 | 28.4 | 29.7 | 30.4 | 29.8 | 29.2 | 28.0 | 26.3 | 27.4 |
| 22.5N | 38.5E | 25.5 | 24.9 | 25.0 | 26.2 | 27.7 | 28.9 | 30.0 | 30.6 | 30.2 | 29.7 | 28.4 | 26.7 | 27.8 |
| 21.5N | 37.5E | 25.7 | 25.1 | 25.3 | 26.4 | 27.9 | 29.0 | 30.1 | 30.8 | 30.4 | 29.9 | 28.7 | 27.0 | 28.0 |
| 21.5N | 38.5E | 25.9 | 25.2 | 25.4 | 26.6 | 28.1 | 29.2 | 30.2 | 30.9 | 30.5 | 30.1 | 28.8 | 27.1 | 28.2 |
| 20.5N | 37.5E | 26.1 | 25.5 | 25.7 | 26.9 | 28.4 | 29.4 | 30.4 | 31.1 | 30.7 | 30.4 | 29.1 | 27.4 | 28.4 |
| 20.5N | 38.5E | 26.2 | 25.6 | 25.8 | 27.0 | 28.6 | 29.5 | 30.5 | 31.1 | 30.8 | 30.6 | 29.2 | 27.5 | 28.5 |
| 20.5N | 39.5E | 26.3 | 25.7 | 25.9 | 27.2 | 28.8 | 29.7 | 30.6 | 31.2 | 30.9 | 30.7 | 29.2 | 27.6 | 28.6 |
| 19.5N | 37.5E | 26.4 | 25.8 | 26.1 | 27.2 | 28.8 | 29.7 | 30.7 | 31.3 | 31.1 | 30.8 | 29.4 | 27.7 | 28.8 |
| 19.5N | 38.5E | 26.4 | 25.8 | 26.0 | 27.2 | 28.8 | 29.7 | 30.7 | 31.3 | 31.0 | 30.8 | 29.3 | 27.7 | 28.7 |
| 19.5N | 39.5E | 26.4 | 25.9 | 26.2 | 27.6 | 29.2 | 30.0 | 30.9 | 31.4 | 31.2 | 31.1 | 29.4 | 27.7 | 28.9 |
| 19.5N | 40.5E | 26.4 | 25.9 | 26.3 | 27.7 | 29.4 | 30.1 | 30.9 | 31.4 | 31.2 | 31.2 | 29.4 | 27.7 | 29.0 |
| 18.5N | 38.5E | 26.6 | 26.1 | 26.4 | 27.7 | 29.4 | 30.2 | 31.1 | 31.6 | 31.4 | 31.2 | 29.6 | 27.9 | 29.1 |
| 18.5N | 39.5E | 26.4 | 26.0 | 26.4 | 27.7 | 29.4 | 30.2 | 31.0 | 31.5 | 31.4 | 31.2 | 29.4 | 27.7 | 29.0 |
| 18.5N | 40.5E | 26.5 | 26.0 | 26.5 | 27.9 | 29.7 | 30.4 | 31.1 | 31.6 | 31.5 | 31.4 | 29.4 | 27.8 | 29.1 |
| 17.5N | 39.5E | 26.6 | 26.1 | 26.6 | 28.0 | 29.8 | 30.5 | 31.3 | 31.8 | 31.7 | 31.5 | 29.5 | 27.8 | 29.3 |
| 17.5N | 40.5E | 26.4 | 26.0 | 26.5 | 28.0 | 29.9 | 30.6 | 31.2 | 31.6 | 31.7 | 31.4 | 29.3 | 27.6 | 29.2 |
| 17.5N | 41.5E | 26.3 | 25.9 | 26.5 | 28.1 | 30.0 | 30.7 | 31.2 | 31.6 | 31.7 | 31.4 | 29.1 | 27.5 | 29.2 |
| 16.5N | 39.5E | 26.5 | 26.1 | 26.6 | 28.0 | 30.0 | 30.8 | 31.5 | 31.9 | 31.9 | 31.5 | 29.4 | 27.7 | 29.3 |
| 16.5N | 40.5E | 26.3 | 25.9 | 26.5 | 28.0 | 30.0 | 30.7 | 31.3 | 31.6 | 31.8 | 31.4 | 29.1 | 27.4 | 29.2 |
| 16.5N | 41.5E | 26.2 | 25.9 | 26.5 | 28.0 | 30.1 | 30.9 | 31.3 | 31.6 | 31.8 | 31.3 | 28.9 | 27.3 | 29.2 |
| 15.5N | 40.5E | 26.2 | 26.0 | 26.6 | 28.0 | 30.1 | 31.0 | 31.5 | 31.8 | 32.0 | 31.4 | 29.0 | 27.3 | 29.2 |
| 15.5N | 41.5E | 26.1 | 25.8 | 26.5 | 28.0 | 30.1 | 31.0 | 31.3 | 31.5 | 31.9 | 31.2 | 28.7 | 27.0 | 29.1 |
| 14.5N | 42.5E | 25.7 | 25.6 | 26.3 | 27.8 | 30.1 | 31.1 | 30.9 | 30.9 | 31.7 | 30.8 | 28.2 | 26.6 | 28.8 |
| <i>Gulf of Aden</i> | | | | | | | | | | | | | | |
| 12.5N | 43.5E | 25.6 | 25.5 | 26.2 | 27.7 | 29.9 | 31.1 | 30.3 | 29.7 | 31.0 | 30.0 | 27.7 | 26.3 | 28.4 |
| 12.5N | 44.5E | 25.6 | 25.5 | 26.3 | 27.8 | 29.9 | 31.1 | 30.1 | 29.5 | 30.8 | 29.7 | 27.5 | 26.2 | 28.3 |
| SST MONTHLY MEAN for RED SEA | | 25.5 | 25.0 | 25.2 | 26.5 | 28.2 | 29.3 | 30.3 | 30.8 | 30.6 | 30.1 | 28.4 | 26.7 | |

¹⁷ Although new, more detailed information on the SST climatology of the Red Sea is now available (cfr. figure 2.18), this 1994 data has been included for comparison with AST data over the open sea.

Consequently, diurnal SST variations are absorbed and the temperature is almost constant or drops only a little. The second sub-layer, underneath, is characterised by sharply decreasing temperatures. This layer forms the main thermocline¹⁸ in the Red Sea. Towards the bottom of the thermocline, the temperature gradient weakens and a third, rather ill-defined, sub-layer is discriminated in which temperature decreases only by about 1°C. This layer merges almost imperceptibly with the isothermal deep water below.

As the upper mixed layer is very important for planktonic life in the ocean, the depth at which the thermocline starts is significant for the primary production in the Red Sea. The top of the thermocline generally is less deep in areas where SST is higher. As a consequence, the thermocline is at its closest to the surface during mid-summer, at depths between 30 and 60m. In winter, the depth of the thermocline increases. North of 25°N, the thermocline is located below 200m in February. As a result, no thermocline is present in the bordering shallow coastal areas of the northern Red Sea during winter. South of the 25°N parallel, the thermocline is situated at less than 90m, with a minimum depth of ca. 30m near 18°N on the eastern side of the Red Sea. When surface waters are extremely cooled, the thermocline is destroyed by convection of the surface water as is often the case in the northern Gulfs where SST may drop well below 21.5°C, the mean deep water temperature, during winter.

These general trends are clearly shown in figures 2.20a and 2.20b. In these graphs, seasonal changes in temperature in function of depth are depicted for two generalised 1° by 1° grid cells from the north and south of the Red Sea respectively. Below 200-300m, the temperature becomes remarkably stable around 21.5-22°C in both cases. Besides, temperature inversion takes place in the upper water column in autumn and winter in both examples as SST is influenced by the cooling effect of the strong seasonal winds. In the north(fig. 2.20a), the top of the thermocline changes seasonally in which it clearly occurs deeper in the winter months, at around 100m, than in the rest of the year when it is situated at ca. 20-30m. The temperature gradient in the upper water layers also changes seasonally, with a more pronounced gradient in summer than in winter. In the south, the temperature gradient is larger throughout the year and is also less influenced by seasonality as the SST varies less. As a consequence, the depth of the thermocline remains more or less stable at about 50m depth (fig. 2.20b).

¹⁸ According to the definition of Robinson *et al.* (1979), the top of the thermocline is specified as the depth at which the temperature is 1.1°C (2°F) lower than the surface temperature (Edwards, 1987).

2.3.2.2 Salinity

2.3.2.2.1 Surface salinity

The salinity in the world's oceans is believed to average 35PSU and generally does not vary widely (Edwards, 1987). The Red Sea forms the exception as in this semi-enclosed basin surrounded by a desertic climate, evaporation dramatically increases salinity. In the Bab el Mandab and the southern part of the Red Sea, mean surface salinity amounts to nearly 37PSU which is similar to the water in the Gulf of Aden. Salinity may however increase to 37-38PSU in late summer and early autumn. Mean salinity steadily increases northwards to an average annual salinity of 40.5PSU at the entrance of the northern Gulfs (fig. 2.21, table 2.5). In the Gulf of Suez, salinity increases even further and concentrations of about 42.5PSU are reached in Suez Bay. This may not only be the result of increased evaporation in the Gulf of Suez, but there may also be a possible source of salts in the rocks underlying part of the Gulf of Suez (Edwards, 1987; Sheppard *et al.*, 1992). In general, salinity also increases inshore due to higher evaporation in the shallow coastal waters (fig. 2.22). In contrast to SST, salinities at any given latitude are higher along the western shores of the Red Sea than along the eastern coast and this difference sometimes amounts to as much as 1PSU (Edwards, 1987) (fig. 2.23).

Overall, seasonal variations in surface salinity in the Red Sea are limited and a clear pattern can not be recognised. Highest salinity levels are recorded in September, while the lowest levels occur in March-April. It seems that minima and maxima follow SST extremes by about a month. Although Edwards (1987) assumed that evaporation -and therefore salinity- is highest in winter, this trend was not detected in the data given in table 2.5.

2.3.2.2.2 Sub-surface salinity

Below a depth of 150m, salinity exceeds 40PSU throughout the entire Red Sea. Below 200-300m, the salinity of the deep water layer in the Red Sea becomes virtually constant at a little more than 40.5PSU. As can also be seen on figures 2.24a and 2.24b for the northern and southern part of the Red Sea respectively, the vertical gradient of salinity is largest in the southern Red Sea. In the north, salinity barely changes with depth and a salinity gradient is almost non-existent near the mouth of the northern Gulfs. Seasonal changes in the vertical distribution of salinity are limited in the south,

whereas salinity levels are overall higher in summer in the northern parts of the Red Sea. The summer profile even depicts an important drop in salinity between 50 and 100m.

Table 2.5. Surface salinity over the Red Sea in 1° by 1° cells (Levitus, 1994)

| Latitude | Longitude | Salinity January | Salinity February | Salinity March | Salinity April | Salinity May | Salinity June | Salinity July | Salinity August | Salinity September | Salinity October | Salinity November | Salinity December | Salinity annual mean |
|-----------------------------------|-----------|------------------|-------------------|----------------|----------------|--------------|---------------|---------------|-----------------|--------------------|------------------|-------------------|-------------------|----------------------|
| °N | °E | PSU | PSU | PSU | PSU | PSU | PSU | PSU | PSU | PSU | PSU | PSU | PSU | PSU |
| 27.5N | 34.5E | 40.3 | 40.1 | 40.5 | 40.0 | 40.0 | 40.1 | 40.6 | 41.6 | 41.8 | 40.3 | 40.1 | 40.4 | 40.5 |
| 26.5N | 34.5E | 40.4 | 40.2 | 40.7 | 40.1 | 40.0 | 40.1 | 40.6 | 41.6 | 41.7 | 40.3 | 40.1 | 40.4 | 40.5 |
| 26.5N | 35.5E | 40.4 | 40.2 | 40.7 | 40.1 | 40.0 | 40.1 | 40.5 | 41.5 | 41.5 | 40.3 | 40.1 | 40.4 | 40.5 |
| 25.5N | 35.5E | 39.9 | 39.9 | 40.4 | 39.7 | 39.7 | 39.7 | 40.0 | 41.0 | 41.0 | 39.9 | 39.7 | 40.0 | 40.1 |
| 25.5N | 36.5E | 39.9 | 39.9 | 40.4 | 39.7 | 39.7 | 39.7 | 40.0 | 40.9 | 40.9 | 39.9 | 39.7 | 40.0 | 40.1 |
| 24.5N | 35.5E | 39.7 | 39.8 | 40.3 | 39.5 | 39.5 | 39.5 | 39.7 | 40.7 | 40.7 | 39.8 | 39.5 | 39.8 | 39.9 |
| 24.5N | 36.5E | 39.7 | 39.8 | 40.3 | 39.5 | 39.5 | 39.6 | 39.7 | 40.7 | 40.7 | 39.8 | 39.6 | 39.8 | 39.9 |
| 23.5N | 36.5E | 39.5 | 39.6 | 40.1 | 39.1 | 39.3 | 39.4 | 39.5 | 40.5 | 40.5 | 39.7 | 39.5 | 39.8 | 39.7 |
| 23.5N | 37.5E | 39.4 | 39.6 | 40.0 | 39.1 | 39.3 | 39.4 | 39.5 | 40.5 | 40.5 | 39.7 | 39.5 | 39.9 | 39.7 |
| 22.5N | 36.5E | 39.2 | 39.3 | 39.7 | 38.8 | 39.0 | 39.2 | 39.2 | 40.2 | 40.3 | 39.5 | 39.3 | 39.8 | 39.5 |
| 22.5N | 37.5E | 39.2 | 39.4 | 39.7 | 38.8 | 39.0 | 39.2 | 39.3 | 40.2 | 40.3 | 39.5 | 39.3 | 39.8 | 39.5 |
| 22.5N | 38.5E | 39.1 | 39.3 | 39.6 | 38.8 | 39.0 | 39.2 | 39.2 | 40.2 | 40.2 | 39.5 | 39.3 | 39.8 | 39.4 |
| 21.5N | 37.5E | 39.0 | 39.2 | 39.4 | 38.6 | 38.9 | 39.0 | 39.0 | 40.0 | 40.1 | 39.4 | 39.2 | 39.7 | 39.3 |
| 21.5N | 38.5E | 39.0 | 39.1 | 39.3 | 38.6 | 38.8 | 39.0 | 39.0 | 40.0 | 40.0 | 39.4 | 39.2 | 39.7 | 39.3 |
| 20.5N | 37.5E | 38.5 | 38.7 | 38.8 | 38.2 | 38.4 | 38.5 | 38.5 | 39.5 | 39.5 | 39.0 | 38.8 | 39.3 | 38.8 |
| 20.5N | 38.5E | 38.6 | 38.8 | 38.8 | 38.3 | 38.5 | 38.6 | 38.6 | 39.6 | 39.6 | 39.1 | 38.9 | 39.4 | 38.9 |
| 20.5N | 39.5E | 38.5 | 38.6 | 38.6 | 38.1 | 38.3 | 38.4 | 38.5 | 39.4 | 39.5 | 38.9 | 38.8 | 39.2 | 38.7 |
| 19.5N | 37.5E | 38.7 | 38.8 | 38.8 | 38.4 | 38.6 | 38.7 | 38.7 | 39.6 | 39.7 | 39.3 | 39.1 | 39.5 | 39.0 |
| 19.5N | 38.5E | 38.5 | 38.6 | 38.5 | 38.1 | 38.4 | 38.4 | 38.4 | 39.4 | 39.5 | 39.0 | 38.8 | 39.2 | 38.7 |
| 19.5N | 39.5E | 38.5 | 38.5 | 38.4 | 38.1 | 38.4 | 38.4 | 38.4 | 39.3 | 39.5 | 38.9 | 38.8 | 39.1 | 38.7 |
| 19.5N | 40.5E | 38.7 | 38.8 | 38.6 | 38.4 | 38.6 | 38.6 | 38.6 | 39.6 | 39.7 | 39.1 | 39.0 | 39.2 | 38.9 |
| 18.5N | 38.5E | 38.2 | 38.3 | 38.1 | 37.9 | 38.1 | 38.1 | 38.1 | 39.0 | 39.1 | 38.7 | 38.5 | 38.9 | 38.4 |
| 18.5N | 39.5E | 38.2 | 38.2 | 38.0 | 37.9 | 38.1 | 38.1 | 38.0 | 38.8 | 39.2 | 38.7 | 38.5 | 38.7 | 38.4 |
| 18.5N | 40.5E | 38.1 | 38.2 | 38.0 | 37.9 | 38.1 | 38.1 | 38.0 | 38.5 | 39.2 | 38.6 | 38.5 | 38.6 | 38.3 |
| 17.5N | 39.5E | 37.8 | 37.9 | 37.5 | 37.6 | 37.8 | 37.7 | 37.7 | 38.2 | 38.9 | 38.4 | 38.1 | 38.2 | 38.0 |
| 17.5N | 40.5E | 37.8 | 37.9 | 37.5 | 37.7 | 37.8 | 37.7 | 37.7 | 38.2 | 39.0 | 38.4 | 38.2 | 38.2 | 38.0 |
| 17.5N | 41.5E | 37.7 | 37.8 | 37.3 | 37.7 | 37.7 | 37.6 | 37.6 | 38.1 | 39.0 | 38.3 | 38.1 | 38.0 | 37.9 |
| 16.5N | 39.5E | 37.8 | 37.7 | 37.1 | 37.7 | 37.8 | 37.7 | 37.6 | 38.1 | 39.1 | 38.4 | 38.3 | 38.1 | 37.9 |
| 16.5N | 40.5E | 37.6 | 37.6 | 37.4 | 37.6 | 37.6 | 37.5 | 37.5 | 38.0 | 38.9 | 38.2 | 38.0 | 37.9 | 37.8 |
| 16.5N | 41.5E | 37.6 | 37.6 | 37.5 | 37.7 | 37.7 | 37.6 | 37.6 | 38.2 | 39.0 | 38.3 | 38.1 | 37.9 | 37.9 |
| 15.5N | 40.5E | 37.1 | 37.3 | 37.3 | 37.2 | 37.2 | 37.0 | 37.1 | 37.7 | 38.5 | 37.8 | 37.6 | 37.3 | 37.4 |
| 15.5N | 41.5E | 37.0 | 37.2 | 37.2 | 37.2 | 37.2 | 37.0 | 37.2 | 37.7 | 38.4 | 37.8 | 37.6 | 37.3 | 37.4 |
| 14.5N | 42.5E | 36.7 | 36.9 | 36.9 | 37.0 | 37.0 | 36.9 | 37.1 | 37.4 | 37.9 | 37.5 | 37.2 | 36.9 | 37.1 |
| Gulf of Aden | | | | | | | | | | | | | | |
| 12.5N | 43.5E | 36.0 | 36.3 | 36.2 | 36.4 | 36.4 | 36.5 | 36.4 | 36.6 | 36.9 | 36.7 | 36.5 | 36.2 | 36.4 |
| 12.5N | 44.5E | 35.9 | 36.2 | 36.2 | 36.3 | 36.4 | 36.5 | 36.3 | 36.5 | 36.7 | 36.6 | 36.5 | 36.1 | 36.3 |
| 12.5N | 45.5E | 35.9 | 36.2 | 36.2 | 36.3 | 36.3 | 36.5 | 36.1 | 36.3 | 36.6 | 36.5 | 36.4 | 36.0 | 36.3 |
| Salinity monthly mean for Red Sea | | 38.7 | 38.8 | 38.8 | 38.5 | 38.6 | 38.6 | 38.7 | 39.5 | 39.8 | 39.1 | 38.9 | 39.1 | |

2.3.2.3 Water flow

2.3.2.3.1 Red Sea – Gulf of Aden water exchange

Most of the water deficit in the Red Sea is made up by inflow from the Indian Ocean through the Bab el Mandab. This thermohaline influx is not a simple northward flow, but is complicated by the different characteristics of the water in the Red Sea and in the Gulf of Aden, by the presence of the shallow Hanish sill, and by the upwelling of cool intermediate water in the Gulf of Aden (GAIW) during summer (Smeed, 1997; Smeed, 2000; Siddall *et al.*, 2002). At greater depth, saline Red Sea outflow water (RSOW) consisting of both normal Red Sea water (RSW) and denser Red Sea deep water (RSDW) is discharged over the sill throughout the year (Edwards, 1987; Sheppard *et al.*, 1992; Smeed, 1997; Johns *et al.*, 1999; Smeed, 2000; Siddall *et al.*, 2002) (fig. 2.25).

In winter, the water flow is least complex as a double-layered contra-flow system (Siedler, 1968) is established (fig. 2.25). At the surface, Gulf of Aden surface water (GASW) is driven through the Bab el Mandab by the general thermohaline circulation, compensating for the evaporation in the Red Sea. The GASW, with a mean temperature of about 26°C and a salinity of around 37 PSU (Smeed, 1997), is clearly less dense than the RSOW, being both cooler (22.5°C) and more saline (40PSU) (Smeed, 1997), and the GASW consequently overflows the RSOW. This double-layered system exists from November to early June (Siddall *et al.*, 2002) and maximum water exchange occurs during this winter system (Johns *et al.*, 1999).

In summer, the system becomes complicated by the upwelling of cooler GAIW (fig. 2.25), resulting from the strong SW monsoon in the Gulf of Aden. During the warmest months, the Red Sea surface water (RSSW) heats up, reaching a temperature of 32°C, and also is more saline (37-38PSU) (Edwards, 1987; Smeed, 1997). As the GAIW is both cooler (18°C) and less saline (36PSU) (Smeed, 1997) than the RSSW, it consequently is less dense and underflows this superficial layer. This GAIW, conversely, is less dense than the RSOW, thus forming an intermediate inflow layer between the RSSW and the RSOW (Sheppard *et al.*, 1992; Smeed, 1997; Smeed, 2000; Siddall *et al.*, 2002). Besides, the relative deep inflow of GAIW reduces the outflow of dense RSOW to about 10-15% of the wintertime flux (Maillard and Soliman, 1986) and, in order to compensate this outflow loss, the superficial RSSW flow is forced to reverse (Siddall *et al.*, 2002). As such, a complex triple-layered flow

system is created in summer. With the subsiding SW Monsoon, and the consequent retreat of the upwelled GAIW, the system gradually reverts back to the double-layered contra-flow system.

Until the mid-1990s, the origin of this three-layered flow system was largely attributed to the seasonally changing wind directions in the southern Red Sea as the winter Northwesterlies and the summer Southeasterlies respectively correspond to the dominant surface flow direction in the Bab el Mandab (Edwards, 1987; Sheppard *et al.*, 1992). Although these winds may contribute to the velocity of the surface layer, they are disregarded as being the driving forces behind the seasonal flow direction shifts (Smeed, 2000).

The inflowing GAIW quickly thins out and at about 18°N, no traces of this water body are found (Smeed, 1997). The inflowing water is believed to become quickly denser due to evaporation as it travels northwards in the Red Sea (Edwards, 1987; Sheppard *et al.*, 1992). As a result, the water sinks and becomes incorporated in the RSDW. The water renewal time in the upper 200m, therefore, is estimated by Sheppard *et al.* (1992) to be in the order of 6 years. RSDW turnover for the entire Red Sea, conversely, could be in the order of 200 years (Sheppard *et al.*, 1992).

2.3.2.3.2 General water flow in the Red Sea

The general water flow system in the Red Sea basically consists of a surface thermohaline drift from south to north and a counterflow underneath, at depths lower than 250-300m. The northward surface flow originates from the gradual decrease and increase in respectively temperature and salinity. As evaporation in the Red Sea largely overclasses freshwater input throughout the year, salinity gradually increases towards the north, from around 37PSU at Bab el Mandab to ca. 40.5PSU at the entrance of the Gulfs of Suez and Aqaba. Meanwhile, SST drops towards the north such that in winter, a temperature gradient between 26°C and 21-22°C prevails from south to north. Water flowing in from the south, thus, becomes denser as it travels to the north.

The RSDW is formed in the northern Red Sea, mainly in winter. In the Gulf of Suez, passing low pressure troughs in winter cool the water to below 18°C, while evaporation remains at the same high level (fig. 2.26). As a result, a salinity level up to 42.5 PSU can be reached in the Suez bay. This dense, heavy water consequently sinks and returns southwards as an underflow through the Gulf of Suez. Meanwhile, it gets

mixed with the warmer and less saline surface water until a homogenous water mass of 21.5°C and 40.5PSU is formed. When this dense, cool and saline water reaches the entrance to the Gulf of Suez, it starts to pour downwards, turns under the thermocline at 250-300m and returns southward in the deep Red Sea (Edwards, 1987; Sheppard *et al.*, 1992) (fig. 2.26).

A similar *turnover* occurs in the Gulf of Aqaba, although the shallow Tiran sill prevents the outflow of the Gulf of Aqaba deep water, created below 200m (Manasrah *et al.*, 2004). Plähn *et al.* (2002) have even traced two separate layers within the RSDW according to their origin in the Gulf of Suez or the Gulf of Aqaba. The deep water originating in the Gulf of Aqaba was found to be denser than Gulf of Suez-related water such that the latter was only found up to 250m above the seafloor. Besides, these authors also estimate that the Gulf of Aqaba contributes to the RSDW formation with an intensity at least 1.5 times greater than the Gulf of Suez (Plähn *et al.*, 2002; Manasrah *et al.*, 2004).

The accordingly formed RSDW is a stable deep water layer with a mean temperature of 21.5°C and a mean salinity level of 40.5PSU¹⁹. This deep water mass is markedly warmer and more saline as compared to most other ocean basins (Plähn *et al.*, 2002; Manasrah *et al.*, 2004). Weikert (1987) report the differences with the Gulf of Aden water masses: at a depth of only 150m, the Red Sea water is already 4.5°C warmer (Smeed, 1997) and 4PSU more saline and at 2000m depth, differences become even higher, being 19°C and 6PSU respectively. These enormous differences form an effective physiological barrier for the migration of mid-water or deep-sea organisms adapted to the cooler and less saline waters of the Indian Ocean and Gulf of Aden (Weikert, 1987).

2.3.2.3.3 Surface currents

Surface currents are generally weak and may vary considerably within the Red Sea. While the northern Red Sea turnover probably is the driving force behind the net water circulation in the Red Sea, surface currents are mostly influenced by the prevailing wind fields in the region. In summer, the northerly winds over the entire Red Sea cause a set of surface waves in a SSE direction in the open waters along the central axis of the Red Sea. This flow increases in speed from about 0.12ms⁻¹ in the northern

¹⁹ Not to be confused with the characteristics of the RSOW which also comprises (intermediate) RSW

two thirds of the Red Sea, to 0.24m s^{-1} south of 16°N and may reach a maximum of 0.60m s^{-1} in Bab el Mandab (Edwards, 1987). During winter, GASW enters the Red Sea through the Bab el Mandab and although this northerly drift soon weakens, it persists to the northern end of the basin. Over the northern end of the Red Sea, the surface currents, therefore, are contrary to the prevailing northwesterly winds (Edwards, 1987).

In addition, this general surface flow pattern is altered by *gyres* which occur along the central axis of the Red Sea (Clifford *et al.*, 1997; Johns *et al.*, 1999) (fig. 2.27). With average horizontal velocities of 0.5ms^{-1} and more, these currents often are more energetic than the overall surface currents (Johns *et al.*, 1999). These gyres are highly correlated with the main wind fields over the region and their interaction with the surrounding orography (Quadfasel and Baudner, 1993; Clifford *et al.*, 1997). Clifford *et al.* (1997) have noted that gyres are markedly better developed when the wind fields are oriented across the basin, hence they interact with the Red Sea Mountains, than when winds blow parallel to the Red Sea axis. In the northern Red Sea, a permanent cyclonic gyre -at least in winter- has been reported by Clifford *et al.* (1997) and Manasrah *et al.* (2004). This gyre, with a diameter of about 50-60km and a maximum velocity of about 0.4ms^{-1} in the upper 200m, is believed to accommodate the formation of intermediate water in this part of the Red Sea (Johns *et al.*, 1999; Manasrah *et al.*, 2004). The central Red Sea is dominated by two anticyclonic gyres regularly occurring near $23\text{-}24^\circ\text{N}$ and $18\text{-}19^\circ\text{N}$ respectively (Johns *et al.*, 1999). In the southern Red Sea, finally, both cyclonic and anticyclonic temporal gyres patterns have been found (Johns *et al.*, 1999).

In shallow coastal waters, currents are mostly influenced by the local seabed topography and sometimes also by tidal streams. Although these tidal streams are largely negligible in the open Red Sea, they may exceed velocities of 1 to 2ms^{-1} in more shallow waters (Sheppard *et al.*, 1992). On the whole, little is yet known about coastal currents, largely due to their local variability.

2.3.2.3.4 Tides and other temporary sea-level changes

The Red Sea is not influenced by a tidal wave originating in the Indian Ocean. Instead, the basin is characterised by a local oscillatory tide of small amplitude and semi-diurnal period. This means that while a water highstand occurs at one end of the Red Sea, low water prevails at the other end. The mean spring tide range increases towards

the two ends of the basin, averaging about 0.6m near the entrance to the Gulf of Suez and about 0.9m in the south. The northward trend of increasing tidal range continues in the Gulf of Aqaba and Gulf of Suez, reaching maxima of 1.2 and 1.5m respectively. This semi-diurnal tide fades out in the central part of the Red Sea, between 19°N and 21°N, with a nodal tide point at about 20°N. There is a second nodal tide point just north of Bab el Mandab, south of which, the Gulf of Aden tides become dominant. In addition, a subsidiary diurnal oscillation amplifies the semi-diurnal tide. Although this diurnal tide has a very small amplitude, it locally dominates, especially near the nodal tide points of the semi-diurnal tide (Edwards, 1987).

The sea level of the Red Sea not only depends on tides but is also seasonally influenced by the rate of evaporation and the balance between inflowing and outflowing water, the latter of both being the most dominant (Sheppard *et al.*, 1992). In winter, the inflow at Bab el Mandab exceeds the combined effects of the outflow and the loss by evaporation. Consequently, mean sea level rises over the whole of the Red Sea. Losses due to outflow and evaporation, conversely, dominate in summer and cause a drop in mean sea level. As a result, the sea level is approximately 0.2-0.3m below annual msl in August and September, while an elevation of 0.1-0.2m above msl occurs in December and January. The abrupt shift from summer low to winter high happens in less than a month (Sheppard *et al.*, 1992). Evaporation, nonetheless, has some effect as well, as mean sea level throughout the year is nearly 0.5m lower in the north of the Red Sea (Sheppard *et al.*, 1992).

Superimposed, the water level may also be influenced by wind stress. The consequences of strong diurnal breezes have already been discussed in section 2.3.1.1.4, but wind may have large-scale effects as well. Edwards (1987), for example, have reported elevated sea levels 2.5m above msl in the Gulf of Suez, due to exceptional, prolonged southerly winds. Besides, the prevailing southeasterly winds in winter drive surface waters southwards and under the influence of Coriolis forces, the sea level may rise on the African coast and decrease on the Arabian side respectively, resulting in local differences of 0.2-0.3m at the same latitude. Atmospheric pressure changes, finally, may influence sea level as well, although these effects are generally small in the narrow Red Sea.

2.3.2.4 Chemical oceanography

2.3.2.4.1 Dissolved-oxygen content

a. Horizontal distribution

The dissolved-oxygen (DO) content in sea water is very important for marine life as the zone of maximum photosynthesis corresponds to the zone of maximum DO concentration (Weikert, 1987). The amount of oxygen required to saturate sea water decreases with both increasing temperature and salinity. The warm and saline surface waters of the Red Sea, therefore, are close to oxygen saturation, although DO concentrations are quite low (Edwards, 1987; Weikert, 1987). Highest annual DO concentrations are found in the northern ($\pm 4.3 \text{ ml-O}^2/\text{l}$) and southern ($\pm 4.5 \text{ ml-O}^2/\text{l}$) parts of the Red Sea (table 2.6). Concentrations are minimal in the central region ($\pm 4.0 \text{ ml-O}^2/\text{l}$) between $17^\circ\text{-}20^\circ\text{N}$, corresponding to the zone of maximum annual SST. Small seasonal changes in surface DO concentrations occur according to the changes in SST and salinity (fig. 2.28).

b. Vertical distribution

DO concentrations vary little with depth in the top 100m of the water column although a sub-surface DO maximum can be distinguished, especially in the northern Red Sea where this layer is clearly recognisable at about 50m depth through most of the year (fig. 2.28a). This sub-surface DO maximum only minimises near the end of winter, most probably linked to the destruction of the thermohalocline and the consequent mixing of the surface layer (Edwards, 1987; Weikert, 1987). The depth of the maximum DO layer gradually decreases towards the south and becomes finally merged with the surface layer south of 17°N (Edwards, 1987; Weikert, 1987). Only in early winter, a small sub-surface layer of maximum DO concentration can be noticed in fig. 2.28b.

Below this sub-surface maximum, DO content rapidly decreases due to the high oxygen consumption by bacteria during the decomposition of POM (Weikert, 1987). At depths between 300-600m, a minimum is reached of about 1.5 to $1.75 \text{ ml-O}^2/\text{l}$ in the north and only 0.5 to $0.6 \text{ ml-O}^2/\text{l}$ in the central part²⁰. Similar to the surface trend, DO concentrations at these depths increases again south of 19°N , to reach values up to

²⁰ based on the analysis of the World Ocean Atlas 1994 (Levitus, 1994) database

1.0ml-O²/l near the Hanish sill, mainly due to the decreasing temperature and the vertical mixing of the water. Underneath the DO minimum level, concentrations slowly increase again and in the RSDW, values of ca. 2.0ml-O²/l have been observed (Weikert, 1987) (fig. 2.28a).

Table 2.6. Surface dissolved oxygen, phosphate, nitrate and silicate concentration in the Red Sea in 1° by 1° cells (Levitus, 1994)

| latitude °N | longitude °E | phosphate μmol | nitrate μmol | silicate μmol | dissolved oxygen ml/l |
|---------------------------------------|-----------------|-------------------|-----------------|------------------|-----------------------------|
| 27.5N | 34.5E | 0.094 | 0.743 | 1.000 | 4.311 |
| 26.5N | 34.5E | 0.072 | 0.403 | 1.000 | 4.337 |
| 26.5N | 35.5E | 0.073 | 0.408 | 1.000 | 4.341 |
| 25.5N | 35.5E | 0.050 | 0.069 | 1.000 | 4.361 |
| 25.5N | 36.5E | 0.051 | 0.075 | 1.000 | 4.370 |
| 24.5N | 35.5E | 0.173 | 0.080 | 1.000 | 4.166 |
| 24.5N | 36.5E | 0.174 | 0.087 | 1.000 | 4.178 |
| 23.5N | 36.5E | 0.040 | 0.099 | 1.000 | 4.289 |
| 23.5N | 37.5E | 0.040 | 0.105 | 1.000 | 4.308 |
| 22.5N | 36.5E | 0.124 | 0.148 | 1.000 | 4.383 |
| 22.5N | 37.5E | 0.103 | 0.159 | 1.000 | 4.318 |
| 22.5N | 38.5E | 0.125 | 0.157 | 1.000 | 4.430 |
| 21.5N | 37.5E | 0.123 | 0.227 | 1.000 | 4.164 |
| 21.5N | 38.5E | 0.124 | 0.230 | 1.000 | 4.184 |
| 20.5N | 37.5E | 0.197 | 0.451 | 2.000 | 4.046 |
| 20.5N | 38.5E | 0.167 | 0.398 | 1.592 | 4.096 |
| 20.5N | 39.5E | 0.200 | 0.455 | 2.000 | 4.066 |
| 19.5N | 37.5E | 0.136 | 0.680 | 1.000 | 4.064 |
| 19.5N | 38.5E | 0.145 | 0.454 | 1.354 | 4.086 |
| 19.5N | 39.5E | 0.160 | 0.499 | 1.454 | 4.067 |
| 19.5N | 40.5E | 0.142 | 0.690 | 1.000 | 4.061 |
| 18.5N | 38.5E | 0.116 | 0.248 | 1.333 | 4.113 |
| 18.5N | 39.5E | 0.153 | 0.415 | 1.445 | 4.056 |
| 18.5N | 40.5E | 0.121 | 0.281 | 1.333 | 4.105 |
| 17.5N | 39.5E | 0.217 | 0.638 | 1.667 | 3.945 |
| 17.5N | 40.5E | 0.188 | 0.718 | 1.651 | 4.063 |
| 17.5N | 41.5E | 0.224 | 0.726 | 1.667 | 3.964 |
| 16.5N | 39.5E | 0.125 | 1.025 | 2.000 | 4.289 |
| 16.5N | 40.5E | 0.194 | 1.232 | 1.943 | 4.227 |
| 16.5N | 41.5E | 0.134 | 1.126 | 1.652 | 4.311 |
| 15.5N | 40.5E | 0.326 | 2.059 | 2.465 | 4.254 |
| 15.5N | 41.5E | 0.330 | 2.093 | 2.444 | 4.267 |
| 14.5N | 42.5E | 0.169 | 1.575 | 12.363 | 4.513 |
| Gulf of Aden | | | | | |
| 12.5N | 43.5E | 0.234 | 0.216 | 13.337 | 4.473 |
| 12.5N | 44.5E | 0.232 | 0.342 | 14.307 | 4.490 |
| 12.5N | 45.5E | 0.230 | 0.656 | 13.264 | 4.546 |
| 11.5N | 43.5E | 0.293 | 2.209 | 6.893 | 4.602 |
| 11.5N | 44.5E | 0.260 | 1.854 | 12.369 | 4.635 |
| 11.5N | 45.5E | 0.290 | 2.481 | 8.086 | 4.661 |
| mean concentration for the Red Sea | | 0.146 | 0.568 | 1.708 | 4.204 |

A vertical DO concentration gradient does not occur in the Gulf of Suez as, because of its limited depth, the entire water column is well oxygenated. In the deeper Gulf of Aqaba, the upper 200m of the water column appears to be fairly homogeneous and

shows only small seasonal variations in DO concentrations (Badran, 2001). Below this surface layer, DO-concentration levels steadily decrease until about 3.0ml-O₂/l near the bottom (Edwards, 1987; Weikert, 1987).

2.3.2.4.2 Nutrient concentrations

a. Horizontal distribution

Similarly to other oceans, both phosphate and nitrate concentrations in the open surface water are low. Compared to the water of the adjacent Indian Ocean, the Red Sea open water even suffers a marked deficiency of nutrients, i.e. the water in the Red Sea is *oligotrophic* or even *ultra-oligotrophic* (Weikert, 1987). Inflow of water from the Gulf of Aden through the Bab el Mandab, therefore, enriches the Red Sea with nutrients and POM. Most nutrients are imported during summer, when the upwelling GAIW enters the Red Sea. In winter, the GASW inflow is poor in nutrients but rich in seston²¹ (Poisson *et al.*, 1984). The remineralisation of this seston, however, is regarded as a potential source of nutrients in the surface water (Beckmann, 1984) and, throughout the year, the water column in the southern part of the Red Sea is relatively rich in nutrients compared to the rest of the basin (Weikert, 1987) (table 2.6).

Because the imported nutrients are rapidly consumed by the plankton, the concentrations in phosphate, nitrate, and silicate steadily decrease from south to north along the axis of the basin (table 2.6). These nutrient gradients, however, are less pronounced in comparison to SST and surface salinity. Although Khmeleva (1970) (in: Weikert, 1987) reported a spectacular drop in nutrient concentrations in the surface waters north of 19°N, table 2.6 suggests that this boundary more likely occurs around 21°N. Differences in concentration between the eastern and western parts are also recorded (Morcos, 1970), but these are of minor importance (Weikert, 1987) (table 2.6).

As with temperature and salinity, the situation in the coastal shallow areas is completely different and higher nutrient concentrations are to be expected (Weikert, 1987). Based on literature review, Badran *et al.* (2005), for example, report significantly higher nutrient concentrations in the reef-bordered Gulf of Aqaba coastal waters.

²¹ Seston comprises the particulate matter (plankton including bacteria, organic and inorganic material) within the water.

b. Vertical distribution

Through the decomposition of POM by bacteria in the water, nutrients are remineralised and released in the water column. As a result, nutrient levels generally rise with increasing depth and decreasing DO concentrations (fig. 2.29). According to Weikert (1987), maximum nutrient concentrations are therefore found at the level of minimal oxygen concentrations. In the deep water, concentrations slightly rise but generally remain at a constant, relatively high level throughout the deep water layer. This trend is more pronounced in the north than in the south where the effects of inflowing GAIW are felt.

As the thermocline, and consequently also the zone of maximum DO concentration, fluctuates throughout the year, seasonal changes in nutrient concentrations are to be expected. In summer, the thermocline in the Gulf of Aqaba and the Red Sea inhibits vertical mixing of large parts of the water column, so that nutrients lost to the deep water body are not re-entering the euphotic²² zone. The surface layer up to about 60-100m (Badran, 2001), as a result, remains poor in nutrients. In winter, the thermocline is destroyed in the Gulf of Aqaba (Badran, 2001) and in the shallower parts of the northern Red Sea. Enhanced by stronger winds, the water column is consequently mixed and nutrient levels reach homogeneously high levels throughout the water column (Badran, 2001). In the Gulf of Suez, a thermocline is totally absent throughout most of the year and nutrient concentrations are homogeneously distributed in the water column. Concentrations at the surface, therefore, are usually higher than in the Red Sea, especially near the northern Suez Bay (Weikert, 1987).

2.3.2.5 Phytoplankton concentrations - primary production

2.3.2.5.1 Horizontal distribution

For most of the year, the development of a stable thermo-halocline in most of the Red Sea prevents the recycling of nutrients from deeper water to the euphotic zone. This loss in nutrients is hardly compensated by terrestrial runoff so the primary production in the Red Sea is expected to be low (Weikert, 1987), somewhat increasing from north to south. In the south, this increased productivity is largely related to the inflow of

²² Euphotic zone: layer between the surface and the compensation depth where photosynthesis can take place (Weikert, 1987).

nutrient- and plankton-rich water from the Gulf of Aden. Highest plankton input is linked to the GASW inflow in winter. Highest annual plankton concentrations are therefore found between 16°N and 18°N. Further north, these immigrating organisms soon die because of an increasingly hostile environment and planktonic concentrations consequently decrease and so does the primary production (Weikert, 1987). Within the central and northern parts of the Red Sea, concentrations, however, remain relatively stable (Weikert, 1987). The northernmost Red Sea and the Gulfs of Suez and Aqaba, conversely, encounter higher productivity levels because of vertical mixing, especially during winter. Evidently, the shallow coastal coral-reef waters show different, more intense (Glorieus, 2006), productivity patterns.

Generally, two periods of increased plankton production occur, one in winter and the other in summer (Weikert, 1987). The winter eutrophication is related to vertical water mixing (Badran, 2001) and predominates in the northern and southern extremities of the Red Sea. The summer eutrophication is confined to the coastal zones and both the northern and southern ends of the Red Sea, whereas the vast oceanic region between 27°N and 18°N is not influenced (Weikert, 1987). Within the central Red Sea and Gulf of Aqaba, blooming of blue-green algae, especially *Oscillatoria erythraeum* may nevertheless occur in summer. As these dinoflagellates are capable of absorbing atmospheric nitrogen dissolved in the surface water, they outcompete other phytoplankton species when nutrients become limited, and thus illustrate the general depletion of nutrients. These patchy algal blooms, also called *sea dust*, produce coloured water which is believed by some to have given rise to the naming of the Red Sea (Weikert, 1987).

With the development of special spaceborne sensors, like SeaWiFS or MODIS, much information is now available on the horizontal distribution of Chlorophyll-*a* (Chl-*a*) concentrations in the upper surface layers of the world's oceans. Although it is not the scope of this work to go into much detail about these datasets, one example of a remote-sensing-derived product is given. Figure 2.30 represents four seasonal composites of Chl-*a* concentrations over the Red Sea for the year 2003. These composites are derived from MODIS level-3 data products with a spatial resolution of 4km²³. In general, a clear difference is seen between the relatively high concentrations in the southern part of the Red Sea and the poorer northern Red Sea waters. On each

²³ available online at: <http://oceancolor.gsfc.nasa.gov>

seasonal composite, the coastal water and the shallow Gulf of Suez show higher Chl-*a* concentrations than the open water. Seasonal trends are not uniform throughout the region: in the northern Red Sea, Chl-*a* concentrations are highest in winter, probably linked to vertical mixing and the winter eutrophication phase recognised by Weikert (1987), while in the south, Chl-*a* concentrations are highest in autumn and possibly also during the summer although this is masked in the image due to persistent cloud cover. Here, Chl-*a* concentrations remain relatively high in winter as well, because of migrating plankton from the Gulf of Aden, but concentrations markedly drop in spring, at least in the central part of the southern Red Sea. As figure 2.30 only depicts a one-year-cycle of the Chl-*a* concentrations in the Red Sea, no general conclusions about inter-annual and/or seasonal changes could be drawn.

2.3.2.5.2 Vertical distribution

During most of the year, light intensities at the surface of the Red Sea and the Gulf of Aqaba are above the optimum for most phytoplankton species, so that photo-inhibition takes place. Most phytoplankton, therefore, occur deeper in the water. In summer, the bulk of the phytoplankton standing stock is situated between 50 to 80m (Weikert, 1987; Badran, 2001). In the Red Sea, Chl-*a* has been found to accumulate within the thermo-halocline, near the bottom of the euphotic zone. The existence of such a *subsurface chlorophyll maximum* is typical of nutrient-poor and warm water masses (Lorenzen, 1976; Weikert, 1987; Badran, 2001). This summer distribution is occasionally changed by the blooming of blue-green algae as these phytoplankton species can resist high light intensities and, therefore, occur closer the surface (Weikert, 1987).

In winter, light intensities are lower and phytoplankton concentrations peak in the upper 50m of the Red Sea (Weikert, 1987). In the Gulf of Aqaba, the water is more turbid and the zone of photo-inhibition is confined to the upper 20m. Underneath, high Chl-*a* and primary production values are recorded down to 200m depth (Badran, 2001), while Coccolithophore blooms occur down to 400m as a result of the mixing of the water (Weikert, 1987). Little is known about the vertical distribution of primary production within the Gulf of Suez (Weikert, 1987). However, as the water is well mixed, the high Chl-*a* concentrations observed at the surface (cfr. fig. 2.30) (Glorieus, 2006) are most probably representative for the entire water column.

2.3.2.5.3 Light absorption

Thanks to the low concentrations of seston in the Red Sea, the euphotic zone extends to about 100m deep during summer. This euphotic zone thus stretches almost to the physical limit of penetration of light in sea water. Some regional differences however occur. Water is clearest in the northern part of the Red Sea, with a horizontal visibility up to 40-60m in the Gulf of Aqaba and along the Egyptian coast. Towards the central Red Sea, visibility decreases to 30-35m and in some places in the southern Red Sea, visibility drops to 5m or less as a result of increasing resuspension of sediments (Hassan *et al.*, 2002).

In winter, the euphotic zone becomes somewhat restricted due to vertical mixing in the northern parts of the Red Sea, the Gulf of Aqaba and the Gulf of Suez. Especially in the Gulf of Suez, the water is more turbid due to its shallowness and soft substrates. Also in the extreme south, in the vicinity of Bab el Mandab, turbidity levels are higher as sediments in the narrow and undep Bab el Mandab are resuspended, and the euphotic layer becomes restricted to about 30-60m (Khmeleva, 1970; Petzold, 1986; Weikert, 1987).

2.3.2.6 Conclusions for coral-reef growth

Coral reefs are formed on the structural highs in the upper 100-150m of the water column. Although conditions in the shallow coastal areas are often more extreme as described before for the open Red Sea water, their physical and chemical characteristics mostly favour coral growth. Salinity and SST fall within the range of physical boundary conditions, although often near the upper limit. As corals are adapted to survive in nutrient-poor marine environments, they are very well suited to the Red Sea. Moreover, as nutrient levels are exceptionally low even compared to other oceans, macro-algae are less competitive in the struggle for the available space; in natural conditions, reefs, therefore, are rarely overgrown by macro-algae. Besides, as tidal sea-level changes are limited, most reefs are able to build up almost to mean sea level. The water column, finally, is very clear because of the low seston content and the restricted input of terrestrial sediments by rivers, except maybe in the northern and southern extremities of the Red Sea. As a result, the euphotic zone almost stretches down to the physical limit of light penetration in sea water at about 100m depth. The higher turbidity levels in the Gulf of Suez, Bab el Mandab, and the southern shelf zones, conversely, translate in reduced coral-reef formation as will be seen in following section. Occasional extreme conditions, on the other hand, may have

devastating effects on coral reef prosperity. Examples are given of strong winds exposing coral reef flats; intense showers bringing sediments to the coastal zone which may locally smother the corals; periodic phytoplankton blooms restricting light conditions in the water column; and extreme temperature rises surpassing the temperature threshold. In general, the Red Sea appears to be a very stable and suitable environment for coral-reef growth.

2.4 COASTAL ECOSYSTEMS

2.4.1 Introduction

Because of its unique configuration, the Red Sea acts biogeographically as a trap for larvae and seeds imported through the Bab el Mandab (Behairy *et al.*, 1992; Sheppard *et al.*, 1992). As a result, the Red Sea appears to have the highest diversity of corals west of India (Veron, 2000). Due to its isolated position and its location amongst deserts, the Red Sea also contains some of the most northerly reefs and mangroves in the world (Head, 1987a). Coral-reef diversity increases south to north, with the exception of the northern Gulf of Suez and Gulf of Aqaba which maintain lower diversity levels, whereas the diversity in mangroves and seagrasses decreases with latitude. Most of the restrictions to species distribution are seemingly related to increased salinity levels, rather than lowering SST (Head, 1987a).

The semi-enclosed, isolated position of the Red Sea might lead one to expect high levels of endemic species, enforced by the extreme physical environment which brings most marine species to the limits of their physiology. The sea-level drop during the Last Glacial Maximum and the associated hypersaline marine environment, however, has killed all marine life. As a result, the Red Sea has only been recolonised in the last 10,000 to 15,000 years, leaving limited time for evolutionary changes. Some scientist, conversely, believe that this sudden colonisation may itself have forced species to adapt, leading to endemism at least at the sub-species level (Head, 1987a; Sheppard *et al.*, 1992). Whatever the cause, only about 17% and 5% of respectively fish and corals are believed to be endemic to the Red Sea (Head, 1987a; Sheppard *et al.*, 1992; Veron, 2000). Care, however, should be taken in interpreting these figures as it is not always straightforward to identify an endemic species and numbers are revised frequently (Veron, 2000).

An interesting new path for species migration to the Red Sea might be the man-made Suez Canal, the so-called *Lessepsian migration*. Some Red Sea fish and mollusc species have migrated to the Mediterranean but very few species have accomplished the reverse migration. The Bitter Lakes with current salinity levels of 41PSU may form an important barrier to the migration of Mediterranean species not used to such high salinity concentrations (Head, 1987a).

Important for the distribution of coastal ecosystems is the type of shores bordering the Red Sea. Shore profiles differ widely in the region, ranging from cliffs, vertically rising 30 to

40m above msl, to wide, horizontal expanses of beach rock and sand (Jones *et al.*, 1987). Most rocky shores along the Red Sea are formed by raised fossil, late Neogene coral reefs. These cliffs are often undercut by *notches* (fig. 2.31a) created by physical erosion due to wave action; bioerosion by molluscs, chemical solution by seawater; or any combination of these. In other places, flat beaches occur, forming plate-like formations which gently slope to the sea. Sandy beaches, commonly, are formed in embayments and in sheltered lagoons or back reefs (fig. 2.31b). In very sheltered occasions, especially in the southern Red Sea, mudflats may be deposited as well. Almost without any exception, sands or muds have been deposited on top of beach rock. Besides, these soft deposits are often thin and the beach rock may appear at the surface, especially towards the low-tide mark (Jones *et al.*, 1987).

2.4.2 Coral reefs

2.4.2.1 Geographical aspects

Until the mid-1970s, it was assumed that fringing reefs line both coasts of the Red Sea over its entire length. Even in 1987, Longhurst and Pauly still wrote that '*the longest fringing reef ... lies along the Red Sea coastline, over a total length of 4500km*' (Sheppard *et al.*, 1992). This general misunderstanding was the result of the limited accessibility to the southern part of the Red Sea and the consecutive extrapolation of the known situation in the north (Behairy *et al.*, 1992; Sheppard *et al.*, 1992). The maps represented in the World Atlas of Coral Reefs (Spalding *et al.*, 2001), which have been derived from satellite data, probably are the first to give a detailed regional overview of the distribution of coral reefs in the Red Sea (fig. 2.32).

2.4.2.1.1 Coral-reef types

The complex geological structure of the Red Sea makes it difficult to apply the general large-scale geomorphological classification presented in section 1.1.4.1 to the reef structures observed. As a result, various additional classes have been proposed by different authors, although most of them merely were specifications of the general categories (Sheppard *et al.*, 1992). Therefore, only two additional geomorphological classes, being *coral carpets* (Riegl and Piller, 1997) and *algal reefs* (Sheppard, 1985a), have been retained as they appear significant for the Red Sea marine environment.

a. Fringing reefs

Fringing reefs have developed near the continental shores as well as on alluvial fan deposits (Behairy *et al.*, 1992). They are the basic reef type in the Red Sea and dominate most of the shorelines in the north. They greatly vary in areal extent from the minimal ‘*contour reefs*’ (Fishelson, 1980) only 3 to 4m wide in the Gulf of Aqaba, to the large fringing reefs offshore Sudan which extend to over 1km offshore and which may have a substantial 10m deep lagoon in behind (Head, 1987b).

b. Barrier reefs

True barrier reefs as defined by Darwin as steady growing reef systems in a subsidence environment, do not occur in the Red Sea (Head, 1987b). Barrier-like structures often extending over several kilometres, conversely, are common off most coasts of Sudan, Egypt and Saudi Arabia (Head, 1987b). Their distribution seems to depend on the Red Sea tectonics as they are mainly founded on the seaward edges of large fault blocks (Berry *et al.*, 1966; Braithwaite, 1982; Head, 1987b; Guilcher, 1988) or on top of elongated salt diapirs (Head, 1987b; Guilcher, 1988; Sheppard *et al.*, 1992). These ‘*elongated, generally narrow frameworks running in a NW-SE direction, i.e. the general trend of that (Red Sea) sea*’ were defined by Guilcher (1988: 399) as ‘*ridge reefs*’. As this term does not imply any significant difference concerning the modern morphology of these reef systems, ‘barrier reef’ is used in the Red Sea context as a generic term for any offshore, linear system of reefs (Behairy *et al.*, 1992).

c. Atolls

Atolls are not well developed in the Red Sea. Different small atoll-like structures are reported along its entire length – e.g. Shaab el Erg reef north of Giftun Island- but only Sanganeb Reef near Port Sudan is generally recognised as a true atoll (Head, 1987b). The formation of most atoll-like reef structures is associated with smaller salt diapirs.

d. Patch reefs

Many reefs without a clear linear structure are defined as patch reefs. In scale, they vary from very small, simple *coral on coral* structures to large patches without clear ecological zonation but extending over tens of square meters and more. The smallest patches –sometimes called *coral heads* or *reef patches*- are commonly found in sheltered areas, such as lagoons or back reef areas, and are more widespread in the

southern Red Sea (Behairy *et al.*, 1992). They reach the low-tide level and are formed by aggregations of a few enormous coral colonies, or sometimes merely of a single *Porites* colony several meters across (Behairy *et al.*, 1992). The larger patch reefs grow in shallow depths, generally less than 20m, in a more exposed hydrodynamic environment (Riegl and Piller, 1999). They are considered by Riegl and Piller (1999) as an intermediate form between a coral reef and a coral carpet.

e. Coral carpets

During their research in the northern part of the Red Sea, Riegl and Piller have encountered extensive framework-building coral communities which, however, had not evolved to real reef structures (e.g. Piller and Pervesler, 1989; Riegl and Piller, 1997). Such coral carpets (*sensu* Reiss and Hottinger, 1984) are defined by Riegl and Piller (1999: 242) as ‘*more or less continuous veneers of coral framework following the existing seafloor morphology ... not distinctly three-dimensional*’ (fig. 2.33).

In the northern Red Sea, three different types of coral carpets are distinguished (Riegl and Piller, 1999) depending on the dominant coral genus: *Porites* carpets, *Faviidae* carpets, and *Stylophora* carpets. The *Porites* carpets are rigid, upward-oriented frameworks built out of numerous adjacent columnar *Porites* colonies growing directly next to each other. They generally are found between 5 and 15m with an average coral cover between 60 and 90%. These carpets are not found in the Gulf of Suez or in the Gulf of Aqaba. At greater depths, the *Porites* carpets are commonly replaced by *Faviidae* carpets. The depth at which this transition takes place depends on the light availability, being deeper in clearer water. The *Faviidae* carpets are made up of a diverse array of small, massive *Faviidae* species forming a compact framework. They generally are smaller in size than the *Porites* carpets but are the most widespread coral community in the northern Red Sea and the Gulf of Aqaba. These coral carpets are mainly situated between 10m and approximately 30-45m depth. The *Stylophora* carpets, finally, are unique to the Gulf of Suez and only occur nearshore, north of Ras Zafarana. These carpets form dense thickets with fused branches entirely made up of coral skeletons of which only the colonies on the edges are still alive (Riegl and Piller, 1999).

f. Algal reefs

In the southern Red Sea, a special reef type is distinguished which has not been built by corals but by algae. These algal reefs (Sheppard, 1985a) are most common in the sheltered environment of the broad, sandy continental shelf along the southern Saudi Arabian Red Sea shores. They are one of the few living examples of algal reefs outside the Caribbean (Sheppard *et al.*, 1992). These algal reefs rise up from 2 to 4m depth, developing steep sides which reach up to the low tide level. Few and sparse coral communities are found on them; most conspicuous are the dense *Sargassum* algae whose fronds float in thick mats at the sea surface (Sheppard *et al.*, 1992).

2.4.2.1.2 Coral-reef distribution

a. Gulf of Suez

The coral reefs in the Gulf of Suez (fig. 2.34) are generally less developed than in the rest of the Red Sea and Gulf of Aqaba (Fouda, 1995). Although the physical environment is extreme for the survival of corals –winter temperatures near 18°C and salinity levels approaching 41PSU- the main constraint appears to be the shallow depth of the Gulf of Suez and its resulting murky waters. This is reflected in the dominance of branching *Acropora* and *Stylophora* colonies which are ideally suited for passive rejection of sediments in low energy conditions (Sheppard *et al.*, 1992; Pilcher and Alsuhaibany, 2000).

In the northernmost part and along the eastern shores, only small patch reefs, 1 to 3m high, occur which are situated on a calcareous sandy and silty substrate up to 600m offshore (Sneh and Friedman, 1980). Along the western coastline, reefs generally are better developed and a continuous fringing reef stretches from around 50km south of Suez to Ain Sukhna. Its reef flat extends 30-40m offshore and slopes gently to a sandy bottom at 4 to 5m depth (Sheppard *et al.*, 1992). Towards the southern end of the Gulf of Suez, coral reefs become more abundant both along the Sinai and the Egyptian coasts. On the eastern shore from El-Tur onwards, different barrier reefs run parallel to the coast at a distance of 200 to 2000m offshore (Sneh and Friedman, 1980). The coral reefs around Ashrafi Islands and the southern tip of Sinai form some of the largest reef complexes in the Red Sea (Sheppard *et al.*, 1992).

b. Gulf of Aqaba

Most of the shorelines of the Gulf of Aqaba (fig. 2.34), up to Ras Mohammad at the southern tip of the Sinai, are made out of cliffs steeply plunging to depths of 1800m and more, leaving only limited space for narrow, so-called contour reefs to develop. In some embayments or in front of old alluvial fans, the reef may extend as much as 1km offshore but it is only near the shallow Tiran sill that extensive soft substrates provide space for a complex of coral reefs and seagrass beds (Sheppard *et al.*, 1992; Pilcher and Abu Said, 2003).

c. Northern Red Sea

In the northern Red Sea (fig. 2.34), the topography becomes more complex and different reef types have developed on the available shallow substrate. Most of the shoreline, however, is bordered with fringing reefs. In the north, they are usually narrow, extending only a few tens of meters offshore (Sheppard *et al.*, 1992; Pilcher and Abu Said, 2003). Here, the outward growth is generally restricted by the absence of sufficient shallow substrate. This is characterised by the typically steep, vertical slopes on most of these reefs (Behairy *et al.*, 1992). Towards the south, the reef flat may broaden and reefs may extend 1km seawards. Besides, large Pleistocene alluvial fans have pushed the fringing reef offshore. On these fans, beaches are well developed and large backreef lagoons parallel to the shoreline are formed (Sheppard *et al.*, 1992). Resultingly, different series of fringing reefs may run parallel to the coast as well (Behairy *et al.*, 1992).

d. Central Red Sea

Coral reefs in the central Red Sea (fig. 2.35) mostly are similar to the ones in the north. The Red Sea basin is widest in this part and offers a correspondingly wide range of reef morphologies. The only true atoll, Sanganeb Reef, recognised in the Red Sea is situated here. In general, the reef flats of fringing reefs tend to broaden and wider, deeper lagoons are developed. From these latitudes towards the south, mangroves become more abundant along the mainland shorelines (Sheppard *et al.*, 1992).

Two remarkable reef structures are situated along the Saudi Arabian coast. One is the *Wadj Bank* which is situated around the islands offshore Al Wadj and contains extensive seagrass beds, coral reefs and mangroves (Al-Muhandiss and Al-Ruweisy, 1984; Ormond *et al.*, 1984a, b, c; Behairy *et al.*, 1992; Spalding *et al.*, 2001). The

other is the so-called *Little Barrier Reef* (Sheppard, 1985b; Behairy *et al.*, 1992; Spalding *et al.*, 2001) consisting of a series of submerged limestone platforms –mostly 1 to 7km wide and at a depth between 30 and 50m- running parallel to the shoreline from Al Wadj in the north to Jeddah in the south, a distance of approximately 500km. These platforms are separated from the coastline by water well over 100m deep and 5 to 20km wide (Behairy *et al.*, 1992). The precise formation of these structures is not yet known.

e. Southern Red Sea

From around 20°N, coral reefs, and especially fringing reefs, become more restricted along the Saudi Arabian coast of the southern Red Sea (fig. 2.36) as the continental shelf broadens and mainly consists out of soft substrates which are less favourable for coral-reef development. Muddy substrates and mangroves, alternatively, become dominant, pushing significant reef development further offshore. Towards the south, more and more fringing reefs are even completely replaced by mangroves or algal reefs inhabiting sandy shores and sandy sub-littoral habitats. A similar situation exists along the Eritrean coast, where only rudimentary reefs are formed. More abundant fringing and patch reefs, conversely, are common around both the limestone and volcanic components of many islands like the Saudi Arabian Farasan Archipelago and the Dahlak Archipelago, offshore Eritrea (Sheppard *et al.*, 1992).

2.4.2.2 Ecological aspects

2.4.2.2.1 Coral diversity

According to the overview given by Veron (2000), 67 genera and 340 species (of which 18 are endemic) of hermatypic zooxanthellate corals are known in the Red Sea (annex II). Species diversity, supposedly, is highest in the central part of the Red Sea as here, annual seawater temperatures are higher compared to the north, while more suitable substrate is available than in the south (Behairy *et al.*, 1992). For the northern part of the Red Sea, Head (1987b) further differentiated between the Gulf of Suez, the Gulf of Aqaba and the northern Red Sea proper. With the exception of a few genera endemic to the Gulf of Aqaba, like *Caulastrea* and *Euphyllia* (Head, 1987b), the coral diversity in the Gulf of Aqaba and the northern Red Sea nearly is similar. Coral

diversity in the Gulf of Suez, in contrast, is remarkably lower due to its less favourable coral-reef environment (Head, 1987b).

Care, however, should be taken when interpreting diversity data as, first of all, they result from different sources and usually date back to the mid 1980s–early 1990s (Head, 1987b; Behairy *et al.*, 1992). Secondly, most information is gathered at some specific localities scattered throughout the Red Sea such that some parts of the Red Sea are relatively undersampled, especially the Gulf of Suez and the southern part of the Red Sea. Some species regarded as endemic for the moment may, accordingly, be found in other locations in future (Veron, 2000).

2.4.2.2 Ecological zonation

As the coral-reef species distribution in the Red Sea varies according to the marine environment, and thus latitude, so will also the constitution of the dominant coral communities²⁴. Sheppard (1988) and Sheppard and Sheppard (1991), for example, have differentiated 13 distinctive coral communities along the Saudi Arabian Red Sea shores, most of them related to their latitudinal position in the Red Sea (Sheppard *et al.*, 1992). The distribution of coral species, moreover, is also determined by their hydrodynamic exposure and the light availability. While wave exposure is related to the horizontal as well as the vertical position on the reef, the light availability is defined by water clarity and depth (Head, 1987a; Sheppard *et al.*, 1992).

Information on the ecological zonation (and related coral-cover percentages) on the coral reefs of the Red Sea has mostly been collected on the fringing reefs of the northern Red Sea (Head, 1987b; Sheppard *et al.*, 1992). While the general trends discussed below may remain valid for other fringing reefs in the region, albeit with a different community composition, care should be taken when applying these schemes to other reef types or in markedly different environments, e.g. the shallow shelfzones in the southern Red Sea.

a. Horizontal zonation

The physical environment of the Red Sea, especially the relatively calm water and the limited tidal changes, favours coral growth up to the mean summer sea level (Head, 1987b). The conditions on the reef flat, however, are often extreme as corals growing

²⁴ community: a collection of species occurring in the same place at the same time (Fauth *et al.*, 1996)

here suffer the full impact of wave exposure, potential photo-inhibition, UV-B radiation, and emersion in the case of catastrophic low sea level (Fishelson, 1973; Head, 1987b). This harsh environment, therefore, excludes more sensitive coral species, while occasionally causing partial or total mortality in the more resistant coral colonies (Head, 1987b). These lethal conditions, fortunately, are not so frequent to totally prohibit coral growth and some of the most resistant species easily grow under these circumstances besides a number of fast-growing, short-lived species (Head, 1987b). The latter species, e.g. the fast-growing branching *Stylophora* (Head, 1987b) and some *Acropora* species (Riegl and Piller, 1999), generally are the most abundant. The top of massive, resistant colonies may be killed as they reach mean sea level, whereas the coral continues to grow laterally, forming *micro-atolls* (Scoffin and Stoddart, 1978) characteristic for many reef flats in the region (Head, 1987b).

Overall, coral diversity and live coral cover (only 20% on average along the Egyptian coast; table 2.7) is low on these reef flats (Sheppard *et al.*, 1992; Pilcher and Abou Zaid, 2003). Conditions usually are least favourable in the central part of the reef flat and the communities in this zone are composed by only a small number of coral species, usually 10% of the total coral diversity in the area. Besides, no single species dominates the community (Head, 1987b). The coral colonies are small and only cover limited substrate, ca. 6% of the total available surface, whereas algae usually are better adapted to this environment and cover many shallow reef flats in the Red Sea with fast-growing lawns (Benayahu and Loya, 1981; Head, 1987b).

The ecological zonation on fringing reef flats is very patchy and probably responds to subtle changes in depth and wave exposure. Seawards from the central reef flat, coral growth improves although it may be interrupted by a storm rubble belt and/or bare rocky substrates where heavy waves constantly break (fig. 2.37). Conditions, conversely, become worse towards the shore as water exchange is greatly reduced, leading to a depletion in oxygen and particulate matter, and a higher diurnal temperature fluctuation. Coral growth, consequently, is greatly reduced and only one coral species, *Stylophora pistillata*, has been frequently recorded in this zone. Soft corals, especially *Tubipora* and *Xenia* species, algae, and seagrass, in contrast, are better adapted to this environment (Head, 1987b).

The water exchange is better on patch and barrier reef flats and coral growth, therefore, is usually more abundant. The windward reef flat communities are similar to those of fringing reef flat as they are also characterised by fast-growing species,

especially *Stylophora* and micro-atolls. On the leeward side, sand becomes more dominant, interspersed with rocky *knolls* mainly composed of *Porites* communities (Head, 1987b) (fig. 2.38). Although the water exchange becomes more restricted in the lagoons, coral growth may still be abundant. Here, coral cover varies considerably, suggesting that the environmental parameters may quickly change both in space and time. In shallow lagoons, rocky outcrops are mostly covered with *Stylophora pistillata* although *Favia*, *Platygyra*, *Cyphastrea*, *Porites*, and *Millepora* species may also be present. In deeper lagoons, small coral heads are formed, mainly by *Porites* colonies (Head, 1987b).

Table 2.7. Average live coral cover percentages estimated on different reef zones along the Egyptian coastline (source: GEF, 1977 in: Pilcher and Abou Zaid, 2003).

| | reef zone | | | |
|------------------------|------------|------------|------------|------------|
| | reef flat | reef edge | reef wall | reef slope |
| north of Hurghada | 30% | 65% | 68% | 35% |
| Hurghada - Safaga | 18% | 25% | 50% | 20% |
| Safaga - El Quseir | 16% | 45% | 33% | 20% |
| El Quseir - Marsa Alam | 14% | 25% | 50% | 5% |
| Marsa Alam - Hamatah | 11% | 20% | 45% | 12% |
| Hamatah - Berenice | 12% | 20% | 22% | 10% |
| Berenice - Shalatein | 20% | 11% | 12% | 45% |
| Shalatein - Halaib | 35% | 48% | 85% | 62% |
| <i>average</i> | <i>20%</i> | <i>32%</i> | <i>46%</i> | <i>26%</i> |

b. Vertical zonation

From the exposed and extreme environment of the reef flat, coral diversity increases with depth along the reef slope. At the upper reef slope, coral growth is still largely restricted by turbulence and excessive wave energy. Light availability, however, starts to decrease with increasing depth and even in the clearest waters a lower depth limit to hermatypic coral growth is set. Besides, loose sediments at the base of the reef slope may become dominant, additionally restricting the area for reef growth (Head, 1987b). A maximum in coral diversity, therefore, is reached between 5 and 30m (Sheppard *et al.*, 1992). In the Gulf of Aqaba, highest diversity numbers are exceptionally found at a depth of 30m which is markedly deeper than other places in the Red Sea and even most regions of the Indo-Pacific. This proves the very low turbidity of the water in the

Gulf of Aqaba and at depths of 110 to 120m, some of the deepest hermatypic, zooxanthellate corals of the world are found (Sheppard *et al.*, 1992).

Live coral cover does not exactly follow this pattern. On most fore reef slopes, live coral cover is usually less than 50%, although coral cover percentages between 60 and 80% are common on some parts depending on the degree of exposure (table 2.7). These high cover percentages are usually formed by a few dominant species, implying that high coral cover is generally not related to high coral diversity. One coral species, on the other hand, rarely dominates the entire community and coral diversity, consequently, is largely independent of coral cover as well (Sheppard *et al.*, 1992).

Head (1987b) has proposed a general model for the distribution of coral communities along a reef slope in the Red Sea based on multivariate analysis of field data, especially from Sudan (fig. 2.39). Although similar to a model proposed by Riegl and Piller (1997) for Egyptian coral reefs (table 2.8, fig. 2.40), it may be subject to changes when more regionally spread data becomes available.

At the reef crest, the coral community is mainly dominated by branching *Acropora* colonies, although *Pocillophora verrucosa* is more common at the most exposed sites. In semi-exposed locations, hermatypic corals may be totally replaced by soft coral species forming a *Millepora* sub-community. On the sheltered upper reef slopes, the fore reef becomes occupied by a sheltered, shallow community dominated by *Porites* species, although other species such as *Acropora hemprichi*, *Pocillopora* species, and various massive *Faviidae* may occur as well. In very sheltered, shallow environments, *Porites*, however, may exclude most other coral species and may dominate up to 80% of the live coral cover (Sheppard *et al.*, 1992). This is especially the case at the leeward side of patch reefs or barrier reefs where a typical *Porites* ridge sub-community is distinguished (Head, 1987b; Riegl and Piller, 1997; Riegl and Luke, 1998; Riegl and Piller, 1999; Riegl and Piller, 2000a)

Many reef crests in the Indo-Pacific region, in contrast, are dominated by a *coralline algal ridge* which is elevated about 0.3 to 0.5m above the reef flat. In the Red Sea, crustose coralline algae may dominate the reef crest as well, covering 50 to 90%, but never rise to form an algal ridge as this requires very high wave energy conditions which are not present in the Red Sea (Sheppard and Sheppard, 1985; Sheppard *et al.*, 1992).

Table 2.8. Vertical ecological zonation (with indicator species) and average live coral cover percentages on northern Red Sea reefs (Riegl and Velimirov, 1994; Riegl and Piller, 1997; Riegl and Piller, 1999; Riegl and Piller, 2000a)

| reef zones | exposed | semi-exposed | sheltered |
|------------|--|--|--|
| reef crest | <i>Pocillopora verrucosa</i> , <i>Acropora gemmifera</i> , <i>Stylophora mordax</i> Average cover: 43±18% | <i>Stylophora pistillata</i> <i>Acropora secale</i> Average cover: 48±10% | <i>Stylophora pistillata</i> , Faviidae Average cover: 24±17% |
| reef edge | <i>Acropora hyacinthus</i> group Average cover: 54±11% | <i>Millepora dichotoma</i> Average cover: 58±16% | <i>Porites lutea</i> Average cover: 68±30% |
| reef slope | Various <i>Acropora</i> , diverse without clear dominance Average cover: 59±18% | <i>Millepora dichotoma</i> and various massive species Average cover: 56±14% | <i>Porites lutea</i> and various massive species Average cover: 85±29% |
| slope base | Tabular <i>Acropora</i> (<i>A. clathrata</i> , <i>A. divaricata</i>) Average cover: 58±25% | <i>Acropora hemprichi</i> Average cover: 29±6% | Tabular <i>Acropora</i> (<i>A. clathrata</i> , <i>A. divaricata</i>) Average cover: 26±11% |

Algal spur and groove systems also require high wave energy conditions, but less than algal ridges (Sheppard, 1981). Although questioned by some (e.g. Walker, 1987), examples in the Red Sea have been reported from the coasts of the Sinai (Sneh and Friedman, 1980), the Egyptian Red Sea coast and the Little Barrier Reef (Sheppard *et al.*, 1992). The spurs, commonly covered with the coralline algae *Porolithon*, form outward projections into the prevailing wave direction. They are built up to the low tide level at their reef crest base, gradually dipping seawards and fading away when wave energy becomes too low. The spurs are very strong calcareous structures which may persist for thousands of years such that spur and groove systems are known from elevated fossil reefs as well as drowned reef crests at 50m depth (Sheppard, 1981; Sheppard *et al.*, 1992). These spurs, 2 to 3m wide, are separated by steep-sided sandy grooves. These grooves dissipate the high wave energy projected on the front reef and form channels along which the reef sediments are removed. As a result, coral cover is generally low in these grooves (Sneh and Friedman, 1980; Sheppard *et al.*, 1992). As the size of these spur and groove systems mainly depend on wave energy and as the Red Sea is not a high wave energy environment, the spur and groove systems recorded, however, are not very large when compared to some systems in the Pacific Ocean (Sheppard *et al.*, 1992).

In medium wave energy sites with light energy values at about 45% of the surface levels, the reef slope is dominated by an intermediate coral community. This is a very

diverse coral community and, depending on local variations in light availability and wave energy, *Acropora*, *Porites*, or another massive coral species may dominate (Head, 1987b). Whenever light-energy levels fall below 45% of the incoming solar energy, the deep coral community prevails. This probably is the richest and most diverse community, consisting of small colonies of several *Porites* species and large polyp Faviids, especially *Goniastrea pectinata*. Branching corals are less common, except for *Acropora hyacinthus*. In the deeper sites, fungiinids such as *Pavona*, *Pachyseris*, and *Leptoseris* become important, forming the Fungiinid sub-community (Head, 1987b). The depth at which these communities occur largely depend on local environmental conditions and approximate boundaries, as proposed by Head (1987b), can not be drawn (Riegl and Piller, 1997).

2.4.3 Algae

Algae comprise a diverse group of aquatic plants, ranging from small *Cyanobacteria* (blue-green algae) and the single-celled *diatoms* (*Bacillariophyta*) which form most of the phytoplankton, to the morphologically more complex benthic green (*Chlorophyta*), brown (*Phaeophyta*), and red algae (*Rhodophyta*). The benthic algae are differentiated based on the pigments they possess and which determine the capability of each group to use specific parts of the available PAR. The green *Chlorophyta* dominantly reflect the green part of the spectrum and mainly use the longer red wavelengths for photosynthesis (fig. 2.41b). As these wavelengths are quickly absorbed in water (fig. 2.41a), green algae commonly occur close to the surface. The large brown algae, e.g. *Turbinaria* or *Sargassum*, have relatively large amounts of non-photosynthesising tissue and, consequently, also occupy shallow substrates. The red algae which usually consist of very thin filaments, conversely, utilise the shorter blue and green wavelengths (fig. 2.41d) and may therefore occur at much greater depths. In the Red Sea, *Rhodophyta* can be found up to depths of 40m and more (Walker, 1987).

As noted in part I, coralline algae are the second most important carbonate-excreting species contributing to the reef framework. Large parts of the exposed reef flats and reef crests are covered with calcareous encrusting algae, mainly *Porolithon* and *Melobasia* species, forming pink coralline patches. Here, the hydrodynamic conditions hinder the growth of most hermatypic and soft corals, as well as less robust, fleshy and filamentous algae (Walker, 1987).

Some algae also live in symbiosis with the coral animals. In part I, attention was given to the endosymbiotic relationship between hermatypic corals and their zooxanthellate guests. But small algae, especially filamentous *Cyanobacteria* and *Chlorophyta*, may also be found as a thin layer below the coenenchyme. These *endolithic algae* have very high concentrations of chlorophyll and may give a greenish appearance to the surface of a coral colony. When these endolithic algae are formed under dead coral rock, *Rhodophyta* may be present as well (Walker, 1987).

Benthic algae are the most important primary producers in many shallow reef habitats (Head, 1987a). One of the most common species in the northern and central part of the Red Sea is the brown algae *Sphacelaria tribuloides* (Sheppard *et al.*, 1992). On the reefs themselves, benthic algae mainly occur in the form of lawns of turf or filamentous algae controlled by grazing fauna (Head, 1987a; Sheppard *et al.*, 1992). In sheltered environments, thin layers of algae may also form mats on top of sandy sediments (Walker, 1987; Roelfsema *et al.*, 2002). Larger species, or *macro-algae*, however, are more prominent in these intertidal and lagoonal environments, whereas they only occur as isolated plants in crevices on the reef structures. The most dominant Red Sea macro-algae are the green algae *Halimeda* and the brown algae *Padina*, *Sargassum*, and *Turbinaria* (Walker, 1987). The green algae are most dominant in the northern Red Sea, while brown algae are most diverse in the south and may dominate extensive parts of the shallow substrate, forming algal reefs in some places (Sheppard *et al.*, 1992). Benthic algae appear to be least diverse in the central part of the Red Sea (fig. 2.42), although this might be due to a lack of information for this part of the region (Sheppard *et al.*, 1992).

In most areas, algal communities show an annual growth cycle (fig. 2.43). Highest algal cover has been observed from February to May, while most algae disappear during the summer months (Mergner and Svoboda, 1977; Walker, 1987; Sheppard *et al.*, 1992). Some species, conversely, follow an opposite cycle as is the case for the endemic species *Turbinaria elatensis* (Walker, 1987).

2.4.4 Seagrasses

Seagrasses are the only group of higher plants that has adapted to a subaquatic environment (Jones *et al.*, 1987). In total, 59 species of seagrass are known, group in 5 genera, all belonging to a single order of *Monocotyledon* (Spalding *et al.*, 2003). In the Red Sea, 11 species have been detected so far (table 2.9), all of tropical origin and belonging to the genera

Hydrocharitaceae and *Cymodoceaceae* (Lipkin *et al.*, 2003). Remark, however, that only one single plant of *Halophila decipiens* has been collected by Jacobs and Dicks (1985) at a depth of 30m along the southwestern shoreline of the Gulf of Suez (Lipkin *et al.*, 2003). All Red Sea species, except for *Halophila stipulacea* which is confined to the western Indian Ocean, are widely distributed throughout the Indo-Pacific region. *Halophila stipulacea* appears to be most abundant towards the higher latitudinal, cooler edges of its distribution. This could account for its predominance in the northern Red Sea and may also be the reason why it is the only seagrass which was able to colonize the Mediterranean Sea through the Suez Canal (Lipkin, 1977; Jones *et al.*, 1987; Green and Short, 2003).

As can be seen on figure 2.44, seagrasses occur along the entire Red Sea coast but tend to be more abundant along the eastern Saudi Arabian coastline and in the southern Red Sea, most probably related to the wider and shallower shelf available for colonisation (Sheppard *et al.*, 1992). Except for *Enhalus acoroides* which seems not to occur north of the Tropic of Cancer, all other species spread to the northern part of the Red Sea (Lipkin *et al.*, 2003). The environmental conditions in the Gulf of Suez and the Gulf of Aqaba appear to be near the temperature limits of most seagrass species, except for *Halophila stipulacea*. In the Gulf of Aqaba and the Gulf of Suez respectively, seven (not *C. serrulata*, *H. ovata*, *H. decipiens*) and five (*H. uninervis*, *H. stipulacea*, *H. ovalis*, *H. decipiens* and *T. ciliatum*) seagrass species have been reported. This number quickly decreases further north and only three species (*H. uninervis*, *H. stipulacea*, *H. ovalis*) are found at the northern extremities of these Gulfs (Jones *et al.*, 1987; Lipkin *et al.*, 2003).

Red Sea seagrasses can be found from the immediate sub-tidal (and even mid-tidal positions on some beaches) up to depths of 70m. *Halophila stipulacea* and *Thalassodendron ciliatum* have the greatest vertical distribution range, while all other species tend to be restricted to between the mean low sea level and about 10m depth (Lipkin, 1977; Jones *et al.*, 1987). Seagrass beds are usually found in more or less sheltered, shallow lagoons behind coral reefs. They colonise unstable sediments, ranging from muds to coarse coral rubble, which may be unsuitable for macro-algal growth. With their extended rhizome and root networks, they stabilise the sediments and a highly productive plant-dominated ecosystem supporting a rich and specialised fauna can develop. The dense seagrass stands locally reduce wave energy and act as traps for fine grained sediments (Jones *et al.*, 1987). As sediments accumulate, the seagrass beds may become elevated by a few centimetres above the surrounding seafloor, and in certain conditions, may even form more substantial mounds (Burrell and Schubel, 1977; Jones *et al.*, 1987).

Table 2.9. Overview of seagrass species found in the Red Sea (after: Lipkin *et al.*, 2003)

| genus | species |
|-------------------------|---|
| <i>Cymodoceaceae</i> | <i>Cymodocea rotundata</i> <i>Cymodocea serrulata</i> <i>Halodule uninervis</i> <i>Syringodium isoetifolium</i> <i>Thalassodendron ciliatum</i> |
| <i>Hydrocharitaceae</i> | <i>Enhalus acoroides</i> <i>Halophila ovalis</i> <i>Halophila ovata</i> <i>Halophila stipulacea</i> <i>Halophila decipiens</i> <i>Thalassia hemprichii</i> |

Most seagrass plants reproduce asexually rather than sexually, although a flowering season has been noted in the northern Red Sea between June and September (Jones *et al.*, 1987). As a result, most seagrass beds are monospecific consisting of a sizeable stand of plants all originating from one single seedling (Lipkin, 1977; Jones *et al.*, 1987). Seagrass beds are usually separated from adjacent coral reefs by a barren *halo* created by reef fish which graze on the seagrasses during part of the day. The only exception is the seagrass *Thalassodendron ciliatum* which may extend on to the coral reefs (Lipkin *et al.*, 2003).

2.4.5 Mangroves

The environmental conditions of the land surrounding the Red Sea make the coastal zone very harsh for mangal²⁵ development. Mangroves, however, do occur (fig. 2.45) but they are generally impoverished if compared with other mangal systems along the Indian Ocean (Head, 1987a). Although poorly developed, these mangals are still important ecosystems as they accumulate and retain sediments, protect the coastline from erosion, provide shelter and nursery grounds for many marine species, and form oases of high primary productivity in an otherwise barren terrestrial region (Jones *et al.*, 1987; Hanafy, 2002).

Four mangrove species were formerly distinguished in the Red Sea -namely *Avicennia marina*, *Rizophora mucronata*, *Brugueira gymnorhiza* and *Ceriops tagal*- but recent surveys

²⁵ mangal: describes the intertidal, mangrove swamp habitat; mangrove: describes the occurring species or genera (Chapman, 1977)

(Ormond *et al.*, 1988), however, were unable to confirm the presence of *Brugueira gymnorhiza* (Sheppard *et al.*, 1992). *Avicennia marina* is the most common (Sheppard *et al.*, 1992). All mangrove stands along the Egyptian Red Sea coast, north of Shalateen, are uniformly composed of *A. marina* (Hanafy, 2002). At Sinai, at about 28°N, the northernmost mangals of the Indo-Pacific can be found (Jones *et al.*, 1987). In the south, mangrove stands are mixed with co-dominant *A. marina* and *Rizophora mucronata* (Hanafy, 2002).

Most mangals in the Red Sea occur in more or less sheltered environments behind fringing reefs, in bays or sharms, and in the lee or on some offshore islands (Ormond *et al.*, 1988; Sheppard *et al.*, 1992). In many places, especially in the northern Red Sea, beach sediments are poorly developed and only form a thin veneer overlaying beach rock, fossil reefs, or uplifted rock (Jones *et al.*, 1987; Sheppard *et al.*, 1992). This may be an additional reason for the reduced distribution of mangroves towards the north (Sheppard *et al.*, 1992). Such mangals are usually called *hard-bottomed* mangals, *reef* mangals (Sheppard *et al.*, 1992), or *Shura* (Jones *et al.*, 1987). These stands are mainly composed of bushy trees less than 2m high (Sheppard *et al.*, 1992) and may extend between tens of meters to several kilometres (Hanafy, 2002). Along the southern Red Sea, mangals are better developed because of the better environmental settings: the continental shelf becomes broader, annual seawater temperatures are higher, the shores are better protected and more composed of loose sediments, rainfall is generally higher, and more nutrients are available from the seawater influx through Bab el Mandab (Jones *et al.*, 1987; Price *et al.*, 1987; Sheppard *et al.*, 1992). These southerly mangals are called *soft-bottomed* or *peat* mangals and mainly consist of tall mangrove trees 5 to 7m high, generally grouped in stands 100 to 500m wide (Sheppard *et al.*, 1992).

2.4.6 Specific threats to Red Sea coastal ecosystems

Until the late 1960s, the Red Sea probably was one of the world's marine areas least affected by human activities. There were only few small cities which were not industrialised, except maybe along the Gulf of Suez where limited oil field development started at the time. Between these urban centres, sparse populations of nomads and fishermen inhabited the desertic coastal areas. Their impact on the Red Sea was restricted to artisanal fishing, most probably at sustainable levels even near the coastal towns. Pollution, consequently, was restricted to the few industrial plants near the cities, the limited oil exploitation, and the

disposal of garbage and waste water by ships passing through the Red Sea and the Suez Canal (Ormond, 1987).

During the 1970s, development along the Red Sea coasts significantly increased as oil exploitation in the Gulf of Suez expanded to a much larger scale and with the reopening of the Suez Canal in 1976, transport across the Red Sea increased (Ormond, 1987). Ship traffic was further enhanced by the opening of trans-Suez and trans-Arabian pipelines, each with oil terminals along the Red Sea (Ormond, 1987). As these activities generated significant foreign income, industry and urbanisation boomed. Coastal development, however, was not uniformly spread across the region as it focused on the existing urban and industrial centres (Fouda, 1998; Hassan *et al.*, 2002). In Saudi Arabia, for example, the population in the cities of Jeddah and Yanbu increased five-fold between 1972 and 1987 (Ormond, 1987). To supply these new urban centres, fishing activities intensified as well. Most human-related threats, however, were mostly restricted to the direct surroundings of these centres (Dicks, 1987; Ormond, 1987; PERSGA, 2001; Hassan *et al.*, 2002). One major exception, nonetheless, was marine pollution which became more widespread with the ever increasing ship traffic (Dicks, 1987; PERSGA, 2001).

From the 1980s onwards, a new phase in the coastal development of the Red Sea started as new urban centres were needed to accommodate the increasing numbers of tourists visiting the region. Unlike previous developments, many of these new tourist centres were no longer related to existing urban centres and spreaded out over the desertic coastal areas (Hassan *et al.*, 2002). These developments especially took place along the northern Red Sea coasts.

Nowadays, more and more coastal environments start to show serious signs of degradation (Ormond, 1987; Fouda, 1995; Gladstone *et al.*, 1999; Hassan *et al.*, 2002). Table 2.10 gives an overview of the main human activities in the region and their effects on the coastal ecosystems in the Red Sea. All these human activities can be found in each country bordering the Red Sea although the levels of impact greatly vary according to the socio-economic wealth and political stability of the riparian country (Pilcher and Alsuhaibany, 2000). More details on these activities and their negative impacts on the Red Sea coastal ecosystems are given in the following sub-sections.

While some parts of the Red Sea are still more or less unaffected and most human impacts are less intense than in many other marine regions (Jameson *et al.*, 1995; Pilcher and Alsuhaibany, 2000; Hassan *et al.*, 2002), the Red Sea as a whole can no longer be seen as a pristine environment (Price *et al.*, 1998; Hassan *et al.*, 2002). This evolution is especially worrisome for the Red Sea as it is a semi-enclosed water body characterised by relatively

extreme conditions. Many fauna and flora, therefore, are near their upper physiological limits which makes them exceptionally vulnerable to additional disturbances (Dicks, 1987; Gladstone *et al.* 1999). Moreover, due to the limited water exchange through the Bab el Mandab, contaminants are not flushed out into the Indian Ocean and become accumulated (Dicks, 1987; Fouda, 1995; Gladstone *et al.*, 1999; Pilcher and Alsuhaibany, 2000; PERSGA, 2001). This is even more important in the Gulf of Suez where industrial development is highest (Dicks, 1987). Remark that because of its isolated position, the Red Sea, conversely, is largely protected from the negative effects of global change. This, unfortunately, may change dramatically in future when the IPCC climate scenarios are correct.

Table 2.10. Overview of the most important human activities in the Red Sea region and their impacts on the coastal ecosystems (sources: Dicks, 1987; Ormond, 1987; Fouda, 1995; 1998; Gladstone *et al.*, 1999; Pilcher and Alsuhaibany, 2000; Gerges, 2002; Hassan *et al.*, 2002)

| human activities | negative effects on coral reefs |
|---|--|
| coastal development | dredging and land-filling, sewage discharge, garbage dumping, water circulation changes |
| mining, quarrying, industrial activity & oil exploitation | oil pollution; thermal pollution; discharges of heavy metals, fertilisers, chemicals; eutrophication |
| tourism | resort construction; sewage discharge; overfishing; souvenir collection; trampling and coral breakage; anchor damage, spearfishing |
| fisheries & mariculture | overfishing; dynamite fishing; seafloor disturbance; coastal habitat destruction; chemical pollution |
| ship traffic | navigational hazards, oil spills; waste water discharges; garbage jettisoning |
| climate change | sea-level rises; coral bleaching |

2.4.6.1 Natural threats

Exceptional low sea levels occur under extreme wind conditions (section 2.3.1.1.4) and occasional flash floods interrupt coral-reef formation in front of large wadi mouths (section 2.3.1.4), but, otherwise, the Red Sea is a relatively stable and sheltered physical environment. The regional climate is similarly benign as tropical storms do not penetrate from the south (Stoddart, 1971) and passing low pressure fronts in the north are already weakened and remain mostly restricted to the Gulf of Suez and the northwestern part of the Red Sea. These cold weather conditions, nevertheless, may have a severe, but

localised impact on the coral reefs in this region (section 2.3.1.1.4) (Fouda, 1995; Fouda, 1998; Jameson *et al.*, 1995; Pilcher and Alsuhaibany, 2000).

Apart from these occasional physical stresses, more and more observations are made of exceptionally large populations of several bio-eroders. Major outbreaks of COTS, for example, have been recorded in most countries along with fast growing populations of different *Echinometra* and *Diadema* sea urchin species (Ormond, 1987; Jameson *et al.*, 1995; Fouda, 1998; Pilcher and Alsuhaibany, 2000; Hassan *et al.*, 2002). In addition, outbreaks of coral-eating snails, mainly *Coralliphylia* and *Drupella* species, are noted in many sites with partial coral mortality ranging from 10 to 70% (Pilcher and Alsuhaibany, 2000; Hassan *et al.*, 2002). Besides, coral diseases like black-band and white-band disease become more prevalent in the Red Sea as well (Pilcher and Alsuhaibany, 2000).

2.4.6.2 Coastal development

The desertic coastal plains along the Red Sea are very unsuitable for agriculture, except along the northern Bay of Suez (UNEP, 1997). As no permanent rivers enter the Red Sea, no negative impacts of inland development projects are therefore known in the region. Urban coastal development, conversely, seems less impeded by the climate. Perhaps the most serious aspect of the increasing urban expansion is the tendency to occur in a strip-like fashion closely bordering the coastal waters, thereby maximising its negative impacts on the coastal habitats (Ormond, 1987; TDA, 1998).

2.4.6.2.1 Land reclamation and water circulation changes

The most extensive coastal development in the region takes place around the major urban centres of Saudi Arabia, large parts of the Egyptian coastline and especially Sinai, and along parts of the Yemen coastline (Pilcher and Alsuhaibany, 2000). It is predominantly related to the construction of oil-platforms, industrial plants, and tourist resorts and frequently results in the alteration of the coastline for the construction of jetties, harbours, marinas, or coastal roads (Jameson *et al.*, 1995). These dredging and land-filling activities not only destroy nearshore habitats directly, they also result in an augmented sediment load in the water (Dick, 1987; Ormond, 1987; Pilcher and Alsuhaibany, 2000) and/or changes in the water circulation pattern. Some parts of the coastal zone, therefore, will become more eroded, while other parts witness reduced water circulation conditions and resulting rises in sedimentation and temperature (Ormond, 1987).

2.4.6.2.2 Sewage

The greatest single input, in volume, from urban coastal settlements to the Red Sea most probably is sewage (Dicks, 1987). It usually is discharged to or just below the intertidal zone via pipelines; often directly on top of fringing reefs (Dicks, 1987; Fouada, 1995; Pilcher and Alsuhaibany, 2000). In addition, considerable amounts of garbage such as plastic and metal drums are dumped near urban, industrial, and recreational areas (Dicks, 1987; Pilcher and Alsuhaibany, 2000; White *et al.*, 1997).

Most sewage is untreated or only partially treated as existing plants are not well suited to deal with irregular effluents (UNEP, 1997) and/or generally lack regular maintenance (Pilcher and Alsuhaibany, 2000; Gerges, 2002). The sewage volume, and consequently the area affected, depends on the number of people in the urban centre or the magnitude and kind of industrial activity. Accurately predicting the zones of damage in relation to the input, however, is often difficult as local underwater topography and related water circulation patterns influence the rate and direction of dispersion (Dicks, 1987).

The most notable effects of sewage are the increases in nutrient and suspended solid loadings (Dicks, 1987; Walker, 1987; Jameson *et al.*, 1995; Gerges, 2002) and the associated problem of nutrification (section 1.3.2.2.2). Nutrification not only results from excessive untreated sewage input, but is also known to occur due to the settlement of phosphate dust during the loading of phosphate rock e.g. in the port of Aqaba (Walker, 1987). This is particularly important in the Red Sea as the input of nutrients in the otherwise nutrient-poor water may quickly lead to dramatic algal blooms (Walker, 1987; Pilcher and Alsuhaibany, 2000). These on their turn may cause considerable coral mortality as was reported by Walker and Ormond (1982) who have noticed a 4 to 5 fold increase in coral mortality after the doubling of algal biomass which was related to sewage and phosphorus pollution.

2.4.6.2.3 Industrial pollution

Chronic industrial pollution has already reduced water quality in many parts of Egypt, Jordan, Saudi Arabia, and around the major port areas in Sudan (Pilcher and Alsuhaibany, 2000). This pollution includes the discharge of untreated sewage and oily wastes from industrial plants and refineries; spills of minerals (mainly manganese and bauxite) during ship loading in the Gulf of Aqaba (Dicks, 1987); phosphate enrichment during ship loading principally at Quseir (Dicks, 1987) and Aqaba

(Walker and Ormond, 1982); and various effluents from the many desalination plants along the Red Sea (Dick, 1987; Jameson *et al.*, 1995, Pilcher and Alsuhaibany, 2000).

Aside from the evident effects of oil spills and oil-rig discharges (section 1.3.2.4), the operation of an oil platform or shore terminal may also affect nearby coral reefs by discharges of drill muds and rock cuttings, and chemicals (Dicks, 1987). In addition, seismic blasts during oil exploration surveys may have significant effects as well, mainly causing physical damage to the reef structure (Fouda, 1983). If the adventurous plans of the 1970s and 1980s to mine the deep sea trough for metals and other commercially valuable elements ever come to action, this most probably would result in additional discharges of heavily polluted sewage and effluents (Dicks, 1987; Karbe, 1987).

To provide the industry and the increasing local population and number of visitors with potable water in this arid climate, many Red Sea governments have built desalination plants near their urban and industrial centres (Dicks, 1987; Pilcher and Alsuhaibany, 2000), while some remote tourist resorts also have small, private desalination facilities (Hafez and El-Manharawy, 2002). As construction and operating costs of such plants are high, most plants are restricted to the more wealthy regions, particularly the tourist centres of Egypt and the urban centres on the Saudi Arabian coast (Hoepner and Latteman, 2002). Municipal desalination plants are often large industrial facilities consuming considerable amounts of space and emitting large amounts of concentrated discharges back into the sea. This concentrate does not only contain hypersaline, warm water but also additives, mostly chlorine, necessary for the desalination process and corrosion by-products like copper (Dicks, 1987; Hoepner, 1999; Hoepner and Latteman, 2002). While the effects of these elements are only noticeable in close proximity to the outlets, they can be very severe as chlorine is already very toxic at low levels and copper tends to accumulate in the marine sediments (Hoepner and Latteman, 2002). As natural salinity levels in the Red Sea are already high, brine discharges will only have negligible effects on the overall salinity level (Hoepner and Latteman, 2002). Most coral species, however, are already near their upper physiological salinity limits so that even small and local increases in salinity may become stressful (Coles and McCain, 1990; Hoepner and Latteman, 2002).

2.4.6.3 Tourism

Many negative impacts of tourism, on the one hand, are related to coastal development issues (Dick, 1987; Jameson *et al.*, 1995), while, on the other hand, damage to coral reefs may also be directly caused by tourists via coral breakage while diving or snorkelling, reef flat trampling, anchor damage, or collection of curio on the reefs (Dick, 1987; Jameson *et al.*, 1995; White *et al.*, 1997; Pilcher and Alsuhaibany, 2000) (section 1.3.2.3). Most tourism-related damage on Red Sea coral reefs occurs in Egypt around the resorts at Hurghada and Sharm-el-Sheikh; in Sudan at Sanganeb reef; and in Djibouti at Sept Frères reef, Moucha, and Maskalia (Pilcher and Alsuhaibany, 2000). As tourism is one of the fastest growing economic sectors in the Red Sea region (PERSGA, 2001), the negative effects related to tourism are more than likely to increase.

2.4.6.4 Marine pollution

Oil pollution stemming from both oil exploitation and transportation undoubtedly is the most important form of marine pollution in the Red Sea since the mid-1970s (Sheppard *et al.*, 1992). Oil extraction is mainly concentrated in the Gulf of Suez and the northwestern part of the Red Sea; in 1999, 37 oil fields were known in the Gulf of Suez and 23 wells were operational (Gladstone *et al.*, 1999; PERSGA, 2001). The local oil consumption, conversely, accounts for only 9% of the total production and refining industries are consequently limited (Dicks, 1987). Except for the Gulf of Suez, marine pollution related to oil exploitation and production, therefore, is largely restricted to the immediate surroundings of oil depots (Loya and Rinkevich, 1980; McClanahan, 2002) and oil-handling ports such as Eilat, Aqaba, Jiddah, Yanbu, and Port Sudan (Dicks, 1987; Pilcher and Alsuhaibany, 2000). With the increasing development of the area, local oil demand, however, will grow, leading to a potential increase in chronic discharges in a much wider area if no adequate environmental standards are imposed (Dicks, 1987).

The Red Sea, however, is first and foremost one of the most important shipping routes since the reopening of the Suez Canal in 1976. About 16,000 ships pass through Bab al Mandab each year (PERSGA, 2001) and many more transit the Red Sea annually (Pilcher and Alsuhaibany, 2000), most of them transporting petrochemical products between the pipeline terminal in Yanbu, the Suez Canal, and the Sumed pipeline entrance in Ain Sukhna, Egypt (Gladstone *et al.*, 1999). Consequently, over 100 million tons of oil is transported through the Red Sea annually (Lintner *et al.*, 1996; Gladstone *et al.*, 1999). As

a result of these high volumes, Awad (1995 in: PERSGA, 2001) estimates the annual volume of oil pollution from shipping in the Red Sea to be 1.5 times the global average.

Since 1982, more than 20 oil spills have been recorded along the Egyptian Red Sea coast and many others have affected Saudi Arabia and to a lesser extent, Yemen and Sudan (Pilcher and Alsuhaibany, 2000). The dense ship traffic is also the cause of other forms of marine pollution such as ship-based dumping of solid wastes and garbage (Pilcher and Alsuhaibany, 2000), tank washings, and uncontrolled discharges of oily ballast waters which result in local accumulations of soft tarry patches and/or tar balls (Dicks, 1987; Pilcher and Alsuhaibany, 2000).

Besides, the shallow, reef-bordered coastlines, especially near major ports such as Djibouti, Jeddah, Port Sudan, and Suakin, and around the narrow entrances to the Gulf of Suez, the Gulf of Aqaba, and Bab el Mandab, augment the chance of major navigation hazards (Lintner *et al.*, 1996; Pilcher and Alsuhaibany, 2000). These ship groundings not only damage the reefs directly, but may also impose indirect chronic stress via the discharge of pollutants, or toxic stress by the anti-fouling paint on the ship (section 1.3.2.4).

2.4.6.5 Fisheries and destructive fishing activities

Fisheries are important for the countries bordering the Red Sea as they are an important source of high grade protein. Economically, the fishing industry represents also an important source of employment and income to the local community (Head, 1987c; Hariri *et al.*, 2000). In 2003, for example, the total value of fish catches in the Red Sea amounted to nearly 340 million USD (SAU, 2006). With the growing population and the increasing national income from tourism and the oil industry in some countries, fishing activities have been steadily intensified over the last three decades (fig. 2.46) and start to threaten the ecological system of the Red Sea (Head, 1987c; Jameson *et al.*, 1995; Hariri *et al.*, 2000).

Figure 2.47 gives an overview of the most important fishing grounds in the Red Sea. These are the broad shelves in the southern part of the Red Sea, the relative shallow Gulf of Suez, and Foul Bay near the Egyptian-Sudanese border. In the south, the water inflow from the Gulf of Aden imports relatively high nutrient levels (section 2.3.2.4.2) which result in higher primary productivity in the water column and consequent higher fish stocks. In addition, the broad, shallow continental shelf zones allow resuspension of bottom sediments which also contribute to increased nutrient levels. Besides, the complex

interplay between sandy bottoms, seagrass beds, mangroves, and coral reefs in this area most likely contributes to the high fish productivity as well (Sheppard *et al.*, 1992). In the north, the high levels of fishery production in the Gulf of Suez and Foul Bay mainly result from the increased nutrient availability via the resuspension of sediments from the shallow seabeds (Sheppard *et al.*, 1992). The continental shelf throughout the rest of the Red Sea is very narrow and nutrients, conversely, are quickly lost to the deep waters.

Fishing in the main fishing grounds is conducted by artisanal subsistence fishermen, local commercial fisheries, and foreign industrial fisheries alike (Hariri *et al.*, 2000). Fishermen in the remainder of the Red Sea, however, need to closely follow the coral reefs near the coasts. Due to the complex topography of this surface, this type of fishing is unsuitable for industrial fishing and, here, most fishing is performed by artisanal fishermen (Head, 1987c; Sheppard *et al.*, 1992). As a result, artisanal fishing dominates the sector (Head, 1987c; Hariri *et al.*, 2000). At least 29,500 fishermen work in the artisanal fishing sector, using around 9,000 mostly small vessels to fish for demersal species on or near the coral reefs (Hariri *et al.*, 2000). They use a whole range of gears, including handlines, longlines, traps, nets, and spears (Sheppard *et al.*, 1992; Hariri *et al.*, 2000). The commercial fishing sector is significantly smaller and only counts about 7,500 fishermen and 1,600 vessels (Hariri *et al.* 2000). The two most important techniques used are purse seining²⁶ and trawling²⁷. According to Head (1987c), industrial fishing is only conducted by Egyptian fishermen in the southern Red Sea. These extractive fisheries are very seasonal and take place from September to May after which stocks become quickly depleted (Head, 1987c; Sheppard *et al.*, 1992).

Catches mainly consists of demersal and pelagic fishes, and invertebrates. Pelagic fish catches are dominated by sardines, Indian mackerel, Spanish mackerel, and yellowfin tuna, whereas demersal fish catches mostly comprise species of snapper, jack, emperor, lizard-fish, grouper, seerfish, rabbitfish, and seabream (Hariri *et al.*, 2000). As most species occur across the entire Red Sea, they are essentially shared stocks (Hariri *et al.*, 2000). Invertebrate fisheries in the Red Sea, finally, concentrate on shrimps and lobster (Sheppard *et al.*, 1992) although some countries also fish for edible seacucumbers and export them to Southeast Asia (Hassan *et al.*, 2002).

²⁶*Purse seining* is a popular form of fishing in which a long, deep net is dragged behind a vessel which steams in a circle. Both ends of the net, subsequently, are recovered, such that the circular form of the set net encloses a large volume of water and fish. A rope runs along the bottom of the net, and when this is tightened, the net closes like a purse, trapping the fish inside (Head, 1987c).

²⁷*Trawling*: fishing method in which a vessel pulls a heavy weighted net across the sea bottom (Head, 1987c).

Total catches from both artisanal and commercial fisheries in the Red Sea amount to about 145,315 ton in 2003, roughly 10,000 ton less than in the previous year (SAU, 2006) (fig. 2.46). Egypt has become the most important fishing country in the Red Sea, accounting for 43% of the total catches in 2003, closely followed by Yemen responsible for 38.6% of the total catches in that year. Other relatively important fishing countries are Saudi Arabia (10.1%), Eritrea (4.6%), and Sudan (3.4%), while the remaining riparian countries only deploy very limited fishing activities in the Red Sea.

At present, overfishing is not considered a big problem for the totality of the Red Sea, although some local problems start to occur (Hariri *et al.*, 2000; Pilcher and Alsuhaibany, 2000) which is shown by declines in catches of especially Indian mackerel, kingfish, cuttlefish, shrimps, and lobster (Sheppard *et al.*, 1992; Jameson *et al.*, 1995; Hariri *et al.*, 2000). These declining catches are mainly the result of overfishing in the northern Red Sea, the Gulf of Suez, and the Gulf of Aqaba; illegal fishing practices; and the ignorance of national fishing laws and regulations (Hariri *et al.*, 2000; Pilcher and Alsuhaibany, 2000). In the case of lobster, overfishing in the Gulf of Aqaba has been attributed by Sheppard *et al.* (1992) to an increasing demand for lobster in the tourist hotels since the mid-1980s. Shrimp trawl fisheries, moreover, have very high unwanted by-catches of fish, turtles, and dolphins (Hariri *et al.*, 2000).

No significant declines in the seacucumber populations, conversely, have been recorded so far (Hassan *et al.*, 2002). A complete other story can be seen in the shark population. Overfishing of sharks results from both local fishermen and foreign vessels, illegally fishing outside their territorial waters, supplying the lucrative Southeast Asian shark fin market (Hariri *et al.*, 2000; Pilcher and Alsuhaibany, 2000). Most problems are encountered in Yemen, Somalia, Djibouti, and Sudan. As with shrimp fishing, high amounts of by-catches including fish, turtles, and dolphins are killed, while local fishermen using nets damage the coral reefs they operate on (Hariri *et al.*, 2000; Pilcher and Alsuhaibany, 2000).

In recent years, the aquarium fish trade has gained increasing importance as a source of foreign income and is expected to increase throughout the region (Gladstone *et al.*, 1999). This will probably be enhanced by the planning of new international airports along the Egyptian coastline to accommodate tourist charters. In 1992, only one aquarium fish trader was known in Egypt (Sheppard *et al.*, 1992). By 2000, Hariri *et al.* (2000) counted at least seven operational aquarium fish exporters in Saudi Arabia. Although this trade can be a sustainable manner of resource extraction, destructive fishing techniques are

often applied. There have been already some unconfirmed reports of the spreading use of cyanide fishing in the Red Sea (Wabnitz *et al.*, 2003). No large-scale international trade in Red Sea corals or ornamental shells is known (Head, 1987c; Sheppard *et al.*, 1992). Collection of curio for tourist sale was known in some areas, especially along the Egyptian Red Sea (Head, 1987c; Sheppard *et al.*, 1992), but these practices have been banned in recent years.

Besides negative effects of overexploitation, destructive techniques are applied in some locations which may cause important damage to the marine ecosystem. Dynamite fishing, for example, is still being used along the Egyptian Red Sea coast (Ormond, 1987; Riegl and Luke, 1998; Pilcher and Alsuhaibany, 2000). Riegl and Luke (1998) note that 65% of the reefs in their study area have signs of dynamite damage, both new and old. The damage varies with the intensity of the blasting, whereas changes in coral and fish community composition on the dynamited sites are noted in most of the cases (Riegl and Luke, 1998). Besides, although spearfishing is officially banned in Sudan, Egypt, and Jordan, it is hard to control as yachts may enter the territorial waters without passing through local immigration controls (Ormond, 1987; Pilcher and Alsuhaibany, 2000). The destruction of the natural habitat, finally, is also known from some ponds constructed for shrimp farming in Egypt and Saudi Arabia, and for pearl-oyster culture in Sudan (Hariri *et al.*, 2000).

2.4.6.6 Global change

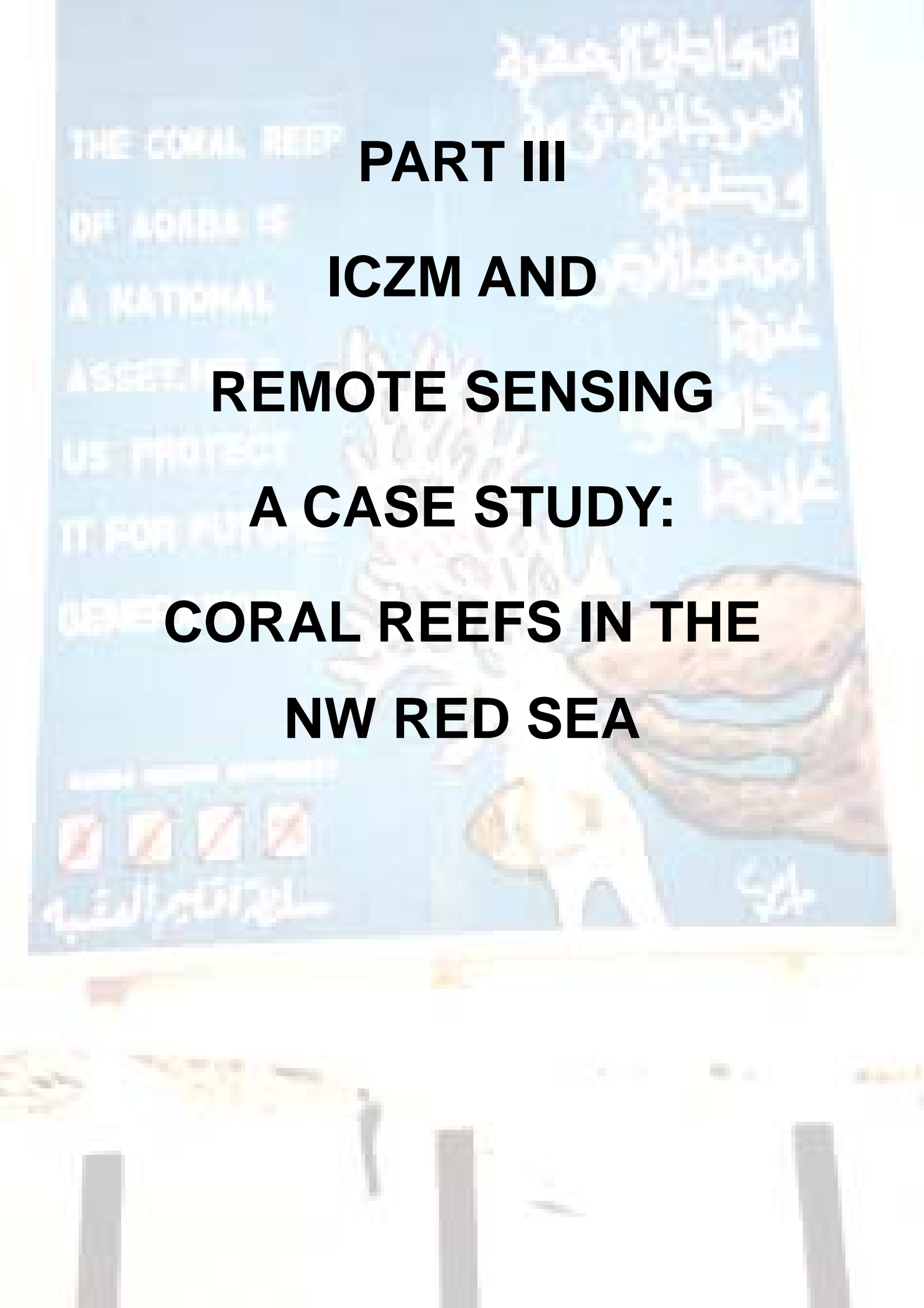
Mass coral bleaching probably is the most important threat to coral reefs linked to global change. During the biggest mass bleaching event on record in 1997-1998, parts of the southern Red Sea witnessed an elevated SST and related coral bleaching from August to September (Spalding *et al.*, 2001). Bleaching, however, was patchy, being more severe towards the south and around human settlements (Vogt, 2000; Schmid, 2000). Reefs north of Jeddah, where coastal development is currently taking place, for example, showed 20 to 30% of bleached reefs, while to the south of the city, where development is limited, only 5 to 10% of the corals showed signs of bleaching (Schmid, 2000).

The worst affected coral reefs were situated in the Yemen and Saudi Arabia, with about half of the live coral cover killed in some places (Pilcher and Alsuhaibany, 2000). In Sudan, bleaching occurred at several locations south of Port Sudan (Pilcher and Alsuhaibany, 2000; Vogt, 2000). In Eritrea, some coral bleaching was reported, predominantly on shallow reefs, although recovery appeared to be fast (Vogt, 2000). No

bleaching was conversely recorded in the Gulf of Suez, the Gulf of Aqaba, and the northern part of the Red Sea, roughly north of Port Sudan on the west coast and north of Yanbu on the Saudi Arabian coast (Vogt, 2000; Spalding *et al.*, 2001).

Besides, as the Red Sea is linked with the Indian Ocean through Bab al Mandab, a global sea-level rise will also have its effects on the Red Sea coastal region. An increase in sea level with 0.09 to 0.88m by 2100 as predicted (section 1.3.3.4), would affect many development sites, as most urban centers, tourist resorts, and industrial facilities are built close to or even beyond the high tide level. Reduced coastline protection and an increased chance of inundation resulting from drowning coral reefs may thus be very devastating in the Red Sea region (Fouda and Gerges, 1994; Gerges, 2002).

On the longer term, the predicted global change will also result in changes in the atmospheric circulation and, particularly important for the tropical and sub-tropical regions, alterations in the monsoon system. As the climate in the Red Sea region is largely determined by the seasonal changes in the Asian monsoon system, global change may modify dominant wind directions and consequent precipitation patterns (Fouda and Gerges, 1994; Gerges, 2002).



PART III

ICZM AND

REMOTE SENSING

A CASE STUDY:

CORAL REEFS IN THE

NW RED SEA

3.1 INTRODUCTION

3.1.1 Integrated Coastal Zone Management and remote sensing

As shown in previous chapters, coral reefs are ecologically and socio-economically very valuable although threatened by a plethora of human-induced and natural factors. The conservation and sustainable development of these natural resources, therefore, are urgently needed. The coastal zone of which many coral-reef systems are part of, however, is an inherently dynamic and complex environment, and consequently difficult to manage. It not only forms the interaction zone between different local land-based and marine processes, but it is also influenced by far-distanced events through river runoff and/or marine transport. In addition, the coastal region typically is subject to the *tragedy of the commons* (Hardin, 1968) as it is a freely accessible resource -usually without specific ownership- of which all take benefit but none take responsibility. Managing the coastal environment, therefore, is seldom if ever an easy and straightforward task (Ormond, 1987; Carney, 1999; Salm *et al.*, 2000; Westmacott, 2002).

The recognition, in the mid-1980s, of the shortcomings of traditional single sector management approaches which were unable to respond to the specific nature of the coastal zone led to the development of a new concept, being *integrated coastal zone management (ICZM)* (Post and Lundin, 1996). This concept, consistent with principles 1 through 19 of the 1992 United Nations Conference on Environment and Development (Rio) Declaration²⁸ and Chapter 17 of Agenda 21²⁹, is most concisely defined in the so-called *Noordwijk Guidelines* set out at the 1993 World Coast Conference (Anonymous, 1993):

ICZM involves the comprehensive assessment, setting of objectives, and planning and management of coastal systems and resources, taking into account traditional, cultural, and historical perspectives and conflicting interests and uses; it is a continuous and evolutionary process for achieving sustainable development.

²⁸ <http://www.un.org/documents/ga/conf151/aconf15126-1annex1.htm>

²⁹ <http://www.un.org/esa/sustdev/documents/agenda21/english/agenda21chapter17.htm>

The core objective of ICZM is to balance socio-economic development and ecological conservation (Cicin-Sain *et al.*, 1995; Post and Lundin, 1996; Kelleher, 1999; Salm *et al.*, 2000; Crosby *et al.*, 2002; Westmacott, 2002; Roberts *et al.*, 2003b). On the one hand, its socio-economic goals are to improve and diversify the current interests of coastal resource users -predominantly in fisheries, recreation, and tourism (Kelleher, 1999; Lubchenco *et al.*, 2003; Roberts *et al.*, 2003b)- and to plan future developments (Carney, 1999; Westmacott, 2002). The environmental processes and ecological functions underlying these economic assets, on the other hand, need to be preserved (Carney, 1999; Westmacott, 2002). This preservation may take the form of conservation of the complete biodiversity, conservation of rare and/or endemic species, maintenance of genetic diversity, maintenance and/or restoration of natural ecosystem functions, or conservation of habitats vital for vulnerable life stages (Lubchenco *et al.*, 2003; Roberts *et al.*, 2003b).

ICZM strives to maximise the economic and social benefits for all stakeholders³⁰ involved, taking into account traditional, cultural, and historical perspectives (Carney, 1999; Turner and Salomons, 1999; Westmacott, 2002; ICRI, 2003). To avoid conflicts between the different stakeholder groups, ICZM necessarily is a participatory and collaborative process in which the voice of all parties is heard (Post and Lundin, 1996; Salm *et al.*, 2000; Westmacott, 2002; UNEP, 2004). The involvement of local stakeholders at all stages of the ICZM planning, implementation and enforcement is essential for the long-term success of ICZM (Kelleher, 1999; Roberts and Hawkins, 2000; ICRI, 2003).

Engaging local stakeholders into ICZM requires education (Carney, 1999; Westmacott, 2002; UNEP, 2004) as all stakeholders, including tourists (Medio *et al.*, 1997), need to understand the concept of sustainable development and how the interests of all stakeholder groups should be maximized without hampering one another or destroying the environment. They must realise that protecting the environment, in the long run, is beneficial to their socio-economic profits. Poverty is a special issue which should be regarded in this respect as it may force people to exploit the coastal zone unsustainably to support their livelihood (Christie and White, 1997; Westmacott, 2002). People, therefore, may turn reluctant to support ICZM if no other means of income are provided. The need to combat poverty and its negative impact on

³⁰ Stakeholders are defined as groups of people with common objectives and sets of interests with regard to the resource in question and the environment (Grimble and Chan, 1995; Brown *et al.*, 2001), including key representatives of the science and management communities, environmental NGOs, local community groups with commercial and recreational interests, tourists, and indigenous people (Brown *et al.*, 2001; Crosby *et al.*, 2002).

the environment is underlined by the 2002 UN Johannesburg Declaration on Sustainable Development (UN, 2003).

Capacity building and institutional strengthening are two other important aspects of ICZM (Salm *et al.*, 2000; Crosby *et al.*, 2002). Management staff at all levels of government (Post and Lundin, 1996) should not only be trained on how to plan and manage the coastal zone, but also on how to develop a legal frame in which the ICZM can work (Kelleher, 1999). In the long run, even with enthusiastic local stakeholders, ICZM needs a tight legal framework to be successful (Roberts and Hawkins, 2000; Westmacott, 2002). In addition, a long-term perspective financial plan laid out at the beginning of the process is also essential (Anonymous, 1993; Turner and Salomons, 1999; McClanahan, 1999; UNEP, 2004). Management staff should therefore be aware of possibilities to sustainably raise money in order to maintain their ICZM activities. ICZM, especially in developing countries, is often initiated by large international donor organisations. These organisations, however, usually inject money over a short period to cover the set-up costs but rarely support the long-term management and enforcement (McClanahan, 1999; Roberts and Hawkins, 2000). Sustainable ways to finance the ICZM plan, e.g. through the levy of taxes or entry fees (McClanahan, 1999), should also be discussed with all stakeholders (Kelleher, 1999).

ICZM intrinsically acknowledges the need for holistic –integrated– research (Post and Lundin, 1996; Carney, 1999; Salm *et al.*, 2000; ICRI, 2003). In order to assess the coastal system and understand its functioning, a multi-disciplinary research approach is required (Turner and Salomons, 1999; UNEP, 2004). This research, in the first place, should be targeted towards the understanding of the diverse set of coastal and far-distanced environmental processes, the interactions between them, the links between human activities and natural processes, and the opportunities these may present (Carney, 1999). Focus should not only be on the ecological aspects of the coastal system but also on its social, economic, and cultural aspects as it is important to understand the driving forces behind the human interaction with the coastal zone (Crosby *et al.*, 2002). Research, consequently, should also be more management-oriented, addressing questions related to the sustainable use and conservation of the coastal zone (Carney, 1999; Kelleher, 1999; Crosby *et al.*, 2002, ICRI, 2003).

ICZM, finally, is a continuous, dynamic and evolutionary process. Monitoring enables managers and policy makers to track changes in the coastal zone and to assess the success of the management programmes. When needed, this allows the adaptation of the ICZM plan to improve its performance (Kelleher, 1999; Roberts and Hawkins, 2000, Westmacott *et al.*,

2000). Moreover, ICZM should be adaptive to changing user's interests or altering environmental conditions (Post and Lundin, 1996; Westmacott *et al.*, 2000; Westmacott, 2002). It should be remarked in this respect that climate change acts globally and can not directly be dealt with through ICZM. Local or regional initiatives, however, may help optimising the conditions for resilience and adaptation of the coral reefs when faced with changing environmental conditions (Wilkinson and Buddemeier, 1994; Hughes *et al.*, 2003; Harley *et al.*, 2006; Schubert *et al.*, 2006). In this way, ICZM gradually evolves from a reactive to a proactive solution (Post and Lundin, 1996; Crosby *et al.*, 2002).

In response to the growing concern about the worldwide decline of the coral reefs, and envisaging the concept of ICZM, several international initiatives have been taken which try to set up a framework wherein the sustainable development of these natural resources can be achieved. One of the first projects established is the International Coral Reef Initiative (ICRI), launched in 1994. As it is recognised that many nations face similar threats to coral reefs and related ecosystems as well as similar management problems, ICRI provides an informal international forum for governments, international organizations, multilateral development banks, environmental and developmental NGOs, the scientific community, and the private sector where ideas and experiences can be shared (ICRI, 2006). In 2000, under the umbrella of ICRI, the International Coral Reef Action Network (ICRAN) was established. ICRAN mainly serves as a platform for the collection and distribution of information concerning local, regional, and global coral-reef monitoring and management. The dissemination of this knowledge is specifically coordinated through the International Coral Reef Information Network (ICRIN)³¹. Besides, ICRAN '*seeks to put financial mechanisms in place that support the translation of findings into direct on-the-ground action throughout the world's major coral reef regions*' (ICRAN, 2006).

Global coral-reef monitoring is also addressed by the Global Coral Reef Monitoring Network (GCRMN) which main aims are to link existing organisations and people to monitor all aspects of coral reefs (ecological, sociological, cultural and economic) within regional networks, to provide a consistent monitoring program, and to disseminate the results at local, regional, and global scales. One important example of the latter is the biannual publication of a '*Status of the Coral Reefs of the World*' report (GCRMN, 2006). Data from the GCRMN, as well as from ICRAN, are distributed through ReefBase³², an online information system.

³¹ <http://www.coralreef.org/>

³² <http://www.reefbase.org>

The United Nations Educational, Scientific and Cultural Organization (UNESCO) is also aware of the need to protect coral reefs and sees its World Heritage Convention (WHC) ‘*as a unique legal tool for achieving conservation of marine and coastal ecosystems and for enhancing international co-operation of such work*’ (WHC, 2003). In 2006, UNESCO enlisted 644 cultural sites, 162 natural sites, and 24 mixed sites on their World Heritage List (WHC, 2006). 19 of them contain coral reefs, although only few are specifically designed to protect them. Besides, UNESCO recognizes 482 Biosphere Reserves in their Man and Biosphere (MAB) program (MAB, 2006). 74 Biosphere Reserves are specifically aimed at the marine environment, with 20 of them including coral reefs (MAB, 2006). Coral-reef-related issues are also addressed by the UNESCO-Intergovernmental Oceanographic Commission (IOC) and specifically through its Integrated Coastal Area Management (ICAM) activities (IOC, 2002). Moreover, a specific ‘Coral Reef Programme’ has been established under the auspices of UNESCO’s CSI-Unit (Environment and Development in Coastal Regions and in Small Islands), which, for example, is responsible for the publication of the ‘*Remote Sensing Handbook for Tropical Coastal Management (Green et al., 2000b)*’.

Marine area management is key topic for the United Nations Environmental Programme (UNEP) as well. Coral-related projects form part of many UNEP programmes, for example the UNEP Programme on Small Island Developing States (UNEP, 2006) and the UNEP Regional Seas Programme (UNEP, 2005), but all are coordinated by the specifically designed Coral Reef Unit (UNEP, 2003). In addition, numerous other international (e.g. ISRS³³), regional (CORDIO³⁴, AGRRA³⁵), national (e.g. the US Coral Reef Task Force³⁶), and non-governmental (e.g. ReefCheck³⁷) initiatives exist, all recognising the specific challenges of sustainably managing coastal zones, and coral reefs in particular.

3.1.1.1 Multi-use marine protected areas

Central in the protection of coral reefs stands the delineation of *marine protected areas* (MPAs) (Crosby *et al.*, 2002; Hughes *et al.*, 2003) which are defined by the IUCN (1988) as ‘*any area of the intertidal or subtidal terrain, together with its overlying water and associated flora, fauna, historical and cultural features, which has been reserved by law or other effective means to protect part or all of the enclosed environment*’.

³³ International Society for Reef Studies (<http://www.fit.edu/isrs/>)

³⁴ Coral Reef Degradation in the Indian Ocean (www.cordio.org)

³⁵ Atlantic and Gulf of Mexico Rapid Reef Assessment (www.agrra.org)

³⁶ <http://www.coralreef.gov/>

³⁷ <http://www.reefcheck.org/>

The demarcation of an MPA on its own, however, does not protect the coral reefs from negative impacts originating outside the MPA boundaries. Other management instruments controlling hinterland and coastal development, marine and land-based pollution, shipping, tourism, and fisheries must therefore be deployed before coral reefs can be effectively protected. Consequently, coral-reef MPAs, ideally, are part of a wider ICZM plan inherently covering all activities potentially impacting coral reefs. As such, MPA planning and management follow the same basic principles of sustainable development, stakeholder involvement, proactive and dynamic approach, and sustainable financing (Kelleher, 1999; Salm *et al.*, 2000; Westmacott *et al.*, 2000; Mascia, 2001; NCEAS, 2001; Crosby *et al.*, 2002; Westmacott, 2002; Hughes *et al.*, 2003; ICRI, 2003; Lubchenco *et al.*, 2003; Tilmant, 2004; IUCN, 2005).

To avoid conflicts between different stakeholder groups, an MPA is often divided into separate zones, each designed for a specific use (Hudgson, 1997, Harvey, 1999, Winer and Harrigan, 1999; Salm *et al.*, 2000; Crosby *et al.*, 2002). A zone of high conservation value, in casu a coral-reef system, is usually situated at the core of such a *multi-use MPA* (fig. 3.1). These central zones, called *marine reserves*, *ecological reserves* or *no-take areas* (Lubchenco *et al.*, 2003), are fully protected and all activities, except limited research, are explicitly prohibited. Surrounding the core, a second zone is delineated which protects associated habitats, such as seagrass beds and mangroves, which are important for the functioning of the central coral-reef system. In this zone, the least damaging activities such as line fishing or diving are allowed on a restricted and sustainable level. At the outside of the MPA, a final buffer zone is designed, protecting the vulnerable and valuable core from eventual negative impacts originating outside the MPA boundaries. Several areas may be delineated within this buffer zone wherein other stakeholder activities such as commercial fishing, harbour activities, or recreation are allowed on a sustainable level. Within the buffer zone, linked habitats such as beaches or dunes may be put under special protection (Salm, 1984; Hudgson, 1997; Kelleher, 1999; ICRI, 2003; Alvarez, 2004). Some activities such as reef mining or oil drilling, however, are incompatible with coastal conservation and are totally prohibited within the MPA boundaries (Salm *et al.*, 2000; Lubchenco *et al.*, 2003).

In order to effectively conserve coral reefs on a regional to global scale, at least 20 to 40% of the coral reefs should be fully protected (Roberts and Hawkins, 2000; Gell and Roberts, 2003; Hastings and Botsford, 2003; Hughes *et al.*, 2003; Tilmant, 2004). Most resentment from local stakeholders, unfortunately, originates from the implementation of

such marine reserves. Several studies, however, have shown the long-term benefits of marine reserves for both biodiversity and economy (NCEAS, 2001). Marine reserves, in the first place, reduce the probability of extinction of the marine species residing within their borders. A review by Halpern (2003: S125) shows that '*creating a reserve appears to double density, nearly triple biomass, and raises organism size and diversity by 20–30% relative to the values for unprotected areas*'. Setting aside some parts of the coral-reef ecosystem, secondly, has also beneficial effects on the zones which are not strictly protected. Allowing the recovery of the stock of valuable exploited species at certain areas helps restocking the fishing grounds through spill-over of juveniles and adults and the export of eggs and larvae. Several studies have shown enhanced fishery catches on an increased sustainable level as compared to the pre-conservation situation (Roberts and Hawkins, 2000; NCEAS, 2001; Gell and Roberts, 2003; Lubchenco *et al.*, 2003). Besides, degrading reef areas lead to declines in overall tourist revenues (Brown *et al.*, 2001), as for example shown in table 1.3. In a similar way, marine reserves may support an increasing biodiversity in sites open to SCUBA diving. Educating stakeholders on these benefits thus is an important task in both ICZM and MPA management.

As with ICZM planning, the objective of an MPA should be clearly stated from the start (Halpern, 2003). Different objectives can be put forward such as: conserving rare and/or endemic species; increasing the overall biodiversity; restoring earlier conditions; research; fisheries management; sustainable tourism; or supporting other economic benefits (Salm *et al.*, 2000; Roberts *et al.*, 2003b). The chosen objective is largely defined by the needs, priorities and abilities of the country where the MPA will be implemented (Salm *et al.*, 2000). Depending on the objective(s) set forward, different criteria will determine the ideal siting of the MPA and the localisation of the core marine reserve in the first place (Salm *et al.*, 2000). These criteria not only concern ecological aspects, but also the political, economic and social dimensions of the MPA. Political criteria usually deal with financial sustainability, enforceability, and/or the maximum reserve size which can be controlled by existing management structures. Economic criteria concern, amongst others, employment, income (both national and personal), fishery yields, and number of tourists allowed. Social criteria are primarily valuing the accessibility of the MPA for traditional uses, the social acceptance of the proposal, and the aesthetic, educational and heritage value of the reserve or MPA (Salm *et al.*, 2000; Roberts *et al.*, 2003a).

Although some authors (e.g. Fernandes *et al.*, 1999; Brown *et al.*, 2001) deal with all aspects simultaneously through a multi-criteria analysis (MCA), Roberts *et al.* (2003a,

2003b) suggest to first delineate marine reserves based on ecological criteria. Several scenarios are subsequently proposed to the stakeholder community, after which the most supported one is chosen based on socio-economic and political criteria. In this evaluation step, MCA seems to be a good approach (Fernandes *et al.*, 1999; Brown *et al.*, 2001). By doing so, designing ecologically valueless and unsustainable marine reserves is avoided without neglecting important socio-economic considerations (Roberts *et al.*, 2003a). This approach can be applied to locate a marine reserve or a multi-use MPA; to design one single reserve or a reserve network.

One single marine reserve usually is not sufficient to help ecosystem recovery nor to enhance fishery yields (NCEAS, 2001). A network of marine reserves, consequently, is needed, covering all major habitat types within a biogeographic region (Westmacott *et al.*, 2000; NCEAS, 2001; Wilkinson *et al.*, 2003) and optimally connected by larval dispersal and/or juvenile and adult migration (ICRI, 2003; Lubchenco *et al.*, 2003; West and Salm, 2003; Wilkinson *et al.*, 2003). Such a network may be obtained through the integration of several marine reserves within one national or regional MPA (Salm *et al.*, 2000), or through the spread of several MPAs over a regional water body. The ultimate goal set forward by the GCRMN is to come to a global network of MPAs optimally protecting coral reefs worldwide (GCRMN, 2004). In the case of a marine reserve network, multiple objectives can also be met simultaneously. The network then constitutes of a number of reserves each supporting a specific goal (Salm *et al.*, 2000; Roberts *et al.*, 2003b).

The size of each marine reserve in a network and the optimal distance between them have different critical levels related to the main objective of the reserve, being conservation or fisheries management (Mascia, 2001; Roberts *et al.*, 2003b). Relatively small reserves are valuable for conservation purposes (NCEAS, 2001; Halpern, 2003) although their success increases with size (Halpern, 2003). From a certain size, however, additional conservation benefits become marginal. This upper limit is determined by the specific characteristics of the coral-reef system: rare and fragmented habitats are at higher risk of being totally lost after a disastrous event so that larger reserves are needed to preserve them as compared to extensive and well-connected habitats. The viability of the marine reserve also depends on the protection status of similar nearby habitats. If these habitats are already highly protected in other marine reserves, a smaller reserve size may be sufficient. To support sustainable fisheries, conversely, marine reserves generally need to be larger in order to sustain viable populations of exploitable fishes with commonly

large dispersal distances (Halpern, 2003). When reserves become too large, however, they lose relevance as the spill-over effect to the fisheries areas decreases.

As with size, optimal distances between marine reserves can not be defined. Much depends on the connectivity rate³⁸ of the species of interest (Palumbi, 2003). Most marine species have dispersal ranges in the order of a few tens of kilometres (Palumbi 2003). If a reserve is designed to be self-seeding, its size should be of the same magnitude. The distance to other reserves is then less important. If the reserve is designed to fit into a network, its size can be smaller but reserves should be designed such that they are not further away than the mean dispersal range of the dominant species (Palumbi 2003; Hughes *et al.*, 2003). When larval dispersal follows major ocean currents, the marine reserves network might be designed to serve as stepping stones linking remote populations (Roberts, 1997; Mascia, 2001; Palumbi, 2003). If reserves, alternatively, are designed to support sustainable fishery, distances between them should be larger, allowing sufficient spill-over effects to the fisheries areas (Roberts *et al.*, 2003b).

Finally, although marine reserves do not stop coral bleaching (Hughes *et al.*, 2003) they may facilitate ecosystem recovery after major human or natural disturbances (Roberts and Hawkins, 2000; Harley *et al.*, 2006; Schubert *et al.*, 2006). In this respect, it is sensible to safeguard those coral reefs which show more resistant or resilient to the threat posed. These reefs may serve as sources of larvae to recolonise damaged areas (Westmacott *et al.*, 2000; West and Salm, 2003; Wilkinson *et al.*, 2003). Conversely, MPAs may explicitly protect those damaged areas where corals are struggling to recover (Westmacott *et al.*, 2000). In either way, all local negative influences on these areas should be minimized. This again shows the importance of embedding MPAs in a wider ICZM.

3.1.1.2 Research and monitoring

The availability of accurate information on coral reefs and the human exploitation of these natural resources is crucial for an effective ICZM and MPA management (Ormond, 1987). Research, therefore, is a fundamental part of any management strategy. The acquisition of fundamental information first requires the collection of baseline data concerning the current status of the coral-reef ecosystem and the present human uses (Knight *et al.*, 1997; ICLARM, 1999; Salm *et al.*, 2000; Mascia, 2001; IUCN, 2005). Such a baseline survey is

³⁸ Connectivity rate is expressed by the mean dispersal range of larvae, recruits and juveniles.

important to understand the natural elements to be protected, to indicate current natural and human threats, to guide future management, and to serve as a reference point to estimate future changes (Tilmant, 2004). Concordantly, a monitoring programme needs to be set up to track such changes over time (Knight *et al.*, 1997; ICLARM, 1999; Salm *et al.*, 2000; Mascia, 2001; IUCN, 2005). Monitoring, in this respect, is defined by Wilkinson *et al.* (2003: 2) as '*the gathering of data and information on coral reef ecosystems and its users on a regular basis, preferably for an extended period of time*', basically repeating the baseline survey every 1 to 3 years. Monitoring gives insight in the natural variability and long-term trends of the coral-reef ecosystem. Against this background, managers can interpret the impact of new natural disturbances or human activities. Monitoring also provides the means to assess the extent and severity of the damage and the rate and degree of recovery afterwards. Moreover, monitoring allows an early detection of changes, permitting a timely management response (Tilmant, 2004). As such, it is an essential instrument to determine the success, or failure, of the management in reaching the stated goals whereby when needed, the management practices can be adapted in time (Mascia, 2001; NCEAS, 2001; Wilkinson *et al.*, 2003; Tilmant, 2004).

The collection of ecological and socio-economical data requires different methods. Both elements, however, can not be regarded separately as the ecological status of the reef is often crucial for the livelihoods of local people. Ecology, therefore, may have a swift and immense impact on the socio-economic behaviour of the people, and vice versa. These data should thus be collected simultaneously (Wilkinson *et al.*, 2003). Collecting ecological data mainly concerns mapping and monitoring the extent and location of the major habitats, coral reefs in particular, and understanding the status of the benthic communities and fish populations (Kelleher, 1999; Wilkinson *et al.*, 2003). This involves studying physical parameters such as depth, sea currents, temperature, water quality, visibility, and salinity, as well as biological parameters expressed by the percentage coverage of the dominant habitats including their health status, the species composition and size structure of the coral communities and fish populations, and the success of settlement or recovery after a disaster (Wilkinson *et al.*, 2003). Socio-economic assessment and monitoring provides information on how people use and value the coastal resources. It helps to understand the motivation of the resource users –e.g. poverty stimulating unsustainable fishing practices- and to identify key stakeholders which need to be involved in the management process. Special attention needs to be paid to traditional uses and the cultural and/or heritage value of the natural resources (Kelleher, 1999).

Social aspects comprise local demographics, levels of employment (with special emphasis on fishers) and incomes, social interaction between different stakeholder groups, community decision making structures, level of education, and the local awareness of the importance of a healthy coastal environment. Economic parameters which may be measured include catch and price statistics for reef fisheries, fishing techniques, level of reef use by outsiders, or the tourists' willingness to pay (Wilkinson *et al.*, 2003).

3.1.1.2.1 Remote sensing

Already since the late 1960s, aerial and space photography has been used to detect submerged features, to retrieve the seabed composition, and to map bathymetry (e.g. Ross, 1969 in: Ackleson, 2003). Since the first Landsat data became available in the mid 1970s, research (e.g. Smith *et al.*, 1975; Hammack, 1977) has explored possible applications of remote sensing in coral-reef science and management (Mumby *et al.*, 1997; Ackleson, 2003). Many studies ever since have shown the usefulness of remote sensing for providing baseline information on and monitoring of coral reefs (Green *et al.*, 1996; Bryant *et al.*, 1998; Mumby and Edwards, 2000a, Tilmant, 2004).

According to Phinn *et al.* (2000), four categories of information can be extracted from remotely sensed data. These include information on the configuration, the composition, and the biophysical parameters of the studied object, as well as on the changes over time of these elements. If this scheme is adapted to coral-reef studies, following data can be obtained:

- Information on the configuration of a coral-reef structure encompasses the localisation of the coral reef (planimetric and bathymetric) as well as a geomorphological classification. As most coral reefs are clearly detectable on satellite images, they can easily be located. Most geomorphological zones extend to large spatial scales and are often associated with a typical depth distribution. The mapping of the geomorphological zonation of a coral reef, therefore, has proven to be one of the most successful reef applications of remote sensing (Mumby *et al.*, 2004). Extracting depth information from remote sensing data is less straightforward, although many methods have already been developed.
- Remote sensing data can also be used to derive information about the reef communities, benthic habitats, or bottom types, which compose the benthic reef system. The level of detail depends on the used data and may range from

broad-scale classifications (e.g. coral, sand, algae, seagrass) to more detailed distinctions between coral species or quantitative assessments of coral and algal cover density, or seagrass standing stock (Green *et al.*, 2000b; Mumby *et al.*, 2004).

- One of the most elaborate applications in marine remote sensing is the investigation of the biophysical parameters of seas and oceans. This data is generally gathered at a relatively coarse scale and may encompass information about SST, water quality (Chl-*a* concentrations, sediments, C-DOM³⁹), salinity, waves, and currents. Besides, information can be derived concerning the marine, tropical atmosphere including data on solar radiation (both PAR and UV-B), cloud coverage, wind speed and direction, and rainfall distribution (Mumby *et al.*, 2004).
- As remote sensing data are available for the last two to three decades and data are still gathered at regular time intervals, they are ideally suited to detect changes over time in the above elements. Especially in the frame of changing climate conditions, remote sensing can be very helpful to monitor and detect shifts in community structure or in the health status of the corals (Mumby *et al.*, 2004). Different operational products have already been developed to predict potential mass bleaching sites based on changes in the biophysical parameters of the seas and oceans in which the coral reefs occur. Besides, remote sensing may be applied to track the evolution of human activities which negatively interfere with the coral-reef environment, for example the expansion of coastal urban centres. More detailed socio-economic data, however, needs to be collected in other ways. A manual for socio-economic surveys supporting coral-reef management has been published by Bunce *et al.* (2000).

The level of detail in which this information is obtained depends on the *descriptive resolution* (Green, 2000) of the remote sensing data. This descriptive resolution is function of the spatial, spectral and radiometric resolution of the data (Green, 2000). If multitemporal analyses are involved, the sensor's temporal resolution is important as well (Phinn *et al.*, 2000).

³⁹ coloured dissolved organic matter, also called *Gelbstoff* or *yellow substances*, which is the result of the breakdown of plant tissue

The use of remote sensing in coral-reef studies clearly has some advantages when compared to in situ survey methods⁴⁰. Regardless of the protocol applied, field-based surveys are spatially very heterogeneously distributed and cover only small fractions of the reefs under investigation (Hochberg and Atkinson, 2003). They, commonly, result in grids of points or in transect information, requiring interpolation to map the entire area of interest. The possibility, unfortunately, exists that objects are missed which are located between adjacent survey sites (Mumby *et al.*, 1999; Mumby *et al.*, 2000). Remote sensing, in contrast, is synoptic by virtue and samples larger areas at once. It therefore is very suitable for mapping coral reefs on a local to global scale (Mumby *et al.*, 2000; Hochberg and Atkinson, 2003). Moreover, to survey an area with equal spatial detail as with remote sensing using a uniquely field-based approach would also involve enormous amounts of staff time as well as logistic expenses. Even if the additional costs of hardware, software and trained employees are taken into account, the remote sensing approach is still more cost-effective⁴¹ than field-survey methods (Mumby *et al.*, 1999; Mumby *et al.*, 2000). This is especially important for developing countries where most of the coral reefs occur.

Besides, remote sensing offers the possibility to study coral reefs which are too remote to visit, or which are inaccessible because of physical constraints (for example reef crests and shallow reef flats (Kutser *et al.*, 2003)), political instability, or other external circumstances. Remote sensing also allows studying the situation in the past decades. In that way, a more elaborate time series of data can be formed in order to follow up possible changing conditions on the reef. Finally, most remote sensing data are in a uniform, digital format which reduces the subjectivity of the interpreter and augments the validity of the results (ICRI, 1997).

Remote sensing also has some drawbacks. The limited depth penetration of visible light in water, gradually increasing with higher turbidity, is a specific constraint for marine applications using optical remote sensing. Even in the clearest waters, only the upper 15 to 30m of the water column can be investigated (Mumby *et al.*, 2004). As most coral reefs occur in clear, shallow waters and usually only the upper parts of the coral reefs are of interest to most stakeholders, this does not prohibits remote sensing from being used in coral-related studies. Secondly, the coarse spectral and spatial resolution of most datasets recorded (Joyce *et al.*, 1995) limits the use of remote

⁴⁰ See Hill and Wilkinson (2004) for an overview of these methods.

⁴¹ Effectiveness is defined in terms of overall map accuracy (Mumby *et al.*, 1999).

sensing to coarse-scale mapping on a regional to global scale (Bryant *et al.*, 1998; Mumby *et al.*, 1999; Mumby *et al.*, 2000). With the development of new, airborne as well as spaceborne sensors having very high spatial (less than 1m) and/or spectral resolutions, these problems are largely overcome and detailed coral-reef studies can be made (Mumby *et al.*, 2004).

Remote sensing, by no means, excludes field surveys from any coral-reef study (Dahdouh-Guebas, 2002) as detailed information such as on community structure, fish size, or fish population dynamics can only be gathered in the field (Wilkinson *et al.*, 2003; Tilmant, 2004). An overview of standard protocols used for in situ surveying of tropical marine resources is given by English *et al.* (1997). Remote sensing data, alternatively, can be used to plan field surveys more cost-effectively, improve their efficiency, and ensure an adequate sampling of all relevant habitats (Salm *et al.*, 2000). The ideal approach would be *multi-level sampling* (Bryant *et al.*, 1998) in which in situ observations are used for detailed, ground-truthing data acquisition in order to calibrate and validate the satellite data (ICLARM, 1999; Salm *et al.*, 2000; Tilmant, 2004). The remote sensing data would then be used to extrapolate this locally gathered information to unsurveyed areas based on physical, i.e. spectral, measurements instead of using interpolation techniques (Mumby *et al.*, 1999; Edwards, 2000; Mumby *et al.*, 2000; Mumby *et al.*, 2004). Current monitoring techniques, therefore, range from underwater observations of coral reefs to analyses of satellite data (Bryant *et al.*, 1998).

Although current research in coral-reef remote-sensing applications is mainly directed towards hyperspectral, airborne data (e.g. Hochberg *et al.*, 2003), this type of data was still very experimental at the start of this research, and was therefore not integrated in this study. Besides, a relatively large area, namely the northwestern Red Sea, is envisaged for investigation. For such spatial dimensions, satellite data is the most cost-effective option (Edwards, 2000). Moreover, as it is the intention to develop a methodology which can be implemented in the Red Sea riparian countries, the price of remote sensing data can not be neglected. Most multispectral data are readily available at relatively low costs, while collecting hyperspectral information requires a specifically planned flight to acquire the data which augments the price drastically. As neither we nor most developing countries possess the financial and/or logistic means to execute such a campaign, multispectral data are the only realistic option. Whenever

more detailed information for specific interest areas is required, hyperspectral data can still be integrated in a later stage.

3.1.1.2.2 *Geographic information system*

Although remote-sensing-derived information is valuable on its own, it has its best use when integrated in a geographic information system (GIS) (fig. 3.2) (Knight *et al.*, 1997; Salm *et al.*, 2000; Thanilachalam and Ramachandran, 2002; Tilmant, 2004). A GIS allows storing, archiving, retrieving and displaying georeferenced datasets from different sources, different moments and different spatial scales (Drummond *et al.*, 1997; Stanbury and Starr, 1999; Salm *et al.*, 2000; Tilmant, 2004). A GIS also permits the integration of data from different economic sectors, areas (marine and land-based) and disciplines (social and natural sciences) (Cicin-Sain, 1993; Knight *et al.*, 1997). As such, a GIS facilitates the linkage between remote-sensing-derived products and additional datasets including: socio-economic data; information on the effective or proposed legislation; data on the urban coastal development; marine and inland pollution data; detailed information gathered during field trips; information about natural hazards; long-term monitoring data; and much more (Salm *et al.*, 2000; Crosby *et al.*, 2002). Additionally, as a GIS is open-ended by definition, newly acquired data can be easily added, while old data might be digitised and integrated as well (Salm *et al.*, 2000; Chapman and Turner, 2004).

At least as important, a *Coral Reef GIS* is useful as a tool to analyse the different data layers. This is very valuable (Knight *et al.*, 1997; Stanbury and Starr, 1999; Salm *et al.*, 2000; Freire, 2001) for example to understand the spatial relations of coral reefs; to detect natural and anthropogenic changes; to indicate areas of high biodiversity or human activity; to model different spatial and temporal processes; or to determine specific risk zones which mark those reefs under potential stress –i.e. *risk assessment mapping* (Bryant *et al.*, 1998)- or most sensitive to stress –being *sensitivity mapping* (El-Raey *et al.*, 1996).

The outcomes of these analyses may be used by coastal managers to support ecosystem-based decisions for example in identifying multi-use MPAs; monitoring coastal development; assessing environmental impacts of natural hazards or legislative decisions; evaluating various proposed management scenarios; oil spill contingency planning (El-Raey *et al.*, 1996; Gayanilo *et al.*, 1998); or accessing new fishing

grounds (Knight *et al.*, 1997; Stanbury and Starr, 1999; Mumby and Edwards, 2000a; Salm *et al.*, 2000; Freire, 2001; Chapman and Turner, 2004; Tilmant, 2004).

As a GIS is a highly visual and interactive system, it also is a very useful tool to communicate with the general public, to raise their environmental awareness, and to educate them on the importance of the coral reefs and the need for conservation. GIS data usually are easily understandable albeit visualising diverse datasets, different proposed management scenarios, or changes in the status of the coastal resources. As such, it augments the role of the stakeholders in management planning as it interactively models the impacts of their proposals (Knight *et al.*, 1997; ICLARM, 1999; Salm *et al.*, 2000; Mascia, 2001; Crosby *et al.*, 2002; Wilkinson *et al.*, 2003; Chapman and Turner, 2004). GIS databases, furthermore, are easily distributable on CD/DVD or over the internet, e.g. through a virtual data management centre such as ReefBase, facilitating networking and the exchange of information amongst researchers and managers dealing with similar coastal-related issues all over the world (Knight *et al.*, 1997; Salm *et al.*, 2000; Crosby *et al.*, 2002).

3.1.2 Study area

As became clear in previous chapters, the Red Sea is an ideal physical environment for coral-reef growth. However, since the 1960s, human interference with the natural environment is steadily increasing, leading to negative impacts on the health and status of these coral reefs (Pilcher and Alsuhaibany, 2000; PERSGA, 2001). The situation becomes especially worrisome in the northwestern part of the Red Sea, i.e. along the Egyptian coastline. While total population growth in Egypt is already very high and varies around 20% per year (Gladstone *et al.*, 1999), the Red Sea coastal population even is expected to double every 10 years (Gladstone *et al.*, 1999; PERSGA, 2001) both as a result of booming tourism and the national policy that encourages resettlement outside the overcrowded Cairo area (Wilson, 1998).

Salem (2002) estimates that already more than 30% of the reefs along the Egyptian Red Sea coast has been damaged, predominantly by human activities. The most threatening impacts in this region are oil exploitation, mainly in the Gulf of Suez; the ship traffic through the Suez Canal and across the Red Sea; the increasing fishing pressure in the Gulf of Suez and Foul Bay; and the booming tourism development. The population and their related activities, however, are not evenly distributed along the Egyptian Red Sea shores, but rather are

concentrated in a few urban settlements (table 3.1) (PERSGA, 2001) such as Hurghada (fig. 3.3). As a result, some parts of the northwestern Red Sea coastal zone are still relatively pristine and largely unaffected by human interference (Spalding *et al.*, 2001).

Table 3.1. Overview of the urban settlements along the Egyptian Red Sea coast with indication of major economic activities (source: PERSGA, 2001)

| governorate/city | population | major economic activities |
|--------------------------------|-------------------|----------------------------------|
| <i>South Sinai Governorate</i> | <i>82,800</i> | |
| Nuweiba | 15,000 | port, tourism |
| Dahab | 10,000 | tourism |
| Sharm el Sheikh | 20,000 | tourism, port, fishing |
| El Tur | 30,800 | tourism, port, fishing |
| Abu Rudees | 7,000 | oil fields |
| <i>Suez Governorate</i> | <i>446,700</i> | |
| Ras Sudr | 5,000 | tourism |
| Suez | 440,000 | port, fishing, industry |
| Ain Sukhna | 500 | tourism, oil |
| Zaafarana | 1200 | tourism |
| <i>Red Sea Governorate</i> | <i>89,050</i> | |
| Ras Gharib | 5,300 | oil fields, industry |
| Hurghada | 46,050 | oil, fishing, tourism, port |
| Safaga | 11,000 | mining, port, fishing |
| El Quseir | 22,000 | fishing, mining, trade |
| Marsa'alam | 1700 | mining, fishing |
| Abu Ghosoon | 2000 | mining |
| Shalateen | 1000 | fishing, camel trade |
| total | 618,550 | |

3.1.2.1 Oil exploitation and transport

The majority of oil and gas exploitation in the Red Sea is concentrated in the Gulf of Suez and the northwestern part of the Red Sea (PERSGA, 2001; Pilcher and Abou Zaid, 2003). Since the major oil spill in 1982 when 75% of the Egyptian Red Sea coast was smothered with oil (PERSGA, 2001), more than 20 other large oil spills occurred in this part of the Red Sea (PERSGA, 2001; Pilcher and Abou Zaid, 2003). Moreover, small spills are reported on a monthly basis, which mostly are the result of inefficient and ineffective

operation of equipment, illegal discharges, and lack of supervision (PERSGA, 2001; Pilcher and Abou Zaid, 2003). Because of the shallow nature of the Gulf of Suez and the prevailing currents, each spill will mostly have a devastating effect on the marine coastal habitats (PERSGA, 2001). The pollution from ships transporting oil or other products may not be underestimated either (Spalding *et al.*, 2001; Pilcher and Abou Zaid, 2003). The construction of a terminal of the Trans-Suez pipeline at Ain Sukhna, for example, significantly augmented the marine pollution in the northern part of the Gulf of Suez (PERSGA, 2001).

3.1.2.2 Fishing pressure

The Red Sea fisheries, which account for nearly 16% of Egypt's marine fisheries (Pilcher and Abou Zaid, 2003), currently comprise 11 to 14% of the total annual Egyptian fish production (Pilcher and Alsuhaibany, 2000; Pilcher and Abou Zaid, 2003). 44% of this catch originates from coral-reef fisheries (Pilcher and Alsuhaibany, 2000). 78% of the total landings is reported in Suez (Pilcher and Abou Zaid, 2003), although only one third of the fishing fleet registered in Suez actually operates in the Gulf of Suez. Most of the fleet is active in the central and southern Red Sea (PERSGA, 2001; Pilcher and Abou Zaid, 2003).

Table 3.2. Number of fishermen active in Egypt's Red Sea fisheries (source: General Authority for Fish Resources Development (GAFRD) in: Hariri *et al.*, 2000)

| Suez | | Hurghada | | El Quseir | | El Tur | | other | | total |
|--------|----|----------|----|-----------|---|--------|---|-------|---|--------|
| # | % | # | % | # | # | # | % | # | % | # |
| 13,376 | 75 | 2,022 | 11 | 1,227 | 7 | 831 | 5 | 462 | 2 | 17,918 |

In terms of employment, 7% of the Egyptian national workforce is involved in the fishing industry (Pilcher and Alsuhaibany, 2000), with nearly 18,000 fishermen active on the Red Sea (table 3.2) (Hariri *et al.*, 2000; PERSGA, 2001). About 53% of the Egyptian fishermen on the Red Sea are predominantly artisanal, using hook and line and/or set nets (Hariri *et al.*, 2000). These artisanal fishermen usually work on the fringing coral reefs along the coast, while the industrial fishing fleet is completely concentrated in the Gulf of Suez and Foul Bay.

Yearly fish catches in the late 1980s and throughout the 1990s were highly irregular ranging between 20,297 tonnes in 1987 and 40,545 tonnes in 1989 (table 3.3). In 1997, the

GAFRD of the Egyptian Ministry of Agriculture developed a strategy to stabilise fish catches and increase the yearly volume to 70,000 metric tonnes by 2017 (PERSGA, 2001). As a result, fish catch volumes increased significantly as of 1999, although still varying considerably from year to year (table 3.3). Fishing pressure in the past was considered low for the northwestern Red Sea (Spalding *et al.*, 2001), although the new GAFRD incentive may become problematic, especially at the most popular fishing grounds, as a supporting fisheries management plan is currently not in place (Pilcher and Alsuhaibany, 2000). Destructive fishing practices are not as widespread as in Southeast Asia, although reports are known of cyanide and dynamite fishing in some parts of the Egyptian Red Sea (e.g. Riegl and Luke, 1998).

Table 3.3. Egyptian Red Sea fish catches (tonnes) between 1980 and 2003 (SAU, 2006)

| | | | | | | | |
|-------------|-------------|-------------|-------------|-------------|-------------|-------------|-------------|
| 1980 | 1981 | 1982 | 1983 | 1984 | 1985 | 1986 | 1987 |
| 6,047 | 12,792 | 10,195 | 11,682 | 10,067 | 19,757 | 16,263 | 20,297 |
| 1988 | 1989 | 1990 | 1991 | 1992 | 1993 | 1994 | 1995 |
| 26,024 | 40,545 | 35,465 | 37,014 | 39,326 | 32,429 | 30,210 | 25,657 |
| 1996 | 1997 | 1998 | 1999 | 2000 | 2001 | 2002 | 2003 |
| 29,953 | 35,272 | 35,110 | 74,605 | 66,272 | 67,394 | 68,009 | 62,626 |

3.1.2.3 Tourism and coastal development

Tourism is the second most important source of revenue for the Egyptian economy and is also one of its largest employers (PERSGA, 2001). As such, it often is utilized by the Egyptian government as an instrument for regional development and population distribution (TDA, 1995 in: PERSGA, 2001). With an ever increasing number of international arrivals each year, e.g. a 16.42% growth between 2002 and 2003 (table 3.4), tourism is also the fastest growing economic activity in Egypt (PERSGA, 2001). Even compared with a mean annual growth of 5.9% in world tourism, this growth is extraordinary (TDA, 1996; in: PERSGA, 2001).

Initially, international tourism was completely focused on the Egyptian antiquities along the Nile valley. Since the mid-1980s, an increasing number of tourists, however, started to visit the Egypt's coasts. Nowadays, about 2.5 million tourists visit Egypt's coastal areas each year, of which 23% are specifically dive tourists and an additional 22% takes part in snorkelling trips (Cesar, 2003 in: Cesar *et al.*, 2003). Most of these activities are concentrated in South Sinai (Sharm el Sheik) and the Red Sea Governorate

(Hurghada) (Smits and Shousha, 1998) while to a much smaller extent, domestic leisure tourism also takes place along the Gulf of Suez and the Mediterranean Sea (Ormond, 1987; PERSGA, 2001).

Table 3.4. Evolution of arrivals and overnight stays of non-resident visitors in Egypt between 1999 and 2003 (source: WTO, 2005)

| | 1999 | 2000 | 2001 | 2002 | 2003 | % change 2003-02 |
|--|------------|------------|------------|------------|------------|---------------------|
| Arrival of non-resident visitors | 4,796,520 | 5,506,179 | 4,648,485 | 5,191,678 | 6,044,160 | 16.42 |
| Overnight stays of non-resident visitors | 31,002,088 | 32,787,881 | 29,813,290 | 32,663,954 | 53,129,907 | 62.66 |

Detailed statistics on tourism in the Egyptian Red Sea region are scarce and should be interpreted with care (Shaalán, 2005). Following figures, nevertheless, give an idea of the proportions to which tourism has grown over the last 20 years:

- Until the mid-1980s, only two hotels were known in Sharm-el-Sheikh (Smits and Shousha, 1998) hosting up to 10,000 snorkellers and divers each year (Ormond, 1987). Since then, an average annual growth rate of 42% in foreign tourism has been estimated for this area (PERSGA, 2001). In 1993, approximately 411,000 tourists were visiting South Sinai (UNEP, 1997), reaching already 500,000 in 1997 of which ca. 60% were snorkellers or divers (Shehata, 1998). In 1988, 600 tourist beds were available in Sharm el Sheikh, rapidly increasing to 6,000 in 1995, 16,000 in 1999 (Spalding *et al.*, 2001) and an estimated 20,000 by 2002 (Felton, 2000). Development in the region still continues unappeased and a ceiling of 160,000 beds is set to be reached in 2017 (Shehata, 1998).
- Hurghada accounted for roughly 1,800 rooms in 1990 (Smits and Shousha, 1998); by 2000, this number had increased to 15,000 (Felton, 2000). In 1980, 16,200 roomnights were booked, rapidly increasing to 207,000 in 1990 of which 70% were foreign tourists (Smits and Shousha, 1998). From 1995 to 2000, international arrivals almost doubled to 1 million (Smits and Shousha, 1998; Felton, 2000).

Inspired by the success of tourism in the Red Sea region and the resulting rise in foreign revenue and employment opportunities, tourism development of the Red Sea coast has

become a prime target for the Egyptian government (PERSGA, 2001). In the Sinai, investments have been augmented at Sharm el Sheikh and new developments are started in Nabq Bay, Nuweiba and Taba (PERSGA, 2001; Spalding *et al.*, 2001). For the western Egyptian Red Sea coast, plans are even more ambitious and a coastal strip of 800km from El Gouna in the north to Ras Banas in the south is reserved for tourism and residential developments (Riegl and Piller, 2000; McEachern, 2002). The goal is to accommodate 16 million tourists per year by 2017 (Shaalan, 2005), concentrated in integrated resort communities (Felton, 2000), like El Gouna⁴² today, each with a maximum capacity of 100,000 transient guests and employees (TDA, 1998).

Large-scale tourism, unfortunately, may have devastating impacts on the vulnerable natural environment which is the main attractor of tourists (PERSGA, 2001). In Hurghada alone, 80 (Jameson *et al.*, 1999; Hanafy, 2000) to 150 (Hassenstein and Hirsch, 2002) dive centres are active, operating over 1000 dive boats on a daily basis (Hanafy, 2000; Hassenstein and Hirsch, 2002). Although a carrying capacity of 10,000 divers per year is regarded as sustainable for Red Sea reefs (Cesar *et al.*, 2003), the most heavily used dive site in Sharm el Sheikh receives up to 50,000 divers a year (Hawkins and Roberts, 1997); in the Hurghada area, this even amounts to well over 100,000 (Cesar *et al.*, 2003). Flipper and anchor damage are therefore noted on most reefs near Hurghada (Riegl and Velimirov; 1991; Cesar *et al.*, 2003), Sharm el Sheikh (Cesar *et al.*, 2003), and even in the Ras Mohammad National Park (Medio *et al.*, 1997). In Hurghada, for example, Abou Zaid (2002, in: Cesar *et al.*, 2003) describes that the most heavily visited sites have only live coral cover percentages between 29 and 34% as compared to a live coral coverage of 69-75% on non-diving control sites. Although prohibited by law, souvenir collection on the reefs remains a problem in popular areas and many marine organisms end up in the illicit curio trade (PERSGA, 2001) (fig. 3.4). During field campaigns between 2000 and 2002, no personal observations were made, but in spring 2003, small curio-sellers were encountered, obviously with illegal stands.

Probably even more problematic, because acting on a much larger scale, are the indirect impacts of the largely uncontrolled development of infrastructure, tourist resorts, and residential accommodations. In the past, coastal development was hardly controlled and coastal development took place in a strip-like fashion along the coastline near Hurghada and Sharm el Sheikh (PERSGA, 2001; Spalding *et al.*, 2001). As a result,

⁴² a large tourist resort north of Hurghada

extensive coastline modifications have been carried out and barely any stretch of coast near the major urban centres is left without alteration by dredging or landfilling operations (UNEP, 1997; PERSGA, 2001). Between 1994 and 1997, an estimated 2,900,000m² of reef flat offshore Hurghada has been landfilled, and the resulting sediment plume extended several kilometres offshore (Pilcher and Abou Zaid, 2003).

As the Red Sea coastal zone is a desertic area, special attention should be paid to the fresh water supply sustaining tourism as well as domestic use (table 3.5). This is of special importance to Egypt as its total annual water use already amounts to 97% of the net annual renewable water available (Gladstone *et al.*, 1999). In the past, water was supplied to Hurghada with water tanks coming from the Nile Valley (Soenen, 1997) (fig. 3.5). Recently, 3 pipelines with a daily capacity of 80,000m³ have been constructed to supply the entire western Egyptian Red Sea coast (table 3.5) (Hafez and El-Manharawy, 2002). In addition, most coastal towns have large government-owned desalination plants and many tourist resorts also rely on private plants to meet their fresh water requirements (UNEP, 1997; Hafez and El-Manharawy, 2002; Hoepner and Latteman, 2002).

Table 3.5. Assessment of fresh-water demand and supply in the Red Sea and South Sinai Governorate (source: Hafez and El-Manharawy 2002; * Abou Rayan *et al.*, 2001)

| | 2001 | | 2020 | |
|-----------------------|--------------------------------------|------------------------------------|--------------------------------------|------------------------------------|
| | Red Sea coast (m ³ /d) | South Sinai (m ³ /d) | Red Sea coast (m ³ /d) | South Sinai (m ³ /d) |
| Nile water pipelines | 80,000 | 0 | 140,000 | 30,000 |
| fresh ground water | 0 | 10,000 | 0 | 25,000 |
| seawater desalination | 97,000 | 40,000* | 250,000 | 150,000 |
| estimated demand | 500,000 | 125,000 | 1,000,000 | 600,000 |
| water shortage | 323,000 | 75,000 | 610,000 | 395,000 |

Further investments in water supply are needed to overcome the water shortage already existing today and which is expected to become worse in the near future (table 3.5) (Hafez and El-Manharawy, 2002). In the next decade, two additional pipelines with a capacity of 60,000m³/day and 30,000m³/day are therefore planned to supply the western Red Sea coast and South Sinai respectively (Hafez and El-Manharawy, 2002). As the Nile water is already used to its maximum, desalination is most probably the only realistic, long-term

solution. The discharge of hot brine by these desalination plants may however negatively affect the coastal environment (see section 2.4.6.2.3).

Besides, sewage water is often only partially treated or even untreated and directly released to the sea (section 2.4.6.2.2) or to inland dumping sites (Soenen, 1997). As a result, pollution due to sewage and consequent coral damage has been noted at most localities along the Egyptian Red Sea coasts (Jameson *et al.*, 1999). Investments in water treatment plants are therefore urgently needed (UNEP, 1997). These plants might probably also resolve part of the water shortage by recycling waste water for domestic use.

3.1.2.4 Management

Due to the rapidly deteriorating environment, there is an urgent need for protection of the ecosystems in the Red Sea, preferably embedded in a framework of ICZM (Ormond, 1987; Gladstone *et al.*, 1999; Pilcher and Alsuhaibany, 2000; Gerges, 2002). At this moment, most required actions are still preventive in nature and less expansive than in other more threatened regions (Gladstone *et al.*, 1999). However, if measures are not taken soon, the ecological integrity of the Red Sea coastal environment will become undermined, leading to major socio-economic and financial consequences for the bordering countries (Gerges, 2002).

Fortunately, the Egyptian government recognises the importance of a healthy coastal environment and the serious problems massive uncontrolled coastal development and tourism may pose. Several responsible Egyptian authorities, like the Egyptian Environmental Affairs Agency (EEAA), the Tourist Development Agency (TDA), and the local Red Sea governorates, therefore, have issued numerous laws and guidelines to stop the unlimited development (Pilcher and Abou Said, 2003). To give just one example, since 1994, an environmental impact assessment study is required by the EEAA before any coastal development is permitted. One of the rules which has to be followed is the creation of a setback zone of 50 to 200m, depending on the topography, to protect the sensitive coastal habitats (TDA, 1998).

Besides, large parts of Egypt's coastal areas are incorporated in MPAs. The most successful initiative is the protection of the coastal zone around the Sinai Peninsula and along the Gulf of Aqaba. The coral reefs at the tip of the Sinai Peninsula became protected in 1983, when the Ras Mohammad MPA, extending over 97km², was declared by Presidential Decree. The Ras Mohammad MPA only existed on paper until it was

renamed the Ras Mohammad National Park in 1990 and an effective management plan became operational (Spalding *et al.*, 2001; Pilcher and Abou Zaid, 2003). In the mean time, the protected area was expanded to 210km². In 1992, two additional coastal areas were protected, namely the Nabq Multiple Use Management Area covering the northernmost mangroves in the Red Sea, and the Abu Galum Multiple Use Management Area. In 1994, these three parks were linked through the protection of the interconnecting coastlines, forming the Ras Mohammad National Park Sector, covering 1470km² of marine and terrestrial habitats (Shehata, 1998; Pilcher and Abou Zaid, 2003).

Along the northwestern Red Sea coast, the Jebel Elba Protectorate was almost simultaneously declared in 1986, being the largest protected area in Egypt as it encompasses 35,000km² of land and coastal zones (Pilcher and Abou Zaid, 2003). In the course of time, seven additional MPAs have been proposed, covering 22 islands in the Red Sea, including Giftun Island, and the important coral reefs near the Brothers Island, Daedalus, Zabargad, and Rocky Island (Spalding *et al.*, 2001; Pilcher and Abou Zaid, 2003). Even more ambitious, plans are being made to integrate all existing protected areas into one big *International Red Sea Marine Park* (Salm *et al.*, 2000). Most of these MPAs, unfortunately, still lack decent management structures securing their implementation and enforcement on the field (Riegl and Piller, 2000).

In Egypt, as in many countries, implementation and enforcement of environmental laws and regulations remain very problematic (Fouda, 1998; Gladstone *et al.*, 1999; Pilcher and Alsuhaibany, 2000; Hassan *et al.*, 2002). As the Government of Egypt is highly sectoral, each department has its own goals and priorities with only a minimal overall structure. Issued laws, therefore, are often overlapping, contradictory or unclear. In addition, controlling agencies lack the technical and/or human capacity for effective monitoring and enforcement, while the determined fines usually are too low to deter from serious violation (PERSGA, 2001).

Moreover, economy and ecology are often in apparent contradiction for the Egyptian government. Tourism is an important economic sector providing jobs for thousands of Egyptians. Besides, the infrastructure and services developed for tourism can be used to stimulate people to relocate outside the overpopulated Nile Valley. Fear, therefore, exists that future developments will follow the same pattern as before (Wilson, 1998; Shaalan, 2005). The ambitious plan to receive 16 million visitors by 2017, for example, puts extra pressure on the coastal zone managers (Shaalan, 2005). As a result, developers and investors are not always enforced to strictly follow the environmental laws. On the

contrary, they are encouraged to accomplish the planned developments in order to fulfil the national economic development plans, regardless of the advice given by the EEAA (Shaalán, 2005).

Besides, with the enormous number of tourists planned to visit the Red Sea coasts, Shaalan (2005) also expects the character of tourism to change from nature-based diving tourism to mass 3S (sea, sun, sand)-package tourism. While tourists interested in diving, generally, are willing to pay extra for the uniqueness of the biodiversity in their destination, most 3S-package tourists are only interested in the lowest prices. This change in tourism approach partly is the result of an already deteriorated environment, forcing tour operators to change their marketing tool. When this evolution sets through, an important incentive may be lost to incorporate ecological guidelines in development plans.

The Ras Mohammad National Park, in contrast, shows a more positive future. The Ras Mohammad National Park managers are able to maintain the integrity of the coral reefs while allowing coastal zone development and tourism through the enforcement of a zero discharge policy and a strict obedience to the environmental rules set forward by the government. This could only be done because local management was sufficiently funded and was provided with technical equipment, staff and training. The income generated by visitor fees currently even succeeds the operating and recurrent costs, making the Ras Mohammad National Park Sector fully self-financed. This MPA, therefore, is nowadays regarded as a benchmark for other protected areas in the region, and joint training exercises are often provided for managers from other Red Sea countries (Salm *et al.*, 2000).

Additionally, small-scale, local initiatives are taken as well. In a project funded by USAID, EEAA, and several NGOs, the Hurghada Environmental Protection and Conservation Agency (HEPCA), for example, has installed hundreds of mooring buoys around Hurghada to prevent further anchor damage to the reefs (Spalding *et al.*, 2001; Hassan *et al.*, 2002; Pilcher and Abou Zaid, 2003). Also, one of the few projects for renewable energy in Egypt is located north of Hurghada. Here, a wind power plant is being tested which supplies electricity to the desalination plants, tourism villages, and other services in the Hurghada region (PERSGA, 2001).

Not all problems, however, can be effectively tackled on the local or national level. Issues such as marine pollution, and oil pollution in particular, can only be dealt with internationally (Ormond, 1987; Fouda, 1998). Egypt, therefore, is signatory to many

international conventions such as the *International Convention for the Prevention of Marine Pollution from Ships* (MARPOL) or the *Protocol for the Regional Cooperation for Combating Pollution by Oil and other Harmful Substances in Cases of Emergency* (Pilcher and Abou Zaid, 2003). A useful opportunity for regional cooperation with the other Red Sea riparian countries is the Regional Organization for the Conservation of the Environment of the Red Sea and Gulf of Aden (PERSGA)⁴³, established in 1995 under the umbrella of the Arab League.

Through this international cooperation, the idea of ICZM has found ground in Egypt. Already in 1996, the National Committee for Integrated Coastal Zone Management (NCICZM) was initiated by the EEAA. Its main objective is to coordinate all coastal activities among the competent authorities in order to harmonise development with the carrying capacity of the coastal ecosystems (PERSGA, 2001; Pilcher and Abou Zaid, 2003). Although still struggling with the sectoral structure of the Egyptian government, the NCICZM gradually evolves to a focal point of ICZM in Egypt (PERSGA, 2001). Besides more effective implementation and enforcement of the existing rules and laws, three major shortcomings have been identified in the status of Egypt's ICZM, being: the lack of appropriate baseline environmental information and a monitoring programme; insufficient ICZM planning; and too little public participation and education (Fouda, 1998; Pilcher and Alsuhaibany, 2000; Pilcher and Abou Zaid, 2003).

At least for collecting baseline information, remote sensing and GIS are recognised as useful tools to improve current knowledge bases (UNEP, 1997; Pilcher and Abou Zaid, 2003). The research presented here may thus be seen as a showcase of how these tools can be applied in the Red Sea context to come to a more elaborate ICZM.

⁴³ <http://www.persga.org>

3.2 DATA AND MATERIALS

3.2.1 Satellite data

3.2.1.1 Landsat 7 ETM+

Table 3.6. Overview of the main characteristics of the Landsat 7 platform and ETM+ sensor (source: USGS, 2006a)

| Landsat 7 Platform | | |
|--|--|-----------------|
| Launched | April 15 th , 1999 | |
| orbit type | sun synchronous, 705km altitude | |
| equator crossing | 10 a.m., descending | |
| Enhanced Thematic Mapper Plus (ETM+) Sensor | | |
| spectral resolution | band # | wavelength (nm) |
| | 1 | 450-520 |
| | 2 | 530-600 |
| | 3 | 630-690 |
| | 4 | 760-900 |
| | 5 | 1550-1750 |
| | 6 (TIR) | 10400-12500 |
| | 7 | 2080-2350 |
| 8 (Pan) | 520-900 | |
| spatial resolution | 30m (MS) 60m (TIR) 15m (Pan) | |
| swath width | 185 by 170km | |
| radiometric resolution | 8 bit | |
| temporal resolution (revisit time) | 16 days | |
| Price | \$600 per scene free of charge: http://glcf.umiacs.umd.edu/data/ | |

Table 3.7. Specific information of the Landsat 7 ETM+ dataset used

| | | |
|----------------------|---|-----------------------------------|
| reseller | USGS, http://edcimswww.cr.usgs.gov/pub/imswelcome/ | |
| data characteristics | scene ID | LE1744041000025450 |
| | processing level | Landsat 7 ETM+ L1G |
| | acquisition date | September 10 th , 2000 |
| | acquisition time | 08:02:46-08:03:13 GMT |
| | sun elevation | 57.6681976 |
| | sun azimuth | 130.1355286 |

3.2.1.2 Landsat 5 TM

Table 3.8. Overview of the main characteristics of the Landsat 5 platform and TM sensor (source: USGS, 2006b)

| Landsat 5 Platform | | |
|---------------------------------------|--|-----------------|
| Launched | March 1 st , 1984 | |
| orbit type | sun synchronous, 705km altitude | |
| equator crossing | 9.45 a.m., descending | |
| Thematic Mapper (TM) Sensor | | |
| spectral resolution | band # | wavelength (nm) |
| | 1 | 450-520 |
| | 2 | 520-600 |
| | 3 | 630-690 |
| | 4 | 760-900 |
| | 5 | 1550-1750 |
| | 6 (TIR) | 10400-12500 |
| 7 | 2080-2350 | |
| spatial resolution | 28.5/30m (MS) 120m (TIR) | |
| swath width | 185 by 185km | |
| radiometric resolution | 8 bit | |
| temporal resolution (revisit time) | 16 days | |
| Price | \$425 per scene free of charge: http://glcf.umiacs.umd.edu/data/ | |

Table 3.9. Specific information of the Landsat 5 TM dataset used

| | | |
|----------------------|---|--------------------------------|
| reseller | Global Land Cover Facility: http://glcf.umiacs.umd.edu/data/ Courtesy of the U.S. Geological Survey | |
| data characteristics | scene ID | 012-953 |
| | processing level | Earthsat Ortho |
| | acquisition date | August 14 th , 1987 |
| | acquisition time | 07:37:00 GMT |
| | sun elevation | 58.33 |
| | sun azimuth | 106.74 |

3.2.1.3 QuickBird

Table 3.10. Overview of the main characteristics of the QuickBird platform and sensor (source: DigitalGlobe, 2004)

| QuickBird Platform | | |
|---------------------------------------|--|-----------------|
| launched | October 18 th , 2001 | |
| orbit type | sun synchronous, 450 km altitude | |
| equator crossing | 10.30 a.m., descending | |
| QuickBird Sensor | | |
| spectral resolution | band # | wavelength (nm) |
| | 1 | 450-520 |
| | 2 | 520-600 |
| | 3 | 630-690 |
| | 4 | 760-900 |
| 5 (Pan) | 450-900 | |
| spatial resolution | 2.44 or 2.88m (multispectral) (MS) 0.61 or 0.72m (panchromatic) (Pan) | |
| swath width | 16.5 by 16.5km (at nadir) min.: 25km ² (archive) – 64km ² (new acquisition) | |
| radiometric resolution | 11 bit (delivered as 8 or 16 bit) | |
| temporal resolution (revisit time) | on demand max. 1-3.5 days (30° off-nadir, depending on latitude) | |
| Price | \$18/km ² (archive) - \$22/km ² (on demand) | |

Table 3.11. Specific information of the QuickBird dataset used

| | | | |
|----------------------|---|---------------------------------|----------------|
| Reseller | GIM nv, http://www.gim.be | | |
| data characteristics | archived image ID | 10100100001A7D01 | |
| | acquisition date | February 5 th , 2002 | |
| | acquisition time | 08:27:03 GMT | |
| | spatial resolution | 2.88m MS | 0.71m Pan |
| | georeference | WGS84 – UTM 36 N RMSE: 14m | |
| | off nadir angle | 9° | |
| | in track view angle | -3.47444 (MS) | -3.29214 (Pan) |
| | cross track view angle | 7.62389 (MS) | 7.63434 (Pan) |
| | target azimuth | 298° | |
| | satellite azimuth | 123.234 (MS) | 122.072 (Pan) |
| | satellite elevation | 80.9462 (MS) | 81.0175 (Pan) |
| | sun elevation | 41.6595 | |
| | sun azimuth | 149.983 | |

3.2.1.4 ASTER

Table 3.12. Overview of the main characteristics of the Terra platform and ASTER sensor (source: ERSDAC, 2003)

| Terra Platform | | | |
|---|---|------------------------------|----------------|
| launched | December 18 th , 1999 | | |
| orbit type | sun synchronous, 705km altitude | | |
| equator crossing | 10.30 a.m., descending | | |
| Advanced Spaceborne Thermal Emission and Reflection Radiometer (ASTER) | | | |
| spectral resolution | band # | central band wavelength (nm) | band with (nm) |
| | Visual and Near InfraRed (VNIR) | | |
| | 1 | 560 | 80 |
| | 2 | 660 | 60 |
| | 3 | 810 | 100 |
| | 3b | 810 | 100 |
| | Short-Wave InfraRed (SWIR) | | |
| | 4 | 16500 | 100 |
| | 5 | 21650 | 40 |
| | 6 | 22050 | 40 |
| | 7 | 22600 | 50 |
| | 8 | 23300 | 70 |
| | 9 | 23950 | 70 |
| | Thermal InfraRed (TIR) | | |
| 10 | 83000 | 350 | |
| 11 | 86500 | 350 | |
| 12 | 91000 | 350 | |
| 13 | 106000 | 700 | |
| 14 | 113000 | 700 | |
| spatial resolution | 15m (VNIR: band 1-3) 30m (SWIR: band 4-9) 90m (TIR: band 10-14) | | |
| swath width | 60 by 60km | | |
| radiometric resolution | 8 bit (band 1-9) 12 bit (band 10-14) | | |
| temporal resolution (revisit time) | 16 days 5 days (off-nadir) | | |
| Price | \$ 55 per scene | | |

Table 3.13. Specific information of the ASTER dataset used

| | | |
|----------------------|---|--|
| reseller | USGS, http://edcimswww.cr.usgs.gov/pub/imswelcome/ | |
| data characteristics | scene ID | SC:AST_L1B.003:2017822535 |
| | processing level | L1B registered radiance at sensor V003 |
| | acquisition date | March 21 st , 2001 |
| | acquisition time | 08:40:26.30 GMT |
| | sun elevation | 58.007487 |
| | sun azimuth | 144.399944 |

3.2.2 Field data

3.2.2.1 Field surveys

Field surveys are essential for any remote sensing application. They are useful to get acquainted with the study area and to gather information which serves as ground truth data and accuracy test points in the processing and validation of the remote-sensing-derived datasets. During the past six years, three field campaigns have been executed in the Hurghada area with more than 650 observations made at sea and 62 ground control points (GCPs) measured on land (table 3.14). The collected data are summarised in annex III.

Table 3.14. Overview of the three field campaigns made in the specific study area

| | Period | # observations at sea | # GCPs on land |
|------------|----------------------------|------------------------------|-----------------------|
| campaign 1 | 08/25/2001 till 08/31/2001 | 159 | 29 |
| campaign 2 | 03/28/2002 till 04/04/2002 | 262 | 30 |
| campaign 3 | 08/23/2003 till 08/27/2003 | 231 | 3 |

The first two field surveys were specifically aimed at depth measurements in order to calibrate the bathymetric map derived from the satellite data. Most points, therefore, were taken over a fairly homogeneous sandy substrate. On each point, depth measurements were taken using a handheld echosounder⁴⁴ which has a precision of 0.3m above and 1.0m below 10m depth. During the third field campaign, special attention was given to gathering detailed information on the distribution of bottom types in the region. This information was collected in a restricted study area, covering the coral reefs depicted on the QuickBird scene, although additional bottom-type information was gathered on adjacent reef systems as well. Though it was the purpose to collect depth information simultaneously, this objective could not be attained because of the failure of the echosounder. Each observation point was also logged using a handheld GPS-system⁴⁵ measuring in a UTM36 – WGS84 coordinate system.

The first objective of the study was to test whether remote sensing can deliver information about the configuration and composition of coral reefs. As only a quick and easy sampling technique is necessary for broad-scale mapping of coral reefs (Mumby and Green, 2000b), qualitatively bottom-type observations were made from the sea surface.

⁴⁴ Manta Dive Ray DR-100

⁴⁵ Garmin GPS 12 XL (campaign 1/2); Garmin eTrex Vista (campaign 3)

Additional detailed ecological surveys, for example quadrats or line transects which give more quantitative information on the composition and cover percentage of each bottom type, were not applied because of their time-consuming character. Besides, such surveys usually provide information on relatively small areas, in the order of a few m². This is not practical for the analysis of the available satellite data which have a minimal instant field of view of 8.29m² and even 900m² in the case of multispectral QuickBird and Landsat 7 ETM+ data respectively.

All observations at sea were made from inside a zodiac. In order to reach remote coral reefs, a daily dive boat from the dive centre 'VooDoo Divers' could be used to 'hitchhike' to their dive spots. The distribution of the observations throughout the study area, therefore, was largely dependent on the action radius of the dive boat, but also on the roughness of the sea which often hindered open water observations, especially in the morning. Nonetheless, a reasonable distribution of marine observations was obtained in the end (fig. 3.6). Secondly, more than 60 GCPs were measured on land in order to georeference the satellite data to the coordinate system used during the field measurements. As much as possible, these GCPs were homogeneously distributed throughout the study area (fig. 3.7). Most points were taken at junctions of roads easily recognisable on the satellite images; at typical coastal features, usually piers or docks; or at specific rock formations. At some locations, height measurements were taken as well. These would be useful for the digital photogrammetrical processing of the ASTER stereopair. These measurements were made with an altimeter⁴⁶ deriving heights depending on barometric pressure and temperature.

3.2.2.2 Tidal correction data

Depth measurements taken during the different field campaigns had to be normalised to a common vertical datum in order to be useful as ground truth for the calibration of a bathymetric map. Daily tidal variations in the northern Red Sea are in the order of 0.6m (Edwards, 1987). Each depth measurement, therefore, needed to be corrected for the tidal effects at the moment of sampling. Information on the tides at Hurghada was not readily available. Tidal data, therefore, were derived from the free tidal prediction program *WXTide32 version 2.6* (©1998-2000, M. Hopper). This program delivers predictions for the tides at 3 stations surrounding Hurghada, being Shadwan Island (27°17' N, 34°02'E)

⁴⁶ SUUNTO with 5m precision

(Tide_S), Quseir (26°06'N, 34°17'E) (Tide_O) and Ashrafi Island (27°47' N, 33° 43'E) (Tide_A). A weighed distance formula was consequently applied to intrapolate the tide (Tide_H) at Hurghada⁴⁷:

$$Tide_H = 0.593Tide_S + 0.280Tide_A + 0.126Tide_O \quad (3.1)$$

Table 3.15. Overview of the tidal heights at the moment of satellite data acquisition

| | date of acquisition | time of acquisition | tide to LAT (m) |
|----------------|---------------------|---------------------|-----------------|
| Landsat 5 TM | 08/14/1987 | 07:38 GMT | + 0.41 |
| Landsat 7 ETM+ | 09/10/2000 | 08:03 GMT | + 0.24 |
| ASTER | 03/21/2001 | 08:40:26.30 GMT | + 0.32 |
| QuickBird | 02/05/2002 | 08:27:03 GMT | + 0.60 |

Using the derived tidal information, each depth measurement was subsequently corrected to datum, being the lowest astronomical tide (LAT) (annex III). Besides, when linking these depths to spectral measurements derived from the satellite data, a compensation for the tide at the moment of data acquisition needed to be performed as well. As both date and time of data acquisition are known for each dataset, corresponding tides could be defined using WXTide32 (table 3.15).

3.2.3 Additional information sources

3.2.3.1 Topographic maps

Egyptian General Survey Authority, 1989. *Sheet NG 36 02b: Al Ghardaqah*. Scale: 1:50,000; Projection: Transverse Mercator; Ellipsoid: Helmert 1906; Datum: National Geodetic Net, Az Zahrā', 1874.

Egyptian General Survey Authority, 1989. *Sheet NG 36 02d: Jazirat Shâkir (South)*. Scale: 1:50,000; Projection: Transverse Mercator; Ellipsoid: Helmert 1906; Datum: National Geodetic Net, Az Zahrā', 1874.

⁴⁷ centred at 27°14'53"N, 33°50'56"; WP025: pier of dive centre 'VooDoo Divers'

3.2.3.2 Admiralty charts

Admiralty Charts, 2001. *Chart 157: Red Sea – Massamirit to Bab el Mandeb*. Scale: 1:750,000; Projection: WGS84.

Admiralty Charts, 2001. *Chart 158: Red Sea – Berenice to Massamirit*. Scale: 1:750,000; Projection: WGS84.

Admiralty Charts, 2001. *Chart 159: Red Sea – Suez (El Suweis) to Berenice*. Scale: 1:750,000; Projection: WGS84.

Admiralty Charts, 1997. *Chart 3043: Ports on the Coast of Egypt: B. Hurghada*. Scale: 1:25,000; Projection: Transverse Mercator.

Admiralty Charts, 1991. *Chart 4704: Red Sea*. Scale: 1:2,250,000; Projection: Mercator.

3.2.3.3 Software

Image processing software:

ITC, RSG/GSD, 2004. *ILWIS3.2 Academic*. <http://www.itc.nl/ilwis>.

PCI Geomatics, 2003. *PCI Geomatica V8.2.0*. <http://www.pcigeomatics.com>.

Digital photogrammetrical software:

Supersoft Inc., ©1999-2000. *VirtuoZo3.2*.

Vector-GIS software:

ESRI Inc., ©1992-2000. *ArcView GIS 3.2a*.

Tidal prediction program:

Michael Hopper, © 1998-2000. *WXTide32 version 2.6*. Available online at: <http://www.GeoCities.com/SiliconValley/1195/>, (Accessed: 20/01/2000).

3.3 DATA PRE-PROCESSING

Raw remote sensing data, the *level-0 product*, consist of the basic spectral information recorded by the sensor onboard the satellite without any correction or adjustment applied. This information, however, is not readily interpretable and most often a basic set of corrections is needed before data processing. Different pre-processing actions are already undertaken by the data provider in order to reduce errors in the remote sensing data delivered, to correct the product from external influences, or to adapt the product to specific users needs. The basic *level-1 product* delivered by the data provider usually consists of the spectral information transcoded to *digital numbers* (DNs) and integrated in a regular raster grid; often, additional corrections for radiometric errors and/or geometric adjustments have been applied. For some datasets, e.g. SeaWiFS or MODIS, *level-2 products* are available. These level-2 products no longer represent the original DN values; instead new information, for example on the Chl-*a* concentration in the water column, has been derived from the level-1 product.

Except for the examples given of the biophysical parameters of the northwestern Red Sea (section 3.7), only level-1 products are used in this study. An overview of the specific corrections applied to each dataset by the data provider was given in section 3.2. Depending on the specific analysis envisaged, these datasets, however, often need additional pre-processing, for example to remove remaining noise and artefacts in the scenes, to match the datasets to the study-specific georeference system, to regain the original physical radiance values recorded by the sensor, or to correct the signal for atmospheric and/or water-column effects. In following sections, details are provided on the different pre-processing steps applied.

Table 3.16. Overview of specific spectral bands used per dataset according to algorithm

| | bathymetry | bottom-type classification | multitemporal analysis | other |
|----------------|-------------------|-----------------------------------|-------------------------------|--------------|
| Landsat 7 ETM+ | 1, 2, 3 | 1, 2, 3 | 1, 2, 3, 4 | 8 |
| Landsat 5 TM | 1, 2, 3 | 1, 2, 3 | 1, 2, 3, 4 | |
| ASTER | 3n, 3b | | | |
| QuickBird | 1, 2, 3 | 1, 2, 3 | | Pan |

Because of the specific optical characteristics of water, especially the resulting differential attenuation of light⁴⁸, spectral bands in the available multispectral datasets which register longer wavelengths in the near-infrared could not be used. The spectral information needed also depended on the specific data analysis. In table 3.16, an overview per dataset is given of the spectral bands used according to the specific analysis performed.

3.3.1 Noise reduction

In some cases, not all noise elements or artefacts in a dataset have been removed by the data provider. The remaining radiometric noise frequently is the result of malfunctions of the sensor or any other component integrated in the data acquisition chain. Artefacts may also result from errors introduced in the digital processing of the data. Some of these artefacts are well known and described in the literature. Different correction algorithms, consequently, have been developed and integrated in most data-processing software. The correction of the noise patterns encountered in two of the datasets, i.e. Landsat 5 TM and QuickBird, was not that straightforward. These noise patterns and the encountered problems are discussed below. Besides, scan-correlated shifts or striping effects (IPLab, 2003) were present in these and other datasets. As these were of limited radiometric magnitude and/or areal extent, corrections for these effects have been omitted.

3.3.1.1 Landsat 5 TM

A well-known scanning problem of the Landsat 5 TM sensor is *banding*, also called the *memory effect*. These artefacts in the multispectral bands are created by relative gain and offset variations between neighbouring forward and reverse scans⁴⁹ of all 16 detectors (Crippen, 1989). This effect occurs when a scan records a sudden, significant change in radiance intensity, such as a land/water boundary (IPLab, 2003): after prolonged periods of saturation, the Landsat 5 TM detector output values tend to be depressed such that scans away from bright targets can be significantly darker than the interleaved scans towards bright targets (Crippen, 1989). This noise is more significant over uniform dark objects, e.g. oceans, and is very unfavourable for quantitative studies, especially for marine coastal applications (Zhang *et al.*, 1999). The memory effect, however, does not

⁴⁸ see section 3.3.5

⁴⁹ scan: 16 lines of image data corresponding to each detector in the sensor (IPLab, 2003)

affect the entire scan and decreases as the scan moves away from the intensity transition (IPLab, 2003).

Many techniques have been developed to solve for the memory effect (see e.g. Crippen, 1989 for an overview). Most techniques are based on the regular occurrence pattern of the memory effect and/or its horizontal orientation in the scene. Unfortunately, the Landsat 5 TM dataset derived from the Earthsat archive has been resampled to fit the WGS84-UTM36 coordinate system. This resulted in scans running diagonal in the scene (fig. 3.8). A second problem was created during resampling, when the spatial resolution was changed from 30m to 28.5m. As a result, the data of the 16 detectors in one scan was spread over approximately 16.85 lines (Crippen, 1989). The edges of each scan, therefore, were smeared and the memory effect was no longer alternating with exactly 16 lines.

Although Crippen (1989) has developed a method for noise reduction on resampled Landsat TM data, his method was aimed at improving the appearance of the imagery for visual interpolation and did not prove very helpful for noise reduction before digital processing (Crippen, 1989). Besides, this method introduces additional artefacts near sharp radiance borders, like the coastline. This could be solved by masking out the land area and replacing each pixel by a mean deep-water DN value (Crippen, 1989; Zhang *et al.*, 1999), but for coral-reef research, this solution was inadequate as similar sharp transitions are also present along the reef structures, for example on the edge of a shallow reef flat.

An alternative approach for *debanding* which is independent of scan direction is based on the implementation of Fourier transformation (e.g. Zhang *et al.*, 1999). After a Fourier transform, the noise pattern is isolated in the frequency domain and subsequently removed before an inverse Fourier transform is applied. The major drawback of this method is the difficult and often subjective identification of the proper noise pattern (Crippen *et al.*, 1989; Zhang *et al.*, 1999). Therefore, this correction approach was not performed.

During further processing of the dataset, this artefact did not significantly affect the bottom-type classification as intra-class variability was higher than the additional variance introduced by the memory effect. Noise removal for this case, therefore, was not necessary. These radiometric errors, conversely, had serious effects on the bathymetric mapping, especially in the nearshore areas as will be further discussed in section 3.4.3.3.

3.3.1.2 QuickBird

A major error in the array calibration was encountered in the QuickBird multispectral bands. If these were stretched as in the example given in figure 3.9a, a clear difference between the DN values on the left and right hand side of the scene was noted. On each multispectral band, the boundary between both parts was located near column # 1124. As the dataset was geometrically transformed to fit the WGS84-UTM36 coordinate system, the originally vertical error was slightly rotated, so that it was no longer aligned with the vertical column direction.

To solve this problem, two sample sets were taken over deep water at each side of but close to the scanning boundary⁵⁰. Assuming that the water column in the study area was homogeneous, the mean DN values of both sample sets over deep water should be identical. Due to the scanning error, this was clearly not the case (table 3.17). Based on the assumption that the left part of the scene was oversaturated in band 1 and 2, formula 3.2 was constructed to normalise this part of the scene to the DN values on the right hand side based on the difference, d , between both mean deep-water values. Remark that although a reverse situation was detected in bands 3 and 4, i.e. an underestimation of the left part of the scene, the same formula was applied.

$$QBband_i_{cor} = iff(QBband_i = 0, 0, iff(\%C = 1124, (QBband_i - d), QBband_i)) \quad (3.2)$$

With: $QBband_i$: DN values in QuickBird multispectral band i

$\%C$: parameter indicating column number in scene

d : parameter representing difference in DN value between left and right part of the scene as determined in table 3.17.

The first *iff-function* of formula 3.2 prevented the transformation of the background values at the borders of the scene. The second, more important *iff-function* corrected the DN values in the original bands, $QBband_i$, if the column number of the pixel, $\%C$, was lower than 1124, thus to the left of the detected boundary. If the column number of the pixel was higher than or equal to 1124, the original DN values were maintained. The result of this correction on the QuickBird band 3 is shown in figure 3.9c.

⁵⁰ the left sample area bordered by scene coordinates: UL: 475-1100; LR: 525-1120 and the right sample area by UL: 475-1140; LR: 525-1160

Table 3.17. Mean DN values calculated in two sample sets at either side of a vertical scan error detected in the QuickBird dataset

| | mean DN left sample | mean DN right sample | difference (d)* |
|-----------|---------------------|----------------------|-----------------|
| QB band 1 | 183.5 | 180.5 | 3 |
| QB band 2 | 179.3 | 175.5 | 3.8 ~ 4 |
| QB band 3 | 64.6 | 67.7 | -3.1 ~ -3 |
| QB band 4 | 34.9 | 35.9 | -1 |

* difference = mean DN left sample – mean DN right sample

A small linear artefact, a couple of pixels wide was still present after correction, especially towards the upper and lower borders of the scene (fig. 3.9d). This resulted from the georeferencing performed by the data provider and could only be solved by reversing this rotation before noise reduction. This, however, would probably affect the DN values in each pixel and as the residual error had only a limited effect in the deep-water area, this additional correction was not performed.

3.3.2 Geometric correction

All remote sensing data have been geometrically corrected by the provider in order to reduce distortions which are mainly due to scanning errors, the rotation and curvature of the Earth, and changes in altitude of the platform during data acquisition. The datasets have been georeferenced as well, based on satellite track parameters. Errors in this georeferencing, however, are often significant and the scenes may not optimally match the GCPs measured during the field campaigns. Hence, the 63 terrestrial GCPs measured were used as tie-points to geocode⁵¹ the different datasets to the specific coordinate system described in table 3.18. The specific algorithms applied and the results obtained are described in following sub-sections.

3.3.2.1 Landsat 7 ETM+

The Landsat 7 ETM+ scene covered more than just the specific study area around Hurghada (fig. 3.10). Geocoding outside the specific study area, however, would be less

⁵¹ geocoding: allocating X, Y coordinates to all pixels based on a polynomial equation without resampling the image

reliable and a subset was consequently made for the Hurghada area. To geocode the Landsat 7 ETM+ subset, 27 GCPs were selected as tie-points (table 3.19) which were as evenly distributed throughout the study area as possible (fig. 3.11). A full second order polynomial equation was derived from these tie-points and the geocoding was performed with a root mean square error (RMSE) of 0.311 pixel. The geocoding of the Landsat 7 ETM+ subset was acceptable, as this error felled well below the 0.5 pixel put forward as the minimum accuracy standard.

Table 3.18. Overview of the parameters used to define the specific coordinate system

| | | |
|---------------------------------|-------------------------------------|-----------|
| coordinate system | WGS84-UTM 36R | |
| projection: | Universal Transverse Mercator (UTM) | |
| | zone: 36 Northern Hemisphere | |
| horizontal datum: | WGS 1984 | |
| ellipsoid: | WGS84 | |
| specific coordinate boundaries: | | |
| min X, Y: | 550.000 | 3.000.000 |
| max. X, Y: | 600.000 | 3.040.000 |

3.3.2.2 Landsat 5 TM

Since 1987, the year the Landsat 5 TM dataset was recorded, the situation on the ground has completely changed and many GCPs measured between 2000 and 2003 did not yet exist. A slave-to-master geocoding method was therefore applied to the Landsat 5 TM dataset in which the geocoded Landsat 7 ETM+ dataset served as the master layer. Besides, for the multitemporal analysis of the two Landsat datasets, the co-registration between the two scenes should be optimal in order to minimise misregistration errors in the change detection result. The slave-to-master method was ideal for this purpose as it offered the opportunity to spread the tie-points in the slave image more homogeneously. As for the Landsat 7 ETM+ dataset, a subset of the Landsat 5 TM dataset was created, covering the specific Hurghada study area. For the geocoding process, a second order polynomial transformation was applied which resulted in a RMSE of 0.339 based on 31 tie-points (fig. 3.12; table 3.20).

An additional problem with the Landsat 5 TM dataset was its different spatial resolution (i.e. 28.5m) compared to the Landsat 7 ETM+ dataset (i.e. 30m). As these spatial resolutions should be similar to perform a multitemporal change detection, the

older Landsat 5 TM dataset needed to be resampled to the master Landsat 7 ETM+ dataset. A nearest neighbour resampling algorithm was applied to optimally preserve the DN values of the original Landsat 5 TM dataset.

Table 3.19. Overview of residual errors for each GCP used for geocoding the Landsat 7 ETM+ subset (X, Y: metric coordinates; Row, Col: scene coordinates; DRow and DCol: error of each point in X and Y expressed in pixel units)

| ID | X | Y | Row | Col | DRow | DCol |
|-------------|--------|---------|------|------|-------|-------|
| 1 | 563764 | 3027669 | 446 | 262 | -0.16 | 0.12 |
| 2 | 558875 | 3036784 | 170 | 55 | 0.04 | -0.11 |
| 3 | 565972 | 3023243 | 581 | 357 | -0.07 | 0.22 |
| 4 | 575651 | 3016217 | 765 | 711 | 0.40 | 0.01 |
| 5 | 577216 | 3012236 | 888 | 782 | 0.15 | -0.30 |
| 6 | 583399 | 3013681 | 809 | 979 | -0.44 | 0.06 |
| 7 | 580106 | 3014054 | 814 | 868 | 0.40 | -0.55 |
| 8 | 572899 | 3006908 | 1085 | 667 | -0.08 | 0.13 |
| 10 | 580169 | 3010639 | 926 | 887 | 0.35 | -0.49 |
| 11 | 582319 | 3011767 | 878 | 953 | 0.23 | 0.25 |
| 12 | 582608 | 3012582 | 849 | 958 | -0.52 | -0.26 |
| 13 | 580914 | 3015523 | 761 | 888 | -0.27 | 0.04 |
| 14 | 580790 | 3015108 | 776 | 886 | 0.47 | 0.09 |
| 15 | 581788 | 2998717 | 1310 | 1000 | -0.34 | -0.28 |
| 16 | 578834 | 2999543 | 1298 | 899 | -0.12 | -0.11 |
| 17 | 575129 | 3004939 | 1139 | 750 | 0.18 | -0.13 |
| 18 | 581951 | 2996914 | 1369 | 1015 | -0.01 | 0.27 |
| 19 | 584007 | 2996367 | 1377 | 1085 | 0.45 | 0.03 |
| 20 | 581469 | 3002687 | 1181 | 970 | -0.04 | 0.13 |
| 21 | 581814 | 3004145 | 1131 | 974 | -0.24 | 0.08 |
| 22 | 583667 | 3008633 | 974 | 1013 | -0.11 | 0.39 |
| 23 | 582976 | 3011313 | 889 | 977 | -0.41 | 0.37 |
| 25 | 596266 | 3007490 | 948 | 1433 | -0.17 | -0.12 |
| 26 | 595324 | 3007223 | 962 | 1403 | 0.30 | -0.38 |
| 27 | 592268 | 3009544 | 901 | 1292 | 0.10 | 0.56 |
| 28 | 585939 | 3003860 | 1120 | 1111 | 0.25 | 0.00 |
| 29 | 585871 | 3004005 | 1115 | 1108 | -0.32 | -0.04 |
| total RMSE: | | | | | 0.311 | |

Table 3.20. Overview of the residual errors for each tie-point used for the geocoding of the Landsat 5 TM dataset

| ID | X | Y | Row | Col | DRow | DCol |
|----|--------|---------|------|-----|-------|-------|
| 1 | 558875 | 3036749 | 171 | 40 | -0.09 | -0.13 |
| 2 | 560927 | 3032886 | 307 | 112 | 0.17 | -0.10 |
| 3 | 561766 | 3024021 | 618 | 141 | 0.18 | -0.40 |
| 4 | 561114 | 3027483 | 496 | 119 | -0.27 | 0.49 |
| 5 | 578958 | 3015973 | 901 | 745 | 0.09 | 0.53 |
| 6 | 580331 | 3015250 | 926 | 793 | -0.25 | 0.41 |
| 7 | 582065 | 3014832 | 941 | 854 | 0.09 | 0.60 |
| 8 | 583457 | 3012224 | 1032 | 902 | -0.12 | 0.00 |

| ID | X | Y | Row | Col | DRow | DCol |
|-------------|--------|---------|------|------|-------|-------|
| 9 | 581307 | 3011030 | 1074 | 827 | 0.11 | 0.52 |
| 10 | 576849 | 3009004 | 1145 | 670 | 0.02 | -0.18 |
| 11 | 577375 | 3008896 | 1149 | 688 | 0.27 | -0.61 |
| 12 | 581472 | 3002686 | 1366 | 832 | -0.16 | 0.00 |
| 14 | 597241 | 3004632 | 1297 | 1385 | 0.14 | 0.36 |
| 15 | 597552 | 3005926 | 1252 | 1396 | 0.29 | 0.21 |
| 16 | 596058 | 3010633 | 1087 | 1344 | -0.63 | -0.20 |
| 18 | 596299 | 3010199 | 1103 | 1353 | 0.24 | 0.40 |
| 21 | 596332 | 3007543 | 1195 | 1353 | -0.39 | -0.23 |
| 22 | 593787 | 3010036 | 1109 | 1264 | 0.53 | -0.31 |
| 27 | 586660 | 3011313 | 1064 | 1014 | 0.05 | -0.31 |
| 28 | 586838 | 3011284 | 1065 | 1020 | 0.03 | -0.56 |
| 30 | 586735 | 3004882 | 1289 | 1016 | 0.18 | -0.32 |
| 31 | 584995 | 3003241 | 1346 | 955 | -0.39 | -0.31 |
| 34 | 561711 | 2996282 | 1594 | 143 | -0.13 | 0.01 |
| 35 | 562323 | 2996883 | 1573 | 164 | 0.17 | -0.15 |
| 36 | 558646 | 2997718 | 1544 | 36 | 0.06 | 0.13 |
| 38 | 559112 | 3000450 | 1447 | 51 | -0.44 | -0.42 |
| 40 | 557774 | 3001439 | 1413 | 5 | 0.31 | 0.41 |
| 43 | 589727 | 3026090 | 549 | 1125 | 0.14 | -0.09 |
| 45 | 581626 | 2994540 | 1652 | 838 | 0.07 | 0.36 |
| 46 | 590733 | 3016114 | 896 | 1158 | -0.47 | -0.15 |
| 47 | 590756 | 3016075 | 898 | 1159 | 0.19 | 0.04 |
| total RMSE: | | | | | 0.339 | |

3.3.2.3 QuickBird

The in-situ-measured GCPs, unfortunately, could not be used to geocode the QuickBird dataset as only a small part of the land, in which 4 GCPs are located, was covered by the scene. As this was insufficient to conduct a thorough transformation, a slave-to-master method was used to geocode the QuickBird multispectral dataset with the geocoded Landsat 7 ETM+ dataset as master layer. In total, 15 tie-points were used (fig. 3.13; table 3.21). Because the QuickBird scene represents an area of roughly 36km², only an affine polynomial transformation was needed. However, as the Landsat 7 ETM+ dataset was used as master layer, each Landsat 7 ETM+ pixel corresponded to more than 100 multispectral QuickBird pixels. Therefore, it was impossible to exactly link the two scenes and only an RMSE of 3.499 could be obtained. This error corresponding to 10.08m, nonetheless, was still smaller than the RMSE of 14m guaranteed on the original georeference by the data provider (DigitalGlobe, 2004).

Because of the different spatial resolution of the panchromatic QuickBird band, this scene was separately geocoded. A slave-to-master method was applied in which the combined geocoded QuickBird multispectral bands were used as master layer. An affine order polynomial was calculated based on 35 tie-points (fig. 3.14; table. 3.22), resulting in

a RMSE of 1.257. This relatively high error was due to the difference in resolution between the slave and master layer. However, as this error was lower than half a pixel of a QuickBird multispectral band, this result was still considered acceptable.

Table 3.21. Overview of the residual errors for each tie-point used for geocoding the multispectral QuickBird bands

| ID | X | Y | Row | Col | DRow | DCol |
|-------------|--------|---------|------|------|-------|-------|
| 1 | 582942 | 3007919 | 27 | 417 | 1.86 | 2.36 |
| 2 | 582675 | 3007389 | 216 | 322 | 1.89 | 0.88 |
| 3 | 582598 | 3007197 | 281 | 294 | -1.48 | -0.42 |
| 6 | 582022 | 3005198 | 992 | 94 | -2.50 | -0.74 |
| 8 | 582479 | 3003791 | 1493 | 266 | -1.21 | 4.38 |
| 9 | 582512 | 3002616 | 1912 | 274 | -0.27 | -2.68 |
| 14 | 585976 | 3005139 | 1006 | 1498 | -3.11 | -4.84 |
| 15 | 585959 | 3005026 | 1050 | 1494 | 0.80 | -3.13 |
| 16 | 585941 | 3004883 | 1096 | 1490 | -4.08 | -1.08 |
| 19 | 585921 | 3004056 | 1390 | 1485 | -4.37 | -1.49 |
| 22 | 586742 | 3004869 | 1100 | 1777 | -3.99 | 0.51 |
| 25 | 586469 | 3005446 | 900 | 1680 | 0.97 | 2.22 |
| 27 | 585871 | 3004005 | 1421 | 1471 | 8.35 | 2.18 |
| 28 | 585939 | 3003860 | 1470 | 1498 | 5.88 | 4.55 |
| total RMSE: | | | | | 3.499 | |

Table 3.22. Overview of the residual errors for each tie-point used for geocoding the panchromatic QuickBird band

| ID | X | Y | Row | Col | DRow | DCol |
|----|--------|---------|------|------|-------|-------|
| 1 | 581828 | 3007939 | 79 | 74 | 0.11 | 0.19 |
| 2 | 582950 | 3007904 | 121 | 1674 | -0.07 | 1.27 |
| 3 | 582663 | 3007385 | 860 | 1267 | -0.91 | -2.08 |
| 8 | 582200 | 3004814 | 4524 | 633 | 1.56 | -1.96 |
| 11 | 582172 | 3003501 | 6389 | 611 | -1.38 | 2.07 |
| 12 | 582472 | 3002529 | 7773 | 1046 | 0.20 | 0.80 |
| 13 | 584916 | 3003218 | 6775 | 4522 | -1.17 | 1.52 |
| 14 | 584925 | 3003246 | 6736 | 4530 | 0.30 | -2.44 |
| 15 | 584988 | 3003141 | 6883 | 4623 | -1.81 | -1.34 |
| 16 | 587500 | 3002375 | 7959 | 8208 | 1.10 | -1.37 |
| 17 | 585868 | 3004034 | 5609 | 5870 | -0.07 | 1.80 |
| 20 | 586715 | 3004911 | 4354 | 7067 | -0.45 | 1.74 |
| 21 | 586458 | 3005428 | 3621 | 6694 | 0.15 | 0.12 |
| 22 | 586418 | 3005434 | 3613 | 6637 | -0.10 | -0.16 |
| 23 | 585972 | 3005130 | 4050 | 6005 | 1.25 | -0.50 |
| 24 | 585975 | 3005174 | 3988 | 6008 | 2.20 | -0.78 |
| 26 | 585940 | 3004956 | 4295 | 5960 | -1.70 | -1.56 |
| 27 | 585951 | 3004938 | 4322 | 5978 | -0.33 | 0.53 |
| 28 | 585925 | 3004868 | 4421 | 5943 | -0.09 | 1.69 |
| 29 | 585928 | 3004837 | 4467 | 5945 | 1.12 | 0.00 |
| 30 | 585907 | 3004692 | 4673 | 5918 | 1.12 | 0.97 |
| 31 | 585892 | 3004573 | 4842 | 5897 | 1.19 | 0.20 |
| 32 | 585889 | 3004609 | 4789 | 5893 | -0.80 | 0.14 |

| ID | X | Y | Row | Col | DRow | DCol |
|-------------|--------|---------|------|------|-------|-------|
| 33 | 585880 | 3004523 | 4911 | 5880 | -1.71 | -0.81 |
| 34 | 585874 | 3004466 | 4994 | 5872 | -0.07 | -0.54 |
| 41 | 584468 | 3007374 | 864 | 3840 | -1.00 | 0.37 |
| 42 | 584098 | 3007471 | 728 | 3313 | -1.14 | 1.81 |
| 43 | 582237 | 3005589 | 3419 | 678 | -0.23 | -1.45 |
| 44 | 582267 | 3005462 | 3603 | 724 | 2.19 | -0.45 |
| 45 | 582271 | 3005534 | 3499 | 730 | 1.02 | 1.45 |
| 47 | 583376 | 3006105 | 2677 | 2296 | -0.47 | -1.52 |
| 48 | 583329 | 3006097 | 2689 | 2229 | -0.01 | -1.12 |
| 49 | 582405 | 3003740 | 6049 | 941 | -0.65 | 2.21 |
| 51 | 581914 | 3003273 | 6716 | 243 | -1.33 | -0.04 |
| 52 | 582341 | 3004488 | 4987 | 839 | 1.99 | -0.78 |
| total RMSE: | | | | | 1.257 | |

3.3.2.4 ASTER

The ASTER scene covered an area of 60 by 60km which largely corresponded to the specific study area. Subsetting, therefore, was not needed as the entire scene could be directly geocoded. 22 GCPs were used for setting up a second order polynomial and the nadir ASTER VNIR bands were geocoded with a RSME of 0.359 (fig. 3.15; table 3.23).

Table 3.23. Overview of the residual errors for each GCP used for the geocoding of the nadir ASTER VNIR bands

| ID | X | Y | Row | Col | DRow | DCol |
|-------------|--------|---------|------|------|-------|-------|
| 1 | 563764 | 3027669 | 1857 | 708 | -0.05 | 0.10 |
| 3 | 575651 | 3016217 | 2494 | 1606 | -0.31 | -0.46 |
| 4 | 577216 | 3012236 | 2741 | 1749 | -0.04 | -0.18 |
| 5 | 583399 | 3013681 | 2584 | 2143 | -0.33 | -0.02 |
| 7 | 572899 | 3006908 | 3135 | 1518 | 0.00 | 0.04 |
| 8 | 576752 | 3011653 | 2784 | 1724 | -0.05 | -0.36 |
| 9 | 580169 | 3010639 | 2817 | 1960 | 0.10 | 0.15 |
| 10 | 582319 | 3011767 | 2721 | 2091 | -0.16 | 0.45 |
| 11 | 580914 | 3015523 | 2488 | 1961 | 0.21 | 0.13 |
| 12 | 580790 | 3015108 | 2517 | 1957 | 0.65 | 0.25 |
| 13 | 581788 | 2998717 | 3586 | 2186 | -0.70 | -0.11 |
| 15 | 575129 | 3004939 | 3243 | 1685 | 0.27 | 0.23 |
| 16 | 581951 | 2996914 | 3704 | 2215 | -0.02 | -0.16 |
| 17 | 584007 | 2996367 | 3720 | 2356 | 0.52 | 0.09 |
| 18 | 581469 | 3002687 | 3328 | 2125 | -0.06 | 0.01 |
| 20 | 583667 | 3008633 | 2914 | 2211 | -0.16 | 0.55 |
| 21 | 582976 | 3011313 | 2745 | 2138 | 0.49 | -0.38 |
| 22 | 584024 | 3014198 | 2544 | 2179 | -0.05 | -0.23 |
| 23 | 596266 | 3007490 | 2863 | 3053 | 0.31 | 0.28 |
| 24 | 594991 | 3006801 | 2921 | 2975 | 0.03 | -0.32 |
| 25 | 595324 | 3007223 | 2890 | 2993 | 0.19 | -0.17 |
| 26 | 592268 | 3009544 | 2767 | 2769 | -0.82 | 0.09 |
| total RMSE: | | | | | 0.359 | |

The backward looking band, *3b*, of the ASTER dataset, however, had different scene boundaries and needed to be separately geocoded from the nadir-taken VNIR bands. Hence, a slave-to-master method was applied with the geocoded ASTER band 3 as reference layer. All reference points were selected on the coral reefs surrounding Big Giftun Island as this would be the test area for the digital photogrammetric processing of the ASTER stereopair. In this way, an ideal match between the two stereo-images was obtained. An affine (first order) polynomial transformation was applied using 27 GCPs (fig. 3.16; table 3.24). With a resulting RMSE of 2.486, this transformation was not ideal. This was mainly caused by the selection of subaquatic GCPs which were not optimally recognisable on both layers. However, this selection of subaquatic reference points was needed for the digital photogrammetric process as will be explained in section 3.4.3.5.

Table 3.24. Overview of the residual errors for each tie-point used in the geocoding of the ASTER 3b scene

| ID | X | Y | Row | Col | DRow | DCol |
|-------------|--------|---------|------|------|-------|-------|
| 1 | 587567 | 3016542 | 1234 | 1908 | -0.36 | -2.12 |
| 2 | 587322 | 3016337 | 1250 | 1894 | -0.27 | -1.92 |
| 3 | 588703 | 3016820 | 1204 | 1980 | -0.66 | -2.34 |
| 4 | 589245 | 3016801 | 1203 | 2031 | 2.55 | 12.75 |
| 5 | 589269 | 3016235 | 1237 | 2023 | -0.48 | -2.25 |
| 6 | 589334 | 3015905 | 1258 | 2031 | -0.54 | -1.72 |
| 7 | 585672 | 3011410 | 1591 | 1833 | 0.01 | -1.16 |
| 8 | 585751 | 3011643 | 1575 | 1836 | 0.13 | -1.19 |
| 9 | 586215 | 3011815 | 1559 | 1865 | 0.13 | -1.16 |
| 10 | 586009 | 3011358 | 1591 | 1866 | 0.02 | 9.12 |
| 11 | 590466 | 3009435 | 1673 | 2169 | 0.25 | -0.22 |
| 12 | 590472 | 3009175 | 1689 | 2172 | -0.81 | -0.11 |
| 13 | 590174 | 3008900 | 1711 | 2155 | 0.10 | -0.07 |
| 14 | 596060 | 3010661 | 1536 | 2526 | 0.04 | -0.34 |
| 15 | 595976 | 3010502 | 1547 | 2522 | -0.28 | -0.35 |
| 16 | 596066 | 3010475 | 1548 | 2528 | -0.14 | -0.53 |
| 17 | 586332 | 3013617 | 1439 | 1855 | -0.19 | -1.61 |
| 18 | 586781 | 3013350 | 1452 | 1887 | -0.21 | -1.75 |
| 19 | 587131 | 3013768 | 1421 | 1905 | -0.24 | -2.88 |
| 20 | 593696 | 3011052 | 1534 | 2366 | 0.03 | -0.73 |
| 21 | 593672 | 3010903 | 1544 | 2366 | -0.02 | -0.57 |
| 22 | 592880 | 3007849 | 1753 | 2344 | 0.13 | 0.50 |
| 23 | 593464 | 3008477 | 1706 | 2376 | 0.32 | -0.04 |
| 24 | 593363 | 3008625 | 1697 | 2368 | 0.02 | 0.01 |
| 25 | 585924 | 3009492 | 1715 | 1869 | 0.39 | -0.16 |
| 26 | 596951 | 3007486 | 1736 | 2616 | 0.11 | 0.53 |
| 27 | 597298 | 3007659 | 1721 | 2637 | -0.04 | 0.31 |
| total RMSE: | | | | | 2.486 | |

3.3.3 Radiometric correction

Radiometric corrections are required when images are compared in time and space, when interactions between the electromagnetic radiation measured by the sensor and the study object are modelled, and when band ratios are used for data analysis (Mumby and Clark, 2000). In contrast, when data processing only involves the multispectral classification of one single dataset, these corrections are not necessary (Mumby and Clark, 2000). As in this study most results were derived from one single dataset, radiometric conversions were only applied when required by the selected processing algorithms.

Radiometric correction encompasses three subsequent steps (Mumby and Clark, 2000). First, the DN values available in the remote sensing datasets are converted to *spectral radiance* values ($\text{W m}^{-2} \text{ster}^{-1} \mu\text{m}^{-1}$) measured at sensor. Digital Numbers are arbitrary values resulting from the conversion of the physical measurements at sensor to an integer value easily transcoded from satellite to receiver and interpretable in most software packages. As each sensor has its own conversion algorithms, reversion to the original physical measurements is needed before radiance values of different sensors can be compared.

Secondly, the spectral radiance values are converted to *apparent reflectance* at the top of the atmosphere (TOA). The spectral radiance measured at the sensor not only depends on the reflectance characteristics of the study object but is also influenced by the degree of solar illumination of the object, the *irradiance*. The measured spectral radiances, consequently, are influenced by the time and date of image acquisition. As apparent reflectance values represent the ratio of radiance to irradiance, they provide a standardised measure which is directly comparable between datasets of different dates.

Finally, the atmospheric effects on the electromagnetic radiance are removed in order to come to reflectance values at the Earth's surface. The first two steps are rather straightforward and only involve intrinsic information about the datasets which is available in the metadata provided by the data manufacturer. Atmospheric corrections, conversely, require ancillary data or estimates about atmospheric conditions at the moment of data acquisition. Radiometric corrections as applied in this study, therefore, only encompass the first two steps, while the removal of atmospheric effects is separately discussed in section 3.3.4.

3.3.3.1. Conversion of DN to spectral radiance

For each band of each sensor, the conversion of DN values to physical measurements of spectral radiance at the sensor involves a specific transformation equation defined by the manufacturer. These equations are based on a calibration curve of DN to radiance as the example shown on figure 3.17 for an 8bit Landsat 5 TM dataset. Because the sensitivity of the sensor changes over time, frequent re-calibrations of the sensor are made (Mumby and Clark, 2000).

3.3.3.1.1 Radiometric calibration of Landsat 7 ETM+

The transformation formula applied in the case of the Landsat 7 ETM+ sensor is described as follows (LPSO, 2004):

$$L_{\lambda} = \left[\frac{(L_{\max_{\lambda}} - L_{\min_{\lambda}})}{(Q_{cal \max} - Q_{cal \min})} \right] \times (DN - Q_{cal \min}) + L_{\min_{\lambda}} \quad (3.3)$$

With: L_{λ} : spectral radiance at sensor
 $Q_{cal \min}$: the minimum quantised calibrated pixel value in DN (corresponding to $L_{\min_{\lambda}} = 0$ (NLAPS⁵²)
 $Q_{cal \max}$: the maximum quantised calibrated pixel value in DN (corresponding to $L_{\max_{\lambda}} = 255$
 $L_{\min_{\lambda}}$: spectral radiance scaled to $Q_{cal \min}$ in $W m^{-2} ster^{-1} \mu m^{-1}$
 $L_{\max_{\lambda}}$: spectral radiance scaled to $Q_{cal \max}$ in $W m^{-2} ster^{-1} \mu m^{-1}$

$L_{\min_{\lambda}}$ and $L_{\max_{\lambda}}$ are the spectral radiance values per band at $Q_{cal \min}$ and $Q_{cal \max}$ respectively. Depending on the moment the dataset was created, i.e. processed after order placement, different $L_{\min_{\lambda}}$ and $L_{\max_{\lambda}}$ apply. Secondly, the sensor can also be configured to measure in low gain or high gain mode⁵³ depending on the date of acquisition and the spectral reflectance properties of the geographical zone registered. For transformation to DN values, however, low gain conversion values are always used (LPSO, 2004). As the available Landsat 7 ETM+ dataset was created after July 1st, 2000, the $L_{\min_{\lambda}}$ and $L_{\max_{\lambda}}$ values listed in table 3.25 should be used.

⁵² NLAPS: National Land Archive Production System: specific processing algorithm used by the provider for this scene (for more details see: LPSO, 2004)

⁵³ for further details about this subject see: LPSO (2004)

Table 3.25. Spectral radiance range (in $W\ m^{-2}\ ster^{-1}\ \mu m^{-1}$) for the ETM+ sensor, specific for the dataset used in this study (LPSO, 2004)

| | L_{min} | L_{max} |
|--------|-----------|-----------|
| band 1 | -6.20 | 293.70 |
| band 2 | -6.40 | 300.90 |
| band 3 | -5.00 | 234.40 |
| band 4 | -5.10 | 241.10 |
| band 5 | -1.00 | 47.57 |
| band 6 | 0.00 | 17.04 |
| band 7 | -0.35 | 16.54 |
| band 8 | -4.70 | 243.10 |

3.3.3.1.2 Radiometric calibration of Landsat 5 TM

In the metadata of the Landsat 5 TM dataset, *gain* and *bias* values were given (table 3.26) in order to convert the DN values to radiance values at sensor according to figure 3.17 and formula 3.4:

$$L_{\lambda} = (Gain \times DN) + Bias \quad (3.4)$$

Table 3.26. Landsat 5 TM calibration parameters to convert DN to radiance values

| | gain | bias |
|--------|-------------|-------------|
| band 1 | 0.6024314 | -1.52 |
| band 2 | 1.1750981 | -2.84 |
| band 3 | 0.8057647 | -1.17 |
| band 4 | 0.8145490 | -1.51 |
| band 5 | 0.1080784 | -0.37 |
| band 6 | 0.0551582 | 1.24 |
| band 7 | 0.0569804 | -0.15 |

3.3.3.1.3 Radiometric calibration of QuickBird

As with the Landsat 7 ETM+ sensor, the transformation parameters used to calibrate the different bands of the QuickBird sensor have been revised. If data is used which has been processed before June 6th, 2003, formula 3.5 should be applied (Krause, 2003):

$$L_{\lambda} = \frac{K(\text{revised})}{\Delta\lambda_{\text{band}}} \times DN \quad (3.5)$$

With: $K(\text{revised})$: absolute radiometric calibration factor (K-factor)

$\Delta\lambda_{\text{band}}$: effective bandwidth in μm

The use of the absolute radiometric calibration factor, K -factor, transforms the DN values to band-integrated radiance values ($\text{W m}^{-2} \text{ster}^{-1}$). Different K-factors should be used, depending on the radiometric resolution of the dataset provided by the manufacturer. In the case of 16bit products, absolute radiometric calibration factors as summarised in table 3.27 must be used. In order to come to spectral radiance values ($\text{W m}^{-2} \text{ster}^{-1} \mu\text{m}^{-1}$), the results should be divided by the appropriate effective bandwidth, $\Delta\lambda_{\text{band}}$ (table 3.27). Only the multispectral bands were processed as these bands were used in further data analyses.

Table 3.27. Revised K-factors for 16bit products and effective bandwidths of the QuickBird multispectral bands

| | K (revised) [$\text{W m}^{-2} \text{ster}^{-1} \text{count}^{-1}$] | $\Delta\lambda_{\text{band}}$ (μm) |
|--------|--|--|
| band 1 | 1.604120 e-02 | 0.068 |
| band 2 | 1.438470 e-02 | 0.099 |
| band 3 | 1.267350 e-02 | 0.071 |
| band 4 | 1.542420 e-02 | 0.114 |

3.3.3.1.4 Radiometric calibration of ASTER

The ASTER dataset was only used for digital photogrammetrical processing. In this application, spectral radiance values were of no importance, so radiometric corrections were not applied on this dataset.

3.3.3.2 Conversion of spectral radiance to apparent reflectance

The apparent reflectance at TOA represents the ratio of the upwelling radiance recorded at the sensor against irradiance from the sun, taking into account the solar elevation at the time of data acquisition (Mumby and Clark, 2000). This, in fact, is a simplification of the atmospheric radiative transfer model developed by Moran *et al.* (1992) (formula 3.6)

which describes the effects of different atmospheric processes on the reflectance received at sensor:

$$\rho_{\lambda} = \frac{[\pi \times (L_{\lambda} - L_{\lambda haze}) \times d^2]}{[T_v \times (ESUN_{\lambda} \times \cos(SZ) \times T_z + E_{down})]} \quad (3.6)$$

With: ρ_{λ} : reflectance at surface (unitless ratio)

π : 3.141593

L_{λ} : spectral radiance at sensor ($\text{W m}^{-2} \text{ster}^{-1} \mu\text{m}^{-1}$)

$L_{\lambda haze}$: correction for path radiance ($\text{W m}^{-2} \text{ster}^{-1} \mu\text{m}^{-1}$)

d : earth-sun distance in astronomical units, calculated as:

$$d = 1 - [0.01674 * \cos(0.9856 * (JD - 4))] \quad (3.7)$$

with: JD : Julian Day of image acquisition

T_v : atmospheric transmittance along the path from surface to sensor

= $\cos(VZ)$

with: VZ : zenith angle of sensor (in radians⁵⁴)

$ESUN_{\lambda}$: mean solar exoatmospheric irradiance in $\text{W m}^{-2} \mu\text{m}^{-1}$

SZ : Sun Zenith angle (in radians) at the moment of image acquisition

$$SZ = \frac{\pi}{2} - SE \quad (3.8)$$

with: SE : sun elevation angle (in radians)

T_z : atmospheric transmittance along the path from sun to ground surface

E_{down} : downwelling spectral irradiance at the surface because of scattering in the atmosphere ($\text{W m}^{-2} \mu\text{m}^{-1}$)

If all atmospheric effects in the above equation are ignored, the apparent reflectance, ρ_{al} , also termed *exoatmospheric reflectance* (Mumby and Clark, 2000), *planetary reflectance*,

⁵⁴ necessary for processing in ILWIS3.2

or *planetary albedo* as the influence of the atmosphere on the signal is not yet removed (Krause, 2003; LPSO, 2004), is calculated as follows:

$$\rho_{a\lambda} = \frac{[\pi \times L_{\lambda} \times d^2]}{[ESUN_{\lambda} \times \cos(SZ)]} \quad (3.9)$$

3.3.3.2.1 Landsat 7 ETM+

All the information needed to convert radiance values at the Landsat 7 ETM+ sensor to apparent reflectance values could be derived from the metadata file provided by the data manufacturer. The date of acquisition of the dataset used -September 10th, 2000- corresponds to Julian Day 254. Mean solar exoatmospheric spectral irradiance values specifically determined for each Landsat 7 ETM+ bandwidth are given in table 3.28. Finally, the sun elevation angle (57.6682°) is also given in the metadata (table 3.7), so that the sun zenith angle could be calculated.

Table 3.28. ETM+ mean solar exatmospheric spectral irradiance values (LPSO, 2004)

| | ESUN (W m ⁻² μm ⁻¹) |
|--------|--|
| band 1 | 1969.00 |
| band 2 | 1840.00 |
| band 3 | 1551.00 |
| band 4 | 1044.00 |
| band 5 | 225.70 |
| band 7 | 82.07 |
| band 8 | 1368.00 |

3.3.3.2.2 Landsat 5 TM

The Landsat 5 TM dataset was taken on August 14th, 1987, which corresponds to Julian Day 226; mean exoatmospheric solar spectral radiance values have been summarised by Chander and Markham (2003) (table 3.29); and the sun elevation angle at the moment of data acquisition (58.33°) was provided in the metadata of the dataset (table 3.9).

3.3.3.2.3 QuickBird

The same information was found in the metadata-files of the QuickBird dataset. The date of acquisition, February 5th, 2002, corresponds to Julian Day 36; the earth-sun

distance then equals 0.9857. The sun elevation angle was 41.6595° (table 3.11) and the mean solar exoatmospheric spectral irradiance values for the QuickBird multispectral bands are given in table 3.30.

Table 3.29. Landsat 5 TM mean solar exatmospheric spectral irradiance values (Chander and Markham, 2003)

| | ESUN ($\text{W m}^{-2} \mu\text{m}^{-1}$) |
|--------|---|
| band 1 | 1957 |
| band 2 | 1826 |
| band 3 | 1554 |
| band 4 | 1036 |
| band 5 | 215.0 |
| band 7 | 80.67 |

Table 3.30. QuickBird mean solar exoatmospheric spectral irradiance values (Krause, 2003)

| | ESUN ($\text{W m}^{-2} \mu\text{m}^{-1}$) |
|--------|---|
| band 1 | 1924.59 |
| band 2 | 1843.08 |
| band 3 | 1574.77 |
| band 4 | 1113.71 |

3.3.4 Atmospheric correction

According to Gitelson and Kondratyev (1991: 373), ‘90% of the contribution to the signal at TOA in the visible light depends on atmospheric and water surface properties’. In other words, the apparent reflectance at TOA is not equal to the reflectance at the earth’s surface partly due to different effects of the atmosphere on the electromagnetic radiance (EMR) (fig. 3.18). Two main atmospheric processes are acting to reduce the signal received at sensor, namely absorption by gases such as water vapour, carbon dioxide, and ozone which reduce the radiance intensity, and scattering by gas molecules and aerosols which alters the direction of the EMR (Mumby and Clark, 2000).

The degree of absorption depends on the wavelength of the light. Most bandwidths for optical remote sensing are selected such that wavelengths are recorded which fall in those parts of the spectrum, the so-called *transmission windows*, where absorption is lowest (fig.

3.19) (Mumby and Clark, 2000). Scattering, in contrast, is mainly influenced by the composition of the atmosphere. Different types of scattering are distinguished based on the size of the aerosols and gas molecules. If particles and molecules are very small, the effect of scattering also varies with wavelength. *Rayleigh scattering*, secondly, is caused by particles and molecules with radii far much smaller than the wavelengths in the optical range and shorter wavelengths, therefore, are the most affected. Third, *Mie scattering* is caused by particles which vary in size between 0.1 and 10 μm , and is also mostly affecting shorter wavelengths. If particles, such as water droplets or ice cores in clouds, have radii larger than 10 μm , all visible wavelengths are equally affected, resulting in a white haze over the scene (Mumby and Clark, 2000).

Besides, as the direction of the light is diverted by scattering, some part of the radiation recorded by the sensor will not have been reflected by the object but by the atmospheric particles. This part of the signal is known as *path radiance*. Moreover, scattering also creates *adjacency effects* in which radiance is recorded over a given pixel that originates from scattered radiance of the adjacent pixels (Mumby and Clark, 2000). This effect becomes more important in very heterogeneous environments and will increase with a decreasing pixel size. Lastly, in the case of marine remote sensing applications, the reflectance of light on the water surface should not be neglected either.

To eliminate these atmospheric effects, a range of correction techniques have been proposed (e.g. Tanré *et al.*, 1990; Chavez, 1996; Vermote *et al.*, 1997; Ouaidrari and Vermote, 1999; Hu *et al.*, 2001). Mumby and Clark (2000) distinguish three main groups, being the simple removal of path radiance; the direct calibration using field-derived reflectance; and atmospheric modelling. Atmospheric modelling is the most sophisticated method to convert apparent reflectance to surface reflectance. It is based on the atmospheric radiative transfer theory (formula 3.6) formulating the impacts of all atmospheric components on the EMR. This correction technique does not require field-measured reflectance values but needs accurate measurements of the atmospheric optical properties, such as aerosol content or atmospheric visibility, at the moment of data acquisition. This information rarely is available or of questionable quality and, therefore, approximated by standard values available in most correction algorithms (Mumby and Clark, 2000; Song *et al.*, 2001), e.g. *6S* (Vermote *et al.*, 1997). The more standards that have to be used, the less precise the atmospheric correction becomes. As in this case, hardly any information was available on the atmospheric characteristics at the different moments of data acquisition, atmospheric modelling should have been performed using the simplest generalisations. As a result, the atmospheric

correction would have affected all pixels equally and the relative relationship among the pixel values would not have been changed. The effects of such atmospheric corrections, thus, would have been minimal (Vogelmann *et al.*, 2001) and atmospheric modelling, therefore, was not applied here.

However, as no direct field-derived reflectances were available, the second atmospheric correction method could not be used either. When information on certain atmospheric characteristics is missing, some authors (e.g. Hu *et al.*, 2001) propose to derive these parameters from other sensors like SeaWiFS or MODIS, especially for marine research. As shown above, atmospheric modelling, unfortunately, does not necessarily lead to improved results (Andréfouët *et al.*, 2001; Song *et al.*, 2001) and especially when only single dataset analyses are performed, empirical atmospheric correction is equally performing (Song *et al.*, 2001).

The applied atmospheric corrections, consequently, only account for the removal of path radiance and sea surface reflection. Basically, the *dark pixel subtraction* method (Chavez, 1988) was used which assumes that in each image a dark object is present which totally absorbs the solar irradiance. The radiance measured over these pixels would then be totally composed of path radiance. This assumption can be made for marine applications as inside optically deep, clear water most of the visual light is absorbed. As a consequence, the signal received at the sensor is nearly entirely composed of atmospheric path radiance and surface reflection. If atmospheric and water surface conditions are assumed to be uniform throughout the scene, the mean deep-water radiance at sensor can be used to remove the atmospheric effect and the effect of sea-surface reflectance (Gordon and Morel, 1983; Tassan, 1996; Mumby and Edwards, 2000b). To determine this mean deep-water radiance, an area was selected for each dataset where, based on the nautical charts, depths were greater than 50m. In addition, two standard variations were subtracted from the mean in order to account for possible overreduction of the reflectance resulting from sensor and/or environmental noise (Armstrong, 1993).

3.3.4.1 Landsat 7 ETM+

On the Landsat 7 ETM+ multispectral bands, the deep-water area was located between scene coordinates: 1, 1450 (UL) and 800, 1800 (LR). Table 3.31 represents minimum, maximum, and mean deep-water radiance derived in this area, as well as the standard deviation and the final, corrected mean deep-water value, L_{si} . The panchromatic band 8 was also atmospherically corrected as it was used to pan-sharpen the multispectral bands

(see section 3.3.7). The same area as for the multispectral bands was selected to determine mean deep-water radiance, but, because of the different spatial resolution, other scene coordinates -1, 2900 (UL); 1600, 3600 (LR)- bordered the area.

Table 3.31. Determination of deep-water radiance on the Landsat 7 ETM+ dataset

| | $L_{\text{deep min}}$ | $L_{\text{deep max}}$ | $L_{\text{deep mean}}$ | st. dev. | L_{si}^* |
|--------|-----------------------|-----------------------|------------------------|----------|-------------------|
| band 1 | 59.66 | 71.42 | 64.55 | 1.37 | 61.81 |
| band 2 | 34.57 | 44.22 | 38.57 | 0.98 | 36.61 |
| band 3 | 19.41 | 29.74 | 24.52 | 1.02 | 22.48 |
| band 8 | 13.76 | 33.20 | 21.47 | 1.60 | 18.27 |

$$* L_{\text{si}} = L_{\text{deep mean}} - (2 \times \text{st. dev.}) \quad (3.10)$$

3.3.4.2 Landsat 5 TM

A specific atmospheric correction approach was applied to the Landsat 5 TM dataset because in multitemporal analysis, differences in viewing geometry, solar illumination, and atmospheric conditions between the images as well as differences in sensor performances usually result in altered measured radiance values which may be unrelated to actual bottom-type changes (Andréfouët *et al.*, 2001; Du *et al.*, 2002). Different authors (Andréfouët *et al.*, 2001; Song *et al.*, 2001) state that there are no real gains in applying a complex atmospheric correction for multitemporal analyses as long as the training data and the images to be classified are on a common relative scale and the classification of each dataset is independently made. For multitemporal change detection, the key point, conversely, is to maintain consistency in the radiometric measurements among the datasets (Song *et al.*, 2001). Consequently, *relative radiometric normalisation* has been used here as a preparation step for the change detection procedure.

Different relative-radiometric-normalisation techniques exist, giving different case-dependent results (Yuan and Elvidge, 1996; Yang and Lo, 2000). Based on the possibilities of the image-processing software, ILWIS 3.2, the *pseudo-invariant feature* (PIF) method (Schott *et al.*, 1988) was applied. This method assumes that some areas covered in each scene remain nearly constant over time. Changes in radiation detected over these areas, thus, are solely the result of changes which are not related to any surface change. These differences in radiation are assumed to be represented by a linear function which, subsequently, can be extrapolated to the entire dataset. The normalised datasets

consequently appear as if they were taken with the reference sensor under the same atmospheric and illumination conditions as for the reference dataset (Yang and Lo, 2000).

The atmospherically corrected Landsat 7 ETM+ dataset (y), in radiance values, was taken as the reference to which the different bands of the Landsat 5 TM dataset (x), converted to radiance values, were normalised. Remark that the Landsat 5 TM dataset has been resampled to the Landsat 7 ETM+ georeference so that pixels would match. In contrast to the original PIF method in which only one sample set -being man-made constructions (Schott *et al.*, 1988)- was used to perform the normalisation, two distinct areas –one over deep water (UL: 100, 1300; LR: 200, 1400) and one over a terrestrial sandy area distant from the urban centre (UL: 1325, 350; LR: 350, 400)- were considered pseudo-invariant over the period 1987-2000. This was in line with the *radiometric-control-sets* method of Hall *et al.* (1991), an adaptation of the original PIF method (fig. 3.20), in order to more accurately determine the linear relationship between the different datasets. In contrast with Hall *et al.* (1991) who selected their samples for land-use applications using a Kauth-Thomas greenness-brightness scattergram (Yang and Lo, 2000), the two samples were arbitrary selected over a bright and a dark sample area based on knowledge of the area under investigation.

The linear relationship between the different bands of each dataset was determined based on the mean radiance values in these two pseudo-invariant areas (Andréfouët *et al.*, 2001; Song *et al.*, 2001). As shown in figures 3.21a, b and c, the following linear equations for each band respectively were determined and applied to normalise the three Landsat 5 TM multispectral bands:

$$\text{Band1: } y = 0.8802x - 43.896 \quad (3.11)$$

$$\text{Band2: } y = 0.8906x - 21.472 \quad (3.12)$$

$$\text{Band3: } y = 0.9366x - 12.316 \quad (3.13)$$

3.3.4.3 QuickBird

A deep-water area on the QuickBird multispectral scenes has been selected between scene coordinates: 200, 1150 (UL) and 1050, 1350 (LR). Table 3.32 gives an overview of minimum, maximum and mean deep-water radiance values as well as the standard deviation and the corrected mean deep-water value, L_{si} .

Table 3.32. Determination of deep-water radiance on the QuickBird dataset

| | $L_{\text{deep min}}$ | $L_{\text{deep max}}$ | $L_{\text{deep mean}}$ | st. dev. | L_{si} |
|--------|-----------------------|-----------------------|------------------------|----------|-----------------|
| band 1 | 40.10 | 45.29 | 42.44 | 0.57 | 41.30 |
| band 2 | 24.27 | 29.79 | 25.43 | 0.35 | 24.73 |
| band 3 | 10.89 | 14.46 | 12.05 | 0.32 | 11.41 |

3.3.5 Water-column correction

In coastal marine applications, not only the atmosphere interferes with the radiance recorded by the remote sensor, but also the water column has an important impact on the reflectance of the seabed (fig. 3.18). As in the atmosphere, attenuation of the light takes place due to the effects of both absorption and scattering. Absorption in seawater mainly is the result of the water molecules, but it is also influenced by phytoplankton, inorganic and organic particulate matter in suspension and C-DOM (Roesler *et al.*, 1989; Mumby and Edwards, 2000b). Scattering in the watercolumn, or *backscatter* (Gould *et al.*, 2001), in addition, is the result of the water itself and the organic and inorganic particulate matter in suspension (Mumby and Edwards, 2000b; Gould *et al.*, 2001).

Attenuation in water, however, is not simply an addition of scattering and absorption, but rather is approached by formula 3.14 (Durand *et al.*, 2000; Ohde and Siegel, 2001). Unlike the atmosphere, scattering in pure water is largely negligible in the visual spectrum (Smith and Baker, 1981; Gould *et al.*, 2001) such that absorption is the most important influence in the water (Jerlov, 1976). Scattering will only take place when the amount of particulate matter in suspension, i.e. *turbidity*, is significantly large.

$$k_{di} = \sqrt{(a_i^2 + 2 a_i b_{bi})} \quad (3.14)$$

With: k_{di} : diffuse attenuation coefficient⁵⁵ for wavelength i
 a_i : total absorption coefficient (m^{-1}) for wavelength i
 b_{bi} : backscatter coefficient (m^{-1}) for wavelength i

The water itself is responsible for a difference in attenuation according to wavelength in which longer wavelengths are more attenuated (fig. 3.22). In contrast, the particulate matter in

⁵⁵ The diffuse attenuation coefficient is an apparent optical property summarising the effects of the inherent optical properties, i.e. absorption and scattering coefficients, on the signal received by e.g. a remote sensing sensor (Gould *et al.*, 2001; Morel and Maritorena, 2001).

suspension and the C-DOM are mainly attenuating shorter wavelengths (Jerlov, 1976; Maritorena, 1996) (fig. 3.22). Depending on their concentrations, a shift in radiance towards longer wavelengths may take place making the water to appear green or yellow-brown. The effects of the water column, thus, are highly wavelength dependent (Jerlov, 1976; Maritorena, 1996; Mumby and Edwards, 2000b; Gould *et al.*, 2001) and will increase with the height of the water column, i.e. depth. The radiance received at sensor, L_i , can consequently be expressed using following, simplified water reflectance model (formula 3.15) (Lyzenga, 1978; Paredes and Spero, 1983):

$$L_i = L_{s_i} + (a_i \times R_{b_i}) e^{-f k_i z} \quad (3.15)$$

With: L_{s_i} : mean deep-water radiance in band i
 a_i : wavelength-dependent constant accounting for the irradiance at the sea surface, the transmittance of the sea surface and atmosphere, and the reduction of the radiance due to refraction at the sea surface (Ji *et al.*, 1992)
 R_{b_i} : bottom reflectance
 f : geometric factor accounting for path length through the water⁵⁶
 k_i : effective attenuation coefficient of water
 z : depth

In this decay model, the intensity of light exponentially decreases with increasing depth. As a consequence, the spectral radiances recorded by the sensor will not only depend on the reflectance of the substrata but also on depth (Mumby and Edwards, 2000b). In other words, if depth increases, the signal will be more attenuated and the spectral separability of the different bottom types will decrease. While in most cases, the effects of the atmosphere can be assumed more or less homogeneous over one scene, this can not be done for the water column as its effects change with depth even if horizontal and vertical homogeneity within the water column is assumed (Lyzenga, 1981). The most confusing effect on the remote sensing signal

⁵⁶ Attenuation should be taken into account on both downwelling and upwelling radiance. Here, a two-flow model is applied assuming attenuation k is similar in both cases and f , consequently, equals 2. This, however, is not always the case, especially not in turbid waters (Maritorena *et al.*, 1994; Durand and Cauneau, 1997; Durand *et al.*, 2000).

for subaquatic bottom-type classification, therefore, is believed to be the interaction with the water column.

If inherent optical properties of the water column and the depth are known for each pixel in the scene, reflectance of the seabed can be reconstructed from the reflectance values at the sea surface (Lyzenga, 1981, Mumby *et al.*, 1998a). This information, however, is rarely, if ever completely available and several methods (e.g. Lyzenga, 1978; Khan *et al.*, 1992; Bierwirth *et al.*, 1993; Tassan, 1996; Durand *et al.*, 2000; Tanis *et al.*, 2002) have been proposed to correct for water-column effects which require only limited or no ancillary data concerning the composition of the water column and/or depth. For this study, the technique developed by Lyzenga (1978; 1981) which does not require any in situ or ancillary data (Spitzer and Dirks, 1987; Maritorena, 1996; Mumby *et al.*, 1998a; Edwards, 1999; Mumby and Edwards, 2000b; Matsunaga *et al.*, 2001; Radiarta *et al.*, 2002) was used to perform the water-column correction. This approach, however, did not reconstruct the reflectance of the seabed as such, but produced a new set of *depth-invariant bottom indices* (DIBs) (Mumby *et al.*, 1998a).

3.3.5.1 DIB correction method

The DIB correction method proposed by Lyzenga (1978; 1981) is based on atmospherically corrected radiance at sensor values. These values have been previously obtained by transforming the DN values to physical radiance values and correcting them for path radiance and surface reflection. As a result, formula 3.15 is transformed so that the left side of formula 3.16 represents the atmospherically corrected radiance values.

$$L_i - L_{si} = (a_i \times R_{bi}) e^{-2k_i z} \quad (3.16)$$

The first step is to linearise the exponential relationship between radiance and depth by taking the natural logarithm of formula 3.16 (Lyzenga, 1978; 1981; Paredes and Spero, 1983; Edwards, 1999; Mumby and Edwards, 2000b; Andréfouët *et al.*, 2001):

$$X_i = LN(L_i - L_{si}) = LN(a_i \times R_{bi}) - 2k_i z \quad (3.17)$$

Following, equation 3.17 can be rearranged to determine the bottom reflectance, R_{bi} :

$$LN(R_{bi}) = \frac{X_i + 2k_i z}{a_i} \quad (3.18)$$

Three variables (i.e. a_i , k_i , z), however, remain unknown. The DIB method does not attempt to solve these unknowns, but calculates the ratio between each pair of log-transformed, atmospherically corrected radiance bands, X_i and X_j . A consequence of the method, however, is that the original spectral radiance values will be transformed into DIBs not related to the spectral characteristics of the bottom type. In order to define the ratios between pairs of X_i bands, a selection of pixels over a uniform substratum, but at different depths, is needed (Edwards, 1999; Mumby and Edwards, 2000b). A sandy bottom type is preferable (Mumby and Edwards, 2000b) as this is fairly recognisable by the interpreter. Lyzenga (1981) and Edwards (1999) select homogeneous areas, while Maritorenna (1996) prefers to determine the ratio as the mean of ratios defined between different pairs of pixels in order to minimise the effect of possible heterogeneity in the selected areas. In the following implementation, these ratios have been determined based on the depth measurements collected during the field work which can be linked to individual pixels.

Next, the atmospherically corrected radiance values for the selected pixels can be represented on a bi-plot of the two log-transformed radiance bands X_i and X_j (fig. 3.23). As the relationship between radiance and depth has been linearised and the substratum is constant, pixel values ideally fall along a straight line. The slope of this 'straight line' represents the relative amounts of attenuation in each band and thus the ratio k_i/k_j (Edwards, 1999). In reality, these points do not fall on a perfect line due to, for example, the natural heterogeneity in the bottom-type reflection, variations in water quality, or surface roughness (Edwards, 1999) (fig. 3.24). Consequently, a regression line needs to be calculated through this cloud of points, representing the ideal straight line. For this purpose, least squares regression, however, is not used as its result depends on which band is used as the dependent variable. Instead, rather than calculating the mean square deviation from the regression line in the direction of the dependent variable, the regression line is placed where the mean square deviation is minimised (Lyzenga, 1981) according to formula 3.19:

$$k_i/k_j = a + \sqrt{a^2 + 1} \quad (3.19)$$

$$\text{With: } a = \frac{\delta_{ii} - \delta_{jj}}{\delta_{ij}} \quad (3.20)$$

With: δ_{ii} : variance of band i
 δ_{ij} : covariance of bands i and j

If different bottom types are represented in such a bi-plot, they will all be represented by another line in which variation along the line is solely indicating changes in depth (fig. 3.23). These lines differ in position, as each bottom type has a different reflectance, whereas their gradients is identical since the ratio of attenuation coefficients is not dependent on the bottom-type reflectance (Edwards, 1999; Mumby and Edwards, 2000b). The y-intercept of each line, finally, refers to a DIB:

$$DIB_{ij} = X_i - \left\{ (k_i/k_j) \times X_j \right\} \quad (3.21)$$

With: band i along the Y axis and band j along the X axis

k_i/k_j : ratio of attenuation coefficients

As not all pixels belonging to one bottom type fall along a single, perfectly straight line (fig. 3.24), each pixel is assigned to an index of bottom type by connecting it to the Y axis along a line of gradient k_i/k_j . In this way, the DIB is scaled to the y-intercept (Edwards, 1999; Mumby and Edwards, 2000b). Based on this y-value, representing the DIB, all pixels can be classified. Although Lyzenga (1978) and Maritorena (1996) have performed an additional orthogonal rotation to align the Y axis along the k_i/k_j gradient, such a refinement does not change the functionality of the process (Mumby and Edwards, 2000b) and was consequently not applied.

A study by Mumby *et al.* (1998a) clearly shows that the classification accuracy is significantly improved for both Landsat TM and CASI datasets when water-column correction is applied. In the case of SPOT data, this beneficial effect, in contrast, is at the expense of the multispectral information as the two useful SPOT bands are transformed into one single DIB layer (Mumby *et al.*, 1998a). Therefore, as already suggested by Lyzenga (1978; 1981), at least three multispectral bands are required.

Another constraint to this technique is its restriction to clear -Type IA, IB and II (Jerlov, 1976)- water (Jerlov, 1976; Spitzer and Dirks, 1987; Tassan, 1996; Mumby and Edwards, 2000b), although modifications to the technique have been developed for more turbid water (e.g. Tassan, 1996). This, however, was not needed for classifying the coral reefs of the Red Sea as, similar to most coral-reef environments (Maritorea, 1996), they occur in clear nutrient-poor waters.

Finally, the selection of pixels over a sandy substrate is most convenient but may also introduce additional problems to the classification process, as demonstrated by Mumby *et al.* (1998a), because the implementation of this correction algorithm only improves the mapping of sandy bottoms while the confusion between other bottom types may increase. Besides, if a dark substrate reflects less than the mean deep-water radiance, Lyzenga's approach can not be used either, since in that case $LN(L_i - L_{si})$ could not be determined (Philpot, 1989; Ji *et al.*, 1992; Durand *et al.*, 2000). This, probably, represents the most fundamental constraint to the technique.

3.3.5.2 Implementation

3.3.5.2.1 Landsat 7 ETM+

To correct the water-penetrating spectral bands of the Landsat 7 ETM+ dataset for the effects of the water column, 319 pixels were selected which correspond to the in situ depth observations over a sandy area. In this way, it was assured that (1) the whole range of depths present in the study area was covered, and (2) the sandy substrate was as homogeneous as possible.

If the radiance values in each band were plotted against the corresponding measured depth, corrected for tidal effects at the moment of image registration (fig. 3.25), the exponential relationship between both became clear. From a certain depth, increasing with decreasing wavelength, the radiance values became more or less constant (roughly corresponding to the mean deep-water radiance) as can be seen in figure 3.25. From this depth onwards, reflection of the seabed, therefore, was no longer recorded by the remote sensor. In shallow (less than 1-2m) water, the influence of the water column, on the other hand, became minimal and a clear difference between the radiance values of all three bands could no longer be made. As saturation or total absorption in the selected pixels for one of the bands should be avoided (Edwards, 1999), pixels in very shallow (< 1 m) and very deep areas were discarded.

Optically deep water for each band was determined by the maximum depth of penetration of each waveband as will be determined in section 3.4.3.1.1 (table 3.47). As a result, 196 ground control points between 1 and 16.8m were selected for the determination of ratio k_1/k_2 , while only 79 GCPs between a depth of 1 and 5.2m remained for the determination of ratios k_1/k_3 and k_2/k_3 . An overview of these GCPs is given in annex IV.

When the natural logarithms taken from the atmospherically corrected radiances were plotted against depth, the effect of this linearization can clearly be noted when comparing figure 3.25 and 3.26. As three wavebands of the Landsat 7 ETM+ dataset were used, three different DIBs could be determined. k_i/k_j ratios were defined according to formulas 3.19 and 3.20 as summarised in tables 3.33a and b. As can be seen on figures 3.27a, b and c, the selected pixels in each of these plots were more or less aligned.

Table 3.33a. Variance within each Landsat 7 ETM+ radiance band

| | band 1 | band2 | band3 |
|-----------------------------|---------------|--------------|--------------|
| variance δ_{ii}^* | 0.259 | 0.451 | / |
| variance δ_{ii}^{**} | 0.065 | 0.130 | 0.462 |

*based on 196 points; ** based on 79 points

Table 3.33b. Determination of the attenuation ratios k_i/k_j for Landsat 7 ETM+ water column correction

| | ratio k_1/k_2 * | ratio k_1/k_3 ** | ratio k_2/k_3 ** |
|--------------------------|-------------------------------------|--------------------------------------|--------------------------------------|
| covariance δ_{ij} | 0.328 | 0.149 | 0.232 |
| a_{ij} | -0.293 | -1.331 | -0.714 |
| k_i/k_j | 0.75 | 0.33 | 0.52 |
| reference k_i/k_j # | 0.93 | 0.31 | 0.39 |
| reference k_i/k_j § | 0.70-0.79 | 0.36-0.37 | 0.46-0.54 |
| reference k_i/k_j § | 0.59-1.02 | 0.34-0.42 | 0.33-0.64 |

*based on 196 points; ** based on 79 points

The obtained ratio values were in accordance with the values summarized by Mumby and Edwards (2000) for the application of Lyzenga's method on Landsat 5 TM bands 1, 2 and 3 in their study area in the Turks and Caicos Islands[#], and for Landsat 5 TM-derived^{\$} and field-measured values^{\$} in the Bahamas (Armstrong, 1993) (table 3.33b). While differences in k_i/k_j ratios between the different sample areas could largely be attributed to local differences in the composition of the water column, the overall agreement between them proves the good performance of the algorithm (Armstrong, 1993).

These k_i/k_j ratios were subsequently applied to convert the multispectral radiances into three DIB bands using formula 3.21. When DIB values for the 79 selected pixels were plotted against depth, the effect of the water-column correction was clearly seen on figure 3.28, especially when compared with figures 3.25 and 3.26. In contrast, some problems were noted when the DIBs for all 196 points were plotted (fig. 3.29). Here, only DIB₁₂ had a relative constant value up to 15m depth. DIB₁₃ and DIB₂₃, in contrast, only remained constant up to depth of about 5m due to the incorporation of the red waveband in the ratio. As a result, differentiation between the bottom types will become more difficult in areas deeper than 5m, which could affect the accuracy of the classification result. However, this would already be the case at much shallower depths if no water-column correction was applied.

The effect of the water-column correction was also estimated by comparing the *coefficient of variation* (CoV) of each DIB band to the mean CoVs⁵⁷ of the original, atmospherically corrected radiance bands (Edwards, 1999) calculated over the 79 points used for the k_i/k_j determination. As can be seen in table 3.34, CoVs for the DIB bands were about one order in magnitude lower than for the corresponding radiance bands. Besides, water-column variances calculated for the mean radiance bands showed that respectively 64, 90 and 91% of the variance in the DIB₁₂-, DIB₁₃- and DIB₂₃-corresponding radiance bands was due to effects of the water column. This high level of confusing variation, thus, was eliminated by the water-column correction technique.

⁵⁷ the mean CoV of radiance band i and j used for the calculation of the corresponding DIB_{ij}

Table 3.34. Comparison of COVs for Landsat 7 ETM+ before and after water column correction

| | mean_{ij} | DIB_{ij} | water-column variance (%)* |
|-----------------|--------------------------|-------------------------|-----------------------------------|
| band 1 – band 2 | 0.281 | 0.101 | 64 |
| band 1 – band 3 | 0.449 | 0.044 | 90 |
| band 2 – band 3 | 0.494 | 0.042 | 91 |

$$* \text{water column variance} = 100 - \left(\frac{DIB_{ij}}{mean_{ij}} \times 100 \right) \quad (3.22)$$

3.3.5.2.2 Landsat 5 TM

A similar process was followed to correct the Landsat 5 TM dataset. Initially, the derivation of the k_i/k_j ratios was based on the same ground control points used for the correction of the Landsat 7 ETM+ dataset, assuming that no large changes in bathymetry had taken place. However, a recognisable change in spectral reflectance was encountered on some locations, pointing to a possible change in bottom type. These points, therefore, were omitted and 171 points were withheld to calculate k_1/k_2 ; and 57 points to determine k_1/k_3 and k_2/k_3 . See annex IV for an overview of these points.

The radiometrically normalised Landsat 5 TM radiance values, RRN_i , derived in section 3.3.4.2 were used as the base values for X_i . Following, natural logarithms were taken of these values and the k_i/k_j ratios were determined as in formula 3.19 (table 3.35a and b). A small adaptation to formula 3.21, however, was needed before the DIBs could be calculated because the radiometrical normalisation resulted in negative values over some areas. As this would cause problems to determine the natural logarithms, an artificial bias of $10 \text{ W m}^{-2} \text{ ster}^{-1} \mu\text{m}^{-1}$ was introduced in each band in order to make all values positive. This did not affect the further processing of the data as the relative differences between the pixel values remained unaltered. The adapted formula then became:

$$DIB_{ij} = LN(RRN_i + 10) - \left[k_i/k_j \times LN(RRN_j + 10) \right] \quad (3.23)$$

Table 3.35a. Variance within each Landsat 5 TM radiance band

| | band 1 | band2 | band3 |
|-----------------------------|---------------|--------------|--------------|
| variance δ_{ii}^* | 0.336 | 0.579 | / |
| variance δ_{ii}^{**} | 0.073 | 0.118 | 0.657 |

*based on 171 points; ** based on 57 points

Table 3.35b. Determination of the attenuation ratios k_i/k_j for Landsat 5 TM water column correction

| | ratio k_1/k_2 * | ratio k_1/k_3 ** | ratio k_2/k_3 ** |
|--------------------------|-------------------------------------|--------------------------------------|--------------------------------------|
| covariance δ_{ij} | 0.413 | 0.158 | 0.254 |
| a_{ij} | -0.294 | -1.845 | -1.062 |
| k_i/k_j | 0.75 | 0.25 | 0.40 |

* based on 171 points; ** based on 57 points

The calculated COVs enlisted in table 3.36 clearly proof the advantage of defining DIBs over the original spectral values, as was the case for the Landsat 7 ETM+ dataset.

Table 3.36. Comparison of COVs for the radiometrically normalized Landsat 5 TM dataset before and after water column correction

| | mean_{ij} | L5_DIB_{ij} | water-column variance (%)* |
|-----------------|--------------------------|----------------------------|-----------------------------------|
| band 1 – band 2 | 0.302 | 0.101 | 67 |
| band 1 – band 3 | 0.521 | 0.050 | 90 |
| band 2 – band 3 | 0.556 | 0.055 | 90 |

3.3.5.2.3 QuickBird

During the third field campaign, numerous bottom-type observations were made for the area covered by the QuickBird scene, whereas the number of depth measurements was limited due to the failure of the bathymetric instrument. Fortunately, Lyzenga's method (1978; 1981) does not strictly require known depth values; it only needs a homogenous substrate at different depths in order to define the k_i/k_j ratios. As it was known from the field campaigns, the observations of the bottom type occurred at

different depths so that this information could also be used for the water-column correction.

Besides, this offered the opportunity to verify the remark of Mumby *et al.* (1998a) who point to a bias in the bottom-type classification resulting from selecting sample pixels over a sandy substrate. To test this hypothesis, the DIB method was once calibrated using depth variations over a sandy bottom type, and a second time using pixels selected over seagrass patches. This could easily be done with the QuickBird dataset as many seagrass patches observed during the field campaigns were easily recognisable on the QuickBird scenes.

a. Sandy substrate sample points

In addition to the available depth-measured GCPs over a sandy substrate, nine extra GCPs were added which were observed during the third field campaign over a sandy substrate. As a result, 69 and 41 GCPs were respectively obtained to determine the k_1/k_2 ratio and the k_1/k_3 and k_2/k_3 ratios (annex IV). The atmospherically corrected QuickBird radiance values corresponding to these GCPs were subsequently logarithmically transformed and the different k_i/k_j ratios were calculated as shown in table 3.37a.

Table 3.37a. Variance within each QuickBird radiance band

| | band 1 | band2 | band3 |
|-----------------------------|--------|-------|-------|
| variance δ_{ii}^* | 0.739 | 1.236 | / |
| variance δ_{ii}^{**} | 0.237 | 0.499 | 1.631 |

*based on 69 points; ** based on 41 points selected over a sandy substrate

Table 3.37b. Determination of the attenuation ratios k_i/k_j for QuickBird water column correction

| | ratio k_1/k_2 * | ratio k_1/k_3 ** | ratio k_2/k_3 ** |
|--------------------------|-------------------|--------------------|--------------------|
| covariance δ_{ij} | 0.934 | 0.591 | 0.864 |
| a_{ij} | -0.266 | -1.180 | -0.656 |
| k_i/k_j | 0.77 | 0.37 | 0.54 |

*based on 69 points; ** based on 41 points selected over a sandy substrate

As the range of wavelengths covered by each QuickBird waveband is very similar to the range of the corresponding Landsat 7 ETM+ wavebands, the k_i/k_j ratios calculated were almost equal. Based on these ratios, the new *QB_DIB* bands were determined following formula 3.21 (table 3.37b).

Here as well, the comparison of the CoVs of the DIBs and the radiance wavebands of the QuickBird dataset showed the importance of correcting the dataset for water-column effects (table 3.38).

Table 3.38. Comparison of COVs for the QuickBird dataset before and after water column correction calibrated with sandy substrate points

| | mean _{ij} | QB_DIB _{ij} | water-column variance (%)* |
|-----------------|--------------------|----------------------|----------------------------|
| band 1 – band 2 | 0.583 | 0.093 | 84 |
| band 1 – band 3 | 0.879 | 0.039 | 96 |
| band 2 – band 3 | 0.968 | 0.054 | 94 |

b. Seagrass substrate sample points

To test the alternative water-column correction approach, a number of pixels over a homogeneous seagrass substrate, at different depths ranging up to 10m, were selected. Unfortunately, the seagrass patches were more heterogeneous than a bare sandy bottom, making it more difficult to select pixels over equally dense seagrass stands. Nevertheless, 92 pixels in total were selected to determine k_1/k_2 ; and 68 pixels to determine k_1/k_3 and k_2/k_3 (see annex IV).

Subsequently, as with the sandy bottom alternative, the log-transformed, atmospherically corrected radiance values of the sample pixels in each band were used to calculate the different k_i/k_j ratios. Tables 3.39a and b enlist the different parameters calculated.

Table 3.39a. Variance within each QuickBird radiance band

| | band 1 | band2 | band3 |
|-----------------------------|--------|-------|-------|
| variance δ_{ii}^* | 0.164 | 0.212 | / |
| variance δ_{ii}^{**} | 0.143 | 0.189 | 0.693 |

*based on 92 points; ** based on 68 points selected over a seagrass substrate

Table 3.39b. Determination of the attenuation ratios k_i/k_j for QuickBird water column correction

| | ratio k_1/k_2 * | ratio k_1/k_3 ** | ratio k_2/k_3 ** |
|--------------------------|-------------------|--------------------|--------------------|
| covariance δ_{ij} | 0.174 | 0.245 | 0.328 |
| a_{ij} | -0.138 | -1.120 | -0.767 |
| k_i/k_j | 0.87 | 0.38 | 0.49 |

*based on 92 points; ** based on 68 points selected over a seagrass substrate

Although the resulting k_i/k_j ratios should be similar to the ones calculated using the sandy samples as the water-column attenuation, theoretically, is independent of bottom type, this was not the case, especially for the k_1/k_2 ratio. If the parameters enlisted in tables 3.37b and 3.39b were compared, the differences in covariance between X_1 and X_2 for the respective algorithms was remarkable. This might be explained by the fact that seagrass has a completely different influence on the reflection of the blue and green wavelengths as compared to a white, calcareous sandy substrate. While over bright sandy substrates, both wavelengths are highly reflected in almost equal proportions, the seagrass absorbs the blue wavelengths more than the green part of the spectrum. The relative relation between both reflectances also varies according to the seagrass species, the growth stage, health status, ..., which greatly reduces the overall covariance between X_1 and X_2 . Alternatively, this could also mean that water-column composition over seagrass is different than over bare sand. Technical equipment and time, unfortunately, was lacking to test this hypothesis.

Table 3.40. Comparison of COVs for the QuickBird dataset before and after water column correction calibrated with seagrass substrate points

| | mean _{ij} | QB_DIBsg _{ij} | water-column variance (%)* |
|-----------------|--------------------|------------------------|----------------------------|
| band 1 – band 2 | 0.418 | 0.494 | -18 |
| band 1 – band 3 | 0.577 | 0.110 | 71 |
| band 2 – band 3 | 0.599 | 0.083 | 86 |

Finally, the DIBs based on these new parameters, QB_DIBsg_{ij} , were calculated following formula 3.21. As with the other datasets, CoVs were calculated to illustrate the effect of the water-column correction (table 3.40). Remarkably, in contrast to the

water-column variance over sandy substrates, variance in QB_DIBsg₁₂ was greater than the mean variance of QuickBird radiance bands 1 and 2. Moreover, the contribution of the water column to the variation in the other radiance bands was also lower than over sandy areas. This led to the conclusion that the variance in reflection of these seagrass beds was greater than the variation added by the water column and that in fact, the water column reduced the original variation in reflection.

3.3.6 Masking

As most applications were only intended to study the marine part of the coastal zone, the terrestrial part of the study area could be masked. An automated method to mask the land was presented by Van Hengel and Spitzer (1991) and Ji *et al.* (1992). Their approach is based on the total absorption of the infrared wavelengths by the water. As terrestrial pixels, consequently, are much more reflective, a slicing could be applied to select only the land-representing pixels. This, however, was not an effective method for this study area as many shallow reef parts had a similar reflection to the land. Alternatively, a land mask for each dataset was created by vectorising the coastline on a true colour composite (TCC) of each dataset. The vector-based land masks were subsequently rasterised and all pixels representing the land area were given the value 0. For the QuickBird dataset, the mask was digitised on the panchromatic band as the very high resolution of this layer allowed a more detailed delineation. Afterwards, this mask layer was rasterised to the multispectral band georeference so that it could be applied on each multispectral QuickBird band.

Secondly, masking out the deep water is advised by some authors (Maritorea, 1996; Edwards, 1999; Matsunaga *et al.*, 2001) as no reflection of the seabed is recorded over these parts. Results, however, were not found to be improved by masking the deep water and, therefore, the deep-water mask was only applied to clean up the final results. This deep-water mask will be defined during the bathymetric mapping algorithm (see section 3.5).

Finally, it was also important to mask out all boats, wrecks, or other artefacts visible in the QuickBird scenes as these covered the underlying seabed. This was not required for the other datasets as their spatial resolution did not allow detecting these features. This specific mask was created by visually digitising all artefacts on screen based on a QuickBird TCC. The multispectral bands were chosen so that all pixels affected by these artefacts were correctly covered. While applying the mask, it was not only necessary to mask the artefacts themselves but also their surroundings, as shadows or changes in surface currents around these obstacles

seriously affected the reflected signal of the seabed. This additional mask layer was subsequently rasterised and applied to the QuickBird multispectral bands in which the masked-out values were given a value of 0.

3.3.7 Pan-sharpening

According to the definition of Van Genderen and Pohl (1994), *image fusion* is ‘*the combination of two or more different images to form a new image by using a certain algorithm*’ aiming at ‘*the integration of disparate and complementary data to enhance the information apparent in the images as well as to increase the reliability of the interpretation*’ (Pohl and Van Genderen, 1998: 827). *Image sharpening*, subsequently, is a special form of image fusion applied to enhance the spatial resolution of a dataset (Pohl and Van Genderen, 1998). *Pan-sharpening*, accordingly, is the spatial enhancement of a multispectral dataset with the higher spatial resolution of a panchromatic image.

From the moment datasets with different characteristics were available, many techniques and methods have been developed to fuse these datasets (for an overview, see e.g. Pohl and Van Genderen, 1998; Ranchin and Wald, 2000). Most of these methods were based on principle component analysis (PCA), Hue-Intensity-Saturation (HIS) transformations, or high pass filters (HPF) but although they enhanced the spatial resolution, none entirely preserved the spectral integrity of the original multispectral dataset (e.g. Chavez *et al.*, 1991; Carter, 1998, Pohl and Van Genderen, 1998, Ranchin and Wald, 2000).

Recently, new fusion algorithms have been developed to merge multispectral data and high-resolution data with maximal preservation of the spectral information (de Béthune *et al.*, 1998b). Based on the analysis of a wide range of statistic parameters such as standard deviation, correlation, deviation index, and entropy, the ARSIS⁵⁸ method (Ranchin and Wald, 2000) proves to achieve the best result for integrating higher spatial resolution with maximal preservation of the spectral integrity of the original dataset (Wald *et al.*, 1997; Ranchin and Wald, 2000). This technique based on the multiresolution analysis of images using wavelet transforms, however, was difficult to implement in the ILWIS 3.2 software and, instead, an alternative method, the adaptive-intensity-matching filter (AIMF) method (de Béthune *et al.*, 1998a), with similar performance was used.

⁵⁸ ARSIS: “Amélioration de la Résolution Spatiale par Injection des Structures” (Ranchin and Wald, 2000)

3.3.7.1 Adaptive-intensity-matching-filter method

The AIMF method developed by de Béthune *et al.* (1998a) aims at adjusting the spectral information of the high-resolution dataset to the radiometry of the low-resolution multispectral bands before the actual pan-sharpening takes place. Therefore, AIMFs are applied which equalise the mean, or the mean and variance of the high-resolution dataset with those of the low-resolution bands, on a pixel by pixel basis, using local image statistics (de Béthune *et al.*, 1998a).

The implementation of this method is divided in four steps, allowing the pan-sharpening of a multidimensional dataset (de Béthune *et al.*, 1998a). The first step involves the georegistration of the low-resolution multispectral wavebands, MS_i , to the high-resolution band, H . The geometric accuracy in this step is of vital importance for the success of the pan-sharpening as misregistration may introduce artefacts into the result which, usually, would lead to misinterpretations (Pohl and Van Genderen, 1998). A bicubic convolution resampling algorithm has been proven to give the best results (Wald *et al.*, 1997).

The second step enables the simultaneous pan-sharpening of a dataset containing several multispectral bands. In order to do so, a low-resolution *global intensity channel*, L , is created to which the spectral intensity of the high-resolution band, H , will be matched in the consequent step. de Béthune *et al.* (1998a) propose following formula 3.24 to create L :

$$L = \sum MS_{iH} \quad (3.24)$$

With: MS_{iH} : resampled low-resolution band MS_i to the high-resolution band H

Subsequently, the spectral intensity of the high-resolution band, H , is matched to the global intensity channel, L , by using a *local mean matching filter*, LMM , (formula 3.25) or a *local mean and variance matching filter*, $LMVM$ (formula 3.26). The size of the filter window, $(w \times h)$, determines how well the spectral values are preserved in the pan-sharpened result. The larger the filtering window, the more structural information from the high-resolution band will be incorporated, but the more the spectral information will be distorted (de Béthune *et al.*, 1998a; b).

$$F_{H>L(l,c)} = \frac{(DN_{H(l,c)} \times M_{L(l,c)(w \times h)})}{M_{H(l,c)(w \times h)}} \quad (3.25)$$

$$F_{H>L(l,c)} = \frac{[(DN_{H(l,c)} - M_{H(l,c)(w \times h)}) \times \sigma_{L(l,c)(w \times h)}]}{\sigma_{H(l,c)(w \times h)}} + M_{L(l,c)(w \times h)} \quad (3.26)$$

- With: $F_{H>L(l,c)}$: fused intensity band at pixel (l, c)
 $DN_{H(l,c)}$: pixel value in the band H at pixel (l, c)
 $M_{H(l,c)(w \times h)}$: local mean value in band H at pixel (l, c) within a kernel with dimensions (w x h)
 $M_{L(l,c)(w \times h)}$: local mean value in the low-resolution band at pixel (l, c) within a kernel (w x h)
 $\sigma_{H(l,c)(w \times h)}$: local standard deviation in H at pixel (l, c) within a kernel (w x h)
 $\sigma_{L(l,c)(w \times h)}$: local standard deviation in the low-resolution band at pixel (l, c) within a kernel (w x h)

In the final step, the resampled low-resolution bands, MS_{iH} , are transformed based on the INR transform⁵⁹, using the fused intensity band, $F_{H>L(l,c)}$, and the low-resolution global intensity channel, L , as shown in formula 3.27:

$$H_i = \frac{(MS_{iH} \times n \times F_{H>L(l,c)})}{L} \quad (3.27)$$

- With: H_i : pan-sharpened multispectral band i
 n : number of multispectral bands involved

As the ARSIS-method⁶⁰ is considered the best method available, de Béthune *et al.* (1998a) use results obtained with this method as a standard to determine the ideal filter size to be applied in their method. In the case of the LMVM, small window sizes (3 to 7) do not integrate the high spatial resolution into the pan-sharpened result and are considered insufficient. The closest match with the ARSIS results is obtained with a LMVM filter

⁵⁹ INR transform: intensity-normalised-ratio transform (de Béthune *et al.*, 1998a)

⁶⁰ although this method was first described in 2000, it already existed several years before (Ranchin and Wald, 2000)

size of 15 pixels, although bigger window sizes produce equally good results. The best matches with the LMM filter, conversely, are produced with window sizes of 3 to 5 pixels (de Béthune *et al.*, 1998a). Comparison of both filters shows that the LMVM filter is the best performing (de Béthune *et al.*, 1998b).

3.3.7.2 Test case: pan-sharpening the Landsat 7 ETM+ dataset

Mumby *et al.* (1999) have merged the multispectral wavebands of a Landsat 5 TM dataset with a SPOT panchromatic scene using a HIS transformation method. In their result, the loss of spectral data was significant and the image sharpening of the dataset actually reduced the accuracies of their bottom-type classification (Green *et al.*, 1998; Mumby *et al.*, 1999). Since then, however, newly developed fusion techniques have become available, as well as new datasets. A Landsat 7 ETM+ dataset, for example, comprises both multispectral bands and a panchromatic band with higher spatial resolution. This reduces the potential errors introduced by pan-sharpening as the radiometric, atmospheric, and water-column conditions at the moment of data acquisition do not differ between the two datasets. Besides, the low-resolution multispectral bands and the high-resolution panchromatic band are exactly matched by the data provider during geometric processing of the level-1 products, so that potential artefacts introduced by georeferencing are avoided.

For these reasons, a test case for the pan-sharpening of the Landsat 7 ETM+ dataset was made. The aim was to investigate whether a pan-sharpened multispectral dataset would give better results for the study of coral reefs. Because of time restrictions, the QuickBird dataset was not pan-sharpened. Besides, the spatial resolution of the multispectral QuickBird wavebands was already assumed to be sufficiently high such that the introduction of the spatial resolution of the QuickBird panchromatic band would not add much to the accuracy of the result.

3.3.7.2.1 Data pre-processing

A subset of the Landsat 7 ETM+ band 8 (UL: 6199, 2199; LR: 9200, 5800) was created which exactly matched the subset of the multispectral bands, taking into account its higher spatial resolution. All sensor-specific pre-processing steps had to be applied prior to image fusion as after pan-sharpening, the contribution of each sensor would no longer be distinguishable (Pohl and Van Genderen, 1998).

To georeference the panchromatic band based on the GCPs measured during the field surveys, however, would potentially introduce misregistration with the multispectral bands. For this reason, as the multispectral bands and the panchromatic bands were already matched by the data provider, the pan-sharpening was performed based on the scene coordinates and the resulting pan-sharpened bands were only georeferenced afterwards. As a result, a scene-specific reference system, defined by the coordinates of the corner pixels, needed to be separately created for the multispectral bands (table 3.41) and the panchromatic band (table 3.42). In this, the 2:1 ratio between the spatial resolution of the multispectral and panchromatic bands was preserved. Afterwards, the multispectral bands were resampled to the panchromatic georeference system using a bicubic convolution resampling algorithm.

Table 3.41. Specific georeference system for the Landsat 7 ETM+ multispectral bands, based on scene characteristics, used in the pan-sharpening procedure

Georeference: corners

Pixel size: 1

Min. X, Y: 0 0

Max. X, Y: 1801 1501

Center of pixels: No

Table 3.42. Georeference system for the Landsat 7 ETM+ panchromatic band, based on scene characteristics, used in the pan-sharpening procedure

Georeference: corners

Pixel size: 0.5

Min. X, Y: 0 0

Max. X, Y: 3600 3000

Center of pixels: No

Finally, each resampled band was radiometrically converted to obtain radiance values using formula 3.3 and the parameters enlisted in table 3.25, and atmospherically corrected using the mean deep-water radiance values as defined in table 3.31. The correction for the effects of the water column, conversely, was only performed after the pan-sharpening process.

3.3.7.2.2 Creation of a global intensity channel

In formula 3.24 proposed by de Béthune *et al.* (1998a), L represented the sum of the intensity values in each multispectral band. During the course of the application, however, a mean intensity value in L proved to enhance the performance of the pan-sharpening process. For this reason, L combining the first three Landsat 7 ETM+ multispectral bands was calculated as follows:

$$L = \frac{\sum MS_{iH}}{n} \quad (3.28)$$

3.3.7.2.3 Application of a LMVM filter

As the LMVM filter has proven to perform best, this adaptive filter has been applied. Because atmospheric and water-column effects already reduced the signal received at sensor, any additional reduction of the spectral information would greatly decrease the accuracy of the outcomes. Therefore, a 15 by 15 filter size was selected to guarantee an ideal compromise between the incorporation of spatial information from the panchromatic band and a maximal preservation of the spectral integrity of the multispectral bands.

3.3.7.2.4 Creation of individual pan-sharpened multispectral bands

Finally, using the fused intensity band, $F_{H>L(l, c)}$, and the global intensity channel, L , each multispectral band was individually sharpened. Because of the adaptation in formula 3.28, formula 3.27 needed to be adapted as well:

$$H_i = \frac{(MS_{iH} \times F_{H>L(l, c)})}{L} \quad (3.29)$$

A detail of the TCC of the pan-sharpened dataset is presented in figure 3.30b. When this image was compared to the TCC of the original Landsat 7 ETM+ radiance bands corrected for atmospheric effects (fig. 3.30a), the influence of pan-sharpening could clearly be noticed. The suitability of the pan-sharpening process, however, was not statistically tested by comparing the spectral information in the original radiance bands with the pan-sharpened results. Instead, the analysis results of the Landsat 7 ETM+ dataset and the pan-sharpened Landsat 7 ETM+ dataset, e.g. the bathymetric

map and the bottom-type classification, will be compared to see whether or not the pan-sharpening of the dataset increased the accuracy of the results.

3.3.7.2.5 Additional pre-processing steps

a. Geometric correction

To perform additional analyses on the pan-sharpened multispectral dataset, it was geocoded to the coordinate system used for the other datasets. In total 24 of the 62 GCPs measured during the field campaigns were used to perform a full second order transformation (fig. 3.31; table 3.43). The geocoding was acceptable as the obtained RMSE of 0.45pixel was lower than the standard 0.5pixel.

Table 3.43. Overview of the residual errors for each GCP used for geocoding the pan-sharpened Landsat 7 ETM+ dataset

| ID | X | Y | Row | Col | DRow | DCol |
|-------------|--------|---------|------|------|-------|-------|
| 1 | 563764 | 3027669 | 893 | 476 | -0.19 | -0.02 |
| 2 | 558875 | 3036784 | 342 | 63 | -0.10 | -0.10 |
| 3 | 565972 | 3023243 | 1163 | 666 | 0.42 | 0.33 |
| 4 | 575651 | 3016217 | 1528 | 1373 | -0.02 | -0.05 |
| 6 | 583399 | 3013681 | 1617 | 1909 | -0.35 | 0.31 |
| 7 | 580106 | 3014054 | 1626 | 1688 | 0.21 | -0.06 |
| 8 | 572899 | 3006908 | 2170 | 1286 | 0.10 | 0.51 |
| 9 | 576752 | 3011653 | 1818 | 1491 | 0.15 | -0.36 |
| 10 | 580169 | 3010639 | 1850 | 1726 | -0.29 | -0.51 |
| 13 | 580914 | 3015523 | 1521 | 1727 | 0.13 | 0.48 |
| 15 | 581788 | 2998717 | 2620 | 1953 | -0.52 | 0.07 |
| 16 | 578834 | 2999543 | 2596 | 1751 | 0.11 | 0.86 |
| 17 | 575128 | 3004939 | 2277 | 1451 | -0.25 | -0.96 |
| 18 | 581951 | 2996914 | 2738 | 1981 | 0.10 | -0.79 |
| 19 | 584007 | 2996367 | 2754 | 2123 | 0.78 | 0.32 |
| 20 | 581469 | 3002687 | 2361 | 1892 | -0.72 | -0.01 |
| 21 | 581814 | 3004145 | 2262 | 1900 | -0.04 | -0.08 |
| 22 | 583667 | 3008633 | 1948 | 1977 | 0.60 | -0.03 |
| 23 | 582976 | 3011313 | 1778 | 1905 | 0.34 | 0.40 |
| 24 | 584024 | 3014198 | 1577 | 1944 | -0.03 | -0.67 |
| 25 | 596266 | 3007490 | 1897 | 2819 | 0.09 | 0.11 |
| 26 | 595324 | 3007223 | 1924 | 2759 | 0.15 | -0.45 |
| 27 | 592268 | 3009544 | 1801 | 2535 | -0.36 | 0.34 |
| 28 | 585939 | 3003860 | 2239 | 2175 | -0.32 | 0.37 |
| total RMSE: | | | | | 0.450 | |

b. Water-column correction

To correct the pan-sharpened bands for the additional effects of the water column on the signal, the same procedure was followed as described for the original Landsat 7

ETM+ dataset (section 3.3.5.2.1). As could be expected, the resulting k_i/k_j ratios presented in table 3.44b were similar to the values derived for the original dataset (table 3.33b). This partly proved the validity of the applied pan-sharpening method to preserve the spectral information of the original dataset. Formula 3.21 was finally applied to derive three pan-sharpened DIB bands, $XL7_DIB_{ij}$.

Table 3.44a. Variance within each pan-sharpened Landsat 7 ETM+ band

| | band 1 | band2 | band3 |
|-----------------------------|---------------|--------------|--------------|
| variance δ_{ii}^* | 0.28 | 0.49 | / |
| variance δ_{ii}^{**} | 0.06 | 0.10 | 0.39 |

*based on 196 points; ** based on 79 points

Table 3.44b. Determination of the attenuation ratios k_i/k_j for pan-sharpened Landsat 7 ETM+ water column correction

| | ratio k_1/k_2 * | ratio k_1/k_3 ** | ratio k_2/k_3 ** |
|--------------------------|-------------------------------------|--------------------------------------|--------------------------------------|
| Covariance δ_{ij} | 0.36 | 0.11 | 0.18 |
| a_{ij} | -0.29 | -1.52 | -0.78 |
| k_i/k_j | 0.75 | 0.30 | 0.49 |

c. Masking

As the spatial resolution of the pan-sharpened multispectral bands is higher than the original Landsat 7 ETM+ dataset, small differences in the delineation of the coast on the land mask occurred. Therefore, a new land mask needed to be created. This mask was based on the vectorisation of the coastline on the pan-sharpened Landsat 7 ETM+ dataset, which was subsequently rasterised and applied to the pan-sharpened dataset in which all pixels representing land were given a value of 0.

3.4 BATHYMETRIC MAPPING

3.4.1 Introduction

A bathymetric map is one of the most important basic documents for coral-reef studies, because, as depth influences the benthic cover of the reef, it provides an insight in the ecology of the coral reef (Green *et al.*, 2000b; Stumpf *et al.*, 2003). Besides, if detailed bathymetric information is available, slope and aspect of the coral-reef structure can be defined and correlations may be determined with coral type and coverage, as shown in section 2.4.2.2.2 (Isoun *et al.*, 2003). Coral reefs, as complex physical structures, also interact with and influence their environment. Knowledge on the depth at which these structures occur will, therefore, also support the understanding of the biophysical processes in the marine environment (Stumpf *et al.*, 2003). Moreover, a bathymetric map is a necessary document for MPA planning and management. In the case of oil pollution or coral bleaching (Stumpf *et al.*, 2003) where the effects usually decrease with depth, for instance, specific prevention and/or remediation activities can be planned more effectively.

Unfortunately, because of the rather shallow depth at which most coral reefs occur and/or their often remote location, it is not always possible to conduct a conventional bathymetric echosounding campaign. Currently, bathymetric information on coral reefs is therefore often non-existing, inaccurate, or out of date (Mumby *et al.*, 1998a; Stumpf *et al.*, 2003). The nautical charts available for the Red Sea, for example, only offer widespread echosounding point data for the navigational deeper parts without any indication of depth on the reefs themselves. Besides, the data provided is often outdated. The detailed 1:25000 scale map of Hurghada (3043B), for example, is largely based on data collected during two Admiralty surveys dating back to 1871-1884 and 1919.

Remote sensing, by virtue, is not restricted by inaccessibility or shallowness. Besides, data is collected synoptically so that large areas are mapped at once. As a result, it is often more cost-effective than shipborne bathymetric mapping campaigns (O'Neill and Miller, 1989; Green *et al.*, 2000a; Liceaga-Correa and Euan-Avila, 2002; Isoun *et al.*, 2003). Remote sensing also offers the opportunity to track changes in depth, making it possible to update existing nautical maps in short time notice. Care must be taken however when applying remote sensing for updating nautical charts as the accuracy of the derived bathymetric maps

must be in the order of tens of centimetres to be adequate for shallow water navigation (Green *et al.*, 2000a).

3.4.2 Bathymetric mapping methods using remote sensing data

3.4.2.1 Active remote sensing bathymetric mapping methods

A first group of bathymetric mapping methods involves active remote sensing with sensors like RADAR (Radar Detection And Ranging) and LIDAR (Light Detection And Ranging). Although the wavelengths emitted by the RADAR are totally attenuated by water, these systems have shown useful to determine water depths (e.g. Calkoen *et al.*, 2000) as changes in sea surface roughness detected by the RADAR system can be correlated to changes in water depth. This technique, however, requires a significantly strong current flowing across a smooth seabed and is, therefore, not applicable in most coral-reef environments (Green *et al.*, 2000a; Purkis *et al.*, 2002).

With the LIDAR approach, a green and infrared laser pulse are emitted by the sensor. The infrared pulse will be almost totally reflected by the sea surface, while the green laser pulse will penetrate the water column (fig. 3.32). Depending on the time difference in recording the reflected pulses, depth estimates can be made with a precision in the order of centimetres (Lillicrop, 1996). In optically very clear water, depths may be determined up to 50m (Guenther *et al.*, 2000). Although a very detailed and accurate technique, only a dozen of LIDAR systems operating aboard airplanes exist worldwide. This limits their cost-effectiveness and global applicability, and lacks the synoptic advantage attributed to spaceborne systems. For these reasons, the LIDAR approach will not be discussed in further detail.

3.4.2.2 Passive remote sensing bathymetric mapping methods

A second group of methods is based on passive sensor, multispectral data. The basic principle is that different wavelengths of light penetrate water to various depths. Longer wavelength light, i.e. red in the visible part of the spectrum, has a higher attenuation coefficient than short wavelengths, e.g. blue. Shorter wavelengths will therefore penetrate deeper into the water column than longer wavelengths before they become completely attenuated (fig. 3.33). When depth further increases, all light will eventually be attenuated

and no reflection will be received at sensor. Even in the clearest case I (Jerlov, 1976) oceanic water, most wavelengths detected by satellite sensors are no longer reflected from depths lower than 30m (Green *et al.*, 2000a). This maximum depth quickly decreases with increasing turbidity (Tanis *et al.*, 2002). Bathymetric mapping using passive, multispectral data, therefore, is limited to this maximum depth (Green *et al.*, 2000a; Stumpf *et al.*, 2003).

Several *radiative transfer models* for visible light in water have been determined, either empirically or based on computer simulations (Maritorena *et al.*, 1994; Ackleson, 2003). Formula 3.30 represents one of these models which has been specifically adapted for remote sensing applications (Maritorena *et al.*, 1994).

$$R_{(0,H)} = R_{\infty} + \left(A_b e^{-\kappa_B H} - R_{\infty} e^{-\kappa_C H} \right) e^{-\kappa_d H} \quad (3.30)$$

With: $R_{(0,H)}$: reflectance at null depth over a bottom at depth H

R_{∞} : reflectance at null depth over an infinitely deep water column

$$R_{\infty} = \frac{b_{bd}}{(k_d + \kappa)} \quad (3.31)$$

With: b_{bd} : diffuse backscattering coefficient for downwelling light (m^{-1})

k_d : vertical attenuation coefficient for downwelling radiance (m^{-1})

κ : vertical attenuation coefficient for flux scattered upward from a thin layer of water (m^{-1})

A_b : bottom albedo

κ_B : attenuation coefficient for upwelling light originating from bottom reflectance (m^{-1})

κ_C : attenuation coefficient for upwelling light originating from water-column reflectance (m^{-1})

When all parameters involved in the radiative transfer model are measured in situ, the model can be solved directly, both for depth and seabed reflectance. However, as the measurement of water-column optical properties is complicated and expensive, this information is seldom complete and often even unavailable as is the case for the Hurghada study area. The remaining unknowns could be approached by tabulated optical parameters (Spitzer and Dirks, 1987), although no recent information concerning water-column

optical properties is available for the study area. Parameters published for other water masses may also be used, but this would introduce errors into the algorithm as water-column optical properties are not the same all over the world (Tanis *et al.*, 2002).

Alternatively, the model may be solved for depth and bottom reflection when there are at least as many spectral bands as there are bottom types in the study area (Paredes and Spero, 1983). With multispectral datasets, this condition is usually not met and too many unknowns remain to be solved simultaneously (Tanis *et al.*, 2002). New hyperspectral sensors, in contrast, record datasets which have become sufficiently large (Sandidge and Holyer, 1998; Tanis *et al.*, 2002; Isoun *et al.*, 2003) to estimate the unknown parameters (Hedley and Mumby, 2003; Lee and Carder, 2005). Unfortunately, as with LIDAR, hyperspectral data is not yet widely available and could not be used in this study.

To derive depth information from multispectral remote sensing data, the theoretical radiative transfer model is often simplified, assuming constant water-column properties. Two of the most common simplifications are the *simple radiative transfer model for optically shallow waters* (Lyzenga 1978; Maritorena, 1996), presented in formula 3.15, and the *single-scattering⁶¹ irradiance (SSI) model* by Philpot (1987; 1989) (formula 3.32):

$$R_{(0,-)} = R_{i\infty} + (A_b - R_{i\infty})e^{-gz} \quad (3.32)$$

With: $R_{(0,-)}$: radiance just below sea surface
 $R_{i\infty}$: irradiance reflectance of an optically deep water column
 g : effective attenuation coefficient of the water
 $1.5k_d < g < 3k_d$ ⁶²
 z : depth

Different methods have been computed to derive depth based on these simplified models. Limited ground-truth data, however, is still required to calibrate the model. In following sub-sections, an overview is given of the most common algorithms. In all cases, natural logarithms are taken from formulas 3.15 or 3.32 in order to linearise the relation between radiance and depth (formula 3.33; 3.34).

⁶¹ Single scattering: no downward reflection of the upward irradiance at the water-air interface is assumed

⁶² in most cases g equals $2k_d$

$$X_i = LN(L_i - L_{i\infty}) = LN(a R_{bi}) - f k_i z \quad (3.33)$$

$$X_i = LN(R_{(0,-)} - R_{i\infty}) = LN(A_b - R_{i\infty}) - g z \quad (3.34)$$

3.4.2.2.1 Bottom-reflection-based bathymetric mapping theory

The theory behind most passive remote sensing methods is based on the fact that up to the maximum penetration depth, part of the signal recorded by the sensor is reflected by the bottom. The assumptions inherent to this *bottom-reflection-based bathymetric mapping theory* (Ji *et al.*, 1992) are that the seabed is highly reflective; that the water column is optically clear; and that the seabed is situated at depths shallower than the maximum penetration depth. Besides, three additional assumptions have to be made to adapt the theory for remote sensing applications: (1) light attenuation is an exponential function of depth (Beer's law) -which implicitly presumes that the water column is vertically homogeneous (Philpot, 1989; Newman and LeDrew, 2001)-; (2) the water column is horizontally homogeneous -i.e. that the sea state and the water quality (hence the attenuation coefficient) do not vary within an image-; and (3) the reflective properties, or *albedo*, of the substrate are constant. This, consequently, limits the application to optically clear coastal water whereas it performs poorly over dark, limited reflective bottom types (Ji *et al.*, 1992).

For a study area in the Turks and Caicos Islands, Green *et al.* (2000a) have evaluated three distinct methods, being the ones proposed by Lyzenga (1978), Benny and Dawson (1983), and Jupp (1988), using a Landsat TM and a hyperspectral CASI dataset. Based on the correlation between computed depth and actual depth of a control area, they conclude that the method developed by Jupp (1988) was the most accurate. Therefore, only this method, taking into account the modifications proposed by Edwards (1999), will be applied in this study. In recent years, different alternative methods have been proposed. One of these methods, being the *ratio-transform method* by Stumpf *et al.* (2003), will be discussed and implemented as well for both the Landsat 7 ETM+ and QuickBird datasets. Other methods are based on neural networks (Sandidge and Holyer, 1998) or on subpixel classification (Huguenin, *et al.*, 2004) and could not be implemented in the available software.

a. Method of Jupp (1988)

The method of Jupp (1988) depends on the differential maximum penetration of light according to its wavelength. For red light, for example, there will be a depth, the maximum *depth of penetration* (DOP), at which all the red wavelengths will be fully attenuated. Some light, however, will still be detectable at this depth in the green and blue part of the spectrum (fig. 3.33). With increasing depth, the maximum DOP for green light will be reached, followed by the maximum DOP of blue light. As a result, exclusive DOP zones can be delineated by the maximum depths of penetration of successive bands with shorter wavelengths (Green *et al.*, 2000a) (fig. 3.33).

These different DOP zones can be defined by the maximum radiance (or reflectance) of each band over optically deep water, $L_{i \infty \max}$. If the radiance value, L_i , of a pixel in band i is higher than $L_{i \infty \max}$, the depth at its location is supposed to be above the maximum DOP of that specific band. If the radiance value for the same pixel in the successive band recording longer wavelengths, L_{i+1} , is lower than $L_{i+1 \infty \max}$, the depth of the water column will be between their corresponding maximum depths of penetration z_i and z_{i+1} . A decision tree can thus be set up to delineate N exclusive DOP zones related to the number of spectral bands in the dataset.

In between the maximum DOP for each band and the surface, assuming the substrate remains constant, the radiance, L_i , is purely a function of depth, z . As a result, equation 3.33 can be transformed to interpolate depth, z , in each DOP zone:

$$z = \frac{(A_i - X_i)}{2 k_i} \quad (3.35)$$

With $A_i = LN(L_i - L_{i \infty \text{mean}})$ being the log-transformed, atmospherically corrected radiance value which ideally remains constant in each waveband for a given bottom type. The minimal X_i value in each DOP zone, $X_{i \min}$, corresponding to the maximum DOP for that waveband, z_i , then is:

$$X_{i \min} = LN(L_{i \min} - L_{i \infty \text{mean}}) = A_i - 2 k_i z_i \quad (3.36)$$

with: $L_{i \min}$: minimum radiance value in DOP zone i .

Consequently, the maximum X_i value in each DOP zone, $X_{i \max}$, is determined as follows:

$$X_{i \max} = LN(L_{i \max} - L_{i \infty \text{mean}}) = A_i - 2k_i z_{i+1} \quad (3.37)$$

with $L_{i \max}$ the maximum radiance value in DOP zone i and z_{i+1} the maximum depth of penetration of the successive waveband recording longer wavelengths.

Combining equations 3.36 and 3.37, A_i and k_i can be determined:

$$A_i = X_{i \min} + 2k_i z_i \quad (3.38)$$

$$k_i = \frac{(X_{i \max} - X_{i \min})}{2(z_i - z_{i+1})} \quad (3.39)$$

$L_{i \min}$ and $L_{i \max}$ can easily be determined via simple data processing. Initial z_i values, as summarised in table 3.45, have been determined by Jupp (1988) for four multispectral TM bands in a study area on the Great Barrier Reef. These depths, however, are likely to vary with water-column characteristics as well as the radiometric resolution of the sensor. Edwards (1999), therefore, proposes an alternative method to derive maximum depths of penetration through the co-analysis of radiance and a large number of in situ depth measurements. Once all parameters are defined in equation 3.35, they can be applied to determine depth for every pixel in each DOP zone. Finally, the successive calibrated DOP zones are to be combined into one single bathymetric map representing the entire study area.

Table 3.45. Maximum DOP for TM bands 1, 2, 3 and 4 in optically clear water of the Great Barrier Reef (Jupp, 1988)

| | maximum depth of penetration z_i (m) |
|--------|--|
| band 1 | 25 |
| band 2 | 15 |
| band 3 | 5 |
| band 4 | 1 |

b. Ratio-transform method

The central assumption of the ratio-transform method proposed by Stumpf *et al.* (2003), besides the basic assumptions inherent to the bottom-reflection-based bathymetric mapping theory, is that with multispectral bands subject to different water attenuation coefficients, a band recording longer wavelengths will have arithmetically lower reflectance values than another band which records shorter wavelengths. In a bi-plot of X_i -values, as already proposed by Lyzenga (1978; 1985)⁶³, reflectance will decrease when depth increases, although X_j of the band with the higher absorption coefficient will decrease proportionally faster than X_i of the band with lower absorption characteristics. Accordingly, the ratio X_i/X_j increases with depth. Secondly, Stumpf *et al.* (2003) assume that a change in bottom albedo affects both bands similarly (Philpot, 1989). The effects of changes in depth on the ratio X_i/X_j are consequently much greater than the effects of changes in bottom albedo. Different bottom albedos at the same depth will therefore result in a similar ratio (fig. 3.34).

If both assumptions apply, the ratio X_i/X_j approximates depth independent of bottom albedo and can be linearly scaled to absolute depth values using equation 3.40 in which m_1 is a tuneable constant, n is a fixed constant introduced to assure positive natural logarithms and linear relationships with depth, and m_0 is the offset for a depth of 0m.

$$z = m_1 \times \left[\frac{LN(n \rho_i)}{LN(n \rho_j)} \right] - m_0 \quad (3.40)$$

To tune the algorithm, a simple linear regression is set up between depths and ratio values for a number of ground-truth sampling points. In the example given by Stumpf *et al.* (2003), only three depth measurements were needed. This method, however, requires atmospherically corrected reflectance values, ρ_λ , rather than radiance or DN values as for the aforementioned method.

3.4.2.2.2 Water-column-scattering-based bathymetric mapping theory

The main restrictions of the abovementioned models are their limited success in turbid water and over dark-coloured bottom types. The *water-column-scattering-based*

⁶³ see section 3.3.5.1 on water column correction

theory has been developed by Ji *et al.* (1992) to perform in such circumstances. This theory states that in turbid water or over weakly reflective bottoms, most part of the signal received by the remote sensor is formed by scattering in the water column. Consequently, the part of equations 3.33 and 3.34 representing the bottom albedo can be ignored, such that these algorithms become:

$$LN(L_i - L_{i\infty}) = -f k_i z \quad (3.41)$$

$$LN(R_{(0,-)} - R_{i\infty}) = -g z \quad (3.42)$$

Reflectance, or radiance, over optically deep water is easily derived from the remote sensing dataset itself. The attenuation coefficient can be determined if in situ reflectance measurements just below the sea surface and near the seabed are taken at minimally two proximate locations at different depths, provided a horizontally homogeneous water column can be assumed (Ji *et al.*, 1992).

Bierwirth *et al.* (1993) have presented an alternative approach in which an estimation of depth, Z , can be made using equation 3.43, with N the number of spectral bands involved.

$$Z = \frac{\sum LN(L_i - L_{i\infty})}{-2 k_i N} \quad (3.43)$$

To determine the attenuation coefficient, k_i , a number of depth measurements over a homogeneous substrate are required. If a bi-plot is constructed of X_i against depth for measured depths located in the dataset, equation 3.33 can be derived by applying a linear regression to this dataset (Bierwirth *et al.*, 1993). In the obtained linear equation ' $y = ax+b$ ', parameter a then represents the attenuation coefficient. Green *et al.* (2000a), instead, propose to co-analyse X_i and log-transformed depth values.

For the coral reefs in the northwestern Red Sea, the assumption of clear coastal water, however, is valid so that a method following the water-column-scattering-based theory was not required.

3.4.2.3 Digital photogrammetrical approach

A third approach to derive bathymetric information is based on the photogrammetric processing of stereoscopically taken remote sensing data. Since the 1960s, the feasibility of ‘*through-water*’ photogrammetry⁶⁴ for mapping subaquatic features has been examined (e.g. Tewinkle, 1963; Rinner, 1969; Höhle, 1971; Harris and Umbach, 1972). Likewise, the use of *underwater photogrammetry*⁶⁵ in coral-reef studies has also become popular (e.g. Bythell *et al.*, 2001; Chong and Stratford, 2002). This form of photogrammetry, however, will not be discussed here.

It was soon recognised that the refraction of the light rays at the air/water interface posed an additional complication to the photogrammetric restitution process. The refraction of the light follows Snellius’ law, represented in formula 3.44, in which i is the angle of incidence of the light ray; r , the refraction angle of the light after passing the air/water interface; and n , the refractive index of the water. In the case of remote sensing where the received ray of light at the sensor is concerned, i can be seen as the angle of emittance at the sea surface (fig. 3.35).

$$\sin(i) = n \sin(r) \quad (3.44)$$

Due to the refraction of the light, a shift in estimated depth occurs and a point, p , on the bottom, is viewed as an apparent point, p_a , which is situated at a shallower depth (fig. 3.35). Based on the geometry of figure 3.35, the true, h , and apparent, h_a , depth can be respectively expressed in terms of the angles of refracted and incident light (Rinner, 1969):

$$h = \frac{x}{\tan(r)} \quad (3.45)$$

$$h_a = \frac{x}{\tan(i)} \quad (3.46)$$

⁶⁴ ‘Through-water photogrammetry is a specific case of two-media photogrammetry where the camera is above the water surface (in air) and the target is in a different medium (water).’ (Butler *et al.*, 2002: 420).

⁶⁵ unlike Höhle (1971), the term underwater photogrammetry is nowadays preserved for photogrammetric data acquisition using submerged cameras

Deriving the unknown parameter x from equation 3.46 and substituting it in formula 3.45 gives:

$$h = \frac{h_a \times \tan(i)}{\tan(r)} \quad (3.47)$$

or after deriving r out of formula 3.44:

$$h = \frac{h_a \times \tan(i)}{\tan\left(\sec\left(\frac{\sin(i)}{n}\right)\right)} \quad (3.48)$$

For all realistic values of i , formula 3.48 can be approximated as (Butler *et al.*, 2002):

$$h = h_a \times \left[\frac{\tan(i)}{\tan\left(\frac{i}{n}\right)} \right] \quad (3.49)$$

Accordingly, the effect of refraction on the accuracy of the bathymetric map increases with depth (Westaway *et al.*, 2001; Butler *et al.*, 2002). The refraction also creates shifts between the planimetric coordinates of p and p_a . Different analogue and analytic correction algorithms have been proposed to account for these positional errors (e.g. Rinner, 1969; Slama, 1980). However, when the depth/height ratio is reasonably small, as is the case for spaceborne sensors, the effects of refraction on the planimetric position of the depth points is negligible (Höhle, 1971; Buchroitner, 1991; Chong and Schneider, 2001).

Problems may also arise due to sea surface roughness, which should ideally be known or modelled (Harris and Umbach, 1972; Westaway *et al.*, 2001; Butler *et al.*, 2002). For moderately calm seas, the influence of random waves and surface roughness on the accuracy of the bathymetric result, nonetheless, is minimal up to depths of 10m (Harris and Umbach, 1972; Okamoto, 1982; Buchroitner, 1991). For this reason, most models assume the air/water interface to be a horizontal, planar surface (Okamoto, 1982; Butler *et al.*, 2002). Related, the time lag between the acquisitions of the two stereo-images may

result in differences of the water surface features (Okamoto, 1982; Butler *et al.*, 2002). These problems can be pragmatically outdone by simultaneous stereo-image capturing (Okamoto, 1982). Finally, image matching may fail in areas where the seabed is invisible or where surface glare occurs (Westaway *et al.*, 2001). Optically deep water and/or areas with a high amount of surface glare are therefore masked as in these areas no reliable depth predictions can be expected (Pasqualini *et al.*, 2001; Westaway *et al.*, 2001).

Recently, through-water photogrammetry has regained interest (e.g. Pasqualini *et al.*, 2001; Westaway *et al.*, 2001; Butler *et al.*, 2002) and the theory has been adapted to digital photogrammetry. In contrast to analogue and analytic photogrammetry in which both planimetric and depth shifts could be corrected during the block adjustment process before the effective photogrammetric restitution was performed, an operator using digital photogrammetry has no longer the possibility to intervene with this part of the restitution process. Butler *et al.* (2002), alternatively, demonstrate that any digital photogrammetric software is capable of creating an apparent DEM surface, without needing initial depth corrections. This apparent DEM can easily be corrected for the depth shift during an additional post-processing step (Butler *et al.*, 2002).

Westaway *et al.* (2001) and Butler *et al.* (2002) have developed a refraction correction algorithm for this post-processing step. The basic idea is to derive true depth, h , out of the apparent depth, h_a , via formula 3.49 and the known angle of incidence, i . As refraction differently influences both images in the stereopair, corrections should be applied on each image separately (Butler *et al.*, 2001; Westaway *et al.*, 2002). The total correction algorithm then becomes (Harris and Umbach, 1972):

$$h = \left(\frac{\sum a_i}{N} \right) \times h_a \quad (3.50)$$

with: a_i : correction parameter for each image: $\left[\frac{\tan(i)}{\tan\left(\frac{i}{n}\right)} \right]$

N : number of images used in the photogrammetric process

An attempt was made to extrapolate the conclusions of Westaway *et al.* (2001) and Butler *et al.* (2002) to the digital photogrammetric processing of an ASTER stereo-pair in order to derive depths on coral reefs (see section 3.4.3.5).

3.4.3 Implementation

3.4.3.1 Landsat 7 ETM+

3.4.3.1.1 Modified DOP-mapping method

DN values, radiance values, or reflectance values, corrected for atmospheric effects or not, can all be used as input values to the algorithm (Green *et al.*, 2000a). For simplicity, uncorrected DN values were used in the processing and only those multispectral bands not totally attenuated by the water column were selected. Although Green *et al.* (2000a) have used Landsat TM bands 1, 2, 3 and 4 in their case study on the Turks and Caicos Islands, earlier attempts to implement the DOP-mapping method on the Landsat 7 ETM+ dataset for the Hurghada study area resulted in large errors over the shallowest parts of the reefs. This was most probably caused by the bathymetric interpolation in DOP zone 4 corresponding to ETM+ band 4. As a consequence, only the first three multispectral Landsat 7 ETM+ bands were retained for the implementation presented here.

a. Methodology

The methodology can be split in two sections, being the determination of the different DOP zones and the interpolation of depth for every pixel in each DOP zone.

- Calculation of DOP zones

A DOP zone can be defined as a region in which light is reflected in one band but not in the next (Green *et al.*, 2000a). For example, the first DOP zone represents those depths in the scene where only band 1 of the ETM+ sensor is still receiving some reflectance of the bottom. DOP zone 2 receives reflection in the blue and green band but not in the red and near infrared, and so on.

Table 3.46. Minimum, maximum and mean deep-water DN values for the original Landsat 7 ETM+ dataset

| | $L_{i \infty \min}$ | $L_{i \infty \max}$ | $L_{i \infty \text{mean}}$ |
|--------|---------------------|---------------------|----------------------------|
| band 1 | 54 | 65 | 60 |
| band 2 | 32 | 41 | 37 |
| band 3 | 25 | 36 | 31 |

First, the maximum depths of penetration for the Landsat 7 ETM+ bands 1 to 3 were calculated. For each band i , this depth was determined by the deepest pixels with a DN value higher than the maximum deep-water DN value⁶⁶, $L_{i \infty \max}$, (Edwards, 1999)⁶⁷ as defined in table 3.46. 242 in situ depth measurements (see annex V) were used to estimate the maximum depth of penetration for each waveband. These points were taken over a homogeneous sandy substrate and selected based on their reliability. Observed depth values referred to datum were corrected for the tide at the moment of image acquisition (i.e. 0.24m above datum). These points were subsequently located on the geocoded dataset and the corresponding DN value in each band for every observation point was derived.

Table 3.47. Determination of the maximum DOP in Landsat 7 ETM + waveband 1, 2 and 3

| | band 1 | band 2 | band 3 |
|--|---------------|---------------|---------------|
| deepest pixel: $L_i > L_{i \infty \max}$ (m) | 31.2 | 19.1 | 13.0 |
| shallowest pixel: $L_i \leq L_{i \infty \max}$ (m) | 15.9 | 15.7 | 2.8 |
| average depth: $L_i > L_{i \infty \max}$ (m) | 20.2 | 17.5 | 5.1 |
| average depth: $L_i \leq L_{i \infty \max}$ (m) | 22.6 | 16.0 | 5.4 |
| max. depth of penetration: z_i (m) | 21.4 | 16.8 | 5.2 |

The derived maximum depths of penetration (table 3.47) were in accordance with the values derived by Jupp (1988) which have been listed in table 3.45. Remarkably, z_1 for the blue band was shallower than the results obtained by Jupp (1988), whereas z_2 for the green ETM+ band was higher. This may point to a higher C-DOM concentration in the Hurghada study area which resulted in higher attenuation of the blue wavelengths (Jerlov, 1976).

Subsequently, the maximum deep-water DN values, $L_{i \infty \max}$, were also used to delineate the different DOP zones. If the DN value in waveband i , L_i , was greater than $L_{i \infty \max}$, some reflectance of the seabed was supposed to be present in the signal received by the sensor (Green *et al.*, 2000a). A decision tree, shown in table 3.48, could thus be formed to determine the successive but exclusive DOP zones.

⁶⁶ Deep water DN values were defined in the same area as deep water radiance values in section 3.3.4.1.

⁶⁷ For a detailed explanation of the imperative method to determine depth of penetration in each multispectral band is referred to Edwards (1999).

Afterwards, the different layers representing each DOP zone were used to mask the corresponding wavebands for consequent processing.

Table 3.48. Decision tree used to delineate the three exclusive DOP zones on the Landsat 7 ETM+ dataset

| | band 1 | band 2 | band 3 | DOP zone |
|----------------|-----------|-----------|-----------|----------------------------------|
| If DN of pixel | ≤ 65 | ≤ 41 | ≤ 36 | then depth > 21.4 (unknown: ?) |
| If DN of pixel | > 65 | ≤ 41 | ≤ 36 | then depth =]16.8, 21.4] (DOP1) |
| If DN of pixel | > 65 | > 41 | ≤ 36 | then depth =]5.2, 16.8] (DOP2) |
| If DN of pixel | > 65 | > 41 | > 36 | then depth = [0, 5.2] (DOP3) |

- Interpolation and calibration of depths within the DOP zones

Each waveband, masked by its corresponding DOP zone, was further analysed to determine $L_{i \min}$ and $L_{i \max}$ of that waveband. A 0.1% confidence interval was respected to eliminate outliers. Using these values, k_i and A_i were determined based on equation 3.39 and 3.38 respectively (table 3.49). The implementation of formula 3.35 resulted in estimated depths for every pixel in each exclusive DOP zone.

Table 3.49. Parameters needed for interpolating depth in each Landsat 7 ETM+ DOP zone

| | band 1 | band 2 | band 3 |
|------------------------------------|----------|----------|-----------|
| $L_{i \min} - L_{i \max}$ in DOP 1 | 66-68 | | |
| $L_{i \min} - L_{i \max}$ in DOP 2 | | 42-63 | |
| $L_{i \min} - L_{i \max}$ in DOP 3 | | | 37-125 |
| k_i | 0.03127 | 0.071063 | 0.264571* |
| A_i | 3.130107 | 3.99715 | 4.543295 |

* Remark: for the calculation of k_3 : z_{3+1} was set to 0m (sea surface)

The three resulting depth layers were subsequently integrated into one bathymetric map using formula 3.51:

$$bathy = ifundef(bathy3, ifundef(bathy2, bathy1, bathy2), bathy3) \quad (3.51)$$

b. Result

The derived depth values were relative to the moment of data acquisition. Therefore, the result was corrected to the common tidal datum. Finally, depths were converted to negative values, and the land surface was given an arbitrary value of 2m, purely for representative reasons. The made-up result of the bathymetric mapping using the modified DOP-mapping method in the case of the Landsat 7 ETM+ dataset is shown in figure 3.36. Depths are represented in shades of blue. Areas which are deeper than the maximum depth of penetration of band 1, i.e. 21.4m, are represented in white. For these areas, no accurate depth information is available. Reef zones generally are shallower than their surroundings. Fringing reefs usually are connected to one another, whereas the more offshore reef structures are clearly more isolated as they are surrounded by relatively deep water.

c. Residual analysis

To assess the accuracy of the resulting bathymetric map, 100 depth observation points not used to calibrate the algorithm were used as validation points. Figure 3.37 gives an overview of the distribution of these control points related to depth. This shows that the validation is slightly biased towards shallower depths. For each point, the computed depth derived from the bathymetric map was compared to the observed depth, corrected to datum. Of the 100 control points selected, 5 did not correspond to a computed depth value and were discarded for validation (annex VI).

Different parameters were calculated to assess potential errors in the result. First, the correlation between the ground truth and the computed depth values was determined. A bi-plot of calculated depths against observed depths was made and the Pearson product moment correlation coefficient (Green *et al.*, 2000a) was defined (table 3.50). This value indicates how good the trend in the seabed topography was detected by the algorithm. With a Pearson product moment correlation coefficient of 93%, the general trend of the seabed was clearly detected and represented by the modified DOP-mapping result. This value was also in accordance with the result obtained by Green *et al.* (2000a) for their test case on the Turks and Caicos Islands using Landsat TM data.

Secondly, a residual analysis was made in which residuals were determined by subtracting computed depths⁶⁸ from the corresponding observed depths. A mean residual was calculated as well as the standard deviation and RMS (table 3.50) (Green *et al.*, 2000a; Liceaga-Correa and Euan-Avila, 2002). Finally, a linear regression (R^2 value) was calculated between observed depths and mean residual errors to detect a possible linear relationship between both. As seen on figures 3.38 and 3.39, computed depth generally overestimated true depth with a mean residual error of -1.13m. Standard deviation and RMS of the residuals were relatively high, indicating significant uncertainty in the error prediction. The very low R^2 correlation between residual error and observed depth (0.26%) indicated that there was no clear linear trend in the relation between depth and errors. This was also obvious in figure 3.39.

Table 3.50. Residual analysis of the Landsat 7 ETM+ bathymetric result

| | |
|--|-------|
| Pearson correlation coefficient (observed –computed depth) | 93% |
| mean residual (m) | -1.13 |
| standard deviation (m) | 1.85 |
| RMS (m) | 1.84 |
| R^2 (observed depth- residual) | 0.26% |

3.4.3.1.2 Ratio-transform method

a. Methodology

The method presented by Stumpf *et al.* (2003) is based on the ratio calculation between two log-transformed reflectance bands. As the algorithm fails when one of these bands is totally attenuated by the water column (Stumpf *et al.*, 2002), Landsat 7 ETM+ bands 1 and 2 were selected to test this algorithm as these bands penetrate deepest into the water column and depths up to 16-17m were expected to be reached.

- DN to atmospherically corrected reflectance conversion

As mentioned, the input values to the algorithm need to be reflectance values corrected for atmospheric effects. An atmospheric correction model proposed by Chavez (1996), similar to the one applied by Stumpf *et al.* (2003) in their case studies, was applied. The *COST-model* (Chavez, 1996) is a simplification of the

⁶⁸ Positive depth values are used in the residual analysis.

model proposed by Moran *et al.* (1992) (formula 3.6) which encompasses following approximations:

- $L_{i\ haze}$ is estimated by the dark pixel radiance, $L_{i\ \infty}$, corrected for sensor noise and overreduction by an assumed one-percent minimum reflectance value, $L_{i, 1\%}$ (formula 3.52). This minimum reflectance value is the radiance expected to be recorded by the sensor if the bottom feature only reflects 1% of the incoming irradiance, taking the atmosphere into account (Skirvin, 2004) (formula 3.53).

$$L_{i\ haze} = L_{i\ \infty} - L_{i, 1\%} \quad (3.52)$$

$$\text{With: } L_{i, 1\%} = \frac{0.01 \times ESUN_i \times \cos^2(SZ)}{\pi d^2} \quad (3.53)$$

Table 3.51. Determination of $L_{i\ haze}$ for the atmospheric correction of the Landsat 7 ETM+ bands 1 and 2

| | $L_{i\ \infty\ mean}$ | $L_{i, 1\%}$ | $L_{i\ haze}$ |
|--------|-----------------------|--------------|---------------|
| band 1 | 59.66 | 4.42 | 55.24 |
| band 2 | 34.57 | 4.13 | 30.44 |

- T_v : for nadir view, the sensor zenith angle becomes 0 and, consequently, TAU_v equals 1.
- E_{down} : the effect of downwelling spectral radiance is regarded minimal and is ignored in the COST-model.
- T_z : the atmospheric transmittance along the path from sun to surface is approximated in the COST-model by the cosine of the solar zenith angle, $\cos(SZ)$.

$L_{i\ haze}$ (table 3.51) was easily determined from the mean deep-water radiance, $L_{i\ \infty\ mean}$, as given in table 3.31 and $\cos(SZ) = 0.845$ as defined from the information available in section 3.3.3.2.1. Subsequently, equation 3.54 was applied to come to reflectance values at surface for waveband 1 and 2 of the Landsat 7 ETM+ dataset:

$$\rho_i = \frac{\pi \times (L_i - L_{ihaze}) \times d^2}{1 \times ESUN_i \times \cos^2(SZ)} \quad (3.54)$$

- ratio-transform

The ratio between the log-transformed reflectance bands 1 and 2 was determined with an arbitrary n-coefficient of 1000. Stumpf *et al.* (2003) showed that n-values between 500 and 1500 did not influence the result markedly. When analysing this ratio layer, it became clear that the central assumption for the ratio-transform method, namely that one band -in casu the blue Landsat 7 ETM+ band- always has higher reflective values, was not valid in this case. Similar to the test by Lubin *et al.* (2001) with Landsat TM bands 1 and 2, reflectances in the green Landsat 7 ETM+ band 2 were higher than in band 1 over most shallow parts, which resulted in ratio-values smaller than 1. Most likely, the shallow water column only minimally attenuated the reflectance of the seabed such that bottom types such as algae or coral could still reflect relatively more green than blue light.

More problematic, however, was the fact that a predominant number of pixels⁶⁹ had similar reflectance values in both band 1 and 2. Consequently, the ratio of log-transformed reflectance values became 1 and depths derived for these pixels were identical. As it was not very likely that more than 25% of a heterogeneous coral-reef environment was situated at the same depth, the ratio-transform method (Stumpf *et al.*, 2003) was not regarded as a good alternative bathymetric mapping method in this specific case.

3.4.3.2 Pan-sharpened Landsat 7 ETM+

As the method of Stumpf *et al.* (2003) did not work out for the original Landsat 7 ETM+ dataset, only the modified DOP-mapping method was applied on the pan-sharpened Landsat 7 ETM+ dataset. As with the original dataset, only the first three multispectral bands were used. This allowed to estimate the advantage or disadvantage of pan-sharpening as compared to the original Landsat 7 ETM+ dataset.

⁶⁹ If land as well as deep water areas were masked out, more than 26% of the ratio values equals 1.

3.4.3.2.1 Methodology

The methodology applied here was almost similar to the one explained for the original Landsat 7 ETM+ dataset, except that the pixels in the pan-sharpened dataset represent radiance values corrected for path radiance. As a consequence, equations 3.35, 3.38 and 3.39 remained valid but equations 3.36 and 3.37 respectively became:

$$X_{i \min} = LN(L_{i \min}) \quad (3.55)$$

$$X_{i \max} = LN(L_{i \max}) \quad (3.56)$$

a. Calculation of DOP zones

The different deep-water radiance values for each pan-sharpened band were individually determined on a subset delineated by image coordinates: UL: 200, 2800; LR: 300, 3500 (table 3.52). A 0.01% confidence interval was respected to eliminate extreme outliers in the sample set which were introduced by errors in the pan-sharpening process. Besides, negative $L_{i \infty \min}$ values were caused by overreduction during the correction for path radiance. As these values only occurred over the deepest parts in the study area, they did not affect the further processing of this dataset.

Table 3.52. Minimum, maximum and mean deep-water radiance values for the pan-sharpened Landsat 7 ETM+ dataset

| | $L_{i \infty \min}$ | $L_{i \infty \max}$ | $L_{i \infty \text{mean}}$ |
|--------|---------------------|---------------------|----------------------------|
| band 1 | -1.09 | 7.63 | 3.06 |
| band 2 | -1.70 | 6.47 | 2.23 |
| band 3 | -1.70 | 7.10 | 2.27 |

Using the same 242 ground control points (see annex VII) as for the original Landsat 7 ETM+ dataset, the maximum DOP for each band was determined (table 3.53). The maximum depths of penetration in all bands were slightly higher than the ones calculated for the original dataset. This probably was due to the disturbing effect of the pan-sharpening process on the spectral content of the dataset which could not be totally prevented.

Subsequently, a decision tree was set up to determine each exclusive DOP zone based on the maximum deep-water radiance, $L_{i \infty \max}$ (table 3.54). Afterwards, each

DOP zone was used as a mask to select the zone of interest on the corresponding radiance layer.

Table 3.53. Determination of the maximum DOP in the pan-sharpened Landsat 7 ETM + waveband 1, 2 and 3

| | band 1 | band 2 | band 3 |
|--|-------------|-------------|------------|
| deepest pixel: $L_i > L_{i \infty \max}$ (m) | 31.1 | 24.3 | 10.7 |
| shallowest pixel: $L_i \leq L_{i \infty \max}$ (m) | 19.9 | 15.7 | 2.8 |
| average depth: $L_i > L_{i \infty \max}$ (m) | 23.4 | 18.7 | 4.6 |
| average depth: $L_i \leq L_{i \infty \max}$ (m) | 24.2 | 20.0 | 6.8 |
| max. depth of penetration: z_i (m) | 23.8 | 19.4 | 5.7 |

Table 3.54. Decision tree used to delineate the three exclusive DOP zones on the pan-sharpened Landsat 7 ETM+ dataset

| | band 1 | band 2 | band 3 | DOP zone |
|----------------|-------------|-------------|-------------|-----------------------------------|
| If DN of pixel | ≤ 7.63 | ≤ 6.47 | ≤ 7.10 | then depth > 23.8 (unknown: ?) |
| If DN of pixel | > 7.63 | ≤ 6.47 | ≤ 7.10 | then depth =] 19.4, 23.8] (DOP1) |
| If DN of pixel | > 7.63 | > 6.47 | ≤ 7.10 | then depth =] 5.7, 19.4] (DOP2) |
| If DN of pixel | > 7.63 | > 6.47 | > 7.10 | then depth = [0, 5.7] (DOP3) |

b. Interpolation and calibration of depths within the DOP zones

Each waveband, masked with its corresponding DOP zone, was analysed to determine $L_{i \min}$ and $L_{i \max}$. Here as well, a 0.1% confidence interval was respected to eliminate outliers. Using these values, k_i and A_i were determined based on equations 3.39 and 3.38 respectively (table 3.55).

Table 3.55. Parameters needed for interpolating depth in each pan-sharpened Landsat 7 ETM+ DOP zone

| | band 1 | band 2 | band 3 |
|------------------------------------|------------|------------|------------|
| $L_{i \min} - L_{i \max}$ in DOP 1 | 7.64-11.88 | | |
| $L_{i \min} - L_{i \max}$ in DOP 2 | | 6.48-34.32 | |
| $L_{i \min} - L_{i \max}$ in DOP 3 | | | 7.11-86.24 |
| k_i | 0.050166 | 0.06084 | 0.218915* |
| A_i | 4.4211288 | 4.229301 | 4.457134 |

* Remark: for the calculation of k_3 : z_{3+1} was set to 0m (sea surface)

The implementation of the adapted equation 3.35 resulted in estimated depths for every pixel in each exclusive DOP zone. The three different layers were subsequently integrated into one bathymetric layer using formula 3.51. Finally, the result was corrected to tidal datum and the depths were converted to negative values. The land surface was given an arbitrary value of 2m, purely for representative reasons.

3.4.3.2.2 Result

The bathymetric information derived from the pan-sharpened Landsat 7 ETM+ dataset is shown in figure 3.40. If compared to figure 3.36 representing the bathymetric map derived from the original Landsat 7 ETM+ dataset, no major differences were noted. If looking into more detail, the enhanced spatial resolution, however, became clear, especially near the borders of distinct reef zones (fig. 3.41a, b). Whether the accuracy of the result was improved as well, is tested in the residual analysis below.

3.4.3.2.3 Residual analysis

To assess the accuracy of the resulting bathymetric map, the same 95 independent depth observations as used before were selected as validation points (annex VIII). All parameters calculated for the original Landsat 7 ETM+ dataset were determined as well and are represented in table 3.56. Bi-plots representing observed depth versus computed depth and residual error against observed depth are respectively given in figures 3.42 and 3.43.

Table 3.56. Residual analysis of the pan-sharpened Landsat 7 ETM+ bathymetric result

| | |
|--|-------|
| Pearson correlation coefficient (observed –computed depth) | 89% |
| mean residual (m) | -1.54 |
| standard deviation (m) | 2.52 |
| RMS (m) | 2.50 |
| R ² (observed depth- residual) | 2.8% |

The Pearson coefficient describing the correlation between observed depth and computed depth indicated that the general trend of the seabed was acceptably represented by the bathymetric result. As can be seen on figures 3.42 and 3.43, computed depths generally overestimated true depth, as was the case for the original

Landsat 7 ETM+ dataset, albeit with a slightly higher mean residual error of -1.54m. Standard deviation and RMS of residuals were relatively high as well, indicating uncertainty in the error prediction. The very low R^2 correlation between residual error and observed depth (2.8%) indicated the lack of correlation between depth and errors in the result. From figure 3.42 might conversely be concluded that with deeper depth, computed depth underestimated true depth, but as only a limited number of control points were located in deeper waters (fig. 3.37), this probably is a biased representation.

3.4.3.3 Landsat 5 TM dataset

As the Landsat 5 TM dataset has similar characteristics as the original Landsat 7 ETM+ dataset, bathymetric mapping was also performed using the first three multispectral bands. As no depth measurements were available for the time of data acquisition in 1987, the same 240 depth measurements used to calibrate the modified DOP algorithm on the original Landsat 7 ETM+ dataset were used, under the assumption that the seabed topography at these points had not drastically changed during the time interval (annex IX).

3.4.3.3.1 Methodology

a. Calculation of DOP zones

Deep-water parameters (table 3.57) were derived in a known deep-water area on the scene bordered by scene coordinates: UL: 500-700; LR: 1350-1550.

Table 3.57. Minimum, maximum and mean deep-water DN values for the Landsat 5 TM dataset

| | $L_{i \infty \min}$ | $L_{i \infty \max}$ | $L_{i \infty \text{mean}}$ |
|--------|---------------------|---------------------|----------------------------|
| band 1 | 83 | 96 | 89 |
| band 2 | 21 | 28 | 24 |
| band 3 | 15 | 23 | 20 |

Secondly, the maximum depths of penetration for the Landsat 5 TM bands 1 to 3 were calculated (table 3.58) following the method proposed by Edwards (1999). In situ depth measurements were corrected for the tide (+0.41m) at the time of data acquisition. The maximum depths of penetration were lower for each band than the ones obtained with the original Landsat 7 ETM+ dataset. The lower radiometric

sensitivity of the TM sensor as compared to the ETM+ sensor (USGS, 2005), resulting in a loss of signal over low radiance features (i.e. deep water), might have caused these differences. Another possible cause might be a more turbid water column in the study area at the moment of data acquisition in 1987 so that light was unable to penetrate as deep as in 2000. As no other indications were noted of a more turbid water column in 1987, the first hypothesis was assumed the most likely.

Table 3.58. Determination of the maximum DOP in the Landsat 5 TM band 1, 2 and 3

| | band 1 | band 2 | band 3 |
|--|---------------|---------------|---------------|
| deepest pixel: $L_i > L_{i \infty \max}$ (m) | 24.4 | 18.4 | 8.6 |
| shallowest pixel: $L_i \leq L_{i \infty \max}$ (m) | 12.0 | 9.5 | 1.3 |
| average depth: $L_i > L_{i \infty \max}$ (m) | 16.0 | 12.1 | 3.0 |
| average depth: $L_i \leq L_{i \infty \max}$ (m) | 19.3 | 13.8 | 4.4 |
| max. depth of penetration: z_i (m) | 17.7 | 13.0 | 3.7 |

The maximum deep-water DN values, $L_{i \infty \max}$, were also used to delineate the different DOP zones using the decision tree presented in table 3.59. As with the Landsat 7 ETM+ dataset, the different DOP zone layers were subsequently used to mask the corresponding wavebands.

Table 3.59. Decision tree used to delineate the three exclusive DOP zones on the Landsat 5 TM dataset

| | band 1 | band 2 | band 3 | DOP zone |
|----------------|---------------|---------------|---------------|-----------------------------------|
| If DN of pixel | ≤ 96 | ≤ 28 | ≤ 23 | then depth > 17.7 (unknown: ?) |
| If DN of pixel | > 96 | ≤ 28 | ≤ 23 | then depth =] 13.0, 17.7] (DOP1) |
| If DN of pixel | > 96 | > 28 | ≤ 23 | then depth =] 3.7, 13.0] (DOP2) |
| If DN of pixel | > 96 | > 28 | > 23 | then depth = [0, 3.7] (DOP3) |

b. Interpolation and calibration of depths within the DOP zones

Each waveband, masked with its corresponding DOP zone, was analysed to determine $L_{i \min}$ and $L_{i \max}$. A 0.1% confidence interval was respected to eliminate outliers. Using these values, k_i and A_i were calculated based on equation 3.39 and 3.38 respectively (table 3.60). The implementation of equation 3.35 resulted in estimated depths for every pixel in each exclusive DOP zone. The three different zones were subsequently integrated into one bathymetric layer using formula 3.51. Finally, the result was

corrected to tidal datum and, for representative reasons, the depth values were converted to negative values, while the land was given an arbitrary value of 2m.

Table 3.60. Parameters needed for interpolating depth in each Landsat 5 TM DOP zone

| | band 1 | band 2 | band 3 |
|------------------------------------|---------------|---------------|---------------|
| $L_{i \min} - L_{i \max}$ in DOP 1 | 97-105 | | |
| $L_{i \min} - L_{i \max}$ in DOP 2 | | 29-53 | |
| $L_{i \min} - L_{i \max}$ in DOP 3 | | | 24-98 |
| k_i | 0.073739 | 0.094508 | 0.401407* |
| A_i | 4.689804 | 4.066659 | 4.356709 |

* Remark: for the calculation of k_3 : z_{3+1} was set to 0m (sea surface)

3.4.3.3.2 Result

At first sight, the Landsat 5 TM bathymetric mapping result was similar to the one obtained by processing the original Landsat 7 ETM+ dataset. Major errors, however, were noticed when looking in more detail as broad bands causing major stepwise shifts in bathymetry were running diagonal over the scene (fig. 3.44). These bands resulted from the memory effect of the Landsat 5 TM sensor. As these errors could not be solved through debanding (section 3.3.1.1) and the banding errors were too significant to ignore, especially in the shallowest parts, the bathymetric map derived from this specific Landsat 5 TM dataset was discarded from further analysis.

3.4.3.4 QuickBird

The spectral resolution of the multispectral QuickBird dataset is similar to the first 4 multispectral bands of the Landsat 7 ETM+ dataset. For the same reason as for the Landsat 7 ETM+ dataset, only the first three wavebands, namely the blue (1), green (2), and red (3) band were used for bathymetric mapping.

3.4.3.4.1 Modified DOP-mapping method

First, the modified DOP-mapping method was applied on the three selected multispectral bands. As only a restricted part of the total study area near Hurghada was covered by the QuickBird scene, not all in situ depth measurements could be used to calibrate the algorithm. As a result, a total of 77 depth measurements over a homogeneous sandy substrate, and corrected for the tide at the moment of data

acquisition, was selected based on the reliability of the depth measurement. DN values were used as input to the algorithm (annex X). Remark that the radiometric resolution of QuickBird, namely 11bit, is higher than the radiometric resolution of Landsat 7 ETM+. DN values, consequently, vary from 0 to 2047 which may augment the accuracy of the depth estimates.

a. Methodology

- calculation of DOP zones

The three main deep-water parameters (table 3.61) were derived from a known deep-water area on the scene bordered by scene coordinates: UL: 200-1150; LR: 1050-1350. No confidence threshold was applied in this case.

Table 3.61. Minimum, maximum and mean deep-water DN values for the QuickBird dataset

| | $L_{i \infty \min}$ | $L_{i \infty \max}$ | $L_{i \infty \text{mean}}$ |
|--------|---------------------|---------------------|----------------------------|
| band 1 | 170 | 192 | 180 |
| band 2 | 167 | 205 | 175 |
| band 3 | 61 | 81 | 68 |

Next, the maximum depths of penetration for the QuickBird bands 1 to 3 were calculated (table 3.62) following the method proposed by Edwards (1999). The maximum DOP in each band was lower than obtained for the original Landsat 7 ETM+ dataset. This was most probably caused by the lack of depth measurements in the deeper parts of this specific study area (fig. 3.45) which biased the calibration of the algorithm over deeper waters.

Table 3.62. Determination of the maximum DOP in QuickBird band 1, 2 and 3

| | band 1 | Band 2 | band 3 |
|--|---------------|---------------|---------------|
| deepest pixel: $L_i > L_{i \infty \max}$ (m) | 24.6 | 14.5 | 4.4 |
| shallowest pixel: $L_i \leq L_{i \infty \max}$ (m) | 12.2 | 12.2 | 2.2 |
| average depth: $L_i > L_{i \infty \max}$ (m) | 16.0 | 13.6 | 3.2 |
| average depth: $L_i \leq L_{i \infty \max}$ (m) | 17.4 | 13.8 | 2.9 |
| max. depth of penetration: z_i (m) | 16.7 | 13.7 | 3.0 |

The maximum deep-water DN values, $L_{i \infty \max}$, were used to delineate the different DOP zones using the decision tree as shown in table 3.63. As in previous applications, the different DOP zones were subsequently used to mask the corresponding wavebands before further processing.

Table 3.63. Decision tree used to delineate the three exclusive DOP zones on the QuickBird dataset

| | band 1 | band 2 | band 3 | DOP zone |
|----------------|---------------|---------------|---------------|-----------------------------------|
| If DN of pixel | ≤ 192 | ≤ 205 | ≤ 81 | then depth > 16.7 (unknown: ?) |
| If DN of pixel | > 192 | ≤ 205 | ≤ 81 | then depth =] 13.7, 16.7] (DOP1) |
| If DN of pixel | > 192 | > 205 | ≤ 81 | then depth =] 3.0, 13.7] (DOP2) |
| If DN of pixel | > 192 | > 205 | > 81 | then depth = [0, 3.0] (DOP3) |

- interpolation and calibration of depths within the DOP zones

Each waveband, masked with its corresponding DOP zone, was subsequently analysed to determine $L_{i \min}$ and $L_{i \max}$. A 0.1% confidence interval was respected to eliminate outliers. Using these values, k_i and A_i were calculated based on equation 3.39 and 3.38 respectively (table 3.64).

Table 3.64. Parameters needed for interpolating depth in each QuickBird DOP zone

| | band 1 | band 2 | band 3 |
|------------------------------------|---------------|---------------|---------------|
| $L_{i \min} - L_{i \max}$ in DOP 1 | 193-216 | | |
| $L_{i \min} - L_{i \max}$ in DOP 2 | | 206-379 | |
| $L_{i \min} - L_{i \max}$ in DOP 3 | | | 82-365 |
| k_i | 0.169762 | 0.088044 | 0.509112* |
| A_i | 8.234987 | 5.846382 | 5.693722 |

* Remark: for the calculation of k_3 : z_{3+1} was set to 0m (sea surface)

The implementation of equation 3.35 resulted in estimated depths for every pixel in each exclusive DOP zone. The three different zones were subsequently integrated into one bathymetric layer using formula 3.51. Finally, the result was corrected to tidal datum and, for representative reasons, depths were converted to negative values, while the land surface was given an arbitrary value of 2m.

b. Result

The result of the bathymetric mapping using QuickBird multispectral bands in a modified DOP-mapping method (Edwards, 1999) is given in figure 3.46. On the one hand, the maximum depth was more restrict than in the Landsat 7 ETM+ results due to the limited DOP of the blue QuickBird multispectral band. Because of the higher spatial resolution, more spatial detail, on the other hand, was noted. Seagrass beds which have been detected during the field campaigns, however, were depicted deeper than their surroundings. As these seagrass beds are generally not situated in topographic depressions, this represented obvious errors introduced by the algorithm.

c. Residual analysis

A statistical residual analysis was performed to estimate the accuracy and validity of the result (table 3.65). As only a limited number of depth-measured observation points were located on the QuickBird scene, no independent dataset could be selected to check the accuracy of the bathymetric result. For this reason, a selection of 64 validation points was employed which have already been used to calibrate the algorithm (annex XI). Care should therefore be taken when interpreting the derived statistics as they might be biased. Bi-plots representing observed depth versus computed depth and residual error against observed depth are respectively given in figures 3.47 and 3.48.

Table 3.65. Residual analysis of the QuickBird DOP-mapping bathymetric result

| | |
|--|--------|
| Pearson correlation coefficient (observed –computed depth) | 90% |
| mean residual (m) | 0.24 |
| standard deviation (m) | 2.20 |
| RMS (m) | 2.16 |
| R ² (observed depth- residual) | 23.19% |

The Pearson product moment coefficient of 90% indicated a good general agreement between the observed depths and the depths computed using the modified DOP-mapping method on the QuickBird multispectral dataset. The mean residual error of 0.24m showed a good agreement as well, although when compared to figure 3.47, it also indicated a general underestimation of depth. In contrast, a trend was noticed on figure 3.48 in which shallow depths were generally overestimated, whereas deeper

areas were rather underestimated. The R^2 value, although higher than for the Landsat 7 ETM+ results, did not indicate a significant correlation between depth and residual errors.

3.4.3.4.2 Ratio-transform method

Secondly, the alternative bathymetric mapping method proposed by Stumpf *et al.* (2003) was tested on the QuickBird dataset. As with the original Landsat 7 ETM+ dataset, the blue and green waveband were selected to calibrate the algorithm as these bands were least attenuated by the water column.

a. Methodology

- DN to atmospherically corrected reflectance conversion

The input values required by the algorithm are reflectance values corrected for atmospheric effects (Stumpf *et al.*, 2003). The COST correction model (Chavez, 1996) was applied to convert DN values to atmospherically corrected reflectance values. The assumption made by Chavez (1996) that T_v equals 0, however, was no longer valid as the QuickBird sensor at the moment the dataset was taken was slightly tilted, both along-track and cross-track. For this reason, a small adaptation to formula 3.54 was needed:

$$\rho_i = \frac{\pi \times (L_i - L_{i \text{ haze}}) \times d^2}{T_v \times ESUN_i \times \cos^2(SZ)} \quad (3.57)$$

$L_{i \text{ haze}}$ for the QuickBird bands 1 and 2 could not be determined using equation 3.52 as this would result in negative ρ_i values in many pixels, making it impossible to calculate the natural logarithms used in the ratio-transform method. Therefore, minimum deep-water radiances, $L_{i \infty \text{ min}}$, were used to define $L_{i \text{ haze}}$ as shown in table 3.66.

Table 3.66. Determination of $L_{i \text{ haze}}$ for the atmospheric correction of the QuickBird multispectral bands 1 and 2

| | $L_{i \infty \text{ min}}$ | $L_{i, 1\%}$ | $L_{i \text{ haze}}$ |
|--------|----------------------------|--------------|----------------------|
| band 1 | 40.103 | 2.754 | 37.349 |
| band 2 | 24.120 | 2.638 | 21.483 |

Tv equals the cosine of the sensor's zenith angle, VZ , which could be determined from the sensor's viewing angle, VE , using following equation:

$$VZ = \frac{\pi}{2} - VE \quad (3.58)$$

The sensor's viewing angle could be derived from both the in track, IT , and cross track, CT , viewing angles (in radians) of the multispectral QuickBird sensor as given in section 3.2.1.3:

$$VE = \cot\left(\sqrt{\tan^2(IT) + \tan^2(CT)}\right) \quad (3.59)$$

The sensor's zenith angle, VZ , was accordingly computed to be 1.425rad and consequently, $TAUv$ equals 0.145. As all other parameters have been defined in section 3.3.3.2.3, equation 3.57 could be used to calculate the atmospherically corrected reflectance values for QuickBird multispectral bands 1 and 2.

- ratio-transform

Based on these reflectance values, the ratio between QuickBird reflectance band 1 and 2 was determined using equation 3.40 with a constant $n = 1000$. To check whether the ratio-transform problem encountered with the Landsat 7 ETM+ dataset was occurring here as well, a binary layer was created in which all values were set to 0 except the ratio values equalling 1. When this binary layer was analysed, less than 0.5% of the pixels had a ratio value of 1. The problem encountered earlier, apparently, did not occur in the QuickBird dataset. This, most probably, resulted from the higher radiometric resolution of the QuickBird sensor so that radiance values in the blue and green range are recorded in more detail and are more likely to differ from one another.

When analysing this ratio-layer, numerous pixels with ratio values less than 1, however, were encountered, especially in the shallowest reef parts as was also the case with the Landsat 7 ETM+ dataset. In these zones, the effects of the water column probably were minimal and the green reflectance was generally higher than the blue reflectance. To solve this problem, the algorithm as proposed by

Stumpf *et al.* (2003) was split up in two parts in which each part, respectively, corresponded to ratio-values ≥ 1 and ratio-values < 1 .

To calibrate the algorithm, only a limited numbers of ground truth depths are required (Stumpf *et al.*, 2002; 2003). A thorough selection was therefore made in the available GCPs and finally, 14 observation points were withheld in the shallow area, which corresponded to ratio values lower than 1, while 54 observation points were used to calibrate the linear equation corresponding to ratio values ≥ 1 (annex XII). The linear correlation equations for each part then became:

$$\text{ratio-values } \geq 1 \text{ (fig. 3.49): } \quad z = (157.54 \times \text{ratio}) - 155.62 \quad (3.60)$$

$$\text{ratio-values } < 1 \text{ (fig. 3.50): } \quad z = (44.072 \times \text{ratio}) - 42.212 \quad (3.61)$$

Finally, both parts were integrated in one provisional formula:

$$z = \text{iff}(\text{ratio} < 1, (44.072 \times \text{ratio} - 42.212), (157.54 \times \text{ratio} - 155.62)) \quad (3.62)$$

As with previous bathymetric maps, the resulting depth estimates were subsequently corrected to LAT and, for cosmetic reasons, all depth values were made negative, while the land area was given an arbitrary value of 2m.

b. Result

The result of the adapted ratio-transform method applied on the QuickBird multispectral bands 1 and 2 is shown in figure 3.51. When compared to the DOP-mapping result of the QuickBird dataset, the ratio-derived result was much noisier and showed less spatial detail in the seabed topography; a shortcoming which was already subscribed by Stumpf *et al.* (2003). Besides, the ratio-transform method did not exclude deep water where reflection of the seabed could no longer be expected. The depth values predicted for these areas, therefore, were not realistic as they were usually higher than the maximum depth attainable with band 2. The problem with the seagrass patches encountered in the DOP-derived result, on the other hand, was less pronounced or even absent in most zones. In other areas, these seagrass beds were even represented as being higher than the surrounding sandy planes. This could be the

effect of the seagrass itself or it might represent the actual seabed topography as seen in section 2.4.4.

c. Residual analysis

As with the other results, a statistical residual analysis was performed. Bi-plots of observed depth and computed depth (fig. 3.52) and observed depth and residuals (fig. 3.53) respectively were made as well. The Pearson product moment correlation coefficient, the mean residual error, and the standard deviation and the RMS of the distribution of these residuals (table 3.67) were calculated based on 64 validation points selected out of the calibration points (annex XIII). Care should thus be taken when analysing the statistical parameters.

The Pearson product moment correlation coefficient as well as the mean residual error pointed to a close relationship between observed depth and computed depth. As was seen on figure 3.52, computed values were almost evenly distributed around the optimal fit. The standard deviation and RMS of the residuals, nonetheless, indicated some deviation. The R^2 value was seemingly low (3.36%), indicating the lack of a relation between depth and residual error in the bathymetric result.

Table 3.67. Residual analysis of the QuickBird ratio-transform bathymetric result

| | |
|--|-------|
| Pearson correlation coefficient (observed –computed depth) | 93% |
| mean residual (m) | -0.03 |
| standard deviation (m) | 1.87 |
| RMS (m) | 1.85 |
| R^2 (observed depth- residual) | 3.36% |

3.4.3.5 ASTER dataset

3.4.3.5.1 Pre-processing

Before the ASTER data were processed in VIRTUOZO 3.2, the stereoscopic images were first contrast-enhanced and rotated in ILWIS 3.2.

a. Contrast enhancement

Enhancing the contrast of the scenes ameliorated the matching process in VIRTUOZO 3.2. In order to equally enhance land and marine areas, each scene was split up into a land and a marine zone based on the arbitrary defined DN value of the brightest pixel

in the sea, i.e. 60. As almost all infrared light is absorbed by the water, this was considered a good separator. Subsequently, each zone, separately, was linearly stretched. A summary of the algorithms used on both the nadir and backward scene is given below. Finally, both contrast-enhanced zones were recombined in each scene.

Nadir scene:

$$n3land = \text{iff}(\text{gifnir}3n \leq 60, 0, \text{gifnir}3n)$$

$$n3landl2 = \text{MapStretchLinear}(n3land, 80 : 128, \text{image})$$

$$n3sea = \text{iff}(\text{gifnir}3n > 60, 0, \text{gifnir}3n)$$

$$n3seal2 = \text{MapStretchLinear}(n3sea, 14 : 35, \text{image})$$

$$n3s = \text{iff}(n3land = 0, n3seal2, n3landl2)$$

Backward scene:

$$b3land = \text{iff}(\text{gifnir}3b \leq 60, 0, \text{gifnir}3b)$$

$$b3landl = \text{MapStretchLinear}(b3land, 100 : 140, \text{image})$$

$$b3sea = \text{iff}(\text{gifnir}3b > 60, 0, \text{gifnir}3b)$$

$$b3seal2 = \text{MapStretchLinear}(b3sea, 12 : 60, \text{image})$$

$$b3s = \text{iff}(b3land = 0, b3seal2, b3landl)$$

b. Rotation

VIRTUOZO 3.2 has a specific internal scene orientation in which the flight line of the sensor parallels the X-axis of the working window, i.e. from left to right. As the ASTER sensor onboard TERRA, in its descending daytime mode, orbits the globe in a N-S direction, the two scenes in the stereo-pair needed to be rotated 90° counterclockwise to match the internal orientation of the photogrammetric package. In this way, the nadir scene became the left-hand image and, consequently, the backward scene became the right-hand image. As a result, the UTM coordinates of the GCPs which will be used for the absolute orientation of the stereoscopic model needed to be

converted as well. Based on the geometric relationship between the UTM reference system and the software specific reference system (fig. 3.54), these new coordinates, X_I and Y_I , were defined as follows:

$$X_I = -Y_{UTM} \quad (3.63)$$

$$Y_I = X_{UTM} \quad (3.64)$$

3.4.3.5.2 VIRTUOZO 3.2 processing

a. Set-up

First, the stereo-model needed to be defined in VIRTUOZO 3.2 (fig. 3.55). As input to the model, the rotated and specifically enhanced nadir and backward scene of the ASTER dataset were indicated. Because ASTER is a digital scanning sensor, the ASTER scenes were regarded as taken by a non-metric camera. Next, the local environment in which each part of the scene will be processed was arbitrary defined as a 5 by 5 kernel. Following, an image overlap of 99% was selected in order to account for the different geometry of the nadir and backward scene. Finally, a DEM spacing of 15m, equalling the spatial resolution of the ASTER scenes, was chosen which defined the spatial resolution of the output DEM.

b. Model orientation

The orientation of a photogrammetric model consists of three consequent steps: internal orientation, relative orientation, and absolute orientation.

- internal orientation

During the internal orientation, the scenes in the model are oriented to the software-specific reference system based on the camera characteristics and the fiducial marks on metric scenes. As the ASTER sensor was considered as a non-metric camera, no internal orientation can be performed. This, however, had no effect on the result.

- relative orientation

During the relative orientation, both scenes in the stereo-model are referred to one another. This image-matching process is an automatic procedure in VIRTUOZO

3.2 in which conjugate points related to distinct points in the left scene are automatically retrieved in the other scene (Zhang *et al.*, 1996). The accuracy of this automatic procedure still needed to be manually checked. After the accuracy test, 161 automatic tie-points were retained with a general RMS of 0.0074pixel.

- absolute orientation

To relate the model reference system to a real-world reference system, a minimum of 6 GCPs measured in X, Y and Z are needed. Butler *et al.* (2002) only selected control points which lie above the water surface. During earlier tests with VIRTUOZO 3.2 and an ASTER stereo-pair, the use of GCPs on land, nevertheless, generated unrealistic depth values -in the order of several tens of meters above and below sea level. In contrast to the findings of Butler *et al.* (2002), subaquatic GCPs were thus found to be beneficial to the accuracy of the bathymetric map. Moreover, the combination of a satellite-mounted sensor at 705km altitude and the restricted water penetration of the infrared wavelengths in which the stereo-pair was acquired ended up in a very small depth/height ratio. Together with the spatial resolution of the ASTER stereoscopic scenes, this resulted in minimal planimetric shifts caused by refraction, allowing the use of subaquatic GCPs.

The depth measurements made during the field campaigns, unfortunately, could not be used as these features were difficult to localise on the ASTER scenes. Besides, as the stereo-pair is recorded in the infrared wavelengths, only the shallowest parts of the reefs which were the least accessible in the field were recognisable on the scenes. To solve this problem, alternative GCPs were determined based on the bathymetric map derived from the modified DOP-mapping on the original LANDSAT 7 ETM+ dataset (section 3.4.3.1.1). Pixels were selected which were recognisable on the Landsat 7 ETM+ bathymetric map and on both the nadir and backward ASTER scenes. X, Y and Z-coordinates for in total 63 GCPs were derived in this way (annex XIV). In addition, X and Y-coordinates were adjusted to fit the internal orientation according to formulas 3.63 and 3.64. Ultimately, 9 GCPs were retained for the absolute orientation of the stereo-model (table 3.68). An overview of the resulting mean errors in X, Y and Z is given in table 3.69.

c. Epipolar images

Once the absolute orientation was performed, left and right epipolar images were calculated in order to remove the redundant y-parallax in the stereo-model. In this way, image matching was only needed for the X dimension (Zhang *et al.*, 1996).

Table 3.68. Overview of the GCPs used in the absolute orientation of the ASTER stereo-pair with the indication of individual errors in X, Y and Z

| GCP ID | X | Y | Z | dX | dY | dZ |
|--------|----------|--------|------|---------|---------|--------|
| 1922 | -3011815 | 586215 | 0.0 | 3.869 | 15.911 | 1.06 |
| 1916 | -3016820 | 588703 | -2.0 | -11.346 | 4.511 | -0.303 |
| 1918 | -3016235 | 589269 | -1.0 | 10.000 | -0.945 | 0.204 |
| 1919 | -3015905 | 589334 | 0.0 | 1.846 | -6.837 | -0.395 |
| 1929 | -3010475 | 596066 | -2.0 | 4.461 | -4.125 | 0.867 |
| 1925 | -3009175 | 590472 | -3.0 | 1.496 | -2.274 | 0.010 |
| 1924 | -3009435 | 590466 | -1.0 | -1.348 | -1.667 | -1.517 |
| 1928 | -3010502 | 595976 | -1.0 | -9.173 | 5.951 | -0.169 |
| 1921 | -3011643 | 585751 | 0.0 | 0.489 | -10.791 | 0.250 |

Table 3.69. Overview of mean RMS-errors of the absolute orientation

| m_x | m_y | m_xy | m_z |
|--------|--------|--------|--------|
| 6.2845 | 7.4412 | 9.7399 | 0.7115 |

d. Image matching

Subsequently, the left and right epipolar images were matched to facilitate the DEM-extraction algorithm. The matching accuracy for each patch was indicated by coloured pegs as shown in figure 3.56. As could be expected (Westaway *et al.*, 2001), the deep-water areas were not correctly matched and these parts, therefore, were masked before further processing.

e. Match editing

In the match editing step, the deep areas were masked and given an arbitrary depth value of 5m as below this depth, no reflection of the seafloor was assumed to be recorded by the ASTER infrared sensors. Besides, as only subaqueous GCPs were used, height estimates for the land surface were invalid and the land surface was therefore assigned an arbitrary value of 0m.

f. DEM calculation

Finally, a regular grid DEM was automatically extracted and an ortho-image of the left-hand scene, i.e. the nadir scene, created. These products could be combined in a 3D screen display, two examples of which are given in anaglyph format on figures 3.57 and 3.58. Last, the DEM raster grid was exported to ILWIS 3.2 and re-oriented to fit the original UTM reference system.

3.4.3.5.3 Post-processing: refraction correction

To account for the underestimation of depth caused by the refraction of the light at the air/water interface, the correction algorithm developed by Westaway *et al.* (2001) and Butler *et al.* (2002) was adapted to the ASTER stereo-configuration (fig. 3.59). The ASTER sensor is equipped with two near-infrared sensors which are configured to take stereo-images: one telescope (3n) is looking at nadir, the other one (3b) looks backwards with an angle of 27.60° relative to the downward looking sensor. Due to the curvature of the earth surface, this results in an angle of 30.96° between the nadir and backward direction at an observing point on the earth surface (ERSDAC, 2003). This angle of 30.96° thus represents the angle of incidence, i , in figure 3.59.

With a known angle of incidence, i , for each telescope, equation 3.49 could be calibrated if also the refraction index of the seawater in the study area was known. As no in situ information on the temperature and salinity of the seawater was available for the moment of data acquisition, no precise estimation of the refraction index could be made. However, regional variations in temperature and salinity of the seawater only have minimal effects on the refraction index (Jerlov, 1976). The refraction index was therefore set to the standard value of 1.340 (Jerlov, 1976).

For the nadir ASTER sensor which has a near-vertical viewing angle and is located at a high flying altitude relative to water depth, equation 3.49 could be simplified to (Westaway *et al.*, 2000; Westaway *et al.*, 2001):

$$h_1 = n \times h_a \quad (3.65)$$

With the refraction index of the seawater, n , set to 1.340, this became:

$$h_1 = 1.340 \times h_a \quad (3.66)$$

i and n were known for the backward looking telescope as well, so the correction algorithm could be defined as follows:

$$h_2 = \left[\frac{\tan(30.96)}{\tan\left(\frac{30.96}{1.340}\right)} \right] \times h_a = 1.41 \times h_a \quad (3.67)$$

According to equation 3.50, the total correction algorithm then became:

$$h = \frac{(1.340 + 1.41)}{2} \times h_a = 1.38 \times h_a \quad (3.68)$$

Equation 3.68, finally, was applied in post-processing on the apparent DEM in ILWIS 3.2 to calculate true depth from the apparent depth.

3.4.3.5.4 Result

The result of the trough-water digital photogrammetric processing of the ASTER stereo-pair is depicted in figure 3.60. The “hill” in the northeast corner of the map, obviously, is a large error in the result. Nonetheless, some topographic variation on the reef flat areas was clearly represented and fell within a reasonable depth range.

3.4.4 Discussion

3.4.4.1 The effect of pan-sharpening the Landsat 7 ETM+ dataset

The visual comparison of the bathymetric results derived from the application of the modified DOP-mapping method on the original and pan-sharpened Landsat 7 ETM+ dataset did not reveal much differentiation between both. The enhanced spatial resolution of the pan-sharpened dataset has increased the detail in which the reef structures are depicted, but has not significantly changed depth predictions. When comparing the statistical residual analyses of both results (based on the same independent validation points), some minor differences were revealed. The Pearson product moment correlation coefficient for the original Landsat 7 ETM+ result was slightly higher, indicating that the

general trend of the seabed topography is better represented in this result. The mean residual error, its standard deviation, and the RMS-error also pointed to a more accurate bathymetric map.

The lesser performance of the pan-sharpened bathymetric map may have been the result of a loss in spectral information during data fusion; a loss which could not be totally excluded by using the LMVM-filter method. This spectral modification may have affected the original exponential relationship between radiance received at sensor and depth, leading to errors in depth predictions. On the other hand, the residual analysis is probably also influenced by the spatial resolution of the pan-sharpened dataset. With a pixel size of 15 by 15m, more variance is introduced into the bathymetric map which may have led to a lower correlation with single-point field observations.

3.4.4.2 Comparison of the modified DOP-mapping results of the Landsat 7 ETM+ and QuickBird dataset

When the results obtained after applying the modified DOP-mapping method to both the original Landsat 7 ETM+ and the QuickBird dataset were visually compared, the difference in spatial resolution could clearly be noted. The QuickBird bathymetric map has much more structural detail and depicts bottom features not visible on the Landsat 7 ETM+ bathymetric map. The problem with the seagrass beds in the QuickBird result, conversely, is less pronounced in the Landsat 7 ETM+ result as most seagrass patches are too small to be detected by the latter sensor. An overestimation of depth over the largest seagrass beds, however, also occurs in the Landsat 7 ETM+ result.

Additionally, a differentiation map (fig. 3.61) was created in which the QuickBird result was subtracted from the Landsat 7 ETM+ result which has previously been resampled to the georeference and spatial resolution of the QuickBird dataset. While the shallow areas show a remarkable similarity on both results -except for the seagrass beds- the deeper areas are notably shallower on the QuickBird result as on the Landsat 7 ETM+ result; i.e. significant negative residuals were calculated as shown in figure 3.61. This most probably is the result of the biased calibration of the DOP-mapping algorithm on the QuickBird dataset due to the limited number of GCPs available over deeper waters in the restricted study area. The area between the mainland and Shaab Magawish, in contrast, shows major positive residuals. Based on the pattern of the errors, they most probably result from a memory effect in the Landsat 7 ETM+ dataset which saturates the reflection over the deeper water between the highly reflective land and the shallow Shaab Magawish

structure. The depth of the water column in these pixels, as a result, is highly underestimated.

In order to make a statistical comparison between the QuickBird and the Landsat 7 ETM+ result, an additional residual analysis for the resampled Landsat 7 ETM+ bathymetric map was performed, based on the same 64 validation points as used for the QuickBird dataset (annex XV). The different statistical parameters are enlisted in table 3.70 and the corresponding bi-plots are given in figures 3.62 and 3.63. The Pearson product moment correlation coefficient indicates a better result derived from the original Landsat 7 ETM+ dataset compared to the QuickBird result. When the mean residual errors and their standard deviations are considered, the QuickBird dataset, conversely, performs best. As with the pan-sharpened Landsat 7 ETM+ result, the higher spatial resolution of the QuickBird dataset may have introduced more variance in the result, which may have reduced the correlation between observed and computed depth. Both the Landsat 7 ETM+ and the QuickBird result thus have their advantages and disadvantages and a clear preference for one of the results can not be stated.

Table 3.70. Specific residual analysis of the resampled Landsat 7 ETM+ bathymetric result

| | |
|--|-------|
| Pearson correlation coefficient (observed –computed depth) | 93% |
| mean residual (m) | -1.26 |
| standard deviation (m) | 1.71 |
| RMS (m) | 1.70 |
| R ² (observed depth- residual) | 4.9% |

3.4.4.3 The applicability of the ratio-transform method

The modified DOP-mapping method has shown its usefulness for both the Landsat 7 ETM+ and the QuickBird dataset. Due to problems encountered with the Landsat 7 ETM+ dataset, a comparison of the bathymetric results obtained with the ratio-transform method and the modified DOP-mapping method could only be made based on the QuickBird multispectral dataset. A small adaptation to the method proposed by Stumpf *et al.* (2003) was however needed to predict depths accurately both in shallow and deeper areas.

During a visual evaluation, two elements became clear. On the one hand, the ratio-transform method delivers a noisier result with less detailed bottom structures. The noise could be reduced by applying a 3 by 3 or 5 by 5 average filter (Stumpf *et al.*, 2003),

although this would lead to a further loss of structural detail. The severe depth errors over seagrass beds encountered in the modified DOP-mapping result, on the other hand, were less apparent in the ratio-transform result in which seagrass patches are situated at equal or slightly shallower depths than the surrounding seabed.

Statistically, the ratio-transform method results in a more accurate bathymetric map as both the mean residual error and the error distribution are markedly better than with the modified DOP-mapping method, as well as the correlation between the observed and computed depth. Care should be taken, however, when interpreting these statistical measures as they may be biased by the use of the dependent GCPs. This is especially important with the ratio-transform method as the linear regression defined to determine depth is exclusively based on these calibration points. In the modified DOP-mapping method, the calibration of the algorithm is less dependent on each individual depth measurement because of the specific calibration method proposed by Edwards (1999).

3.4.4.4 General remarks on multispectral bathymetric methods

To summarise, some general remarks concerning bathymetric mapping using passive, multispectral data can be made. First, the general depth restriction of the passive, multispectral approach to about 30m is not only influenced by the turbidity of the water column but also depends on the radiometric resolution of the satellite sensor used. As the signal reflected from the seabed is already attenuated to a great extent by the water column and the atmosphere, a high signal-to-noise ratio is essential to extract useful information (O'Neill and Miller, 1989; Sandidge and Holyer, 1998). Besides, the amount of radiance reflected by the seabed and recorded at sensor depends on the dynamic range, i.e. the minimum and maximum radiance recorded, and the sensitivity of each sensor (O'Neill and Miller, 1989; Philpot, 1989; Ji *et al.*, 1992). As most high-resolution sensors, like the Landsat series, are primarily developed for terrestrial applications, their dynamic ranges are not specifically designed to be sensitive in typical low radiance levels reflected by the seabed in relatively deep water. Another important element in this respect is the quantisation to DN values of the radiance recorded by the sensors which links one DN value to a fixed range in radiance values (Philpot, 1989; Ji *et al.*, 1992). Due to the finite sensitivity of the sensor, a large range of lower radiance values from deep-water areas is normally combined into one single DN value, while a similar radiance range in more reflective, shallow parts or over land is distributed over a range of DN values.

Consequently, the uncertainty in the bathymetric result dramatically increases with depth (Philpot, 1989).

Secondly, the assumptions inherent to most passive, multispectral bathymetric mapping methods do not always represent reality. The assumption of horizontal homogeneity of the water-column optical properties and the atmospheric composition covered by one scene might be valid for oceanic coral-reef environments, where many bathymetric models have been developed, but in a coastal setting, this is likely not the case. This inevitably introduces errors in the bathymetric model (O'Neill and Miller, 1989; Philpot, 1989; Van Hengel and Spitzer, 1991; George, 1997; Stumpf *et al.*, 2003; Huguenin *et al.*, 2004). However, unless all atmospheric and water-column parameters can be measured in the field or can be derived from the satellite data itself, this assumption needs to be made. A possible solution proposed by Philpot (1989) is to partition the scene into regions of uniform water type prior to bathymetric mapping. This, nonetheless, still requires information about the variation of the water-column optical properties in the scene which is not available for this study.

A related problem is the determination of mean deep-water radiances which are used to correct radiance values for atmospheric path radiance. As stated by Stumpf *et al.* (2003: 555), '*the determination of mean deep-water radiance probably induces more uncertainty in the linear algorithm than any other coefficient*'. If chosen inappropriate, errors may be introduced in optically shallow water over low albedo surfaces or in water with a higher attenuation coefficient than expected. Here, the radiance recorded at sensor, L_i , may be lower than or equal to the determined mean deep-water radiance, $L_{i \infty mean}$, resulting in a zero or negative value for $(L_i - L_{i \infty mean})$. These values can consequently not be used to calculate valid natural logarithms necessary in equation 3.33 and depth for these pixels can not be estimated (Ji *et al.*, 1992; Stumpf *et al.*, 2003). Results, therefore, may be improved with more elaborate atmospheric corrections.

The assumption of a homogeneous substrate covering the entire study area is most certainly not valid in a heterogeneous coral-reef environment (Liceaga-Correa and Euan-Avila, 2002). As a consequence, depending on the spatial resolution of the data used, a generalisation of reflectance over a very heterogeneous area is made. This creates some radiometric uncertainty about which bottom type exactly is represented by the recorded DN value and inevitably leads to problems in depth estimations (O'Neill and Miller, 1989; Sandidge and Holyer, 1998; Green *et al.*, 2000b; Tanis *et al.*, 2002; Huguenin *et al.*, 2004). Moreover, the applied algorithms are usually calibrated with depth measurements

over a bright sandy substrate (Ji *et al.*, 1992) and dark substrates like seagrass beds, therefore, are often interpreted as deep water (Bierwirth *et al.*, 1993). As with horizontal water-column heterogeneity, this problem can be circumvented if each bottom type with a different albedo is separately analysed (Green *et al.*, 2000; Tanis *et al.*, 2002). This, however, requires a very precise bottom-type classification which can only be made based on detailed field studies or based on remote sensing if detailed bathymetric information is a priori available. In addition, the reflection characteristics of the bottom type already influence the accuracy of the estimated depth. The darker the bottom type, the smaller the variation in radiance values which will be observed over a range of water depths. Correspondingly, the less reflective bottom types automatically result in less depth precision and accuracy (Ji *et al.*, 1992; Tanis *et al.*, 2002).

The third assumption of an exponential decay of water-leaving radiance with depth, and inherently the assumption of vertical homogeneity of the water column, has long been considered valid. Recent studies, however, prove that vertical changes in water-column composition are more widespread than expected (Newman and LeDrew, 2001) and that inelastic scattering processes (such as fluorescence) which were considered negligible (e.g. Spitzer and Dirks, 1987), have an important effect on the radiance received at sensor (Ackleson, 2003). Based on this new information, the basic radiative transfer models may need to be adapted in future.

Other errors are generated by the characteristics of the field measurements, the sampling method applied, and/or the spatial uncertainty of the satellite data used. The precision of the depth-measuring instrument, i.e. 0.3m above and 1m below 10m depth, already restricts the maximum possible accuracy obtained with any method relying on these data (Van Hengel and Spitzer, 1991). Besides, the time lag between the date of remote sensing data acquisition and the period of field sampling may also introduce errors (Van Hengel and Spitzer, 1991; Sandidge and Holyer, 1998).

An effective calibration of the algorithm also depends on the distribution and the density of the depth measurements (O'Neill and Miller, 1989). As the shallowest parts of the reefs are not easily accessible, even with a zodiac, depth measurements in waters shallower than approximately 1m are not equally represented in the dataset. This may result in poorly performing algorithms over these shallow reef zones and may already have attributed to the poor results obtained with the N-IR bands of the Landsat 7 ETM+ and QuickBird datasets. Specific for the QuickBird dataset, a problem was encountered for deep water due to the limited number of GCPs available in deep water. This probably

resulted in the limited depths of penetration calculated as compared to the values obtained for the Landsat 7 ETM+ dataset and, consequently, the underestimation of depth over deeper areas.

Finally, while making depth measurements from the zodiac, the position of the vessel is very variable due to current and wave motions, while the standard location error of the hand-held GPS receiver for a fixed position was also in the order of 4 to 5m. Moreover, the geocoding of the satellite datasets introduces additional location errors. The Landsat 7 ETM+ scene was geocoded with a RMSE of 0.311pixel, corresponding to approximately 10m; while the QuickBird scene was geocoded with a RMSE of 3.499pixel or 10.08m. Taking the standard GPS location error into account, this means that the precise location of a reference point may vary within a radius of 14-15m on average. In the case of the Landsat 7 ETM+, this is not so much of a problem as this radius equals half the pixel size, meaning that most reference points corresponded to the correct pixel. On a QuickBird scene, however, this radius corresponds to approximately 100 pixels. These positional uncertainties thus make it difficult to match each depth measurement to a unique DN value. This may also explain the lower correlation coefficients obtained for the QuickBird and pan-sharpened Landsat 7 ETM+ datasets. The low spatial resolution of the Landsat 7 ETM+ dataset, conversely, makes it more difficult to match the in situ depth measurement with the generalised area covered by one single pixel, i.e. 900m². This is especially problematic for coral-reef bathymetry which may change rapidly within a few meters (Edwards, 1999).

3.4.4.5 Through-water digital photogrammetric approach

To the advantage of the through-water digital photogrammetric approach, the abovementioned assumptions concerning the water-column optical properties need not to be made. As this approach, however, still requires multispectral data, it remains limited in maximum depth predictability. Especially with ASTER stereo-data which are recorded in the N-IR spectral range, the depth penetration is highly restricted. Some additional problems have also to be solved before this procedure can become operational.

First, the errors introduced by the mismatching of deep-water areas have to be eliminated as this greatly biases the overall result. Different solutions are possible: (1) improving the matching of the deep-water areas by manually adding relative tie-points to these areas (Chong *et al.*, 2001). This, however, is very difficult as conjugate pixels on both scenes in the stereo-model are almost impossible to find; (2) ameliorating the

matching process by resampling the backward scene coordinates to the nadir scene coordinates. In this way, conjugate pixels will be located in the same relative position on both scenes and more tie-points may be automatically found by the software; or (3) refining the masking procedure over deep water because many errors in the deep water originate along the borders of the scene as can be seen on in figure 3.60.

The second main problem is that local errors occur on the shallow coral reef parts, most probably as a consequence of the lack of absolute GCPs which have been directly measured in situ. Such field-based measurements, unfortunately, are difficult to make as large parts of the shallow reef flats are hardly accessible and maybe more important, field locations are often very difficult to retrieve on both ASTER scenes. Buchroitner (1991) proposes a solution by using relative GCPs derived with a conventional mirror stereoscope. Although this improves the stereo restitution (Buchroitner, 1991), additional in situ measurements are still needed to perform a full absolute orientation. An alternative solution may be to replace the nadir N-IR scene with the green band of the same dataset. This would enhance the contrast in the marine area, and potentially improve the image matching and the positioning of field-based measurements. This, however, only forms a partial solution to the problem, as the backward N-IR scene can not be replaced.

3.4.5 Conclusions

The conventional approach to multispectral bathymetric mapping is limited by the optical properties of the water column. Specifically for the study area, depths up to 20m are determined by using the modified DOP-mapping method, with an accuracy of $\pm 1\text{m}$ for both the Landsat 7 ETM+ and QuickBird dataset. This depth restriction most probably is the result of the high C-DOM concentration in the study area. Some additional problems occur with both datasets. Major problems were noted over seagrass patches which were interpreted as sandy substrate at much greater depths. This problem was more pronounced on the QuickBird result as more seagrass beds were detected by the very-high-resolution sensor. Specifically for the Landsat 7 ETM+ dataset, a memory effect has been detected over deep waters surrounded by highly reflective features, resulting in an underestimation of depth for these areas. The calibration of these algorithms also requires a sufficiently large number of ground truth data well distributed over the total depth range in the study area. This was exemplified in the poor performance of the method with the QuickBird dataset over the deeper area. Nevertheless,

coral reefs are still largely mapped with an acceptable accuracy, indicating the usefulness of the modified DOP-mapping method.

The alternative ratio-transform method could only be used with the QuickBird dataset, although modifications were needed to apply the technique to the shallowest reef parts. A visual comparison of the bathymetric maps derived using the modified DOP-mapping method and the adapted ratio-transform method indicates higher structural detail obtained with the modified DOP-mapping method. The problem with erroneously estimated depths over seagrass beds, in contrast, is less pronounced with the ratio-transform method, though predicted depths for these areas are not correct either. The residual error analyses, conversely, indicate the ratio-transform method as the best performing. However, this may be biased by the use of dependent validation points. For these reasons, the modified DOP result is preferred over the ratio-transform result.

For highly heterogeneous environments such as coral reefs, the spatial resolution of the dataset has been defined as an important factor for bathymetric mapping of coral reefs. It is clearly noted that the QuickBird dataset results in a more detailed bathymetric map, although it is more restricted in spatial extent and the result is seriously biased by errors over dark substrates. Pan-sharpening the Landsat 7 ETM+ dataset also improves the structural detail, although introducing some minor additional errors.

As the stereo-information of the ASTER sensor is acquired in the near-infrared range of wavelengths, only the shallowest parts of a coral-reef system are depicted. Despite the problems encountered during data processing, the through-water photogrammetric approach might prove to be a valid alternative for the more conventional, passive remote-sensing-based bathymetric mapping methods. With the development of the CHRIS/PROBA, a spaceborne sensor acquiring a set of 18 hyperspectral bands under 5 different angles, or the availability of stereoscopic QuickBird and IKONOS datasets, the applicability of the digital photogrammetric approach may be expanded.

3.5 GEOMORPHOLOGICAL CLASSIFICATION

3.5.1. Introduction

As reviewed in section 1.1.4, the physical structure of a coral reef is defined by a number of distinct medium- to small-scale geomorphological zones depending on the dominant physical and ecological processes taking place. These geomorphological zones usually have distinct boundaries (Mumby, 2000) and are therefore easily recognised on a remote sensing image. As depth also plays an important role in the characterisation of most coral-reef geomorphological zones, the integration of this information is beneficial to the geomorphological classification process (Houhoulis Smit, 2001). For this reason, a *depth-improved colour composite* (DCC) is created before digitising the geomorphological zones. This specific colour composite is constructed by merging the topographic information of the bathymetric map with the spectral information of the multispectral dataset (Bierwirth *et al.*, 1993) using the AIMF method (de Béthune *et al.*, 1998a). The topographic information is obtained by applying hill-shading to the raster-DEM (Bierwirth *et al.*, 1993; Houhoulis Smith, 2001). On this DCC, the different geomorphological features are delineated based on their spectral and geomorphologic, i.e. bathymetric, characteristics following the geomorphological classification scheme (Mumby and Harborne, 1999a; b; Coyne *et al.*, 2003) presented in table 3.71. The level of detail mostly depends on the spatial resolution of the dataset under investigation.

Table 3.71. Specific geomorphological classification scheme for the Hurghada study area (adapted from: Mumby and Harborne, 1999a; b; Coyne *et al.*, 2003)

| class | | description |
|-----------|--------------------|---|
| level 1 | level 2 | |
| 1. land | | as defined by the land mask |
| 2. lagoon | | shallow area (relative to the deeper bank/shelf) between the shoreline and the back reef or the reef crest, or the shallow area encircled by an atoll; protected from high-energy waves by a reef crest |
| | 2.1 shallow lagoon | depth \leq 12m |
| | 2.2 deep lagoon | depth $>$ 12m |

| class | | description |
|--------------------------|------------------------|---|
| level 1 | level 2 | |
| 3. patch reef | | relative small coral formations with unclear morphology formed by hard corals or dead coral colonised by new organisms |
| | 3.1 dense patch reef | areas of aggregated coral colonies where colonies cover more than 70% of the benthos (Mumby and Harborne, 1999a) |
| | 3.2 diffuse patch reef | areas of dispersed coral colonies where less than 30% of the benthos is covered by coral colonies (Mumby and Harborne, 1999a) |
| 4. back reef / reef flat | | shallow zone between reef crest and lagoon often formed by a pavement of hard substratum with or without rubble and frequently covered with algae; in the case of a fringing reef, the shallow area between the landward edge of the reef crest and the shore is called the reef flat (Coyne <i>et al.</i> , 2003) |
| 5. reef crest | | the shallowest and often emergent part of a reef; it separates fore reef from back reef and lagoon |
| 6. fore reef | | the zone from the seaward edge of the reef crest downwards (often difficult to distinguish from bank/shelf) |
| | 6.1 spur and groove | spurs are usually formed by accreting hard coral and calcified green algae whereas grooves usually contains sand or bare bedrock (Green <i>et al.</i> , 2000b) |
| 7. bank/shelf | | relative undep area –specifically that part still visible on satellite images- of the continental shelf which is not in direct relation to the reef morphology |
| 8. mudflat | | land-derived mud depositions |
| 9. deep water | | zone where no significant spectral reflectance is recorded by the satellite sensor |
| 10. unknown | | class containing areas of undefined nature |

3.5.2. Implementation

3.5.2.1 Original Landsat 7 ETM+ dataset

As spectral input data, the blue, green, and red Landsat 7 ETM+ bands were selected as these bands contain information concerning the submerged coral reefs. The bathymetric result obtained from the modified DOP-mapping method (section 3.4.3.1.1) was used as additional bathymetric input layer.

3.5.2.1.1 Hill-shading of the bathymetric map

To visualise the topographic information contained in the bathymetric map, hill-shading was applied to the bathymetric Landsat 7 ETM+ result shown in figure 3.36. Best results were obtained with a 3 by 3 shadow filter (ILWIS 3.2) (see below) initialising the sun in the northeast, corresponding to the dominant direction of the surface currents in the study area. In this way, most reef fronts were highlighted, while the more gradual back-reef slopes were displayed in shadow.

| | | |
|----|----|----|
| -1 | -2 | -3 |
| 2 | 1 | -2 |
| 4 | 2 | -1 |

The hill-shaded map was subsequently rescaled to an 8bit image domain in order to fit the radiometric resolution of the Landsat 7 ETM+ spectral bands. During this rescaling, an additional linear stretch with a 0.5% threshold was performed to improve the contrast in the hill-shaded DEM.

3.5.2.1.2 Construction of the DCC

Secondly, the contrast-enhanced hill-shaded raster DEM was merged with the three Landsat 7 ETM+ spectral bands. As the final merged product will be mainly used for the visual delineation of the geomorphological features, the structural information of the bathymetric map should be integrated as much as possible. For this reason, a 7 by 7 LMM filter (de Béthune *et al.*, 1998a) was applied.

The data fusion procedure was largely similar to the one described in section 3.3.7, so that the different steps will only be briefly illustrated here. Because both datasets have the same spatial resolution, the pre-processing step in which the low-resolution

datalayers are resampled to the high-resolution data-layer, could be omitted. Consequently, formula 3.28 as described in section 3.3.7.2.2 was applied to derive a global intensity channel, L , representing the mean spectral information of the three Landsat 7 ETM+ spectral bands. The LMM-filter (formula 3.25), however, needed to be adapted to allow the merging of the spectral bands with the hill-shaded bathymetric model:

$$F_{(l,c)} = \frac{(DN_{b(l,c)} \times M_{L(l,c)(7 \times 7)})}{M_{b(l,c)(7 \times 7)}} \quad (3.69)$$

With: $F_{(l,c)}$: fused intensity band at pixel (l, c)
 $DN_{b(l,c)}$: value in the converted, hill-shaded raster DEM at pixel (l, c)
 $M_{L(l,c)(7 \times 7)}$: average value of the global intensity channel, L , calculated in a 7 by 7 kernel, at pixel (l, c)
 $M_{b(l,c)(7 \times 7)}$: average value in the converted, hill-shaded raster DEM, calculated in a 7 by 7 kernel, at pixel (l, c)

Finally, three data-merged bands containing both topographic information and blue, green, and red spectral information were respectively derived using formula 3.29. These bands were then combined to form the DCC and in addition, a land mask was applied.

3.5.2.1.3 Geomorphological zonation

The made-up DCC, a detail of which is presented in figure 3.64a, formed the base for the geomorphological mapping. When compared to a conventional TCC of the same area (fig. 3.64b), the advantage of integrating bathymetric information for the delineation of geomorphological zones was clearly noted. Although some loss of spectral information was inevitable, more importantly, the physical structures of the reef geomorphological zones were highlighted. Specifically in this example, the back-reef slopes could be easily recognised as well as some secondary reef-flat structures. The use of a bathymetric map derived from passive, multispectral data, however, limits the depth to which geomorphologic structures can be delineated. Here, all areas deeper than 21.4m, i.e. the maximum depth of penetration of the blue Landsat 7 ETM+ spectral band, were automatically masked out and received value 0 in the DCC.

3.5.2.1.4 Result

The result of the geomorphological mapping of the Hurghada study area using the original Landsat 7 ETM+ dataset is shown in figure 3.65a. For comparison with the QuickBird geomorphological zonation map, a detail over the restricted study area is also given (fig. 3.65b). Most mainland shores are aligned with reef structures. The crests of these fringing reefs generally were too narrow to be recognised with the spatial resolution of the sensor and could therefore only be delineated in some places. Alternatively, these coral-dominated reef crests may have been destroyed by human-activities.

The fringing reefs are often connected to large patch reef structures further offshore. Here, the dominance of coral could not always be deduced from the DCC and these structures were alternately classified as back reef, dense, or diffuse patch reefs according to the spectral information on the Landsat 7 ETM+ TCC and ground truth information. For many structures, the reef crest could be better delineated than was the case for the fringing reefs. This might indicate the validity of the hypothesis suggesting the human-induced destruction of the reef crests on the fringing reef structures. The lagoons associated with these patch reefs are often shallow, in the order of 2-5m, and characterised by bright uncovered carbonate sands⁷⁰ and smaller seagrass patches. Due to the steepness of the front reef, most of them could not be delineated on the Landsat 7 ETM+ DCC.

The reef structures are especially well developed around the Giftun Islands and Abu Minqar. In most cases, a clear reef crest could be delineated, often projecting seawards from the islands and forming large, irregular reef flats or back reefs. Special reference should also be given to two reef structures, being Shaab el Erg and El Gouna Reef, in the northern part of the study area which may be classified as ‘horseshoe reefs’ and eventually may form atoll-like reefs in future.

3.5.2.2 Pan-sharpened Landsat 7 ETM+ dataset

A similar workflow as described for the original Landsat 7 ETM+ dataset was followed with the pan-sharpened dataset. Remark, however, that input spectral values were radiance values corrected for atmospheric effects as these resulted from the pan-sharpening process performed in section 3.3.7. The geomorphological zonation map derived from the visual

⁷⁰ Sands derived from eroded reef structures.

analysis of the pan-sharpened Landsat 7 ETM+ DCC, and a detail over the restricted study area, are respectively given in figures 3.66a and 3.66b. In general, the same structures as on the original Landsat 7 ETM+ geomorphological classification were detected, although more spatial detail could be added in some places.

3.5.2.3 QuickBird dataset

3.5.2.3.1 Methodology

For the QuickBird geomorphological classification, the workflow as abovementioned was also followed. Input bands were the first three QuickBird spectral bands represented as 11bit DN values. The result of the modified DOP-mapping method application on the QuickBird dataset was used as bathymetric input as this result showed more spatial detail in bottom features than the result obtained with the ratio-transform method.

Care should be taken when delineating geomorphological zones based on this DCC as, due to the inherent shortcomings of the applied bathymetric mapping technique, seagrass and other dark substrates resulted in false depressions in the seabed topography (section 3.4.3.4). Knowledge on the bottom-type distribution was therefore derived from the field observation data.

3.5.2.3.2 Result

The QuickBird-derived geomorphological zonation map is represented in figure 3.67. As could be expected, the large-scale reef structures seen on the Landsat 7 ETM+ geomorphological zonation map were also detected on the QuickBird result but the delineation of each zone was performed with much more spatial detail. The reef crests bordering the northwestern edges of the Abu Magawish fringing reef and the Shaab Magawish reef structure could almost continuously be tracked; this was not the case with the lower spatial resolution of the Landsat 7 ETM+ dataset. These reef crests, remarkably, do not occur along the northeastern side of the reef structures as is predominantly the case in the study area. This difference most probably is caused by a change in current direction due to the occurrence of the Giftun Islands towards the northeast of this specific study area. As a result, the currents are forced through the channel between the mainland and Abu Minqar Island, obtaining a more N-NW direction in this specific study area.

A major difference with the Landsat 7 ETM+ geomorphological zonation map is the addition of mudflats along the mainland shores which were characterised in the field by the occurrence of fine terrestrial muds and sands rather than carbonate reef sands. The coral cover of these parts was also minimal. These specific characteristics could not be recognised on the Landsat 7 ETM+ colour composites.

Apart from the geomorphological zones shown on figure 3.67, some small spur and groove systems along the eastern side of the Shaab Magawish reef structure were detected on the original QuickBird bathymetric map as shown on the enhanced detail in figure 3.68. According to the bathymetric map, these features are located between 10 and 15m deep. Spur and grooves, conversely, are normally formed near the surface (see section 1.1.4.2.4). If these features are actually spur and grooves and not another geomorphological feature, they most likely are fossilised structures representing a submerged Pleistocene carbonate surface. These structures are not represented in the final QuickBird geomorphological zonation map as they do not form part of the modern coral-reef system.

3.5.3 Discussion

3.5.3.1 Effect of pan-sharpening

As could be expected, the geomorphological map derived from the pan-sharpened Landsat 7 ETM+ dataset showed somewhat more spatial detail than the one derived from the original dataset. Several zones were more accurately delineated and some features too small to be detected with the original 30m spatial resolution became apparent in the pan-sharpened DCC. Other narrow, elongated zones, conversely, could no longer be recognised on the pan-sharpened dataset, most probably due to a loss of spectral information during the data merging procedure. The differences in delineation between bank/shelf and deep-water areas on both results, was not so much a result of the increased spatial resolution, rather it represented the subjectivity in the visual interpretation of a DCC.

The high spatial resolution of the QuickBird multispectral dataset obviously led to the spatially most detailed geomorphological classification. When the three results for the same specific study area were compared, the original Landsat 7 ETM+ result, however, still represented the same large-scale geomorphological features although at a lower spatial resolution. With the advantage of synoptically covering a much bigger study area

than the QuickBird sensor at a much lower cost, the Landsat 7 ETM+ sensor can definitely be used to delineate large geomorphological zones. The advantage of pan-sharpening the dataset was only minimal and the benefit of this additional pre-processing step could thus be questioned.

3.5.3.2 General observations

The Red Sea reefs clearly are very complex and often lack a distinct geomorphological zonation. Only in few places, a clear distinction between fringing reef and barrier reef could be made. In large, the narrow and structurally complex Red Sea shelf is illustrated by this classification. The detectible shallow bank/shelf zone (i.e. < 22m) is 7 to 8km wide at most, after which it steeply drops to depths of 100m and more as seen e.g. on Admiralty Chart 159. The continental shelf becomes much more restricted towards the southern part of the study area where it only extends for some hundreds of metres. Further offshore, secondary individual undep areas occur on which coral-reef growth is possible. These shallow zones are mostly related to structural blocks and salt diapirs such as Giftun Island and the Shaab el Erg reef structure (Orsbag-Sperber *et al.*, 1998).

The alignment of the offshore reef structures is not only determined by the occurrence of shallow substrates but also by the dominant currents in this part of the Red Sea. The coral-dominated reef crests are usually built into the strongest current direction as most available nutrients could then be captured by the corals. In this way, the coral structures also protect the leeward parts from the harshest effects of the waves and sand could settle to form shallow lagoons. Most reef crests, therefore, are situated along the northeastern edge of the structures although local differences may occur as was seen on the QuickBird geomorphological zonation map.

A geomorphological zonation map will also give insight in the ecological processes taking place on a coral-reef as these are highly influenced by the physical environment of the reef. The position on the reef will thus determine the distribution of bottom types or habitats in a coral-reef system. The distinctive geomorphological zonation maps will thus contribute to the classification of these bottom types as shown in following section.

3.6 BOTTOM-TYPE CLASSIFICATION

3.6.1 Introduction

According to Mumby and Harborne (1999a), a *coral-reef habitat* is defined by both a specific coral-reef community and its location in the geomorphological structure of the reef. Confusion may occur with the ecological meaning of a community as it is often defined as ‘*a collection of species occurring in the same place at the same time*’ (Fauth *et al.*, 1996: 283). A benthic community, however, only refers to the composing species –faunal as well as floral- and not explicitly to the position in the geomorphological structure. A habitat, additionally, may also be dominated by bare substrate. Therefore, as an alternative for community, the term *bottom type* was launched which is defined as a ‘*basic set of organisms and substrates*’ (Hochberg *et al.*, 2003: 159). The spectral reflectance of these bottom types also composes the signal received by a remote sensor, making it a convenient working tool for image classification (Mumby and Harborne, 1999a; Hochberg and Atkinson, 2003; Hochberg *et al.*, 2003). A coral-reef habitat is consequently described by a comprehensive combination of a specific bottom type at a specific location in the geomorphological reef structure.

Each bottom type can be defined on different levels of detail depending on the applied field sampling technique, the descriptive resolution of the available remote sensing data, the technical expertise, and the thematic user’s needs (Mumby and Harborne, 1999a). The general classification scheme presented in table 3.72 is built up hierarchically, so that more detail can be added if new information becomes available. This hierarchical structure also expresses the uncertainty in differentiating bottom types in detail (Congalton, 1991; Mumby, 2000): at one end, the level-1 bottom-type classes are clearly distinguishable from one another and confusion is minimal; going into more detail, bottom types may share similar characteristics, e.g. low density seagrass is dominated by both seagrass and bare substrate, and misclassification, as a result, becomes more likely (Mumby, 2000).

Optimally, each bottom-type class should be (semi-)quantitatively described (Mumby and Harborne, 1999a; Mumby, 2000). Some examples of quantitative, detailed subdivisions are indicated in table 3.72. The broad-scale field sampling method used for this study, however, did not allow detailed quantitative bottom-type assessments.

Table 3.72. General hierarchical bottom-type classification scheme

| level 1 | level 2 | level 3 | |
|-------------------|----------------------|---|--|
| bare substrate | terrigenous sediment | | |
| | carbonate sand | sand intertidal* sand subtidal* | |
| benthic community | coral rubble | | |
| | coral-dominated | density / % cover coral morphology dominant species spectral characteristics | |
| | | algae-dominated | density / % cover typology** species |
| | | | seagrass-dominated |
| | land | | |
| | deep water | | |
| no data | | | |

* distinction between intertidal and subtidal sand is based on the different spectral reflectance of wet and dry carbonate sands

** differentiation between turf algae, encrusting or coralline algae, fleshy algae, ...

*** leaf area index (e.g. Dierssen *et al.*, 2003)

The potential to discriminate these different bottom types and the level of detail attainable with remote sensing depends on two principle conditions (Chauvaud *et al.*, 1998; Mumby and Harborne, 1999a; Mumby and Edwards, 2002; Hochberg and Atkinson, 2003; Hochberg *et al.*, 2003). First, each bottom type needs to have its own specific spectral signature and the spectral and radiometric resolution of the sensor used must be suited to detect the differences in spectral reflectance. Secondly, but not less important, the spatial resolution of the sensor must be adapted to the complexity of the coral-reef environment.

In situ spectrometry has proven that most coral-reef bottom types have typical spectral signatures with pronounced differences between one another (e.g. Hochberg and Atkinson, 2000; Hochberg *et al.*, 2003; Werdell and Roesler, 2003; LeDrew *et al.*, 2004). In the case of seagrasses, Fyfe (2003) has shown that spectral reflectance values may even be used to

discriminate different species. With coral species, intra-species variability, in contrast, is generally as high as inter-species variability and except for some distinct species, differentiation onto the species level is not expected to be possible (Minghelli-Roman *et al.*, 2002; Kutser *et al.*, 2003).

Spectral differences between bottom types, however, are subtle and often only result from small variations in chlorophyll-pigment concentration and/or composition (Kutser *et al.*, 2003). As these spectral differences usually occur within narrow spectral ranges, the spectral resolution of the sensor should be capable of retrieving these minor variations. Moreover, the reflectance received by an airborne or spaceborne sensor is influenced by the intervening atmosphere and water column. As a result of predominantly water-column attenuation and atmospheric Rayleigh scattering (Lubin *et al.*, 2001; Mumby and Edwards, 2002), the working spectral range is reduced to 400-600nm (Lubin *et al.*, 2001; Minghelli-Roman *et al.*, 2002). This greatly limits the separability of bottom types as the most marked spectral differences occur within the red and near-infrared spectral ranges ($> 570\text{nm}$) (Mumby *et al.*, 1997; Joyce and Phinn, 2002; Kutser *et al.*, 2003). Some spectral differences, however, do occur in the green part of the spectrum, making the differentiation not totally impossible (Lubin *et al.*, 2001; IGOS, 2003; Kutser *et al.*, 2003).

Coral reefs are also very heterogeneous and consist of many intermingled bottom types varying on a sub-metre to metre scale (Hopley, 1996; Dobson and Dustan, 2000; Maeder *et al.*, 2002). Most passive, multispectral remote sensors, in contrast, operate with spatial resolutions ranging from 1 to 30m. Attributing a label to each pixel based on pure spectra therefore is practically impossible, as most pixels record a mixture of bottom types, a so-called *mixel*. The thematic detail of the resulting bottom-type classification will thus vary depending on the spatial resolution of the chosen sensor.

3.6.2 Methodology

3.6.2.1 Pre-processing

3.6.2.1.1 Correction for water-column effects

The correction for the confusing effect of the water column on the spectral reflectance of the seabed has been explained in section 3.3.5 and the positive effects of these corrections were shown. The method of Lyzenga (1978) has been used to transform the original radiance bands into three different DIBs per dataset on which the bottom-

type classification was performed. Specifically for the QuickBird dataset, DIBs have been calibrated once using reference points situated on a sandy bottom type, and once using reference points situated on seagrass beds. In this way, the dependence of the bottom-type classification on the initial water-column correction technique could be tested.

3.6.2.1.2 *Texture analysis*

A classification solely based on the spectral information of a remote sensing dataset omits potentially valuable information incorporated in the dataset concerning the spatial organisation of the coral-reef bottom types (Mumby and Edwards, 2002; Schaale *et al.*, 2002). This spatial information, frequently expressed as a measure of *texture* (Dustan *et al.*, 2001; Joyce and Phinn, 2001; Cuevas-Jiménez *et al.*, 2002; Mumby and Edwards, 2002; Andréfouët *et al.*, 2003), may help to discriminate spectrally similar bottom types. Seagrass beds and coral-dominated parts of a reef, for example, have similar spectral reflectances, especially when recorded by broadband multispectral sensors, but significantly differ in their spatial organisation: while coral-dominated bottom types are typically very heterogeneous, seagrass beds are relatively homogeneous (Dustan *et al.*, 2001; Mumby and Edwards, 2002).

LeDrew *et al.* (2004) even suggest a classification uniquely based on this spatial information. This, however, is very difficult as, to date, no spatial statistical parameters characteristic for each bottom type have been defined (Hochberg and Atkinson, 2003). Texture, therefore, only gives a relative indication of bottom type and for this reason, a combination of spectral information, represented by the DIBs, and the additional texture components is preferred (Joyce and Phinn, 2001; Chen and Stow, 2002; Cuevas-Jiménez *et al.*, 2002; Mumby and Edwards, 2002; Andréfouët *et al.*, 2003; Hochberg and Atkinson, 2003).

Textural information is usually derived by applying a local variance filter to the dataset (Dustan *et al.*, 2001; Joyce and Phinn, 2001; Chen and Stow, 2002; Mumby and Edwards, 2002) although more elaborate methods, such as GETIS statistics (LeDrew *et al.*, 2004), exist. Variance is defined after the correction for water-column effects has been applied (Mumby and Edwards, 2002), in order not to incorporate bathymetric effects. To avoid artefacts in these *textural neo-channels* (Andréfouët *et al.*, 2003), the variance filter also is applied before a land mask is imposed as this

would affect the variance values along the edges of the mask (Mumby and Edwards, 2002).

In order to create a texture layer coinciding with the spatial complexity of the study area, Mumby and Edwards (2002) differentiate the kernel size of the filter depending on the spatial resolution of the dataset used. As Mumby *et al.* (1999) have defined a 20m mean boundary spacing between fine-level bottom types in the Turks and Caicos Islands, they apply a 5 by 5 variance filter on their IKONOS dataset, while using a 3 by 3 filter on the Landsat TM dataset (Mumby and Edwards, 2002). As no information was available on the characteristic patchiness of bottom types in the northwestern Red Sea, a 3 by 3 kernel size has been used on each dataset, irrespective of its spatial resolution.

Determining the benefits of adding textural information to the classification process is difficult as much depends on the spatial complexity of the area under investigation (Andréfouët *et al.*, 2003). While Mumby and Edwards (2002) consider this only worthwhile when using a very-high-resolution dataset to discriminate detailed bottom types in their study area, the situation for the northwestern Red Sea may be completely different. For this reason, the effect of incorporating textural information was tested on the Landsat 7 ETM+, the pan-sharpened Landsat 7 ETM+ and the QuickBird dataset.

3.6.2.2 Processing

3.6.2.2.1 Bottom-type classification

Studies by Mumby and Edwards (2002) and Capolsini *et al.* (2003) indicate that the maximum-likelihood classification algorithm performs best in the case of bottom-type classifications. This classification algorithm is based on image statistics derived from training pixels, representative for each bottom type, which have been determined in the dataset by the interpreter.

In order to be statistically significant, each bottom-type training set should contain at least 30 pixels. The number of training pixels attributed to each bottom type also depends on the heterogeneity of the class and the spatial resolution of the dataset used. Spectrally homogeneous classes only need a minimal number of training pixels to determine reliable training statistics. Heterogeneous classes, conversely, require a larger training set in order to incorporate their characteristic variance. Secondly, the

higher the spatial resolution of the dataset, the more pixels are required as with higher resolution, the intra-class variance of each class will rise (Chen and Stow, 2002).

Based on the information about the coral-reef composition gathered during the three field campaigns, a representative training set for each bottom type could be defined for each dataset. Remark, however, that these training pixels do not necessarily correspond to specific field observation points as these do not equally represent each bottom type. The selection of training pixels was therefore based on circumstantial evidence like, for example, the position in the reef structure or the spectral characteristics of the bottom type.

3.6.2.2.2 Accuracy assessment

An important element in data classification is the final accuracy assessment. A bottom-type classification map can only be used for management purposes after its quality has been estimated. Generally, the thematic accuracy measures refer to the extent to which the classification result agrees with a set of reference data (Ma and Redmond, 1995). Usually, a number of independent field observation points, i.e. points which were not used to calibrate the classification algorithm, are used as reference sample units. Here, these reference sample units have not been collected using a strict probabilistic sample design (Congalton, 1991; Stehman, 1997) as the relative inaccessibility of many parts of the study area made it almost impossible to implement such a sample design.

Table 3.73. Schematic representation of an error matrix

| | reference data | | | | $total\ x_{i+}$ | user accuracy |
|---------------------|----------------|----------|-----|----------|------------------|---------------|
| classification data | x_{11} | x_{12} | ... | x_{1i} | | |
| | x_{21} | x_{22} | | | | |
| | ... | | ... | | | |
| | x_{i1} | | | x_{ii} | | |
| $total\ x_{+i}$ | | | | $total$ | overall accuracy | |
| producer accuracy | | | | N | | |

Different statistical methods and parameters have been developed to estimate the accuracy of a classification⁷¹. The basis for almost all methods is the determination of an *error matrix* or *contingency table* (table 3.73) (Story and Congalton, 1986; Stehman, 1997). In such matrices, the reference data, conventionally represented in the columns, are compared to the classification results, lined in rows, for each corresponding sample unit. Using this error matrix, three basic accuracy parameters are determined (Story and Congalton, 1986):

- *User accuracy*: the probability that a pixel classified on the image actually represent that category in situ. This parameter is calculated as the ratio between the number of correct classifications for class i , x_{ii} , and the total number of observations in row i , x_{i+} . The complementary error, i.e. the number of observations wrongly attributed to class i , is called the *commission error*.
- *Producer accuracy*: the probability that any pixel in that category has been correctly classified. This parameter is calculated as the ratio between the number of correct classifications for class i , x_{ii} , and the total number of reference sample units for that class, x_{+i} . The complementary error, i.e. the number of observations of class i not attributed to that class, is called the *omission error*.
- *Overall accuracy*: this measure represents the total number of pixels correctly classified. This parameter is calculated by dividing the sum of correctly classified observations, $\sum x_{ii}$, by the total number of reference samples, N .

Note that the accuracy assessment has to be performed on the classification results before any post-processing is applied, as this may obscure the basic shortcomings of the classification method (Mumby *et al.*, 1998a).

These measures, however, are case specific and can not be used to statistically compare different classification results. For this aim, the *Tau coefficient* was developed (Ma and Redmond, 1995) which basically expresses the proportionate reduction in error generated by the classification process as compared to the errors generated in a completely random classification. A Tau coefficient of 0.80, for example, indicates that 80% more pixels were classified correctly than would be expected by chance alone (Mumby and Edwards, 2002). As it is a readily interpretable

⁷¹for an overview see e.g. Congalton (1991) and Stehman (1997)

measure, the Tau coefficient usually is a more suitable parameter than the similar Kappa coefficient (Ma and Redmond, 1995; Mumby and Green, 2000a).

If the classification is based on an equal probability of occurrence of each bottom-type class, Tau is determined as follows (Ma and Redmond, 1995):

$$T_e = \frac{(P_o - P_r)}{(1 - P_r)} \quad (3.70)$$

With: P_o : overall accuracy

$$P_r = \frac{\sum(x_{i+} \times x_{ii})}{N^2} \quad (3.71)$$

This parameter not only represents the overall accuracy but also takes into account the number of misclassifications. Therefore, it is generally lower than the overall accuracy measure (Mumby and Green, 2000a) and probably underestimates the true probability of a correct classification (Stehman, 1997). The distribution of the Tau coefficient, however, approaches a Gaussian distribution (Ma and Redmond, 1995) which allows statistical *Z-tests* to be performed to examine the similarity between two classifications. Formula 3.72 represents a Z-test adapted to a two-sample Tau comparison case (Ma and Redmond, 1995; Stehman, 1997). If Z-values higher or equal to 1.96 are attained, the Tau coefficients and by extension also the classification results have a 95% probability of being different (Mumby and Green, 2000a).

$$Z = \frac{(T_1 - T_2)}{\sqrt{(\sigma_1^2 + \sigma_2^2)}} \quad (3.72)$$

With: T_i : Tau coefficient for classification i

$$\sigma_i^2 = \frac{P_{oi} \times (1 - P_{oi})}{N \times (1 - P_{ri})^2} \quad (3.73)$$

i : the number of the classification.

3.6.2.3 Post-processing

3.6.2.3.1 Contextual editing

Because of the spectral similarities of many bottom types, even after the conversion to DIBs and the potential positive effects of incorporating textural information, discriminating the different bottom types remains difficult using datasets derived from sensors with a low spectral resolution. Coral reefs, however, often exhibit predictable geomorphological and ecological zonation patterns according to gradients of depth and wave exposure (Huston, 1994; Mumby *et al.*, 1998a) (see section 2.4.2.2.2). Applying post-processing classification rules based on these zonation patterns thus reduces known misclassifications (Groom *et al.*, 1996; Mumby *et al.*, 1998a; Mumby and Edwards, 2002; Andréfouët *et al.*, 2003; Hochberg *et al.*, 2003), as already shown for coarse-level mapping of coral reefs (Mumby *et al.*, 1998a; Mumby and Edwards, 2002).

Such contextual editing rules must be applicable throughout the entire study area and not only to those regions most familiar to the interpreter in order not to create bias or misleading improvements to the classification result (Hutchinson, 1982; Mumby *et al.*, 1998a). For this reason, only general decision rules can be used which are based on ecological zonation patterns confirmed by worldwide observations.

Seagrass, for example, generally occurs in sheltered environments (section 2.4.4). Pixels which have been classified as seagrass and occur on a fore reef or reef crest zone as defined by the corresponding geomorphological zonation map are therefore very likely misclassifications. These zones highly exposed to wave energy, in contrast, are favourable to coral growth. As coral-dominated and dense seagrass-covered bottom types are spectrally very similar, pixels classified as seagrass in these cases are assumed to represent a coral-dominated bottom type in reality. A contextual editing rule can subsequently be set up which reclasses seagrass-dominated pixels on the fore reef or reef crest zone to the coral-dominated class (Mumby *et al.*, 1998a; Mumby and Harborne, 1999a; Mumby and Edwards, 2002; Hochberg and Atkinson, 2003).

Seagrasses also live almost solely in the subtidal range (section 2.4.4). In the Caribbean, seagrass beds were usually not found on reef flats or back reefs shallower than 1.2m (Mumby and Harborne, 1999a; Palandro, 2000; Hochberg and Atkinson, 2003). This upper depth limit remains valid for the northwestern Red Sea, where many shallow zones are dominated by algae and some coral species (Purkis *et al.*, 2002). As spectral confusion may exist between seagrass- and algae-dominated bottom types, a

similar contextual rule as described before was developed. This rule changes seagrass-dominated pixels to the algae-dominated class if they occur on a back reef/reef flat zone shallower than 1.2m. This depth, corresponding to the maximal tidal range recorded for the entire Red Sea (Edwards, 1987), was derived from the bathymetric maps created in section 3.4.

Two additional editing rules will finally be applied to mask the land and deep water. The land is labelled using the same mask utilised on the individual DIBs, whereas the elimination of deep water is based on the deep-water areas defined on the geomorphological zonation map.

3.6.2.3.2 Coastal habitat mapping

To conclude, the resulting bottom-type classification map is coupled to the geomorphological zonation map derived for the same dataset in order to obtain a coastal habitat map (Mumby and Harborne, 1999a). Each polygon in this habitat map is assigned two independent labels, one for the bottom type and one for the geomorphological zone. The combined classification scheme is both hierarchical and open-ended as are the composing classification schemes.

3.6.3. Implementation

3.6.3.1 Original Landsat 7 ETM+ dataset

3.6.3.1.1 Pre-processing

a. Water-column correction

The three depth-invariant bottom-index bands (DIB_{12} , DIB_{13} and DIB_{23}) as determined in section 3.3.5.2.1 were used to classify the original Landsat 7 ETM+ dataset. As the classification scripts integrated in ILWIS 3.2 only accept 8bit input data, the DIBs were converted following formula 3.74 which was based on the specific distribution of values in each band as enlisted in table 3.74.

$$DIB_{ij,clas} = IFF(DIB_{ij} = 0, 0, ROUND[(DIB_{ij} + 3) \times 33.33]) \quad (3.74)$$

With: DIB_{ij}^{clas} : depth-invariant bottom index ij after 8bit conversion

DIB_{ij} : original DIB_{ij} value

ROUND: round value to the nearest positive integer

Table 3.74. Minimum and maximum original Landsat 7 ETM+ DIB values

| | minimum | maximum |
|------------|---------|---------|
| DIB_{12} | -2.98 | 3.11 |
| DIB_{13} | -2.57 | 3.76 |
| DIB_{23} | -2.48 | 3.61 |

b. Texture analysis

As stated before, the textural neo-channels were derived from the original Landsat 7 ETM+ DIBs using a 3 by 3 variance filter which is based on formula 3.75. The value ranges of the textural neo-channels were subsequently converted to the 8bit domain using a histogram equalisation stretch with a 0% interval. A land mask was added afterwards.

$$Var = \frac{\sum (x - x_m)^2}{(N - 1)} \quad (3.75)$$

With: x : pixel value in the centre of the kernel

x_m : mean pixel value in the kernel (3 x 3)

N : number of pixels in the kernel (3 x 3)

An excerpt from the textural neo-channel derived from DIB_{12} is shown in grey-scale in figure 3.69. In this figure, dark colours represent low variance, i.e. homogeneous substrate, while brighter colours represent high variance, i.e. heterogeneous bottom types. The blocky appearance resulted from the use of a 3 by 3 filter.

3.6.3.1.2 Processing

a. Bottom-type classification

Due to the relatively coarse descriptive resolution of the Landsat 7 ETM+ dataset, only a broad-level bottom-type classification could be achieved. Table 3.75 gives an overview of the bottom-type classes distinguished with this particular dataset.

Table 3.75. Hierarchical bottom-type classification scheme applied on the Landsat 7 ETM+ dataset

| level 1 | level 2 | level 3 |
|-------------------|--------------------|-----------------|
| bare substrate | carbonate sand | sand intertidal |
| | | sand subtidal |
| benthic community | coral-dominated | |
| | algae-dominated | |
| | seagrass-dominated | |
| land | | |
| deep water | | |
| no data | | |

A colour composite combining the three DIBs -i.e. DIB₁₂clas, DIB₁₃clas and DIB₂₃clas represented respectively in blue, green and red- was used to define training pixels for each bottom type. On the feature spaces (fig. 3.70), two-dimensionally representing the DIB values for each training pixel, each bottom-type class could be clearly distinguished. Although characterised by a high standard deviation, no major problems were to be expected with the deep-water and sand subtidal classes as these were clearly separated from the other classes. Some overlap between the different benthic community classes and the sand intertidal class, in contrast, did occur. This overlap could be explained by the possibility that sandy substrates are covered by a thin layer of algae or by the occurrence of low-density benthic stands. Overlap between the three benthic-community classes was explained by the spectral similarity of these bottom types. Although each benthic community was represented by a distinctive cluster, difficulties were to be expected when separating these classes.

Table 3.76 and figure 3.71 give an overview of the statistics derived for each bottom type based on the samplesets defined for both the DIBs and the textural neo-channels. Each bottom type could statistically be separated based on the mean DIB-values although differences between coral, algae, and seagrass-dominated bottom types were minimal. In the textural neo-channels, these benthic community classes were more distinct. As could be expected, the coral-dominated bottom type was characterised by the highest textural values, i.e. the highest spatial heterogeneity. Remarkably, the seagrass-dominated bottom type was more heterogeneous than the

algae-dominated class. This resulted from the incorporation of different seagrass densities into one training set. The training statistics for these texture neo-channels were unfortunately characterised by high standard deviation values, which complicated the distinction between the three benthic community classes (fig. 3.71).

Table 3.76. Mean and standard deviations for each bottom-type class derived from the original Landsat 7 ETM+ training sets

| | sand intertidal | | sand subtidal | | coral-dominated | | algae-dominated | | seagrass-dominated | | deep water | |
|------------------------|-----------------|-------|---------------|-------|-----------------|-------|-----------------|-------|--------------------|-------|------------|-------|
| | mean | stdev | mean | stdev | mean | stdev | mean | stdev | mean | stdev | mean | stdev |
| DIB ₁₂ clas | 124.4 | 3.1 | 137 | 3.4 | 113.4 | 3.3 | 120.8 | 1.7 | 118.3 | 1.5 | 105.5 | 11.7 |
| DIB ₁₃ clas | 185.8 | 4.4 | 181.3 | 12.4 | 163 | 5 | 178.6 | 2.2 | 172.2 | 1.8 | 129.5 | 11.1 |
| DIB ₂₃ clas | 172.3 | 2.6 | 156.8 | 16.1 | 159.7 | 3.3 | 168.3 | 2.2 | 165.3 | 2.1 | 130 | 8.6 |
| Texture12 | 106.6 | 29.4 | 145.3 | 23 | 155.9 | 14 | 120.5 | 21.8 | 138.5 | 17.1 | 181.8 | 8.6 |
| Texture13 | 137.7 | 26.9 | 171.5 | 25.9 | 183.4 | 16 | 149.1 | 17.1 | 170.3 | 17.5 | 208.9 | 9.7 |
| Texture23 | 123.7 | 26.5 | 182.1 | 25.9 | 170.4 | 15.6 | 136.7 | 17.7 | 160.9 | 11.8 | 202.2 | 9.4 |
| # samples | 83 | | 261 | | 110 | | 70 | | 52 | | 88 | |

These sample statistics were subsequently used to classify the original Landsat 7 ETM+ dataset. A maximum-likelihood classification algorithm was applied with an empirically determined threshold of 30. This classification was separately performed for a data collection containing only the three DIBs as well as for a collection containing both the DIBs and textural neo-channels. This allowed the estimation of the added value of the textural neo-channels.

b. Accuracy assessment

Out of a total of 222 field observations, 171 validation sample units were selected to test the accuracy of the resulting bottom-type classifications (annex XVI). The remaining field data points were omitted as these were taken over small patches which were not detectable with the Landsat 7 ETM+ spatial resolution. Error matrices for the DIB-based classification and the DIB-texture-based classification are represented in table 3.77 and 3.78 respectively.

Both error matrices resulted in an overall accuracy of 60%. This measure could therefore not be used to determine the best classification method. Although individual user and producer accuracy values for each class were different for both classification results, they showed the same trend and could not be used either. Remark also that the number of validation points for each class is too low to make any comments on the individual producer and user accuracies. Tau coefficients showed that for both

approaches, 45% more pixels were correctly classified as would be expected from a random classification. This, at least, illustrated that the classification approach had some value. As these coefficients were identical, a Z-test to define the best classification approach, however, was not relevant.

Table 3.77. Error matrix for the classification of the original Landsat 7 ETM+ dataset based on the DIB layers

| | sand | coral | algae | seagrass | <i>total</i> | user accuracy |
|--------------------------|-------------|------------|------------|------------|--------------|-------------------------|
| sand | 65 | 11 | 2 | 25 | 103 | 63% |
| coral | 1 | 8 | 0 | 5 | 14 | 60% |
| algae | 8 | 3 | 3 | 5 | 19 | 16% |
| seagrass | 1 | 7 | 0 | 27 | 35 | 77% |
| <i>total</i> | 75 | 29 | 5 | 62 | 171 | |
| producer accuracy | 87% | 30% | 60% | 44% | | 60% |
| Tau coefficient | 0.45 | | | | | overall accuracy |

Table 3.78. Error matrix for the classification of the original Landsat 7 ETM+ dataset based on the DIBs and the textural neo-channels

| | sand | coral | algae | seagrass | <i>total</i> | user accuracy |
|--------------------------|-------------|------------|------------|------------|--------------|-------------------------|
| sand | 66 | 9 | 2 | 29 | 106 | 62% |
| coral | 1 | 10 | 0 | 7 | 18 | 56% |
| algae | 4 | 3 | 3 | 3 | 13 | 23% |
| seagrass | 4 | 7 | 0 | 23 | 34 | 68% |
| <i>total</i> | 75 | 29 | 5 | 62 | 171 | |
| producer accuracy | 88% | 34% | 60% | 35% | | 60% |
| Tau coefficient | 0.45 | | | | | overall accuracy |

The validity of these statistical accuracy assessments, however, might be questioned. As not all parts of the reef systems were equally accessible during the field campaigns, a statistical field sampling method could not be performed. Moreover, those areas most subject to misclassifications between coral, algae and seagrass, i.e. the reef crests and reef flats, were least represented in the ground truth data. Therefore, only a limited number of reference sample units were available for the algae-dominated and coral-dominated bottom types. Besides, a minimum of 50 sample units per class is required for a sound statistical accuracy assessment (Hay, 1979; Congalton, 1991). This minimum even augments to 75 or 100 samples if a large area is covered (Congalton,

1991). As this minimum requisite was not met, the statistical validity of the parameters calculated was greatly limited (Stehman and Czaplewski, 1998). The statistical measures should therefore not be strictly interpreted but rather be seen as indicators of possible trends in the accuracy of the classification result (Andréfouët *et al.*, 2003; Capolsini *et al.*, 2003). Consequently, these statistics were considered inappropriate to define the best classification approach and a visual comparison of both results was performed.

c. Visual validation of integrating textural information

Figures 3.72 and 3.73 respectively represent a subset of the classification of the original Landsat 7 ETM+ DIB dataset and the DIB + texture layers dataset. Based on a visual analysis, important differences were noted. The incorporation of textural information did improve the separation between coral-dominated and seagrass-dominated bottom types as expected. Especially along the reef crests and on the fringing back reefs, pixels classified as seagrass-dominated in the result based only on the DIBs dataset, were classified as coral-dominated in the result incorporating both DIBs and textural neo-channels. Unfortunately, some pixels correctly classified as seagrass-dominated were transformed to the coral-dominated class as well. Contrarily, some artefacts were created in the DIB-texture-based result. The border between two adjacent bottom types, for example, was displaced because of the use of the 3 by 3 variance filter.

Some pixels remained unclassified due to errors introduced during the water-column correction, but also partly due to the classification threshold. Most of these artefacts and voids, however, were limited to the deep water. These errors were therefore considered of less importance and the classification method incorporating the textural neo-channels was considered to be slightly superior to the method solely based on the DIBs. Post-processing was therefore restricted to this result.

3.6.3.1.3 Post-processing

a. Contextual editing

Although the classification result was visually improved by the integration of textural information, numerous errors remained. Therefore, the contextual rules stated below were applied to minimize known misclassification errors. The general rules described in section 3.6.2.3.1 were implemented in contextual rule 1, 2 and 4. Contextual rule 3

was added to improve classifications over dense patch reefs. It was assumed that pixels labelled as seagrass-dominated on these geomorphological zones, were in reality dominated by corals. Contextual rules 5 and 6, respectively, mask out deep water and land.

```
Context1 = iff (((classification = "seagrass-dominated") AND (geomorphology = "fore reef")), "coral-dominated", classification)

Context2 = iff (((classification = "seagrass-dominated") AND (geomorphology = "reef crest")), "coral-dominated", context1)

Context3 = iff (((classification = "seagrass-dominated") AND (geomorphology = "patch reef dense")), "coral-dominated", context2)

Context4 = iff (((classification = "seagrass-dominated") AND (geomorphology = "back reef/reef flat") AND (bathymetry > -1.2)), "algae-dominated", context3)

Context5 = ifundef(bathymetry, (iff(geomorphology = "deep water", "deep water", context4)), context4)

Context6 = iff(geomorphology = "land", "land", context5)
```

Figure 3.74a shows the resulting contextually edited classification, while figure 3.74b shows a subset of this map. The effects of contextual editing can clearly be noted. Most misclassifications between the coral-dominated and seagrass-dominated classes on the reef crests as seen in figure 3.73 were removed. The shallowest parts of the back reef/reef flats were also appropriately assigned to an algae-dominated or sand intertidal bottom type. The use of a deep-water mask, i.e. contextual rule 5, cleared up the noisy classification result as shown in figure 3.73.

Not all problems, though, could be solved. Confusion between seagrass and coral remained a problem over diffuse reef patches. As these reef patches may eventually become colonised by seagrasses, no general contextual rule could be set up. Problematic was also the diffuse pattern of seagrass-dominated and coral-dominated pixels in medium deep waters, for example between the coastline and the Shaab Magawish reef (figure 3.74b). These pixels, potentially, represent the coral carpets as defined by Riegl and Piller (2000) with the seagrass-dominated pixels being misclassifications of coral-dominated bottom types. Alternatively, these patterns might result from the memory effect over this area in the Landsat 7 ETM+ dataset as already discussed in section 3.4.4.2. Ground-truth information for these areas was unfortunately lacking to check these hypotheses.

The classification of the dredged coastal areas, especially in El Gouna (fig. 3.74a), was problematic as well. Some of these recently dredged parts were classified as coral-dominated whereas the turbid environment and the limited time span since the dredging make coral colonisation less probable. Errors in the ancillary datasets were also responsible for some remaining problems. Delineation errors on the different geomorphological zones allowed seagrass-dominated pixels to remain in the reef crest zones. With a mean residual error of 1.13m on the bathymetric model, uncertainty was also introduced in the contextual rule separating seagrass-dominated and algae-dominated pixels in the shallow back reef/reef flats.

b. Coastal habitat mapping

The contextually edited classification result based on three water-column-corrected bands and three additional textural neo-channels was finally combined with the geomorphological zonation map derived in section 3.5.2.1 to form a coastal habitat map. For representation reasons, an additional 3 by 3 majority filter was applied to the result. Although this removed some of the detail, it improved the overall readability of the coastal habitat map. An unfiltered subset could always be created to represent a more detailed view on specific reef structures. The filtered map was subsequently vectorised and each label was assigned a double code. An example of part of the coastal habitat map is given in figure 3.75. The colours represent the geomorphological zonation, while the symbols indicate the dominant bottom type.

The bank/shelf is predominantly covered with sand and an occasional seagrass bed. This largely reflects the actual composition of the bank/shelf area although at greater depths, the influence of the water column might hinder an accurate classification. The reef crests are dominated by coral which reflects reality, but largely result from the applied contextual editing. The reef flat/back reef areas, conversely, are mostly covered by algae and sand. Some seagrass stands, however, do occur on the deeper parts of these geomorphological zones. The nearshore diffuse coral-reef patches are composed of sand, algae and seagrass. It was not possible to discriminate coral-dominated bottom types although these were encountered on these patches in the field. Some of the seagrass-dominated pixels are therefore considered as misclassifications. Other erroneous classifications remained as well, especially along the coastline. This zone appeared difficult to classify using the original Landsat 7 ETM+ dataset. All areas deeper than 21m have been masked out and are represented

as deep-water areas. This is logical as below these depths, reflectance of the seabed is no longer expected and any classification result for these parts is likely to be erroneous. Some parts are also represented in the no data class. Usually, these pixels result from a malfunctioning of the vectorisation process. Those pixels, fortunately, are rather restricted and usually occur in deeper waters, so they do not significantly influence the classification result.

3.6.3.2 Pan-sharpened Landsat 7 ETM+ dataset

3.6.3.2.1 Pre-processing

a. Water-column correction

As for the original Landsat 7 ETM+ dataset, the DIBs calculated for the pan-sharpened Landsat 7 ETM+ dataset in section 3.3.7.2.5 needed to be converted to the 8bit domain. For this purpose, formula 3.76 was constructed based on the specific range of values in these bands (table 3.79).

Table 3.79. Minimum and maximum pan-sharpened Landsat 7 ETM+ DIB values

| | Minimum | maximum |
|-----------------------|---------|---------|
| XL7_DIB ₁₂ | -5.839 | 5.483 |
| XL7_DIB ₁₃ | -5.060 | 5.227 |
| XL7_DIB ₂₃ | -5.365 | 5.295 |

$$XL7_DIB_{ij}clas = IFF(XL7_DIB_{ij} = 0, 0, ROUND[(XL7_DIB_{ij} + 6) \times 20]) \quad (3.76)$$

With: XL7_DIB_{ij}: DIB_{ij} value for the pan-sharpened dataset

b. Texture analysis

Textural neo-channels were derived from the pan-sharpened DIBs using the 3 by 3 variance (formula 3.75) filter before the land mask was applied. These textural layers were subsequently transformed to the 8bit domain using a histogram equalisation stretch with a 0% confidence interval.

3.6.3.2.2 Processing

a. Bottom-type classification

The same bottom-type classes as for the original Landsat 7 ETM+ dataset were distinguished. Training pixels were selected at the same locations as well, although in higher amounts to avoid spatial autocorrelation (Capolsini *et al.*, 2003) (table 3.80).

Table 3.80. Mean and standard deviations for each bottom-type class derived from the pan-sharpened Landsat 7 ETM+ training sets

| | sand intertidal | | sand subtidal | | coral-dominated | | algae-dominated | | seagrass-dominated | | deep water | |
|------------------------|-----------------|-------|---------------|-------|-----------------|-------|-----------------|-------|--------------------|-------|------------|-------|
| | Mean | stdev | mean | stdev | mean | stdev | mean | stdev | mean | stdev | mean | stdev |
| DIB ₁₂ clas | 133.5 | 1.6 | 141.6 | 2 | 127.4 | 2.6 | 131 | 1.6 | 130.6 | 1 | 122.9 | 4.8 |
| DIB ₁₃ clas | 174.5 | 2.2 | 169.6 | 7.3 | 160.4 | 4.4 | 169.6 | 3 | 166.6 | 1.9 | 138.9 | 4.4 |
| DIB ₂₃ clas | 166.8 | 1.3 | 155 | 9.2 | 158.4 | 3 | 164.2 | 2.4 | 162.2 | 1.5 | 139.8 | 4.3 |
| Texture12 | 80.7 | 28.1 | 135.8 | 12.1 | 132.2 | 17.6 | 107.8 | 19.7 | 119.2 | 18.3 | 164.5 | 18.5 |
| Texture13 | 100.5 | 26.8 | 151.6 | 24.4 | 139 | 16.5 | 115.8 | 14.7 | 133.3 | 12.5 | 168.4 | 19.7 |
| Texture23 | 99.6 | 25.7 | 148.7 | 21.4 | 131.3 | 12.6 | 109.9 | 15.8 | 128 | 9.6 | 163.6 | 16.3 |
| # samples | 284 | | 1041 | | 372 | | 237 | | 217 | | 329 | |

As was the case for the original Landsat 7 ETM+ dataset, the deep-water and sand subtidal classes were clearly distinguishable in each DIB feature space (fig. 3.76), although some overlap occurred with the benthic community samples. The three benthic community classes and the sand intertidal class were also more intermingled. Most important, however, was the almost total overlap between the algae-dominated and seagrass-dominated classes which might seriously hinder the classification process. The same trends were exemplified by the sample statistics shown in table 3.80 and figure 3.77. Remark that the mean values in table 3.80 were not similar to the values given in table 3.76 for the original Landsat 7 ETM+ dataset. This was caused by the larger number of pixels involved and the inevitable spectral changes in the pan-sharpening process.

As classification algorithm, a maximum-likelihood method using an empirically determined threshold of 30 was applied. The classification was separately performed on the DIBs and on a combination of DIBs and textural neo-channels.

b. Accuracy assessment

The same 171 reference sample units as used for the original Landsat 7 ETM+ dataset were selected to construct error matrices (annex XVI). Tables 3.81 and 3.82 respectively depict the error matrix for the classification solely based on the DIBs and

the error matrix for the classification based on both DIBs and textural neo-channels. The overall accuracy equalled 61% and 60% respectively, similar values as for the original Landsat 7 ETM+ datasets. Although the result solely based on the DIBs had a higher overall accuracy, its Tau coefficient was slightly lower than obtained for the DIB-texture classification. The Z-test ($Z = 0.114$), however, revealed that this was not a significant ($p < 0.05$) difference.

Table 3.81. Error matrix for the classification of the pan-sharpened Landsat 7 ETM+ dataset based on the DIBs

| | sand | coral | algae | seagrass | <i>total</i> | user accuracy |
|--------------------------|-------------|------------|------------|------------|--------------|-------------------------|
| sand | 60 | 13 | 2 | 24 | 99 | 61% |
| coral | 1 | 10 | 0 | 3 | 14 | 71% |
| algae | 9 | 1 | 2 | 2 | 14 | 14% |
| seagrass | 5 | 5 | 1 | 33 | 44 | 75% |
| <i>total</i> | 75 | 29 | 5 | 62 | 171 | |
| producer accuracy | 80% | 34% | 40% | 53% | | 61% |
| Tau coefficient | 0.47 | | | | | overall accuracy |

Table 3.82. Error matrix for the classification of the pan-sharpened Landsat 7 ETM+ dataset based on the DIBs and textural neo-channels

| | sand | coral | algae | seagrass | <i>total</i> | user accuracy |
|--------------------------|-------------|------------|------------|------------|--------------|-------------------------|
| sand | 55 | 11 | 2 | 18 | 86 | 64% |
| coral | 1 | 10 | 0 | 5 | 16 | 63% |
| algae | 9 | 3 | 2 | 3 | 17 | 12% |
| seagrass | 10 | 5 | 1 | 36 | 52 | 69% |
| <i>total</i> | 75 | 29 | 5 | 62 | 171 | |
| producer accuracy | 73% | 34% | 40% | 58% | | 60% |
| Tau coefficient | 0.48 | | | | | overall accuracy |

c. Visual validation of integrating textural information

As the statistical tests did not reveal significant differences between the two classification approaches for the pan-sharpened Landsat 7 ETM+ dataset, a visual analysis of two subsets (fig. 3.78 and fig. 3.79) was performed. This, however, did not allow preferring one of the results either, as the introduction of textural neo-channels into the classification process did not improve the result to the same extent as for the original Landsat 7 ETM+ dataset. Moreover, there was notably more confusion

between other classes, especially between seagrass-dominated and algae-dominated bottom types.

d. Validation of the pan-sharpening process

To test whether the pan-sharpening of the Landsat 7 ETM+ dataset did improve the classification, each result was statistically and visually compared with the corresponding original Landsat 7 ETM+ classification. Z-tests checking the differences between the classifications of the original and the pan-sharpened Landsat 7 ETM+ dataset for both the classification only based on the DIBs ($Z = 0.271$) and the classification based on both DIBs and textural neo-channels ($Z = 0.370$) revealed that the pan-sharpening of the dataset did not significantly ($p < 0.05$) improve the classification accuracy.

The visual comparison was restricted to the best result of the original Landsat 7 ETM+ dataset -being the DIB-texture-based classification (fig. 3.73)- and the corresponding pan-sharpened Landsat 7 ETM+ classification (fig. 3.79). This did not reveal significant improvements either. Both classifications represented the major coral-reef composition in the study area in a similar way, although the higher spatial resolution of the pan-sharpened dataset allowed some more detail. These spatial improvements, however, were minimal while additional artefacts were introduced by scanning errors occurring in the panchromatic Landsat 7 ETM+ band and the loss of spectral integrity during the pan-sharpening process. More reef-flat/back reef zones and reef crests, for example, were classified as seagrass-dominated in the pan-sharpened result. More bank/shelf areas were also classified as being coral-dominated, e.g. between the land and the Shaab Magawish reef, which were likely to be misclassifications.

On the whole, the pan-sharpening of the Landsat 7 ETM+ dataset did not markedly improve the classification result and this approach was therefore discarded from further analysis.

3.6.3.3 QuickBird dataset

3.6.3.3.1 Pre-processing

a. Water-column correction

As stated in section 3.6.2.1.1, two different water-column corrections were applied on the QuickBird dataset. One was based on pixels selected over a homogeneous sandy bottom type (QB_DIB), while the other was calibrated with pixels collected over homogeneous seagrass patches (QB_DIBsg). The aim was to test whether the latter approach would improve the discrimination between coral-dominated and seagrass-dominated bottom types.

Table 3.83. Minimum and maximum QuickBird DIB values calibrated over sand (QB_DIB) and seagrass (QB_DIBsg)

| | minimum | maximum |
|------------------------|---------|---------|
| QB_DIB ₁₂ | -1.97 | 2.83 |
| QB_DIB ₁₃ | -1.80 | 5.16 |
| QB_DIB ₂₃ | -2.49 | 5.60 |
| QB_DIBsg ₁₂ | -2.05 | 3.10 |
| QB_DIBsg ₁₃ | -1.81 | 5.20 |
| QB_DIBsg ₂₃ | -2.45 | 5.37 |

Similar to the Landsat 7 ETM+ dataset processing, the DIBs determined in section 3.3.5.2.3 needed to be converted to the 8bit domain. Based on the specific range of values in each DIB (table 3.83), conversion formula 3.77 was determined in order to optimize the contrast in the resulting bands. As all negative values in the dataset occurred in deep-water areas, they were omitted from further processing. The same formula was applied on the DIBs calibrated over seagrass as the range of values in these bands was similar (table 3.83).

$$QB_DIB_{ij}^{clas} = IFF(QB_DIB_{ij} = 0, 0, ROUND[(QB_DIB_{ij} \times 40)]) \quad (3.77)$$

b. Texture analysis

Textural neo-channels for both DIB datasets were determined following the procedure applied on the Landsat 7 ETM+ dataset. DIBs were calculated without the application of a land mask and, subsequently, a 3 by 3 variance filter was applied. Finally, each textural layer was converted to the 8bit domain by the application of a histogram equalisation stretch with a 0% confidence interval.

3.6.3.3.2 Processing**a. Bottom-type classification**

With the QuickBird dataset, more detailed bottom-type classes could be determined because of the significantly higher spatial resolution (table 3.84). As noted by Roelfsema *et al.* (2002), Stephens *et al.* (2003) and Heil *et al.* (2004), sandy bottoms may be colonised by a thin layer of algae which alter the spectral reflectance of that bottom type. For this reason, a separation in the algae-dominated class was introduced covering the transition between a dense algal coverage and a bare sandy substrate. Due to the lack of ground truth data, this transition could not be quantified, although clear differences occurred in the spectral reflectance. Similarly, a distinction was made between two densities of seagrass stands. In addition, a coral-rubble class was added to the bare substrate group as this bottom type was frequently encountered during field sampling. The coarse structure of this bottom type was expected to influence its spectral reflection so that it could be discriminated from the finer, more homogeneous carbonate sands.

For each DIB dataset, a differentiation was made between a classification solely based on the DIBs and one based on a combination of DIBs and textural neo-channels. A maximum-likelihood classification algorithm was applied on all datasets with the use of an empirically determined threshold of 10. As the QuickBird scene only covered part of the entire study area, other training pixels were selected as the ones used for the classification of the Landsat 7 ETM+ datasets. The selection of training sets was based on field knowledge without specific relation to the collected ground truth data. The same training pixels were used to classify both DIB datasets.

Table 3.84. Hierarchical bottom-type classification scheme applied on the QuickBird dataset

| level 1 | level 2 | level 3 | |
|-------------------|--------------------|-------------------|--|
| bare substrate | carbonate sand | sand intertidal | |
| | | sand subtidal | |
| benthic community | coral rubble | | |
| | coral-dominated | density / % cover | |
| | algae-dominated | high density | |
| | | medium density | |
| | | low density | |
| | seagrass-dominated | high density | |
| | low density | | |
| land | | | |
| deep water | | | |
| no data | | | |

- classification based on QB_DIB

Figure 3.80 represents the three feature spaces in the QB_DIB space. Note the different scale for the third feature space. Each class was represented by a distinct cluster although some overlap occurred, especially between the different benthic-community classes. As with the Landsat 7 ETM+ dataset, no problems were expected with the deep-water and 'sand subtidal' classes. The 'sand intertidal' and coral-rubble bare-substrate classes were both characterised by a distinct cluster, although some overlap existed with the 'algae: low density' class. Some overlap also existed between the coral-dominated and 'seagrass: high density' classes.

High-density and low-density seagrass classes were separable on each feature space, with the 'seagrass: low density' class having the highest QB_DIB values. The same relation to density was noted for the three algae-dominated subdivisions. Significant overlap, though, existed between the seagrass-dominated classes and the algae-dominated bottom types. There could especially be confusion between the 'algae: high density' and the 'seagrass: high density' classes and between the 'algae: medium density' and 'seagrass: low density' classes. However, they still had different mean QB_DIB-values, so they could be separated by the classification algorithm.

Table 3.85 and figure 3.81 represent the statistics derived from the training pixels for each bottom type in the QB_DIB dataset. Each class had specific characteristics which were distinct from one another. The bare surface classes obviously had the highest mean QB_DIB values. A clear distinction could also be made between the different level-2 benthic-community classes and even for the more detailed subdivisions, the mean QB_DIB values showed detectable differences. If the benthic cover decreases, more bare substrate becomes part of the signal received by the sensor and, consequently, mean QB_DIB values rise.

Table 3.85. Mean and standard deviations for each bottom-type class derived from the QB_DIB training sets

| | sand intertidal | | sand subtidal | | coral rubble | | coral- dominated | | algae: high density | |
|------------------------|--------------------------------|-------|-------------------------------|-------|-----------------------------------|-------|----------------------------------|-------|--------------------------------|-------|
| | mean | stdev | mean | stdev | mean | stdev | mean | stdev | mean | stdev |
| DIB ₁₂ clas | 37.3 | 0.7 | 44.7 | 2.5 | 33.6 | 1.1 | 7.6 | 5.7 | 20.2 | 1.3 |
| DIB ₁₃ clas | 109.3 | 1.3 | 113.6 | 11.8 | 105.1 | 1.6 | 52.1 | 10.2 | 76.9 | 1.6 |
| DIB ₂₃ clas | 91.8 | 1.4 | 93.5 | 16.2 | 92.5 | 1.2 | 57.9 | 5.2 | 72.1 | 1.2 |
| Texture ₁₂ | 8.1 | 3.9 | 98.1 | 40.6 | 42.3 | 27.2 | 183 | 20.3 | 79.3 | 26.5 |
| Texture ₁₃ | 7.3 | 2.8 | 162.8 | 56.7 | 33 | 17.8 | 180.2 | 29.7 | 55.1 | 26.1 |
| Texture ₂₃ | 9 | 3.7 | 177.2 | 52.7 | 32.7 | 13.9 | 134.1 | 32.9 | 35 | 13.1 |
| <i># samples</i> | 748 | | 2362 | | 126 | | 462 | | 72 | |
| | algae: med. density | | algae: low density | | seagrass: high density | | seagrass: low density | | deep water | |
| | mean | stdev | mean | stdev | mean | stdev | mean | stdev | mean | stdev |
| DIB ₁₂ clas | 30 | 1.2 | 33 | 2 | 17.7 | 3.6 | 26 | 2 | 32.2 | 5.3 |
| DIB ₁₃ clas | 94.4 | 1.7 | 101 | 2.3 | 71.3 | 4.9 | 89 | 3.5 | 69.9 | 9.4 |
| DIB ₂₃ clas | 81.8 | 1.1 | 88 | 2 | 71.5 | 4.1 | 82 | 3.1 | 50.5 | 7.1 |
| Texture ₁₂ | 25.8 | 20.4 | 43 | 22.4 | 153.3 | 27.4 | 72 | 40.7 | 153 | 40.9 |
| Texture ₁₃ | 18.6 | 11.2 | 32 | 20.1 | 121.3 | 34.6 | 74 | 38.5 | 128 | 38.4 |
| Texture ₂₃ | 18.2 | 11.3 | 43 | 25.1 | 103.7 | 36.8 | 60 | 27.7 | 131 | 44.2 |
| <i># samples</i> | 457 | | 253 | | 810 | | 653 | | 326 | |

The different classes were also discriminated using the textural neo-channels (table 3.85 and figure 3.81), although the higher standard deviation values made the differentiation more difficult. Except for the sand subtidal class, the coral-dominated bottom type clearly was the most heterogeneous. As with the Landsat 7 ETM+ dataset, it was followed by the seagrass-dominated bottom type, while the

algae-dominated bottom types were more homogeneous. The high density benthic community classes were remarkably more heterogeneous than the corresponding low density classes, although dense stands were expected to be more homogeneous than sparse patches composed of a mixture of benthic cover and bare substrate.

Table 3.86. Mean and standard deviations for each bottom-type class derived from the QB_DIBsg training sets

| | sand intertidal | | sand subtidal | | coral rubble | | coral- dominated | | algae: high density | |
|--------------------------|--------------------------------|-------|-------------------------------|-------|-----------------------------------|-------|----------------------------------|-------|--------------------------------|-------|
| | mean | stdev | mean | stdev | mean | stdev | mean | stdev | mean | stdev |
| | DIBsg ₁₂ clas | 15.6 | 0.7 | 33.3 | 4.2 | 14.5 | 1 | 0.3 | 1 | 2.8 |
| DIBsg ₁₃ clas | 107.9 | 1.4 | 113.7 | 11.8 | 104.1 | 1.5 | 51.3 | 10.2 | 75.7 | 1.6 |
| DIBsg ₂₃ clas | 98.8 | 1.3 | 93 | 16.1 | 97.7 | 1.2 | 62 | 5.6 | 77.8 | 1.2 |
| Texturesg ₁₂ | 8.7 | 4.7 | 104.7 | 41.2 | 44.3 | 28 | 178.9 | 21 | 80 | 24.6 |
| Texturesg ₁₃ | 7.3 | 2.7 | 163.5 | 57 | 31.8 | 16.4 | 179.2 | 30 | 53.8 | 25.5 |
| Texturesg ₂₃ | 8.1 | 3.4 | 175 | 52.4 | 33.8 | 14.3 | 139.2 | 33.2 | 38.3 | 13.2 |
| <i># samples</i> | 748 | | 2362 | | 126 | | 462 | | 72 | |
| | algae: med. density | | algae: low density | | seagrass: high density | | seagrass: low density | | deep water | |
| | mean | stdev | mean | stdev | mean | stdev | mean | stdev | mean | stdev |
| | DIBsg ₁₂ clas | 10.2 | 1 | 17 | 3.2 | 6.6 | 3.5 | 9.9 | 1.8 | 24.6 |
| DIBsg ₁₃ clas | 93.1 | 1.7 | 100 | 2.4 | 71.1 | 4.9 | 88 | 3.5 | 69.8 | 9.3 |
| DIBsg ₂₃ clas | 88.4 | 1.1 | 92 | 2 | 72.8 | 3.9 | 86 | 2.9 | 51.2 | 7 |
| Texturesg ₁₂ | 27.9 | 22.2 | 45 | 23 | 155.7 | 25.7 | 92 | 38.9 | 158 | 38.2 |
| Texturesg ₁₃ | 18.9 | 11.5 | 32 | 20.5 | 121.9 | 34.2 | 74 | 38.2 | 129 | 38.4 |
| Texturesg ₂₃ | 18.3 | 11.2 | 40 | 24.4 | 103.5 | 36.1 | 61 | 28.9 | 129 | 44.7 |
| <i># samples</i> | 457 | | 253 | | 810 | | 653 | | 326 | |

- classification based on QB_DIBsg

Table 3.86 and figure 3.83 represent the classification statistics for each bottom type based on the QB_DIBsg dataset. Similar trends as with the QB_DIB dataset were noted. As could be expected, the textural neo-channels had similar characteristics for each bottom type as no changes were made to the spatial structure of the bottom-type sample sets. When the mean and standard deviation values were compared between tables 3.85 and 3.86, mean values, however, were consequently lower for DIB₁₂ and DIB₁₃ in the QB_DIBsg case. Mean DIB₂₃ values, in contrast, were higher when using QB_DIBsg-defined parameters. These

differences resulted from the different water-column correction parameters defined in section 3.3.5.2.3: because of the slightly higher k_1/k_2 ratio determined over the seagrass bottom type, resulting DIB values were lower than the corresponding values determined over a homogeneous sandy substrate. The reverse counts for the k_2/k_3 ratio. These differences, however, did not markedly influence the differentiation between the bottom types so that an improved classification result was not expected.

The three QB_DIBsg feature spaces (fig. 3.82), contrarily, gave a different view. Although similar trends and problems were noted as with the QB_DIB dataset, a better separation between the algae-dominated and seagrass-dominated classes was obtained. In contrast, more overlap was noted between the 'sand intertidal' and coral-rubble classes. This already may indicate the influence of calibrating the water-column correction algorithm over a dark bottom type, rather than over a bright substrate.

b. Accuracy assessment

Because of the limited areal coverage of the QuickBird scene, only 111 GCPs could be used to test the accuracy of the different results (annex XVII). As a result, only a limited number of reference sample units were available for each level-3 class. The detailed bottom-type classes were therefore grouped onto the higher detail level before checking the thematic accuracy. Although some bottom-type classes remained underrepresented, this allowed the comparison with the Landsat 7 ETM+ results.

- QB_DIB case

Table 3.87 and table 3.88 respectively represent the error matrices determined for the classifications based on the QuickBird DIB-dataset and on the combination of QB_DIB and textural information. With an overall accuracy of 64%, the integration of textural neo-channels apparently improved the QB_DIB classification (overall accuracy of 60%). The performance of a Z-test (0.261) on the Tau coefficients, however, revealed no significant ($p < 0.05$) difference.

- QB_DIBsg case

Table 3.89 and table 3.90 respectively represent the error matrices determined for the classifications based on the QuickBird DIBsg-dataset and the combination of

QB_DIBsg and textural information. The texture-integrated approach resulted in a higher overall accuracy (65% as compared to 60% overall accuracy) although the Z-test (0.326) again showed that this improvement was statistically insignificant ($p < 0.05$). A Z-test between the QB_DIB and the QB_DIBsg results was not performed as the corresponding Tau coefficients were almost equal.

Table 3.87. Error matrix for the classification based on the QB_DIBs

| | bare substrate | coral | algae | seagrass | <i>total</i> | user accuracy |
|--------------------------|----------------|-----------|-------------|------------|--------------|-------------------------|
| bare substrate | 17 | 6 | 0 | 19 | 42 | 40% |
| coral | 0 | 1 | 0 | 1 | 2 | 50% |
| algae | 4 | 3 | 2 | 3 | 12 | 17% |
| seagrass | 1 | 7 | 0 | 47 | 55 | 85% |
| <i>total</i> | 22 | 17 | 2 | 70 | 111 | |
| producer accuracy | 77% | 6% | 100% | 67% | | 60% |
| Tau coefficient | 0.45 | | | | | overall accuracy |

Table 3.88. Error matrix for the classification based on the QB_DIBs and textural neo-channels

| | bare substrate | coral | algae | seagrass | <i>total</i> | user accuracy |
|--------------------------|----------------|------------|------------|------------|--------------|-------------------------|
| bare substrate | 16 | 7 | 0 | 17 | 40 | 40% |
| coral | 0 | 4 | 0 | 2 | 6 | 67% |
| algae | 1 | 1 | 1 | 1 | 4 | 25% |
| seagrass | 5 | 5 | 1 | 50 | 61 | 82% |
| <i>total</i> | 22 | 17 | 2 | 70 | 111 | |
| producer accuracy | 73% | 24% | 50% | 71% | | 64% |
| Tau coefficient | 0.48 | | | | | overall accuracy |

c. Visual validation

As was the case with the statistical analysis of the Landsat 7 ETM+ bottom-type classification, the number of reference sample units was inappropriate to separately test the statistical accuracy of each bottom type. The validity of the overall accuracy measures to determine the best classification approach might therefore be questioned. The dominance of reference points over a seagrass-dominated bottom type, 70 out of a

total of 111, probably biased the overall accuracy and Tau coefficient as well. Visual analysis was therefore needed to validate the necessity to incorporate textural information and/or to calibrate the water-column correction algorithm over a seagrass-dominated bottom type.

- necessity of the textural integration

In contrast to the Landsat 7 ETM+ results, the integration of the textural neo-channels did not apparently improve the QB_DIB bottom-type classification (fig. 3.84a and fig. 3.84b). Overall, most confusion existed between the ‘seagrass: low density class’ and the different algae-dominated classes. Much more seagrass-dominated pixels were also allocated to the reef crests and reef flats when textural information was integrated.

Table 3.89. Error matrix for the classification based on the QB_DIBsgs

| | bare substrate | coral | algae | seagrass | <i>total</i> | user accuracy |
|--------------------------|----------------|-----------|-------------|------------|-------------------------|---|
| bare substrate | 17 | 9 | 0 | 16 | 42 | 40% / 15% 86% |
| coral | 0 | 0 | 0 | 0 | 0 | |
| algae | 3 | 2 | 2 | 6 | 13 | |
| seagrass | 2 | 6 | 0 | 48 | 56 | |
| <i>total</i> | 22 | 17 | 2 | 70 | 111 | |
| producer accuracy | 77% | 0% | 100% | 69% | 60% | |
| Tau coefficient | 0.45 | | | | overall accuracy | |

Table 3.90. Error matrix for the classification based on the QB_DIBsgs and textural neo-channels

| | bare substrate | coral | algae | seagrass | <i>total</i> | user accuracy |
|--------------------------|----------------|------------|------------|------------|-------------------------|---|
| bare substrate | 17 | 7 | 0 | 17 | 41 | 41% 100% 17% 84% |
| coral | 0 | 3 | 0 | 0 | 3 | |
| algae | 2 | 1 | 1 | 2 | 6 | |
| seagrass | 3 | 6 | 1 | 51 | 61 | |
| <i>total</i> | 22 | 17 | 2 | 70 | 111 | |
| producer accuracy | 77% | 18% | 50% | 73% | 65% | |
| Tau coefficient | 0.49 | | | | overall accuracy | |

The shallow fringing reef areas, conversely, were more allocated to the 'algae: high density' class when texture was added, which may indicate a positive effect. Additional artefacts on all parts of the reefs, however, were introduced into the texture-incorporated result due to the use of the 3 by 3 variance filter.

A visual comparison of both QB_DIBsg results (fig. 3.84c and 3.84d) revealed similar problems. The integration of texture into the classification augmented the number of pixels classified as seagrass (sparse and dense) on the reef crests and reef flats which were clear misclassifications. In contrast, more pixels appeared to be erroneously classified as coral-dominated in some dense seagrass patches when textural layers were not integrated; but these errors were less pronounced.

- necessity of the seagrass-based water-column correction approach

To check the appropriateness of calibrating the water-column correction algorithm on pixels gathered over a seagrass bottom type, the QuickBird classification results without the integration of textural information were compared. Apparently, the QB_DIBsg classification performed best. There was markedly less confusion between seagrass-dominated bottom types and other bottom types on the reef crests and reef flats. The QB_DIBsg-based classification result was also less noisy.

To conclude, the QuickBird classification result based on the three DIBs corrected for water-column effects using pixels sampled over a seagrass-dominated bottom type but without the integration of textural information seemed to depict the coral-reef composition the most reliable. This result was therefore used during further post-processing.

3.6.3.3.3 Post-processing

a. Contextual editing

As with the Landsat 7 ETM+ processing, some known misclassifications remained in the QuickBird bottom-type classification. Because the classification was performed on a higher detail level, the contextual editing rules applied on the Landsat 7 ETM+ classification needed to be refined. A distinction, for example, had to be made between high- and low-density seagrass misclassifications. Contextual rules 4 and 5 were separated based on the similarities in figure 3.82 in which was noted that

‘seagrass: high density’ corresponded most to ‘algae-dominated: high density’; while there were more similarities between ‘seagrass: low density’ and ‘algae-dominated: medium density’. Contextual rule 8 was added to mask out all ships on the classification result as no information about the reef composition could be gathered on these places. All other editing rules remained the same as the ones described for the Landsat 7 ETM+ contextual editing.

```

QB_context1 = iff (((classification = "seagrass: high density") OR (classification =
    "seagrass: low density")) AND (geomorphology = "fore reef")), "coral-
    dominated", classification)

QB_context2 = iff (((classification = " seagrass: high density ") OR (classification = "
    seagrass: low density ") ) AND (geomorphology = "reef crest")), "coral-
    dominated", QB_context1)

QB_context3 = iff (((classification = " seagrass: high density ") OR (classification = "
    seagrass: low density ") ) AND (geomorphology = "patch reef dense")), "coral-
    dominated", QB_context2)

QB_context4 = iff (((classification = " seagrass: high density ") AND (geomorphology
    = "back reef/reef flat") AND (bathymetry > -1.2)), "algae-dominated: high
    density", QB_context3)

QB_context5 = iff (((classification = " seagrass: low density ") AND (geomorphology =
    "back reef/reef flat") AND (bathymetry > -1.2)), "algae-dominated: medium
    density", QB_context4)

QB_context6 = ifundef(bathymetry, (iff(geomorphology = "deep water", "deep water",
    QB_context5)), QB_context5)

QB_context7 = iff(geomorphology = "land", "land", QB_context6)

QB_context8 = iff(QB_shipmask =1, "unknown", QB_context7)

```

The contextually edited QB_DIBsg classification is shown in figure 3.85. The contextual editing clearly improved the classification of the reef crests and back

reef/reef flats. Because of the higher spatial detail of the classification, a separation could be made between the seaward part of the reef crest, i.e. the reef slope, which is dominated by coral, and the upper and backward parts of the crest which are predominantly covered by high density algal stands.

Although contextual editing solved most misclassifications between coral and seagrass on many reef parts, the reverse problem, being seagrass stands erroneously attributed to the coral-dominated class, occurred in some dense seagrass patches. Unfortunately, no additional contextual rule could be set up as seagrass patches do not form part of the geomorphological reef structure. They can only be delineated after the bottom-type classification has been made. The occurrence of a fringe of high-density seagrass at the border of the deep water may also be questioned. Although a less reflective substrate was seen in situ as well as on the original QuickBird TCC, the employed field sampling technique did not allow to determine whether this bottom type actually is a seagrass bed, a deep coral formation i.e. a coral carpet, or any other bottom type. Additional ground truth is needed to deal with this uncertainty.

Problems also occurred in nearshore areas and predominantly on the mud flats determined in the QuickBird geomorphological classification map. The spectral signature of these dark-coloured muds could not be isolated from other bottom types, especially the coral-dominated and 'algae: high density' classes. Similarly, the dense seagrass patches depicted on the QuickBird bottom-type classification were not encountered in the field. Possibly, these classification errors result from a difference in water quality in between nearshore and offshore areas. As the relatively sheltered nearshore area is fringed by hotels and tourist resorts and is heavily used as a yacht mooring zone, the water might be more turbid than the open water east of the Shaab Magawish reef. As such, the bottom reflectance would appear 'darker', resulting in more confusion between bare substrate and a benthic-community bottom type. The same problem was encountered in recently dredged zones where the turbid waters were classified as a coral-dominated bottom type.

b. Coastal habitat mapping

In order to obtain a comprehensive coastal habitat map (fig. 3.86), the contextually edited QuickBird bottom-type classification was finally combined with the geomorphological zonation map derived in section 3.5.2.3. Similar steps were taken as for the creation of the Landsat 7 ETM+ coastal habitat map: each polygon was

assigned a double code in which the colours represent the geomorphological zonation and the symbols depict the bottom types occurring on these zones. A 3 by 3 majority filter was additionally applied to obtain a more readable map (fig. 3.86).

Magawish Island is clearly surrounded along its northern and western edge by fringing reefs with a clear reef crest. The reef front is dominated by coral, while the shallowest parts are covered by a dense algal layer. This corresponds to the observations made by Purkis *et al.* (2002) along reefs in southern Egypt. The back reef is dominated by less dense algal stands. Towards the northeastern edge of the island, part of the bank/shelf area is sheltered by a protruding part of the reef crest. This shallow zone is largely covered with seagrass patches. The co-occurrence of dominant algae most likely is a misclassification as such stands were not encountered in the field. The eastern and southern back reefs are more degraded without distinct coral-dominated parts but with a diffuse cover of algae instead.

The same patterns could be recognised along the Shaab Magawish reef structure. Its northern and eastern edge show clear reef crest structures dominated by coral and high-density algae along the shallow top. The reef flat itself is largely dominated by less dense algae intermingled with sandy patches. The reef structure is almost completely surrounded by seagrass beds, both with high and low density.

The mainland shores are more complex and consist of mudflats, fringing reefs and reef patches. Although the mudflats are mostly dominated by very sparse seagrass stands as seen during the field survey, they are classified as a composition of coral, dense algae and seagrass. Due to the dark nature of the muddy substrate, the distinction between the three benthic-cover classes could not be made using QuickBird multispectral data. This is also the reason why the newly dredged areas between the piers and marinas along the central part of the coast are classified as a coral-dominated bottom type. The patch reefs further offshore, on the other hand, are correctly classified as a combination of coral, algae and seagrass. The 'no data' polygons along the coastline represent yachts and diving vessels moored in front of the many tourist resorts situated along this part of the Hurghada coastline.

3.6.4 Discussion

Statistical accuracy assessment of the Landsat 7 ETM+ and QuickBird bottom-type classifications revealed that both datasets resulted in a similar overall accuracy of ca. 60%. To

reject or accept the results based on these values is very difficult as it is almost impossible to determine an acceptable accuracy threshold (Mumby *et al.*, 1997; Mumby and Green, 2000a). Although an overall accuracy of 80% is generally considered as a minimum, much depends on the final use of the bottom-type classification map. If this map will have legal consequences, it should be as accurate as possible and the 80% minimum norm may even be too low (Mumby and Green, 2000a). If the map, on the other hand, is only intended as a reconnaissance survey of an unknown area, even a rough indication of what occurs may be valuable. Besides, the optimal 80% norm has been determined for land use applications. When applying optical remote sensing in subaquatic conditions, the recorded signal is additionally attenuated by the water column such that, even after water-column correction, the minimum accuracy of 80% is not likely attainable. In any case, the overall accuracy obtained approaches the range of accuracies described in other studies. For their study area in the Turks and Caicos Islands, Mumby *et al.* (1997) created a coarse level 4-classes bottom-type map using Landsat TM data with an overall accuracy of 73%. For a bottom-type classification discriminating 4-5 classes, Andréfouët *et al.* (2003) obtained an overall accuracy of 77% with IKONOS (a sensor with similar spectral and spatial characteristics as QuickBird), and an average overall accuracy of 56% discriminating 5 to 10 classes using Landsat data.

As discussed before, the relevance of the calculated statistical parameters, however, may be questioned because the field sampling method and the number of reference sample units for each bottom type did not meet minimal statistical norms. Besides, the assessment of the accuracy of the output map is complicated by the unknown reliability of the ground-truth data (Congalton, 1991), by the time lag between field survey and the moment of image acquisition (Hay, 1979; Luczkovich *et al.*, 1993; Michalek *et al.*, 1993; Hopley, 1996; Mumby *et al.*, 1997; Wagner *et al.*, 2001; Purkis *et al.*, 2002; Palandro *et al.*, 2003), and by difficulties in matching these ground data points to specific pixels in the scene (Hay, 1979).

Mumby and Edwards (2002), however, have shown that most bottom types do not shift more than 10m in a couple of years. As the Landsat 7 ETM+ scene and the QuickBird scene respectively date of September 10th, 2000 and February 5th, 2002 and the field surveys were performed in August 2001, March 2002, and August 2003, the time effect was considered minimal. The seasonal difference between the moment of the QuickBird data acquisition and the third field campaign may have caused additional problems, although such difficulties were not encountered during processing.

More problematic was the matching of pixels to exact locations of ground truth data points, especially for the QuickBird scene as already mentioned in the discussion of the

bathymetric mapping results (section 3.4.4). As the coral-reef environment is very heterogeneous, this may introduce large errors in the accuracy assessment as well. An attempt was made to account for these effects during the accuracy assessment: when a seagrass-dominated reference sample unit, for example, was located over a sandy substrate while a clear seagrass patch was recognised within the positional error range, it was assumed a correct classification. This approach, however, is very subjective and can not be uniformly used throughout the study area.

Irrespective of the appropriateness of the accuracy assessment performed, a coral-reef classification could never be 100% accurate (Luczkovich *et al.*, 1993; Mumby, 2000). First of all, the boundaries of ecological habitats tend to be gradiential and are not clear distinct lines. The delineation and definition of habitats will therefore always be slightly arbitrary (Mumby, 2000). This is exemplified by the difficulty in separating different densities of algae and seagrasses in the QuickBird data classification. The more diffuse a benthic community becomes, the more the reflectance will be dominated by the underlying bare substrate. A strict boundary to determine whether or not an algal or seagrass cover was present could thus not be drawn. This uncertainty is reflected by the hierarchical structure of the classification scheme.

Not only the ecological gradient is important, also the complex structural composition and geomorphology of the reef influences the classification performance as its accuracy is limited by the slope and aspect of the benthic topography (Holden and LeDrew, 2002), the 3-D arrangement of the reef (Joyce and Phinn, 2002; Hochberg *et al.*, 2003), and the resulting effect of light and shadow (Zainal *et al.*, 1993; Hopley, 1996; Joyce and Phinn, 2002; Hochberg *et al.*, 2003). These effects, however, are usually minimal and for a broad-scale classification using multispectral remote sensing data, the assumption of a fairly homogeneous, flat substrate surface parallel to a flat air/water interface can be accepted (Mobley and Sundman, 2003; Mobley *et al.*, 2003). One element of the reef topography, however, does limit the usefulness of remote sensing data for coral-reef mapping irrespective of the spatial characteristics of the sensor. Front reef slopes are usually very steep and in many instances almost vertical or even over-hanging. Obviously, these coral-dominated zones can not be mapped using a vertically positioned platform (Hopley, 1996; IGOS, 2003).

The heterogeneity of the reef structure, alternatively, may enhance the classification performance via the inclusion of textural information. Much however depends on the level of heterogeneity in the area under investigation. The higher the spatial complexity, the more difficult it becomes to determine specific textural characteristics for each bottom type. Based on the visual analysis of the different Landsat 7 ETM+ and QuickBird results, the integration

of textural information in the Landsat 7 ETM+ classification is considered beneficial while in the QuickBird case, adding textural neo-channels into the classification process did not markedly improved the results.

Mumby and Edwards (2002) indicate that the incorporation of a texture layer in the IKONOS data analysis is only beneficial when a detailed classification is envisaged. The advantage of the textural neo-channels becomes minimal when a broad-scale classification is performed (Mumby and Edwards, 2002). They also have found that textural information does not improve their Landsat TM bottom-type classification in any case (Mumby and Edwards, 2002). At first sight, this is contradictory to the findings in this study. However, the effects of incorporating textural neo-channels in the Landsat 7 ETM+ classification are only minimal and distinct statistical characteristics for each bottom type could not be determined. Although the coral-dominated bottom type was in general more heterogeneous than the seagrass-dominated bottom type, the standard deviations for each layer within the datasets were too high to clearly separate each class. Besides, contextual editing was still needed to correct many misclassifications between coral and seagrass. So, although the textural information did improve the Landsat 7 ETM+ classification result to some extent, it is not considered of primary importance.

The relative importance of spatial resolution, spectral resolution and radiometric resolution is considered to be site specific and scale dependent (IGOS, 2003). While Andréfouët *et al.* (2003) have found a clear improvement of 15 to 20% in overall accuracy by using IKONOS instead of Landsat data, others (Mumby and Edwards, 2002; Capolsini *et al.*, 2003) consider IKONOS and Landsat data equally performing for a coarse-level bottom-type classification. These conflicting conclusions are attributed to a difference in habitat complexity of the study sites investigated (Andréfouët *et al.*, 2003). More complex coral-reef structures require a higher spatial resolution as the spatial resolution of the sensor must be suited to record the intra-variability of each bottom type rather than the inter-variability caused by the very heterogeneous spatial organisation. The area studied by Andréfouët *et al.* (2003) is consequently more heterogeneous than the one used by Mumby and Edwards (2002) and Capolsini *et al.* (2003) where the Landsat spatial resolution is sufficient to perform a broad-scale mapping of the coral-reef composition.

For the specific focus area under investigation this means that the level of spatial heterogeneity is situated between the Landsat and QuickBird pixel size. While the Landsat 7 ETM+ spatial resolution mainly contains information on the inter-variability between the different bottom types, the QuickBird spatial resolution also provides information on the

intra-variability of each bottom type which allows a more detailed differentiation of the bottom types. When visually comparing a subset of the contextually edited Landsat 7 ETM+ result (fig. 3.74b) and the contextually edited QuickBird classification result (fig 3.85), the advantages of the higher spatial resolution of the QuickBird dataset become clear. This is not only shown in the more detailed delineation of the coastline but also in the discovery of some smaller reef structures, for example the three dense reef patches in the S-SW of the focus area. Because of the higher spatial resolution, more 'pure' pixels are available, facilitating the differentiation between the different benthic cover classes. Furthermore, a differentiation in density of the algae-dominated and seagrass-dominated bottom types could be made. Field data was unfortunately lacking to describe these classes quantitatively. The contextual editing of the QuickBird dataset also appears to have performed better which probably results from the more accurate delineation of the different geomorphological zones.

Although the very high spatial resolution of the QuickBird dataset did improve the classification, major errors still occurred, especially on the coastal fringing reefs and mudflats where clear misclassifications between coral, algae and seagrass remained. The spatial resolution of the satellite data is thus not the only key for a higher classification accuracy (Mumby and Edwards, 2002; Capolsini *et al.*, 2003). Also the finer radiometric resolution of the QuickBird sensor, i.e. 11bit as compared to 8bit for the Landsat 7 ETM + sensor, did not significantly improve its classification accuracy (Capolsini *et al.*, 2003). This points to the relative importance of the spectral resolution of the remote sensing datasets for mapping and classifying the spectrally complex coral-reef environment.

First, the different benthic-community bottom types already are spectrally very similar as their reflectance curves are all dominated by photosynthetic organisms (Andréfouët *et al.*, 1999; Mumby and Edwards, 2002; Kutser *et al.*, 2001; 2003). Seagrass and algae obviously are both chlorophyll-containing and broadly have the same spectral reflectance patterns as illustrated on the different feature spaces (fig. 3.70, 3.80, 3.82). Healthy coral spectral signatures as well are dominated by chlorophyll absorption effects as the endosymbiotic algae, more than the animal tissue or the calcareous skeleton, determine the reflectance. This explains the many misclassifications encountered between seagrass and coral. Even bare substrates are often covered with a thin layer of algae, transforming their otherwise clearly distinguishable spectral signature (Purkis *et al.*, 2002; Roelfsema *et al.*, 2002; Stephens *et al.*, 2003; Heil *et al.*, 2004).

In addition, the difficult spectral separation of the bottom types is complicated by the effects of the intervening atmosphere and water column. Vertical and horizontal heterogeneity

of the atmosphere; variable water quality, wave action, or air/water interface reflection patterns may all influence the spectral signature of a bottom type (Luczkovich *et al.*, 1993; Hopley, 1996; Holden and LeDrew, 2002; Maeder *et al.*, 2002; Hochberg *et al.*, 2003). Especially the differential attenuation of consecutive wavelengths hinders an optimal optical classification approach. Generally, a multispectral classification is limited to about 10-20m depth (Andréfouët *et al.*, 1999; Kutser *et al.*, 2001; Lubin *et al.*, 2001; Hochberg *et al.*, 2003). When using information recorded in the red part of the spectrum, the classification is even restricted to approximately 5-6m (Minghelli-Roman *et al.*, 2002; IGOS, 2003). This red light information, conversely, is essential to reveal significant differences in chlorophyll content and activity, and thus for detailed classifications. Deeper, only blue and green wavelengths are available for classification which limits the possibilities to detecting sand (Hochberg and Atkinson, 2003) and prominent reef features (Tassan, 1996; Mumby *et al.*, 1999; Maeder *et al.*, 2002). This depth effect may explain the occurrence of coral-dominated pixels between the mainland and the Shaab Magawish reef seen on the Landsat 7 ETM+ classification, while the QuickBird classification indicates deep water for this area. The continuous fringe of seagrass at the boundary of the deep-water area noticed on the QuickBird classification result may also be caused by this effect. Ground truth data was unfortunately lacking to clarify these ambiguities. The upper parts of the reef systems may thus be more accurately mapped such that the accuracy of the classification will alter with depth. Remark that the mentioned depths are maximum depths for optically clear water and become greatly reduced with increasing turbidity (Tassan, 1996).

One possibility to improve the classification potential of a moderate spectral resolution dataset, such as Landsat 7 ETM+ or QuickBird, is to spectrally unmix the reflectance recorded for each pixel. The spectral unmixing technique assumes that '*the measured spectral signal is the linear sum of a set of pure endmember spectra weighted by their relative abundance*' (Hedley and Mumby, 2003: 480). In the case of aquatic systems, the confounding effects of the water column, however, hinder the conventional approach. Hedley and Mumby (2003) have therefore developed a specific technique for spectral unmixing in subaquatic applications. As basic input, the spectral reflectance at zero depth of each bottom type needs to be known, as well as the attenuation coefficients of the water column in each spectral band. The technique, however, has only proven useful for unmixing signals received by a sensor recording at least two spectral bands more than the total number of bottom types present (cfr. Paredes and Spero, 1983). This restricts the unmixing technique to hyperspectral datasets.

Kutser *et al.* (2003) recognise three main advantages of hyperspectral sensors: (1) they possess a large number of narrowband channels capable of discriminating bottom types in more detail (Mumby and Edwards, 2002); (2) their large number of bands increase the capacity to unmix spectral signatures (Hedley and Mumby, 2003); and (3) they are capable of distinguishing more bottom types in deeper water. For these reasons, current coral-reef research puts more and more emphasis on a reef-up classification approach using narrowband hyperspectral data in combination with in situ spectral measurements (Holden and LeDrew, 1999; 2001; 2002; Hochberg and Atkinson, 2003; Hochberg *et al.*, 2003; Kutser *et al.*, 2003). Mumby and Edwards (2002), for example, have proven the great advantage of the *Compact Airborne Spectrographic Imager* (CASI) over Landsat and IKONOS for the classification of coral-reef bottom types on any scale. For the same study area, discriminating nine classes, a thematic accuracy of 81% was obtained using CASI data at 1m spatial resolution, as compared to 64% and 31% (Mumby *et al.*, 1998b) for IKONOS and Landsat TM data respectively.

The higher the spectral and spatial resolution of the sensor, the more detail thus can be provided. A very detailed reef mapping onto the species level nonetheless is not attainable with current air- and/or spaceborne sensors (Lubin *et al.*, 2001; Kutser *et al.*, 2003). Hochberg and Atkinson (2003) show that even with a bottom-up classification using in situ spectral measurements and a full spectral resolution of 1nm over a spectral range from 400 to 700nm, a maximum accuracy of 83% was reached for discriminating 12 bottom types.

Besides, airborne hyperspectral sensors are expensive in their exploitation and are only capable of covering relatively small areas as compared to spaceborne sensors (Mumby and Edwards, 2002). This approach also needs an ancillary spectral library of coral-reef bottom-type reflectances which is still not widely available (Hochberg *et al.*, 2003), especially not for typical Red Sea bottom types. As a result, it is impractical to use in many regions. There is therefore need for a specific 'coral-reef-tailored', spaceborne hyperspectral sensor (Hochberg and Atkinson, 2003). An interesting initiative, in this respect, is the fund collection by the Planetary Coral Reef Foundation to develop a new sensor and satellite specifically aimed at studying coral reefs (PCRF, 2002). The sensor, planned to be launched in 2008, will have a spatial resolution of 10m, as proposed by Joyce and Phinn (2001), and 14 spectral bands optimally differentiating between the most relevant coral-reef bottom types (Goeke, 2004).

The classic sensor-down approach in which scene-specific image statistics form the base for the classification (Hochberg *et al.*, 2003; Kutser *et al.*, 2003), nonetheless, still has its merits. Although the descriptive resolution of the available datasets, i.e. Landsat 7 ETM+ and

QuickBird, is not able to detect subtle differences between bottom types, they are at least capable of detecting general bottom-type classes (Holden and LeDrew, 1999; 2001; Lubin *et al.*, 2001; Kutser *et al.*, 2001; Maeder *et al.*, 2002; Andréfouët *et al.*, 2003). This is especially interesting for developing countries which are in need of coral-reef maps and inventories as they are highly dependent on these coastal resources (Luczkovich *et al.*, 1993), but lack the necessary funds and equipment to conduct either extensive field data sampling (Stoffle and Halmo, 1991; Luczkovich *et al.*, 1993) or detailed hyperspectral campaigns.

As QuickBird and Landsat 7 ETM+ performed almost equally over the specific Hurghada study area, the decision to use one or the other is largely constrained by the cost-effectiveness of the sensor (Mumby *et al.*, 1999; Andréfouët *et al.*, 2003). For large-scale surveys, Landsat 7 ETM+ data is considered more cost-effective, while QuickBird may be useful for well-documented, detailed mapping of relatively small areas (< 500km²) (Mumby and Edwards, 2002; Andréfouët *et al.*, 2003; Capolsini *et al.*, 2003). This shows the opportunity of multi-level remote sensing sampling in which Landsat data is used for broad-level overview mapping while IKONOS or QuickBird data may be integrated for more specific, complex areas (Andréfouët *et al.*, 2003). The regional-scale coral-reef inventories obtained in this way are also important to bridge the gap between detailed field studies and monitoring efforts studying processes and threats acting on the global scale (Mumby and Harborne, 1999; Clayton *et al.*, 2002; IGOS, 2003). In addition, the synoptic view presented over an entire regional reef system helps to understand the spatial structure of the reef (Andréfouët *et al.*, 1999) as well as to give an insight into the population dynamics and ecological connectivity of different local reefs in this regional scheme (Mumby and Harborne, 1999a). As such, this regional information also allows managers to plan detailed monitoring sites or field campaigns (Andréfouët *et al.*, 1999; Clayton *et al.*, 2002) and to set up networks of marine protected areas in order to protect biodiversity at multiple levels (Mumby and Harborne, 1999a). Moreover, these regional coastal habitat maps deliver important baseline information to establish management plans (Cendrero, 1989; Mumby and Harborne, 1999a) as they can be used to make an inventory of the habitat types present in an area; to identify patterns and hotspots of habitat diversity (Loehle and Wein, 1994; Mumby *et al.*, 1998b); to identify areas representative of typical coastal habitats worthwhile preserving (McNeill, 1994; Mumby *et al.*, 1998a; Mumby and Harborne, 1999a); to identify sensitive areas; or to demarcate multiple-use zonation schemes (see section 3.10) (Kenchington and Claasen, 1988; Mumby and Harborne, 1999a). Another important issue, in this respect, is the ability to follow up changes in habitat dynamics and to monitor the effects of disturbances on the habitat coverage

(Mumby *et al.*, 1998b). The specific potential for multitemporal analyses using broadband multispectral datasets is discussed in section 3.8.

3.6.5 Conclusions

Landsat 7 ETM+ data has proven useful for mapping the distribution and occurrence of broad-level bottom-type classes, being coral, algae, seagrass, and sand. Although some confusion between the three benthic communities can not be avoided, the result shown in this study clearly indicates the main reef structures with a relevant distribution of the bottom types over the different geomorphological zones. Reef crests are dominated by coral, while the leeward, shallow back reef/reef flats are generally dominated by algae and sand. The deeper bank/shelf and lagoons are usually bare sandy habitats, while the more sheltered parts regularly form a suitable environment for seagrasses. Although some subtle detailed variations are missed due to the spatial resolution of the Landsat 7 ETM+ dataset, this largely represents the broad-scale ecological environment as witnessed during the field campaigns.

As the QuickBird and Landsat 7 ETM+ datasets have a similar broadband spectral resolution suitable for aquatic applications, the misclassifications between the different benthic community classes remain a problem. This is partly reflected by the overall accuracy of 60% obtained for both the Landsat 7 ETM+ and QuickBird analyses. It should, however, be remarked that the validity of this statistical parameter is questioned and can consequently not be used to accept or reject the derived classification. It merely gives an indication of the validity of the results. Visually, the higher spatial resolution of the QuickBird dataset allowed to refine the bottom-type classification spatially as well as thematically. A more detailed classification of the reef crest, for example, is obtained as they could be spatially better delineated and thematically, a distinction could be made between the coral-dominated front reef slopes and the shallow, flat crests which are covered with dense, highly resistant algae.

Based on this observation, the Landsat 7 ETM+ dataset was pan-sharpened to test whether this would improve the classification result. This procedure based on the AIMF technique, however, reduces the accuracy of the bottom-type classification. This negative effect most probably results from the loss in spectral integrity of the dataset during the pan-sharpening process. This is of specific importance to coral-reef studies, as the atmosphere and the water column already largely attenuate the signal reflected by the seabed. Any additional loss in spectral information thus has a large impact on the analysis of the dataset.

From a technical point of view, the classification methodology could be refined in three ways. First, additional, quantitative and detailed ground truth data may improve the classification as well as the validity of the accuracy assessment as this study proves the importance of a ground truth dataset covering each bottom type with a sufficiently large number of GCPs. This, however, is not straightforward on coral reefs having many areas which are not easily accessible. Besides, the precise localisation of the GCPs taken at sea has proven problematic, especially when used for analysing high spatial resolution remote sensing data. The problems encountered might justify the additional costs of using differential GPS. The instability of the research vessel, conversely, forms a second problem which is not that easily overcome. Secondly, based on the QuickBird experience, the calibration of the DIBs over a dark benthic community improves the classification result. Applying this calibration method to the Landsat 7 ETM+ analysis could thus improve the accuracy of this result. A sufficient number of Landsat pixels corresponding to field observations of seagrass beds was unfortunately lacking to test this hypothesis. Thirdly, the integration of textural information apparently improves the Landsat 7 ETM+ bottom-type classification although this is not the case when processing the QuickBird dataset. This means that for the specific focus area under investigation, the level of spatial heterogeneity is situated between the Landsat and QuickBird pixel. Consequently, it might prove valuable to increase the filter size applied on the QuickBird dataset to a 5 by 5 kernel as did Mumby and Edwards (2002). This study, nevertheless, points to the value of textural information for coral-reef classifications.

The final application of contextual editing as a post-processing step proves very valuable. When new information becomes available on the reef structure or on the coral-reef ecology in the Red Sea, the applied editing rules can be refined or supplemented to further improve the bottom-type classification. Remark that the effects of this contextual editing are not integrated in the statistical accuracy assessment so that the final coastal habitat maps presumably are more accurate than represented by the overall accuracy measure. Whether or not the habitat maps are statistically acceptable and notwithstanding the misclassifications which can never be totally avoided, these maps are valuable contributions to the knowledge of the ecology of the reefs along the northwestern shores of the Red Sea. The best approach proves to be multi-level sampling in which Landsat 7 ETM+ data is used for regional scale mapping, while QuickBird data is integrated where more spatial detail is needed on a specific coral-reef site.

3.7 REMOTE SENSING AND BIOGEOPHYSICAL PARAMETERS

The possibilities of satellite remote sensing for monitoring the world's seas and oceans are already acknowledged since the mid-1970s. As the oceans cover more than 2/3s of the Earth, it is difficult to evenly map their characteristics with research vessels (fig. 3.87). Additional research buoys may be deployed but these still only give detailed information for a limited number of point locations (fig. 3.88a, b) (Lagerloef *et al.*, 1995; Llewellyn-Jones *et al.*, 2001; Le Vine *et al.*, 2004; GSFC, 2005). In the case of *sea surface salinity* (SSS) for example, taking 1° by 1° grid cells, more than 73% of the ice free ocean has received less than 10 salinity observations over the past 125 years and about 25% has even never been sampled at all (GSFC, 2005).

Satellite sensors, in contrast, synoptically map large surfaces, providing one-moment-takes covering many thousands of square kilometres without the problem of measurement inconsistencies encountered when combining traditional data sources (Llewellyn-Jones *et al.*, 2001). Sensors designed for oceanographic applications, therefore, were intentionally designed to cover the entire ocean surface on a (bi-)daily basis. To attain this prerequisite, the spatial resolution of the sensor had to be decreased and most oceanographic datasets, as a result, have a typical basic pixel size of 1km². Satellite data also allow capturing sudden changes in the water characteristics which are often missed by research vessels (Andréfouët *et al.*, 2002). Besides, as there is a large data archive from the end of the 1970s onwards, these datasets are very useful for long-term analyses as well.

Most biogeophysical parameters of importance to coral-reef growth can be monitored by satellite sensors. Water transparency is often not directly determined but can be derived from ocean-colour or *total-suspended-matter* (TSM) products (Woodruffe *et al.*, 1999). Ocean-colour products on their own give insight in the nutrient content of the water, while TSM may indicate potential sedimentation risks. The monitoring of these parameters as well as SST, nowadays, is fully operational and widely available. Monitoring SSS, on the other hand, has only recently become technically possible and in the coming years, two sensors are planned to be launched. Recent studies are also examining the possibilities to derive information on *sea surface currents* (SSC) from ASAR⁷², radar altimetry, and/or scatterometer data.

⁷² ASAR: along-track synthetic aperture radar

As most oceanographic products deliver a quantitative assessment of biogeophysical concentrations, special attention needs to be paid to the atmospheric correction. In order to perform an absolute correction, a priori information needs to be available concerning the constitution of the atmosphere as well as its horizontal and vertical variability. New-generation sensors, therefore, usually have a set of near-infrared bands which do not penetrate the water column but can be used to estimate atmospheric parameters (Antoine *et al.*, 2003).

Most algorithms linking remotely sensed radiance to biogeophysical properties, however, have been developed for Case-1 open water, while in shallow, Case-2 coastal water where many coral reefs are situated, the radiance values are additionally influenced by dissolved materials and/or the seabed (Antoine *et al.*, 2003). For this reason, these shallow coastal areas are often masked out in many oceanographic satellite products and the standard algorithms, therefore, need to be altered when coastal areas are investigated (Sathyendranath, 2000). To do so, additional site-specific information needs to be available to calibrate and validate these altered algorithms. As these datasets are not available, a ‘*coastal Red Sea algorithm*’ could not be developed. This section, therefore, only gives a brief overview of the current and near-future oceanographic products which are of interest to coral-reef science. When possible, examples for the Red Sea are given. These open-water products, nonetheless, may already indicate the general conditions of the seas and oceans in which the coral reefs occur, even without providing details on the coastal waters.

3.7.1 Ocean colour

As explained in section 3.3.5, the inherent optical properties of the water are influenced by its constituent elements, being the pure water particles, phytoplankton (expressed by Chl-*a* concentrations), suspended inorganic matter (commonly expressed as TSM if algae are included), and C-DOM. Hence, the colour of the water gives an indication of the concentrations of these elements at the sea surface. In addition, remote-sensing ocean-colour data can also be used to track changes in ocean acidification (see section 1.3.3.1) as it allows to estimate the global distribution of particulate inorganic carbon (PIC) (Kleypas *et al.*, 2006). Current sensors and techniques are still limited to coccolithoporid blooms in the upper few meters of the water column and can only estimate CaCO₃ standing stock as shown in recent studies for example by Balch *et al.* (2005) with MODIS data and Gordon *et al.* (2001) with SeaWiFS data. In future, long-term changes may be tracked and CaCO₃ production may also be quantified (Kleypas *et al.*, 2006).

Already in 1978, the *Coastal Zone Colour Scanner* (CZCS) was launched aboard NASA's Nimbus-7 satellite. For the first time, this sensor specifically dedicated to monitoring Chl-*a* and TSM showed the full potential of remote sensing for oceanographic applications. Albeit the CZCS already ceased in 1986, only in August 1997 a similar sensor, i.e. SeaWiFS, was deployed. Nowadays, the SeaWiFS system is still operational and has been supplemented by two MODIS sensors on the Terra (1999) and Aqua (2002) platform respectively. Simultaneously, ESA launched the MERIS sensor aboard Envisat in 2002 (IOCCG, 2005).

Some examples of MODIS-derived Chl-*a* products over the Red Sea have been discussed in section 2.3.2.5.1, also showing the multitemporal possibilities of these datasets. Ocean-colour data from different satellites however are not easily comparable as the instruments, the data-processing algorithms, and the calibration techniques all are different (Antoine *et al.*, 2003). NASA, fortunately, is currently re-processing all their archived ocean-colour data for its Ocean Colour Time-Series Project in order to produce a consistent, seamless time series of ocean-colour products from 1978 to the present (Esaias *et al.*, 1998).

Apart from the direct benefits of these datasets for studying the biochemical characteristics of the seas and oceans, they may also be further processed to obtain coral-specific parameters, for example water transparency/turbidity and hence the PAR available for the zooxanthellae; the risk of smothering as derived from the TSM products (Miller and Cruise, 1995); or nutrient-content estimations based on Chl-*a* concentrations which may indicate a potential phase shift from coral-dominated to algae-dominated reefs. Although ocean-colour data is already available since the end of the 1970s, only few researchers have specifically applied these data to coral-reef studies. Some of the key studies are Hallock *et al.* (1993) who have used CZCS data to show the influence of terrestrial runoff from the Amazon and Orinoco river on the Caribbean coral reefs; Gabric *et al.* (1990) who have examined Chl-*a* distribution in the Great Barrier Reef with CZCS data; and Andréfouët *et al.* (2002) who have studied the effects of Hurricane Mitch on the Caribbean coral reefs using SeaWiFS.

3.7.2 Sea surface temperature

Monitoring SST probably is one of the most routine oceanographic analyses of satellite data. NOAA has been producing SST maps from satellite data since 1972. Beginning 1982, SST became derived from multichannel infrared data collected by the *Advanced Very High Resolution Radiometer* (AVHRR) as the recording of thermal radiance in different bands made it possible to correct more accurately for atmospheric effects (Llewellyn-Jones *et al.*,

2001; NOAA/NESDIS, 2005). Currently, near-realtime SST data with a spatial resolution of 1km are still provided by AVHRR sensors aboard NOAA's *Geostationary Operational Environmental Satellites* (GOES) and *Polar Orbiting Environmental Satellites* (POES), as well as by the MODIS sensor (NOAA/NESDIS, 2005). Since 1991, ESA also has a series of thermal sensors in orbit (Llwelllyn-Jones *et al.*, 2001). Their latest sensor, the *Advanced Along-Track Scanning Radiometer* (AATSR) aboard the Envisat satellite is capable of acquiring very high precision SST data because of its two-angle viewing geometry which allows an advanced atmospheric correction by viewing the same surface from two different angles at nearly the same time (Llwelllyn-Jones *et al.*, 2001).

All sensors typically have one⁷³ thermal band centred around 3.7 μm for day-time SST retrieval and 2 bands in the 10-13 μm window for night-time SST derivation (Llwelllyn-Jones, 2001; NOAA/SIS, 2005). The night-time spectral interval is believed to be the most reliable as it is less affected by atmospheric absorption and therefore more sensitive to relatively small changes in SST (Llwelllyn-Jones *et al.*, 2001). Although highly performant, these IR-based systems can only be operated in cloud-free conditions. In areas with persistent cloud coverage, SST can be alternatively derived using passive microwave sensing such as e.g. the TMI (TRMM Microwave Imager) sensor aboard the Tropical Rainfall Measuring Mission (TRMM) satellite (REMSS, 2003). The coarse resolution of the TMI-like datasets, i.e. between 20 and 100km, is a major drawback to this approach, making it totally unsuitable for applications in the coastal zone (fig. 3.89).

Remote-sensing-derived SST products give valuable insight in the annual and seasonal changes of SST and its role in the biogeographical distribution of coral reefs. Moreover, as thermal stress is often regarded as a prime trigger for coral bleaching, monitoring SST may help to predict mass bleaching events and to tailor management actions to those specific conditions and sites. Such a coral-bleaching alert system has been developed by NOAA's *Coral Reef Watch* (CRW) team (CRW, 2005). This system is based on the twice-weekly, 50km averaged, global night-time SST products (fig. 3.90) derived from POES AVHRR. Night-time observations are being used to eliminate the diurnal variation in SST due to solar heating at the sea surface (CRW, 2005). From these products, *SST anomalies* (fig. 3.91) are determined which deviate from the *monthly mean SST climatology*. This long-term SST climatology is based on night-time observations from 1984 to 1993, with SST observations from the years 1991 and 1992 being omitted due to aerosol contamination from the eruption

⁷³ four in the case of MODIS (MODIS Web, 2005)

of Mount Pinatubo. In situ SSTs from drifting and moored buoys were used to remove biases (NOAA/OSDPD, 2005). For coral-bleaching prediction, only positive SST anomalies are of importance and *coral bleaching HotSpots* (fig. 3.92) are determined which highlight SST anomalies that are higher than the *SST maximum monthly climatology* (MMM). This MMM which is static in time, but variable in space (Strong *et al.*, 1997), is defined using the abovementioned long-term climatology dataset.

SST, however, must not only be higher than MMM, the anomaly must also last for several weeks. Consequently, *degree heating week products* (DHWs) (fig. 3.93) have been developed which indicate the accumulation of thermal stress over the past 12 weeks. In this, one DHW is equivalent to one week of SST being one degree Celsius higher than the expected MMM; two DHWs, subsequently, are equivalent to two weeks at one degree above the expected MMM or one week of two degrees above the expected MMM (NOAA/OSDPD, 2005). Field observations indicate that corals start to bleach when DHW values of 4.0 have been reached. By the time DHW values reach 8.0, widespread bleaching is likely and some mortality can be expected (Liu *et al.*, 2003). Based on these thresholds, bleaching reports are published on the *Tropical Ocean Coral Bleaching Indices* web page⁷⁴ for 24 selected reef sites. Since July 2005, CRW's *satellite bleaching alert* (SBA) system automatically sends out e-mail alerts when coral bleaching is likely to occur (CRW, 2005). Several studies have already shown the effectiveness and utility of such tropical-ocean coral-bleaching indices and the according warning system (Wellington *et al.*, 2001; Liu *et al.*, 2003). Recently, some adaptations to the system have been proposed taking the preceding temperature history (Klaus and Turner, 2006) or the local coral adaptability (McClanahan *et al.*, 2006) into account. Other parameters such as wind condition or solar irradiance must also be recognised as these may enhance or reduce the bleaching potential (NOAA/OSDPD, 2005).

3.7.3 Sea surface salinity

The principle of measuring SSS with passive microwave sensors has been recognized since the mid-1980s (Swift and McIntosh, 1983; Lagerloef *et al.*, 1995). Measuring SSS is physically based on the dependence of the *dielectric constant* of seawater on salinity at microwave frequencies. This dielectric constant also determines the *surface emissivity*, ϵ , of the water which in turn defines the relationship $T_b = \epsilon (SST)$ between SST and the *brightness*

⁷⁴ http://www.osdpd.noaa.gov/PSB/EPS/CB_indices/coral_bleaching_indices.html

temperature, T_b , which is measurable by a remote radiometer. Although the effect of salinity on T_b is small for typically open-ocean SSS and SST, it is detectable with microwave sensors operating in the 1-3GHz interval (Swift and McIntosh, 1983; Lagerloef, 1998; GSFC, 2005).

In order to obtain a reasonable footprint, large receiving antennas, however, need to be constructed. To obtain a 10km footprint size, for example, a 10 to 20m antenna aperture is needed, its size depending on the orbit altitude (Lagerloef, 1998). Besides, different other factors such as sea roughness, SST, the presence of foam, or the incidence angle influence the brightness temperature (Lagerloef, 1998; Gabarró *et al.*, 2004). All these parameters, therefore, should be known and understood before SSS can be measured with reasonable accuracy. These technical and scientific difficulties have recently been solved and two satellite sensors, being SMOS (Soil Moisture and Ocean Salinity) and AQUARIUS, are respectively being developed by ESA and NASA (Berger *et al.*, 2002; ESA, 2005b; GSFC, 2005). A technical overview of both sensors is given in table 3.91.

Table 3.91. Overview of the technical details of the SMOS and AQUARIUS sensors

| | AQUARIUS (GSFC, 2005) | SMOS (ESA, 2005b) |
|---------------------|--|---|
| sensor type | L-Band Radiometer operating at 1.4 GHz | 2-D interferometric radiometer operating at 1.4 GHz |
| estimated launch | 2009 | 2007 |
| life expectancy | 3 years | 3 years |
| orbit | 657km sun synchronous | 763km polar-orbiting |
| temporal resolution | 7 days | 3 days (at equator) |
| spatial resolution | 100km | 200km |
| PSU accuracy | 0.2PSU (monthly averaged) | 0.1PSU (monthly averaged) |

The main reason for monitoring SSS is to understand its role in the formation of water masses and the meridional overturning circulation (Le Vine *et al.*, 2004). Changes in the pattern of this global ocean circulation will affect the climate and vice versa. A good knowledge of the global and temporal distribution of SSS will thus advance climate models which track and predict future climate changes. To monitor the global SSS distribution pattern and its seasonal and interannual variations, a sensor needed to be designed which is able to measure SSS at a 7 to 30 days time interval with an accuracy in the order of 0.1-0.2PSU and a spatial resolution of 100-300km (Lagerloef, 1998; Le Vine *et al.*, 2004). Although both designed sensors have a

temporal resolution of several days, delivered SSS products will be averaged in monthly, global composites in order to augment their accuracy (ESA, 2005b; GSFC, 2005).

This temporal and spatial resolution, unfortunately, is not ideally suited for the variable and heterogeneous coral-reef environment. Nevertheless, global SSS products may bring a better insight in the importance of salinity in the biogeographical distribution of hermatypic corals. Besides, airborne microwave sensors are available making more detailed studies, but at much larger costs, possible (Le Vine *et al.*, 1998; 2000). One example is the study of Burrage *et al.* (2003) who investigate the role of freshwater input from river plumes on the coral-reef and seagrass ecosystems in the Great Barrier Reef using airborne salinity measurements.

3.7.4 Sea surface currents

Different other ocean-related topics are monitored by satellite sensors, e.g. *sea surface heights* (SSH) and *surface winds*. *Sea surface topography* is determined using *radar altimeters* such as the ones aboard Jason-1 (JPL, 2005a) and Envisat (ESA, 2005a), whereas *vector winds* and *velocity* are derived using *scatterometers* like NASA's QuikSCAT (JPL, 2005b). OSCAR (Ocean Surface Current Analysis in Real-time) is a pilot project which investigates how to derive information on SSC in near real-time by combining information derived from satellite altimeters and scatterometers over the tropical Pacific Ocean (NOAA/OSCAR, 2005). The end product will be a daily updated velocity map with a grid resolution of 100km basin-wide (NOAA/OSCAR, 2005). A preliminary example of such a product is given in figure 3.94. An alternative approach to monitor SSC uses ASAR (Johannessen *et al.*, 2006). This method is also under development and results can not yet be shown.

Such SSC products with relatively high spatial and temporal resolution could be used for identifying meso-scale ocean features like fronts and eddies; for monitoring the spatial and temporal dynamics of these features; for modelling the transport of various particles in the ocean including larvae, marine debris, and oil spills; and for improving global climate models (NOAA/OSCAR, 2005; Johannessen *et al.*, 2006). These products could also be used to model the dispersion patterns of coral larvae and/or pathogens. As such, it will improve our understanding of the connectivity between oceanic coral reefs as was already partly demonstrated by Andréfouët *et al.* (2002) using ocean-colour data.

3.8 MULTITEMPORAL ANALYSIS

3.8.1 Introduction

Because, remote sensing data is available at a repeatable time-interval from the mid-1970s onwards, it can be used to track changes in the environment. The two main prerequisites are that changes on the terrain result in changes in radiance detectable by the sensor and that these changes are larger than changes caused by other factors, such as varying atmospheric conditions or differences in sun angle (Singh, 1989). It, however, is not only important to detect that changes have occurred, but also to identify the nature of the change and to determine the areal extent and the spatial pattern of this change (Macleod and Congalton, 1998).

Different methods and techniques have been developed to monitor environmental changes using remote sensing (for an overview see e.g. Singh, 1989; Civco *et al.*, 2002). Two of the most widely used methods are *image differencing* and *post-classification comparison* (Singh 1989). With the image-differencing technique, two spatially registered images (or bands) from different dates are subtracted. Resulting pixel values close to the mean are indicative of no-change areas, while pixel values which significantly differ from the mean indicate areas of change. With the post-classification comparison method, previously produced, independent classifications for each date in the dataset are compared and changes identified.

Both methods, however, have some important shortcomings. Although the image differencing method gives a relatively accurate determination of the areal extent of the changes, it provides little or no information on the nature of these changes (Pilon *et al.*, 1988; Singh, 1989; Macleod and Congalton, 1998). Besides, the image differencing method is sensitive to changes in atmospheric conditions between the different dates, to misregistration between the different data layers, and to the occurrence of mixels in the images (Singh, 1989; Macleod and Congalton, 1998; Andréfouët *et al.*, 2001). The selection of appropriate threshold boundaries to differentiate change and no-change values is therefore very critical. The post-classification comparison method, in contrast, results in a 'from-to' change map clearly indicating what changes have occurred. No thresholds need to be defined and the effects of changed atmospheric conditions and differences in sun angle are minimal (Singh, 1989). This method, unfortunately, is still sensitive to misregistration and it risks low

accuracy because it combines the errors from each independent classification (Pilon *et al.*, 1988; Singh, 1989; Macleod and Congalton, 1998).

Pilon *et al.* (1988), therefore, propose a multi-component change detection procedure incorporating both the image differencing and the post-classification comparison techniques. In this method, the image-differencing technique first delineates the areas of change after which the classification technique is applied to define the nature of these changes. Consequently, only one reference dataset needs to be completely classified, while all other images in the multitemporal dataset are only classified for those areas showing significant change. This greatly reduces the chance of misclassification inherent to the post-classification comparison technique (Pilon *et al.*, 1988; Macleod and Congalton, 1998). The classified changed pixels are finally combined with the unchanged pixels to create a single 'from-to' change map.

Although multitemporal analysis has already been successfully applied in land use/land cover (LULC) monitoring (see e.g. Singh, 1989), remote-sensing-based change detection on coral reefs has only recently become examined (e.g. Michalek *et al.*, 1993; Zainal *et al.* 1993; Andréfouët *et al.* 2001, Dustan *et al.* 2001, Matsunaga *et al.* 2002, Palandro *et al.* 2003, LeDrew *et al.* 2004; Yamano and Tamura, 2004). More and more, the intrinsic qualities of remote sensing data to monitor changes on coral reefs, and especially coral bleaching, are recognised (Holden and LeDrew, 1998a). When coral bleach, they expel their zooxanthellae and turn white. This transformation results in an increase in spectral reflectance detectable by airborne and satellite sensors (Michalek *et al.*, 1993; Holden and LeDrew, 1998a; Clark *et al.*, 2000; Andréfouët *et al.*, 2001). Since the coral tissue is not necessarily death, it should still be distinguishable from coral rubble and/or carbonate sands (Holden and LeDrew, 1998a). After a couple of weeks, the bleached coral, however, becomes quickly colonised by algae which reduces the spectral reflectance of the substrate, making the discrimination between healthy coral, bleached coral and algae-dominated substrates more complicated (Holden and LeDrew, 1998b; Clark *et al.*, 2000; Dustan *et al.*, 2001; Phinney *et al.*, 2001). This complexity, as well as the general difficulties in spectrally separating different bottom types using satellite remote sensing data (see section 3.6), questions the utility of these datasets for coral health monitoring (Andréfouët *et al.*, 2001).

Some studies (e.g. Dustan *et al.*, 2001; Yamano and Tamura, 2004), nonetheless, have shown that Landsat TM data at least can give an indication of major shifts in coral-reef composition. Using a radiative-transfer simulation, Yamano and Tamura (2004) prove that the blue and green bands of Landsat TM are able to detect bleaching if at least 23% of the coral

surface in a pixel has been bleached on a shallow (less than 3m) homogeneous reef flat. Total bleaching of a purely coral-composed pixel could even be detected to depths up to 17m. Alternatively, in order to bypass the spectral complexity problem, coral bleaching may be determined based on changes in the textural complexity of the reef structure. With this method, a healthy coral reef is assumed to exhibit spatial heterogeneity of the spectral reflectance due to its highly variable structure, while a stressed coral reef will be spatially more homogeneous due to the uniform nature of the bleached and algae-colonised corals (Dustan *et al.*, 2001; Maeder *et al.*, 2002; LeDrew *et al.*, 2004). This approach, however, is still in its testing phase and no proven results are presented yet (LeDrew *et al.*, 2004).

No extensive bleaching appeared to have occurred in the northern Red Sea (Vogt, 2000; Spalding *et al.*, 2001) and changes in coral-reef composition are mainly related to human activities. Locally, severe damage has already been indicated around Hurghada (e.g. Riegl and Velimirov, 1991; Pilcher and Alsuhaibany, 2000; PERSGA, 2001; Cesar *et al.*, 2003) but no detailed regional study has been performed. The main objective of this multitemporal analysis therefore is to investigate the possibilities of remote sensing to link urban development to bottom-type changes in the offshore reefs on a broader scale. As an indication of urban development, the extensions of the road network and the urban areas were determined. Changes in the position of the coastline were also examined and linked to the urban expansion in order to determine whether these coastline changes were human induced or natural. Changes in coral-reef composition, possibly resulting from changes in LULC, were determined by employing the multi-component change detection procedure on the available Landsat 5 TM dataset of 1987 and the Landsat 7 ETM+ dataset of 2000. The Landsat 7 ETM+ image was selected as reference image as contemporary field data was available to calibrate this dataset. Since both datasets are almost from the same time of the year, the confusing effects of seasonal changes in bottom type and different sun angles were considered minimal (Pilon *et al.*, 1988; Singh 1989, Zainal *et al.* 1993). The preparation of both datasets was described in section 3.3. For both datasets, DIBs have been determined without applying a land mask as this would have biased the change detection of landfilled and/or dredged areas.

3.8.2 Data processing

3.8.2.1 Indication of LULC change

The road network and the extension of the urban areas on both the 1987 and 2000 datasets were vectorised on screen. Due to the spatial resolution of both datasets, only the major

roads and large agglomerations could be detected. In addition, the coastlines were digitized and a cross map was made between the 1987 and 2000 datasets in order to determine the areas of coastline change. A distinction could be made between landfill/sedimentation processes on the one hand and dredging/erosion processes on the other hand.

3.8.2.2 Changes in coral-reef composition

3.8.2.2.1 Image-differencing sub-procedure

The first step of the multi-component change detection procedure is to determine the significant areas of change. On each pair of corresponding DIBs of 1987 and 2000, image differencing was therefore conducted. A land mask indicating coastal areas which have not changed during the intervening period was applied to exclude these difference values from the statistics. This mask was derived from the coastline change detection map. Besides, a deep-water mask was applied as changes in this area only represent differences in sea surface roughness, water-column characteristics, or atmospheric conditions not solved by the relative radiometric normalisation (Zainal *et al.*, 1993; Macleod and Congalton, 1998). This deep-water mask was created based on the Landsat 7 ETM+ classification.

The histogram of each difference layer is presented in figures 3.95a, b and c. For each difference layer, an empirically determined threshold of half a standard deviation was chosen to define the areas where significant changes occurred. All pixels with values falling within this range were thus regarded as no-change areas. Next, to select the major change areas, only pixels which were identified as changed in all three difference layers, were retained. The three difference layers were therefore combined into one binary map using an 'AND' logical function. This approach, however, omitted some pixels along the shoreline which had clearly changed as indicated on the LULC change map. These pixels were therefore added to the combined binary map.

3.8.2.2.2 Landsat 5 TM classification

a. Geomorphological classification

A similar workflow was followed for the geomorphological classification of the Landsat 5 TM dataset as described in section 3.5.2 for the other datasets. However, as no bathymetric model could be developed because of the banding in the scenes, a

DCC could not be created. The geomorphological zonation was therefore only defined on a TCC which might have slightly affected the result. The resulting geomorphological zonation map is shown in figure 3.96.

b. Bottom-type classification

The classification process applied on the Landsat 5 TM dataset was similar to the one described for the Landsat 7 ETM+ dataset (section 3.6.3.1). The three Landsat 5 TM DIBs were converted to the 8bit domain based on the values in table 3.92 and formula 3.78. Additionally, three textural neo-channels were derived as described in section 3.6.3.1 for the Landsat 7 ETM+ dataset. Using the histogram equalisation technique, these texture bands were also converted to the 8bit domain.

Table 3.92. Minimum and maximum Landsat 5 TM DIB values

| | minimum | maximum |
|----------------------|---------|---------|
| L5_DIB ₁₂ | 0 | 1.406 |
| L5_DIB ₁₃ | 0 | 3.631 |
| L5_DIB ₂₃ | 0 | 3.092 |

$$L5_DIB_{ij,clas} = IFF(L5_DIB_{ij} = 0, 0, ROUND(L5_DIB_{ij} \times 70)) \quad (3.78)$$

In theory, the Landsat 5 TM dataset needed only to be classified in those areas where change was indicated by the binary change map. Unfortunately, no contemporary ground truthing was available to identify training sets in these changed areas. Training pixels were therefore selected in the no change area as, here, they could be linked to the Landsat 7 ETM+ classification. An overview of the statistical characteristics of the trainingsets in the DIB feature space and for both the DIBs and textural neo-channels is respectively given in figures 3.97a, b and c and table 3.93.

Remark that an additional unknown class was added to the classification. This feature could clearly be distinguished on the DIB colour composite and has clear spectral characteristics in the different feature spaces (fig. 3.97). This class, however, did not occur on the Landsat 7 ETM+ classification and a defined label could therefore not be assigned. This also meant that this class, which probably is a specific seagrass type, has at least severely degraded in the intervening time interval. The other ‘conventional’ classes could clearly be separated from one another and confusion

between the different benthic cover classes was even expected to be less than was the case for the Landsat 7 ETM+ dataset.

Table 3.93. Mean and standard deviations for each bottom-type class derived from the Landsat 5 TM training sets

| | sand | | sand | | coral | | algae | | seagrass | | deep | | unknown | |
|---------------------------|------------|-------|----------|-------|-----------|-------|-----------|-------|-----------|-------|-------|-------|---------|-------|
| | intertidal | | subtidal | | dominated | | dominated | | dominated | | water | | unknown | |
| | mean | stdev | mean | stdev | mean | stdev | mean | stdev | mean | stdev | mean | stdev | mean | stdev |
| L5_DIB ₁₂ clas | 58.1 | 3.6 | 72.4 | 7.4 | 35.7 | 3.5 | 41.0 | 2.6 | 46.8 | 3.1 | 45.3 | 5.9 | 34.6 | 3.7 |
| L5_DIB ₁₃ clas | 223.5 | 6.2 | 193.2 | 7.9 | 168.5 | 6.9 | 195.1 | 5.1 | 180.2 | 5.0 | 129.6 | 4.5 | 141.5 | 3.6 |
| L5_DIB ₂₃ clas | 201.5 | 3.8 | 149.8 | 8.2 | 162.2 | 6.0 | 186.8 | 3.7 | 164.4 | 3.7 | 101.5 | 5.1 | 131.0 | 3.5 |
| L5_Texture ₁₂ | 104.2 | 21.3 | 139.2 | 16.6 | 192.7 | 59.0 | 136.5 | 11.2 | 152.2 | 18.8 | 206.3 | 30.4 | 171.4 | 31.6 |
| L5_Texture ₁₃ | 114.4 | 20.5 | 133.7 | 16.7 | 202.8 | 40.8 | 169.5 | 36.0 | 205.9 | 30.9 | 189.4 | 32.7 | 173.2 | 41.8 |
| L5_Texture ₂₃ | 113.1 | 12.1 | 158.5 | 26.9 | 182.9 | 39.5 | 136.0 | 21.7 | 170.1 | 34.3 | 199.5 | 34.0 | 160.7 | 33.8 |
| # samples | 127 | | 822 | | 110 | | 73 | | 54 | | 624 | | 83 | |

Finally, a maximum-likelihood algorithm with an empirically determined threshold of 30 was used to classify the dataset. Unfortunately, ground-truth data was lacking to perform a statistical accuracy assessment. Subsequently, contextual editing was applied to ameliorate the result. As no bathymetric model for the Landsat 5 TM dataset was available, only the following five rules could be applied:

Context1 = iff (((classification = "seagrass-dominated") AND (geomorphology = "fore reef")), "coral-dominated", classification)

Context2 = iff (((classification = "seagrass-dominated") AND (geomorphology = "reef crest")), "coral-dominated", context1)

Context3 = iff (((classification = "seagrass-dominated") AND (geomorphology = "patch reef dense")), "coral-dominated", context2)

Context4 = iff(geomorphology = "deep water", "deep water", context3)

Context5 = iff(geomorphology = "land", "land", context5)

3.8.2.2.3 Post-classification comparison

Before the post-classification comparison was performed, the binary change map was used as a mask in order to retain only the classified Landsat 5 TM pixels in the 'change' areas. This masked Landsat 5 TM classification result was finally combined with the Landsat 7 ETM+ classification into a 'from-to' change map. If one of the classification layers indicated deep water, the pixel was assigned the 'deep water/no data' label as all changes occurring in deep water were considered irrelevant.

3.8.3 Results

3.8.3.1 LULC and coastline changes

In table 3.94, an overview is given of the changes in the road network and urban area between 1987 and 2000 as derived from the vectorised layers. These numbers clearly show the rapid urban development of Hurghada during this period. Figure 3.98 indicates the major urban expansion of Hurghada during the period covered. Not only the old city centres have grown, almost the entire coastline stretching several tens of kilometres north and south of the centre has become built-up, mainly by tourist resorts. Moreover, the large quantity of roads points to the enormous development plans the Egyptian government has made for the Red Sea coastal area. Since September 2000, the date the Landsat 7 ETM+ dataset was acquired, even more highways have been constructed. A second ring road, for example, has been laid around Hurghada and the inclosed desert is prepared for future industrial and urban development. The expansion of the flight strip indicates the growing number of touristic flights frequenting Hurghada all year through.

Table 3.94. Extension of road network and urban areas in 1987 and 2000 as derived from the analysis of the Landsat 5 TM and Landsat 7 ETM+ datasets

| | 1987 | 2000 |
|--------------------------------|-------|-------|
| road network extension (km) | 106.7 | 251.2 |
| urban areas (km ²) | 4.87 | 36.11 |

The areal extent of the coastline changes in the entire study area is given in table 3.95. Solely based on the analysis of these coastline changes, a clear distinction between natural and human-induced changes could not be made. However, when compared to the urban expansion data, most of these changes could be attributed to urban development, mainly for tourist accommodation. Most of the dredging, for instance, occurred with the construction of the El Gouna resort (figure 3.99a), while most of the landfill effects were associated with the construction of hotels, marinas, piers, and roads along the entire coastline north and south of Hurghada (figure 3.99b).

Table 3.95. Coastline changes between 1987 and 2000 as derived from the analysis of the Landsat 5 TM and Landsat 7 ETM+ datasets

| landfill/sedimentation (m ²) | dredging/erosion (m ²) | total change (m ²) |
|--|------------------------------------|--------------------------------|
| 4,009,782 | 2,028,319 | 6,038,101 |

3.8.3.2 Coral-reef bottom-type change map

An excerpt from the coral-reef bottom-type change map showing part of the fringing-reef system adjacent to the centre of Hurghada is presented in figure 3.100. For representation reasons, a 3 by 3 majority filter (Macleod and Congalton, 1998) was applied and the change classes vectorised. This resulted in a loss of detail, but was needed to obtain a readable overview map. For more detailed analysis, small unfiltered subsets could still be used. The base colours represent the coral-reef composition in 1987, while the hatching shows the changed bottom type in 2000.

The effects of the landfill and dredging activities along the shoreline could clearly be noted. Some fringing reefs and reef flats covered with coral and algae were directly lost due to these construction activities. Some significant bottom-type changes further offshore could also be noted. Especially the loss of two complex habitats, respectively between Abu Minqar and Big Giftun Island and near the SW of Big Giftun Island, was remarkable. Other bottom-type changes occurred as well but at a much smaller scale.

3.8.4 Discussion

Considering both the errors due to misregistration (Singh, 1989; Carmel *et al.*, 2001) and misinterpretation during digitalisation, approximately 6km² of the fringing-reef ecosystem has been altered by direct impacts of the changing LULC between 1987 and 2000. According to Pilcher and Abou Said (2003), the majority of these changes took place between 1994 and 1997. Dewidar (2002) used two Landsat TM datasets of 1984 and 1997 respectively to detect landfill in the same area. He calculated the landfill areas only to be 2.3km². The difference in results could be largely attributed to the dredging/erosion impacts which were not accounted for in the study made by Dewidar (2002). Dewidar (2002) also estimated the urban area to have grown from 0.96km² to 12.82km² between 1984 and 1997. The deviation from the results enlisted in table 3.94 could again be explained by a difference in methodology. Dewidar's (2002) results were based on image classification, while in this study, estimates were derived from a visual digitalisation. Notwithstanding the different estimates for both the

coastline changes and the expansion of the urban area, the conclusion remains that urban development has dramatically increased during the last two decades in Hurghada and the surrounding areas and that this has altered the coastline.

The accuracy of the coral-reef bottom-type change map was difficult to assess. Not only the errors generated in each single-date classification had to be taken into account, but also the errors generated by the change-detection algorithm, by possible misregistration, and by remaining radiometric differences between the two datasets (Macleod and Congalton, 1998). Therefore, to date, no standard, quantitative accuracy-assessment technique is available (Macleod and Congalton, 1998; Carmel *et al.*, 2001). Macleod and Congalton (1998), however, propose an adapted error matrix to test the accuracy of the resulting change-detection map. This *change-detection error matrix* is similar to a normal error matrix but entries are not single classes but changes in bottom-type classes as detected on the field (columns) and on the change classification (rows). The difficulty is that ground-truth data is needed for each date in the analysis (Macleod and Congalton, 1998; LeDrew *et al.*, 2004). As no ancillary ground-truth data was available for the Landsat 5 TM classification, the accuracy could not be statistically tested.

The overall accuracy of the single-date Landsat 7 ETM+ classification was estimated at 60%. This likely is the maximum overall accuracy attainable in the coral-reef bottom-type change detection map as additional errors are introduced by the change-detection procedure. Some of these errors, however, were reduced by the application of a multi-component change-detection algorithm (Macleod and Congalton, 1998). The errors associated with change detection can be divided in two groups, namely location errors and classification errors (Carmel *et al.*, 2001). The location error represents the misalignment between the various dataset layers (Carmel *et al.*, 2001). Even a misregistration error of less than a quarter of a pixel could lead to artefacts along the edges of the features which are more important than the actual change in the area (Townsend *et al.*, 1992). This misregistration effect is even more important in spatially heterogeneous areas (Townsend, 1992; Stow, 1999) like coral reefs and is related to the spatial resolution of the remote sensing dataset. Dai and Khorram (1997) show that for accurate change detection based on Landsat TM data, the misregistration error should be less than 0.2 pixel (Stow, 1999). Accurate spatial co-registration of the different datasets therefore is critical (Singh, 1989; Crowell *et al.*, 1991; Macleod and Congalton, 1998; Stow, 1999). As the RMSE obtained for the co-registration of the Landsat 5 TM and Landsat 7 ETM+ was 0.339pixel, some location errors are likely to occur in the change-detection result.

Change-detection classification errors have the same causes as described in section 3.6 for the single-date classifications. Of particular importance for change detection are errors resulting from differences in viewing geometry, solar illumination and atmospheric conditions between both images, as well as differences in sensor performances (Andréfouët *et al.*, 2001; Carmel *et al.*, 2001). These particularly affect the image-differencing sub-procedure. To account for the different atmospheric settings, only relative radiometric normalisation could be applied because ancillary atmospheric data was unavailable for the time of data acquisition. This, however, would not necessarily affect the result as there are no real gains in applying a complex atmospheric correction as long as the training data and the datasets to be classified are on a common relative scale and the classification of both datasets is made independently (Andréfouët *et al.*, 2001; Song *et al.*, 2001). For multitemporal change detection, therefore, the key point is to maintain consistency in the radiometric measurements among the datasets (Song *et al.*, 2001).

In the case of subaquatic applications, differences in water-column attenuation and water-surface reflectance may also influence the change-detection result (Michalek *et al.*, 1993). Different techniques could be applied to reduce the effect of depth and water quality. In contrast to most studies in which the change detection is bounded to shallow water (Clark *et al.*, 2000; Andréfouët *et al.*, 2001; Dustan *et al.*, 2001; Phinney *et al.*, 2001; Palandro *et al.*, 2003), here, the effect of the water column was limited by transforming the original datasets into sets of DIBs. In that way, a classification of the seabed up to 10-20m could be made. This approach, however, could be disadvantageous for detecting coral-reef bleaching (Yamano and Tamura, 2004). As extensive coral bleaching has not occurred in the study area, this was not considered a major problem.

A delicate point in the change-detection procedure was the determination of threshold values to differentiate between change and no-change areas in the image-differentiation sub-procedure. When placing a threshold, *'the type of change occurring should be determined in order to adequately place the threshold without a lot of trial and error'* (Macleod and Congalton, 1998: 214). As no ground-truth data was available for 1987, the type of change could not be exactly determined. The coastline change-detection map at least indicated some areas of known change along the shores. These areas were therefore *a fortiori* included in the binary mask. No information, however, was available on offshore changes. For this reason, an AND logical function was used to combine the three difference layers so that only those areas which showed significant changes in each difference layer were considered.

Smaller changes may have been overlooked, but these would also be more difficult to separate from confusing ancillary effects.

Nonetheless, the coral-reef bottom-type change map indicated some important shifts in the composition of the coral-reef ecosystems in the study area. The alteration of the coastline due to urban coastal development clearly affected many fringing reefs. The change map also indicated significant shifts in coral-reef bottom types further offshore. Dewidar (2002) also pointed to a reduction in areal coverage of the coral reefs, although what he defined as coral reef is in fact the shallow seafloor of which the spectral reflectance is not totally attenuated by the water. The quantification of these alterations was more difficult due to the lack of adequate ground data. Moreover, these changes were difficult to relate to possible negative indirect effects of the changed LULC. Notwithstanding these difficulties, the change map indicated the replacement of different benthic communities by an ecologically less complex, sandy bottom type.

3.8.5 Conclusions

To summarise, these change-detection results show both significant coastline changes as well as changes in coral-reef composition which have occurred during the period 1987-2000. The coastal urban development projects clearly have had direct negative effects on the fringing coral-reef systems along the entire coastline in the study area. Approximately 6km² of shallow, coastal habitats have been altered, predominantly by landfill and dredging activities. Moreover, the coral-reef bottom-type change map shows some important offshore changes. It was more difficult to link these changes to indirect effects of the coastal development without adequate ground data. Further research is needed to explore the effects of the different image-processing steps on the final change result, and to discover possible links between indirect impacts of LULC changes and changes in the coral-reef composition.

3.9 RISK ASSESSMENT MAPPING

This section exemplifies the use of remote sensing data and a Coral Reef GIS to produce a risk assessment map in which is shown to what level of stress the coral reefs are potentially up to due to human activities in the coastal area. Such a map greatly supports management decision making, for example in guiding multi-use MPA zoning. The delineation of risk zones is largely based on the 'Reefs at Risk'-project by Bryant *et al.* (1998).

3.9.1 'Reefs at Risk' decision rules

Bryant *et al.* (1998) have developed a set of indicators measuring the potential risk that a coral reef is affected by human activities in its vicinity. Largely, four categories of threats have been distinguished, originating from (1) coastal development, (2) overexploitation and destructive fishing, (3) the impact of inland pollution and erosion, and (4) marine pollution. Distance rules defining the extent to which the negative influence of a certain threat is expected to reach have been created for each component indicator, using knowledge on known reef sites degraded by human activity. Minimum distances have been established such that at least two-thirds of the known degraded sites affected by a certain activity were encompassed. These distance rules are subsequently utilized to define three different zones, being a 'low risk', 'medium risk', and 'high risk' zone.

The decision rules for each component indicator are summarised in annex XVIII. Component indicators for coastal development are urban centres, airports and military bases, mines, and tourist resorts which also include diving facilities; each incorporating the likely threat from pollution and sedimentation associated with coastal development. Most stressing are considered those cities with a population of more than 100,000 inhabitants, further differentiated according to their size and the level of sewage treatment. Additionally, an embayment or lagoon identified as being under medium threat from any individual coastal-development component is reclassified to the high risk class to reflect the heightened threat to reefs in enclosed waters. Proxies for marine pollution have been developed to reflect likely threats associated with pollution from oil rigs, tanks and wells, and ports; as well as threats associated with intensive shipping. Shipping hazards are only identified along known major shipping routes situated in relatively narrow passages, like the Gulf of Suez, or passing near shallow reefs. Next, threats related to overexploitation are linked to the population density in the coastal area, while destructive fishing is only identified in expert-defined areas where

blast or cyanide fishing occurs. Threat factors associated with inland pollution and erosion, finally, reflect the danger of sedimentation and chemical pollution through runoff. These impacts are determined based on hydrologic modelling and the analysis of topography, land-use classification, and precipitation data. For a more detailed discussion of this approach is referred to Bryant *et al.* (1998).

3.9.2 Application to the Hurghada study area

The general decision-rules scheme of Bryant *et al.* (1998) has been translated to the specific setting of the Hurghada study area (table 3.96). According to PERSGA (2001), the city of Hurghada had a resident population of 46,050 in 2001 (table 3.1). Besides, as was indicated by Soenen (1997), sewage water is collected by trucks and dumped inland. In the short term, the influence of sewage pollution could therefore be considered less of a threat. Subsequently, a medium risk zone of 8km from the city has been applied. One civilian and military airport is located near Hurghada which is heavily used by tourist charter flights throughout the year. A 10km medium risk zone, therefore, needed to be created. Other military bases also occur in the study area, but these are usually situated further inland and do not immediately threaten the coral-reef ecosystem. Tourist resorts, in contrast, stretch out along the coastline north and south of Hurghada and pose immediate threats to the coastal zone which are therefore incorporated in the 8km wide medium threat zone associated with them.

Concerning marine pollution, the port activities in Hurghada include small-scale fishing, ferry services, and military operations. Therefore, only a 10km medium risk zone needed to be defined. In addition, two oil-drilling platforms were identified in the north of the study area. These are classified under the 'oil tanks and wells' component indicator. A threat from intensive shipping is not considered relevant for the study area as the main shipping routes in the Red Sea are located further offshore. The threats related to the access route to the Hurghada port are implicitly addressed by the port component indicator.

The ecological pressure from fishing overexploitation is difficult to define in the case of Hurghada, first of all because population-density data is not available. Fishing pressure, however, is not yet considered problematic for the Red Sea (section 3.1.2.2) and the absence of data, therefore, does not affect the validity of the analysis. Besides, the population density would probably not exceed 20 persons per km² as the population is highly concentrated in the urban centres which are surrounded by vast stretches of barren desert. This parameter, thus, would not ideally reflect fishing pressure; even more because tourists, not incorporated in that

number, probably are the largest group of consumers. Destructive fishing practices are not widespread, although they have been reported in several occasions e.g. by Riegl and Luke (1998), and certainly not systematically applied, so that a distinctive ‘problem area’ must not be defined.

Table 3.96. Specific decision rules used to delineate risk zones in the Hurghada study area (adapted from: Bryant et al., 1998; *Dixon et al., 1994)

| component indicator | qualifier | high risk | medium risk |
|--|--------------------------------|------------------|--------------------|
| <i>threat factor: coastal development</i> | | | |
| cities | population < 100,000 | / | within 8km |
| airports and military bases | military and civilian airports | / | within 10km |
| tourist resorts | including diving facilities | / | within 8km |
| <i>threat factor: marine pollution</i> | | | |
| ports | small size | / | within 10km |
| oil tanks and wells | any size | within 4km | within 10km |
| <i>threat factor: overexploitation and destructive fishing</i> | | | |
| population density | information lacking | | |
| <i>threat factor: inland pollution and erosion</i> | | | |
| not relevant for Hurghada study area | | | |
| <i>threat factor: physical damage by SCUBA-diving and snorkelling*</i> | | | |
| mooring site | any type | within 100m | within 300m |

As Hurghada is located in an arid environment (see section 2.3.1) and distant from any important source of freshwater, there is hardly any agriculture. The problem with inland pollution and river runoff, therefore, is not relevant. Conversely, sometimes hazardous ephemeral floods deposit large volumes of sediment in the sea, smothering patches of fringing reefs. These events, however, are difficult to account for and are not immediately related to human activities either.

Diving and snorkelling, in contrast, are important threat factors in the study area, but they are not explicitly incorporated in the ‘Reefs at Risk’ analysis. For this reason, a parameter addressing the physical damage caused by SCUBA divers and snorkellers was added to the decision scheme. The distance rule for this parameter is based on the observations by Dixon *et al.* (1994) in the Bonaire National Park (Jameson *et al.*, 1999). They notice that most divers seldom go further than 300m from the mooring site. Therefore, a perimeter around each main

mooring site was constructed in which a zone of high risk was delineated up to 100m from the mooring site, while a zone of medium risk was created between 100 and 300m.

For each threat summarized in table 3.96, the risk zones were subsequently defined. First, all component indicators, except for the mooring sites which were located based on field observations, were identified and digitised using the Landsat 7 ETM+ TCC dating of September 2000. Distances were consequently calculated from these polygons –in which the land is seen as an unsurpassable barrier and given a negative weight– and sliced into a high risk, medium risk and low risk zone. Figures 101a, b and c show the examples of each consecutive step for the oil-drilling platforms.

Next, these individual component layers were combined to form an overall risk assessment map (fig. 102) following Bryant *et al.* (1998): if the reef area is assigned to the high or medium risk class for at least one of the threat factors, this area is classified to the overall high, respectively medium, risk class; only areas which are assigned to the low risk class for all indicators are attributed to the overall low risk class. Finally, to exclude ‘non-reef’ environments in their analysis, Bryant *et al.* (1998) made their analysis only for known reef locations. To simulate this, here, the analysis was restricted to the shallowest part of the coastal zone, above 21m depth, which is visible on the Landsat 7 ETM+ dataset (fig. 103). In the Red Sea, deeper areas mainly constitute of sand and are also likely to be less affected by human activities.

3.9.3 Results and discussion

Two main risk zones are discriminated on the overall risk assessment map shown in figure 103. Most important is the general medium risk zone stretching out along the entire coastline, up to 10km offshore. This zone is mainly related to the almost continuous coastal strip of tourist resorts and urban settlements. Secondly, a high risk zone is present in the north of the study area due to the occurrence of two nearshore oil-drilling platforms. In addition, the small spots of high and medium risk distributed over the area are linked to the main known diving sites. This shows that physical damage caused by divers is relatively localised but potentially severe. Only those reef systems further offshore are less endangered by devastating human activities.

A ‘no risk’ zone was not distinguished. Several reasons may be stated. First, although the study area is not considered to be at high risk from shipping accidents, the Red Sea still is an important shipping route and oil-exploitation area, so that the reefs along the entire Red Sea

coast are threatened to some extent by a potentially large shipping hazard. Secondly, the impacts of global change and natural threats are not included in this risk-assessment analysis (Bryant *et al.*, 1998). The effects of global change usually have similar impacts over large areas and can not be clearly linked to local activities. The low risk zone thus also incorporates the threat by global change, especially as the northwestern part of the Red Sea is not considered at immediate risk of climate changes (section 2.4.6.6). Other, natural, threats to the reefs are not addressed either. Although such events, e.g. flash floods, may have a serious impact on the coastal reefs, they are usually less frequent and can therefore be implicitly addressed by the overall low-risk zone.

Table 3.97. Overall risk assessment for the main bottom types occurring in the study area

| | low risk (%) | medium risk (%) | high risk (%) |
|----------|--------------|-----------------|---------------|
| coral | 12 | 77 | 11 |
| algae | 12 | 78 | 10 |
| seagrass | 5 | 83 | 12 |
| sand | 16 | 80 | 4 |

By combining the overall risk assessment map with the Landsat 7 ETM+ bottom-type classification (fig. 3.74a), more detail is provided on the threatened coastal habitats (table 3.97). Seagrass appears to be the most threatened ecosystem in this area (95% at medium or high risk), closely followed by coral and algae (88% at medium or high risk). These high values can be explained by the relatively narrow continental shelf in this part of the Red Sea, so that most ecosystems are within short distance of the coastline and thus become subject to the potential negative influences of the coastal human activities.

Table 3.98. Overall risk assessment percentages for the study area, the Middle East*, and the world* (*Bryant *et al.*, 1998)

| | low risk (%) | medium risk (%) | high risk (%) |
|--------------------------------|--------------|-----------------|---------------|
| study area | 14 | 80 | 6 |
| Middle East (Red Sea and Gulf) | 39 | 46 | 15 |
| World | 42 | 31 | 27 |

When compared to the global and regional risk assessments made by Bryant *et al.* (1998) (table 3.98), the marine coastal area in the study area in general, i.e. when the high and

medium risk class are combined, is seriously endangered by human activities; 86% in comparison to 61% and 58% for the Middle East and the world respectively. The restricted occurrence of highly stressed areas (6%) could be explained by the absence of highly damaging activities such as oil drilling (except in the north of the study area), large industrial ports, and/or densely populated cities. Smaller urban development sites and tourist resorts, in contrast, are situated all along the coastline of the study area, so that hardly any part of the coastline remains unaffected.

3.10 MULTI-USE MPA ZONING

The core of most ICZM plans is formed by a multi-use MPA which, commonly, is based on a zoning scheme geographically organising allowable and prohibited activities within the marine coastal zone (Winer and Harrigan, 1999). MPA zoning largely consists of three consecutive steps (Harvey, 1999): (1) the collection of baseline information on the natural resource and the human use, including a public consultation round; (2) the creation of an initial draft zoning plan based on this information; and (3) the revision of the initial draft based on public and government commentaries followed by the issue and implementation of the final zoning plan.

The use of remote sensing and GIS to collect baseline information on the natural resources and to prepare management support products has been shown in previous chapters. Here is demonstrated how these data products can be utilized to prepare the initial draft MPA zoning plan. The bottom-type classification maps and bathymetric models, for example, can be used to delineate the most vulnerable and/or valuable marine habitats in the area. The GIS-derived risk assessment map, additionally, indicates those areas currently under threat by human activities. The most endangered habitats could be assigned the highest protection to allow their recovery or enhance their capacity to overcome an eventual disaster. Alternatively, the least threatened areas could be assigned the highest protection in order to conserve their relatively pristine biodiversity. The remote-sensing data also provides a synoptic view of the entire area, allowing the creation of an interconnected network of marine reserves within one single multi-use MPA.

3.10.1 Specific multi-use MPA zoning scheme

The scheme defining the different MPA zones and the level of protection given to each zone should best be determined after consultation with the local stakeholders. As part of a USAID-funded project aimed to develop a '*Policy Framework for Developing an Environmentally Sustainable Tourism Strategy for the Egyptian Red Sea Coast*', Winer and Harrigan (1999) work out such a MPA zoning scheme after consulting different local stakeholder groups including fishermen, dive operators, hotel owners, HEPCA, the Hurghada City Council, TDA, fisheries and defence authorities, and the EEAA. This resulted in a zoning scheme consisting of seven MPA zones which can be grouped into three main classes according to their primary

objective, being conservation, tourism, or fishing and other activities. The main characteristics⁷⁵ of each zone are reviewed below (Winer and Harrigan, 1999):

- conservation

Two zones are specifically designed to optimally preserve the marine habitat:

o Scientific Reserve Zone

The scientific reserve zone defines the area of maximum protection with the aim to preserve the most valuable marine coastal habitats; to allow recovery of extensively damaged areas (through the delineation of permanent zones as well as imposing temporary emergency closures); or to select areas which act as replenishment zones. All activities are prohibited except for limited research. Scientists, however, need to apply for a permit to access the scientific reserve.

o Sanctuary Zone

A sanctuary zone only allows limited, very low impact visitation under the guidance of an EEAA ranger or an EEAA-certified guide. These zones may be conceptualised as buffer zones surrounding the scientific reserves.

- tourism

ICZM, however, not only aims to preserve the environment, it also searches for ways to develop the natural resources sustainably. As tourism, and especially diving- and snorkelling-related tourism, is the most important economic activity in the region, its needs should be optimally met by setting aside specific tourism zones. This will also minimise conflicts with other activities such as fishing. By identifying different zones for specific tourism activities, potential conflicts between each group are avoided as well (Salm *et al.*, 2000). Access to these areas is regulated according to ecological monitoring data.

o Diving Zone

The diving zones are restricted to diving and associated snorkelling. To reduce the environmental impact of these activities, only trained and certified divers are allowed. In addition, a diving etiquette consistent with the conservation goals of the MPA is promoted. All this should lead to an enhanced diving quality which would attract new, experienced divers.

⁷⁵ for a full description is referred to annex XIX

- Snorkelling Zone

In snorkelling zones, visitors without previous diving training or limited water skills are allowed. These zones, therefore, are open for snorkelling trips, dive training, glassbottom boats and submarines. All other motorised and non-motorised water sports remain prohibited. As the permitted activities have a potentially large environmental impact, snorkelling zones are located in shallow areas where the natural disturbance of the marine habitats is already high.
- Beach Sports Zone

Beach sports zones facilitate diving, snorkelling and all other water sport activities, except fishing, directly associated with coastal tourist resorts. A 'reasonable degree' of environmental protection is foreseen. These zones are conceptualised as narrow stretches of mainland beaches, shallow sandy environments and 'house reefs' in front of the resorts. Resort managers may further subdivide these zones at their own discretion.
- Island Access Zone

Island Access Zones are constructed to allow limited access to selected, small areas of nearshore islands for low impact activities such as sunbathing, outdoor cooking or short-term camping. The concept of '*take nothing but pictures, leave nothing but footsteps*' is envisaged.
- fishing and other activities

Most other activities, when sustainably exploiting the natural resources, are allowed in a general 'Fishing and Multiple Activity Zone'. No specific reference is made to traditional uses as, until the 1980s, only few nomadic Bedouins lived along the Red Sea coasts taking only limited use of the marine resources. Low-impact activities, such as fishing, remain largely unrestricted although the use of small mesh nets and spears is prohibited as well as obviously destructive or polluting activities. Potentially more damaging activities such as anchoring, shipping, military operations and petroleum production are only allowed when meeting the above restrictions and a specific set of agreed-upon best practices. Petroleum production activities, for example, are prohibited within 5km of any other zone; when having a visible impact, even within 10km.

3.10.2 Initial draft MPA zoning plan

The draft MPA zoning plan presented in figure 104 was largely based on the zoning scheme developed by Winer and Harrigan (1999), as well as following a number of general guidelines:

- balance should be sought between conservation and development; and between one use and another (Winer and Harrigan, 1999; Salm *et al.*, 2000; Mascia, 2001; Alvarez, 2004);
- planning areas should be as large as possible (Harvey, 1999), although the maximally protected areas should be restricted to the smallest zones in the plan (Winer and Harrigan, 1999);
- maximally protected zones should be buffered from harmful activities by surrounding them with zones with limited activity (Salm, 1984; Harvey, 1999; Winer and Harrigan, 1999; Salm *et al.*, 2000; Mascia, 2001; Alvarez, 2004);
- equal levels of protection should be provided to (inter)connected resources (Winer and Harrigan, 1999);
- zone boundaries should be clear and easily recognisable on site with geographically demarcated lines, eventually marked by signs and/or buoys (Winer and Harrigan, 1999; Salm *et al.*, 2000; Mascia, 2001; Alvarez, 2004).

The offshore boundary of the multi-use MPA roughly follows the 20m bathyline. This boundary has been pragmatically defined as below 20m no information could be derived from the remote sensing datasets. As biodiversity is quickly decreasing at greater depths, this limit is also ecologically meaningful. Depth as outer boundary of the MPA also has the advantage that fishermen or dive-boat captains can quite easily identify this boundary. Some deeper areas have been included in the MPA as they are almost completely surrounded by a shallower shelf. This, however, does not mean that the remainder of the deep marine areas are not controlled or associated activities not regulated. This zone, conversely, falls under the jurisdiction of Egypt's and international maritime law and does not need to be administered by local MPA managers.

The oil platforms in the northern part of the study area will most likely not be aborted in the coming years, so these petroleum facilities have received special attention in the MPA zoning plan. As the risk assessment map indicates a 10km wide high-risk zone surrounding these facilities, it is pointless to create a highly protected area in the northern part of the study

area (e.g. Salm *et al.*, 2000; Roberts *et al.*, 2003a; b). Consequently, opposite to the concept of the Winer and Harrigan (1999) scheme in which petroleum activities with a visible impact are not allowed within 10km of any other zone, here, most activities are prohibited within a 10km buffer zone surrounding the petroleum facilities (fig. 104, red hatching). Some activities such as fishing or motorised water sports could be allowed provided a strict monitoring of potential oil pollution. For this reason, the El Gouna resort which has been built close to the petroleum-activities perimeter could also be granted part of its Beach Sports Zone within that buffer zone. No new tourist resorts, though, should be allowed north of El Gouna.

Due to the ribbon-like development of tourist resorts along the coastline north and south of the Hurghada city centre, almost no unaffected fringing reefs remain. The few patches which are still relatively unaltered should therefore receive maximal protection. For this reason, a first Scientific Reserve Zone has been designated south of the El Gouna resort, comprising a stretch of ca. 7km of coastline (fig. 104, A). This Scientific Zone must be complemented with at least a complete ban on urban development along the shoreline, ideally with an adjacent terrestrial conservation area.

A second Scientific Reserve should comprise Abu Minqar Island (fig. 104, B) and its nearshore waters as this island is home to one of the last mangrove stands along this stretch of coast. As the island falls within the general medium risk zone identified on the risk assessment map, this scientific reserve is additionally buffered from outside influences by the surrounding Sanctuary Zone (fig. 104, 1) encompassing the bordering coral reefs and shallow sand areas.

Some reef systems further offshore, luckily, are largely protected from the negative impacts of the coastal activities and at least part of them should be considered for Scientific Reserve status. One of those areas is the zone between the two Giftun Islands which has already been designated as a marine park (fig. 104, black hatching). In order to improve the management of this park, a suggestion has been made to divide it into several zones as to better separate its multiple uses. The Little Giftun barrier reef, north of the island, (fig. 104, C.II) is defined as a Scientific Reserve for its unique geomorphologic structure and its assumed high level of biodiversity. The lagoon-like reef structures in the southwest of Big Giftun Island (fig. 104, C.I) have also been assigned a Scientific Reserve status. Total protection of this area could help its recovery after the significant changes it underwent during the last two decades as shown by the multitemporal analysis in section 3.8. With the exception of two small areas, the remainder of the current marine park has been designated as a Sanctuary Zone (fig. 104, 2) allowing limited visitation. These exceptions have been

designed to accommodate current tourism activities respectively in a Diving Zone along the SE shores of the Little Giftun Island and an Island Access Zone to the south of Big Giftun Island.

The remote reefs of Umm Qamar (fig. 104, D) and Shaab El Erg (fig. 104, E) have also been designated as Scientific Reserve Zones. Because of their less threatened status and the main NE direction of the water currents, they may serve as replenishment zones for the downstream coastal reefs. The Shaab el Erg reef, moreover, has a unique geomorphology, not frequently found in the northern Red Sea. The Scientific Reserves in the Umm Qamar area are connected to one another via a larger Sanctuary Zone (fig. 104, 3) in which two areas, being Careless Reef in the south and the east coast of Umm Qamar Island, have been designed as Diving Zones.

Two additional areas have been proposed as Sanctuary Zones. One is the Shaab Magawish Sanctuary Zone (fig. 104, 4) which protects the dense concentration of seagrasses and the second is the El Gouna sanctuary zone (fig. 104, 5) in front of the El Gouna resorts, protecting the reefs against excessive tourism activities. Limited and guided access to both areas, however, should still be allowed to point tourists to the importance of sustainable use of these natural resources.

As tourism is the most important economic activity in the region, sustaining the livelihoods of many thousands of people, an important part of the multi-use MPA should be reserved for tourism activities, mainly diving, snorkelling, and boat trips. Several Diving Zones have been designated on the more remote reefs encompassing the currently most popular dive sites. By reserving these sites for the more experienced divers which also follow an ecological diving etiquette, these areas should become more sustainably used than they are today. Snorkelling zones have been defined closer to shore while selecting shallower areas which still have some attractive coral reefs. Care, however, should be taken not to surpass the carrying capacity of each reef individually and profound ecological monitoring of these sites, therefore, is required.

Furthermore, two Island Access Zones have been respectively provided along the southern edge of Big Giftun and Magawish Island as these parts of the islands are already visited by tourists. Access to any of the other islands, however, should be strictly limited. Beach Sports Zones, finally, have been defined in front of tourist resorts and public beaches. Some deeper parts have been included in the Beach Sport Zones to facilitate water sports such as jetskiing or surfing. As the resorts already organise many popular activities in their nearshore waters, it

would be very difficult to gain their support for severe restrictions. More training, instead, should be provided on how to minimize the effects of beach sports on the environment.

The remaining part of the multi-use MPA has been designated as the general Fishing and Multiple Activities Zone. Nowadays, fishermen also take use of areas designated for conservation or tourism. They should, therefore, be convinced of the advantages of closing some parts of the marine area as this will augment catches in the adjacent fishing areas. Diving and snorkelling are still allowed in this general zone, although strict regulations and visiting schemes should also be applied.

To conclude, it should be remarked that this draft initial MPA zoning plan should not be regarded in any way as '*the*' optimal plan for the region. It is only presented here to illustrate the possibilities of remote sensing and GIS to support the ICZM decision making process. Other zoning plans are possible, e.g. after consultation with local stakeholders and regional and national government, or when additional information such as on the carrying capacity of the different dive sites becomes available. Within the ICZM strategy, this MPA plan should be complemented with a development plan for the land such as the ones developed by the TDA. Lack of information, however, should not delay the designation of an initial MPA in the short term as, especially in the light of the increasing growth of tourism in the region, '*an imperfect reserve is better than no reserve*' (Roberts and Hawkins, 2000: 79).

GENERAL CONCLUSIONS

Coral reefs, as meant in this text, are massive carbonate structures build up by carbonate-excreting coral organisms in tropical and subtropical marine waters. The key to the success of hermatypic corals most probably is the symbiotic relation with the zooxanthellae living inside their gastrodermis. The photosynthetic products of these algae provide the coral host with additional energy which it uses to sustain in generally nutrient-poor waters and to form its calcareous exoskeleton at such high rates that massive structures can be formed. The global distribution of coral reefs is largely defined by the coral physiology which poses strict boundaries to physical parameters such as temperature and salinity, while the symbiotic relationship limits zooxanthellate coral growth to the upper 100m of relatively clear water.

The Red Sea forms an ideal environment for coral reefs although, with its generally high temperature, high salinity and low primary production, it may be considered an extreme water body when compared to other oceans and seas. As corals are adapted to survive in nutrient-poor marine environments, they are very well suited to the Red Sea notwithstanding the fact that SST and SSS often are near the upper physiological limits of the corals. Because the nutrient levels are exceptionally low, macro-algae, in contrast, are less competitive in the struggle for the available space so that in natural conditions, Red Sea coral reefs are rarely overgrown by macro-algae. Suitable substrate is provided by the geological setting of the Red Sea. Even though the shallow continental shelf is generally narrow, except in the southern Red Sea, many structural highs such as fault blocks, salt diapirs and ancient wadi and alluvial fan deposits form ideal colonisation grounds in the upper water column. Moreover, due to the arid climate of the Red Sea region and the orographic structure of the basin, no permanent rivers mouth to the Red Sea so that sedimentation hardly obstructs coral settlement. The oligotrophic water and the restricted input of terrestrial sediments also result in an euphotic zone which almost stretches down to the physical limit of light penetration in sea water at about 100m depth. Most reefs, in addition, are able to grow up almost to mean sea level as tidal sea-level changes are limited.

Although the Red Sea forms an ideal natural environment for coral-reef growth, the status of the Red Sea coral reefs has become seriously threatened during the last two to three decades and many reefs have already seriously degraded. This phenomenon is seen all over the world and is related to a large array of causes, mainly associated with human activities and global change. The corals in the Red Sea are predominantly threatened by urban coastal development, tourism activities and marine pollution, whereas the isolated position of the Red Sea appears to protect its environment from the harshest effects of global change. During the mass bleaching event of 1997/1998, only a limited number of corals were for example

affected and most of them were able to recover afterwards. The situation in Hurghada is very illustrative for the northwestern part of the Red Sea. As shown by the multi-component change detection analysis of two remote sensing datasets of 1987 and 2000 respectively, the urban centre has expanded by an estimated 740%, roughly from 5 to 36km². Most problematic are the ribbon-like extensions along the coastline related to the construction of tourist resorts which have altered ca. 6km² of coastline and destroyed many fringing reefs. Although the indirect effects of tourism probably are the most devastating, many direct effects of SCUBA diving and snorkelling have also been reported in the region. Some important, offshore bottom-type changes have been detected with the remote sensing data as well, but information is lacking to link these to the human coastal activities.

Future coastal developments, nevertheless, are highly encouraged by the Egyptian government as tourism is one of the most important sources of foreign income. Because the coral reefs are the main tourist attraction in the region, ICZM is required to balance the socio-economic development of the Red Sea coast and the conservation of the valuable, but vulnerable, coral reefs. One of the cornerstones for a successful ICZM is the collection of relevant baseline data on the current status of the coral reefs and the level of exploitation of this natural resource as well as the monitoring of trends and evolutions in these elements. Here, remote sensing comes to the aid. Fortunately, the ecological requirements of the corals and the physical characteristics of the Red Sea allow the use of passive, optical remote sensing. The main advantages of spaceborne remote sensing are that datasets which have been synoptically collected over relatively large areas in a standardised digital format are readily available; that in this way, information may be obtained from remote or inaccessible reef areas; and this very cost-effectively. As shown, remote sensing provides information on the configuration of the coral-reef structures (i.e. on the localisation and depth of the reef structures and their geomorphological zonation), on the benthic habitat composition (being a combination of the dominant bottom types and the geomorphological zones on which they occur), and on the biogeophysical characteristics of the seas and oceans in which the coral reefs occur. Newly acquired remote sensing data also contribute to the monitoring aspect of ICZM research, while archived datasets may offer a historical perspective on the former status of the coral reefs.

Concerning bathymetric mapping, the DOP-mapping method by Jupp (1988), modified by Edwards (1999), has proven to deliver the best results. Depths up to ca. 20m, with a mean residual error of ± 1 m and a Pearson product moment correlation coefficient of at least 90%, have been determined with both the Landsat 7 ETM+ and QuickBird dataset. Main problems

are encountered with the inherent shortcoming of the bottom-reflection-based bathymetric theory which overestimates depth over dark-coloured substrate types. As a result, the bathymetric model fails over dense seagrass patches. An attempt has been made to overcome this problem by applying the ratio-transform method (Stumpf *et al.*, 2003), adapted for very shallow zones. Although the problem with the seagrass beds is less pronounced, the obtained result depicts the bottom features in less detail and is also very noisy; therefore, it is considered of less quality. Besides, the possibilities of bathymetric mapping using digital photogrammetry and an ASTER stereopair have also been investigated. Even though many errors still need to be overcome before an acceptable bathymetric model can be obtained, this approach looks very promising. The bathymetric maps obtained with the DOP-mapping method, nevertheless, provide a general and relatively accurate view on the seabed topography of the coral-reef environment; information which is difficult to obtain using conventional bathymetric techniques.

Coastal habitat mapping consists of both geomorphological zonation mapping and bottom-type classification. Geomorphological zonation mapping probably is the most straightforward remote-sensing application and largely depends on the knowledge of the interpreter. The visual delineation of the different geomorphological zones, however, is greatly enhanced by the introduction of the previously derived bathymetric maps. The remarkably complex geomorphological structure of the Red Sea coastal area is clearly illustrated in the Landsat 7 ETM+ and QuickBird-derived zonation maps. With the image classification, distinction is made between the dominant bottom types occurring in the study area, being corals, algae, seagrasses and sand. The Landsat 7 ETM+ classification has been enhanced by the integration of textural information, but this has not been the case for the QuickBird result. The calibration of the pre-processing water-column correction with data collected over a dark substrate, in contrast, has improved the separability of the different benthic-community classes in the QuickBird result. Both results, however, still needed post-processing contextual editing based on general ecological zonation rules and the geomorphological zonation maps to deal with some major misclassifications between the different benthic communities. As the general trends in the bottom-type distribution are detected on these edited classifications, the bottom-type classification approach is considered acceptable, at least for broad-level mapping of coastal habitats.

The level of detail which has been obtained depends on the descriptive resolution of the data. First, the higher spatial resolution of the QuickBird dataset allowed a more detailed delineation of the seabed features, which was especially noticed on the bathymetric models

and the geomorphological zonation maps. This is of special interest for heterogeneous environments such as coral reefs because important ecological changes may occur over only a few meters or less. Moreover, the QuickBird bottom-type classification is not only spatially more detailed, a higher thematic detail level is also attained with a differentiation in bare-substrate types as well as in densities of seagrass and algae.

Based on these observations, the possibility of pan-sharpening the multispectral Landsat 7 ETM+ dataset with the concurrently acquired panchromatic Landsat 7 ETM+ band has been tested. This pan-sharpening procedure, however, only delivers limited advantages when compared to the results created with the original Landsat 7 ETM+ dataset. Although some more spatial detail has been obtained with the pan-sharpened dataset, the loss of spectral information inherent to most pan-sharpening techniques introduces additional errors in the geomorphological zonation map and especially in the bottom-type classification. Even a minimal decrease in spectral information may have serious effects for marine remote sensing as already 90% of the signal recorded by the sensor has been altered by the intervening atmosphere and the water column.

For this reason, the radiometric resolution of the data is also important as a broader radiometric range and a higher signal-to-noise ratio allow a better discrimination of the generally low-reflectance characteristics of submerged features. The 11bit QuickBird data is therefore considered superior to the 8bit Landsat 7 ETM+ dataset, especially for the bottom-type classification. The ILWIS 3.2 software, unfortunately, only accepts 8bit input data for its classification algorithm, such that this potential advantage could not be tested.

Probably of more consequence for the bottom-type classification, however, is the spectral resolution of the dataset especially in a coral-reef environment where the different benthic communities are closely intermingled and the spectral differences often subtle. The broad multispectral bands of all used datasets, therefore, are only capable of detecting the large-scale distribution of the most dominant bottom types. Even though the very high spatial resolution of the QuickBird dataset allows more thematic detail, its accuracy has not been significantly improved when compared to the Landsat 7 ETM+ result at the same detail level. It, for example, remains problematic for both datasets to discriminate between dense benthic communities such as seagrass and coral. Also the ecological gradient between bare substrate and a benthic community such as seagrass still causes problems when differentiating both, visually distinctive, classes. This stresses the need for a hierarchical classification scheme in which the uncertainty about the classification is expressed by the detail level at which the classification has been made.

The attenuation of light by water probably is the largest disadvantage of using passive, optical remote sensing. First, this limits the depth of survey to maximally the upper 20 to 30m of the water column; a value which becomes quickly reduced by increasing turbidity. In the Hurghada study area, the maximum depth of penetration is restricted to ca. 21m. As the blue wavelengths are apparently more affected than the green wavelengths, this probably results from a relatively high C-DOM concentration in the coastal water. However, as the maximal coral diversity zone is usually situated between 5 and 30m depth, this depth limit is not totally devaluing the remote-sensing-derived products. Detailed bottom-type classifications, in contrast, are more hindered by the differential attenuation of light so that red wavelengths can only be used in the upper 5m of the water column. Because the most pronounced spectral differences between the benthic communities are situated in this spectral range, their discrimination becomes severely restricted below this depth. The accuracy of the bottom-type classification thus probably is inversely related to depth. Remark, however, that the differential attenuation of the light is the basis for the bathymetric mapping methods relying on passive, optical sensors.

The applied techniques, obviously, also require an important amount of ground-truth data both to calibrate and validate the processing algorithms. During three field campaigns, 650 observations were made at sea, covering depth measurements and bottom-type determinations. This number of observations, however, is still inadequate to optimally calibrate the bathymetric model (e.g. too little depth measurements over very shallow areas which probably excluded the NIR band of being used and too little depth measurements in deep water covered by the QuickBird scene) or to test a number of questions raised during the study (e.g. Is there a different bottom type at ca. 15m depth or is this an artefact of the water-column correction?). Concerning the bottom-type classification, the bottom-type observations were not evenly spread over the different classes such that a thorough statistical classification has not been applied. Data are also lacking to quantify the bottom-type characteristics or the spatial heterogeneity of the environment. Detailed field surveys to collect all these data, however, are expensive and time- and labour-intensive and do not fit the frame of this study. Therefore has been opted for a more broad-scale surveying technique, taking into account its inherent shortcomings. One additional problem is encountered due to the uncertainty of the location of the ground truth observations which is related to the combination of GPS location errors, errors introduced during image georeferencing and errors generated by the instability and drifting of the research vessel. This problem is especially noticeably with very-high-

resolution datasets like QuickBird in combination with the heterogeneous coral-reef environment.

This has had effects on the accuracy assessment as well. To start with, no probabilistic sampling design has been applied mainly due to the inaccessibility of the shallowest and enclosed parts of the reef. This has also led to the underrepresentation of mainly coral- and algae-dominated bottom types in the validation datasets, whereas the bare-substrate and seagrass classes are better represented. The number of validation points per bottom type, therefore, was inappropriate to guarantee the relevance of the individual user and producer accuracies, and could certainly not be used to assess the accuracy of the detailed QuickBird classification. Besides, the lack of ground-truth information for the 1987 Landsat 5 TM dataset prevents the statistical accuracy assessment of the change-detection map. Overall, the validity of the statistical parameters may be questioned and care should be taken when interpreting them. These measures, therefore, can only be seen as an indicator rather than a determinant of accuracy. Besides, the additional influence of the water column makes it very difficult to achieve the 80% accuracy standard set forward for LULC classifications, especially in the heterogeneous coral-reef environment. Moreover, the accuracy of the classifications is most likely augmented by the application of post-processing contextual editing. This can be determined through visual analysis of the different results, as the statistical validation dataset, again, is not suited to check these improvements, especially in the coral-dominated bottom type.

Taking everything into account, the use of optical, passive remote sensors has its merits as these datasets are readily available at relatively low costs making them more cost-effective than intensive field surveys to cover the same area. As such, they are ideal information providers for developing countries which often lack the financial and human capital for intensive field surveying or the acquisition of more elaborate data from airborne hyperspectral data or LIDAR data. Expensive processing software is not strictly needed either as has been proven by the use of the ILWIS 3.2 software. The use of datasets like the Landsat series and QuickBird, nevertheless, remain limited to relatively broad surveys of bathymetry and bottom-type composition on a regional to local scale. The ideal research approach should therefore be a multi-level sampling in which information from different sources and levels of detail is combined to obtain a more complete view on the coral-reef environment. In such a sampling strategy, Landsat datasets could be implemented to cost-effectively collect baseline data on the regional-scale distribution of coral reefs as well as to track major changes over time, whereas very-high-resolution data, such as QuickBird or IKONOS data, can be

integrated for more detailed inventories of specific focus areas (<500km²) supplemented with specialised information from in situ observations. Information derived from oceanographic sensors, such as MODIS, SeaWiFS or AVHRR, could as well be involved to monitor the conditions of the seas and oceans in which the coral reefs occur, even though the biogeophysical products are not yet totally validated over coastal areas.

A GIS is ideal to collect and archive these remote-sensing-derived data products and other information concerning the status of the coral reefs, the socio-economic uses of these natural resources and the changes of these elements over time. The 'Coral Reef GIS' is also perfectly suited to further analyse this collection of data to derive new information supporting ICZM decision-makers in planning and organising the coastal zone. The example of a risk assessment map has been given which delineates and visualises the marine coastal areas potentially affected by human activities. Besides illustrating the extremely threatened status of the coral reefs in the northwestern Red Sea, as almost the entire coral-reef zone is included in a medium risk zone stretching out over the entire study area, such map could be taken into account when planning a multi-use MPA as well as when implementing specific environmental rules to eliminate these potentially negative influences.

The initial draft multi-use MPA zoning plan has finally illustrated how the baseline information collected with remote sensing and the derived information, such as the risk assessment map, can support ICZM planning. It represents a possible scenario to accommodate nature conservation with sustainable development as well as different resource uses such as tourism, fishing and marine transportation. It should certainly not be interpreted as *the* optimal multi-use MPA solution as it is only based on remote sensing data and additional information is required concerning the socio-economic aspects of the coastal zone as well as more specific data from field surveys such as on fish population dynamics. Moreover, involvement of the government and the local stakeholders is needed before it could ever be sustainably implemented. However, it could form an ideal working document to involve the local stakeholders in the ICZM process and to come to a productive discussion about the future of the Red Sea coastal zone.

Globally, coral reefs have already seriously degraded and their future looks grim. Many individual disturbances directly or indirectly affect the coral reef, but most concern rises about the way these factors may interact to pose an even greater synergetic stress on the coral-reef ecosystem. Due to the links between the different elements in the seascape, interference with other tropical marine ecosystems may also have its effects on the coral reefs and vice versa. With the recognition of climate change as an increasing threat the '*coral reef crisis*'

(Buddemeier *et al.*, 2004) has become a global issue. On the one hand, people at the other end of the globe, where no reefs are present, indirectly affect the environment in which coral reefs occur, while, on the other hand, they may witness the direct effects of the degradation of this ecosystem (e.g. through the loss of the biochemical potential of coral organisms) as well. Because most coral species are not believed to be able to adapt or acclimate to the changing conditions, the composition of the reef may shift to more resistant, tolerant species or a phase shift may occur in which corals as dominant reef species are replaced by non-reefbuilding species, mainly fleshy macro-algae. Ultimately, coral reefs as an ecosystem will likely not become totally extinct, but on a space- and time-scale interesting for people who rely on the coral reef as a resource, this will have devastating effects. The situation is especially worrisome in developing countries, as people there already heavily depend on the coral reefs for at least part of their livelihoods and national governments often see the development of the coastal zone as a means to increase the wealth and welfare in their country. As the very complex interaction of disturbances threatening the survival of coral reefs is not yet fully understood, research is primarily needed on the exact effects of the disturbance on the coral-reef functioning and on the manner how different threats may interact. This will guide managers to take more effective measures which could eliminate or mitigate these threats. We, however, are quickly running out of time so that efforts are urgently required to protect coral reefs worldwide from further deterioration and to actively manage and conserve them for future generations. More and more detailed and management-oriented information on the global status of the coral reefs will thus become needed as well as tools to monitor the evolution of their status both under managed and unmanaged scenarios. Remote sensing is a valuable instrument to cost-effectively provide such information from the local to the global scale and should thus be promoted accordingly. To provide more accurate and detailed information, future research in the field of remote sensing for coral reef mapping should especially focus on the digital photogrammetric processing of stereoscopic remote sensing data, particularly with the availability of SPOT 5, IKONOS, QuickBird or Chris/Proba stereoscopic data which contain information in more workable wavelengths; on improving the bottom-type classification results derived from multispectral data through the determination of quantitative textural indicators or improved water-column correction algorithms; and on exploring the possibilities of hyperspectral remote sensing. Nowadays, this data is still very expensive and not ubiquitously employable but these restrictions may become reduced -e.g. by the development of the 'coral reef-specific satellite mission' or the use of UAVs- in future and these datasets may come in reach of studying coral reefs worldwide. These opportunities,

again, emphasise the importance multi-level sampling and the use of an open-ended hierarchical classification scheme so that current habitat maps can be updated with more detailed information derived from remote sensing data with a higher descriptive resolution, from field surveys, or from other ancillary sources.

REFERENCES

REFERENCES PART I

- Abram, N.J., Gagan, M.K., McCulloch, M.T., Chappell, J. and Hantoro, W.S., 2003. Coral reef death during the 1997 Indian Ocean dipole linked to Indonesian wildfires. *Science*, **301**: 952-955.
- Achituv, Y. and Dubinsky, Z., 1990. Evolution and zoogeography of coral reefs. In: Dubinsky, Z. (Ed.), *Coral Reefs: Ecosystems of the World 25*. Elsevier Science Publishers B.V. (Amsterdam: The Netherlands), pp. 1-10.
- Adey, W.H., 1998. Coral reefs: algal structured and mediated ecosystems in shallow, turbulent, alkaline waters. *Journal of Phycology*, **34**(3): 393-406.
- Adey, W.H., 2000. Coral reef ecosystems and human health: biodiversity counts! *Ecosystem Health*, **6**(4): 227-236.
- Anderson, S., Zepp, R., Machula, J., Santavy, D., Hansen, L. and Mueller, E., 2001. Indicators of UV exposure in corals and their relevance to global climate change and coral bleaching. *Human & Ecological Risk Assessment*, **7**(5): 1271-1282.
- Andersson, A.J., Mackenzie, F.T. and Lerman, A., 2006. Coastal ocean CO₂-carbonic acid-carbonate sediment system of the Anthropocene. *Global Biogeochemical Cycles*, **20**(1), GB1S92.
- Andrews, J.C. and Pickard, G.L., 1990. The physical oceanography of coral-reef systems. In: Dubinsky, Z. (Ed.), *Coral Reefs: Ecosystems of the World 25*. Elsevier Science Publishers B.V. (Amsterdam: The Netherlands), pp. 11-48.
- Baker, A.C., 2001. Reef corals bleach to survive change. *Nature*, **411**: 765-766.
- Barber, R.T., Hilting, A. and Hayes, M., 2001. The changing health of coral reefs. *Journal of Human and Ecological Risk Assessment*, **7**(5): 1255-1270.
- Barnes, D.J. and Chalker, B.E., 1990. Calcification and photosynthesis in reef-building corals and algae. In: Dubinsky, Z. (Ed.), *Coral Reefs: Ecosystems of the World 25*. Elsevier Science Publishers B.V. (Amsterdam: The Netherlands), pp. 109-131.
- Beer, T., 1983. *Environmental Oceanography – An Introduction to the Behaviour of Coastal Waters*. Pergamon Press Ltd. (Oxford: UK), pp. 169-189.
- Behairy, A.K.A., Sheppard, C.R.C. and El-Sayed, M.K., 1992. *A Review of the Geology of Coral Reefs in the Red Sea*. UNEP Regional Seas Reports and Studies No. 152, UNEP-PERSGA, 36p.
- Bellwood, D.R., Hughes, T.P., Folke, C. and Nyström, M., 2004. Confronting the coral reef crisis. *Nature*, **429**: 827-833.
- Berg, H., Öhman, M.C., Troëng, S. and Lindén, O., 1998. Environmental economics of coral reef destruction in Sri Lanka. *Ambio*, **27**(8): 627-634.
- Berkelmans, R. and Willis, B.L., 1999. Seasonal and local spatial patterns in the upper thermal limits of corals on the inshore Central Great Barrier Reef. *Coral Reefs*, **18**(3): 219-228.

- Best, B. and Bornbusch, A. (Eds.), 2001. *Global Trade and Consumer Choices: Coral Reefs in Crisis*. 2001 Annual Meeting of the American Association for the Advancement of Science, San Francisco, California, 19/02/2001. AAAS (Washington DC: USA), 32p.
- Birkeland, C., 1997a. Introduction. In: Birkeland, C. (Ed.), *Life and Death of Coral Reefs*. Chapman & Hall (New York: USA), pp. 1-12.
- Birkeland, C., 1997b. Implications for resource management. In: Birkeland, C., (Ed.), *Life and Death of Coral Reefs*. Chapman & Hall (New York: USA), pp. 411-435.
- Bormann, F.H. and Likens, G.E., 1979. *Pattern and Process in a Forested Ecosystem*. Springer-Verlag (New York: USA).
- Broecker, W.S., 2000. Abrupt climate change: causal constraints provided by the paleoclimatic record. *Earth Science Reviews*, **51**: 137-154.
- Broecker, W.S., 2003. Does the trigger for abrupt climate change reside in the ocean or the atmosphere? *Science*, **300**: 1519-1522.
- Brown, B.E., 1997a. Adaptations of reef corals to physical environmental stress. *Advances in Marine Biology*, **31**: 221-299.
- Brown, B.E., 1997b. Disturbances to reefs in recent times. In: Birkeland, C. (Ed.), *Life and Death of Coral Reefs*. Chapman & Hall (New York: USA), pp. 354-379.
- Bryant, D., Burke, L., McManus, J. and Spalding, M. (Eds.), 1998. *Reefs at Risk - a Map-Based Indicator of Threats to the World's Coral Reefs*. World Resources Institute (Washington: USA), 56p.
- Buddemeier, R.W. and Fautin, D.G., 1993. Coral bleaching as an adaptive mechanism: a testable hypothesis. *BioScience*, **43**(5): 320– 326.
- Buddemeier, R.W., Kleypas, J.A. and Aronson, R.B., 2004. *Coral Reefs & Global Climate Change - Potential Contributions of Climate Change to Stresses on Coral Reef Ecosystems*. Pew Center on Global Climate Change (Arlington, Virginia: USA), 56p.
- Caldeira, K. and Wickett, M.E., 2005. Ocean model predictions of chemistry changes from carbon dioxide emissions to the atmosphere and ocean. *Journal of Geophysical Research – Oceans*, **110**: C09S04.
- Carte, B.K., 1996. Biomedical potential of marine natural products. *BioScience*, **46**(4): 271-286.
- Central Intelligence Agency (CIA), 11/05/2004. *The World Fact Book*. Available online at: <http://www.cia.gov/cia/publications/factbook/geos/ps.html>, (Accessed: 26/07/2004).
- Cesar, H., 1996. *Economic Analysis of Indonesian Coral Reefs*. World Bank (Washington DC: USA), 103p.
- Cesar, H., Burke, L. and Pet-Soede, L., 2003. *The Economics of Worldwide Coral Reef Degradation*. Cesar Environmental Economics Consulting (Arnhem: The Netherlands), 24p.

- Chisholm, J.R.M. and Barnes, D.J., 1998. Anomalies in coral reef community metabolism and their potential importance in the reef CO₂ source-sink debate. *Proceedings of the National Academy of Science USA*, **95**: 6566-6569.
- Coch, N.K., 1995. *Geohazards – Natural and Human*. Prentice Hall Inc. (Englewood Cliffs, New Jersey: USA), pp. 370-392.
- Coffroth, M.A. and Santos, S.R., 2005. Genetic diversity of symbiotic dinoflagellates in the genus *Symbiodinium*. *Protist*, **156**: 19-34.
- Connell, J.H., 1978. Diversity in tropical rain forests and coral reefs. *Science*, **199**: 1302-1310.
- Connell, J.H., 1997. Disturbance and recovery of coral assemblages. *Coral Reefs*, **16**: 101-113.
- Coral Reef Information System (CoRIS), 2004a. *Glossary*. Available online at: <http://coris.noaa.gov/glossary/>, (Accessed: 19/07/2004).
- Coral Reef Information System (CoRIS), 2004b. *What are Coral Reefs?* Available online at: <http://coris.noaa.gov/glossary/>, (Accessed: 19/07/2004).
- Costanza, R., d'Arge, R., de Groot, R., Farber, S., Grasso, M., Hannon, B., Limburg, K., Naeem, S., O'Neil, R.V., Paruelo, J., Raskin, R.G., Sutton, R. and van den Belt, M., 1997. The value of the world's ecosystem services and natural capital. *Nature*, **387**: 253-260.
- Coyne, M.S., Battista, T.A., Anderson, M., Waddell, J., Smith, W., Jokiel, P., Kendall, M.S. and Monaco, M.E., 2003. *Benthic Habitats of the Main Hawaiian Islands*. NOAA Technical Memorandum NOS NCCOS CCMA 152. Available online at: <http://biogeo.nos.noaa.gov/projects/mapping/pacific/>, (Accessed: 04/04/2003).
- Cubash, U. and Meehl, G.A. (Eds.), 2001. Projections of future climate change. In: Houghton, J.T., Ding, Y., Griggs, D.J., Noguer, M., van der Linden, P.J. and Xiaosu, D. (Eds.), *IPCC Third Assessment Report: Climate Change 2001: The Scientific Basis*. Available online at: http://www.grida.no/climate/ipcc_tar/index.htm, (Accessed: 04/12/2002).
- Daly, R.A., 1915. The glacial-control theory of coral reefs. *Proceedings of the American Academy of Arts and Science*, **51**: 155-251.
- Darwin, C., 1842. On the distribution of coral reefs with reference to the theory of their formation. Smith, Elder and Co. (London: UK). In: van Wyhe, J. (Ed.), *The Writings of Charles Darwin on the Web*. Available online at: http://pages.britishlibrary.net/charles.darwin4/coral/coral_fm.html, (Accessed: 22/07/2004).
- Davenport, J. and Davenport, J.L., 2006. The impact of tourism and personal leisure transport on coastal environments: A review. *Estuarine, Coastal and Shelf Science*, **67**(1-2): 280-292.
- Davis, R.A. Jr. and FitzGerald, D.M., 2004. *Beaches and Coasts*. Blackwell Science Ltd. (Malden, Maryland: USA), pp. 353-370.
- Davis, W.M., 1923. The marginal belts of the coral seas. *Proceedings of the National Academy of Science USA*, **9**(8): 292-296.

- Done, T.J., 1992. Phase shifts in coral reef communities and their ecological significance. *Hydrobiologia*, **247**: 121–132
- Done, T.J., 1999. Coral community adaptability to environmental change at the scales of regions, reefs and reef zones. *American Zoologist*, **39**(1): 66-79.
- Donner, S.D., Skirving, W.J., Little, C.M., Oppenheimer, W. and Hoegh-Guldberg, O., 2005. Global assessment of coral bleaching and required rates of adaptation under climate change. *Global Change Biology*, **11**(12): 2251-2265.
- Donohue, M.J., Boland, R.C., Sramek, C.M. and Antonelis, G.A., 2001. Derelict fishing gear in the north-western Hawaiian Islands: diving surveys and debris removal in 1999 confirm threat to coral reef ecosystems. *Marine Pollution Bulletin*, **42**(12): 1301-1312.
- Dorenbosch, M., van Riel, M.C., Nagelkerken, I. and van der Velde, G., 2004. The relationship of reef fish densities to the proximity of mangrove and seagrass nurseries. *Estuarine, Coastal and Shelf Science*, **60**(1): 37-48.
- Douglas, A.E., 2003. Coral bleaching – how and why? *Marine Pollution Bulletin*, **46**(4): 385-392.
- Eaton, P. and Radojevic, M., 2001. *Forest Fires and Regional Haze in Southeast Asia*. Nova Science Publishers (New York: USA), 280p.
- Emanuel, K., 2005. Increasing destructiveness of tropical cyclones over the past 30 years. *Nature*, **436**: 686-688.
- Fabricius, K.E., 2005. Effects of terrestrial runoff on the ecology of corals and coral reefs: Review and synthesis. *Marine Pollution Bulletin*, **50**: 125-146.
- Fabricius, K.E. and Wolanski, E., 2000. Rapid smothering of coral reef organisms by muddy marine snow. *Estuarine, Coastal and Shelf Science*, **50**(1): 115-120.
- Faure, G., 1989. Degradation of coral reefs at Moorea Island (French Polynesia) by *Acanthaster planci*. *Journal of Coastal Research*, **5**(2): 295-305.
- Fautin, D.G. and Mariscal, R.N., 1991. Cnidaria: Anthozoa. In: Harrison, F.W. and Westfall, J.A. (Eds.), *Microscopic Anatomy of Invertebrates, Volume 2: Placozoa, Porifera, Cnidaria, and Ctenophora*. Wiley-Liss Inc. (New York: USA), pp. 267-358.
- Fautin, D.G. and Romano, S., 1997. *Cnidaria*. Tree of Life Web Project. Available online at: <http://tolweb.org/tree?group=Cnidaria&contgroup=Animals>, (Accessed: 12/07/2004).
- Fautin, D.G. and Romano, S., 2000. *Anthozoa*. Tree of Life Web Project. Available online at: <http://tolweb.org/tree?group=Anthozoa&contgroup=Cnidaria>, (Accessed: 12/07/2004).
- Fautin, D.G., Romano, S.L. and Oliver, W.A. Jr., 2000. *Zoantharia*. Tree of Life Web Project. Available online at: <http://tolweb.org/tree?group=Zoantharia&contgroup=Anthozoa>, (Accessed: 12/07/2004).
- Falkowski, P.G., Jokiel, P.L. and Kinzie, R.A. III, 1990. Irradiance and corals. In: Dubinsky, Z. (Ed.), *Coral Reefs: Ecosystems of the World 25*. Elsevier Science Publishers B.V. (Amsterdam: The Netherlands), pp. 89-107.

- Fenical, W., 1996. Marine biodiversity and the medicine cabinet: the status of new drugs from marine organisms. *Oceanography*, **9**: 23-27.
- Fernando, H.J.S., McCulley, J.L., Mendis, S.G. and Perera, K., 2005. Coral poaching worsens tsunami destruction in Sri Lanka. *Eos Transactions*, **86**: 301-304.
- Fitt, W.K., 2004. The sublethal bleaching response. In: Hendee, J. (Ed.), *The Effects of Combined Sea Temperature, Light, and Carbon Dioxide on Coral Bleaching, Settlement, and Growth*. The First Annual Combined Effects Think Tank to Support CREWS Modeling, NOAA, pp. 43-46.
- Fitt, W.K., Brown, B.E., Warner, M.E. and Dunne, R.P., 2001. Coral bleaching: Interpretation of thermal tolerance limits and thermal thresholds in tropical corals. *Coral Reefs*, **20**(1): 51-65.
- Fitt, W.K., McFarland, F.K., Warner, M.E. and Chilcoat, G.C., 2000. Seasonal patterns of tissue biomass and densities of symbiotic dinoflagellates in reef corals and relation to coral bleaching. *Limnology and Oceanography*, **45**(3):677-685.
- Folland, C.K. and Karl, T.R. (Eds.), 2001. Observed climate variability and change. In: Houghton, J.T., Ding, Y., Griggs, D.J., Noguer, M., van der Linden, P.J. and Xiaosu D. (Eds.), *IPCC Third Assessment Report: Climate Change 2001: The Scientific Basis*. Available online at: http://www.grida.no/climate/ipcc_tar/index.htm, (Accessed: 04/12/2002).
- Fox, H.E., Pet, J.S., Dahuri, R. and Caldwell, R.L., 2003. Recovery in rubble fields: long-term impacts of blast fishing. *Marine Pollution Bulletin*, **46**(8): 1024-1031.
- Freiwald, A., 2002. Reef-forming cold-water corals. In: Wefer, G., Billett, D., Hebbeln, D., Jørgensen, B.B., Schlüter, M. and van Weering, T. (Eds.), *Ocean Margin Systems*, Springer-Verlag (Berlin Heidelberg, Germany), pp. 365-385.
- Fujiwara, S., Shibuno, T., Mito, K., Nakai, T., Sasaki, Y., Dai, C.F. and Chen, G., 2000. Status of coral reefs of East and North Asia: China, Japan and Taiwan. In: Wilkinson, C. (Ed.), *Status of Coral Reefs of the World: 2000*. Australian Institute for Marine Science (Townsville: Australia), pp. 131-140.
- Gleason, D.F., 2004. Effect of light on coral reproduction and recruitment. In: Hendee, J. (Ed.), *The Effects of Combined Sea Temperature, Light, and Carbon Dioxide on Coral Bleaching, Settlement, and Growth*. The First Annual Combined Effects Think Tank to Support CREWS Modeling, NOAA, pp. 53-56.
- Gleason, D.F. and Wellington, G.M., 1993. Ultraviolet radiation and coral bleaching. *Nature*, **365**: 836-838.
- Glynn, P.W., 1991. Coral reef bleaching in the 1980s and possible connections with global warming. *Trends in Ecology and Evolution*, **6**(6): 175-179.
- Goreau, T., McClanahan, T., Hayes, R. and Strong, A., 2000. Conservation of coral reefs after the 1998 global bleaching event. *Conservation Biology*, **20**(1): 5-15.
- Green, E.P. and Bruckner, A.W., 2000. The significance of coral disease epizootiology for coral reef conservation. *Biological Conservation*, **96**(3): 347-361.

- Grigg, R.W. and Dollar, S.J., 1990. Natural and anthropogenic disturbance on coral reefs. In: Dubinsky, Z. (Ed.), *Coral Reefs: Ecosystems of the World 25*. Elsevier Scientific Publishers B.V. (Amsterdam: The Netherlands), pp. 439-452.
- Guinotte, J.M., Buddemeier, R.W. and Kleypas, J.A., 2003. Future coral reef habitat marginality: Temporal and spatial effects of climate change in the Pacific basin. *Coral Reefs*, **22**(4): 551-558.
- Guzmán, H.M. and Holst, I., 1993. Effects of chronic oil-sediment pollution on the reproduction of the Caribbean reef coral *Siderastrea siderea*. *Marine Pollution Bulletin*, **26**(5): 276-282.
- Häder, D.-P., Worrest, R.C., Kumar, H.D. and Smith, R.C., 1994. Effects of increased solar ultraviolet radiation on aquatic ecosystems. In: UNEP, *Environmental Effects of Ozone Depletion: 1994 Assessment*. Available online at: <http://sedac.ciesin.org/ozone/UNEP/chap4.html>, (Accessed: 13/08/2004).
- Hallock, P., 1997. Reefs and reef limestones in earth history. In: Birkeland, C. (Ed.), *Life and Death of Coral Reefs*. Chapman & Hall (New York: USA), pp. 13-42.
- Harriott, V.J., 1999. Coral growth in subtropical eastern Australia. *Coral Reefs*, **18**(3): 281-291.
- Hatcher, B.G., 1997. Coral reef ecosystems: how much greater is the whole than the sum of the parts? *Proceedings of the 8th International Coral Reef Symposium*, Vol. **1**: 43-56.
- Harley, C.D.G., Hughes, A.R., Hultgren, K.M., Miner, B.G., Sorte, C.J.B., Thomber, C.S., Rodriguez, L.F., Tomanek, L., and Williams, S.L., 2006. The impacts of climate change in coastal marine systems. *Ecology Letters*, **9**(2): 228-241.
- Harvell, C.D., Kim, K., Burkholder, J.M., Colwell, R.R., Epstein, P.R., Grimes, D.J., Hofmann, E.E., Lipp, E.K., Osterhaus, M.E., Overstreet, R.M., Porter, J.W., Smith, G.W. and Vasta, G.R., 1999. Emerging marine diseases – Climate links and anthropogenic factors. *Science*, **285**: 1505-1510.
- Harvell, C.D., Mitchell, C.E., Ward, J.R., Altizer, S., Dobson, A.P., Ostfeld, R.S. and Samuel, M.D., 2002. Climate warming and disease risks for terrestrial and marine biota. *Science*, **296**: 2158-2162.
- Head, S.M., 1987a. Introduction. In: Edwards, A.J. and Head, S.M. (Eds.), *Key Environments: Red Sea*. Pergamon Press (Oxford: UK), pp. 1-21.
- Head, S.M., 1987b. Corals and coral reefs of the Red Sea. In: Edwards, A.J. and Head, S.M. (Eds.), *Key Environments: Red Sea*. Pergamon Press (Oxford: UK), pp.128-151.
- Hendee, J. (Ed.), 2004. *The Effects of Combined Sea Temperature, Light, and Carbon Dioxide on Coral Bleaching, Settlement, and Growth*. The First Annual Combined Effects Think Tank to Support CREWS Modeling. NOAA, 126p.
- Herre, E.A., Knowlton, N., Mueller, U.G. and Rehner, S.A., 1999. The evolution of mutualisms: exploring the paths between conflict and cooperation. *Trends in Ecology and Evolution*, **14**(2): 49-53.
- Hessinger, D.A. and Lenhoff, H.M., 1988. Preface. In: Hessinger, D.A. and Lenhoff, H.M. (Eds.), *The Biology of Nematocysts*. Academic Press (San Diego: USA), pp. xi-xii.

- Hinrichsen, D., 1997. Requiem for reefs? *International Wildlife*. Available online at: <http://www.nwf.org/internationalwildlife/contma97.html>, (Accessed: 25/07/2004).
- Hodgson, G., 1997. Resource use: conflicts and management solutions. In: Birkeland, C. (Ed.), *Life and Death of Coral Reefs*. Chapman & Hall (New York: USA), pp. 386-410.
- Hoegh-Guldberg, O., 2000. *Climate Change, Coral Bleaching and the Future of the World's Coral Reefs*. Greenpeace, 27p.
- Hoegh-Guldberg, O., Jones, R.J., Ward, S. and Loh, W.K., 2002. Is coral bleaching really adaptive? *Nature*, **415**: 601-602.
- Hoegh-Guldberg, O. and Smith, G. J., 1989. The effect of sudden changes in temperature, irradiance and salinity on the population density and export of zooxanthellae from the reef corals *Stylophora pistillata* Esper and *Seriatopora hystrix* Dana. *Journal of Experimental Marine Biology and Ecology*, **129**(3): 279-303.
- Hoepner, T. and Latteman, S., 2002. Chemical impacts from seawater desalination plants - a case study of the northern Red Sea. *Desalination*, **152**(1-3): 133-140.
- Holling, C.S. and Meffe, G.K., 1996. Command and control and the pathology of natural resource management. *Conservation Biology*, **10**(2): 328-337.
- Holling, C.S., Schindler, D.W., Walker, B.W. and Roughgarden, J., 1995. Biodiversity in the functioning of ecosystems: an ecological synthesis. In: Perrings, C., Mähler, K.-G., Folke, C., Holling, C.S. and Jansson, B.-O. (Eds.), *Biodiversity Loss: Ecological and Economical Issues*. Cambridge University Press (Cambridge: UK), pp. 44-83.
- Holmes, K.E., Edinger, E.N., Hariyadi, Limmon, G.V. and Risk, M.J., 2000. Bioerosion of live massive corals and branching coral rubble on Indonesian coral reefs. *Marine Pollution Bulletin*, **40**(7): 606-617.
- Holthus, P.F. and Maragos, J.E., 1995. Marine ecosystem classification for the tropical island Pacific. In: Maragos, J.E., Peterson, M.N.A., Eldredge, L.G., Bardach, J.E. and Takeuchi, H.F. (Eds.), *Marine and Coastal Biodiversity in the Tropical Island Pacific Region*. East-West Center (Honolulu: USA), pp. 239-278.
- Hubbard, D.K., 1997. Reefs as dynamic systems. In: Birkeland, C. (Ed.), *Life and Death of Coral Reefs*. Chapman & Hall (New York: USA), pp. 43-67.
- Hughes, T.P., Baird, A.H., Bellwood, D.R., Card, M., Connolly, S.R., Folke, C., Grosberg, R., Hoegh-Guldberg, O., Jackson, J.B.C., Kleypas, J., Lough, J.M., Marshall, P., Nyström, M., Palumbi, S.R., Pandolfi, J.M., Rosen, B. and Roughgarden, J., 2003. Climate change, human impacts, and the resilience of coral reefs. *Science*, **301**: 929-933.
- Huntington, T.G., 2006. Evidence for intensification of the global water cycle: Review and synthesis. *Journal of Hydrology*, **319**: 83-95.
- Huston, M.A., 1985. Patterns of species diversity on coral reefs. *Annual Review of Ecology and Systematics*, **16**: 149-177.

- International Coral Reef Information Network (ICRIN), 2002. *Coral Reefs Fact Sheet*. Available online at: <http://www.coralreef.org/factSheets/coralreef.html>, (Accessed: 14/07/2004).
- Jackson, J.B.C., Kirby, M.X., Berger, W.H., Bjorndal, K.A., Botsford, L.W., Bourque, B.J., Bradbury, R.H., Cooke, R., Erlandson, J., Estes, J.A., Hughes, T.P., Kidwell, S., Lange, C.B., Lenihan, H.S., Pandolfi, J.M., Peterson, C.H., Steneck, R.S., Tegner, M.J. and Warner, R.R., 2001. Historical overfishing and the recent collapse of coastal ecosystems. *Science*, **293**: 629-637.
- Jameson, S.C., McManus, J.W. and Spalding, M.D., 1995. *State of the reefs: regional and global perspectives*. Available online at: <http://www.ngdc.noaa.gov/paleo/outreach/coral/sor/>, (Accessed: 25/07/2004).
- Jokiel, P.L., 1980. Solar ultraviolet radiation and coral reef epifauna. *Science*, **207**: 1069-1071.
- Jones, R.J. and Hoegh-Guldberg, O., 1999. Effects of cyanide on coral photosynthesis: Implications for identifying the cause of coral bleaching and for assessing the environmental effects of cyanide fishing. *Marine Ecology Progress Series*, **177**: 83-91.
- Jones, R.J., Hoegh-Guldberg, O., Larkum, A.W.D. and Schreiber, U., 1998. Temperature induced bleaching of corals begins with impairment of the CO₂ fixation mechanism in zooxanthellae. *Plant, Cell & Environment*, **21**(12): 1219-1230.
- Kennedy, D. and Woodroffe, C.D., 2002. Fringing reef growth and morphology: A review. *Earth-Science Reviews*, **57**(3-4): 255-277.
- Kinzie, R.A. III, Takayama, M., Santos, S.R. and Coffroth, M.A., 2001. The adaptive bleaching hypothesis: experimental tests of critical assumptions. *Biological Bulletin*, **200**(1): 51-58.
- Kleypas, J.A., Buddemeier, R.W., Archer, D., Gattuso, J.P., Langdon, C. and Opdyke, B.N., 1999a. Geochemical consequences of increased atmospheric carbon dioxide on coral reefs. *Science*, **294**: 118-120.
- Kleypas, J.A., Buddemeier, R.W. and Gattuso, J.-P., 2001. The future of coral reefs in an age of global change. *International Journal of Earth Sciences*, **90**: 426-437.
- Kleypas, J.A., Feely, R.A., Fabry, V.J., Langdon, C., Sabine, C.L. and Robbins, L.L., 2006. *Impacts of Ocean Acidification on Coral Reefs and Other Marine Calcifiers: A Guide for Future Research*. Report of a workshop held 18-20 April 2005, St. Petersburg (Florida), sponsored by NSF, NOAA and USGS, 88pp.
- Kleypas, J.A., McManus, J.W. and Meñez, L.A.B., 1999b. Environmental limits to coral reef development: where do we draw the line? *American Zoologist*, **39**(1): 146-159.
- Knowlton, N., 1992. Thresholds and multiple stable states in coral reef community dynamics. *American Zoologist*, **32**: 674-682.
- Knowlton, N., 2001. The future of coral reefs. *Proceedings of the National Academy of Science*, **98**(10): 5419-5425.
- Knowlton, N. and Rowher, F., 2003. Multispecies microbial mutualisms on coral reefs: the host as a habitat. *The American Naturalist*, **162** suppl.: S51-S62.

- Koop, K., Booth, D., Broadbent, A., Brodie, J., Bucher, D., Capone, D., Coll, J., Dennison, W., Erdmann, M., Harrison, P., Hoegh-Guldberg, O., Hutching, P., Jones, G.B., Larkum, A.W.D., O'Neil, J., Steven, A., Tentori, E., Ward, S., Williamson, J. and Yellowlees, D., 2001. ENCORE: the effect of nutrient enrichment on coral reefs - Synthesis of results and conclusions. *Marine Pollution Bulletin*, **42**(2): 91-120.
- Kushmaro, A., Rosenberg, E., Fine, M., Ben-Haim, Y. and Loya, Y., 1998. Effect of temperature on bleaching of the coral *Oculina patagonica* by *Vibrio* AK-1. *Marine Ecology Progress Series*, **171**: 131-137.
- Ladd, H.S. and Schlanger, S.O., 1960. *Drilling operations on Enewetak Atoll*. USGS Professional 260-Y, U.S. Gov. Printing Office (Washington D.C.: USA).
- LaJeunesse, T., 2002. Diversity and community structure of symbiotic dinoflagellates from Caribbean coral reefs. *Marine Biology*, **141**(2): 387-400.
- Langdon, C., 2004. Effects of CO₂ on coral growth and calcification. In: Hendee, J. (Ed.), *The Effects of Combined Sea Temperature, Light, and Carbon Dioxide on Coral Bleaching, Settlement, and Growth*. The First Annual Combined Effects Think Tank to Support CREWS Modeling, NOAA, pp. 105-110.
- Lesser, M.P., 1996. Exposure of symbiotic dinoflagellates to elevated temperatures and ultraviolet radiation causes oxidative stress and inhibits photosynthesis. *Limnology and Oceanography*, **41**: 271-283.
- Lesser, M.P., 2004a. Experimental biology of coral reef ecosystems. *Journal of Experimental Marine Biology and Ecology*, **300**: 217-252.
- Lesser, M.P., 2004b. Response of corals to solar radiation and temperature. In: Hendee, J. (Ed.), *The Effects of Combined Sea Temperature, Light, and Carbon Dioxide on Coral Bleaching, Settlement, and Growth*. The First Annual Combined Effects Think Tank to Support CREWS Modeling, NOAA, pp. 37-42.
- Lesser, M.P., Stochaj, W.R., Tapley, D.W. and Shick, J.M., 1990. Bleaching in coral reef Anthozoans: effects of irradiance, ultraviolet radiation, and temperature on the activities of protective enzymes against active oxygen. *Coral Reefs*, **8**: 225-232.
- Levinton, J.S., 1982. *Marine Ecology*. Prentice-Hall Inc. (Englewood Cliffs, New Jersey: USA), pp. 394-418.
- Lewis, S.M., 1986. The role of herbivorous fishes in the organization of a Caribbean reef community. *Ecological Monographs*, **56**(3), 183-200.
- Lipp, E., Jarrell, J.L., Griffin, D.W., Lukasik, J., Jacukiewicz, J. and Rose, J.B., 2002. Preliminary evidence for human faecal contamination in corals of the Florida Keys, USA. *Marine Pollution Bulletin*, **44**(7): 666-670.

- Liu, P.L.-F., Lynett, P., Fernando, H., Jaffe, B.E., Fritz, H., Higman, B., Morton, R., Goff, J. and Synolakis, C., 2005. Observations by the International Tsunami Survey Team in Sri Lanka. *Science*, **306**: 1595.
- Loya, Y., Sakai, K., Yamazato, K., Nakano, Y., Sambali, H. and van Woesik, R., 2001. Coral bleaching: The winners and the losers. *Ecology Letters*, **4**(2): 122–131.
- Maddison, D.R. and Schulz, K.-S. (Eds.), 2006. *The Tree of Life Web Project*. Available online at: <http://tolweb.org>, (Accessed: 22/08/2006).
- Madronich, S., McKenzie, R.L., Björn, L.O. and Caldwell, M.M., 1998. Changes in biologically active ultraviolet radiation reaching the Earth's surface. *Journal of Photochemistry and Photobiology B: Biology*, **46**: 5– 19.
- Manabe, S. and Stouffer, R.J., 1993. Century-scale effects of increased atmospheric CO₂ on the ocean-atmospheric system. *Nature*, **364**: 215-218.
- Maragos, J.E., Crosby, M.P. and McManus, J.W., 1996. Coral reefs and biodiversity: a critical and threatened relationship. *Oceanography*, **9**: 83-99.
- Maxwell, W.G.H. and Swinchart, J.P., 1970. Great Barrier Reef: regional variation in a terrigenous-carbonate province. *Geological Society of America Bulletin*, **81**: 691-724.
- McClanahan, T.R., 1995. A coral reef ecosystem-fisheries model: impacts of fishing intensity and catch selection on reef structure and processes. *Ecological Modelling*, **80**(1): 21-26.
- McClanahan, T.R., 2002. The near future of coral reefs. *Environmental Conservation*, **29**(4): 460-483.
- McClanahan, T.R., Cokos, B.A. and Sala, E., 2002. Algal growth and species composition under experimental control of herbivory, phosphorus and coral abundance in Glovers Reef, Belize. *Marine Pollution Bulletin*, **44**(6): 441-451.
- McClanahan, T.R., Sala, E., Mumby, P.J. and Jones, S., 2004. Phosphorus and nitrogen enrichment do not enhance brown frondose "macroalgae". *Marine Pollution Bulletin*, **48**(1-2): 196-199.
- McCook, L.J., 1999. Macroalgae, nutrients and phase shifts on coral reefs: scientific issues and management consequences for the Great Barrier Reef. *Coral Reefs*, **18**(4): 357–367.
- McKenzie, R.L., Björn, L.O., Bais, A. and Ilyasd, M., 2002. Changes in biologically active ultraviolet radiation reaching the Earth's surface. In: UNEP, *Environmental effects of ozone depletion and its interactions with climate change: 2002 assessment*. (Reprinted in: *Photochemical & Photobiological Sciences*, 2: 5-15). Available online at: <http://www.gcric.org/UNEP2002/6unep2002UVrad.pdf>, (Accessed: 13/08/2004).
- McLean, R.F. and Tsyban, A. (Eds.), 2001. Coastal zones and marine ecosystems. In: McCarthy, J.J., Canziani, O.F., Leary, N.A., Dokken, D.J. and White, K.S. (Eds.), *IPCC Third Assessment Report: Climate Change 2001: Impacts, Adaptation, and Vulnerability*. Available online at: http://www.grida.no/climate/ipcc_tar/index.htm, (Accessed: 04/12/2002).

- McManus, J.W., Meñez, L.A.B., Kesner-Reyes, K.N., Vergara, S.G. and Ablan, M.C., 2000. Coral reef fishing and coral-algal phase shifts: implications for global reef status. *ICES Journal of Marine Science*, **57**(3): 572-578.
- McManus, J.W. and Polsenberg, J.F., 2004. Coral-algal phase shifts on coral reefs: ecological and environmental aspects. *Progress in Oceanography*, **60**(2-4): 263-279.
- McManus, J.W. and Vergara, S.G., 1998. *Reef base: a global database on coral reefs and their resources*. Version 3.0 CD-ROM and user's guide. ICLARM (Manila: Philippines), 180p.
- McLaughlin, C.J., Smith, C.A., Buddemeier, R.W., Bartley, J.D. and Maxwell, B.A., 2003. Rivers, runoff, and reefs. *Global and Planetary Change*, **39**(1-2): 191-199.
- Miller, M.W., Hay, M.E., Miller, S.L., Malone, D., Soka, E.E. and Szmant, A.M., 1999. Effects of nutrients versus herbivores on reef algae: a new method for manipulating nutrients on coral reefs. *Limnology and Oceanography*, **44**(8): 1847-1861.
- Milliman, J.D., 1974. *Marine Carbonates*. Springer-Verlag (Berlin: Germany), 373p.
- Moberg, F. and Folke, C., 1999. Ecological goods and services of coral reef ecosystems. *Ecological Economics*, **29**: 215-233.
- Moore, F. and Best, B., 2001. Coral reef crisis: causes and consequences. In: Best, B. and Bornbusch, A. (Eds.), *Global Trade and Consumer Choices: Coral Reefs in Crisis*. 2001 Annual Meeting of the American Association for the Advancement of Science, San Francisco, California, 19/02/2001. AAAS (Washington DC: USA), pp. 5-9.
- Muller-Parker, G. and D'Elia, C., 1997. Interactions between corals and their symbiotic algae. In: Birkeland, C. (Ed.), *Life and Death of Coral Reefs*. Chapman & Hall (New York: USA), pp. 96-113.
- Mumby, P.J., Edwards, A.J., Arias-González, J.E., Lindeman, K.C., Blackwell, P.G., Gall, A., Górczynska, M.I., Harborne, A.R., Pescod, C.L., Renken, H., Wabnitz, C.C.C. and Llewellyn, G., 2004. Mangroves enhance the biomass of coral reef fish communities in the Caribbean. *Nature*, **427**: 533-536.
- Mumby, P.J. and Harborne, A.R., 1999a. Development of a systematic classification scheme of marine habitats to facilitate regional management and mapping of Caribbean coral reefs. *Biological Conservation*, **88**: 155-163.
- Mumby, P.J. and Harborne, A.R., 1999b. *Classification Scheme for Marine Habitats of Belize* (fifth draft). UNDP/GEF Belize Coastal Zone Management Project. Available online at: http://www.birdlist.org/downloads/Coral_classification_scheme.pdf, (Accessed: 29/10/2002).
- Muscantine, L., 1990. The role of symbiotic algae in carbon and energy flux in reef corals. In: Dubinsky, Z. (Ed.), *Coral Reefs: Ecosystems of the World 25*. Elsevier Science Publishers B.V. (Amsterdam: The Netherlands), pp. 75-87.

- Negri, A.P., Smith, L.D., Webster, N.S. and Heyward, A.J., 2002. Understanding ship-grounding impacts on a coral reef: potential effects of anti-foulant paint contamination on coral recruitment. *Marine Pollution Bulletin*, **44**(2): 111-117.
- Neil, D., 1990. Potential for coral stress due to sediment resuspension and deposition by reef walkers. *Biological Conservation*, **52**(3), 221–227.
- Neumann, A.C. and Macintyre, I., 1985. Reef response to sea-level rise: keep-up, catch-up, or give-up. *Proceedings of the 5th International Coral Reef Congress*, Tahiti, Vol. **3**: 105-110.
- Nixon, S.W., 1995. Coastal marine eutrophication: a definition, social causes and future concerns. *Ophelia*, **41**: 199-219.
- Nybakken, J.W. and Bertness, M.D., 2005. *Marine Biology – An Ecological Approach*. Pearson – Benjamin Cummings (San Francisco, USA), pp. 407-453.
- Nyström, M., Folke, C. and Moberg, F., 2000. Coral reef disturbance and resilience in a human-dominated environment. *Trends in Ecology and Evolution*, **15**(10): 413-417.
- Obura, D. and Abdulla, A., 2005. *Assessment of Tsunami Impacts on the Marine Environment of the Seychelles*. CORDIO and IUCN, 17p.
- Odum, H.T., 1971. *Environment, Power and Society*. Wiley-Interscience (New York: USA), 331p.
- Odum, H.T. and Odum, E.P., 1955. Trophic structure and productivity of a windward reef community on Eniwetok Atoll. *Ecological Monographs*, **25**(3): 291-320.
- Ogden, J.C., 1987. Cooperative coastal ecology at Caribbean marine laboratories. *Oceanus*, **30**: 9-15.
- Ogden, J.C., 1997. Ecosystem interactions in the tropical coastal seascape. In: Birkeland, C. (Ed.), *Life and Death of Coral Reefs*. Chapman & Hall (New York: USA), pp. 288-297.
- Ogden, J.C. and Gladfelter, E.H. (Eds.), 1983. Coral reefs, seagrass beds and mangroves: Their interaction in coastal zones of the Caribbean. *UNESCO Reports in Marine Science*, **23**: 133p.
- Orr, J. C., Fabry, V.J., Aumont, O., Bopp, L., Doney, S.C., Feely, R.A., Gnanadesikan, A., Gruber, N., Ishida, A., Joos, F., Key, R.M., Lindsay, K., Maier-Reimer, E., Matear, R., Monfray, P., Mouchet, A., Najjar, R.G., Plattner, G.-K., Rodgers, K.B., Sabine, C.L., Sarmiento, J.L., Schlitzer, R., Slater, R.D., Totterdell, I.J., Weirig, M.-F., Yamanaka, Y. and Yool, A., 2005. Anthropogenic ocean acidification over the twenty-first century and its impact on calcifying organisms. *Nature*, **437**: 681-686.
- Pandolfi, J.M., Bradbury, R.H., Sala, E., Hughes, T.P., Bjorndal, K.A., Cooke, R.G., McArdle, D., McClanachan, L., Newman, M.J.H., Paredes, G., Warner, R.R. and Jackson, J.B.C., 2003. Global trajectories of the long-term decline of coral reef ecosystems. *Science*, **301**: 955-958.
- Pet-Soede, L., Cesar, H. and Pet, J., 2000. Blasting away: the economics of blast fishing on Indonesian coral reefs. In: Cesar, H. (Ed.), *Collected Essays on the Economics of Coral Reefs*, CORDIO (Kalmar: Sweden), pp. 77-84.

- Precht, W.F. and Aronson, R.B., 2003. Climate flickers and range shifts of corals. *Geological Society of America Abstracts with Programs*, **35**(6): 84. Available online at: http://gsa.confex.com/gsa/2003AM/finalprogram/abstract_58069.htm, (Accessed: 14/08/2004).
- Reaka-Kudla, M.L., 1996. The global biodiversity of coral reefs: a comparison with rain forests. In: Reaka-Kudla, M.L., Wilson, D.E. and Wilson, E.O. (Eds.), *Biodiversity II: Understanding and Protecting Our Biological Resources*. Joseph Henry Press (Washington: USA), pp. 83-108.
- Reaser, J.K., Pomerance, R. and Thomas, P.O., 2000. Coral bleaching and global climate change: scientific findings and policy recommendations. *Conservation Biology*, **14**(5): 1500-1511.
- Richardson, L.L., 1998. Coral diseases: What is really known? *Trends in Ecology and Evolution*, **13**(11): 438-443.
- Riegl, B. and Luke, K.E., 1998. Ecological parameters of dynamited reefs in the northern Red Sea and their relevance to reef rehabilitation. *Marine Pollution Bulletin*, **37**(8-12): 488-498.
- Risk, M.J., Sammarco, P.W. and Edinger, E.N., 1995. Bioerosion in *Acropora* across the continental shelf of the Great Barrier Reef. *Coral Reefs*, **14**(2): 79-86.
- Roberts, C.M., 1995. Effects of fishing on the ecosystem structure of coral reefs. *Conservation Biology*, **9**(5): 988-995.
- Rodgers, K.S. and Cox, E.F., 2003. The effects of trampling on Hawaiian corals along a gradient of human use. *Biological Conservation*, **112**(3): 383-389.
- Romano, S.L. and Cairns, S.D., 2002. *Scleractinia*. Tree of Life Web Project. Available online at: <http://tolweb.org/tree?group=Scleractinia&contgroup=Zoantharia>, (Accessed: 12/07/2004).
- Rosenberg, E. and Ben-Haim, Y., 2002. Microbial diseases of corals and global warming. *Environmental Microbiology*, **4**(6): 318-326.
- Rouphael, A.B. and Inglis, G.J., 1997. Impacts of recreational SCUBA diving at sites with different reef topographies. *Biological Conservation*, **82**(3): 329-336.
- Russ, G.R., 1984. A review of coral reef fisheries. *UNESCO Reports in Marine Science*, **27**: 74-92.
- Salih, A., Larkum, A., Cox, G., Kühl, M. and Hoegh-Guldberg, O., 2000. Fluorescent pigments in corals are photoprotective. *Nature*, **408**: 850-853.
- Sargent, M.C. and Austin, T.S., 1949. Organic productivity of an atoll. *Transactions of the American Geophysical Union*, **30**: 245-249.
- Scheffer, M. and Carpenter, S.R., 2003. Catastrophic regime shifts in ecosystems: linking theory to observation. *Trends in Ecology and Evolution*, **18**(12): 648-656.
- Schlichter, D., Weber, W. and Fricke, H.W., 1985. A chromatophore system in the hermatypic, deep-water coral *Leptoseris fragilis* (Anthozoa : Hexacorallia). *Marine Biology*, **89**: 143-147.
- Schubert, R., Schellnhuber, H.-J., Buchmann, N., Epiney, A., Griesshammer, R., Kulesa, M., Messner, D., Rahmstorf, S. and Schmid, J., 2006. *The Future Oceans - Warming Up, Rising High, Turning Sour*. German Advisory Council on Global Change (WBGU) (Berlin: Germany), xii + 110p.

- Scientific Committee on Oceanic Research (SCOR) and Intergovernmental Oceanographic Commission (IOC), 2004. *Priorities for Research on the Ocean in a High-CO₂ World*. Symposium on the Ocean in a High-CO₂ World, Paris, 10-12 May 2004, 12p. Available online at: <http://ioc.unesco.org/iocweb/co2panel/Docs/Research%20Priorities%20Report-Final.pdf>, (Accessed: 02/08/2004).
- Shigenaka, G., 2001. *Toxicity of Oil to Reef-Building Corals: A Spill Response Perspective*. NOAA Technical Memorandum NOS OR&R 8, NOAA (Seattle, Washington: USA), 95p.
- Siegert, F., Ruecker, G., Hinrichs, A. and Hoffmann, A., 2001. Increased damage from fires in logged forests during droughts caused by El Niño. *Nature*, **414**: 437-440.
- Skirving, W., 2004. The hydrodynamics of a coral bleaching event: The role of satellite and CREWS measurements. In: Hendee, J. (Ed.), *The Effects of Combined Sea Temperature, Light, and Carbon Dioxide on Coral Bleaching, Settlement, and Growth*. The First Annual Combined Effects Think Tank to Support CREWS Modeling, NOAA, pp. 33-36.
- Smith, S.V. and Buddemeier, R.W., 1992. Global change and coral reef ecosystems. *Annual Review on Ecology and Systematics*, **23**: 89-118.
- Smith, S.V., Kimmerer, W.J., Laws, E.A., Brock, R.E. and Walsh, T.W., 1981. Kaneohe Bay sewage diversion experiment: perspective on ecosystem responses to nutritional perturbation. *Pacific Science*, **35**(4): 279-402.
- Snead, R.E., 1982. *Coastal Landforms and Surface Features – A Photographic Atlas and Glossary*. Hutchinson Ross Publishing Company (Stroudsburg, Pennsylvania: USA), pp. 42-45.
- Souter, D.W. and Lindén, O., 2000. The health and future of coral reef systems. *Ocean & Coastal Management*, **43**: 657-688.
- Spalding, M.D., Ravilious, C. and Green, E.P., 2001. *World Atlas of Coral Reefs*. UNEP-WCMC, University of California Press (Berkeley: USA), 424p.
- Spencer, T. and Viles, H., 2002. Bioconstruction, bioerosion and disturbance on tropical coasts: coral reefs and rocky limestone shores. *Geomorphology*, **48**(1-3): 23-50.
- Stafford-Smith, M.G., 1993. Sediment-rejection efficiency of 22 species of Australian scleractinian corals. *Marine Biology*, **115**: 229-243.
- Stanley, G.D. Jr., 2003. The evolution of modern corals and their early history. *Earth Science Reviews*, **60**: 195-225.
- Steers, J.A. and Stoddart, D.R., 1977. The origin of fringing reefs, barrier reefs and atolls. In: Jones, O.A. and Endean, R. (Eds.), *Biology and Geology of Coral Reefs*. Academic Press (New York: USA), Vol. IV: Geology 2, pp.21-57.
- Steffen, W., Sanderson, A., Tyson, P.D., Jäger, J., Matson, P.A., Moore III, B., Oldfield, F., Richardson, K., Schellnhuber, H.-J., Turner II, B.L. and Wasson, R.J., 2004. *Global Change and the Earth System: A Planet Under Pressure*. Springer, (Berlin, Germany).

- Stimson, J., 1997. The annual cycle of density of zooxanthellae in the tissues of field and laboratory-held *Pocillopora damicornis* (Linnaeus). *Journal of Experimental Marine Biology and Ecology*, **214**(1-2): 35–48.
- Stoddart, D.R., 1971. Coral reefs and islands and catastrophic storms. In: Steers, J.A. (Ed.), *Applied Coastal Geomorphology*. MacMillan and Co Ltd. (London: UK), pp. 155-197.
- Stone, L., Huppert, A., Rajagopalan, B., Bhasin, H. and Loya, Y., 1999. Mass coral reef bleaching: A recent outcome of increased El Niño activity? *Ecology Letters*, **2**(5): 325-330.
- Szmant, A.M., 2002. Nutrient enrichment on coral reefs: is it a major cause of coral reef decline? *Estuaries*, **25**(4b): 743-766.
- Thompson, F.L., Hoste, B., Thompson, C.C., Huys, G. and Swings, J., 2001. The coral bleaching *Vibrio shiloi* Kushmaro *et al.* 2001 is a later synonym of *Vibrio mediterranei* Pujalte and Garay 1986. *Systematic and Applied Microbiology*, **24**: 516-519.
- Tratalos, J.A. and Austin, T.J., 2001. Impacts of recreational SCUBA diving on coral communities of the Caribbean Island of Grand Cayman. *Biological Conservation*, **102**(1): 67-75.
- United Nations Development Programme (UNDP), 2004. *Human Development Report 2004: Cultural Liberty in Today's Diverse World*. Available online at: <http://hdr.undp.org/reports/global/2003/>, (Accessed: 26/07/2004).
- United Nations Environment Programme (UNEP) – Regional Organisation for the Conservation of the Environment of the Red Sea and the Gulf of Aden (PERSGA), 1997. *Assessment of Land-based Sources and Activities Affecting the Marine Environment in the Red Sea and Gulf of Aden*. UNEP Regional Seas Reports and Studies No. 166, UNEP (Nairobi: Kenya), 67p.
- van Woessik, R., Ayling, A.M. and Mapstone, B., 1991. Technical communication: impact of tropical cyclone 'Ivor' on the Great Barrier Reef, Australia. *Journal of Coastal Research*, **7**(2): 551-558.
- Vellinga, M. and Wood, R.A., 2002. Global climatic impacts of a collapse of the Atlantic Thermohaline Circulation. *Climatic Change*, **54**(3): 251-267.
- Veron, J.E.N., 1986. *Corals of Australia and Indo-Pacific*. Angus and Robertson (London: UK), 644p.
- Veron, J.E.N., 2000. *Corals of the World*. Australian Institute of Marine Science and CRR Qld Pty Ltd. (Townsville: Australia), 1382p.
- Vörösmarty, C.J. and Sahagian, D., 2000. Anthropogenic disturbance of the terrestrial water cycle. *BioScience*, **50**(9): 753-765.
- Wabnitz, C., Taylor, M., Green, E. and Razak, T., 2003. *From Ocean to Aquarium - The Global Trade in Marine Ornamental Species*. UNEP-WCMC (Cambridge: UK), 65p.
- Ware, J.R., Smith, S.V. and Reaka-Kudla, M.L., 1992. Coral reefs: sources or sinks of atmospheric CO₂? *Coral Reefs*, **11**(3): 127-130.
- Watson, R.T. and Core Writing Team (Eds.), 2001. *IPCC Third Assessment Report: Climate Change 2001: Synthesis Report – Summary for Policy Makers*. Available online at: http://www.grida.no/climate/ipcc_tar/index.htm, (Accessed: 04/12/2002).

- Wellington, G.M., Glynn, P.W., Strong, A.E., Navarrete, S.A., Wieters, E. and Hubbard, D., 2001. Crisis on coral reefs linked to climate change. *EOS*, **82**(1): 7p. Available online at: <http://www.agu.org/pubs/eos.html>.
- West, J.M. and Salm, R.V., 2003. Resistance and resilience to coral bleaching: Implications for coral reef conservation and management. *Conservation Biology*, **17**(4): 956-967.
- Westmacott, S., Cesar, H., Pet-Soede, L. and Lindén, O., 2001. Assessing the socio-economic impacts of the coral bleaching event in the Indian Ocean. In: Schuttenberg, H. (Ed.), *Coral Bleaching: Causes, Consequences, and Response. Selected Papers presented at the 9th International Coral Reef Symposium on "Coral Bleaching: Assessing and Linking Ecological and Socioeconomic Impacts, Future Trends and Mitigation Planning*. Coastal Resources Center, University of Rhode Island, **Part I**, pp.31-40.
- Whittingham, E., Campbell, J., and Townsley, P., 2003. *Poverty and reefs - Volume 1: A global overview*. DFID-IMM-IOC/UNESCO, 260 p.
- Wilkinson, C.R., 1993. Coral reefs of the world are facing widespread devastation: can we prevent this through sustainable management practices? *Proceedings of 7th International Coral Reef Symposium*, Vol. **I**: 11-21.
- Wilkinson, C. (Ed.), 1998. *Status of Coral Reefs of the World: 1998*. AIMS (Townsville: Australia), 145p. Available online at: <http://www.aims.gov.au/pages/research/coral-bleaching/scr1998>, (Accessed: 19/02/2001).
- Wilkinson, C. (Ed.), 2000a. *Status of Coral Reefs of the World: 2000*. AIMS (Townsville: Australia), xii + 363p.
- Wilkinson, C., 2000b. The 1997-98 mass coral bleaching and mortality event: 2 years on. In: Wilkinson, C. (Ed.), *Status of Coral Reefs of the World: 2000*. AIMS-GCRMN (Townsville: Australia), pp. 21-34.
- Wilkinson, C. (Ed.), 2002a. *Status of Coral Reefs of the World: 2002*. AIMS-GCRMN (Townsville: Australia), x + 378p.
- Wilkinson, C., 2002b. Coral bleaching and mortality – The 1998 event 4 years later and bleaching to 2002. In: Wilkinson, C. (Ed.), *Status of Coral Reefs of the World: 2002*. AIMS-GCRMN (Townsville: Australia), pp.33-44.
- Wilkinson, C.R. and Buddemeier, R.W., 1994. *Global Climate Change and Coral Reefs: Implications for People and Reefs*. Report of the UNEP-IOC-ASPEI-IUCN Global Task Team on the implications of climate change on coral reefs, IUCN (Gland: Switzerland), x+124p.
- Wilkinson, C., Souter, D. and Goldberg, J. (Eds.), 2006. *Status of Coral Reefs in Tsunami Affected Countries: 2006*. AIMS (Townsville, Australia), 154p.
- Williams, E.H. Jr. and Bunkley-Williams, L., 1990. The world-wide coral reef bleaching cycle and related sources of coral mortality. *Atoll Research Bulletin*, **335**: 1-71.

-
- Woolfe, K.J. and Larcombe, P., 1999. Terrigenous sedimentation and coral reef growth: a conceptual framework. *Marine Geology*, **155**(3-4): 331-345.
- Yentsch, C.S., Yentsch, C.M., Cullen, J.J., Lapointe, B., Phinney, D.A. and Yentsch, S.W., 2002. Sunlight and water transparency: cornerstones in coral research. *Journal of Experimental Marine Biology and Ecology*, **268**: 171-183.
- Zakai, D. and Chadwick-Furman, N.E., 2002. Impacts of intensive recreational diving on reef corals at Eilat, northern Red Sea. *Biological Conservation*, **105**(2): 179-187.
- Zilinskas, R.A. and Lundin, C.G., 1993. *Marine Biotechnology and Developing Countries*. World Bank Discussion Paper No. 210, World Bank (Washington DC: USA), xv + 115p.

REFERENCES PART II

- Al-Muhandiss, A.A. and Al-Ruweissy, M.A., 1984. Distribution of coral reefs along the Saudi Coast of the Red Sea. *Symposium on Coral Reef Environments in the Red Sea*, Jeddah, January 1984.
- Andres, W. and Radtke, U., 1988. Quartäre Strandterrassen an der Küste des Gebel Zeit (Golf von Suez/Ägypten). *Erdkunde*, **42**: 7-16.
- Angelier, J., 1985. Extension and rifting: the Zeit region, Gulf of Suez. *Journal of Structural Geology*, **7**: 605-612.
- Awad, H., 1995. Oil pollution in the Red Sea – a state of the art assessment. *PERSGA/IOC/UNEP Workshop on Oceanographic Inputs in Coastal Zone Management in the Red Sea and Gulf of Aden*, October 12, 1995, Jeddah (Saudi Arabia).
- Badran, M.I., 2001. Dissolved oxygen, Chlorophyll a and nutrients: Seasonal cycles in waters of the Gulf of Aqaba, Red Sea. *Aquatic Ecosystem Health & Management*, **4**(2): 139-150.
- Badran, M.I., Rasheed, M., Manasrah, R. and Al-Najjar, T., 2005. Nutrient flux fuels the summer primary productivity in the oligotrophic waters of the Gulf of Aqaba, Red Sea. *Oceanologia*, **47**(1): 47-60.
- Bartov, Y., Steinitz, G., Eyal, M. and Eyal, U., 1980. Sinistral movement along the Gulf of Aqaba – its age and relation to the opening of the Red Sea. *Nature*, **285**: 220-221.
- Beckman, W., 1984. Mesozooplankton distribution from the Gulf of Aden to the central Red Sea during winter monsoon. *Oceanologica Acta*, **7**: 87-102.
- Behairy, A.K.A., Sheppard, C.R.C. and El-Sayed, M.K., 1992. *A Review of the Geology of Coral Reefs in the Red Sea*. UNEP Regional Seas Reports and Studies, No. 152, UNEP (Nairobi: Kenya), 36p.
- Benayahu, Y. and Loya, Y., 1981. Competition for space among coral-reef sessile organisms. *Bulletin of Marine Science*, **31**: 514-522.
- Berry, L., Whiteman, A.J., and Bell, S.V., 1966. Some radiocarbon dates and their geomorphological significance, emerged reef complex of the Sudan. *Zeitschrift für Geomorphologie*, **10**: 119-143.
- Bosence, D.W.J., 1998. Stratigraphic and sedimentological models of rift basins. In: Purser, B.H. and Bosence, D.W.J. (Eds.), *Sedimentation and Tectonics in Rift Basins: Red Sea - Gulf of Aden*. Chapman & Hall, University Press (Cambridge: UK), pp. 9-26.
- Bosworth, W., 1994. A high-strain rift model for the southern Gulf of Suez (Egypt). In: Lambiase, J.J. (Ed.), *Hydrocarbon Habitat in Rift Basins*. Geological Society of London Special Publication, **80**: 75-102.
- Bosworth, W., 1995. Structure, sedimentation and basin dynamics during the early Gulf of Suez rifting. *Proceedings of Rift Sedimentation and Tectonics in the Red Sea-Gulf of Aden Region*, University of Sana'a, Yemen, October, p. 13.

- Bosworth, W., Crevello, P., Winn, R.D. Jr. and Steinmetz, J., 1998. Structure, sedimentation, and basin dynamics during rifting of the Gulf of Suez and north-western Red Sea. In: Purser, B.H. and Bosence, D.W.J. (Eds.), *Sedimentation and Tectonics in Rift Basins: Red Sea - Gulf of Aden*, Chapman & Hall, University Press (Cambridge: UK), pp. 77-96.
- Bosworth, W. and Taviani, M., 1996. Late Quaternary reorientation of stress field and extension direction in the southern Gulf of Suez, Egypt: Evidence from uplifted coral terraces, mesoscopic fault arrays, and borehole breakouts. *Tectonics*, **15**(4): 791-802.
- Brachert, T.C. and Dullo, W.-C., 1990. Correlation of deep sea sediments and forereef carbonates in the Red Sea: An important clue for basin analysis. *Marine Geology*, **92**: 255-267.
- Braithwaite, C.J.R., 1982. Patterns of accretion of reefs in the Sudanese Red Sea. *Marine Geology*, **46**: 297-325.
- Braithwaite, C.J.R., 1987. Geology and Palaeogeography of the Red Sea Region. In: Edwards, A.J. and Head S.M. (Eds.), *Key Environments: Red Sea*, Pergamon Press (Oxford: UK), pp. 22-44.
- Burrell, D.C. and Schubel, J.R., 1977. Seagrass ecosystem oceanography. In: McRoy, C.P. and Helfferich, C. (Eds.), *Seagrass ecosystems: A Scientific Perspective*, Dekker (New York: USA), pp. 195-232.
- Chapman, V.J., 1977. *Wet Coastal Ecosystems*. Elsevier Scientific Publishing Company (Amsterdam: The Netherlands), 458p.
- Chappell, J., 1983. Evidence for smoothly falling sea level relative to North Queensland, Australia, during the past 6,000 years. *Nature*, **302**: 406-408.
- Clifford, M., Horton, C., Schmitz, J. and Kantha, L.H., 1997. An oceanographic nowcast /forecast system for the Red Sea. *Journal of Geophysical Research*, **102**(C11): 25101-25122.
- Cochran, J.R., 1983. Model for development of the Red Sea. *American Association of Petroleum Geologists Bulletin*, **67**: 41-69.
- Cochran, J.R., Martinez, F., Steckler, M.S. and Hobart, M.A., 1986. Conrad Deep, a new northern Red Sea deep, origin and implications for continental rifting. *Earth and Planetary Science Letters*, **78**: 18-32.
- Coleman, R.G. and McGuire, A.V., 1988. Magma systems related to the Red Sea opening. *Tectonophysics*, **150**: 77-100.
- Coles, S.L. and McCain, J.C., 1990. Environmental factors affecting benthic infaunal communities in the western Persian Gulf. *Marine Environmental Research*, **29**(4): 289-315.
- Colletta, B., Le Quellec, P., Letouzy, J. and Moretti, I., 1988. Longitudinal evolution of the Suez rift structure (Egypt). *Tectonophysics*, **153**: 221-233.
- da Silva, A., Young, A.C. and Levitus, S., 1994. *Atlas of Surface Marine Data 1994, Volume 1: Algorithms and Procedures*. NOAA Atlas NESDIS **6**, Washington D.C. (USA). Available online at: <http://iridl.ldeo.columbia.edu/SOURCES/.DASILVA/.SMD94/.climatology/.sat>, (Accessed: 6/10/2004).

- Dagget, P.H., Morgan, P., Boulos, F.K., Hennin, S.F., El Sherif, A.A., El Sayed, A.A., Basta, N.Z. and Melek, Y.S., 1986. Seismicity and active tectonics of the Egyptian Red Sea margin and the northern Red Sea. *Tectonophysics*, **125**: 313-324.
- Dewey, J.F. and Sengor, A.M.C., 1979. Aegean and surrounding regions: Complex multi-plate and continuous tectonics in a convergent zone. *Geological Society of America Bulletin*, **90**: 82-91.
- Dicks, B., 1987. Pollution. In: Edwards, A.J. and Head, S.M. (Eds.), *Key Environments: Red Sea*, Pergamon Press (Oxford: UK), pp. 383-404.
- Dullo, W.-C., 1990. Facies, fossil record, and age of Pleistocene reefs from the Red Sea (Saudi Arabia). *Facies*, **22**: 1-46.
- Dullo, W.-C., Hötzl, H. and Jado, A.R., 1983. New stratigraphical results from the Tertiary sequence of the Midyan area, NW Saudi Arabia. *Newsletter Stratigraphy*, **12**: 75-83.
- Dullo, W.-C. and Montaggioni, L., 1998. Modern Red Sea coral reefs: A review of their morphologies and zonation. In: Purser, B.H. and Bosence, D.W.J. (Eds.), *Sedimentation and Tectonics in Rift Basins: Red Sea - Gulf of Aden*, Chapman & Hall, University Press (Cambridge: UK), pp. 583-594.
- Edwards, F.J., 1987. Climate and oceanography. In: Edwards, A.J. and Head, S.M. (Eds.), *Key Environments: Red Sea*, Pergamon Press (Oxford: UK), pp. 45-69.
- Evans, A.L., 1988. Neogene tectonics and stratigraphic events in the Gulf of Suez rift area, Egypt. *Tectonophysics*, **153**: 235-247.
- Fauth, J.E., Bernardo, J., Camara, M., Resetarits, W.J. Jr., Van Buskirk, J. and McCollum, S.A., 1996. Simplifying the jargon of community ecology: a conceptual approach. *The American Naturalist*, **147**(2): 282-286.
- Fawzy, H. and Abdel Aal, A., 1984. Regional study of Miocene evaporates and Pliocene-Recent sediments in the Gulf of Suez. *Proceedings of the 7th Petroleum Exploration Seminar, EGPC, Cairo*, pp. 49-74.
- Fishelson, L., 1973. Ecological and biological phenomena influencing coral-species composition on the reef tables at Eilat (Gulf of Aqaba, Red Sea). *Marine Biology*, **19**: 183-196.
- Fishelson, L., 1980. Marine reserves along the Sinai Peninsula (northern Red Sea). *Helgoländer Wissenschaftliche Meeresuntersuchungen*, **33**: 624-640.
- Fouda, M.M., 1983. Oil pollution in the Red Sea. *Cairo Today*: 33-34.
- Fouda, M.M., 1995. *Regional Report on the Middle East Seas: Issues and Activities Associated with Coral Reefs and Related Ecosystems*. Regional report for the International Coral Reef Initiative Workshop, Dumaguete, Philippines, 48p.
- Fouda, M.M., 1998. Status of coral reefs in the Middle East. In: Wilkinson, C. (Ed.), *Status of coral reefs of the world: 1998*, AIMS (Townsville: Australia).
- Fouda, M. and Gerges, M., 1994. *Implications of Climate Change in the Red Sea and Gulf of Aden Region: An Overview*. UNEP Regional Seas Reports and Studies, No. 156, 58p.

- Freytet, P., Baltzer, F. and Conchon, O., 1993. A Quaternary piedmont on an active margin: the Egyptian coast of the NW Red Sea. *Zeitschrift für Geomorphologie*, **37**(2): 215-236.
- Friedman, G.M., 1985. Gulf of Elat (Aqaba). Geological and sedimentological framework. In: Friedman, G.M. and Krumbein, W.E. (Eds.), *Hypersaline Ecosystems. The Gavish Sabkha*, Springer Verlag (Berlin: Germany), pp. 39-71.
- Frostick, L.E. and Read, I., 1989. Is structure the main control of river drainage and sedimentation in rifts? *Journal of African Earth Science*, **8**: 165-182.
- Furon, R., 1963. *The Geology of Africa*. Oliver & Boyd (London: UK), 337p.
- Garfunkel, Z. and Bartov, Y., 1977. The tectonics of the Suez rift. *Geological Survey of Israel Bulletin*, **71**: 1-44.
- Gerges, M.A., 2002. The Red Sea and Gulf of Aden Action Plan - Facing the challenges of an ocean gateway. *Ocean & Coastal Management*, **45**(11-12): 885-903.
- Ghebream, W., 1998. Tectonics of the Red Sea region reassessed. *Earth-Science Reviews*, **45**: 1-44.
- Girdler, R.W., 1991. The Afro-Arabian Rift System, an overview. *Tectonophysics*, **197**: 139-153.
- Girdler, R.W. and Styles, P., 1974. Two-stage *seafloor* spreading. *Nature*, **247**: 7-11.
- Gladstone, W., Tawfiq, N., Nasr, D., Andersen, I., Cheung, C., Drammeh, H., Krupp, F. and Lintner, S., 1999. Sustainable use of renewable resources and conservation in the Red Sea and Gulf of Aden: Issues, needs and strategic actions. *Ocean & Coastal Management*, **42**(8): 671-697.
- Global Environment Facility (GEF), 1997. *Report 2-Baseline Studies*. Egyptian GEF Red Sea Coastal and Marine Resource Management Project. 109p.
- Glorieus, B., 2006. *Studie van Chlorofyl- en Oppervlaktetemperatuurpatronen in de Rode Zee aan de hand van een Tijdsreeks MODIS-Beelden*. MSc. Dissertation, Ghent University, 138pp.
- Green, E.P. and Short, F.T. (Eds.), 2003. *World Atlas of Seagrasses*. UNEP-WCMC, University of California Press (Berkeley: USA), 298p.
- Guilcher, A., 1988. A heterofore neglected type of coral reef: the ridge reef. Morphology and origin. *Proceedings of the 6th International Coral Reef Symposium*, Australia, **3**: 399-402.
- Gvirtzman, G., 1994. Fluctuations of sea level during the past 400 000 years: The record of Sinai, Egypt (Northern Red Sea). *Coral Reefs*, **13**: 203-214.
- Gvirtzman, G., Buchbinder, B., Sneh, A., Nir, Y. and Friedman, G.M., 1977. Morphology of the Red Sea fringing reefs: A result of erosional pattern of the last-glacial-low-stand sea level and the following Holocene recolonization. 2nd Symposium international sur les coraux et récifs coralliens fossils. *Mémoires des Bureau de Recherches Géologiques et Minières*, **89**: 480-491.
- Hafez, A. and El-Manharawy, S., 2002. Economics of seawater RO desalination in the Red Sea region, Egypt. Part 1. A case study. *Desalination*, **153**(1-3): 335-347.
- Hanafy, M.H., 2002. Red Sea mangroves. *Abstractbook of the First Egyptian-International Conference on Protected Areas and Sustainable Development*, October 23-26, 2002, Sharm-el-Sheikh (Egypt), pp. 69-70.

- Hariri, K.I., Nichols, P., Krupp, F., Mishrigi, S., Barrania, A., Ali, A.F. and Kedidi, S.M., 2000. *Status of the Living Marine Resources in the Red Sea and Gulf of Aden Region and their Management*. PERSGA, 151p.
- Hassan, F. and El-Dashlouti, S., 1970. Miocene evaporites of Gulf of Suez region and their significance. *American Association of Petroleum Geologists Bulletin*, **54**: 1686-1696.
- Hassan, M.A. and Hashad, A.H., 1990. Precambrian of Egypt. In: Said, R. (Ed.), *The Geology of Egypt*, A.A. Balkema (Rotterdam: The Netherlands), pp. 201-245.
- Hassan, M., Kotb, M.M.A. and Al-Sofyani, A.A., 2002. Status of coral reefs in the Red Sea-Gulf of Aden. In: Wilkinson, C. (Ed.), *Status of the Coral Reefs of the World: 2002*, AIMS (Townsville: Australia), pp. 45-52.
- Hayward, A.B., 1982. Coral reefs in a clastic sedimentary environment: Fossil (Miocene, SW Turkey) and modern (recent, Red Sea) analogues. *Coral Reefs*, **1**(2): 109-114.
- Head, S.M., 1980. *The Ecology of Corals in the Sudanese Red Sea*. Ph.D. Thesis, University of Cambridge.
- Head, S.M., 1987a. Introduction. In: Edwards, A.J. and Head, S.M. (Eds.), *Key Environments: Red Sea*, Pergamon Press (Oxford: UK), pp.1-21.
- Head, S.M., 1987b. Corals and coral reefs of the Red Sea. In: Edwards, A.J. and Head S.M. (Eds.), *Key Environments: Red Sea*, Pergamon Press (Oxford: UK), pp. 128-151.
- Head, S.M., 1987c. Red Sea fisheries. In: Edwards, A.J. and Head, S.M. (Eds.), *Key Environments: Red Sea*, Pergamon Press (Oxford: UK), p. 363-383.
- Hoepner, T., 1999. A procedure for environmental impact assessments (EIA) for seawater desalination plants. *Desalination*, **124**(1-3): 1-12.
- Hoepner, T. and Latteman, S., 2002. Chemical impacts from seawater desalination plants - A case study of the northern Red Sea. *Desalination*, **152**(1-3): 133-140.
- Hopley, D., Slocombe, A.M., Muir, F. and Grant, C., 1983. Nearshore fringing reefs in North Queensland. *Coral Reefs*, **1**(3): 151-160.
- Hume, W.R., 1921. Relations of the northern Red Sea and associated Gulf areas to the 'rift' theory. *Proceedings of the Geological Society of London*, **77**: 96-101.
- International Commission on Stratigraphy (ICS), 2006. *Stratigraphic Charts*. Available online at: <http://www.stratigraphy.org>, (Accessed: 28/11/2006).
- IRI/LDEO, 2000. *IRI/LDEO Climate Data Library: NOAA NCDC GCPS Monthly Gridded*. Available online at: <http://ingrid.ldeo.columbia.edu>, (Accessed: 15/04/2000).
- Ivanova, E.V., 1985. Late Quaternary biostratigraphy and paleotemperatures of the Red Sea and the Gulf of Aden based on planktonic foraminifera and pteropods. *Marine Micropaleontology*, **9**: 335-364.

- Jackson, J.A., White, N.J., Garfunkel, Z. and Anderson, H., 1988. Relations between normal-fault geometry, tilting and vertical motions in extensional terrains: an example from the southern Gulf of Suez. *Journal of Structural Geology*, **10**: 155-170.
- Jacobs, R.P.W.M. and Dicks, B., 1985. Seagrasses in the Zeit Bay area and at Ras Gharib (Egyptian Red Sea coast). *Aquatic Botany*, **23**: 137-147.
- Jameson, S.C., McManus, J.W. and Spalding, M.D., 1995. *Status of the Reefs: Global and Regional Perspectives – Regional Perspectives: Seas of the Middle East*. Available online at: http://www.ngdc.noaa.gov/paleo/outreach/coral/sor/sor_mideast.html, (Accessed: 25/07/2004).
- Jarrige, J.J., Ott d'Estevou, P., Burollet, P.F., Icart, J.C., Montenat, C., *et al.*, 1986a. Inherited discontinuities and Neogene structure: the Gulf of Suez and NW edge of the Red Sea. *Philosophical Transactions of the Royal Society of London*, **317**: 129-139.
- Jarrige, J.J., Ott d'Estevou, P. and Sehans, P., 1986b. Etude structurale sur la marge occidentale de la Mer Rouge: le secteur du Gebel Duwi près de Quseir (Egypte). *Documents et Travaux de l'Institut Géologique Albert de Lapparent*, **10**: 17-127.
- Jarrige, J.J., Ott d'Estevou, P., Burollet, P.F., Montenat, C., Richert, J.-P. and Thiriet, J.P., 1990. The multistage tectonic evolution of the Gulf of Suez and northern Red Sea continental rift from field observations. *Tectonics*, **9**: 441-465.
- Johns, W.E., Jacobs, G.A., Kindle, J.C., Murray, S.P. and Carron, M., 1999. *Arabian Marginal Seas and Gulfs – Report of a Workshop held at Stennis Space Center, Mississippi*. University of Miami Technical Report 2000-01, 60p.
- Jones, D.A., Ghamrawy, M. and Wahbeh, M.I., 1987. Littoral and shallow subtidal environments. In: Edwards, A.J. and Head S.M. (Eds.), *Key Environments: Red Sea*, Pergamon Press (Oxford: UK), pp. 169-193.
- Karbe, L., 1987. Hot brines and the deep sea environment. In: Edwards, A.J. and Head S.M. (Eds.), *Key Environments: Red Sea*, Pergamon Press (Oxford: UK), pp. 70-89.
- Kazmin, V., Shiferaw, A. and Balcha, T., 1978. The Ethiopian basement, stratigraphy and possible manner of evolution. *Geologische Rundschau*, **67**: 531-546.
- Kebeasy, R.M., 1990. Seismicity. In: Said, R. (Ed.), *The geology of Egypt*, Balkema (Rotterdam: The Netherlands), pp.51-59.
- Kerdany, M.T. and Cherif, O.F., 1990. Mesozoic. In: Said, R. (Ed.), *The Geology of Egypt*, A.A. Balkema (Rotterdam: The Netherlands), pp. 407-438.
- Khmeleva, N.N., 1970. On the primary production in the Red Sea and Gulf of Aden. *Biologiya morja, Kiev*, **21**: 107-133.
- Klitzsch, E., 1990. Paleozoic. In: Said, R. (Ed.), *The Geology of Egypt*, A.A. Balkema (Rotterdam: The Netherlands) pp. 393-406.

- LaBreque, J.L. and Zitellini, N., 1985. Continuous *seafloor* spreading in Red Sea, an alternative interpretation of magnetic anomaly pattern. *American Association of Petroleum Geologists Bulletin*, **69**: 513-524.
- Levitus, S. (Ed.), 1994. *World Ocean Atlas 1994*. Available online at: <http://ingrid.ldeo.columbia.edu/SOURCES/LEVITUS94>, (Accessed: 6/10/2004).
- Lintner, S.F., Arif, S. and Hatzios, M., 1996. *The Experience of the World Bank in the Legal, Institutional and Financial Aspects of Regional Environmental Programs. Potential Applications of Lessons Learned for the ROPME and PERSGA Programs*. The World Bank (Washington D.C.: USA), 46p.
- Lipkin, Y., 1977. Seagrass vegetation of Sinai and Israel. In: McRoy, C.P. and Helfferich, C. (Eds.), *Seagrass ecosystems: A Scientific Perspective*, Dekker (New York: USA), pp. 263-293.
- Lipkin, Y., Beer, S. and Zakai, D., 2003. The seagrasses of the Eastern Mediterranean and the Red Sea. In: Green, E.P. and Short, F.T. (Eds.), *World Atlas of Seagrasses*, UNEP-WCMC, University of California Press (Berkeley: USA), pp. 65-73.
- Longhurst, A.R. and Pauly, D., 1987. *The Ecology of Tropical Oceans*. Academic Press (London: UK), 407p.
- Lorenzen, C.J., 1976. Primary production in the sea. In: Cushing, D.H. and Walsch, J.J. (Eds.), *The Ecology of the Seas*, Blackwell Scientific Publications (Oxford: UK), pp.173-185.
- Loya, Y., 1976. Recolonisation of Red Sea corals affected by natural catastrophes and man-made perturbations. *Ecology*, **57**: 278-289.
- Loya, Y. and Rinkevich, B., 1980. Effects of oil pollution on coral reef communities. *Marine Ecology Progress Series*, **3**: 167-180.
- Maillard, C. and Soliman, G., 1986. Hydrography of the Red Sea and exchanges with the Indian Ocean in summer. *Oceanologica Acta*, **9**: 249-269.
- Manasrah, R., Badran, M., Lass, H.U. and Fennel, W., 2004. Circulation and winter deep-water formation in the northern Red Sea. *Oceanologia*, **46**(1): 5-23.
- McClanahan, T.R., 2002. The near future of coral reefs. *Environmental Conservation*, **29**(4): 460-483.
- Mergner, H. and Svoboda, A., 1977. Productivity and seasonal changes in selected reef areas in the Gulf of Aqaba (Red Sea). *Helgoländer Wissenschaftliche Meeresuntersuchungen*, **30**: 383-399.
- Meshref, W.M., 1990. Tectonic framework. In: Said, R. (Ed.), *The Geology of Egypt*, A.A. Balkema (Rotterdam: The Netherlands), pp. 113-155.
- Milliman, J.D. and Emery, K.O., 1968. Sea levels during the past 35,000 years. *Science*, **162**: 1121-1123.
- Montenat, C., Orszag-Sperber, F., Plaziat, J.-C. and Purser, B.H., 1998a. The sedimentary record of the initial stages of Oligo-Miocene rifting in the Gulf of Suez and the northern Red Sea. In: Purser, B.H. and Bosence, D.W.J. (Eds.), *Sedimentation and Tectonics in Rift Basins: Red Sea - Gulf of Aden*, Chapman & Hall, University Press (Cambridge: UK), pp. 146-161.

- Montenat, C., Ott d'Estevou, P., Jarrige, J.-J. and Richtert, J.-P., 1998b. Rift development in the Gulf of Suez and the north-western Red Sea: structural aspects and related sedimentary processes. In: Purser, B.H. and Bosence, D.W.J. (Eds.), *Sedimentation and Tectonics in Rift Basins: Red Sea - Gulf of Aden*, Chapman & Hall, University Press (Cambridge: UK), pp. 97-116.
- Montenat, C., Ott d'Estevou, P., Purser, B.H., Burollet, P.F., Jarrige, J.-J., Orszag-Sperber, F., Philobos, E., Plaziat, J.-C., Prat, P., Richert, J.-P., Roussel, N. and Thiriet, J.-P., 1988. Tectonic and sedimentary evolution of the Gulf of Suez and the northwestern Red Sea. *Tectonophysics*, **153**: 161-177.
- Morcos, S.A., 1970. Physical and chemical oceanography of the Red Sea. *Oceanography and Marine Biology*, **8**: 73-202.
- Moretti, I. and Colletta, B., 1987. How does a block tilt: The Gebel Zeit example, Gulf of Suez. *Journal of Structural Geology*, **100**: 9-19.
- Morgan, P., 1990. Egypt in the framework of global tectonics. In: Said, R. (Ed.), *The Geology of Egypt*, A.A. Balkema (Rotterdam: The Netherlands), pp. 91-111.
- Morley, N.J.F., 1975. The coastal waters of the Red Sea. *Bulletin of the Marine Research Centre, Saudi Arabia*, No. 5, 19p.
- NASA, 2006. *Ocean Color Web*. Available online at: <http://oceancolor.gsfc.nasa.gov>, (Accessed: 10/06/2004).
- Omar, G.I., Steckler, M.S., Buck, R. and Kohn, B.P., 1989. Fission-track analysis of basement apatites at the western margin of the Gulf of Suez rift, Egypt: Evidence for synchronicity of uplift and subsidence. *Earth and Planetary Science Letters*, **94**: 316-328.
- Ormond, R.F.G., 1987. Conservation and management. In: Edwards, A.J. and Head, S.M. (Eds.), *Key Environments: Red Sea*, Pergamon Press (Oxford: UK), pp. 405-423.
- Ormond, R.F.G., Price, A.R.G. and Shepherd, D.A.R., 1988. The distribution and character of mangroves in the Red Sea, Arabian Gulf and southern Arabia. *Proceedings of the Symposium on New Perspectives in Research and Management of Mangrove Ecosystems*, 11-14 November 1986, Colombo, Sri Lanka, pp.125-130.
- Ormond, R.F.G., Shepherd, A.D., Price, A. and Pitts, R.G., 1984a. *Report on the distribution of habitats and species in the Saudi Arabian Red Sea 1*. IUCN, Meteorological and Environmental Protection Agency, Kingdom of Saudi Arabia, 123p.
- Ormond, R.F.G., Shepherd, A.D., Price, A. and Pitts, R.G., 1984b. *Report on the distribution of habitats and species in the Saudi Arabian Red Sea 2*. IUCN, Meteorological and Environmental Protection Agency, Kingdom of Saudi Arabia, 151p.
- Ormond, R.F.G., Shepherd, A.D., Price, A. and Pitts, R.G., 1984c. *Management of Red sea coastal resources: recommendations for protected areas*. IUCN, Meteorological and Environmental Protection Agency, Kingdom of Saudi Arabia, 123p.

- Orszbag-Sperber, F., Purser, B.H., Rioual, M. and Plaziat, J.-C., 1998. Post-Miocene sedimentation and rift dynamics in the southern Gulf of Suez and northern Red Sea. In: Purser, B.H. and Bosence, D.W.J. (Eds.), *Sedimentation and Tectonics in Rift Basins: Red Sea - Gulf of Aden*, Chapman & Hall, University Press (Cambridge: UK), pp. 427-447.
- Patton, T.L., Moustafa, A.R., Nelson, R.A. and Abdine, S.A., 1994. Tectonic evolution and stratigraphic setting of the Suez rift. *American Association of Petroleum Geologists Special Publication*, **59**: 7-55.
- Perrin, C., Plaziat, J.-C. and Rosen, B.R., 1998. Miocene coral reefs and reef corals of the southwestern Red Sea: distribution, diversity and regional environmental controls. In: Purser, B.H. and Bosence, D.W.J. (Eds.), *Sedimentation and Tectonics in Rift Basins: Red Sea - Gulf of Aden*, Chapman & Hall, University Press (Cambridge: UK), pp. 296-319.
- Perry, C.T., 2006. Holocene reef development and carbonate production in nearshore, siliciclastic-dominated environments. In: *International Society for Reef Studies European Meeting: Programme and Abstracts*, 19-22 September 2006, Bremen (Germany), p. 11.
- PERSGA, 2001. *Strategic Action Programme of the Red Sea and Gulf of Aden – Country Reports*. World Bank (Washington: USA), 217p.
- Petzold, M., 1986. *Untersuchungen zur Horizontalen und Vertikalen Verteilung des Phytoplanktons im Roten Meer*. Diplomarbeit, Institut für Hydrobiologie und Fischereiwissenschaft, Universität Hamburg.
- Physical Oceanography Distributed Active Archive Center (PODAAC), 2006. *NSIPP AVHRR Pathfinder and Erosion 9km SST Climatology*. Available online at: <http://podaac.jpl.nasa.gov/products/products112.html>, (Accessed: 5/09/2006).
- Pilcher, N. and Abou Zaid, M.M., 2003. Coral reefs of Egypt. In: PERSGA, *Coral Reefs in the Red Sea and Gulf of Aden – Surveys 1990 to 2000 Summary and Recommendations*. PERSGA Technical Report No. 7, pp. 1-12.
- Pilcher, N. and Alsuhaibany, A., 2000. Regional status of coral reefs in the Red Sea and the Gulf of Aden. In: Wilkinson, C. (Ed.), *Status of Coral Reefs in the World: 2000*, AIMS (Townsville: Australia), pp. 35-54.
- Piller, W.E. and Pervesler, P., 1989. The northern Bay of Safaga (Red Sea, Egypt): an actuopaleontological approach I. Topography and bottom facies. *Beiträge zur Paläontologie von Österreich*, **15**: 103-147.
- Plähn, O., Baschek, B., Badewien, T.H., Walter, M. and Rhein, M., 2002. Importance of the Gulf of Aqaba for the formation of bottom water in the Red Sea. *Journal of Geophysical Research*, **107**(C8), 3108, doi: 10.1029/2000JC000342.
- Plaziat, J.-C., Baltzer, F., Choukri, A., Conchon, O., Freytet, P., Orszag-Sperber, F., Purser, B., Raguideau, A. and Reyss, J.-L., 1995. Quaternary changes in the Egyptian shoreline of the Northwestern Red Sea and Gulf of Suez. *Quaternary International*, **274**(29-30): 11-22.

- Plaziat, J.-C., Baltzer, F., Choukri, A., Conchon, O., Freytet, P., Orszbag-Sperber, F., Raguideau, A. and Reyss, J.-L., 1998. Quaternary marine and continental sedimentation in the northern Red Sea and Gulf of Suez (Egyptian coast): Influences of rift tectonics, climatic changes and sea-level fluctuations. In: Purser, B.H. and Bosence, D.W.J. (Eds.), *Sedimentation and Tectonics in Rift Basins: Red Sea - Gulf of Aden*, Chapman & Hall, University Press (Cambridge: UK), pp.537-573.
- Poisson, A., Morcos, S., Souvermezoglou, E., Papaud, A. and Ivanoff, A., 1984. Some aspects of biochemical cycles in the Red Sea with special reference to new observations made in summer 1982. *Deep-Sea Research*, **A31**: 707-718.
- Price, A.R.G., Jobbins, G., Shepherd, A.R.D. and Ormond, R.F.G., 1998. An integrated environmental assessment of the Red Sea coast of Saudi Arabia. *Environmental Conservation*, **25**(1): 65-76.
- Price, A.R.G., Medley, P.A.H., McDowall, R.J., Shepherd, D.A.R., Hogarth, P.J. and Ormond, R.F.G., 1987. Aspects of mangal ecology along the Red Sea coast of Saudi Arabia. *Journal of Natural History*, **21**:449-464.
- Purser, B.H. and Bosence, D.W.J., 1998. Organisation and scientific contributions in sedimentation and tectonics of rift basins: Red Sea – Gulf of Aden. In: Purser, B.H. and Bosence, D.W.J. (Eds.), *Sedimentation and Tectonics in Rift Basins: Red Sea - Gulf of Aden*, Chapman & Hall, University Press (Cambridge: UK), pp. 3-8.
- Purser, B.H. and Hötzl, H., 1988. The sedimentary evolution of the Red Sea rift: a comparison of the northwest (Egyptian) and northeast (Saudi Arabian) margins. *Tectonophysics*, **153**: 193-208.
- Purser, B.H. and Philobos, E.R., 1993. The sedimentary expressions of rifting in the NW Red Sea, Egypt. In: Philobos, E.R. and Purser, B.H. (Eds.), *Geodynamics and Sedimentation of the Red Sea-Gulf of Aden Rift System*, Geological Society of Egypt Special Publication, **1**: 1-45.
- Purser, B.H., Philobos, E.R. and Soliman, M., 1990. Sedimentation and rifting in the NW parts of the Red Sea: A review. *Geological Society of France Bulletin*, **8**: 371-384.
- Quadfasel, D. and Baudner, H., 1993. Gyre-scale circulation cells in the Red Sea. *Oceanologica Acta*, **16**: 221-229.
- Quennell, A.M., 1984. The western Arabian rift system. In: Dixon, J.E. and Robertson, H.F. (Eds.), *The geological evolution of the eastern Mediterranean*, Blackwell Scientific Publishers (Oxford: UK), pp.775-788.
- Reiss, Z. and Hottinger, L., 1984. *The Gulf of Aqaba. Ecological Micropaleontology*. Springer (Berlin: Germany), 360p.
- Riegl, B. and Luke, K.E., 1998. Ecological parameters of dynamited reefs in the northern Red Sea and their relevance to reef rehabilitation. *Marine Pollution Bulletin*, **37**(8-12): 488-498.
- Riegl, B. and Piller, W.E., 1997. Distribution and environmental control of coral assemblages in northern Safage Bay (Red Sea, Egypt). *Facies*, **36**: 141-162.
- Riegl, B. and Piller, W.E., 1999. Coral frameworks revisited – reefs and coral carpets in the northern Red Sea. *Coral Reefs*, **18**: 241-253.

- Riegl, B. and Piller, W.E., 2000a. Mapping of benthic habitats in northern Safaga Bay (Red Sea, Egypt): A tool for proactive management. *Aquatic Conservation: Marine and Freshwater Ecosystems*, **10**: 127-140.
- Riegl, B. and Piller, W.E., 2000b. Reefs and coral carpets in the northern Red Sea as models for organism-environment feedback in coral communities and its reflection in growth fabrics. In: Insalaco, E., Skelton, P.W. and Palmer, T.J. (Eds.), *Carbonate Platform Systems: components and interactions*, Geological Society of London Special Publications, **187**: 71-88.
- Riegl, B. and Velimirov, B., 1994. The structure of coral communities at Hurghada in the northern Red Sea. *Marine Ecology*, **15**(3/4): 213-233.
- Roberts, H.H. and Murray, S.P., 1983. Controls on reef development and the terrigenous-carbonate interface on a shallow shelf, Nicaragua. *Coral Reefs*, **2**: 71-80.
- Robinson, M.K., Bauer, R.A. and Schroeder, E.H., 1979. *Atlas of Northern Atlantic Ocean – Indian Ocean Monthly Mean Temperatures and Mean Salinities of the Surface Layer*. United States Naval Oceanographic Office Reference publication, **18**.
- Robson, D.A., 1971. The structure of the Gulf of Suez (Clysmic) rift, with special reference to the eastern side. *Journal of the Geological Society of London*, **127**: 247-276.
- Roelfsema, C.M., Phinn, S.R. and Dennison, W.C., 2002. Spatial distribution of benthic microalgae on coral reefs determined by remote sensing. *Coral Reefs*, **21**(3): 264-274.
- Roeser, H.A., 1975. A detailed magnetic survey of the southern Red Sea. *Geological Journal*, **D13**: 131-153.
- Said, R., 1990a. *The Geology of Egypt*. A.A. Balkema (Rotterdam: The Netherlands), ix + 734p.
- Said, R., 1990b. Cretaceous paleogeographic maps. In: Said, R. (Ed.), *The Geology of Egypt*, A.A. Balkema (Rotterdam: The Netherlands), pp. 439-449.
- Schandelmeier, H. and Reynolds, P.-O. (Eds.), 1997. *Paleogeographic-Paleotectonic Atlas of North-Eastern Africa, Arabia and Adjacent Areas*. A.A. Balkema (Rotterdam: The Netherlands), 398p.
- Schmid, H., 2000. Paradise in Peril. *Al-Sanbouk*, **12**. Available online at: <http://www.persga.org/publications/alsanbouk/sam12.doc>, (Accessed: 07/03/2003).
- Scoffin, T.P. and Stoddart, D.R., 1978. Nature and significance of microatolls. *Philosophical Transactions of the Royal Society of London B*, **288A**: 99-122.
- Sea Around Us (SAU), 2006. *A Global Database on Marine Fisheries and Ecosystems*. Available online at: <http://www.seaaroundus.org>, (Accessed: 11/09/2006). Fisheries Centre, University of British Columbia, Vancouver (British Columbia, Canada).
- Searle, R.C. and Ross, D.A., 1975. A geophysical study of the Red Sea axial trough between 20.5°N and 22°N. *Royal Astronomical Society Geophysical Journal*, **43**: 555-572.
- Sellwood, B.E. and Netherwood, R.W., 1984. Facies evolution in the Gulf of Suez area: sedimentation history as an indicator of rift initiation and development. *Modern Geology*, **9**: 43-69.

- Sengor, A.M.C., 1979. Mid-Mesozoic closure of Permo-Triassic Thetys and its implications. *Nature*, **279**: 590-593.
- Sheppard, C.R.C., 1981. The reef and soft-substrate coral fauna of Chagos, Indian Ocean. *Journal of Natural History*, **15**: 607-621.
- Sheppard, C.R.C., 1985a. Reefs and coral assemblages of Saudi Arabia 2. Fringing reefs in the southern region, Jeddah to Jizan. *Fauna of Saudi Arabia*, **7**: 37-58.
- Sheppard, C.R.C., 1985b. The unspoiled Little Barrier Reef of Saudi Arabia. *Sea Frontiers*, **31**: 94-103.
- Sheppard, C.R.C., 1988. Similar trends, different causes: Responses of corals to stressed environments in Arabian seas. *Proceedings of the 6th International Coral Reef Symposium*, Townsville (Australia), **3**: 297-302.
- Sheppard, C.R.C., Price, A. and Roberts, C., 1992. *Marine Ecology of the Arabian Region – Patterns and Processes in Extreme Tropical Environments*. Academic Press (London: UK), 359p.
- Sheppard, C.R.C. and Sheppard, A.L.S., 1985. Reefs and assemblages of Saudi Arabia 1. The central Red Sea at Madinat al Sinaiyah. *Fauna of Saudi Arabia*, **7**: 17-36.
- Sheppard, C.R.C. and Sheppard, A.L.S., 1991. Corals and coral communities of Arabia. *Fauna of Saudi Arabia*, **12**: 3-191.
- Siddall, M., Smeed, D.A., Matthiesen, S. and Rohling, E.J., 2002. Modelling the seasonal cycle of the exchange flow in Bab El Mandab (Red Sea). *Deep-Sea Research I*, **49**(9): 1551-1569.
- Siedler, G., 1968. Schichtungs- und bewegungsverhältnisse am südausgang des Roten Meeres. *“Meteor” Forschungsergebnisse*, **A4**: 1-76.
- Smeed, D.A., 1997. Seasonal variation of the flow in the strait of Bab el Mandab. *Oceanologica Acta*, **20**(6): 773-781.
- Smeed, D.A., 2000. Hydraulic control of three-layer exchange flows: application to the Bab al Mandab. *Journal of Physical Oceanography*, **30**(10): 2574-2588.
- Sneh, A. and Friedman, G.M., 1980. Spur and groove patterns on the reefs of the northern Gulf of the Red Sea. *Journal of Sedimentary Petrology*, **50**(3): 981-986.
- Soepri Hantoro, W., 1992. Etude des Terrasses Récifales Quaternaries Soulevées entre le Détroit de la Sonde et l’Ile de Timor, Indonésie. Mouvements Verticaux de la Croûte Terrestre et Variations du niveau de la mer. Thesis Science, Marseille-Luminy.
- Sofianos, S.S., Johns, W. and Murray, S.P., 2002. Heat and freshwater budgets in the Red Sea from direct observations at Bab el Mandab. *Deep-Sea Research II*, **49**(7-8): 1323-1340.
- Spalding, M.D., Ravilious, C. and Green, E.P., 2001. *World Atlas of Coral Reefs*. UNEP-WCMC, University of California Press (Berkeley: USA), 424p.
- Spalding, M., Taylor, M., Ravilious, C., Short, F. and Green, E., 2003. Global overview – The distribution and status of seagrasses. In: Green, E.P. and Short, F.T. (Eds.), *World Atlas of Seagrasses*, UNEP-WCMC, University of California Press (Berkeley: USA), pp. 5-26.

- Steckler, M.S., 1985. Uplift and extension at the Gulf of Suez: indications of induced mantle convection. *Nature*, **317**: 135-139.
- Steckler, M.S., Berthelot, F., Lyberis, N. and Le Pichon, X., 1988. Subsidence in the Gulf of Suez: implications for rifting and plate kinematics. *Tectonophysics*, **153**: 249-270.
- Steckler, M.S. and ten Brink, U.S., 1986. Lithospheric strength variations as a control on new plate boundaries: examples from the northern Red Sea region. *Earth and Planetary Science Letters*, **79**: 120-132.
- Stoddart, D.R., 1971. Coral reefs and islands and catastrophic storms. In: Steers, J.A. (Ed.), *Applied Coastal Geomorphology*, MacMillan and Co Ltd. (London: UK), pp. 155-197.
- Sun, Q. and Esteban, M., 1994. Paleoclimatic controls on sedimentation and diagenesis and reservoir quality: Lessons from Miocene carbonates. *American Association of Petroleum Geologists Bulletin*, **78**: 519-543.
- Taviani, M., 1998. Post-Miocene reef faunas of the Red Sea: Glacio-eustatic controls. In: Purser, B.H. and Bosence, D.W.J. (Eds.), *Sedimentation and Tectonics in Rift Basins: Red Sea - Gulf of Aden*, Chapman & Hall, University Press (Cambridge: UK), pp. 574-582.
- Tourism Development Authority (TDA), 1998. *Best Practices of Tourism Center Development along the Red Sea Coast*. Cairo (Egypt), 107p.
- UNEP, 1997. *Assessment of Land-Based Sources and Activities Affecting the Marine Environment in the Red Sea and Gulf of Aden*. UNEP Regional Seas Reports and Studies, No. 166, 67p.
- Veron, J.E.N., 2000. *Coral Reefs of the World*. Australian Institute of Marine Science and CRR Qld Pty Ltd. (Townsville: Australia), 1382p.
- Vogt, H., 2000. Coral reefs and coral bleaching in the region. *Al-Sanbouk*, **12**. Available online at: <http://www.persga.org/publications/alsanbouk/sam12.doc>, (Accessed: 07/03/2003).
- Wabnitz, C., Taylor, M., Green, E. and Razak, T., 2003. *From Ocean to Aquarium - The global trade in marine ornamental species*. UNEP-WCMC (Cambridge: UK), 65p.
- Walker, D.I., 1987. Benthic algae. In: Edwards, A.J. and Head S.M. (Eds.), *Key Environments: Red Sea*, Pergamon Press (Oxford: UK), pp. 152-168.
- Walker, D.I. and Ormond, R.F.G., 1982. Coral death from sewage and phosphate pollution at Aqaba, Red Sea. *Marine Pollution Bulletin*, **13**(1): 21-25.
- Weikert, H., 1987. Plankton and the pelagic environment. In: Edwards, A.J. and Head, S.M. (Eds.), *Key Environments: Red Sea*, Pergamon Press (Oxford: UK), pp. 90-111.
- White, A.T., Fouda, M.M. and Rajasuriya, A., 1997. Status of coral reefs in south Asia, Indian Ocean and Middle East Seas (Red Sea and Persian Gulf). *Proceedings of the 8th International Coral Reef Symposium*, **I**: 301-306.

REFERENCES PART III

- Abou Rayan, M., Djebedjian, B. and Khaled, I., 2001. Water supply and demand and desalination option for Sinai, Egypt. *Desalination*, **136**: 73-81.
- Abou Zaid, M., 2002. *Impact of Diving Activities on the Coral Reefs along the Red Sea Coast of Hurghada*. mimeo Marine Biology and Fish Science Section, Zoology Department, Al-Azhar University, Cairo.
- Ackleson, S.G., 2003. Light in shallow waters: A brief research review. *Limnology & Oceanography*, **48**(1, 2): 323-328.
- Argo Information Centre (AIO), 2006. *Argo Real Time Status*. Available online at: <http://wo.jcommops.org/cgi-bin/WebObjects/Argo>, (Accessed: 16/10/06).
- Alvarez, O., 2004. Community-based coastal resource management and marine biodiversity conservation: Lessons from Punta Allen, Sian Ka'an Biosphere Reserve, Mexico. In: UNEP, *People and Reefs: Successes and Challenges in the Management of Coral Reef Marine Protected Areas*. UNEP Regional Seas Reports and Studies, No. 176, pp. 25-28.
- Andréfouët, S., Kramer, P., Torres-Pulliza, D., Joyce, K.E., Hochberg, E.J., Garza-Pérez, R., Mumby, P.J., Riegl, B., Yamano, H., White, W.H., Zubia, M., Brock, J.C., Phinn, S.R., Naseer, A., Hatcher, B.G. and Muller-Karger, F., 2003. Multi-site evaluation of IKONOS data for classification of tropical coral reef environments. *Remote Sensing of Environment*, **88**(1-2): 128-143.
- Andréfouët, S., Muller-Karger, F., Hochberg, E., Hu, C. and Carder, K., 2001. Change detection in shallow coral reef environments using Landsat 7 ETM+ data. *Remote Sensing of Environment*, **78**: 150-162.
- Andréfouët, S., Muller-Karger, F. and Hu, C., 1999. Using SPOT and Landsat images for mapping, inventory and monitoring of reefs. In: *International Workshop on the Use of Remote Sensing Tools for Mapping and Monitoring Coral Reefs*, June 7-10, 1999, Honolulu (Hawaii: USA). Available online at: http://reef.aoml.noaa.gov/corvil/coral_reefs/abstracts.html, (Accessed: 02/05/2001).
- Andréfouët, S., Mumby, P.J., McField, M., Hu, C. and Muller-Karger, F.E., 2002. Revisiting coral reef connectivity. *Coral Reefs*, **21**(1): 43-48.
- Anonymous, 1993. *World Coast Conference Statement 1993*. Available online at: <http://www.netcoast.nl/projects/netcoast/info/history/downloadwcc.htm>, (Accessed: 26/08/2004).
- Antoine, D., Morel, A., Gentiù, B., Gordon, H.R., Banzon, V.F., Evans, R.H., Brown, J.W., Walsh, S., Baringer, W. and Li, A., 2003. In search of long-term trends in ocean color. *EOS*, **84**(32): 301, 308-309.
- Armstrong, R.A., 1993. Remote sensing of submerged vegetation canopies for biomass estimation. *International Journal of Remote Sensing*, **14**(3): 621-627.

- Balch, W.M., Gordon, H.R., Bowler, B.C., Drapeau, D.T. and Booth, E.S., 2005. Calcium carbonate measurements in the surface global ocean based on Moderate-Resolution Imaging Spectroradiometer data. *Journal of Geophysical Research*, **110**, doi:10.1029/2004JC002560.
- Benny, A.H. and Dawson, G.J., 1983. Satellite imagery as an aid to bathymetric charting in the Red Sea. *The Cartographic Journal*, **20**(1): 5-16.
- Berger, M., Camps, A., Font, J., Kerr, Y., Miller, J., Johannessen, J., Boutin, J., Drinkwater, M.R., Skou, N., Floury, N., Rast, M., Rebhan, H. and Attema, E., 2002. Measuring ocean salinity with ESA's SMOS mission – Advancing the science. *ESA Bulletin*, **111**: 113-121.
- Bierwirth, P.N., Lee, T.J. and Burne, R.V., 1993. Shallow sea-floor reflectance and water depth derived by unmixing multispectral imagery. *Photogrammetric Engineering and Remote Sensing*, **59**(3): 331-338.
- Brown, K., Adger, W.N., Tompkins, E., Bacon, P., Shim, D. and Young, K., 2001. Trade-off analysis for marine protected area management. *Ecological Economics*, **37**(3): 417-434.
- Bryant, D., Burke, L., McManus, J. and Spalding, M., 1998. *Reefs at Risk – A Map-Based Indicator of Threats to the World's Coral Reefs*. WRI (Washington: USA), 56p.
- Buchroitner, M.F., 1991. Three-dimensional survey of submarine sedimentary trails by means of spaceborne remote sensing. *GeoJournal*, **24**(1): 93-101.
- Bunce, L., Townsley, P., Pomeroy, R. and Pollnac, R., 2000. *Socioeconomic Manual for Coral Reef Management*, 2nd edition. GCRMN and AIMS (Townsville:Australia), 251p.
- Burrage, D.M., Heron, M.L., Hacker, J.M., Miller, J.L., Stieglitz, T.C., Steinberg, C.R. and Prytz, A., 2003. Structure and influence of tropical river plumes in the Great Barrier Reef: application and performance of an airborne sea surface salinity mapping system. *Remote Sensing of Environment*, **85**: 204-220.
- Butler, J.B., Lane, S.N., Chandler, J.H. and Porfiri, E., 2002. Through-water close range digital photogrammetry in flume and field environments. *Photogrammetric Record*, **17**(99): 419-439.
- Bythell J.C., Pan P. and Lee J., 2001. Three-dimensional morphometric measurements of reef corals using underwater photogrammetry techniques. *Coral Reefs*, **20**: 193-199.
- Calkoen, C.J., de Valk, C.F., Wensink, G.J., Vernemmen, C. and Verstraeten, J., 2000. *Towards the Operational Use of ERS SAR for Bathymetric Mapping in Belgium using the Advanced Bathymetry Assessment System: BABEL2*. Final report of ESA project A 165, ESA, ESRIN, 55p.
- Capolsini, P., Andréfouët, S., Rion, C. and Payri, C., 2003. A comparison of Landsat ETM+, SPOT HRV, Ikonos, ASTER, and airborne MASTER data for coral reef habitat mapping in South Pacific islands. *Canadian Journal of Remote Sensing*, **29**(2): 187-200.
- Carmel, Y., Dean, D.J. and Fletcher, C.H., 2001. Combining location and classification error sources for estimating multitemporal database accuracy. *Photogrammetric Engineering & Remote Sensing*, **67**(7): 865-872.

- Carney, D. (Ed.), 1999. *Key Sheets for Sustainable Livelihoods: Resource Management 3: Integrated Coastal Management*. Available online at: <http://www.odi.org.uk/keysheets/>, (Accessed: 14/11/2002).
- Carter, D.B., 1998. *Analysis of Multiresolution Data Fusion Techniques*. Master of Science in Geography Thesis, Virginia Polytechnic Institute and State University, Blacksburg (Virginia: USA). 61p.
- Cendrero, A., 1989. Mapping and evaluation of coastal areas for planning. *Ocean and Shoreline Management*, **12**(5-6): 427-462.
- Cesar, H., 2003. *Economic valuation of the coral reefs of Egypt*. Report prepared for the MVE-unit of EEPP, funded by USAID. Preliminary version, January 2003 (mimeo).
- Cesar, H., Burke, L. and Pet-Soede, L., 2003. *The Economics of Worldwide Coral Reef Degradation*. Cesar Environmental Economics Consulting (CEEC) (Arnhem: The Netherlands), 24p.
- Chander, G. and Markham, B., 2003. Revised Landsat-5 TM radiometric calibration procedures and post-calibration dynamic ranges. *IEEE Transactions on Geoscience and Remote Sensing*, **41**(11): 2674-2677.
- Chapman, B. and Turner, J.R., 2004. Development of a Geographical Information System for the marine resources of Rodrigues. *Journal of Natural History*, **38**: 2937-2957.
- Chauvaud, S., Bouchon, C. and Manière, R., 1998. Remote sensing techniques adapted to high resolution mapping of tropical coastal marine ecosystems (coral reefs, seagrass beds and mangrove). *International Journal of Remote Sensing*, **19**(18): 3625-3639.
- Chavez, P.S., 1988. An improved dark-object subtraction technique for atmospheric scattering correction of multispectral data. *Remote Sensing of Environment*, **24**, 459-479.
- Chavez, P.S. Jr., 1996. Image-based atmospheric corrections - Revisited and improved. *Photogrammetric Engineering & Remote Sensing*, **62**(9): 1025-1036.
- Chavez, P.S. Jr., Sides, S.C. and Anderson, J.A., 1991. Comparison of three different methods to merge multiresolution and multispectral data: Landsat TM and SPOT Panchromatic. *Photogrammetric Engineering and Remote Sensing*, **57**(3): 295-303.
- Chen, D. and Stow, D., 2002. The effect of training strategies on supervised classification at different spatial resolutions. *Photogrammetric Engineering & Remote Sensing*, **68**(11): 1155-1161.
- Chong, A.K. and Schneider, K., 2001. Two-medium photogrammetry for bottlenose dolphin studies. *Photogrammetric Engineering and Remote Sensing*, **67**(5): 621-628.
- Chong, A.K. and Stratford, P., 2002. Underwater digital stereo-observation technique for Red Hydrocoral study. *Photogrammetric Engineering & Remote Sensing*, **68**(7): 745-751.
- Christie, P. and White, A., 1997. Trends in development of coastal area management in tropical countries: From central to community orientation. *Coastal Management*, **25**: 155-181.
- Cicin-Sain, B., 1993. Sustainable development and integrated coastal management. *Ocean & Coastal Management*, **21**(1-3): 11-43.

- Cicin-Sain, B., Knecht, R.W. and Fisk, G.W., 1995. Growth in capacity for integrated coastal management since UNCED: An international perspective. *Ocean & Coastal Management*, **29**(1-3): 93-123.
- Civco, D.L., Hurd, J.D., Wilson, E.H., Song, M. and Zhang, Z., 2002. A comparison of land use and land cover change detection methods. In: *2002 ASPRS-ACSM Annual Conference and FIG XXII Congress*, 22-26 April 2002.
- Clark, C.D., Mumby, P.J., Chisholm, J.R.M., Jaubert, J. and Andréfouët, S., 2000. Spectral discrimination of coral mortality states following a severe bleaching event. *International Journal of Remote Sensing*, **21**(11): 2321-2327.
- Clayton, T.D., Brock, J.C. and Worl, R.G., 2002. Application of Aster satellite imagery to regional reef threat assessment, monitoring and outreach: An example from the Eastern Red Sea. In: *Proceedings of the Seventh International Conference on Remote Sensing for Marine and Coastal Environments*, 20-22 May 2002, Miami (Florida: USA), CD-ROM.
- Congalton, R.G., 1991. A review of assessing the accuracy of classifications of remotely sensed data. *Remote Sensing of Environment*, **37**(1): 35-46.
- Coral Reef Watch (CRW), 2005. *NOAA's Coral Reef Watch*. Available online at: <http://coralreefwatch.noaa.gov/satellite/index.html>, (Accessed: 26/10/2005).
- Coyne, M.S., Battista, T.A., Anderson, M., Waddell, J., Smith, W., Jokiell, P., Kendall, M.S. and Monaco, M.E., 2003. *Benthic Habitats of the Main Hawaiian Islands*. NOAA Technical Memorandum NOS NCCOS CCMA, 152. Available online at: <http://biogeo.nos.noaa.gov/projects/mapping/pacific/>, (accessed: 04/04/2003).
- Crippen, R.E., 1989. A simple spatial filtering routine for the cosmetic removal of scan-line noise from Landsat TM P-Tape imagery. *Photogrammetric Engineering and Remote Sensing*, **55**(3): 327-331.
- Crosby, M.P., Brighthouse, G. and Pichon, M., 2002. Priorities and strategies for addressing natural and anthropogenic threats to coral reefs in Pacific Island Nations. *Ocean & Coastal Management*, **45**: 121-137.
- Crowell, M., Leatherman, S.P. and Buckley, M.K., 1991. Historical shoreline change: Error analysis and mapping accuracy. *Journal of Coastal Research*, **7**(3): 839-852.
- Cuevas-Jiménez, A., Ardisson, P.-L. and Condal, A.R., 2002. Mapping of shallow coral reefs by colour aerial photography. *International Journal of Remote Sensing*, **23**(18): 3697-3712.
- Dahdouh-Guebas, F., 2002. The use of remote sensing and GIS in the sustainable management of tropical coastal ecosystems. *Environment, Development and Sustainability*, **4**(2): 93-112.
- Dai, X. and Khorrarn, S., 1997. Quantification of the impact of misregistration on the accuracy of remotely sensed change detection. In: *Proceedings of the IEEE Geosciences and Remote Sensing Symposium*, Texas, pp. 1763-1765.

- de Béthune, S., Muller, F. and Binard, M., 1998a. Adaptive intensity matching filters: A new tool for multi-resolution data fusion. In: *Proceedings of the AGARD Conference: multi-sensor systems and data fusion for telecommunications, remote sensing and radar*, 29/09-02/10 1997, Lisbon (Portugal), pp.28-1 – 28-15.
- de Béthune, S., Muller, F. and Donnay, J.-P., 1998b. Fusion of multispectral and panchromatic images by Local Mean and Variance Matching filtering techniques. In: *Proceedings of Second International Conference "Fusion of Earth: merging point measurements, raster maps and remotely sensed images Data"*, Sophia Antipolis (France), 28-30 January 1998, pp. 31-36.
- Dewidar, K.M., 2002. Landfill detection in Hurghada, North Red Sea, Egypt, using Thematic Mapper images. *International Journal of Remote Sensing*, **23**(5): 939-948.
- Dierssen, H.M., Zimmerman, R.C., Leathers, R.A., Downes, T.V. and Davis, C.O., 2003. Ocean color remote sensing of seagrass and bathymetry in the Bahamas Banks by high-resolution airborne imagery. *Limnology & Oceanography*, **48**(1-2): 444-455.
- DigitalGlobe, 2004. *Product Information – Standard Imagery*. Available online at: http://www.digitalglobe.com/product/standard_imagery.shtml, (Accessed: 01/12/2004).
- Dixon, J.A., Scura, L.F. and van 't Hof, 1994. Valuation of a marine resource. In: Perrings, C., Mäler, K.-G., Folke, C., Holling, C.S. and Jansson, B.-O. (Eds.), *Biodiversity Conservation: Problems and Politics*. Kluwer Academic Press (Dordrecht: The Netherlands).
- Dobson, E.L. and Dustan, P., 2000. The use of satellite imagery for detection of shifts in coral reef communities. In: *Proceedings of the American Society for Photogrammetry and Remote Sensing*, 22-26 May 2000, Washington D.C. (USA), CD-ROM.
- Drummond, J.E., Tait, D.A. and Zamlope, Z., 1997. Building a coastal GIS using digital photogrammetry. *The Photogrammetric Record*, **15**(90): 863-873.
- Du, Y., Teillet, P.M. and Cihlar, J., 2002. Radiometric normalisation of multitemporal high-resolution satellite images with quality control for land cover change detection. *Remote Sensing of Environment*, **82**: 123-134.
- Durand, D. and Cauneau, F., 1997. Diffuse attenuation in turbid shallow-water: Influence on water-leaving radiance measured by airborne spectrometers. In: *Proceedings of the 3rd International Airborne Remote Sensing Conference and Exhibition*, ERIM (Ann Arbor, MI: USA), **Vol.2**:543–544.
- Durand, D., Bijaoui, J. and Cauneau, F., 2000. Optical remote sensing of shallow-water environmental parameters: A feasibility study. *Remote Sensing of Environment*, **73**(2): 152-161.
- Dustan, P., Dobson, E. and Nelson, G., 2001. Landsat Thematic Mapper: Detection of shifts in community composition of coral reefs. *Conservation Biology*, **15**(4): 892-902.
- Earth Remote Sensing Data Analysis Center (ERSDAC), 2003. *ASTER User's Guide*. Available online at: http://www.science.aster.ersdac.or.jp/en/documnts/users_guide/index.html, (Accessed: 09/10/2006).

- Edwards, A.J. (Ed.), 1999. Applications of satellite and airborne image data to coastal management. *Coastal Region and Small Island Papers*, 4. UNESCO (Paris: France), 185pp.
- Edwards, A.J., 2000. Guidelines for busy decision makers. In: Green, E.P., Mumby, P.J., Edwards, A.J. and Clark, C.D. (Eds.), *Remote Sensing Handbook for Tropical Coastal Management*. Coastal Management Sourcebooks, 3, UNESCO (Paris: France), pp. 5-16.
- Edwards, F.J., 1987. Climate and oceanography. In: Edwards, A.J. and Head, S.M. (Eds.), *Key Environments: Red Sea*. Pergamon Press (Oxford: UK), pp. 45- 69.
- El-Raey, M., Abdel-Kader, F.A., Nasr, S.M. and El-Gamily, H.I., 1996. Remote sensing and GIS for an oil spill contingency plan, Ras-Mohammed, Egypt. *International Journal of Remote Sensing*, 17(11): 2013-2026.
- English, S., Wilkinson, C. and Baker, V. (Eds), 1997. *Survey Manual for Tropical Marine Resources, 2nd Edition*. AIMS (Townsville: Australia), 390p.
- Esaias, W.E., Abbott, M.R., Barton, I., Brown, O.B., Campbell, J.W., Carder, K.L., Clark, D.K., Evans, R.L., Hoge, F.E., Gordon, H.R., Balch, W.P., Letelier, R. and Minnett, P.J., 1998. Overview of MODIS capabilities for ocean science observations. *IEEE Transactions on Geoscience and Remote Sensing*, 36(4): 1250-1265.
- European Space Agency (ESA), 2005a. *Envisat Instruments: RA-2*. Available online at: <http://envisat.esa.int/instruments/ra2/>, (Accessed: 27/10/2005)
- European Space Agency (ESA), 2005b. *SMOS –Earth Explorers*. Available online at: <http://www.esa.int/esaLP/LPsmos.html>, (Accessed: 07/11/2005).
- Fauth, J.E., Bernardo, J., Camara, M., Resetarits, W.J. Jr., Van Buskirk, J. and McCollum, S.A., 1996. Simplifying the jargon of community ecology: A conceptual approach. *The American Naturalist*, 147(2): 282-286.
- Felton, J., 2000. *Tourism and Terrorism - The Road to Recovery in Egypt*. Available online at: http://www.hotel-online.com/Trends/Andersen/2001_Egypt.html, (Accessed: 22/04/2004).
- Fernandes, L., Ridgley, M.A. and van't Hof, T., 1999. Multiple criteria analysis integrates economic, ecological and social objectives for coral reef managers. *Coral Reefs*, 18: 393-402.
- Fouda, M.M., 1998. Status of coral reefs in the Middle East. In: Wilkinson, C. (ed.), *Status of coral reefs of the world: 1998*, AIMS (Townsville: Australia).
- Freire, F.F.M., 2001. The application of Geographic Information System to the coral reef of Southern Okinawa. In: *22nd Asian Conference on Remote Sensing*, 5-9 november 2001, Singapore. Available online at: <http://www.crisp.nus.edu.sg/~acrs2001/pdf/194freire.pdf>, (Accessed: 17/01/2002).
- Fyfe, S.K., 2003. Spatial and temporal variation in spectral reflectance: Are seagrass species spectrally distinct? *Limnology & Oceanography*, 48(1, 2): 464-479.

- Gabarró, C., Vall-Llossera, M., Font, J. and Camps, A., 2004. Determination of sea surface salinity and wind speed by L-band microwave radiometry from a fixed platform. *International Journal of Remote Sensing*, **25**(1): 111-128.
- Gabric, A.J., Hoffenberg, P. and Broughton, W., 1990. Spatio-temporal variability in surface chlorophyll distribution in the central Great Barrier Reef as derived from CZCS imagery. *Australian Journal of Freshwater Research*, **41**:313–324.
- Gayanilo, F.C., Silvestre, G.T. and Pauly, D., 1998. A low-level Geographic Information System for coastal zone management, with applications to Brunei Darussalam. Part III: Simulation and tracking of oil spills. *NAGA, The ICLARM Quaternary*, **21**(1): 41-43.
- Gell, F.R. and Roberts, C.M., 2003. Benefits beyond boundaries: the fishery effects of marine reserves. *TRENDS in Ecology and Evolution*, **18**(9): 448-455.
- George, D.G., 1997. Bathymetric mapping using a Compact Airborne Spectrographic Imager (CASI). *International Journal of Remote Sensing*, **18**(10): 2067-2071.
- Gerges, M.A., 2002. The Red Sea and Gulf of Aden action plan: Facing the challenges of an ocean gateway. *Ocean & Coastal Management*, **45** (11-12): 885-903.
- Gitelson, A.A. and Kondratyev, K.Y., 1991. Optical models of mesotrophic and eutrophic water bodies. *International Journal of Remote Sensing*, **12**(3): 373-385
- Gladstone, W., Tawfiq, N., Nasr, D., Andersen, I., Cheung, C., Drammeh, H., Krupp, F. and Lintner, S., 1999. Sustainable use of renewable resources and conservation in the Red Sea and Gulf of Aden: issues, needs and strategic actions. *Ocean & Coastal Management*, **42**(8): 671-697.
- Global Coral Reef Monitoring Network (GCRMN), 2004. *Global Coral Reef Monitoring Network*. Available online at: <http://www.gcrmn.org/>, (Accessed, 02/09/2006).
- Goddard Space Flight Centre (GSFC), 2005. *AQUARIUS – Sea Surface Salinity from Space*. Available online at: <http://aquarius.gsfc.nasa.gov/>, (Accessed: 26/10/2005).
- Goeke, R.F., 2004. The Coral Reef Satellite Mission. In: *Proceedings of the 11th SPIE international symposium on remote sensing*. Available online at: <http://snebulos.mit.edu/projects/crm/docs/spie-0904.pdf>, (Accessed: 12/10/2004).
- Gordon, H.R., Boynton, G.C., Balch, W.M., Groom, S.B., Harbour, D.S. and Smyth, T.J., 2001. Retrieval of coccolithophore calcite concentration from SeaWiFS imagery. *Geophysical Research Letters*, **28**(8): 1587-1590.
- Gordon, H.R. and Morel, A., 1983. *Remote Assessment of Ocean Color for Interpretation of Satellite Visible Imagery*. Springer (New York: USA).
- Gould, R.W. Jr., Arnone, R.A. and Sydor, M., 2001. Absorption, scattering and remote-sensing reflectance relationships in coastal waters: Testing a new inversion algorithm. *Journal of Coastal Research*, **17**(2): 328-341.

- Green, E., 2000. Satellite and airborne sensors useful in coastal applications. In: Green, E.P., Mumby, P.J., Edwards, A.J. and Clark, C.D., *Remote Sensing Handbook for Tropical Coastal Management*. Coastal Management Sourcebooks, 3, UNESCO (Paris: France), pp.41-56.
- Green, E.P., Clark, C.D., Mumby, P.J., Edwards, A.J. and Ellis, A.C., 1998. Remote sensing techniques for mangrove mapping. *International Journal of Remote Sensing*, **19**: 935-956.
- Green, E., Edwards, A. and Mumby, P., 2000a. Mapping bathymetry. In: Green, E.P., Mumby, P.J., Edwards, A.J. and Clark, C.D., *Remote Sensing Handbook for Tropical Coastal Management*. Coastal Management Sourcebooks, 3, UNESCO (Paris: France), pp. 219–235.
- Green, E.P., Mumby, P.J., Edwards, A.J. and Clark, C.D., 1996. A review of remote sensing for the assessment and management of tropical coastal resources. *Coastal Management*, **24**: 1-40.
- Green, E.P., Mumby, P.J., Edwards, A.J. and Clark, C.D., 2000b. *Remote Sensing Handbook for Tropical Coastal Management*. Coastal Management Sourcebooks, 3, UNESCO (Paris: France), x + 316p.
- Grimble, R. and Chan, M.-K., 1995. Stakeholder analysis for natural resource management in developing countries. *Natural Resources Forum*, **19**(2): 113–124.
- Groom, G.B., Fuller, R.M. and Jones, A.R., 1996. Contextual correction: Techniques for improving land cover mapping from remotely sensed images. *International Journal of Remote Sensing*, **17**(1): 69-89.
- Guenther, G.C., Cunningham, A.G., LaRocque, P.E. and Reid, D.J., 2000. Meeting the accuracy challenge in airborne LIDAR bathymetry. In: *EARSEL eProceedings*, **1**(1). Available online at: <http://las.physik.uni-oldenburg.de/projekte/earsel/#workshops>, (Accessed: 22/11/2004).
- Hafez, A. and El-Manharawy, S., 2002. Economics of seawater RO desalination in the Red Sea region, Egypt - Part 1: A case study. *Desalination*, **153**(1-3): 335-347.
- Hall, F.G., Strebel, D.E., Nickeson, J.E. and Goetz, S.J., 1991. Radiometric rectification: toward a common radiometric response among multi-date, multisensor images. *Remote Sensing of Environment*, **35**(1): 11-27.
- Hallock, P., Muller-Karger, F.E. and Halas, J.C., 1993. Coral reef decline. *National Geographic Explorer*, **9**: 358–378.
- Halpern, B.S., 2003. The impact of marine reserves: Do reserves work and does reserve size matter? *Ecological Applications*, **13**(1-suppl.): S117-S137.
- Hammack, J.C., 1977. Landsat goes to sea. *Photogrammetric Engineering & Remote Sensing*, **43**: 683-691.
- Hanafy, M.H., 2000. Egypt Red Sea experiment. Pan-African Conference on Sustainable Integrated Coastal Management (PACSICOM), Proceedings of the Workshops: an integrated approach, Maputo (Mozambique), 18-25 July 1998, UNESCO (Paris: France). *IOC Workshop Report*, No. 165: 97-106.
- Hardin, G., 1968. The Tragedy of the Commons. *Science*, **162**: 1243-1248.

- Hariri, K.I., Nichols, P., Krupp, F., Mishrigi, S., Barrania, A., Ali, A.F. and Kedidi, S.M., 2000. *Status of the Living Marine Resources in the Red Sea and Gulf of Aden Region and their Management*. PERSGA, 151p.
- Harley, C.D.G., Hughes, A.R., Hultgren, K.M., Miner, B.G., Sorte, C.J.B., Thomber, C.S., Rodriguez, L.F., Tomanek, L., and Williams, S.L., 2006. The impacts of climate change in coastal marine systems. *Ecology Letters*, **9**(2): 228-241.
- Harris, W.D. and Umbach, M.J., 1972. Underwater mapping. *Photogrammetric Engineering*, **38**(8): 765-772.
- Harvey, N., 1999. Australian integrated coastal management: A case study of the Great Barrier Reef. In: Salomons, W., Turner, R.K., de Lacerda, L.D. and Ramachandran, S. (Eds.), *Perspectives on Integrated Coastal Zone Management*. Springer-Verlag (Berlin: Germany), pp.279-296.
- Hassan, M., Kotb, M.M.A. and Al-Sofyani, A.A., 2002. Status of coral reefs in the Red Sea-Gulf of Aden. In: Wilkinson, C. (Ed.), *Status of the Coral Reefs of the World: 2002*, AIMS (Townsville: Australia), pp. 45-52.
- Hassenstein, W. and Hirsch, E., 2002. Invasion der Ignoranten. *Greenpeace Magazin*, **1**/02: 26-35.
- Hastings, A. and Botsford, L.W., 2003. Comparing designs of marine reserves for fisheries and for biodiversity. *Ecological Applications*, **13**(1-suppl.): S65-S70.
- Hawkins, J.P. and Roberts, C.M., 1997. Estimating the carrying capacity of coral reefs for SCUBA diving. In: *Proceedings of the 8th International Coral Reef Symposium*, **Vol. 2**: 1923-1926.
- Hay, A.M., 1979. Sampling designs to test land-use map accuracy. *Photogrammetric Engineering & Remote Sensing*, **45**(4): 529-533.
- Hedley, J.D. and Mumby, P.J., 2003. A remote sensing method for resolving depth and subpixel composition of aquatic benthos. *Limnology & Oceanography*, **48**(1, 2): 480-488.
- Heil, C.A., Chaston, K., Jones, A., Bird, P., Longstaff, B., Costanzo, S. and Dennison, W.C., 2004. Benthic microalgae in coral reef sediments of the southern Great Barrier Reef, Australia. *Coral Reefs*, **23**(3): 336-343.
- Hill, J. and Wilkinson, C., 2004. *Methods for Ecological Monitoring of Coral Reefs - Version 1*. AIMS (Townsville: Australia), vi + 117p.
- Hochberg, E.J. and Atkinson, M.J., 2000. Spectral discrimination of coral reef benthic communities. *Coral Reefs*, **19**(2): 164-171.
- Hochberg, E.J. and Atkinson, M.J., 2003. Capabilities of remote sensors to classify coral, algae, and sand as pure and mixed spectra. *Remote Sensing of Environment*, **85**(2): 174-189.
- Hochberg, E.J., Atkinson, M.J. and Andréfouët, S., 2003. Spectral reflectance of coral reef bottom types worldwide and implications for coral reef remote sensing. *Remote Sensing of Environment*, **85**(2): 159-173.
- Hoepner, T. and Latteman, S., 2002. Chemical impacts from seawater desalination plants - a case study of the northern Red Sea. *Desalination*, **152**(1-3): 133-140.

- Höhle, J., 1971. Reconstruction of the underwater object. *Photogrammetric Engineering*, **37**(9): 948-954.
- Holden, H. and LeDrew, E., 1998a. The scientific issues surrounding remote detection of submerged coral ecosystems. *Progress in Physical Geography*, **22**(2): 190-221.
- Holden, H. and LeDrew, E., 1998b. Spectral discrimination of healthy and non-healthy corals based on cluster analysis, principal components analysis, and derivative spectroscopy. *Remote Sensing of Environment*, **65**(2): 217-224.
- Holden, H. and LeDrew, E., 1999. Hyperspectral identification of coral reef features. *International Journal of Remote Sensing*, **20**(13): 2545-2563.
- Holden, H. and LeDrew, E., 2001. Multi - versus hyperspectral characteristics of common coral reef features. *Sea Technology*, **42**(2): 63-70.
- Holden, H. and LeDrew, E., 2002. Measuring and modelling water column effects on hyperspectral reflectance in a coral reef environment. *Remote Sensing of Environment*, **81**(2-3): 300-308.
- Hopley, D., 1996. Coral reefs: The problem child of environmental monitoring and remote sensing. In: *Coral Remote Sensing Workshop: Proceedings and Recommendations*, 17-18 September 1996, Miami (Florida: USA), pp.13-28.
- Houhoulis Smit P., 2001. Maximizing information content of Landsat imagery for coastal zone applications. *Photogrammetric Engineering & Remote Sensing*, **67**(7): 769-771.
- Hu, C., Muller-Karger, F., Andréfouët, S. and Carder, K., 2001. Atmospheric correction and cross-calibration of LANDSAT-7/ETM+ imagery over aquatic environments: A multiplatform approach using SeaWiFS/MODIS. *Remote Sensing of Environment*, **87**: 99-107.
- Hudgson, G., 1997. Resource use: conflicts and management solutions. In: Birkeland, C., (Ed.), *Life and Death of Coral Reefs*. Chapman & Hall (New York: USA), pp.386-410.
- Hughes, T.P., Baird, A.H., Bellwood, D.R., Card, M., Connolly, S.R., Folke, C., Grosberg, R., Hoegh-Guldberg, O., Jackson, J.B.C., Kleypas, J., Lough, J.M., Marshall, P., Nyström, M., Palumbi, S.R., Pandolfi, J.M., Rosen, B. and Roughgarden, J., 2003. Climate change, human impacts, and the resilience of coral reefs. *Science*, **301**: 929-933.
- Huguenin, R.L., Wang, M.H., Biehl, R., Stoodley, S. and Rogers, J.N., 2004. Automated subpixel photobathymetry and water quality mapping. *Photogrammetric Engineering and Remote Sensing*, **70**(1): 111-123.
- Huston, M.A., 1994. *Biological Diversity: The Coexistence of Species on Changing Landscapes*. Cambridge University Press (Cambridge, UK), 708p.
- Hutchinson, C.F., 1982. Techniques for combining Landsat and ancillary data for digital classification improvement. *Photogrammetric Engineering and Remote Sensing*, **48**(1): 123-130.
- ICRI, 1997. *Report of the Middle East Seas Regional Strategy Workshop for the International Coral Reef Initiative*, 21-25 September 1997, Aqaba (Jordan), 28p. Available online at: <http://international.nos.noaa.gov/report/mers.html>.

- ICRI, 2003. *Second International Tropical Marine Ecosystems Management Symposium Action Statement*. 15p. Available online at: http://www.icriforum.org/itmems/presentations/ITMEMS2_ActionStatement.doc, (Accessed: 09/11/2005).
- ICRI, 2006. *About ICRI*. <http://www.icriforum.org/>, (Accessed: 02/09/2006).
- Integrated Global Observation Strategy (IGOS), 2003. *IGOS Coral Reef Sub-Theme Report*. IGOS, 40p.
- International Center for Living Aquatic Resources Management (ICLARM), 1999. *Advancing Remote Sensing Technologies for the Sustainable Management of Coral Reefs. Resolution for Action*. Available online at: http://www.coral.noaa.gov/corvil/coral_reefs/resolution.html, (Accessed: 02/05/2001).
- International Coral Reef Action Network (ICRAN), 2006. *International Coral Reef Action Network*. Available online at: <http://www.icran.org/>, (Accessed: 02/09/2006).
- International Ocean Colour Coordinating Group (IOCCG), 2005. *Ocean-Colour Sensors*. Available online at: http://www.ioccg.org/sensors_ioccg.html, (Accessed: 28/10/2005).
- Intergovernmental Oceanographic Commission (IOC), 2002. *Marine Sciences and Observations for Integrated Marine Area Management*. Available online at: <http://ioc3.unesco.org/icam/>.
- IPLab (Image Processing Laboratory, South Dakota State University), 2003. *Landsat TM Artefacts – Memory Effects*. Available online at: <http://iplab2out.sdstate.edu/projects/landsat45/tmcal/artefacts/me/index.htm>, (Accessed: 10/07/2003).
- Isoun, E., Fletcher, C., Frazer, N. and Gradie, J., 2003. Multi-spectral mapping of reef bathymetry and coral cover - Kailua Bay, Hawaii. *Coral Reefs*, **22**(1): 68-82.
- IUCN, 1988. *Proceedings of the 17th Session of the General Assembly of IUCN and 17th Technical Meeting*. San Jose, Costa Rica, 1-10 February, 1988. IUCN (Gland: Switzerland).
- IUCN, 2005. Riding the tide - Experts chart a course for marine protected areas. In: *Report of the First International Marine Protected Areas Congress*, Geelong (Australia), 23-28 October 2005, 2p. Available online at: http://www.iucn.org/en/news/archive/2005/10/pr_impac_closing.pdf, (Accessed: 16/11/2005).
- Jameson, S.C., Ammar, M.S.A., Saadalla, E., Mostafa, H.M. and Riegl, B., 1999. A coral damage index and its application to diving sites in the Egyptian Red Sea. *Coral Reefs*, **18**: 333-339.
- Jerlov, N.G., 1976. *Marine Optics*. Elsevier Oceanographic Series, **14**, Elsevier Scientific Publishing Company (Amsterdam: The Netherlands), 231p.
- Jet Propulsion Laboratory (JPL), 2005a. *Ocean Surface Topography from Space*. Available online at: <http://topex-www.jpl.nasa.gov/mission/jason-1.html>, (Accessed: 27/10/2005).
- Jet Propulsion Laboratory (JPL), 2005b. *Winds – Measuring Ocean Winds from Space*. Available online at: <http://winds.jpl.nasa.gov/missions/quikscat/index.cfm>, (Accessed: 27/10/2005).
- Ji, W., Civco, D.L. and Kennard, C., 1992. Satellite remote bathymetry: A new mechanism for modeling. *Photogrammetric Engineering and Remote Sensing*, **58**(5): 545-549.

- Johannessen, J.A., Kudryavtsev, V., Chapron, B., Collard, F., Akimov, D. and Dagestad, K.-F., 2006. Backscatter and Doppler signals of surface current in SAR images: A step towards inverse modelling. In: *Proceedings of SEASAR 2006*, 23-26 January 2006, Frascati (Italy), CD-ROM.
- Joyce, K., Stanford, M. and Phinn, S., 1995. Remote sensing for coral reef monitoring: What is required? Available online at: <http://www.geosp.uq.edu.au>, (accessed: 03/10/2001).
- Joyce, K.E. and Phinn, S.R., 2001. Optimal spatial resolution for coral reef mapping. In: *IGARSS Proceedings 2001: 'Scanning the Present and Resolving the Future'*, 9-13 July 2001, University of New South Wales, Sydney (Australia), CD-ROM.
- Joyce, K.E. and Phinn, S.R., 2002. Bi-directional reflectance of corals. *International Journal of Remote Sensing*, **23**(2): 389-394.
- Jupp, D.L.B., 1988. Background and extensions to depth of penetration (DOP) mapping in shallow coastal waters. In: *Proceedings of the Symposium on Remote Sensing of the Coastal Zone*, September 1988, Gold Coast (Queensland: Australia), pp. IV.2.1 – IV.2.19.
- Kelleher, G., 1999. *Guidelines for Marine Protected Areas*. IUCN (Gland, Switzerland), xxiv +107p.
- Kennington, R.A. and Claasen, D.R., 1988. Australia's Great Barrier Reef - Management technology. In: *Proceedings of the Symposium on Remote Sensing of the Coastal Zone*, Gold Coast Queensland, Brisbane, Department of Geographic Information, pp. KA2.2-2.13.
- Khan, M.A., Fadlallah, Y.H. and Al-Hinai, K.G., 1992. Thematic mapping of subtidal coastal habitats in the western Arabian Gulf using Landsat TM data - Abu Ali Bay, Saudi Arabia. *International Journal of Remote Sensing*, **13**(4): 605-614.
- Klaus, R. and Turner, J., 2006. Improved early warning of coral bleaching using seasonally centred sea surface temperature developed from AVHRR data. In: *International Society for Reef Studies European Meeting: Programme and Abstracts*, Center for Tropical Marine Ecology, 19-22 September 2006, Bremen (Germany), p. 86.
- Kleypas, J.A., Feely, R.A., Fabry, V.J., Langdon, C., Sabine, C.L. and Robbins, L.L., 2006. *Impacts of Ocean Acidification on Coral Reefs and Other Marine Calcifiers: A Guide for Future Research*. Report of a workshop held 18-20 April 2005, St. Petersburg (Florida), sponsored by NSF, NOAA and USGS, 88p.
- Knight D., LeDrew, E. and Holden, H., 1997. Mapping submerged corals in Fiji from remote sensing and in situ measurements: Applications for integrated coastal management. *Ocean & Coastal Management*, **34**(2): 153-170.
- Kutser, T., Dekker, A.G. and Skirving, W., 2003. Modeling spectral discrimination of Great Barrier Reef benthic communities by remote sensing instruments. *Limnology & Oceanography*, **48**(1, 2): 497-510.
- Krause, K., 2003. *Radiance Conversion of QuickBird Data – Technical Note*. Digital Globe Inc., 5p.

- Kutser, T., Dekker, A.G. and Skirving, W., 2003. Modeling spectral discrimination of Great Barrier Reef benthic communities by remote sensing instruments. *Limnology & Oceanography*, **48**(1, 2): 497-510.
- Kutser, T., Skirving, W., Parslow, J., Clementson, L., Done, T., Wakeford, M. and Miller, I., 2001. Spectral discrimination of coral reef bottom types. In: *IGARSS Proceedings 2001: 'Scanning the Present and Resolving the Future'*, 9-13 July 2001, University of New South Wales, Sydney (Australia), CD-ROM.
- Lagerloef, G.S.E., 1998. *Final Report of the First Workshop Salinity Sea Ice Working Group*. La Jolla, California (USA), 7-8 February 1998. Available online at: <http://www.esr.org/lagerloef/ssiwg/ssiwgprep1.v2.html>, (Accessed:24/10/2005).
- Lagerloef, G., Swift, C. and Le Vine, D., 1995. Sea surface salinity: The next remote sensing challenge. *Oceanography*, **8**: 44-50.
- Landsat Project Science Office (LPSO), 2004. *Landsat 7 Science Data Users Handbook*. Available online at: http://ltpwww.gsfc.nasa.gov/IAS/handbook/handbook_toc.html, (Accessed: 10/27/2004).
- LeDrew, E.F., Holden, H., Wulder, M.A., Derksen, C. and Newman, C., 2004. A spatial statistical operator applied to multivariate satellite imagery for the identification of coral reef stress. *Remote Sensing & Environment*, **91**(3-4): 271-279.
- Lee, Z. and Carder, K.L., 2005. Hyperspectral remote sensing. In: Miller, R.L., Del Castillo, C.E. and McKee, B.A. (Eds.), *Remote Sensing of Coastal Aquatic Environments – Technologies, Techniques and Applications*. Remote Sensing and Digital Image Processing, 7, Springer (Dordrecht: The Netherlands), pp.181-204.
- Le Vine, D.M., Kao, M., Garvine, R. and Sanders, T., 1998. Remote sensing of ocean salinity: Results from the Delaware Coastal Current Experiment. *Journal of Atmospheric and Oceanic Technology*, **15**: 1478-1484.
- Le Vine, D., Koblinsky, C., Pellerano, F., Lagerloef, G., Chao, Y., Yueh, S. and Wilson, W., 2004. A sensor to measure salinity in the open ocean from space. *International Journal of Remote Sensing*, **25**(7-8): 1313-1318.
- Le Vine, D.M., Zaitzeff, J.B., D'Sa, E.J., Miller, J.L., Swift, C. and Goodberlet, M., 2000. Sea surface salinity: Toward an operational remote sensing system. In: Halpern, D. (Ed.), *Satellites, Oceanography and Society*, Elsevier Science B.V. (Amsterdam: The Netherlands), pp.321-335.
- Liceaga-Correa, M.A. and Euan-Avila, J.I., 2002. Assessment of coral reef bathymetric mapping using visible Landsat Thematic Mapper data. *International Journal of Remote Sensing*, **23**(1): 3-14.
- Lillesand, T.M. and Kiefer, R.W., 2000. *Remote Sensing and Image Interpretation*. John Wiley & Sons, Inc. (New York: USA), xii+724p.

- Lillicrop, J., 1996. The U. S. army corps of engineers SHOALS airborne LIDAR. In: *Coral Remote Sensing Workshop: Proceedings and Recommendations*, 17-18 September 1996, Miami (Florida: USA), pp.29-32.
- Liu, G., Strong, A.E. and Skirving, W., 2003. Remote sensing of sea surface temperatures during 2002 Barrier Reef coral bleaching. *EOS*, **84**(15): 137-144.
- Llewellyn-Jones, D., Edwards, M.C., Mutlow, C.T., Birks, A.R., Barton, I.J. and Tait, H., 2001. AATSR: Global-change and surface-temperature measurements from Envisat. *ESA Bulletin*, **105**: 10-21.
- Loehle, C. and Wein, G., 1994. Landscape habitat diversity: A multi-scale information theory approach. *Ecological Modelling*, **73**(3-4): 311-329.
- Lubchenco, J., Palumbi, S.R., Gaines, S.D. and Andelman, S., 2003. Plugging a hole in the ocean: the emerging science of marine reserves. *Ecological Applications*, **13**(1 suppl.): S3-S7.
- Lubin, D., Li, W., Dustan, P., Mazel, C.H. and Stamnes, K., 2001. Spectral signatures of coral reefs: Features from space. *Remote Sensing of Environment*, **75**(1): 127-137.
- Luczkovich, J.J., Wagner, T.W., Michalek, J.L. and Stoffle, R.W., 1993. Discrimination of coral reefs, seagrass meadows, and sand bottom types from space: A Dominican Republic case study. *Photogrammetric Engineering & Remote Sensing*, **59**(3): 385-389.
- Lyzenga, D., 1978. Passive remote sensing techniques for mapping water depth and bottom features. *Applied Optics*, **17**(3): 379-383
- Lyzenga, D.R., 1981. Remote sensing of bottom reflectance and water attenuation parameters in shallow water using aircraft and Landsat data. *International Journal of Remote Sensing*, **2**(1): 71-82.
- Lyzenga, D.R., 1985. Shallow water bathymetry using combined lidar and passive multispectral scanner data. *International Journal of Remote Sensing*, **6**: 115-125.
- Ma, Z. and Redmond, R.L., 1995. Tau coefficients for accuracy assessment of classification of remote sensing data. *Photogrammetric Engineering & Remote Sensing*, **61**(4): 435-439.
- Macleod, R.D. and Congalton, R.G., 1998. A quantitative comparison of change-detection algorithms for monitoring Eelgrass from remotely sensed data. *Photogrammetric Engineering & Remote Sensing*, **64**(3): 207-216.
- Maeder, J., Narumalani, S., Rundquist, D.C., Perk, R.L., Schalles, J., Hutchins, K. and Keck, J., 2002. Classifying and mapping general coral-reef structure using Ikonos data. *Photogrammetric Engineering & Remote Sensing*, **68**(12): 1297-1305.
- Man and Biosphere (MAB), 2006. *Biosphere Reserves: Reconciling the Conservation of Biodiversity with Economic Development*. Available online at: <http://www.unesco.org/mab/BRs.shtml>, (Accessed: 14/09/2006).
- Maritorena, S., Morel, A. and Gentili, B., 1994. Diffuse reflectance of oceanic shallow-waters: Influence of water depth and bottom albedo. *Limnology & Oceanography*, **39**(7): 1689-1703.

- Maritorena, S., 1996. Remote sensing of the water attenuation in coral reefs: A case study in French Polynesia. *International Journal of Remote Sensing*, **17**(1): 155-166.
- Matsunaga, T., Hoyano A. and Mizukami, Y., 2001. Monitoring of coral reefs on Ishigaki Island in Japan using multitemporal remote sensing data. In: Frouin, R.J., Kawamura, H. and Kishino, M. (Eds.), *Hyperspectral Remote Sensing of the Ocean, Proceedings of SPIE*, **4154**: 212-222.
- Mascia, M.B., 2001. *Designing Effective Coral Reef Marine Protected Areas - A Synthesis Report based on Presentations at the 9th International Coral Reef Symposium (Bali, Indonesia, October 2000)*. IUCN (Gland: Switzerland), 22p.
- McClanahan, T.R., 1999. Is there a future for coral reef parks in poor tropical countries? *Coral Reefs*, **18**(4): 321 -325.
- McClanahan, T., Ateweberhan, M., Sebastian, C.R., Graham, N.A.J., Wilson, S.K., Bruggemann, H. and Guillaume, M.M., 2006. Synoptic view of coral bleaching predictability and effects. In: *International Society for Reef Studies European Meeting: Programme and Abstracts*, Center for Tropical Marine Ecology, 19-22 September 2006, Bremen (Germany), p.79.
- McEachern, J., 2002. The Red Sea marine protected area conservation project. In: *Abstractbook of the First Egyptian-International Conference on Protected Areas and Sustainable Development*, October 23-26, 2002, Sharm-el-Sheikh (Egypt), p. 10.
- McNeill, S.E., 1994. The selection and design of marine protected areas: Australia as a case study. *Biodiversity and Conservation*, **3**(7): 586-605.
- Medio, D., Pearson, M. and Ormond, R.F.G., 1997. Effects of briefing on rates of damage to corals by scuba divers. *Biological Conservation*, **79**(1): 91-95.
- Michalek, J.L., Wagner, T.W., Luczkovich, J.J. and Stoffle, R.W., 1993. Multispectral change vector analysis for monitoring coastal marine environments. *Photogrammetric Engineering & Remote Sensing*, **59**(3): 381-384.
- Miller, R.L. and Cruise, J.F., 1995. Effects of suspended sediments on coral growth: Evidence from remote sensing and hydrologic modeling. *Remote Sensing of Environment*, **53**(3): 177-187.
- Minghelli-Roman, A., Chisholm, J.R.M., Marchioretti, M. and Jaubert, J.M., 2002. Discrimination of coral reflectance spectra in the Red Sea. *Coral Reefs*, **21**(3): 307-314.
- Mobley, C.D. and Sundman, L.K., 2003. Effects of optically shallow bottoms on upwelling radiances: Inhomogeneous and sloping bottoms. *Limnology & Oceanography*, **48**(1, 2): 329-336.
- Mobley, C.D., Zhang, H. and Voss, K.J., 2003. Effects of optically shallow bottoms on upwelling radiances: Bidirectional reflectance distribution function effects. *Limnology & Oceanography*, **48**(1, 2): 337-345.
- Moran, M.S., Jackson, R.D., Slater, P.N. and Teillet, P.M., 1992. Evaluation of simplified procedures for retrieval of land surface reflectance factors from satellite sensor output. *Remote Sensing of Environment*, **41**: 169-184.

- Morel, A. and Maritorena, S., 2001. Bio-optical properties of oceanic waters: A reappraisal. *Journal of Geophysical Research*, **106**(4): 7163-7180.
- Mumby, P.J., 2000. Methodologies for defining habitats. In: Green, E.P., Mumby, P.J., Edwards, A.J. and Clark, C.D. (Eds.), *Remote Sensing Handbook of Tropical Coastal Management*. Coastal Management Sourcebooks, 3, UNESCO (Paris: France), pp. 131-140.
- Mumby, P. and Clark, C., 2000. Radiometric correction of satellite and airborne images. In: Green, E.P., Mumby, P.J., Edwards, A.J. and Clark, C.D. (Eds.), *Remote Sensing Handbook for Tropical Coastal Management*. Coastal Management Sourcebooks, 3, UNESCO (Paris: France), pp.109-120.
- Mumby, P.J., Clark, C.D., Green, E.P. and Edwards, A.J., 1998a. Benefits of water column correction and contextual editing for mapping coral reefs. *International Journal of Remote Sensing*, **19**(1): 203-210.
- Mumby, P.J. and Edwards, A.J., 2000a. Remote sensing objectives for coastal managers. In: Green, E.P., Mumby, P.J., Edwards, A.J. and Clark, C.D., *Remote Sensing Handbook for Tropical Coastal Management*, Coastal Management Sourcebooks, 3, UNESCO (Paris: France), pp.31-40.
- Mumby, P. and Edwards, A., 2000b. Water column correction techniques. In: Green, E.P., Mumby, P.J., Edwards, A.J. and Clark, C.D. (Eds.), *Remote Sensing Handbook for Tropical Coastal Management*. Coastal Management Sourcebooks, 3, UNESCO (Paris: France), pp. 121-128.
- Mumby, P.J. and Edwards, A.J., 2002. Mapping marine environments with IKONOS imagery: Enhanced spatial resolution can deliver greater thematic accuracy. *Remote Sensing of Environment*, **82**(2-3): 248-257.
- Mumby, P.J. and Green, E.P., 2000a. Field survey: Building the link between image and reality. In: Green, E.P., Mumby, P.J., Edwards, A.J. and Clark, C.D. (Eds.), *Remote Sensing Handbook of Tropical Coastal Management*. Coastal Management Sourcebooks, 3, UNESCO (Paris: France), pp. 57-65.
- Mumby, P.J. and Green, E.P., 2000b. Mapping coral reefs and macroalgae. In: Green, E.P., Mumby, P.J., Edwards, A.J. and Clark, C.D. (Eds.), *Remote Sensing Handbook of Tropical Coastal Management*. Coastal Management Sourcebooks, 3, UNESCO (Paris: France), pp.155-174.
- Mumby, P.J., Green, E.P., Clark, C.D. and Edwards, A.J., 1998b. Digital analysis of multispectral airborne imagery of coral reefs. *Coral Reefs*, **17**(1): 59-69.
- Mumby, P.J., Green, E.P., Edwards, A.J. and Clark, C.D., 1997. Coral reef habitat mapping: How much detail can remote sensing provide? *Marine Biology*, **130**: 193-202.
- Mumby, P.J., Green, E.P., Edwards, A.J. and Clark, C.D., 1999. The cost-effectiveness of remote sensing for tropical coastal resources assessment and management. *Journal of Environmental Management*, **55**(3): 157-166.
- Mumby, P.J., Green, E.P., Edwards, A.J. and Clark, C.D., 2000. Cost-effectiveness of remote sensing for coastal management. In: Green, E.P., Mumby, P.J., Edwards, A.J. and Clark, C.D., *Remote*

- Sensing Handbook for Tropical Coastal Management*. Coastal Management Sourcebooks, 3. UNESCO (Paris: France), pp.271-286.
- Mumby, P.J. and Harborne, A.R., 1999a. Development of a systematic classification scheme of marine habitats to facilitate regional management and mapping of Caribbean coral reefs. *Biological Conservation*, **88**(2): 155-163.
- Mumby, P.J. and Harborne, A.R., 1999b. *Classification Scheme for Marine Habitats of Belize (fifth draft)*. UNDP/GEF Belize Coastal Zone Management Project. Available online at: http://www.birdlist.org/downloads/Coral_classification_scheme.pdf, (Accessed: 29/10/2002).
- Mumby, P.J., Skirving, W., Strong, A.E., Hardy J.T., LeDrew, E.F., Hochberg, E.J., Stumpf, R.P. and David, L.T., 2004. Remote sensing of coral reefs and their physical environment. *Marine Pollution Bulletin*, **48**(3-4): 219-228.
- NASA, 2005. *MODIS Web*. Available online at: <http://modis.gsfc.nasa.gov/>, (Accessed: 07/11/2005).
- National Center for Ecological Analysis and Synthesis (NCEAS), 2001. *Scientific Consensus Statement on Marine Reserves and Marine Protected Areas*. Available online at: <http://www.nceas.ucsb.edu/consensus/consensus.pdf>, (Accessed: 17/11/2005).
- Newman, C.M. and LeDrew, E.F., 2001. Assessment of Beer's law of logarithmic attenuation for remote sensing of shallow tropical waters. In: *Proceedings of the 21th IEEE symposium*, Canberra (Australia), CD-ROM.
- NOAA-AOML (Atlantic Oceanographic and Meteorological Laboratory), 2006. *The Global Drifter Program*. Available online at: <http://www.aoml.noaa.gov/phod/dac/gdp.html>, (Accessed:16/10/2006).
- NOAA/NESDIS (National Environmental, Satellite, Data and Information System), 2005. *Satellites*. Available online at: <http://www.nesdis.noaa.gov/satellites.html>, (Accessed: 07/11/2005).
- NOAA/OSCAR, 2005. *OSCAR - Ocean Surface Current Analysis Real-time*. Available online at: <http://www.oscar.noaa.gov/>, (Accessed: 16/10/2006).
- NOAA/OSDPD (Office of Satellite Data Processing and Distribution), 2005. *Operational Satellite Coral Bleaching Monitoring Products Methodology*. Available online at: <http://www.OSDPDd.noaa.gov/PSB/EPS/SST/methodology.html>, (Accessed: 07/11/2005).
- NOAA/OSDPD, 2006a. *Sea Surface Temperature (SST) Contour Charts*. Available online at: <http://www.osdpd.noaa.gov/PSB/EPS/SST/contour.html>, (Accessed: 16/10/2006).
- NOAA/OSDPD, 2006b. *Current Operational SST Anomaly Charts for the Year 2006*. Available online at: <http://www.osdpd.noaa.gov/PSB/EPS/SST/climo.html>, (Accessed: 16/10/2006).
- NOAA/OSDPD, 2006c. *Current Operational Coral Bleaching HotSpots for the Year 2006*. Available online at: <http://www.osdpd.noaa.gov/PSB/EPS/SST/climohot.html>, (Accessed: 16/10/2006).
- NOAA/OSDPD, 2006d. *Degree Heating Week Charts for the Year 2006*. Available online at: http://www.osdpd.noaa.gov/PSB/EPS/SST/dhw_retro.html, (Accessed: 16/10/2006).

- NOAA/SIS (Satellite and Information Service), 2005. *Advanced Very High Resolution Radiometer – AVHRR*. Available online at: <http://noaasis.noaa.gov/NOAASIS/ml/avhrr.html>, (Accessed: 07/11/2005).
- Ohde, T. and Siegel, H., 2001. Correction of bottom influence in ocean colour satellite images of shallow water areas in the Baltic Sea. *International Journal of remote Sensing*, **22**(2-3): 297-313.
- Okamoto, A., 1982. Wave influences in two-media photogrammetry. *Photogrammetric Engineering & Remote Sensing*, **48**(9): 1487-1499.
- O'Neill, N.T. and Miller, J.R., 1989. On calibration of passive optical bathymetry through depth soundings – Analysis and treatment of errors resulting from the spatial variation of environmental parameters. *International Journal of Remote Sensing*, **10**(9): 1481-1501.
- Optech, 2004. *About LIDAR*. Available online at: <http://www.optech.ca/aboutlaser.htm>.
- Ormond, R., 1987. Conservation and Management. In: Edwards, A.J. and Head, S.M. (Eds.), *Key Environments: Red Sea*. Pergamon Press (Oxford: UK), pp.405-423.
- Orszbag-Sperber, F., Purser, B.H., Rioual, M. and Plaziat, J.-C., 1998. Post-Miocene sedimentation and rift dynamics in the southern Gulf of Suez and northern Red Sea. In: Purser, B.H. and Bosence, D.W.J. (Eds.), *Sedimentation and Tectonics in Rift Basins: Red Sea - Gulf of Aden*, Chapman & Hall, University Press (Cambridge: UK), pp. 427-447.
- Ouaidrari, H. and Vermote, E.F., 1999. Operational atmospheric correction of Landsat TM data. *Remote Sensing of Environment*, **70**(1): 4-15.
- Palandro, D., 2000. *Coral Reef Change Detection Using Landsats 5 and 7: A Case Study Using Carysfort Reef In The Florida Keys*. Unpublished Master Thesis, College of Marine Sciences, University of South Florida, 61p.
- Palandro, D., Andréfouët, S., Muller-Karger, F.E., Dustan, P., Hu, C. and Hallock, P., 2003. Detection of changes in coral reef communities using Landsat-5 TM and Landsat-7 ETM+ data. *Canadian Journal of Remote Sensing*, **29**(2): 201-209.
- Palumbi, S.R., 2003. Population genetics, demographic connectivity, and the design of marine reserves. *Ecological Applications*, **13**(1-suppl.): S146-S158.
- Paredes, J.M. and Spero, R.E., 1983. Water depth mapping from passive remote sensing data under a generalized ratio assumption. *Applied Optics*, **22**(8): 1134-1135.
- Pasqualini, V., Pergent-Martini, C., Clabaut, P., Marteel, H. and Pergent, G., 2001. Integration of aerial remote sensing, photogrammetry, and GIS technologies in seagrass mapping. *Photogrammetric Engineering and Remote Sensing*, **67**(1): 99-105.
- PERSGA, 2001. *Strategic Action Programme for the Red Sea and Gulf of Aden. Volume 2: Country Reports*. World Bank (Washington D.C.: USA), 217p.
- Philpot, W.D., 1987. Radiative transfer in stratified waters: A single-scattering approximation for irradiance. *Applied Optics*, **26**: 4123.

- Philpot, W.D., 1989. Bathymetric mapping with passive multispectral imagery. *Applied Optics*, **28**(8): 1569-1578.
- Phinn, S.R., Menges, C., Hill, G.J.E. and Stanford, M., 2000. Optimizing remotely sensed solutions for monitoring, modelling, and managing coastal environments. *Remote Sensing of Environment*, **73**(2): 117-132.
- Phinney, J.T., Muller-Karger, F., Dustan, P. and Sobel, J., 2001. Using remote sensing to reassess the mass mortality of *Diadema antillarum* 1983-1984. *Conservation Biology*, **15**(4): 885-891.
- Pilcher, N. and Abou Zaid, M.M., 2003. Coral Reefs of Egypt. In: PERSGA, Coral Reefs in the Red Sea and Gulf of Aden – Surveys 1990 to 2000 Summary and Recommendations. *PERSGA Technical Report*, No. 7: 1-12.
- Pilcher, N. and Alsuhaibany, A., 2000. Regional status of coral reefs in the Red Sea and the Gulf of Aden. In: Wilkinson, C. (Ed.), *Status of Coral Reefs in the World: 2000*. AIMS (Townsville: Australia), pp. 35-54.
- Pilon, P.G., Howarth, P.J. and Bullock, R.A., 1988. An enhanced classification approach to change detection in semi-arid environments. *Photogrammetric Engineering & Remote Sensing*, **54**(12): 1709-1716.
- Planetary Coral Reef Foundation (PCRF), 2002. *The Planetary Coral Reef Foundation*. Available online at: <http://www.pcrf.org/>, (Accessed: 12/10/2004).
- Pohl, C. and Van Genderen, J.L., 1998. Multisensor image fusion in remote sensing: Concepts, methods and applications. *International Journal of Remote Sensing*, **19**(5): 823-854.
- Post, J.C. and Lundin, C.G. (Eds.), 1996. Guidelines for integrated coastal zone management. *Environmentally Sustainable Development Studies and Monographs Series*, No. 9, World Bank (Washington DC: USA), 16p.
- Purkis, S., Kenter, J.A.M., Oikonomou, E.K. and Robinson, I.S., 2002. High resolution ground verification, cluster analysis and optical model of reef substrate coverage on Landsat TM imagery (Red Sea, Egypt). *International Journal of Remote Sensing*, **23**(8): 1677-1698.
- Radiarta, I.N., Tripathi, N.K., Borne, F. and Jensen, K.R., 2002. *Coral Reef Habitat Mapping: A Case Study in Mensanak Island - Senayang Lingga, Riau Province, Indonesia*. GISdevelopment.net, Available online at: <http://www.gisdevelopment.net/application/nrm/coastal/mnm/>, (Accessed: 12/01/2003).
- Ranchin, T. and Wald, L., 2000. Fusion of high spatial and spectral resolution images: The ARSIS concept and its implementation. *Photogrammetric Engineering and Remote Sensing*, **66**(1): 49-61.
- Remote Sensing Systems (REMSS), 2003. *Description of TMI Data Products*. Available online at: http://www.smmi.com/tmi/tmi_description.html, (Accessed: 16/10/2006).
- Riegl, B. and Luke, K.E., 1998. Ecological characteristics of dynamited reefs in the northern Red Sea and their relevance to reef rehabilitation. *Marine Pollution Bulletin*, **37**(8-12): 488-498.

- Riegl, B. and Piller, W.E., 2000. Mapping of benthic habitats in northern Safaga Bay (Red Sea, Egypt): A tool for proactive management. *Aquatic Conservation: Marine and Freshwater Ecosystems*, **10**: 127-140.
- Riegl, B. and Velimirov, B., 1991. How many damaged corals in Red Sea reef systems? *Hydrobiologia*, **216/217**: 249-256.
- Rinner, K., 1969. Two media photogrammetry. *Photogrammetric Engineering*, **35**(3): 275-282.
- Roberts, C. M., 1997. Connectivity and management of Caribbean coral reefs. *Science*, **278**:1454–1457.
- Roberts, C.M., Andelman, S., Branch, G., Bustamante, R.H., Castilla, J.C., Dugan, J., Halpern, B.S., Lafferty, K.D., Leslie, H., Lubchenco, J., McArdle, D., Possingham, H.P., Ruckelshaus, M. and Warner, R.R., 2003a. Ecological criteria for evaluating candidate sites for marine reserves. *Ecological Applications*, **13**(1-suppl.): S199-S214.
- Roberts, C.M., Branch, G., Bustamante, R.H., Castilla, J.C., Dugan, J., Halpern, B.S., Lafferty, K.D., Leslie, H., Lubchenco, J., McArdle, D., Ruckelshaus, M. and Warner, R.R., 2003b. Application of ecological criteria in selecting marine reserves and developing reserve networks. *Ecological Applications*, **13**(1-suppl.): S215-S228.
- Roberts, C.M. and Hawkins, J.P., 2000. *Fully-Protected Marine Reserves: A Guide*. WWF and the University of York, 131p. Available online at: http://www.panda.org/resources/publications/water/mpreserves/mar_dwnld.htm, (Accessed: 01/03/2002).
- Roelfsema, C.M., Phinn, S.R. and Dennison, W.C., 2002. Spatial distribution of benthic microalgae on coral reefs determined by remote sensing. *Coral Reefs*, **21**(3): 264-274.
- Roesler, C.S., Perry, M.J. and Carder, K.L., 1989. Modeling *in situ* phytoplankton absorption from total absorption spectra in productive inland marine waters. *Limnology and Oceanography*, **34**(8): 1510-1523.
- Ross, D.S., 1969. Color enhancement of ocean cartography, In: Badgley, P.C., Miloy, L. and Childs, L. (Eds.), *The Oceans from Space*. Gulf Publishing, pp.50–63.
- Salem, S., 2002. Impact of tourism on marine habitats. *Abstractbook of the First Egyptian-International Conference on Protected Areas and Sustainable Development*. October 23-26, 2002, Sharm-el-Sheikh (Egypt), p.55.
- Salm, R.V., 1984. Ecological boundaries for coral-reef reserves: Principles and guidelines. *Environmental Conservation* **11**(3): 209-215.
- Salm, R.V., Clark, J. and Siirila, E., 2000. *Marine and Coastal Protected Areas: A Guide for Planners and Managers*. IUCN (Washington DC: USA), xxi + 371p.
- Sandidge, J.C. and Holyer, R.J., 1998. Coastal bathymetry from hyperspectral observations of water radiance. *Remote Sensing of Environment*, **65**(3): 341-352.

- Sathyendranath, S. (Ed.), 2000. Remote sensing of ocean colour in coastal, and other optically-complex, waters. *Reports of the International Ocean-Colour Coordinating Group*, No. 3, IOCCG, Dartmouth (Canada), 145p.
- Schaale, M., Fischer, J. and Keller, I., 2002. Classification of remotely sensed images by textural information. In: *Proceedings of the Fifth International Airborn Remote Sensing Conference and Exhibition*, 22-24 May 2002, Miami (Florida: USA), CD-ROM.
- Schott, J.R., Salvaggio, C. and Volchok, W.J., 1988. Radiometric scene normalisation using pseudoinvariant features. *Remote Sensing of Environment*, **26**(1): 1-16.
- Schubert, R., Schellnhuber, H.-J., Buchmann, N., Epiney, A., Griesshammer, R., Kulesa, M., Messner, D., Rahmstorf, S. and Schmid, J., 2006. *The Future Oceans - Warming Up, Rising High, Turning Sour*. German Advisory Council on Global Change (WBGU) (Berlin: Germany), xii + 110p.
- Sea Around Us (SAU), 2006. *A Global Database on Marine Fisheries and Ecosystems*. Available online at: <http://www.searoundus.org>, (Accessed: 11/09/2006). Fisheries Centre, University of British Columbia, Vancouver (British Columbia, Canada).
- Shaan, I.M., 2005. Sustainable tourism development in the Red Sea of Egypt threats and opportunities. *Journal of Cleaner Production*, **13**(2): 83-87.
- Shehata, A., 1998. Protected areas on the Gulf of Aqaba, Egypt: A mechanism of integrated coastal management. In: *International Tropical Marine Ecosystems management Symposium Proceedings*, November 1998, GBMPA (Townsville: Australia), pp.310-319.
- SOOP, 2006. *Ship of Opportunity Programme*. Available online at: http://www.jcommops.org/soopip/soopip_overview.html, (Accessed: 16/10/2006).
- Singh, A., 1989. Digital change detection techniques using remotely-sensed data. *International Journal of Remote Sensing*, **10**(6): 989-1003.
- Skirvin, S., 2004. Atmospheric and radiometric correction of Landsat Thematic Mapper data using the COST model of Chavez, 1996. Available online at: http://www2.erdas.com/SupportSite/downloads/Models/user_models/user_model_2.html, (Accessed: 16/11/2004).
- Slama, C.C. (ed.), 1980. *Manual of Photogrammetry – 4th Edition*. American Society of Photogrammetry, Falls Church (Virginia: USA), xvi + 1056p.
- Smith, R.C. and Baker, K.S., 1981. Optical properties of the clearest natural waters. *Applied Optics*, **20**(2): 177-184.
- Smith, V.E., Rogers, R.H. and Reed, L.E., 1975. Automated mapping and inventory of Great Barrier Reef zonation with Landsat data. In: *Ocean '75 conference record*, Institute of Electrical and Electronics Engineers Inc. (New York: USA).
- Smits, R. and Shousha, N., 1998. *Egypt's Red Sea Resorts ... trends and opportunities....* Available online at: http://www.hotel-online.com/Neo/Trends/Andersen/1998_EgyptResorts.html#Development, (Accessed: 22/04/2004).

- Soenen, M., 1997. *Fysisch milieu en ontwikkeling: de degradatie van de koraalriffen. Een overzichtsstudie*. Licentiaatsthesis, Vakgroep Geografie, Faculteit Wetenschappen, Universiteit Gent, 169p.
- Song, C., Woodcock, C.E., Seto, K.C., Lenney, M.P. and Macomber, S.A., 2001. Classification and change detection using Landsat TM data. When and how to correct atmospheric effects? *Remote Sensing of Environment*, **75**(2): 230-244.
- Spalding, M.D., Ravilious, C. and Green, E.P., 2001. *World Atlas of Coral Reefs*. Prepared at the UNEP World Conservation Monitoring Centre, University of California Press (Berkeley: USA), 424p.
- Spitzer, D. and Dirks, R.W.J., 1987. Bottom influence on the reflectance of the sea. *International Journal of Remote Sensing*, **8**(3): 279-290.
- Stanbury, K.B. and Starr, R.M., 1999. Applications of Geographic Information Systems (GIS) to habitat assessment and marine resource management. *Oceanologica Acta*, **22**(6): 699-703.
- Stehman, S.V., 1997. Selecting and interpreting measures of thematic classification accuracy. *Remote Sensing of Environment*, **62**(1): 77-89.
- Stehman, S.V. and Czaplewski, R.L., 1998. Design and analysis for thematic map accuracy assessment: Fundamental principles. *Remote Sensing of Environment*, **64**(3): 331-344.
- Stephens, F.C., Louchard, E.M., Reid, R.P. and Maffione, R.A., 2003. Effects of microalgal communities on reflectance spectra of carbonate sediments in subtidal optically shallow marine environments. *Limnology & Oceanography*, **48**(1, 2): 535-546.
- Stoffle, R. and Halmo, D. (Eds.), 1991. *Satellite Monitoring of Coastal Marine Ecosystems: A Case from the Dominican Republic*. Consortium for International Earth Science Information Network, University Center, Michigan (USA), 269p.
- Story, M. and Congalton, R.G., 1986. Accuracy assessment: A user's perspective. *Photogrammetric Engineering and Remote Sensing*, **52**(3): 397-399.
- Stow, D.A., 1999. Reducing the effects of misregistration on pixel-level change detection. *International Journal of Remote Sensing*, **20**(12): 2477-2483.
- Strong, A.E., Barrientos, C.S., Duda, C. and Sapper, J., 1997. Improved satellite techniques for monitoring coral reef bleaching. In: *Proceedings of the 8th International Coral Reef Symposium*, Smithsonian Tropical Research Institute (Panama), **Vol. 1**: 1495-1498
- Stumpf, R.P., Holderied, K. and Sinclair, M., 2002. Mapping coral reef bathymetry with high resolution, multispectral satellite imagery. In: *Proceedings of the Seventh International Conference on Remote Sensing for Marine and Coastal Environments*, 20-22 may 2002, Miami (Florida: USA), CD-ROM.
- Stumpf, R.P., Holderied, K. and Sinclair, M., 2003. Determination of water depth with high-resolution satellite imagery over variable bottom-types. *Limnology and Oceanography*, **48**(1, part 2): 547-556.

- Swift, C.T. and McIntosh, R.E., 1983. Considerations for microwave remote sensing of ocean salinity. *IEEE Transcripts on Geosciences and Remote Sensing*, **GE-21**: 480-491.
- Tanis, F.J., Malinas, N.P., Holland, D. and Albasini, J., 2002. Shallow water extraction algorithm for bathymetry and bottom features. In: *Proceedings of the 7th International Conference on Remote Sensing for Marine and Coastal Environments*, 20-22 May 2002, Miami (Florida: USA), CD-ROM.
- Tanré, D., Deroo, C., Duhaut, P., Herman, M., Morcrette, J.J., Perbos, J. and Deschamps, P.Y., 1990. Description of a computer code to simulate the satellite signal in the solar spectrum: The 5S code. *International Journal of Remote Sensing*, **11**(4): 659-668.
- Tassan, S., 1996. Modified Lyzenga's method for macroalgae detection in water with nonuniform composition. *International Journal of Remote Sensing*, **17**(8): 1601-1607.
- TDA, 1995. *Investment Prospective – Annual Report*. Ministry of Tourism, Tourism Development Authority, 12p.
- TDA, 1996. *Investment Prospective – Annual Report*. Ministry of Tourism, Tourism Development Authority, 12p.
- TDA, 1998. *Best Practices for Tourism Center Development along the Red Sea Coast*, 107p.
- Tewinkle, G.C., 1963. Water depths from aerial photographs. *Photogrammetric Engineering*, **29**(6): 1037-1042.
- Thanilachalam, M. and Ramachandran, S., 2002. Management of coral reefs in Gulf of Mannar using remote sensing and GIS techniques - With reference to coastal geomorphology and land use. *Map Asia 2002*. Available online at: <http://www.gisdevelopment.net/application/nrm/coastal/mmm/>, (Accessed: 12/01/2003).
- Tilmant, J. (Ed.), 2004. *Coral Reef Protected Areas: A Guide for Management*. U.S. Coral Reef Task Force, Department of the Interior (Washington DC: USA), 14p.
- Townsend, P.A., Justice, C.O., Gurney, C. and McManus, J., 1992. The impact of misregistration on change detection. *IEEE Transaction on Geoscience and Remote Sensing*, **30**: 1054-1060.
- Turner, R.K. and Salomons, W., 1999. Introduction and overview. In: Salomons, W., Turner, R.K., de Lacerda, L.D. and Ramachandran, S. (Eds.), *Perspectives on Integrated Coastal Zone Management*. Springer-Verlag (Berlin: Germany), pp.1-10.
- UN, 2003. *World Summit on Sustainable Development – Plan of Implementation*. Johannesburg, 26/08-04/09/2002, Available online at: http://www.un.org/esa/sustdev/documents/WSSD_POI_PD/English/WSSD_PlanImpl.pdf, (Accessed: 21/11/2005).
- UNEP, 1997. Assessment of land-based sources and activities affecting the marine environment in the Red Sea and Gulf of Aden. *UNEP Regional Seas Reports and Studies*, No. 166: 67p.
- UNEP, 2003. <http://corals.unep.org/>, (Accessed: 02/09/2006).
- UNEP, 2004. People and reefs: Successes and challenges in the management of coral reef marine protected areas. *UNEP Regional Seas Reports and Studies*, No. 176.

- UNEP, 2005. <http://www.unep.org/regionalseas/default.asp>, (Accessed: 02/09/2006).
- UNEP, 2006. <http://islands.unep.ch/>, (Accessed: 02/09/2006).
- United States Geological Survey (USGS), 2005. *Landsat Project Website*. Available online at: <http://landsat.usgs.gov/>, (Accessed: 13/04/2005).
- USGS, 2006a. *Landsat 7 history*. Available online at: http://landsat.usgs.gov/project_facts/history/landsat_7.php, (Accessed: 24/10/2006).
- USGS, 2006b. *Landsat 5 history*. Available online at: http://landsat.usgs.gov/project_facts/history/landsat_5.php, (Accessed: 24/10/2006).
- Van Genderen, J.L. and Pohl, C., 1994. Image fusion: Issues, techniques and applications. In: *Proceedings of the EARSeL Workshop "Intelligent Image Fusion"*, 11 September 1994, Strasbourg (France), pp.18-26.
- Van Hengel, W. and Spitzer, D., 1991. Multitemporal water depth mapping by means of Landsat TM. *International Journal of Remote Sensing*, **12**(4): 703-712.
- Vermote, E.F., Tanré, D., Deuze, J.L., Herman, M. and Morcrette, J.J., 1997. Second simulation of the satellite signal in the solar spectrum, 6S: An overview. *IEEE Transactions on Geoscience and Remote Sensing*, **35**: 675-686.
- Vogelmann, J.E., Helder, D., Morfitt, R., Choate, M.J., Merchant, J.W. and Bulley, H., 2001. Effects of Landsat 5 Thematic Mapper and Landsat 7 Enhanced Thematic Mapper Plus radiometric and geometric calibrations and correction on landscape characterization. *Remote sensing of Environment*, **78**(1-2): 55-70.
- Vogt, H., 2000. Coral reefs and coral bleaching in the region. *Al-Sanbouk*, **12**. Available online at: <http://www.persga.org/publications/alsanbouk/sam12.doc>, (Accessed: 07/03/2003).
- Wagner, T.W., Michalek, J.L. and Laurin, R., 1991. Remote sensing applications in the coastal zone. In: Stoffle, R. and Halmo, D. (Eds.), *Satellite Monitoring of Coastal Marine Ecosystems: A Case from the Dominican Republic*, Consortium for International Earth Science Information Network, Michigan (USA), pp. 17-56.
- Wald, L., Ranchin, T. and Mangolini, M., 1997. Fusion of satellite images of different spatial resolutions: Assessing the quality of resulting images. *Photogrammetric Engineering and Remote Sensing*, **63**(6): 691-699.
- Wellington, G.M., Glynn, P.W., Strong, A.E., Navarrete, S.A., Wieters, E. and Hubbard, D., 2001. Crisis on coral reefs linked to climate change. *EOS*, **82**(1): 7p.
- Werdell, P.J. and Roesler, C.S., 2003. Remote assessment of benthic substrate composition in shallow waters using multispectral reflectance. *Limnology & Oceanography*, **48**(1, 2): 557-567.
- West, J.M. and Salm, R.V., 2003. Resistance and resilience to coral bleaching: Implications for coral reef conservation and management. *Conservation Biology*, **17**(4): 956-967.

- Westaway, R.M., Lane, S.N. and Hicks, D.M., 2000. The development of an automated correction procedure for digital photogrammetry for the study of wide, shallow gravel-bed rivers. *Earth Surface Processes and Landforms*, **25**: 209-226.
- Westaway, R.M., Lane, S.N. and Hicks, D.M., 2001. Remote sensing of clear-water, shallow, gravel-bed rivers using digital photogrammetry. *Photogrammetric Engineering & Remote Sensing*, **67**(11): 1271-1281.
- Westmacott S., 2002. Where should the focus be in tropical integrated coastal management? *Coastal Management*, **30**(1): 67-84.
- Westmacott, S., Teleki, K., Wells, S. and West, J.M., 2000. *Management of Bleached and Severely Damaged Coral Reefs*. IUCN (Gland: Switzerland), vi+37p.
- Wilkinson, C.R. and Buddemeier, R.W., 1994. *Global Climate Change and Coral Reefs: Implications for People and Reefs*. Report of the UNEP-IOC-ASPEI-IUCN Global Task Team on the implications of climate change on coral reefs, IUCN (Gland: Switzerland), x+124p.
- Wilkinson, C., Green, A., Almany, J. and Dionne, S., 2003. *Monitoring Coral Reef Marine Protected Areas*. AIMS and IUCN, 72p.
- Wilson, M., 1998. The GEF Egyptian Red Sea coastal and marine resource management project - A decade of effort, experience and trade-offs required to achieve marine tourism and conservation goals. In: *International Tropical Marine Ecosystems management Symposium Proceedings*, November 1998, GBRMPA (Townsville: Australia), pp. 239-250.
- Winer, N. and Harrigan, W.J., 1999. *Zoning for the Sustainable Use of the Red Sea's Marine Resources*. USAID and Government of Egypt, 17p.
- Woodruff, D.L., Stumpf, R.P., Scope, J.A. and Paerl, H.W., 1999. Remote estimation of water clarity in optically complex estuarine waters. *Remote Sensing of Environment*, **68**: 41-52.
- World Heritage Centre (WHC), 2003. *Biodiversity Partnerships*. Paris (France).
- World Heritage Centre (WHC), 2006. *World Heritage List*. Available online at: <http://whc.unesco.org/en/list>, (Accessed: 14/09/2006).
- World Tourism Organisation (WTO), 2005. *Yearbook of Tourism Statistics – data 1999-2003: Volume I*. WTO (Madrid: Spain), pp.232-239.
- Yamano, H. and Tamura, M., 2004. Detection limits of coral reef bleaching by satellite remote sensing: Simulation and data analysis. *Remote Sensing of Environment*, **90**: 86-103.
- Yang, X. and Lo, C.P., 2000. Relative radiometric normalization performance for change detection from multi-date satellite images. *Photogrammetric Engineering & Remote Sensing*, **66**(8): 967-980.
- Yuan, D. and Elvidge, C.D., 1996. Comparison of relative radiometric normalization techniques. *ISPRS Journal of Photogrammetry & Remote Sensing*, **51**(3): 117-126.

- Zainal, A.J.M., Dalby, D.H. and Robinson, I.S., 1993. Monitoring marine ecological changes on the east coast of Bahrain with Landsat TM. *Photogrammetric Engineering & Remote Sensing*, **59**(3): 415-421.
- Zhang, M., Carder, K., Muller-Karger, F.E., Lee, Z. and Goldgof, D.B., 1999. Noise reduction and atmospheric correction for coastal applications of Landsat Thematic Mapper imagery. *Remote Sensing of Environment*, **70**: 167-180.
- Zhang, J., Zhang, Z., Shen, W. and Wang, Z., 1996. Virtuozo digital photogrammetry system and its theoretical foundation and key algorithms. In: *Proceedings of the XVII Congress of ISPRS*, 9p.

